AD NUMBER

AD904310

NEW LIMITATION CHANGE

TO

Approved for public release, distribution unlimited

FROM

Distribution authorized to U.S. Gov't. agencies only; Test and Evaluation; Mar 1972. Other requests shall be referred to U.S. Tank Automotive Command, Warren, MI.

AUTHORITY

USATAC ltr, 11 Jul 1974

TECHNICAL REPORT NO. 11398

Engine Simulation Studies

conducted at
The University of Wisconsin

MARCH 1972

Contract No. DAAE07-70-C-3336

by
G. L. Borman
P. S. Myers
O. A. Uyehara

The University of Wisconsin
Department of
Mechanical Engineering
Madison, Wisc.

TACOM

PROPULSION SYSTEMS LABORATORY

U.S. ARMY TANK AUTOMOTIVE COMMAND Warren, Michigan

Unclassified

TECHNICAL REPORT NO. 11398

Engine Simulation Studies

conducted at
The University of Wisconsin

MARCH 1972

Contract No. DAAE07-70-C-3336

by

G. L. Borman
P. S. Myers
O. A. Uyehara

The University of Wisconsin
Department of
Mechanical Engineering
Madison, Wisc.

TACOM

PROPULSION SYSTEMS LABORATORY

U.S. ARMY TANK AUTOMOTIVE COMMAND Warren, Michigan

REPORT NO. 11398

FINAL REPORT

ON

ENGINE SIMULATION STUDIES

conducted at the

UNIVERSITY OF WISCONSIN

for the

ARMY TANK AND AUTOMOTIVE COMMAND

BY

Professor G.L. Borman

Professor P.S. Myers

Professor O.A. Uyehara

The Department of Mechanical Engineering
The University of Wisconsin
Madison, Wisconsin

Contract No.

DAAE07-70-C-3336

MARCH 1972

SUMMARY

The report covers work done at the University of Wisconsin to develop an engine simulation program at the University of Wisconsin for use by the Army Tank and Automotive Command in their engine development program. Such a program is needed as an engine development tool as well as an aid in evaluating proposed unusual engine configurations.

At the start of the contract an engine simulation program was written using the best available information. At the end of the contract this program was rewritten to update it and make it compatible with the more modern computer the Univac 1108. Full details including the computer program are given for this final program.

In addition to the writing and rewriting of the program, considerable effort was expended in comparing the program with experimental data and in developing new data. Areas that were studied included a parameter study of an engine, the development of a data acquisition and handling system, studies in both convective and radiant heat transfer and in the effect of heat transfer on intake manifold oscillations and studies in obtaining rates of heat release and in developing a model for combustion in a diesel engine.

The current status of engine simulations and recommendations as to ways in which TACOM can benefit by using the program are given.

TABLE OF CONTENTS

I. INTRODUCTION

A. Reasons for Developing the Program (TACOM)

The Army Tank and Automotive Command (TACOM) has a continuing need for power sources which occupy less space, consume less fuel, reject less heat and have less audible and exhaust emissions. In general, the needs of TACOM have been more demanding and in advance of current industrial requirements. Thus an active ahead-of-the-state-of-the-art engine development program has been and must in the future be conducted by TACOM if their needs are to be met. This program involves evaluation of new approaches and configurations as well as major changes and advances in existing configurations. Because the program is in advance of the state-of-the-art there is a strong need for analytical extrapolation techniques to support and correct intuitive judgments based on experience and "know how".

Simplified analytical representations of the thermodynamic, fluid flow, heat transfer and chemical reaction processes occurring in engines have been used for many years as a means of extrapolating to new configurations but simplicity and detailed predictions are incompatible. The advent of computers opened up new computational possibilities and made feasible much more detailed representations of engine processes with correspondingly more detailed predictions. These detailed predictions typically include predictions of pressure-time diagrams, metal temperatures, instantaneous flow rates, etc., as well as the customary performance parameters of fuel flow rates and power output and are called engine simulation.

The Army Tank and Automotive Command recognized the potential of this approach as well as the necessity for basic data to improve and support more detailed simulations. Consequently, they have supported work to provide and strengthen a simulation program at the University of Wisconsin. This report is a detailed summary of the work done under Contract No. DA-11-022-AMC-1385(T) covering a period of approximately six years.

At the start of the contract (1964) there was limited activity in industry in developing engine simulation programs. Because such computer programs were in their infancy and because of their proprietary nature only one computer program was available to TACOM. However complete detail as to the assumptions made in this computer program was not available and the extent of agreement between experimental and computed results was not clear. Consequently, the Army Tank and Automotive Command could obtain the use of a tested program with known assumptions only by their own development efforts.

It was recognized from the beginning that there would of necessity be two parts to the development program. The first part would consist of writing an initial computer program using the best available mathematical correlations and comparing it with experimental data while the second part would consist of obtaining and correlating basic heat transfer, fluid flow and thermodynamic data needed to strengthen and improve the initial program. It was further recognized that the second part would be a time-consuming effort involving instrumentation development as well as obtaining and correlating data to prove or disprove theoretical models.

Because the personnel at the University of Wisconsin had been concerned with engine simulation developments at International Harvester (IH) and Continental Aviation and Engineering (CAE) it was judged most expeditious to conduct the first part of the development program in cooperation with these two companies. Thus the initial computer program was written as a doctoral thesis by Gary Borman for Continental Aviation under their contract with TACOM. This computer program benefited from initial computer program efforts and data developed by International Harvester. In turn, International Harvester received the benefit of the improved program. While Continental Aviation provided some experimental data, the primary evaluation of the initial computer program was conducted in cooperation with International Harvester.

Coincidentally with the computer program TACOM in cooperation with International Harvester developed a single cylinder diesel test engine suitable for experimental combustion and engine simulation studies. One of these engines was obtained on a rental basis by the University of Wisconsin, instrumented and used to develop supporting data. The details of these studies as well as the studies conducted cooperatively are presented later in this report.

B. Format of the Report

As indicated earlier the work has covered a span of approximately six years. During this time TACOM has been kept well informed about the progress being made via personal visits and discussions, periodic reports, copies of master's and doctoral theses and copies of published papers. However, it seemed appropriate to summarize at this time the work done and the current status of the engine simulation programs. This is the objective of this report.

Because the work covered a number of years, theses and papers, it is voluminous. The current program which has just been rewritten to be compatible with the UNIVAC 1108 will be presented first in this report. The presentation will briefly cover the model and equations used, the flow diagram and the considerations that should be taken into account in using the program. Following this a concise, but moderately complete, resume of all of the work done under the contract will be presented. The Appendices will include the current computer program plus instructions as to its use as well as the information in the papers presented to technical groups describing in detail the work done.

This method of presentation was chosen to meet the needs of different readers. The reader who wants only information about the current program may read only up to that point in the report and study Appendix I. The reader who would like to obtain a concise summary of all of the work done may read only the main body of the report. The reader who wishes to know more detail about any or all of the work will find additional detail in the Appendices and, if sufficiently interested, can obtain copies of the theses supported by this contract from the University of Wisconsin Library. The large physical size of the report is eloquent testimony—both as to the amount of work done and the wisdom of not including copies of the theses as part of the report.

II. PRESENTATION OF THE CURRENT PROGRAM

The current program is intended to represent in detail the in-cylinder events of a single cylinder four stroke engine plus the associated inlet and exhaust gas dynamic processes of a single cylinder engine. It is written for use with the UNIVAC 1108 and to provide maximum flexibility in use for both spark- and compression ignition and pre- and open-chamber engines. Full details are given in Appendix I.

A. Description of the Physical Model

For analysis, the single cylinder engine is divided into five systems: the intake port, the exhaust port, the engine cooling system and the engine cylinder which in some cases is subdivided in two parts. In the case of the pre chamber diesel engine, the two subdivisions of the cylinder are the pre and main chamber. In the case of spark ignition engine, the two subdivisions of the cylinder are the burned and unburned mixture, the division occurring only during the combustion period. In the case of open chamber diesel engine, the entire cylinder is considered to be one system i.e., a total of four systems.

Five equations are available to describe the behaviour of any one of these systems. These five equations are:

1. Conservation of Mass

   a. The time derivative of mass of gases, M, in a system can be written as

$$\dot{M} = \sum \dot{M}_f \qquad (1)$$

   where

   $\dot{M}_f$ is the mass flow rate between two system and the summation is carried over all the mass flow quantities for the system.

   b. The rate of mass flow, $\dot{M}_f$, between two systems, is computed from the steady flow relationship.

$$\dot{M}_f = A_e p_1 \sqrt{\phi g_c / R_1 T_1} \qquad (2)$$

where:

A_e is the effective flow area,

g_c is the dimensional constant,

R is the gas constant,

T is the temperature,

p is the pressure, and

$$\phi = \frac{2k}{k-1}\left[\left(\frac{p_2}{p_1}\right)^{2/k} - \left(\frac{p_2}{p_1}\right)^{(k+1)/k}\right],$$

where k is the specific heat ratio

Subscripts 1 & 2 denote upstream and downstream conditions respectively. Note that when the pressure ratio is critical sonic conditions prevail.

2. Conservation of Energy

The time derivative of the total internal energy, both sensible and chemical, of a system can be obtained from the energy balance as

$$\frac{d}{dt}(Mu) = \sum h_f \dot{M}_f + \sum \dot{Q}_i - \frac{p}{J}\dot{V} \tag{3}$$

where:

u is the internal energy per unit mass,

h_f is the flow enthalpy per unit mass, the summation being carried over all the flow surfaces for the system,

$\dot{Q}_i$ is the heat transfer rate to the metal wall for the ith surface, the summation being carried over all the heat transfer surfaces.

J is Joule's constant and

$\dot{V}$ is the time derivative of the volume of the system.

3. Conservation of Momentum

For unsteady isentropic flow in a straight pipe of constant cross-sectional area, the equations used are

$$\frac{\partial v}{\partial t} + v\frac{\partial v}{\partial x} + \frac{C^2}{\rho} = 0 \tag{4}$$

$$\frac{\partial \rho}{\partial t} + v\frac{\partial \rho}{\partial x} + \rho\frac{\partial v}{\partial x} = 0 \tag{5}$$

where:

v is the local velocity of gas stream

ρ is the local density,

C is the local speed of sound, and

x is the longitudinal position

4. Equation of State

The relationship between the pressure, temperature and volume is

$$pV = MRT \tag{6}$$

R, in turn, is a known function of p, T and F, the equivalence ratio of the mixture.

5. Internal Energy Equation

The equilibrium composition internal energy, u, including both the sensible and chemical energy, can be computed as a function of pressure, temperature and the composition of the gas,

$$u = u(p, T, F) \tag{7}$$

and

$$\dot{u} = \frac{\partial u}{\partial p}\dot{p} + \frac{\partial u}{\partial T}\dot{T} + \frac{\partial u}{\partial F}\dot{F} \tag{8}$$

where:

F is the equivalence ratio = f/f_s

f is the actual fuel air ratio, and

f_s is the stoichiometric fuel air ratio

Equilibrium thermodynamic properties of the products of combustion for C_nH_{2n}, as computed by E.S. Starkman and H.K. Newhall at the University of California, Berkeley, are used. As a means of interpolating in these tables, mathematical expressions were developed to give internal energy as function of pressure, temperature and equivalence ratio.

B. Systems and Assumptions

For each system thermodynamic equilibrium is assumed at each instant of time for the calculation of the thermodynamic properties of the gases in the system. The rate of heat transfer from the gas to wall is calculated for each part area using an instantaneous heat transfer coefficient, a uniform metal wall surface temperature, and an instantaneous mass-averaged system gas temperature. The model assumes no deposits on the inside surface of the walls. The other assumptions and the rate equations for various systems are described below.

1. Engine Cylinder

The instantaneous mass flow rate through either valve is computed using the steady flow equations. The flow coefficient is obtained from steady flow experiments and the valve area from the engine geometry taking into account valve dynamics and expansion effects due to temperature changes. Blow-by around the piston is neglected.

As stated above, the engine cylinder is treated differently for three different types of engines.

a. Open Chamber Diesel Engine: The engine cylinder, not having been subdivided in this case, forms only one system. The heat transfer model assumes five different surfaces. These are intake valve front area, exhaust valve front area, the cylinder head, the piston surface and the sleeve area exposed to gases at any time. The temperatures for these five surfaces are each different but assumed to be uniform for each surface.

A fictitious rate of fuel injection is specified for the combustion period and from it, the rate of heat release is computed with the assumption of instantaneous burning.

The various equations are simplified:

$$\frac{d}{dt}(M_1 u_1) = \dot{M}_I h_I + \dot{M}_E h_E + \dot{M}_{f_1} h_{f_1} + \sum_{i=1}^{5} \dot{Q}_i - \frac{p_1}{J}\dot{V}_1$$
$$\dot{M}_1 = \dot{M}_I + \dot{M}_E + \dot{M}_{f_1}$$
$$p_1 V_1 = M_1 R_1 T_1 \tag{9}$$

or

$$\frac{\dot{p}_1}{p_1} + \frac{\dot{v}_1}{v_1} = \frac{\dot{M}_1}{M_1} + \frac{\dot{R}_1}{R_1} + \frac{\dot{T}_1}{T_1} \tag{10}$$

and

$$\dot{u}_1 = \left.\frac{\partial u}{\partial p}\right)_1 \dot{p}_1 + \left.\frac{\partial u}{\partial T}\right)_1 \dot{T}_1 + \left.\frac{\partial u}{\partial F}\right)_1 \dot{F}_1 \tag{11}$$

where:

Subscript 1 is the properties in the engine cylinder, i.e., System 1,

I is flow quantities through the intake valve,

E is flow quantities through the exhaust valve, and

f is fuel.

The equation for F is obtained from the mass balances of air and fuel constituents of the mixture.

$$F_1 = \frac{\left(\frac{M_o F_o}{1+f_o}\right)_1 + \int_o^t \left[\frac{\dot{M}_I F_I}{1 + f_I} + \frac{\dot{M}_E F_E}{1 + f_E} + \frac{\dot{M}_{f_1}}{f_s}\right] dt}{\frac{M_o}{1 + f_o} + \int_o^t \left[\frac{\dot{M}_I}{1 + f_I} + \frac{\dot{M}_E}{1 + f_E}\right] dt} \tag{12}$$

where:

f is the actual fuel air ratio,

f_s is the stoichiometric fuel air ratio, and

o is initial value.

Simplification of the above equations results in the following equation for temperature derivative.

$$\dot{T}_1 = \frac{A - \frac{p_1}{D} \left.\frac{\partial u}{\partial p}\right)_1 \left[\frac{\dot{M}_1}{M_1} - \frac{\dot{V}_1}{V_1} + \frac{\dot{F}_1}{R_1} \left.\frac{\partial R}{\partial F}\right)_1\right] - \left.\frac{\partial u}{\partial F}\right)_1 \dot{F}_1}{\left.\frac{\partial u}{\partial T}\right)_1 + \left.\frac{\partial u}{\partial p}\right)_1 \frac{p_1}{T_1} \frac{C}{D}} \tag{13}$$

where:

$$A = -R_1 T_1 \frac{\dot{V}_1}{V_1} + \frac{1}{M_1}\left[\sum_{i=1}^{5} Q_i + \dot{M}_I h_I + \dot{M}_E h_E + \dot{M}_{f_1} h_{f_1} - u_1 \dot{M}_1\right],$$

$$C = 1 + \frac{T_1}{R_1} \left.\frac{\partial R}{\partial T}\right)_1, \text{ and}$$

$$D = 1 - \frac{p_1}{R_1} \left.\frac{\partial R}{\partial p}\right)_1.$$

b. Pre Chamber Diesel Engine: The engine cylinder is subdivided in two parts, main chamber (denoted by subscript "1") and the pre chamber (denoted by subscript "2"). There is gas flow between the two chambers which is computed from the steady flow equation. In addition to the five heat transfer surfaces in the main chamber, one heat transfer surface at a uniform surface temperature is assumed to exist in the pre chamber. Part of the fuel injected in the pre chamber is assumed to flow with the exiting gases to the main chamber and burn in it. Thus the heat release model specifies two different fuel burning rates for the two systems.

i. *Main Chamber* - The equations are similar to the open chamber except for additional flow term between the pre-chamber and the main chamber in the equations for energy conservation, mass conservation and equivalence ratio.

ii. *Pre Chamber* - Since the volume of the pre chamber does not change, $\dot{V}_2$ is equal to zero. The equations for the pre chamber are derived in the usual way:

$$\dot{T}_2 = \frac{A - \frac{p_2}{D}\left.\frac{\partial u}{\partial p}\right)_2\left[\frac{\dot{M}_2}{M_2} + \frac{\dot{F}_2}{R_2}\left.\frac{\partial R}{\partial F}\right)_2\right] - \left.\frac{\partial u}{\partial F}\right)_2 \dot{F}_2}{\left.\frac{\partial u}{\partial T}\right)_2 + \left.\frac{\partial u}{\partial p}\right)_2 \frac{p_2}{T_2}\frac{C}{D}}$$

where:

$$A = \frac{1}{M_2}\left[\dot{Q}_2 + \dot{M}_{f_2}h_{f_2} + \dot{M}_{12}h_{12} - u_2\dot{M}_2\right],$$

$$C = 1 + \frac{T_2}{R_2}\left.\frac{\partial R}{\partial T}\right)_2$$

$$D = 1 - \frac{p_2}{R_2}\left.\frac{\partial R}{\partial p}\right)_2$$

$\dot{M}_{12}$ is mass flow rate between pre and main chamber, and

h_{12} is the flow enthalpy

Conservation of mass for the pre chamber gives

$$\dot{M}_2 = \dot{M}_{f_2} + \dot{M}_{12} \tag{15}$$

The equation for equivalence ratio is

$$F_2 = \frac{\left(\frac{M_oF_o}{1+f_o}\right)_2 + \int_o^t\left[\frac{\dot{M}_{12}F_{12}}{1+f_{12}} + \frac{\dot{M}_{f_2}}{f_s}\right]dt}{\left(\frac{M_o}{1+f_o}\right)_2 + \int_o^t\left(\frac{\dot{M}_{12}}{1+f_{12}}\right)dt} \tag{16}$$

c. <u>Spark Ignition Engine</u>: During combustion, the spark-ignition engine combustion chamber is divided into two parts, the unburnt air-fuel mixture and the burnt products each of which are treated differently.

i. *Before Combustion* - The gases are assumed to be a homogeneous mixture of air, fuel vapor and the product of combustion from the previous cycle. Hence the internal energy, u, of the mixture can be computed as follows:

$$u = w_a u_a(T) + w_v u_v(T) + w_p u_p(p,T,F) \tag{17}$$

where

w is mass fraction of various constituents, and

u is internal energy per unit mass of various constituents.

Subscripts a is air

v is the fuel vapor, and

p is the products of combustion

The equivalence ratio, F, of the products of the combustion remains constant during the cycle. Thus, its time derivative is always zero.

Differentiating the above equation, we get

$$\dot{u} = [\dot{w}_a u_a + \dot{w}_v u_v + \dot{w}_p u_p] + \left[w_a \frac{\partial u_a}{\partial T}\dot{T} + w_v \frac{\partial u_v}{\partial T}\dot{T} + w_p\left(\frac{\partial u_p}{\partial p}\dot{p} + \frac{\partial u_p}{\partial T}\dot{T}\right)\right] \quad (18)$$

The time derivatives of the mass fractions can be computed from the mass balance for each constituent using the mass flow rates.

Substitution of the above equation in the energy equation leads us to the time derivative of the temperature of gases. The rest of the procedure is similar to an open chamber diesel engine cylinder case.

ii. *During Combustion* - From the start of the spark until the end of the burning, the engine cylinder is divided into two parts - burned and unburned. At the specified rate, a corresponding mass of the charge transfers from the unburned zone to the burned zone with an instantaneous conversion to products. Thus the mass and the volume of the burned zone monotonically increases while that of the unburned zone monotonically decreases. The mass of gases in the burned system consists only of the products of combustion. Although it is not a completely accurate assumption, the heat transfer areas of the cylinder head and the piston, assumed to be exposed to both zones, are divided in proportion to the volume, and the heat transfer areas of the sleeve and two valves are assumed to be exposed only to the unburned gas. Thus, though the unburned zone still has five heat transfer areas, the burned zone has only two. If the total mass burned, at the end of the combustion mass burning schedule, is less than 100% of the charge, the remaining part of the unburned mixture is assumed to oxidize, in the cylinder, linearly with time before exiting through the exhaust port.

The rates of change of temperatures, mass and the volumes are computed from the energy and mass balance together with the equation of state.

2. Intake Port

This system is treated differently for diesel and spark ignition engines.

a. Diesel Engine: The conservation of mass and momentum equations (Eqs. 4 and 5) with two boundary conditions - one at the open end of the intake system and the other at the valve end - are solved. The solution of these equations permits the computation of an average pressure, at that instant, for the intake port thermodynamic equations. The heat transfer model has two areas. These are the port wall and the intake valve back surfaces.

For temperatures below 3000°R, dissociation is negligible so $\partial u/\partial p$ is zero. Hence the temperature derivative simplifies to

$$\dot{T} = \left[A - \frac{\partial u}{\partial F}\dot{F}\right] \Big/ \frac{\partial u}{\partial T}$$

where:

$$A = \frac{1}{M}\left[\sum_{i=1}^{2} Q_i + \sum h_i \dot{M}_i - u\dot{M}\right] \quad (19)$$

The equivalence ratio of the gases in the port may not be zero as a result of back flow of gases from the engine cylinder to the port. The rest of the procedure is similar to that of the open chamber diesel engine cylinder case.

A simplified model of the above system can be obtained by assuming constant pressure in the intake port. The momentum equation is not solved for this alternative.

b. Spark Ignition Engine: Intake dynamics are not simulated in the spark ignition engine because the effect of the carburetor is not known. Since the carburetor is not simulated the intake system consists of an orifice followed by a volume and then the intake valve. The volume can represent the intake manifold and port as desired.

The internal energy equation is modified for the three constituent mixture and the equivalence ratio derivative is zero. The pressures in the intake manifold and the intake port are assumed to be constant. The rest of the procedure is similar to the diesel engine.

3. Exhaust Port

For both spark and compression ignition engines the properties of the gases in the exhaust port are computed from the equations for the products of combustion. In all cases the gases coming into the port system are assumed to mix instantaneously with gases already in the port system. Heat transfer is handled in a manner analogeous to that for the intake port. The exhaust port pressure is assumed to be constant. The derivation of the various rate equations follows from open chamber diesel engine cylinder.

4. Engine Coolant

Only the liquid cooling case is considered. The coolant enters the engine at a specified temperature. The rate of heat transfer to the coolant from the coolant side of the metal walls is computed from the heat transfer coefficient based on the coolant properties and the engine geometry. As the geometry of the cooling system is quite complicated, judgement is involved in determining the heat transfer coefficients.

At the end of the cycle, the total heat transfer from the gases to the walls must be equal to the total heat transfer from the walls to the coolant for the assumption of constant wall temperatures to be valid. If they are not equal, new metal wall temperatures are estimated, using an equivalent, one-dimensional, metal path length for heat transfer assigned to each part. The effect of friction between sleeve and the piston rings is also taken into account.

C. Input Data

Input data for the program is specified in detail in Appendix I but can be divided into several categories.

1. Engine Geometry

A complete physical description of the engine is required. Some of the data, such as bore, stroke, connecting rod length, etc., are easily obtained but judgements are involved in getting some of the other data such as heat transfer path lengths.

2. Valve

The flow areas through the two valves can be computed from the flow rates obtained experimentally for the particular port and valve combination by a steady flow bench test. An effective flow area as a function of valve lift is then computed. The program also needs the valve train geometry data to calculate the valve lift at the given operating conditions. Valve lifts are used to compute the effective flow area.

3. Heat Release

For the diesel engine the fuel injection rate and for the spark ignition engine the burning rate, are needed before using the program. They can either be computed from an empirical correlation or from the energy and mass balance with known cylinder pressure-time curves from similar engines.

4. Heat Transfer

As mentioned previously, the heat transfer is assumed to be one-dimensional through the metal and an equivalent one-dimensional heat transfer path length must therefore be assigned to each engine part under consideration. As the engine head geometry is very complicated, judgement must be used in assigning equivalent path lengths. In the case of the valve, it can be cooled by the valve seat as well as the valve stem when the valve is closed. Thus, the effective path lengths should be adjusted to give correct results.

On the gas side, various choices for convective heat transfer correlation in the engine cylinder are available. The program requires the desired correlation to be specified as an input item. For radiation, the radiative part of Annand's correlation with some modifications is used. For the intake and exhaust port, a choice between Eichelberg and pipe-flow type expression is made in the program with the larger value being chosen. Because of our imprecise knowledge of heat transfer a multiplying factor for each heat transfer surface is a specified input item in order to match the total heat transfer rates with either the experimental or empirical data.

5. Engine Coolant

Flow data for the coolant must be specified. The determination of the hydraulic diameter and the velocity of the cooling fluid involves a knowledge of the flow rate, inspection of the water passages and judgment as to the Reynolds number to be used. For the liquid coolant, the heat transfer coefficient is computed by a combination of boiling and convective formulas.

6. Engine Friction

Determination of brake performance from the computed indicated performance involves the estimate of friction losses. Friction due to rubbing has been assumed to be proportional to maximum pressure during the cycle and the accessories friction proportional to the mean piston speed.

7. Error Limits and Initial Values

Error limits for rate variables such as T, F etc., and for cyclic variables such as initial pressure, temperature are needed. Also the initial values of the cyclic variables are needed.

D. *Considerations in Applying the Program*

The current program provides the most detail of incylinder events of any simulation that now exists. Because it does provide so much detail there is a natural tendency to "ask questions" of the program that is is not programmed to answer. Before using the program it is essential therefore to understand both the power and limitations of the program.

First of all, information about the details of combustion are not included in the current program. Note carefully, however, that questions about the effect of changing rates of heat release can be answered with the program even though no information about how to achieve the change can be obtained. For example, no predictions about the change in the form of the rate of heat release with a change in speed can be made. At the same time the effect of engine speed on performance, assuming the variation in the rate-of-heat release to be non-existent or known, can be predicted.

A similar situation exists in the area of heat transfer. Even after considerable work done under this contract we do not have a reliable heat transfer correlation that includes the effect of engine geometry - swirl, intake turbulence, etc. Thus the detailed effect of engine geometry on heat transfer cannot be predicted.

Information regarding the detailed factors that affect engine friction is also not well established. Thus, prediction of small changes in performance due to detailed design changes is not feasible.

There is of course the danger that in pointing out the deficiencies of the program that we shall lose sight of its usefulness. The program is useful in single cylinder design and development effort that is justified. For example, using the program one can determine with useful precision the effect of changing the shape of the heat release curve. If the simulation studies show little or no benefit from changing the shape of the heat release curve the lengthy expensive laboratory studies required to determine this experimentally need not be undertaken.

In a similar manner the effect of large or radical changes in engine design or in the engine cycle can be best estimated by use of the simulation program. It is true that estimations of input items will have to be made, but in comparison with the alternative of building an experimental design, the information is speedy and inexpensive. Thus, the admonitions previously given were those given in connection with any powerful tool—use it in the way it is intended and designed for and it will be very helpful. Use in other ways can be misleading.

III. WORK DONE UNDER THE CONTRACT CULMINATING IN THE CURRENT PROGRAM

A. *Description and Evaluation of Initial Program*

Only one simulation program was available to TACOM when this contract was under consideration for initiation. Furthermore, the details of the assumptions underlying this program were not available to TACOM or its consultants. At the same time the advent of computers and the increasing demands on TACOM powerplants for higher output with lower fuel consumption emphasized the need for and the potential usefulness of a simulation program.

Personnel at Wisconsin had been instrumental in initiating a proprietary simulation program at International Harvester Company. At the initiation of the contract these same personnel were serving as consultants to Continental Aviation who, under contract with TACOM, were attempting to evaluate lean fuel-air ratio engines. By mutual understanding among all concerned a decision was made to use the expertise developed at International Harvester to write a program which would incorporate the best available information and be as complete as possible with regard to in-cylinder events. Both Continental Aviation and International Harvester would contribute experimental data to aid in evaluating the extent of agreement between computed and experimental results and both Continential Aviation and International Harvester (as well as TACOM of course) would have the resulting program available to them. Accordingly a simulation program was written and comparisons made with experimental data. While the details of the program and of the comparisons are reported in Appendix II and in some of the references given in Appendix II a concise summary of the work will be presented here.

The writing of the initial program was done by Dr. G.L. Borman. The fact that it was not necessary to rewrite the program until recently and that even then no major changes were necessary is a tribute to the excellence of the initial program.

1. Similarities and Differences between the Initial and Current Programs.

The two programs are alike in that both use the same set of basic thermodynamic relations. The differences between the two programs are as follows:

a. The current program can treat any one of the following three cases for a single-cylinder, four-stroke engine.

   i. Open chamber diesel engine
   ii. Prechamber diesel engine
   iii. Spark ignition engine

   The old program treated only the open chamber diesel engine

b. The current program is streamlined and parts of it, like valve flow area, heat transfer, the combustion model, port dynamics etc., can be changed easily.

c. The current program, as did the initial program, uses the modified Euler technique for numerical solution of the set of first order ordinary differential equations with initial values. However the current program can be easily changed to use other methods such as Runga-Kutta or Hamming's method.

d. The current program has more flexibility in using different types of heat transfer correlations. Where the old program used only Annand's convective correlation and Borman's radiative equation, the current program can use any one of the four—Annand, Woschni, Eichelberg and Pflaum—convective correlations and one of the two—Borman and Flynn—radiative formulas. It is to be noted that Flynn's radiation formula in the present form has only been verified for the TACOM experimental single cylinder diesel engine.

e. The initial program could compute the properties of products of combustion only on the lean side of the mixture. However the present program can compute the properties on both the lean and rich side of the mixture as well as the properties of fuel vapor alone.

f. The present program has three combustion models for three different types of engines. Also the input for the heat release can be either in the Weibe equation form or the tabulated form.

2. Comparison of Experimental and Calculated Performance Data

Once the initial program was written it seemed desirable to evaluate the sensitivity of the computed data to small variations in input items—for example, heat transfer correlations. The program computes events in great detail as shown in Table 1 and Table 2. Because of this detail it is necessary to choose comparison data. Table 3 shows the input items varied and the resulting change in selected output items.

The results of these computations are described in detail in Appendix II but can be summarized from Table 3 as follows:

a. Using the present homogeneous combustion model dissociation is not significant at lean mixtures until stoichiometric fuel-air ratio are approached. It is significant for rich mixtures.

b. Varying the effective heat transfer path length of one of the surfaces markedly affects the metal temperature but does not dramatically affect performance parameters such as volumetric efficiency.

c. Inclusion of the effects of inlet gas dynamics significantly changes air flow. Thus, if the effects are present in the experimental set up they must be included in the program producing the computational results if agreement of results is to be achieved.

d. In general, increased total heat rejection increases metal temperatures and lowers volumetric efficiency and thus power output.

e. Engine performance data are not tremendously sensitive to choice of heat transfer correlations although metal temperatures are relatively sensitive to the choice of correlations.

With these comparisons as background, experimental data were taken for comparison with computed results. The care and attention to detail required when obtaining this experimental data cannot be overemphasized. Obtaining such data are necessary, tedious and expensive.

Again complete details are presented in Appendix II and only selected comparisons will be presented here. Figure 1 presents a comparison of calculated and experimental performance data. Figure 2 presents data showing how well the computed heat balance agreed with the experimentally determined heat balance. Figure 3 presents a comparison between the experimental and computed pressure-time diagrams.

In summary, after the comparisons between computed and experimental data were completed it was felt that the agreement was within the accuracy of the experimental data. To put it another way it was not obvious whether the disagreements that existed were the result of inaccurate assumptions or inaccurate measurements. This again emphasizes the great care necessary in obtaining experimental comparison data or data to be used to develop correlations.

Basically, the initial program was judged successful. In addition, it was judged desirable to obtain additional experimental data to clarify and improve some of the assumptions used in the program.

B. Use of Initial Program for Parameter Study

The initial program was used to study the effects produced by changing some of the engine design parameters. The results helped to illustrate the use of the program as a design tool as well as to give a better understanding of the casual relationships between design changes and the resulting changes in performance. A complete resume of the studies is given in Appendix III.

1. Effects of Valve Diameter and Valve Timing on Performance

The first engine design parameters that were studied was the effects of valve diameter and valve timing on performance. During these studies the mass rate of burning, the total fuel introduced per cycle, the inlet temperatures and pressure and all engine geometry except that noted were kept constant.

The sum of the valve diameters was kept constant corresponding to a fixed engine bore. However the respective port cross sectional areas were changed as the valve areas were changed. In order to minimize the number of variables involved the shape of the valve lift curves was kept constant.

In order to minimize the number of computer runs required the techniques of surface response methodology were used. The use of this technique is illustrated in Fig. 4 which shows the variation in volumetric efficiency when the valve intake diameter (VID), the crank angle at which the intake valve opens (CAIVO) and the crank angle at which the exhaust valve opens (CAEVO) were varied with engine speed constant at 2000 rpm. By studying Fig. 4 it can be seen that the volumetric efficiency increases in the direction of decreasing intake valve diameter, retarded exhaust valve timing, and advanced intake valve timing.

Computations of volumetric efficiency at constant speed were performed 20 different conditions and the resulting surface was fit with a second degree polynomial. Differentiation of the resulting equation with respect to each variable gave the maximum point on the surface and therefore the following engine parameter values:

Intake valve diameter = 1.963 in.
Intake valve opening = 513.54 deg.
Exhaust valve opening = 24.68 deg.

The values were arrived at on the basis of constant speed computer runs. Many additional runs at different speeds would be required to completely optimize the volumetric efficiency of the engine. However the initial computations improved the volumetric efficiency of the engine at all speeds as shown in Fig. 5. The "optimum" curve in Fig. 5 was obtained using the engine parameter values shown above. The results clearly show that the use of the computer program to study engine parameter changes will show an optimum region where detailed laboratory tests can be concentrated to achieve maximum improvement at minimum total cost.

Because of the great detail of the computations and because one parameter can be varied at a time the simulation program has the additional advantage of telling *why* an effect occurred as well as the fact that it did occur. For example Fig. 6 shows the effect of variable exhaust valve timing with all else held constant. Figure 6 shows that volumetric efficiency drops off rapidly as exhaust timing is advanced. A detailed study of the computed pressure time diagrams shows that the cylinder pressure at exhaust valve closing rises quickly with advanced exhaust timing because the high pressure at the end of exhaust (and therefore at intake valve opening) causes backflow into the intake port increasing the mass averaged intake port temperature as shown.

Table 4 shows a comparison of the original and optimized performance. It will be noted in Table 4 that the optimum design had a greater pumping mep than did the original design in spite of its higher volumetric efficiency. Also note that an increased volumetric efficiency does not inevitably mean a higher bmep.

2. Effect of Shape of Heat Release Curve

As previously indicated the similation program cannot tell if a change in operating conditions or engine parameters will cause a change in the shape of the heat release curve. However the simulation will predict the effects of different combustion heat releases on engine performance and thus indicate the effort that is justified in an attempt to change the heat release rate. Table 5 shows the results of changing both heat release rate and compression ratio. The figures referred to in Table 5 will be found in Appendix III. Note that a reduction in peak pressure could be achieved at the same compression ratio with only a loss of 2.5 imep—and probably less bmep loss because of effect of peak pressure on friction. It appears there may be ways to increase performance without resorting to higher peak pressures.

3. Effect of Ambient Conditions

The simulation program can also be used to predict the effect of changing ambient conditions on engine performance. The results of the computations show not unexpectedly that atmospheric pressure and temperature affect performance but emphasize that they do not affect performance in the same way. The formula developed to correct the indicated horsepower was

$$\frac{IHP}{IHP_o} = \left(\frac{P}{P_o}\right)^{1.03}\left(\frac{T_o}{T}\right)^{0.855}$$

When all heat losses were reduced to zero (constant inlet pressure), the following relationship was obtained:

$$\frac{IHP}{IHP_o} = \left(\frac{T_o}{T}\right)^{1.04}$$

indicating that heat loss affected the temperature relationship.

4. Effect of Bore-Stroke Ratio

Assuming unchanged heat release rates the effect of bore-stroke ratio can also be studied. While the volumetric efficiency was not optimized for value size and timing for each bore-stroke ratio the results show significant effects on brake horsepower and volumetric efficiency.

In summary the simulation program is very valuable in predicting effects of engine parameter changes in air flow but would be even more useful if it simulated the combustion process in detail.

C. Data Acquisition and Processing System for Instantaneous Engine Data

During the comparison of experimental and computed results it became quite clear that large amounts of data would have to be handled as data were taken to improve the program. For example, rapid changes in the pressure-time diagram plus cycle-to cycle irreproducibility indicated the desirability—almost necessity—of taking data every crankangle degree and averaging the results of as many as several hundred. If only 50 cycles are used, this represents 18,000 measurements to obtain one item of data such as a pressure time record at one operating condition. Clearly some sort of mechanized data reduction system was necessary!

The overall systems requirements are detailed in Appendix IV but briefly include a wide frequency response, good signal-to-noise ratio, multi-channel capability, automatic scaling, flexible operation and visual observation of data before and after recording. Figure 7 shows the conceptual view of the overall system developed.

As indicated in Fig. 7 transducers generate a signal which is a function of the parameter being studied. The transducers used include pressure pickups, surface thermocouples, photo tubes, crankangle timing markers, etc. The signal from the transducer was appropriately conditioned by suitable amplifiers and networks and finally recorded on tape with simultaneous visual observation by oscilloscope being possible both before, during and after recording. Figure 8 shows, as a specific example, the network used for the surface thermocouples.

The tape recorder used was a Model 7784 Sangamo. While its complete specifications are shown in Appendix IV briefly it has 11 frequency modulated channels and 3 direct record channels with modular transistorized electronics and tape speeds ranging from 15/16 ips to 120 ips. The tape recorder is in a central location and connected by coaxial cable to various test sites as well as the hybrid computer used for scaling and initial data processing.

In general, data were recorded at the highest tape speed (120 ips) and played back at lower tape speeds (usually 7.5 ips) for digitizing purposes. At least 200 consecutive cycles of engine data were recorded per run. The data were first played back into a Brush recorder and visually inspected. If no obvious faults were found the data were then processed through the hybrid computer. Although a portion of the three units (analog, interface, and digital) of the hybrid computer were needed, the hybrid computer facilities were not used to full capability. The iterative analog equipment was used for signal conditioning, the interface for the analog-to-digital function and the digital computer for storage, calculation, control and output. The net result was that the following functions could be performed:

1. Individual cycles of engine data could be identified and sampled at each crankangle degree.
2. A number of engine cycles could be identified, sampled and averaged.
3. The results from either item 1 and 2 could be converted to meaningful measurements of pressure, temperature, etc. In addition these items could be presented in listed form and/or written on magnetic tape for later use.

While not a part of the hybrid computer a subroutine (called GAUSHAUS), which is available on call from the UW function library, was used often in the data reduction and presentation processes. The purpose of GAUSHAUS is to obtain a least squares squares estimate of parameters entering non-linearly into a mathematical model.

In summary, development of the data recording and processing system was a necessary prerequisite to the studies hereinafter described. The studies would have been impractical without the system. The system has worked very satisfactorily and accomplished its desired objective.

D. Heat Transfer Studies

One's intuitive feels that heat transfer is important to practical engines was reinforced by the studies conducted using the simulation program. Heat transfer during the induction process decreases the density and consequently the mass flow of air. Heat transfer increases the operating temperature and thus decreases the strength of engine parts and, when lubrication is involved, may cause lubrication failure. Heat transfer in the exhaust system adversely affects turbine power in a turbocharged engine plus the ability to further oxidize hydrocarbons and carbon monoxide. Thus precise detailed information regarding rates of heat transfer are an inherent part of an accurate simulation.

However, detailed information regarding heat transfer rates in an engine are difficult to obtain and even harder to analyze from a theoretical standpoint. Waves and surges are imposed on intermittent flow in the intake and exhaust ports. Insofar as is known no measurements of instantaneous heat transfer rates have been made in intake and exhaust systems. Prior to this program no heat transfer rates had been measured for the gas flowing over the intake and exhaust valves. Experimental measurements of instantaneous gas velocities in the cylinder are unavailable although it is known that velocities vary markedly between engine designs because of squish and swirl. It is also known that because the boundary layer is alternately compressed and expanded the temperature profile in the boundary layer is distorted from that observed in constant pressure flow. This distortion of the temperature profile in the boundary layer can momentarily cause heat transfer from the surface to the boundary layer even though the bulk gas temperature is higher than the surface temperature. In spite of much speculation no known measurements of instantaneous radiant heat

transfer rates had been made prior to these studies. Because our ignorance of heat transfer rates is so large the studies reported herein, while significant, have not solved all of the problems. The work done on heat transfer is presented in detail in Appendix V.

1. Heat Transfer From a Poppet Valve

The rate of heat transfer from the intake valve is of interest from three standpoints. In the first place if significant heat transfer occurs it will heat the incoming air and reduce volumetric efficiently. Secondly, calculation of flow rates thru the valve is based on an adiabatic model. Thirdly, the temperature of the valve is affected by heat transfer to the incoming charge. Consequently, one of the first heat transfer studies was concerned with the intake valve and is reported in detail in Appendix VA.

The basic arrangement used for the study is shown in Fig. 9. The basic concept of the experiments was to run conventional steady flow tests on a given poppet valve and to then run the same tests with the valve heated. The valve was heated electrically and steps taken to minimize loss by conduction including a guard heater so that the electrical energy supplied would equal the heat losses from the valve. Appropriate measurements and adjustments were made to insure that thermal expansion did not change the flow area and thus the results.

The results of the tests were initially expressed as a percentage change in effective flow area as a function of valve lift as shown in Fig. 10. Note that two different heat transfer rates are shown in Fig. 10. The data can also be plotted as a function of heat transfer rate as shown in Fig. 11. Figure 11 indicates that at small lifts heat transfer significantly affects flow rate but that there is but little effect at high flow rates.

Although the experiment was designed to yield data on the effect of heat transfer on flow rates it can be used to obtain estimates of heat transfer coefficients for the back of the valve. The correlation found was

$$Nu = 1.012 \times 10^{-4} (Re)^{1.27} \tag{20}$$

with data points as shown in Fig. 12. The exponent of 1.27 is higher than the usual 0.8.

Although not a part of this study it might be commented that General Motors in 1970 reported more extensive studies of heat transfer coefficients from valves in SAE Paper 70051, "Correlation of Convective Heat Transfer for Steady Intake - Flow Through a Poppet Valve" by G.T. Engh and C. Chiang. Their correlation was of this form

$$Nu = f(Re)^{a}\left(\frac{H}{D}\right)^{b} \tag{21}$$

where

H = valve opening, and

D = valve diameter

Note that the characteristic length in Eq. 20 is defined as the square root of the difference between the seat and valve area and that the H/D in Eq. 21 is a non-dimensional valve lift.

The data developed in this study were used in the simulation program and showed not much effect on volumetric efficiently. However the intake valve was somewhat oversized for the engine for which the computer runs were made. Thus larger effects might be found on other engines.

2. Instantaneous Heat Flux Measurements

As indicated in Appendix VB there are a number of heat transfer correlations available for instantaneous heat transfer rates. However, as one studies the literature the proliferation of correlations and the paucity of experimental data to justify old correlations or develop new ones is very striking. Eichelberg (Ref. 4, Appendix VB) is the primary source of measurements of

instantaneous heat transfer rates. However his results were obtained from measurements in a slow speed engine which were made below the surface of the metal where the high frequency component would have been damped out. It seemed imperative therefore to make surface temperature measurements in the modern high speed TACOM diesel engine.

Figure 13 shows the type of surface thermocouple used. Figure 8 shows the basic circuit used and Fig. 14 shows the location of the thermocouples. Figure 15 shows the basic data recorded - surface temperature versus time. From this basic data instantaneous rates of heat transfer could be obtained.

The first observation that was made was that there was considerable difference in heat transfer between the different thermocouple locations. This effect is shown in Fig. 16. The second observation came from the fortuitous location of thermocouple four in the cylinder sleeve and shows that the thermocouples can be used to indicate piston ring location. Figure 17 shows the temperature-time record for thermocouple four at different operating conditions. The rapid temperature rise is due to the passage of the piston rings over the thermocouple. Note that when the intake density is greater than atmospheric only five spikes are generated during the compression-expansion process as compared to six during the exhaust-intake process.

After taking considerable data using the previously described data system the first use of the experimental heat transfer data was to make comparisons with existing correlations. While more comparisons are shown in Appendix VB, Fig. 18 shows a comparison between the experimental data and two popular correlations - Annand and Woschni. Because of the variation between locations as illustrated in Fig. 16 experimental data for two locations are shown in Fig. 18. The final conclusion reached was that none of the experimental correlations adequately predicted the experimental data at any location and certainly none predicted the experimentally observed differences between different locations.

A conduction-compression model for heat transfer in a non-turbulent motored engine was developed at Wisconsin as part of another study (Ref. 21, Appendix IVB). Basically the model divides the gas into equal-mass slabs parallel to the piston top with the slabs exchanging heat by conduction only along the axis of piston motion while the entire cylinder mass is being heated and cooled by the compression expansion and work, plus conduction to the piston and head. This model is applicable only to a motored engine and is compared with motored engine data in Fig. 19. While the shape of the computed and experimental curves are comparable the computed curve is obviously too low even when the conductivity of all of the gas except that immediatly adjacent to the head was increased by a factor of five. Furthermore, this model is also incapable of predicting the observed differences between the two thermocouples. This model does, however, incorporate the effects of pressure work and variable density in the boundary layer.

In an attempt to predict the observed different heat transfer at the different thermocouple positions a boundary layer model with swirl was constructed with the Reynolds number in this case being defined as the product of the radius from the center of swirl (center of the cylinder axis in this case) and the angular velocity divided by the kinematic viscosity. This model gave good agreement with motored data for both thermocouples as shown in Figs. 20 and 21. Good agreement was also found when the speed and manifold pressure were varied. However extension of the model to fired data gave fair agreement for one thermocouple (Fig. 22) but poor agreement with the experimental data for the other thermocouple (Fig. 23). Apparently squish, gas motion and radiation due to combustion further complicate the heat transfer picture in fired operation. The different effects have not yet been sorted out although further mention of this will be made in the next section on radiant heat transfer.

3. Radiant Heat Transfer

The paucity of data regarding radiant heat transfer rates at the start of the contract was even more striking than the situation for total heat transfer. No instantaneous radiant heat transfer rate measurements were known to the authors although a measurement of time-averaged radiant heat transfer had been made at Wisconsin (Ref. 3, Appendix VC). This study indicated that time-

averaged radiant heat transfer could be as much as 40% of the total heat transfer which suggests that instantaneous radiant heat transfer could be an even higher percentage. Thus a study was undertaken to develop a suitable technique to measure radiant heat transfer and to use the developed instrument to study the effect of different operating variables on radiant heat transfer. The details of this study are reported in Appendix VC.

The first requirement, of course, is viewing access to the combustion chamber. This was achieved via a window that could be changed during engine operations to provide a nearly clean window when taking data. Provision was also made for determination of the transmittance of the window immediately after use.

The scheme to measure the intensity of the radiation passing thru the window is shown in Fig. 24. Basically, it consisted of a monochromator to permit selection of radiation having different wavelengths and a lead solenoid detector to measure radiation intensity at the chosen wavelengths. A built-in calibration system permitted calibration of the window immediately upon its removal from use in the engine. The output from the photo tube was conditioned electronically and recorded via the previously described data reduction system. Seven wavelength values (1, 1.5, 2, 2.5, 3, 3.5, and 4 microns) were chosen for data recording as the best compromise between number of wavelengths recorded, detector sensitivity and fraction of radiation received. Data were recorded at one wavelength for several hundred cycles and then, at constant operating conditions, the monochromator moved to a new wavelength setting. It was found that consistent reproducible readings could be obtained if all data at different wavelengths were taken without stopping the engine but that the data were less reproducible if the engine were stopped and then reset to nominally the same operating conditions during a series of different wavelength runs.

Taking data in the manner specified above permitted a plot to be made of radiation intensity versus wavelength with the radiant heat transfer being the area under the curve when it was extrapolated to zero and infinite wavelengths. In order to mathematically represent the area under the curve the concept of black body radiation modified by an emissivity factor was used. The emissivity factor first used was a function of wavelength, i.e.,

$$\varepsilon_\lambda = 1 - e^{-\frac{kL}{\lambda^{.95}}} \tag{22}$$

where

ε_λ = emissivity at wavelength

k = soot concentration, number per unit path length

L = path length

However, this expression was used to define a pseudo-grey body emissivity ε_a which ultimately was determined to be a function of the radiation temperature, T_R and kL with precision adequate for present purposes. Since the rate of radiant heat transfer $\dot{q}_R$ is given by

$$\dot{q}_R = \varepsilon_a \sigma T_R^4$$

where

σ = Stefan-Boltzman constant

The analysis of the data were simplified by use of this relationship.

A large number of engine and fuel variables were studied and are reported in Appendix VC. Thus only a few results will be shown here. The effect of variable injection timing is shown in Fig. 25 since the results from this variable are readily observable. Note that early injection gave significantly higher optical thicknesses (kL), peak radiant heat flux and apparent rate of heat release. It should not be concluded however that radiant heat flux and apparent rate of heat release correlate with each other. For example, Fig. 26 shows the effect of different cetane number fuels. Note that the higher cetane number fuel had higher radiant heat flux and optical thickness but lower rates of heat release.

For comparison purposes the total heat transfer, measured as previously described by the surface thermocouple, are shown in Fig. 27. Note that the peak radiant heat fluxes shown in Figs. 25 and 26 are a significant fraction of the heat flux in Fig. 27. Although there is some question as to whether the data are directly comparable the measured radiant heat fluxes for the same operating conditions were subtracted from those given in Fig. 27 to give the convective heat transfer with the result shown in Fig. 28.

Table 6 presents further comparisons including comparisons of time averaged values. In general, the ratio of the time-averaged radiant heat flux to the time-averaged total heat flux is not quite as large as that found by Ebersole who found ratios as high as 0.4 but clearly radiant heat transfer is significant.

It is of course necessary to find some way to correlate and express radiant heat transfer rates if they are to have maximum utility in the simulation program. Because of the shape of the curve of radiant heat flux versus time the Wiebe function was used to characterize the curve. The expression finally developed (Appendix VC) gives $\dot{q}$ as a function of engine speed, inlet manifold pressure, inlet air temperature and compression ratio (these last two functions were not evaluated), beginning of injection and equivalence ratio. For comparison purposes Fig. 29 presents computed radiant heat transfer flux which, if the expression is accurate, should be identical to the experimental data of Fig. 25. The comparison is favorable. However, it should be realized that the equation has not been tested on other engine designs. One must also estimate the size and location of the flame in the combustion chamber and assign values for the area and absorptivity of each of the combustion chamber parts. Nevertheless, for the first time a reasonable estimation of radiant heat transfer can be made.

Finally, let us summarize the status of computing heat transfer in engines and the work done under this contract. At the start of the contract only one or two reliable measurements of instantaneous cylinder heat transfer rates were available to serve as the basis for formulating correlations. As a result most proposed correlations had not been compared with experimental data. The studies provided considerable experimental data and clearly showed the deficiencies of existing correlations. Attempts to develop better correlations were not wholly successful but clearly pointed out the need for instantaneous gas velocity measurements in the cylinder. For the first time instantaneous radiant heat transfer rates were experimentally determined and shown to be significant in comparison with total heat transfer rates. A correlation with engine operating variables was developed but lack of other comparison data prevented determination of its universality. Expressions for heat transfer to the intake valve were also developed from experimental data. No studies were conducted to determine heat transfer rates in manifolds. The simulation program is dependent solely on estimates for these data.

E. Work Done on Rate of Burning

One of the necessary and important input items to the simulation program is the rate of burning or rate of heat release which affects markedly the pressure time diagram. Ideally one would construct a complete model of the very complicated physical and chemical phenomena that occur during the introduction and burning of the fuel and this model would automatically produce the desired rate of burning curve. While such a model would markedly increase the utility of predictions from the program the facts are that the details of the processes are so poorly understood that, prior to the study, no one had attempted to construct a detailed model and, as shown in Sec. III-E-2, even the work done under this contract included only a portion of the details. Thus the first approach to obtaining a rate of burning curve was to use the pressure-time diagram as an input item to the program and to obtain a rate of burning curve as an output item. If a number of such curves are obtained they then can be used as input items for similar engines under similar operating conditions.

In summary, the work done under this contract basically consisted of two parts—determining rates of burning from pressure-time diagrams and attempting to construct a theoretical model to predict rate of burning in a diesel engine.

1. Rate of Burning From Pressure-Time Diagrams

Appendix XIA and VIB give the details of the techniques used to determine rate of burning from pressure-time diagrams. The starting point for the computation is the energy equation (Eq. 3) which is solved for the rate of mass transfer $\dot{M}$. In the diesel engine $\dot{M}$ physically represents the space averaged rate at which fuel is burnt in the cylinder. Note that $\dot{M}$ is not the rate at which fuel is introduced (injected) into the cylinder unless the ignition delay is zero. In the case of a spark ignition engine the charge is divided into two parts—a completely burned and an completely unburned part and $\dot{M}$ physically represents the rate at which mass is transferred between the two. If the mass of charge plus P and $\dot{P}$ are known $\dot{M}$ can be determined using the relations given in the first part of this report.

One of the first problems that is encountered is how to determine $\dot{P}$ since P is measured as discrete points. Dividing ΔP by Δt seems too simplistic and gives large discontinuities in $\dot{P}$. In practice pressure values are calculated from a smoothed pressure-time table by using a second-degree Lagrangian interpolation formula.

One of the next problems is caused by the observed cyclic irreproducibility of the pressure-time diagrams. This irreproducibility raises a question as whether you determine the rate of burning for each cycle and average these to determine the average rate of burning or whether you average the pressure-time records to obtain an average pressure time record and from this determine an average rate of burning.

Using the average pressure-time diagram has the advantage that it gives an average indicated power. Since an investigation showed that the two techniques did not give markedly different results and because of decreased computational time the average pressure time diagram was used.

The third problem comes from the desire to normalize the results and to plot the fraction of the mass burned rather than the actual mass burned. This procedure requires division by the total mass burned in the cycle. This total mass can be determined as the integral of the computed $\dot{M}$ or from the measured fuel mass in a unit time plus the measured number of revolutions during that same time. If the latter procedure is followed it was found that 100% mass burned was never quite achieved in a spark ignition engine presumably because of the quench zone but possibly because of experimental error or other things such as inaccurate heat transfer correlations.

Appendices VIIA and IIB show the effect of experimental errors on $\dot{M}$. For example, if the pressure-time diagram is shifted two degrees either way $\dot{M}$ is affected as shown in Fig. 30. Figure 31 shows the differences in the mass fraction burned curves when the maximum peak pressure trace, the minimum peak pressure and the average pressure time curve are used.

Data were obtained for a spark-ignition engine showing the effect of operating variables on the shape of the mass burned fraction versus crankangle curves. Fuel-air ratio and engine speed were found to have a relatively minor effect on the shape of such curves although if speed were plotted on a time basis the effect would be major. Spark timing obviously affects the location of the curves but also has a shape effect possibly in part due to changes in combustion chamber shape (Fig. 32). Engine load was also found to have an effect (Fig. 33).

The previously described data collection system permitted a study to be made of the cyclic irreproducibility as evidenced for example by the plot in Fig. 34 of the frequency of cylinder pressure at 9 deg ATDC versus cylinder pressure. A study of the data showed an essentially normal distribution of the pressures with the values for the average and standard deviation increasing with the number cycles studied up to about 300 cycles after which the value varied less than 1%. Interestingly enough the deviation of the imep was much smaller than the pressure deviation. As an example, for one run where 350 cycles were analyzed the calculated average IMEP was 119 psi with a standard deviation of 1.05 psi while in Fig. 34 the average pressure is 360 psi with a standard deviation of 53.3 psi.

Studies of apparent rates of burning were also conducted for the diesel engine but since an attempt was made to construct a theoretical model of combustion they will be reported in the next section.

2. A Spray-Droplet Model for Diesel Combustion

While it is possible to use a rate of burning curve obtained as described above as an input item to the program it would be much more useful to be able to predict the rate of burning curve from the geometry of the injection system plus ignition lag data. Since considerable work has been done in simulating injection systems it was judged that the area of maximum ignorance lay in computing rates of burning given a pressure-time history at the nozzle tip. Accordingly the TACOM engine was fitted with a means of measuring injection pressure at the nozzle tip and this pressure, plus cylinder pressures, recorded using the data collection system. An attempt was then made to construct a theoretical model that, using the observed tip pressure, would predict the apparent rate of heat release computed as previously described from the observed pressure time diagrams. Complete details are reported in Appendix VIC and VD.

The pressure-time diagrams used for the computed apparent rate of heat release (AROHR) was the average of approximately 50 cycles since the cyclic irreproducibility is smaller in the diesel engine. In spite of this there are wide swings in the AROHR curve if the discrete points are used for the computations as shown in Fig. 35. It is not known if these swings are real or are caused by cyclic irreproducibility and/or the data processing system. Note that the rate of fuel addition curve is also shown in Fig. 35. To characterize and compare the AROHR curves a mathematical expression called the Wiebe function (Appendix VIC) was used which gives the smoothed curve shown in Fig. 35. The smoothed curves were used in the analysis.

While data showing AROHR for many operating variables are given in Appendix VIC only one injection timing will be shown here. Injection timing is shown since it had been used as the variable for illustration in the heat transfer studies. The resulting data are shown in Fig. 36. Figure 37 shows the effect of changing the rate of injection as well as the nozzle tip as an illustration of the wide range of AROHR curves covered in the study.

As indicated previously, a model of combustion was set up as follows: Using the injection pressure, a mean droplet size is calculated. The droplets are assumed to vaporize according to a simple steady-state formula for single droplets in air. Ignition delay is calculated by an empirical ignition delay formula. At the end of the delay period the vaporized fuel is arbitrarily assumed to burn in one crankangle degree. The unburned fuel is assumed to burn according to a spray burning law developed by Tanasawa for gas turbine sprays.

This theoretical model was modified by an experimentally determined coefficient. It was found that there was only a small dependence of this coefficient on pressure, on oxygen and on speed. There did, however, seem to be a larger dependence of this coefficient on gas temperature so this effect was included as shown in Appendix VID.

This model then permitted an AROHR curve to be computed from a rate-of-injection (ROI) curve. As previously indicated, moderately realistic predictions of ROI curves can be made using techniques available in the literature. Thus the model permits prediction of an AROHR curve from engine geometry. A comparison of the predicted and experimentally observed AROHR curves are shown in Fig. 38.

As shown in Fig. 38 a reasonably good prediction is made for the TACOM engine. However, the model has not been tested on other engines and it is not known whether or not it is widely applicable. In addition, it does not include prediction of emissions which is increasingly desired from a combustion model in today's real world.

F. Intake and Exhaust System Simulation

It was known that Prof. Rowland Benson at the University of Manchester, England and others were studying the complex unsteady-flow phenomena in intake and exhaust

systems. Under the assumption that their efforts would eventually be available as inputs to the program only minimal work was done in this area. (Note—under the latest TACOM contract with Wisconsin Prof. Benson's program has been made available.) The work that was done was an attempt to explain some of the discrepancies found in comparisons with the simulation as reported in Appendix I.

The most apparent discrepancy was the marked difference in experimental and computed damping rates of the waves in the intake manifold of the single cylinder engine. This difference is shown in Fig. 39. The computed waves assume no heat transfer from the manifold or valve to the air in the intake manifold while experimentally there is heat transfer especially from the back of the intake valve. It was thought that the heat transfer might act as an energy source to maintain wave amplitude. Complete details are given in Appendix VII.

Two basic types of experiments were conducted using the apparatus described in Fig. 40. The first type of experiment used the cam mechanism to close the valve. The second type allowed the valve to snap shut with no cam control. Such closing insured that the valve would stay closed and was devised to allow a longer time to observe the pressure oscillations. A third experiment used the arrangement shown in Fig. 41. In this experiment the copper bar was heated and, after the heated air was blown out of the pipe, the open end was sealed with a rubber stopper thru which a tube from a compressed air tank passed. The pipe was then pressurized to a few psig, the rubber stopper pulled out quickly and the pressure oscillations observed. Essentially no effect of heat transfer on damping ratio was observed in any of the experiments.

The second problem studied was the magnitude of the temperature rise in the port as measured by the temperature probe shown in Fig. 40. The results are shown in Fig. 42 and indicate that there is a significant temperature increase due to the heated valve.

G. *Status and Use of Program*

During the period covered by this contract most engine companies as well as University people have found engine simulation useful. Consequently any evaluation of engine simulation today must recognize these other studies and uses being made of simulation programs.

The program developed for ATAC at Wisconsin is believed to be the most detailed and accurate program available for predicting in-cylinder events for a single-cylinder engine. The studies at Wisconsin have not so far been expanded to include multi-cylinder engines. However, Professor Rowland Benson at Manchester, England has a multi-cylinder program which emphasizes and is reported to adequately represent the gas dynamics in the intake and exhaust system of multi-cylinder engines but includes much less detail on in-cylinder events. This program has been obtained for TACOM evaluation and use under the current contract with the University of Wisconsin. Thus, as a result of the contract, TACOM has at its disposal the best of engine simulations available any place in the world.

CAV in England and FIAT in Italy have conducted in-depth studies of injection system simulation. The studies at Wisconsin have not so far included the injection system but the CAV or FIAT studies could be adapted to the program. Injection system simulation should be added as methods of predicting heat release from injection data are verified and improved for other engines designs.

As indicated in Appendix VIII we are not yet at the ideal state where, from detailed drawings of the engine, one can predict multi-cylinder engine performance. Nevertheless, engine simulations in their current state have real utility and their use can "pay off" at their present state of development. To illustrate this statement let us consider three different ways in which it is judged that engine simulation can "pay off" for TACOM.

1. <u>The simulation can be used as a design tool during single-cylinder engine development</u>

Many questions and ideas occurring during single-cylinder engine work can be evaluated and prescribed by engine simulation. The effect of valve size and valve timing can be quite adequately predicted by present programs—in fact,

almost more accurately than experiments where varying a single variable is usually impossible because details like the effect of piston cutouts, etc., becloud the answer. While the effect of combustion changes cannot be predicted their potential can be evaluated in terms of effect on peak pressures, fuel rates, etc. before costly experiments to achieve them are started. Reasonable estimates of the relative effect of operating variables on metal temperatures can be obtained. Thus it is judged that the continual use during development of the current in-depth single cylinder simulation program will "pay off" at its present stage of development.

2. The simulation can be used as a tool to predict radical design changes in existing engines.

A good historical example of this use is the VCR program on the 1100 engine. If, at the time this development program was started, a simulation program had been available it could have been used to estimate performance data under the radically different proposed operating conditions. It is true that combustion simulation is not possible but reasonable estimates and studies of limits could yield valuable performance estimates. The performance estimates could be extremely valuable both in deciding whether or not to embark on the adventure and the limits to which the venture should be extended.

3. The simulation can be used as an evaluation of unusual cycles and configurations.

TACOM is always confronted with the problem of evaluating proposed unusual cycles and configurations. TACOM cannot afford to ignore these both from the standpoint of potential use and political pressures. At the same time because of their unusual configurations, judgments are difficult to make and defend. Again, it is believed that by assuming reasonable heat transfer coefficients, rates of combustion, etc., engine simulation can be the basis for valid and defendable performance estimates.

In summary, in our opinion the work that TACOM has sponsored at Wisconsin plus developments elsewhere have brought engine simulation to the point where it is now useful to TACOM. However, a remaining problem is how does TACOM avail itself of this tool. Ideally TACOM should have an individual in its organization who is familiar with engine simulations and could use them as well as guide their use and coordinate the obtaining of needed additional information. If this is not currently possible, knowledgeable people at Wisconsin or elsewhere could be used temporarily.

H. Further Program Improvement

As indicated in the previous section, engine simulation programs are judged to be useful to TACOM at the present time. As indicated in Appendix VII there are, however, areas where the program still needs improvement and where addition data and information are needed. These fall into two broad categories.

1. Adaptation and coordination of existing information and inclusion in TACOM program.

Current examples of this are the exhaust-intake manifold program of Professor Benson and the injection system simulation of CAV. Also, as information on combustion simulation becomes available this should be included. Again, this points out the need for TACOM to have some individual who is actively using and improving TACOM's engine simulation program. While such work may be done temporarily at a University, the work in the next category is much more in line with University objectives, capabilities and available manpower.

2. Obtaining basic data to improve program.

There are several areas where additional basic data are needed. A partial list includes:

a. Determination of rates of burning in a pre-chamber engine and evaluation of the pre-chamber program. Work on this aspect is being done under our current TACOM contract.

b. Expand the simulation to include prediction of emission particularly NO_x. The theory is fairly well established in the case of the spark-ignition engine. However in the case of the compression ignition engine considerable experimental data would have to be taken to establish the correct physical model for both NO_x and particulates.

c. Measurement of instantaneous gas velocities and corresponding heat transfer rates in the cylinder. Such data as necessary in establishing heat transfer correlations.

d. Establishment of heat transfer correlations for different combustion chamber configurations.

e. Measurement of instantaneous gas velocities and corresponding in manifolds and establishment of a heat transfer correlation.

f. Determination and correlation of factors affecting engine friction.

Table 1 - Cycle Analysis of Single-Cylinder 4 Stroke Diesel Engine Fired Prob 1

Engine	ER-1	INT OP	529.0	CADEG	Speed	3200.0 rpm	INT	T	552.0 R	CAGRS	165
Bore	4.125	INT CL	59.0	CADEG	Coolant Temp	635.5 R	INT	P	14.08 psia	CAPHR	180
Stroke	4.313	EXH OP	295.0	CADEG	Coolant Flow	1.3390 lb/sec	EXH	P	14.08 psia	CAHRE	260
Comp Ratio	16.000	EXH CL	549.0	CADEG	Fuel	10.67 lb/hr	0. CADEG = BDC				

Crank Angle	Pres Cyl psia	Temp Cyl R	Mass Cyl 10^6 lbm	Equiv. Ratio	Temp Int. Port R	Flow IV lbm /hr	Temp EP R	Flow EV lbm /hr	Tot. Ht. Tr. Cyl 10^4 B/CA	Tot. Ht. Tr. IP 10^4 B/CA	Tot. Ht. Tr. EP 10^3 B/CA	Pres. Int. Port Ot. Port psia	Vol. $in.^3$
529.	19.39	1865.	73.	0.849	647.		1717.	-90.	-0.669	0.1747	-0.1714	14.11	4.52
547.	15.40	1713.	58.	0.849	662.	-39.	1659.	-1.	-0.454	-0.2303	-0.1500	14.42	4.12
549.	14.26	1678.	57.	0.849	663.	-9.	1653.		-0.405	-0.2187	-0.1458	14.22	4.29
550.	13.81	1660.	57.	0.844	663.	36.	1650.		-0.110	-0.0716	-0.1449	14.00	4.40
560.	11.11	1355.	77.	0.617	653.	239.	1619.		0.129	-0.0491	-0.1361	13.00	6.05
580.	9.32	920.	103.	0.247	621.	531.	1567.		0.437	0.0146	-0.1212	11.54	12.23
600.	8.79	774.	377.	0.130	601.	740.	1522.		0.608	0.0503	-0.1090	11.57	21.24
620.	9.05	720.	619.	0.081	594.	917.	1484.		0.755	0.0664	-0.0987	12.75	31.53
650.	10.05	694.	1042.	0.049	581.	999.	1436.		0.915	0.0919	-0.0861	13.63	46.04
710.	13.17	701.	1796.	0.029	571.	658.	1363.		1.056	0.1149	-0.0675	14.58	61.16
20.	15.37	724.	1997.	0.026	577.	223.	1334.		1.081	0.1065	-0.0604	15.84	60.20
30.	16.19	735.	2016.	0.026	581.	43.	1326.		1.078	0.1014	-0.0583	16.24	58.61
40.	17.08	748.	2011.	0.026	585.	-65.	1317.		0.807	0.2752	-0.0563	18.21	56.38
59.	19.91	783.	2002.	0.026	577.		1303.		0.767	0.3296	-0.0528	14.49	50.43
80.	26.16	848.	2002.	0.026	564.		1288.		0.688	0.3348	-0.0493	12.77	41.53
110.	40.22	1011.	2002.	0.026	578.		1269.		0.395	0.3191	-0.4448	13.77	26.33
140.	139.91	1336.	2002.	0.026	596.		1252.		-0.917	0.2976	-0.0409	15.12	12.23
170.	546.69	1876.	2002.	0.027	590.		1237.		-7.662	0.2959	-0.0375	13.87	4.40
186.	1202.45	3686.	2053.	0.407	589.		1230.		-40.240	0.2942	-0.0358	13.37	4.04
200.	836.31	3797.	2074.	0.558	592.		1224.		-34.300	0.2887	-0.0344	13.49	6.05
230.	287.79	3517.	2101.	0.760	606.		1212.		-17.890	0.2702	-0.0317	14.50	16.48
260.	138.47	3221.	2113.	0.849	609.		1201.		-11.600	0.2607	-0.0293	14.31	31.53
296.	78.79	2821.	2113.	0.849	610.		1188.	-9.	-7.455	0.2534	-0.1897	13.71	48.52
310.	68.58	2725.	2100.	0.849	614.		1230.	-152.	-6.672	0.2471	-0.1714	13.90	53.52
330.	55.71	2588.	1967.	0.849	620.		1973.	-842.	-5.496	0.2370	-0.3198	14.27	58.61
360.	36.30	2335.	1490.	0.849	624.		2300.	-1161.	-3.422	0.2270	-0.3744	14.23	61.47
390.	23.60	2103.	1026.	0.849	626.		2083.	-949.	-1.985	0.2201	-0.2850	13.89	58.61
420.	17.10	1937.	689.	0.849	632.		1912.	-599.	-1.214	0.2089	-0.2264	14.06	50.06
480.	16.26	1873.	288.	0.849	640.		1784.	-433.	-0.774	0.1903	-0.1891	14.03	21.24
520	17.88	1855.	91.	0.849	646.		1738.	-183.	-0.638	0.1780	-0.1762	14.06	6.05

Table 2 - Cycle Analysis of a Single-Cylinder 4 Stroke Diesel Engine Prob No. 1.0

Performance Data Fired at 3200 rpm with a Fuel/Air Ratio of 0.0576 = 0.85 Eq Ratio

Horsepower				Mean Pressure, psi			
NIHP	31.62	IHP	33.35	NIMEP	135.77	GIMEP	143.20
BHP	18.08	PHP	-1.73	BMEP	77.64	PMEP	-7.43
RAHP	13.54	RAHP/BHP	0.75	RAMEP	58.13	RMEP	-27.00

Flow Rates	Lb/cycle	Lb/hr	Temperatures, F		Efficiencies	
Intake	0.0019375	186.003	Mass ave int temp	127.4	Volumetric	82.8%
Exhaust	0.0020486	196.670	Mass ave exh temp	1566.5	Mechanical	54.2%
Blowby	-0.0000000	0.000	Time ave exh temp	1060.1	I Thermal	43.3%
Fuel	0.0001111	10.670	Peak temp	3340.2	B Thermal	23.4%
			Peak press	1202.0 psi	ISFC	0.3200
					BSFC	0.5901

Energy Balance	Btu/cycle		Wall Temp (Gas Side) F	Heat Transfer (Gas to Wall) Btu/Cycle	Effective Gas Temp, F
Net work on piston	0.838	Piston	686.7	0.1478348	1995.9
Heat transfer sum	0.360	Cyl head	509.6	0.0664871	1995.9
Blowby	0.000	Cyl sleeve	616.4	0.0480521	1531.4
Net intake and exhaust	-1.283	Int valve	803.8	0.0190501 (face)	1977.5
				-0.0157012 (back)	198.3
Fuel total enthalpy	0.086	Int port	168.6	-0.0031827	146.6
Balance error	-0.001	Ex valve	1369.0	0.0080898 (face)	1995.9
Sum				-0.0021407 (back)	1307.1
LHV fuel input	2.041	Ex port	435.8	0.0914701	1092.6

Energy Distribution		Coolant Temperature Rise		
% Brake work	23.4	Head	3.3 F	1.3390 lb/sec
% Heat transfer	16.8	Barrel	4.2 F	1.3390 lb/sec
% Exhaust	42.3	Friction	1.4 F out of 4.2	
% Friction and Acces.	17.5	Total	7.5 F	

Table 3 - Selected Parameters Showing Results of Computations for Single-Cylinder Engine

Run	Volumetric Efficiency	NIMEP	PMEP	Mass Average Int. Temp. F	Mass Average Exh. Temp. F	Time Average Exh. Temp. F	Peak Temp., F	Peak Pressure, psia	Piston Temp., F	Cylinder Head Temp., F	Cylinder Sleeve Temp., F	Intake Valve Temp., F	Exhaust Valve Temp., F	At Intake Valve Closing P psia	At Intake Valve Closing T °F	At 160 deg Crank Angle P psia	At 160 deg Crank Angle T °F	Total Heat Transfer, q (Btu/cycle)
3200 rpm, 0.0001111 lb fuel/cycle, coolant flow = 1.339 lb/sec																		
A	82.8	135.8	-7.43	127	1567	1060	3347	1202	688	510	616	804	1369	19.91	323	359	1233	0.360
B	82.1	133.9	-7.32	129	1536	1047	3372	1202	740	555	659	884	1396	19.94	331	360	1253	0.396
C	79.5	133.9	-7.07	144	1621	1091	3455	1189	703	522	630	437	1412	19.97	359	357	1293	0.368
D	80.2	134.6	-7.66	128	1602	1081	3407	1184	694	513	623	811	1395	19.44	329	350	1295	0.368
E	82.5	135.7	-7.40	128	1570	1061	3353	1199	687	510	617	799	1370	20.93	335	357	1232	0.361
F	82.9	136.5	-7.44	127	1565	1069	3369	1205	681	505	612	795	1364	19.90	322	359	1231	0.356
G	77.1	136.3	-5.89	131	1632	1098	3437	1145	691	509	620	814	1406	17.94	298	326	1190	0.370
H	82.7	135.9	-7.42	127	1572	1063	3356	1203	737	511	609	807	1373	19.91	325	359	1239	0.357
I	83.0	135.8	-7.45	127	1563	1058	3341	1203	686	508	615	769	1366	19.90	321	359	1229	0.360
J	81.2	131.7	-7.21	129	1542	1047	3385	1197	763	575	679	908	1398	20.08	395	362	1231	0.414
K	82.9	135.8	-7.44	127	1562	1057	3341	1202	663	508	593	801	1365	19.88	321	358	1228	0.362
L	82.9	135.7	-7.45	127	1574	1063	3350	1069	677	501	609	788	1362	19.89	322	358	1229	0.355
M	84.2	139.2	-7.58	125	1555	1049	3322	1210	653	468	593	738	1349	19.70	362	356	1191	0.334
N	82.3	134.4	-8.64	129	1579	1075	3359	1201	691	512	621	813	1386	19.91	327	359	1239	0.366
O	82.2	133.4	-7.27	129	1499	1020	3365	1204	781	574	698	912	1392	19.91	328	360	1249	0.422
2600 rpm, 0.0001128 lb fuel/cycle, coolant flow = 1.165 lb/sec																		
A	84.6	139.7	-4.77	128	1520	997	3300	1206	637	476	576	753	1307	19.58	301	354	1188	0.382
G	78.5	139.5	-3.72	131	1590	1039	3417	1149	644	478	582	769	1353	17.70	281	323	1156	0.395
2000 rpm, 0.0001068 lb fuel/cycle, coolant flow = 1.09 lb/sec																		
A	83.3	135.2	-2.65	130	1398	906	3266	1149	573	434	525	670	1190	18.69	273	338	1132	0.388
B	82.4	132.7	-2.62	132	1362	891	3290	1148	623	475	567	746	1212	18.71	282	339	1153	0.433
C	78.0	132.5	-2.47	153	1473	947	3422	1125	592	448	541	400	1246	18.51	315	331	1203	0.402
G	79.7	135.2	-2.12	132	1435	927	3327	1117	576	435	528	678	1212	17.63	262	320	1113	0.395
J	81.2	130.7	-2.58	133	1374	894	3299	1138	636	486	579	758	1213	18.74	293	339	1174	0.447
M	84.5	136.9	-2.69	131	1367	886	3247	1158	579	428	533	662	1181	18.65	261	339	1110	0.388
O	81.4	129.2	-2.58	134	1308	859	3293	1144	694	521	630	821	1223	18.71	289	340	1174	0.495
1400 rpm, 0.000959 lb fuel/cycle, coolant flow = 0.625 lb/sec																		
A	80.0	124.7	-1.28	129	1223	803	3055	942	529	405	498	553	1026	17.96	243	326	1071	0.366
G	79.7	125.0	-1.06	129	1225	804	3058	940	529	405	498	553	1028	17.87	242	325	1069	0.365

A. With intake dynamics and dissociation.
B. Radiation temperature increased 30%, that is, T = 1.3 Tg.
C. Intake valve and port heat transfer coefficient increased by factor of 5.
D. Intake effective valve flow area reduced by 10%.
E. Intake valve opens and closes 5 crank angle degrees later.
F. Without dissociation.
G. With constant port pressure.
H. Piston metal heat transfer path 50% longer.
I. Intake valve metal heat transfer path 67% of original length.
J. Cylinder gas-side heat transfer coefficient increased by 30%.
K. No frictional heating at sleeve-piston interface.
L. Shape of heat release curve changed.
M. Eichelberg heat transfer coefficient ; q same at 2000 as Run A-2000.
N. Exhaust effective valve flow area reduced by 10%.
O. Eichelberg heat transfer coefficient ; q nearly same at 3200 as Run J-3200.

Table 4 - Comparison of Original and Proposed Optimum Engine Performance

	Original	Optimum w/cons. F/A Ratio	Optimum w/cons. Fuel Rate
Performance			
Imep, psi	138.69	140.95	139.16
Ind. thermal efficiency, %	0.4437	0.4443	0.4452
Isfc, lb/bhp-hr	0.3124	0.3120	0.3114
Mass avg. int. temp, F	129.70	124.70	124.50
Vol. eff., %	83.30	84.56	84.58
Pumping mep, psi	-3.02	-3.91	-3.89
Friction mep, psi	-44.94	-45.20	-45.06
Brake mep, psi	90.72	91.84	90.20
Pcyl at st. inj., psi	229.98	232.38	232.29
Tcyl at st. inj., R	1428.00	1428.00	1426.00
Engine Conditions			
Speed, rpm	2000.00	2000.00	2000.00
Fuel air ratio	0.0540	0.0540	0.0531
Fuel rate, lb/hr	7.831	7.948	7.831
Caivo, deg	520.00	514.00	514.00
Caivc, deg	50.00	44.00	44.00
Caevo, deg	310.00	322.00	322.00
Caevc, deg	560.00	572.00	572.00
Int. valve dia., in.	2.00	1.962	1.962
Exh. valve dia., in.	1.70	1.738	1.738
P atm, psi	14.08	14.08	14.08
T atm, F	95.00	95.00	95.00

Table 5 - Effects of Heat Release Shape and Compression Ratio

Compression Ratio	16.00	16.00	16.00	16.00	18.19
Peak cyl. temp., R	3737.1	3750.5	3758.7	3764.1	3550.5
Peak cyl. pressure, psi	1130.0	1110.0	966.0	1112.0	1110.0
Max. pressure rise, psi/deg	88.38	81.03	50.82	70.64	56.19
Imep, psi	137.85	138.92	135.32	138.56	137.98
Heat transfer sum, Btu/cycle	0.423	0.421	0.413	0.432	0.415

Column	Heat Release Curve
1	Original (Fig. 10)
2	Simplified (Fig. 10)
3	Modified, 75% peak (Fig. 11)
4	Modified, w/7 deg advance (Fig. 12)
5	Modified, 75% peak (Fig. 11)

TABLE 6

COMPARISON OF RADIANT TO OVERALL HEAT TRANSFER RATES

Radiant Heat Transfer			Total Heat Transfer*		
RUN NO.	INSTANTANEOUS PEAK RATE**	AVERAGE RATE**	RUN NO.	INSTANTANEOUS PEAK RATE**	AVERAGE RATE**
20	388000	27297	133	not available	137950
27	391155	14729	144	560000	69190
54	337435	15009	136	1080000	83250
62	414507	23362	137	930000	99450
70	334663	24747	138	1540000	134060
77	214531	23254	145	1650000	167570
34	366360	22957	132	1270000	119790
91	416445	28442	154	1420000	138170
98	407392	14893	152	1100000	88000
125	524143	31467	151	780000	122060
132	306001	23498	150	1250000	121090

*Data from the work of LeFeuvre. Information from runs at engine conditions similar to those of this author. Data presented represents LeFeuvre's data for thermocouple No. 1 located in the cylinder head deck.

**BTU/hr-ft^2

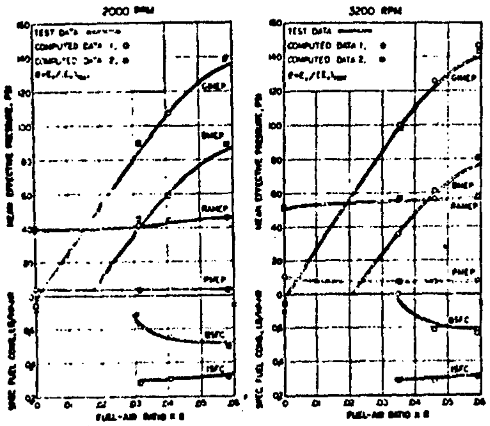

Fig. 1 Comparison of Calculated and Experimental Performance Data.

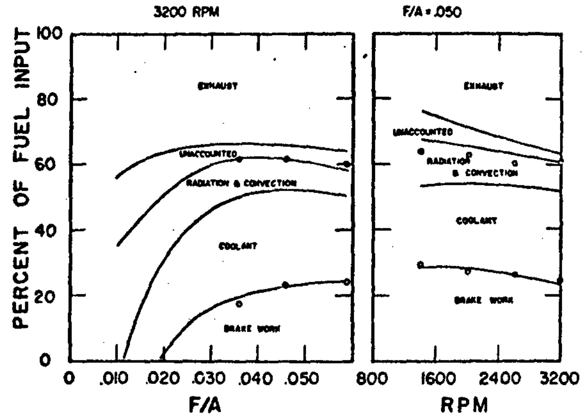

Fig. 2 Comparison of Calculated and Experimental Heat Balance.

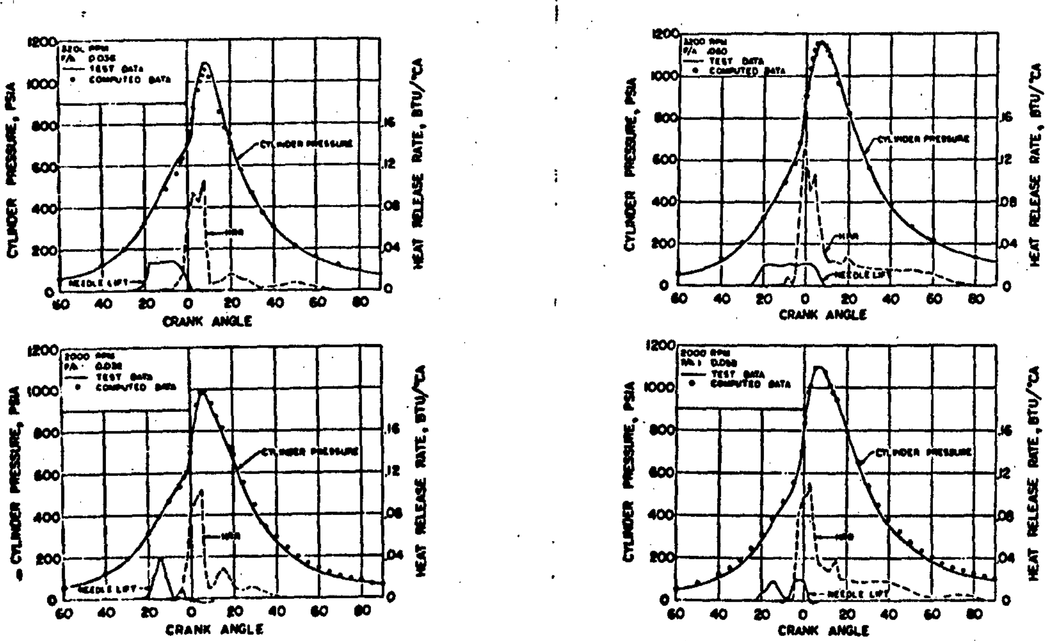

Fig. 3 Comparison Between the Experimental and Computed Pressure-Time Diagrams.

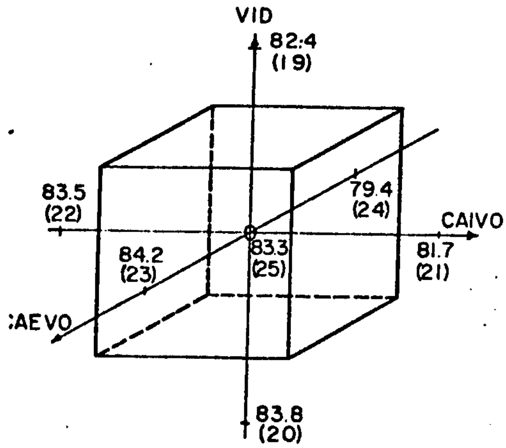

Fig. 4 Volumetric efficiency at 2000 rpm for various values of valve diameter and valve timing

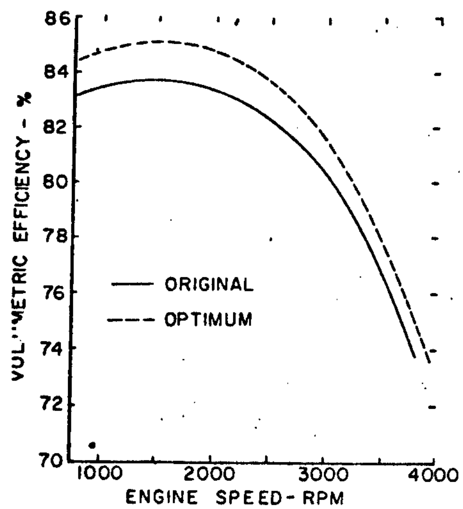

Fig. 5 Comparison of original and predicted optimum volumetric efficiency versus engine speed.

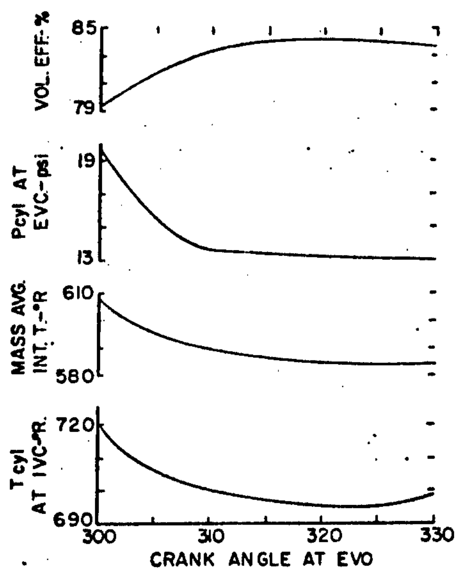

Fig. 6 Various computed values versus crankangle when exhaust valve opens.

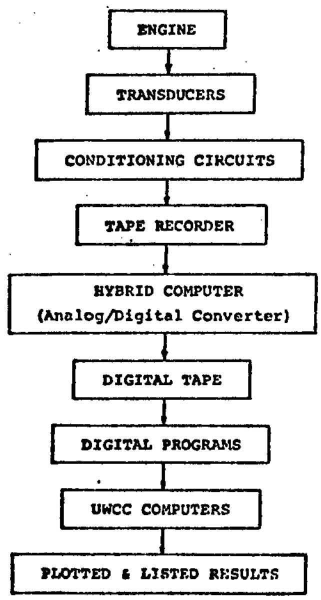

Fig. 7 Overall system used.

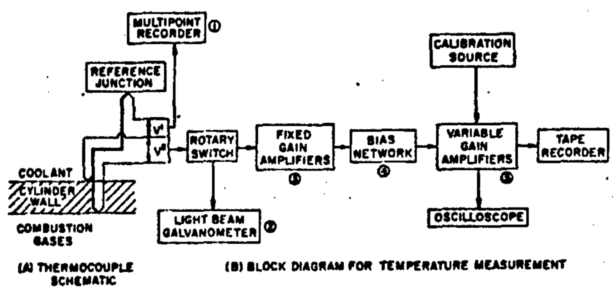

Fig. 8 Thermocouple schematic and instrumentation for surface temperature measurement.

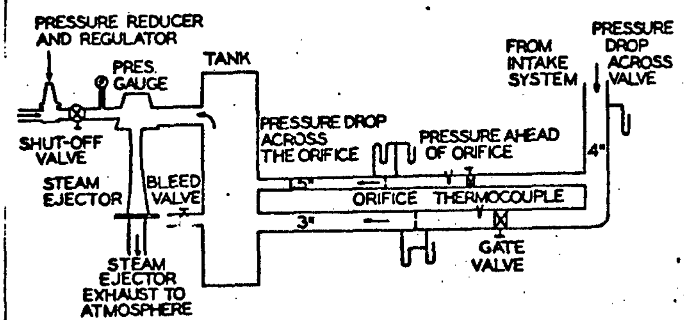

Fig. 9 Schematic representation of flow system apparatus.

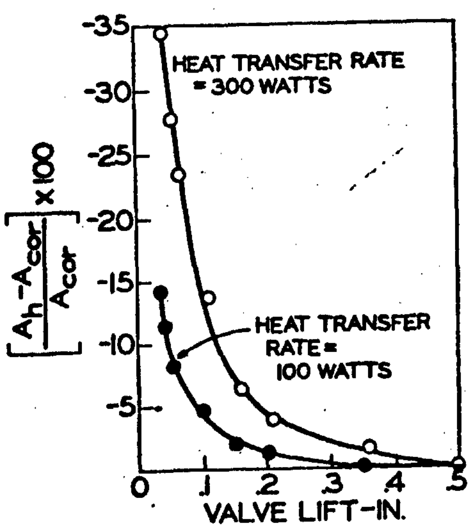

Fig. 10 Percentage change in effective flow area for two different heat transfer rates. Lift was corrected for linear expansion.

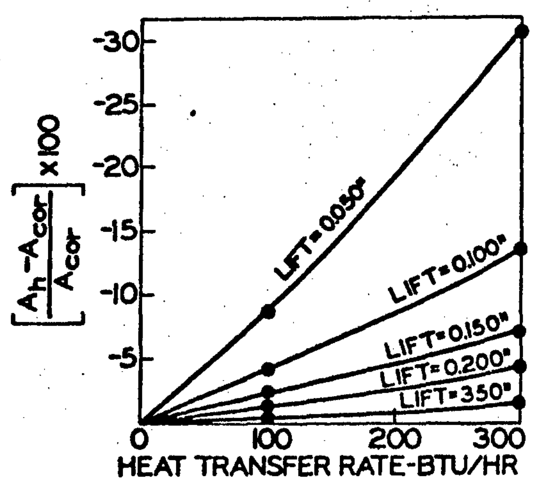

Fig. 11 Percentage change in effective flow area as function of heat transfer rate. Lines of constant lift with lift values corrected for expansion.

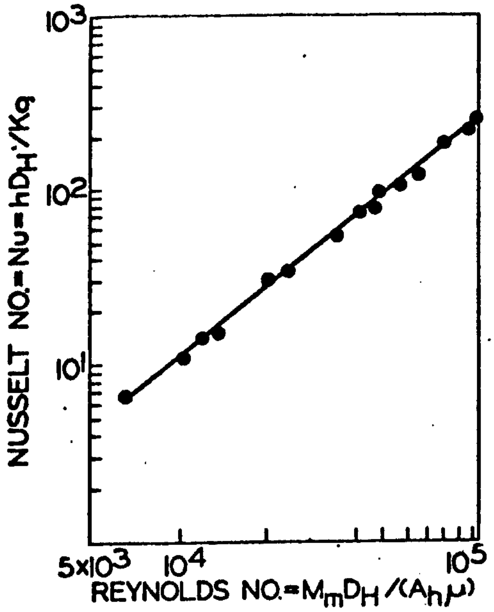

Fig. 12 Nusselt number as function of Reynolds number for valve heat transfer.

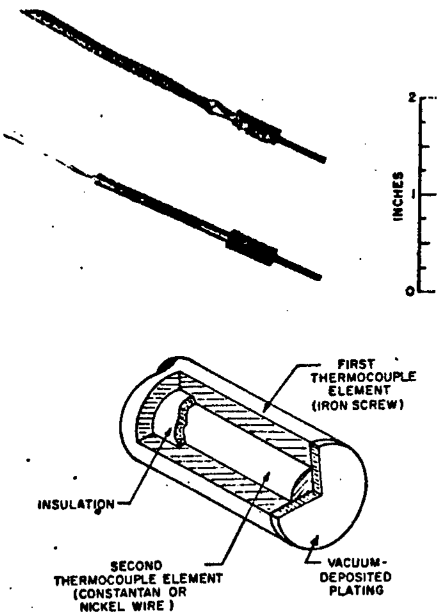

Fig. 13 Surface thermocouple.

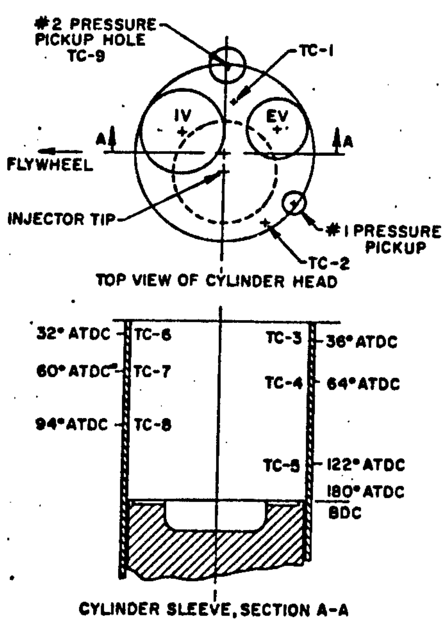

Fig. 14 Cylinder head and sleeve geometry showing thermocouple locations.

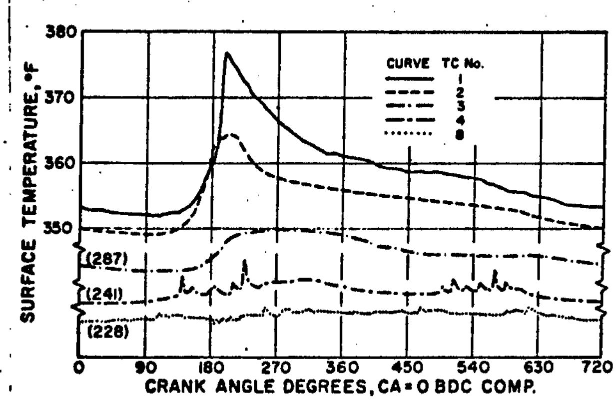

Fig. 15 Cyclic surface temperature at five locations in cylinder for SOC operation.

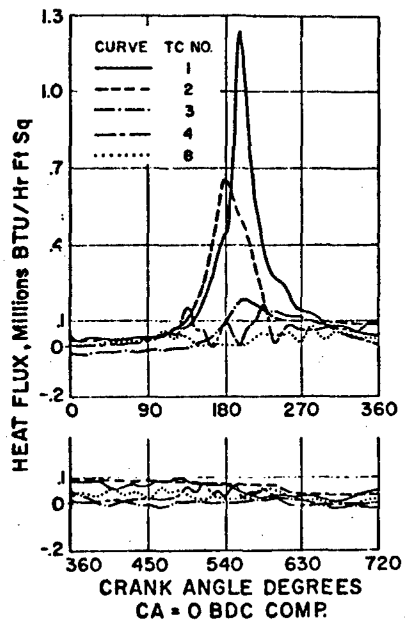

Fig. 16 Cyclic surface heat flux at five locations in cylinder for SOC operation.

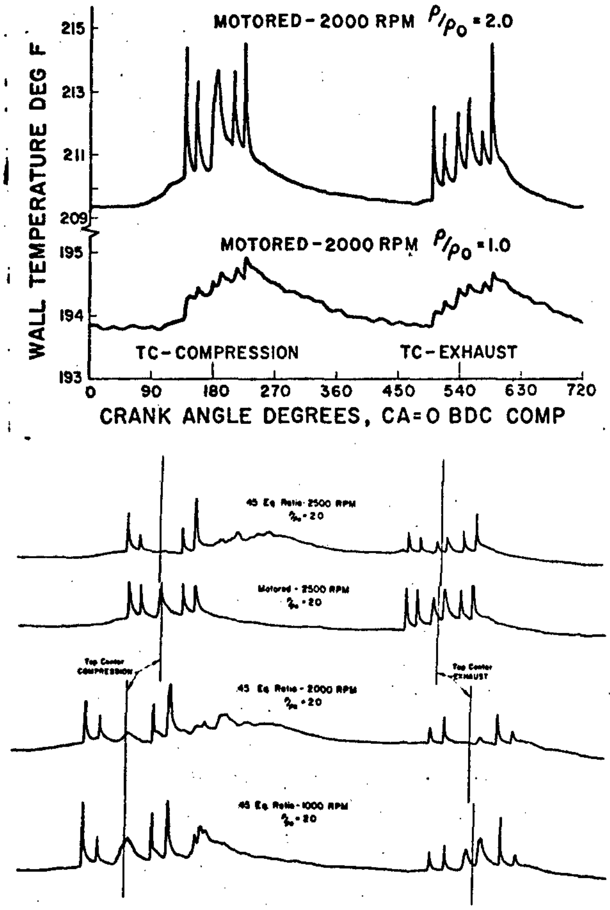

Fig. 17 Cyclic surface temperature-time records from TC-4 on cylinder sleeve.

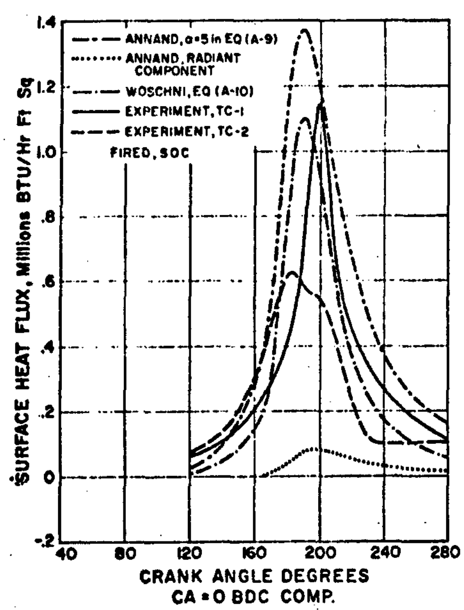

Fig. 18 Comparisons of predictions of Annand and Woschni with experimental data from cylinder head for fired operation.

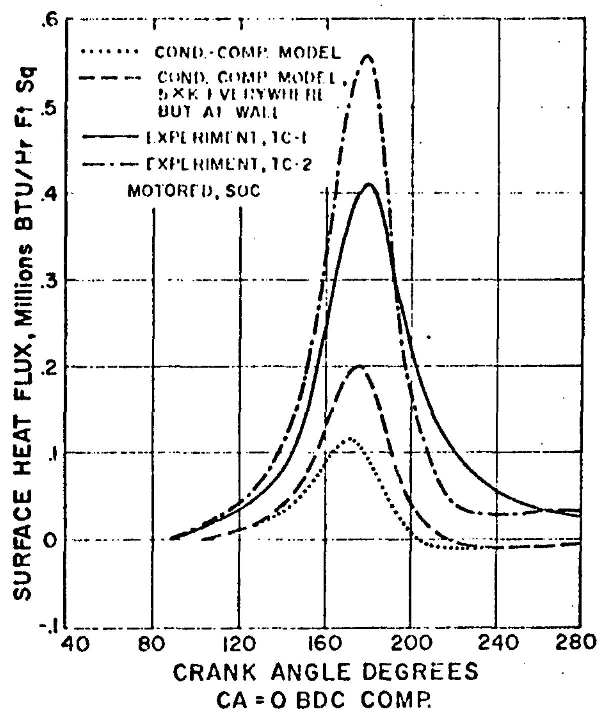

Fig. 19 Comparisons of the results from the conduction-compression model with experimental data for motored operation.

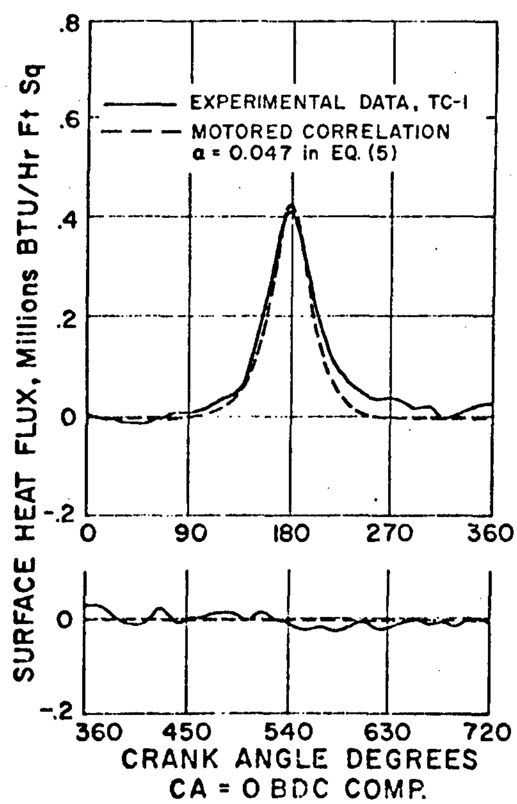

Fig. 20 Boundary layer model fit of motored (SOC) data at TC-1.

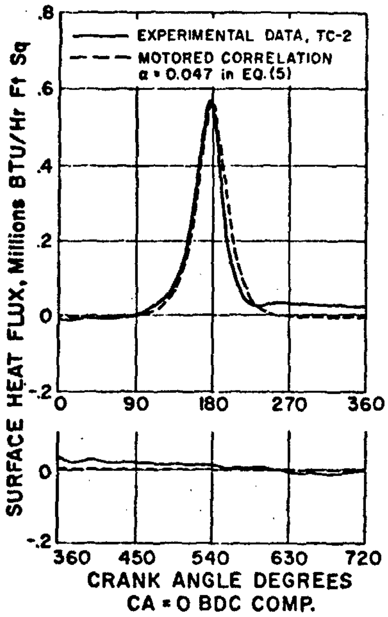

Fig. 21 Boundary layer model fit of motored (SOC) data at TC-2.

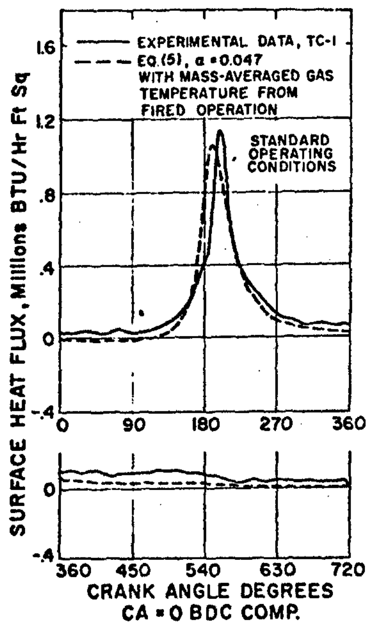

Fig. 22 Extension of motored correlation to fired operation (SOC) at TC-1.

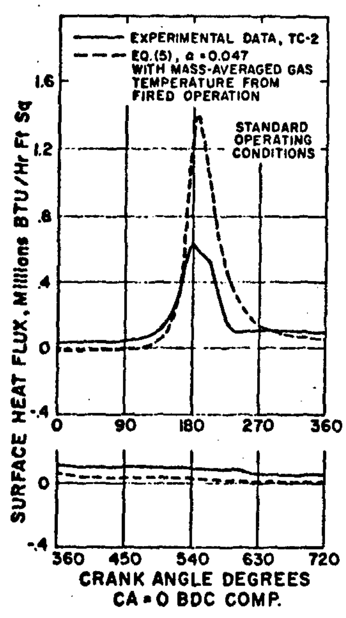

Fig. 23 Extension of motored correlation to fired operation (SOC), at TC-2.

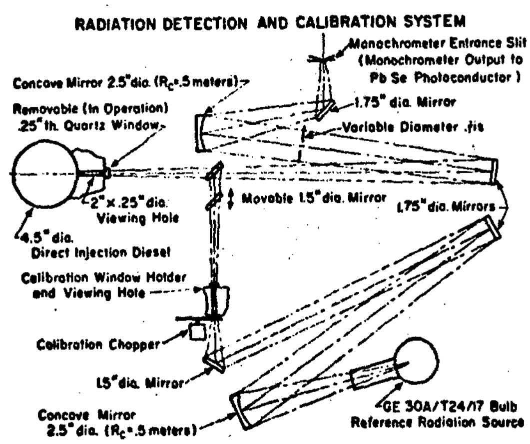

Fig. 24 Radiation detection and calibration system.

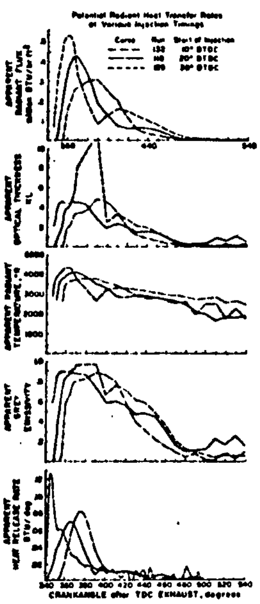

Fig. 25 Radiant emissions and heat release rates when injection timing is varied.

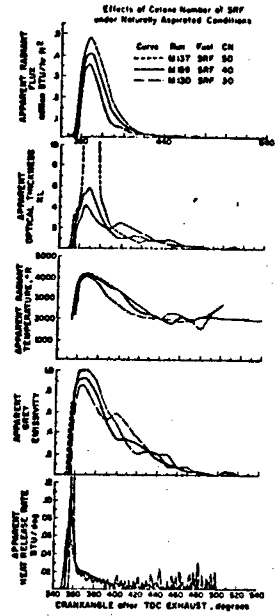

Fig. 26 Radiant emissions and heat release rates for various cetane number fuels under naturally aspirated conditions.

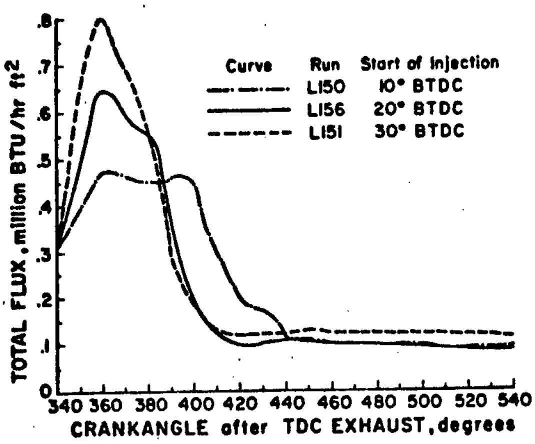

Fig. 27 Total heat flux for various injection timings as reported by LeFeuvre.

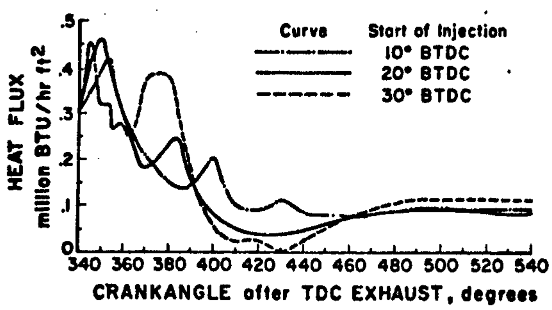

Fig. 28 Convective heat flux portion of LeFeuvre's total heat flux.

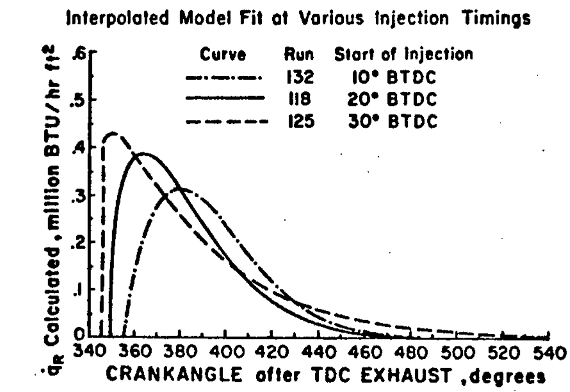

Fig. 29 Representation of Eq. 16 for runs of Fig. 13 in Appendix VC.

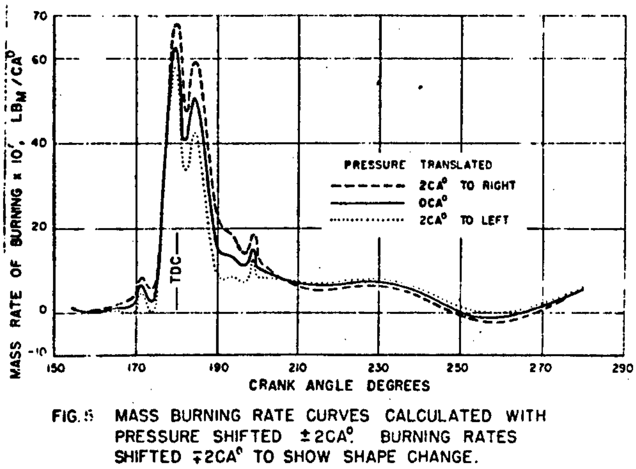

Fig. 30 Mass burning rate curves calculated with pressure shifted ±2 CA°. Burning rates shifted ±2 CA° to show shape change.

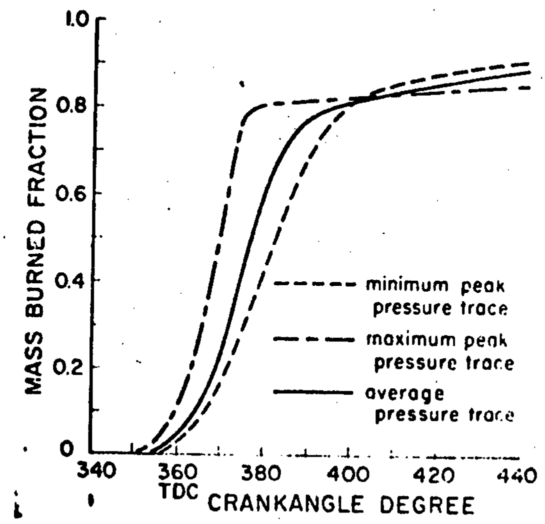

Fig. 31 Mass burned fraction versus crankangle for three cycles of data run No. 7.

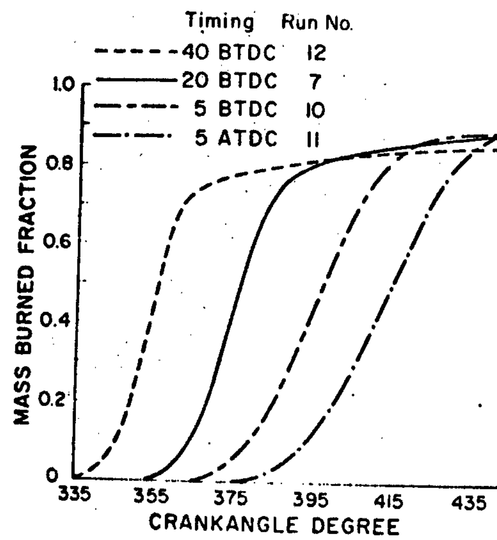

Fig. 32 Mass burned fraction versus crankangle for different spark timings using average pressure-time diagrams.

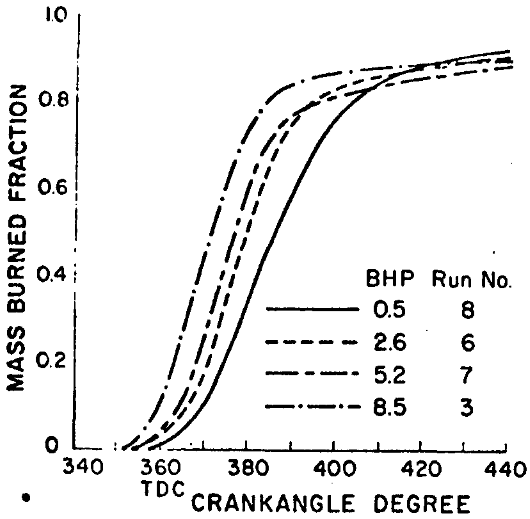

Fig. 33 Mass burned fraction versus crankangle for different engine loads using average pressure-time diagrams.

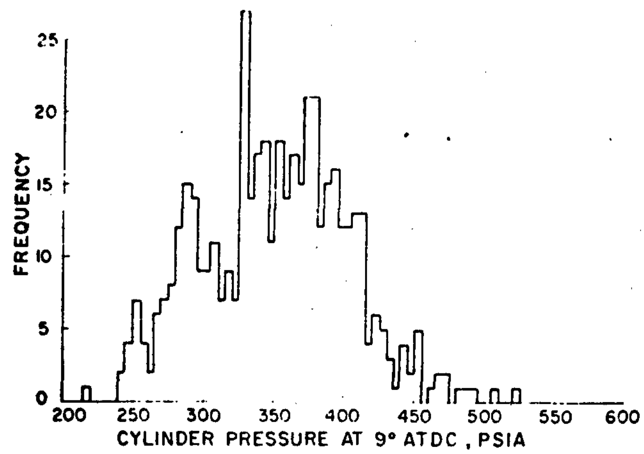

Fig. 34 Frequency plot of cylinder pressure for data run No. 1.

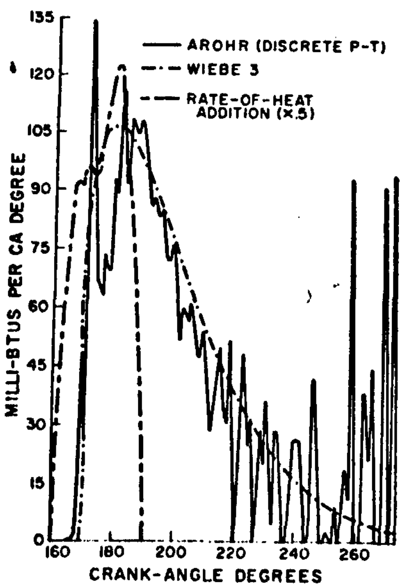

Fig. 35 AROHR computed from discrete p-t diagram and smooth curve fitted to AROHR using three Wiebe parameters.

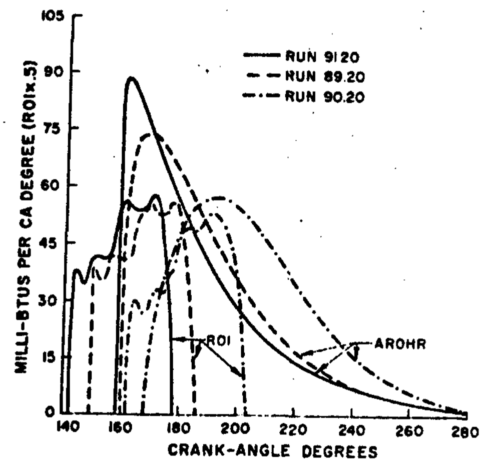

Fig. 36 Effect of INJ timing on AROHR with small (0.0118) nozzle tip and low ROI.

Run 90	18 deg btc
Run 89	30 deg btc
Run 91	40 deg btc

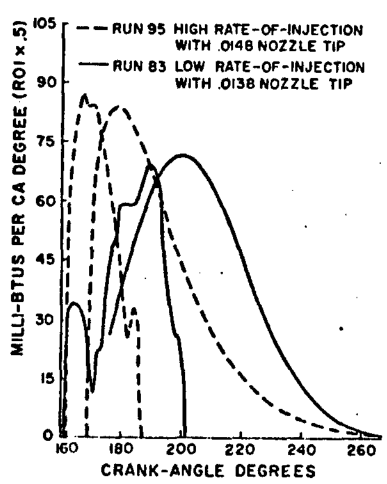

Fig. 37 Comparison of AROHR obtained with two different rates of INJ.

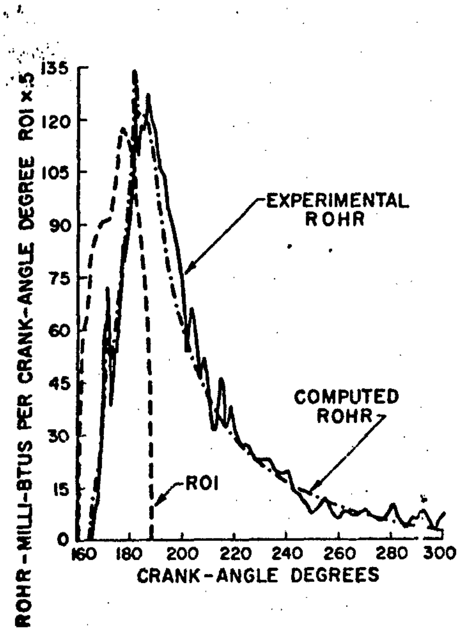

Fig. 38 Comparison of ROHR predicted with Model Tanas II with $C_E \propto T^{0.33}$ and experimental ROHR.

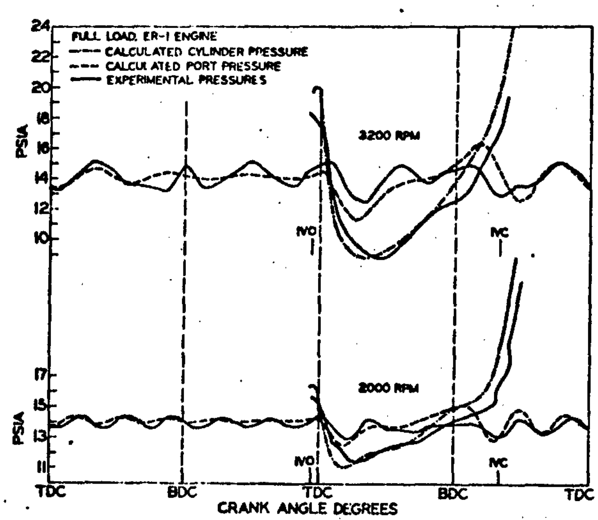

Fig. 39 Some comparisons of experimental and calculated intake port pressures. (International Harvestor Co. Data).

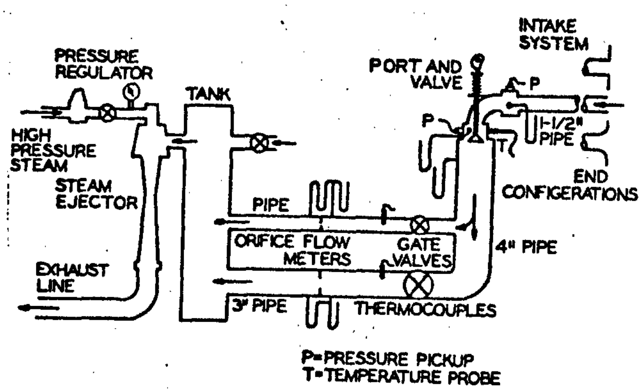

Fig. 40 Schematic diagram of flow system apparatus,

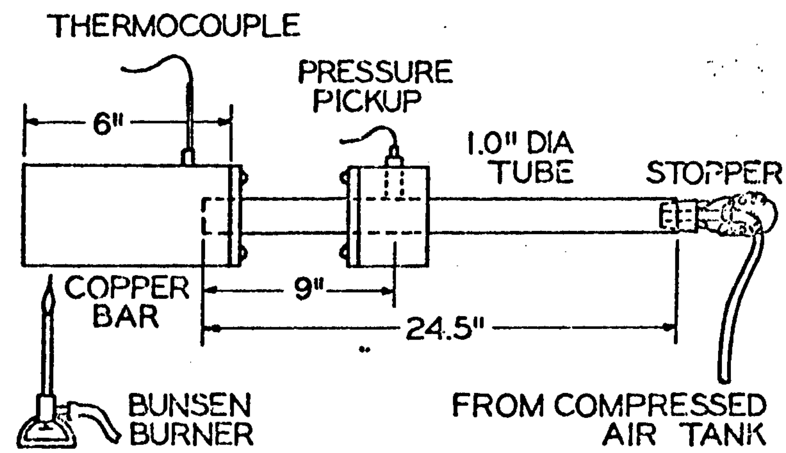

Fig. 41 Schematic of pressurized pipe bench test apparatus.

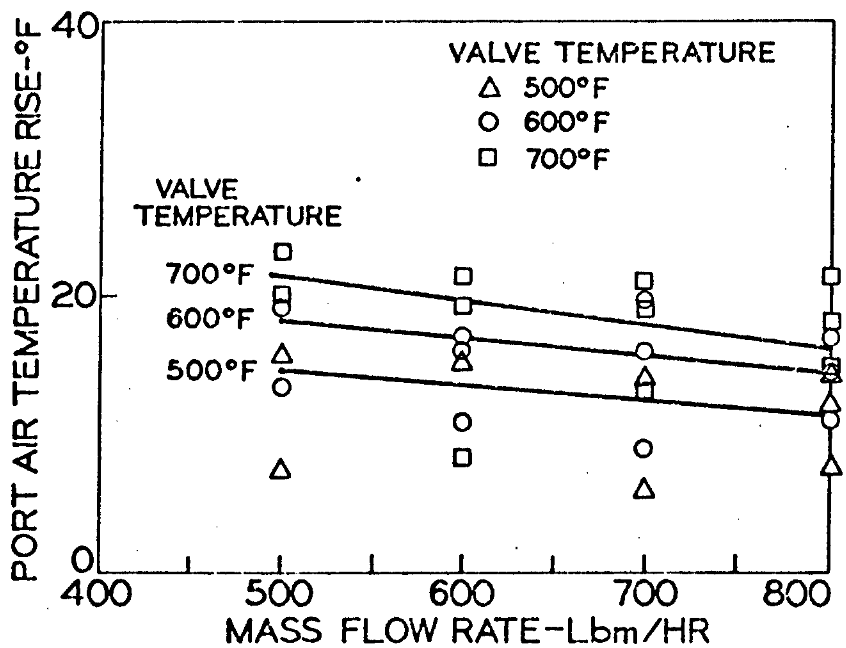

Fig. 42 Air temperature rise in port as function of valve temperature and mass flow rate.

APPENDIX I

DETAILS OF CURRENT ENGINE PROGRAM

Computer Program for Single Cylinder Internal Combustion Engine

A digital computer simulation has been rewritten in FORTRAN V language for the UNIVAC 1108 computer. The program can be used to simulate any one of the following types of single cylinder engines:

1. Four stroke open chamber diesel engine.
2. Four stroke per chamber diesel engine
3. Four stroke spark ignition engine.

The work on mathematical modeling and the development of time dependent differential equations for open chamber diesel engine and spark ignition engine is given in the following Appendices. The work on the pre chamber diesel engine has not yet been completed but is covered in principle in the main body of this report.

As indicated in the main body of this report, the engine is divided in several thermodynamic systems and two basic assumptions are made. They are:

1. Existence of thermodynamic equilibrium at each instant of the cycle.
2. No spacial variation of thermodynamic variables, e.g., pressure and temperature, in the system.

Consequently, the only independent variable is time, except in the case of wave dynamics for long intake pipes, and the differential equations for the system are reduced to ordinary type. The various systems are explained below:

1. Ports - There are two different systems for ports, intake and exhaust. The instantaneous flow rates of gases to and from the ports are computed using conventional steady state flow equations. The flow coefficient can be found either by using empirical relationships or can be experimentally determined. The pressures in the ports can be assumed to be constant or in the case of a long intake pipe for diesel engines the one dimensional wave equation is solved. For instantaneous heat transfer rate purposes, each port is divided into two parts -- port wall and valve back. It should be noted that the intake port may contain products of combustion in case of back flow from cylinder for diesel as well as spark ignition engine but that the exhaust port may not contain air or fuel vapor in the case of spark ignition engine.

2. Cylinder - Two cases can be considered for the cylinder—with combustion and no combustion. In case of spark ignition engines during combustion the cylinder is divided into two subsystems—burnt and unburnt. The pressure is also assumed to be the same in the two systems but the temperature is different. In the case of diesel engines, the fuel is injected at some known rate and assumed to burn instantaneously. The rate of fuel burning can be either found empirically or computed from a pressure-time diagram for a similar engine using the heat release program. The cylinder is divided into five different parts for computing instantaneous heat transfer rates. They are: (*i*) Piston, (*ii*) Cylinder head, (*iii*) Sleeve, (*iv*) Intake valve front, and (*v*) Exhaust valve front. The five wall temperatures, assumed to be constant during a cycle, and mass averaged gas temperature are used to calculate heat transfer rates using various heat transfer correlations. The properties of products of combustion are computed for the type C_nH_{2n} fuel using analytical expressions fitted to tabulated data of Starkman and Newhall.

3. Prechamber - This is used only in case of pre chamber diesel engine. Fuel is assumed to be injected and burnt in this system also, in addition to the cylinder. The two systems are coupled by a throat between them through which gases can flow. Pre chamber wall temperature is assumed to be constant during a cycle. Development of equations in this system is similar to the cylinder.

4. Coolant - Water cooling is assumed. Using one dimensional heat conduction models for various walls and a correlation for the heat transfer coefficient on coolant side, a cyclic heat balance is written. From it, new wall temperatures are computed to be used in the next cycle. Simplification of geometry is essential for the one dimensional model.

The computer program consists of a main program with 17 subroutines, all of which may not be called for in some cases. A listing of the program can be found in Appendix I. Most of the subroutines can be divided into two main parts. The first part is initialization which takes place at the start of the program execution and/or at the beginning of each cycle iteration. The second part of the subroutine is called during execution of the cycle. A subroutine is divided into different parts by various entry points which is a feature of higher order FORTRAN languages. A flow chart showing the logic of the program is on page . The function of each subprogram with its important features is given below.

1. MAIN ... The main program calls the subroutines for input variables and the initialization at the starting crankangle. It starts the program and provides 720 increments of 1 degree crankangle each. It also controls the print output of ØUTPUT subroutine in various cases as follows:

   a. List of input variables
   b. Tabular form output for cyclic variables
   c. Output at the end of unsuccessful cycle
   d. Output in case of error
   e. Final output

2. INPUT ... This is the *only* subprogram which reads the input information in card form and transmits the respective values of input variables to their respective subroutines by common blocks. It has been structured in such a way that the order of cards in the input deck does not affect the values of the variables. The first ten columns of each input card consists of the alphanumeric identifying name (6 columns) and numeric branching information. The list of input variables with units is the Appendix 10.

3. INITIAL ... This subprogram is divided into three parts. The first is initialization of variables at the start of execution and the second is initialization of cyclic variables at the beginning of each cycle. The third part is the print output of cyclic variables at the end of unsuccessful cycle.

4. SØLVE ... This subprogram provides crankangle increment of 1 degree or 0.1 degree, in case of nonconvergence, and calls the subroutine for solving ordinary coupled differential equations.

5. IDIFF ... This subprogram solves time dependent coupled ordinary differential equations in state variables by Modified Euler Predictor Corrector method. The variables are pressure, temperature, mass and equivalence ratio of volume for spark ignition engine during combustion.

6. IRATE ... The function of this subprogram is to calculate the time derivatives of state variables during the cycle. It can be divided into four parts. The first part initializes the variables and sets the constants. It also generates switch variables for various branches. The second part calculates the mass flow rates between various systems and time derivatives for solving differential equations. The third part calculates the accumulated sum of mass and energy flow quantities and piston work during a cycle. The fourth and last part calculates output quantities such as horsepower, efficiencies etc., and prints the output.

7. IVLUME ... This subprogram evaluates the geometrical variables such as compression ratio, cylinder gas volume, its rate of change, sleeve area open to gas side heat transfer etc., as a function of crankangle during the cycle.

8. IAREA ... The function of this subprogram is to calculate the flow areas for gases between the valves and the engine cylinder as functions of crankangle. The effective flow areas at the reference speed of 1200 rpm are known from experimental results and then using polydyne cam theory, the effective flow areas can be calculated at different speeds. This subprogram can be replaced for different engines.

9. IENGRY ... This subprogram calculates the internal energy, the gas constant and their partial derivatives with pressure, temperature and equivalence ratio for the products of combustion. It is divided into two parts. The first part is for lean mixtures. In this part, the internal energy and gas constant are written as functions of pressure, temperature and equivalence ratio. In the second part, for rich mixture, the properties of products of combustion are functions of pressure and temperature at five equivalence ratios (1.0, 1.1, 1.2, 1.4 and 1.6). The values at other equivalence ratios are found by interpolation formula.

10. IAVRGY ... This subprogram calculates properties of air and fuel vapor as function of temperature. It is used only for the spark ignition engine.

11. IFLWCØ ... The function of this subprogram is to find the coefficient of discharge of flow areas for inlet valve, exhaust valve, intake manifold and the throat between precup and engine cylinder.

12. IHEAT ... This subprogram calculates the instantaneous rates of heat transfer on gas side for various engine parts. It can be subdivided into five parts. The first part initializes, sets the constants and generates switch variables for various branches. The second part calculates the instantaneous heat transfer rates using various types of correlations. The third part accumulates the sum of the heat transfer rates of all engine parts to be used for the cyclic energy balance. The fourth part finds the mean wall temperatures at the end of the cycle using a one dimensional heat conduction model. Finally, the fifth part calculates the output variables and prints the output.

13. ICØMB ... This subprogram determines the combustion period during the cycle and calculates the apparent fuel burning rate. For spark ignition engines, it also changes the total number of systems in the engine cylinder at the beginning and end of the combustion.

14. LAGINT ... It uses a Lagrangian interpolation scheme to find the apparent fuel burning rate at various crankangles. It is called by the INCØMB subroutine.

15. MASS ... This subprogram calculates the mass flow rate for an area opening using orifice flow equation. It is called by the IRATE subroutine.

16. ICYCLE ... This subprogram checks for the cyclic variables such as pressure temperature, equivalence ratio and various wall temperatures, at the end of cycle and stops the program in case of convergence.

17. IDYNIP ... The first part of this subprogram initializes the variables and the second part solves the one dimensional wave equation for the intake system. The equations are hyperbolic and solved by the method of characteristics. It calculates the mean port pressure and its time derivative as functions of crankangle. There is provision in the program to skip this subroutine in case of constant port pressure assumption.

18. ØUTPUT ... This subroutine prints the list of input variables before starting the cyclic calculations and then at the end of the cycle, prints either the cyclic variables in case of nonconvergence or the final output for the convergent cycle. It is controlled by the MAIN program. A sample output with the corresponding input list is attached in the appendix.

INPUT VARIABLE LIST

N1	N2	VARIABLE NAME	DESCRIPTION	UNITS
1	1	NRUN	Integer variable for identification	[-]
		RPM	Engine Speed	[rev/min]
		BØRE	Cylinder diameter	[in.]
		STRØKE	Length of piston stroke	[in.]
		CØNRD	Length of the piston connecting rod	[in.]
	2	SCL	Sleeve height uncovered at TDC	[in.]
		VLPCL	Volume added to the combustion chamber volume due to the curvature of the top of the piston (piston bowl volume)	[in.^{3}]
		VLVCL	Volume added to the combustion chamber volume by taking the head and valve configuration into account. Combustion chamber volume $= (\pi/4)(BØRE)^2 SCL + VLPCL + VLVCL$	[in.^{3}]
		VØLP2	Volume of the pre chamber for a pre chamber diesel engine (includes throat volume)	[in.^{3}]
		APM	Cross-sectional area of the throat between the pre chamber and the main chamber of a pre chamber diesel engine	[in.^{2}]
		AIM	Cross-sectional area of the inlet manifold of S.I. engine	[in.^{2}]
	3	AH1	Heat transfer area of the head for System 1 - gas side	[in.^{2}]
		AP	Heat transfer area of the top of the piston - gas side	[in.^{2}]
		AH2	Heat transfer area of the head in System 2 for pre chamber engine - gas side	[in.^{2}]
	4	AH1C	Heat transfer area of the head for System 1 - coolant side	[in.^{2}]
		APC	Heat transfer area of the underside of the piston - coolant side	[in.^{2}]
		ASC	Heat transfer area of the sleeve - coolant side	[in.^{2}]
		APSC	Heat transfer area used in determining the thermal resistance between the center of the piston and the sleeve	[in.^{2}]
		ASBC	Heat transfer area used in determining the thermal resistance between the center of the piston and the coolant side of piston	[in.^{2}]
		AH2C	Heat transfer area of the head in System 2 for pre chamber engine - coolant side	[in.^{2}]
	5	DIV	Diameter of the inlet valve	[in.]
		DEV	Diameter of the exhaust valve	[in.]

N1 N2	VARIABLE NAME	DESCRIPTION	UNITS
1 5	AIVF	Heat transfer area of the front side of the inlet valve - gas side	[in.^{2}]
	AIVB	Heat transfer area of the back side of the inlet valve in the intake port - gas side	[in.^{2}]
	AEVF	Heat transfer area of the front side of the exhaust valve - gas side	[in.^{2}]
	AEVB	Heat transfer area of the back side of the exhaust valve in the exhaust port - gas side	[in.^{2}]
6	AIVC	Not used	
	AEVC	Not used	
7	DMIP	Mean hydraulic diameter of the inlet port	[in.]
	DMEP	Mean hydraulic diameter of the exhaust port	[in.]
	AIP	Average cross-sectional area of the intake port	[in.^{2}]
	AEP	Average cross-sectional area of the exhaust port	[in.^{2}]
	VIP	Volume of the intake port	[in.^{3}]
	VEP	Volume of the exhaust port	[in.^{3}]
8	AIVP	Heat transfer area of the intake port - gas side	[in.^{2}]
	AEVP	Heat transfer area of the exhaust port - gas side	[in.^{2}]
	AIPC	Heat transfer area of the intake port - coolant side	[in.^{2}]
	AEPC	Heat transfer area of the exhaust port - coolant side	[in.^{2}]

The following lengths are used in a one dimensional heat transfer model of the cylinder and port areas. This model is used for determining the wall temperatures.

9	XH1	Thickness of the head between the gases in System 1 and the coolant	[in.]
	XPGI	Distance from the top of the piston to an intermediate point within the piston	[in.]
	XPIS	Distance from the intermediate point within the piston to the sleeve	[in.]
	XPIC	Distance from the intermediate point within the piston to the bottom of the piston	[in.]
	XSGC	Thickness of the sleeve	[in.]
	XH2	Thickness of the head between the gases in system and the coolant for pre chamber engine	[in.]
10	XIP	Thickness of the intake port wall	[in.]

DQIP.

N1	N2	VARIABLE NAME	DESCRIPTION	UNITS
1	10	XEP	Thickness of the exhaust port wall	[in.]
		XIVØ	Average distance through the intake valve from the port gases to the coolant while the valve is open	[in.]
		XEVØ	Same as XIVØ except for the exhaust valve	[in.]
		XIVC	Average distance through the intake valve from the port gases to the coolant while the valve is closed	[in.]
		XEVC	Same as XIVC except for the exhaust valve	[in.]

The following crankangles are measured from top-dead-center of the exhaust stroke.

2	1	CAEVØR	Crankangle exhaust valve opening ramp	[°CA]
		CAEVØ	Crankangle exhaust valve opens	[°CA]
		CAEVC	Crankangle exhaust valve closes	[°CA]
		CAEVCR	Crankangle exhaust valve closing ramp	[°CA]
	2	CAIVØR	Crankangle intake valve opening ramp	[°CA]
		CAIVØ	Crankangle intake valve opens	[°CA]
		CAIVC	Crankangle intake valve closes	[°CA]
		CAIVCR	Crankangle intake valve closing ramp	[°CA]

The following 12 variables are used in determining valve motion. The model used is a one mass, two spring system. Equivalent mass and spring constant terms are calculated for the valve side of the rocker arm.

3	YIVM	Maximum displacement of inlet valve at reference speed	[in.]
	YEVM	Maximum displacement of exhaust valve at reference speed	[in.]
	YCIR	Clearance and initial deflection of inlet valve at reference speed	[in.]
	YCER	Clearance and initial deflection of exhaust valve at reference speed	[in.]
	RALI	Rocker arm ratio for inlet valve	[-]
	RALE	Rocker arm ratio for exhaust valve	[-]
4	WIVT	Equivalent weight of the intake valve train	[lb_m]
	WEVT	Equivalent weight of the exhaust valve train	[lb_m]
	SRSI	Spring constant for the return spring on the inlet valve	[lb_f/in.]
	SRSE	Spring constant for the return spring on the exhaust valve	[lb_f/in.]

N1	Nz	VARIABLE NAME	DESCRIPTION	UNITS
2	4	SVTI	Equivalent spring constant for the intake valve train	[lb_f/in.]
		SVTE	Equivalent spring constant for exhaust valve train	[lb_f/in.]

The following values are error limits for certain parameters used to determine if further iteration is required at a given crankangle. The cyclic error values set the error limits of parameters from cycle to cycle and are used to determine if the program must make another cyclic iteration.

		VARIABLE NAME	DESCRIPTION	UNITS
3	1	ERP1	Error limit for the pressure in System 1	[psi]
		ERT1	Error limit for the temperature in System 1	[°R]
		ERF1	Error limit for the equivalence ratio of the fuel air mixture in System 1 (for diesel engines only) or error limit for volume of System 1 during combustion of S.I. engine	[-] or [in.^{3}]
		ERW1	Relative error limit for the mass in System 1	[-]
		ERP1C	Cyclic error limit for the pressure in System 1	[psi]
		ERT1C	Cyclic error limit for the temperature in System 1	[°R]
		ERF1C	Cyclic error limit for the equivalence ratio in System 1 for diesel engine	[-]
	2	ERP2	Error limits for System 2, same as for System 1	[psi]
		ERT2		[°R]
		ERF2		[-] or [in.^{3}]
		ERW2		[-]
		ERP2C		[psi]
		ERT2C		[-]
		ERF2C		[-]
	3	ERPIP	Error limits for the intake port, same as for System 1	[psi]
		ERTIP		[°R]
		ERFIP		[-]
		ERWIP		[-]
		ERPIPC		[psi]
		ERTIPC		[°R]
		ERFIPC		[-]
	4	ERPEP	Error limits for the exhaust port, same as for System 1	[psi]
		ERTEP		[°R]
		ERFEP		[-]
		ERWEP		[-]
		ERPEPC		[psi]
		ERTEPC		[°R]
		ERFEPC		[-]

Metal temperatures are considered constant over a cycle. Therefore the following error limits are cyclic error limits.

		VARIABLE NAME	DESCRIPTION	UNITS
	5	ERTWH1	Error limit for the wall temperature of the head in System 1	[°R]

N1	N2	NAME	DESCRIPTION	UNITS
3	5	ERTWS	Error limit for the temperature of the sleeve	[°R]
		ERTWP	Error limit for the temperature of the top of the piston	[°R]
		ERTWIV	Error limit for the temperature of the intake valve	[°R]
		ERTWEV	Error limit for the temperature of the exhaust valve	[°R]
		ERTWIP	Error limit for the wall temperature in the intake port	[°R]
		ERTWEP	Error limit for the wall temperature in the exhaust port	[°R]
	6	ERTWH2	Error limit for the wall temperature of the head in System 2 (Needed for a pre chamber diesel engine only)	[°R]
		ERRVØL	Error limit for volume used to stop combustion for S.I. engine	[in.^{3}]

The following are integer variables used for giving engine type and whether printed output is desired from some of the subroutines.

N1	N2	NAME	DESCRIPTION	UNITS
4	1	NENG	1 - designates open chamber diesel engine 2 - designates pre chamber diesel engine 3 - designates spark ignition engine	[-]

In the following 9 variables, a value of 1 designates yes and 2 designates no.

N1	N2	NAME	DESCRIPTION	UNITS
		NØUT1	Tabulated output for each degree crankangle at the end of the cycle	[-]
		NDBSØL	Print out the number of iterations required for convergence at each crankangle	[-]
		NDBRT	Printed output from RATE subroutine giving the values calculated within the routine each time it is called	[-]
		NVLDBG	Printed output from the VØLUME subroutine	[-]
		NARDBG	Printed output from the AREA subroutine	[-]
		NEGDBG	Printed output from the ENERGY subroutine	[-]
	2	NAVDBG	Printed output from the AVERGY subroutine	[-]
		NDBFLØ	Printed output from the FLØWCØ subroutine	[-]
		NHTDBG	Printed output from the HEAT subroutine	[-]
		ICYCLE	The maximum number of cyclic iterations for cycle convergence	[-]
		IDVS	The maximum number of iterations for computing rates of port systems	[-]
		ICA1	Crankangle at which the program is to start, measured from TDC on the exhaust stroke	[°CA]
		ICA2	Crankangle at which the program is to stop. Negative value means complete cycle calculations	[°CA]

N1 N2

VARIABLE NAME	DESCRIPTION	UNITS
	The following integer variables are used to determine which heat and flow correlations are used in the program.	
4 3 NHTC1	Type of convective heat transfer correlation for System 1 11 1 - Annand or Woschni (See NHTCAW) 2 2 - Eichelberg 3 3 - Pflaum 4 4 - (Open)	5 [-]
NHTCAW	Convective heat transfer for System 1 (Needed only if NHTC1=1) 1 2 1 - Annand 2 - Woschni	[-]
NHTR1	Radiative heat transfer correlation for System 1 1 - Modified 2 - Flynn 3 - Open	3 [-]
NHT2	Integer variable for System 2 1 - yes 2 - no	[-]
NHTC2	Convective heat transfer correlation for System 2 1 - Eichelberg 2 - Open	[-]
NHTR2	Radiative heat transfer correlation for System 2 1 - Open	[-]
NHTP	Flow and heat transfer correlation for the ports 1 - Eichelberg and pipe flow 2 - Open	[-]
	The following values are used to start the program. They should be measured values or best estimated of the parameter values at the beginning crankangle.	
5 1 P1	Pressure in System 1 *	[psia]
T1	Temperature in System 1 *	[°R]
F1	Fuel air equivalence ratio in System 1	[-]
P2	Pressure in System 2 *	[psia]
8 1(5) CHCEVF	GO TO Pg53 Convective heat transfer coefficient for the exhaust valve face and System 1 gases	[-]
8 2 CØHRH1 1	Radiation heat transfer coefficient for the head and System 1 gases	[-]

N1	N2	VARIABLE NAME	DESCRIPTION	UNITS
8	2	CØHRP1 2	Radiation heat transfer coefficient for the piston and System 1 gases	[-]
		CØHRS 3	Radiation heat transfer coefficient for the sleeve and System 1 gases	[-]
		CHRIVF 4	Radiation heat transfer coefficient for the inlet valve face and System 1 gases	[-]
		CHREVF 5	Radiation heat transfer coefficient for the exhaust valve face and System 1 gases	[-]
	3	CØHCH2	Convective heat transfer coefficient for the head and System 2 gases	[-]
		CØHCP2	Convective heat transfer coefficient for the piston and System 2 gases	[-]
		CØHRH2	Radiation heat transfer coefficient for the head and System 2 gases	[-]
		CØHRP2	Radiation heat transfer coefficient for the piston and System 2 gases	[-]
	4	CHCIVB	Convective heat transfer coefficient for the inlet valve back	[-]
		CHCIP	Convective heat transfer coefficient for the intake port	[-]
		CHCEVB	Convective heat transfer coefficient for the exhaust valve back	[-]
		CHCEP	Convective heat transfer coefficient for the for the exhaust port	[-]
	5	CHCEIP	Eichelberg convective heat transfer coefficient for intake port	[-]
		CHCEEP	Eichelberg convective heat transfer coefficient for exhaust port	[-]
		CHCEIB	Eichelberg convective heat transfer coefficient for inlet valve back	[-]
		CHCEEB	Eichelberg convective heat transfer coefficient for exhaust valve back	[-]
	6	CØVJ	Coefficient for jet velocity through inlet valve	[-]
		CØHCA1	Constant coefficient in Annand's correlation	[-]
		CØHCA2	Exponential coefficient in Annand's correlation	[-]
		THCNR	Thermal conductivity of air at reference temperature	[Btu/hr-ft-°R]
		TRTHC	Reference temperature in Annand's correlation	[°R]
		PRRA	Prandtl No. of air @ reference temperature	[-]

N1 N2

	VARIABLE NAME	DESCRIPTION	UNITS
	The following 7 variables are used for Woschni correlation.		
8 6 7	VØLR	Volume @ reference crankangle	[in.^{3}]
	PR	Pressure @ reference crankangle	[psia]
	TR	Temperature @ reference crankangle	[°R]
	CAWSS	Crankangle when blowdown starts	[°CA]
	CAWSE	Crankangle when exhaust flow ends	[°CA]
	CAWCS	Crankangle when compression period starts	[°CA]
	CAWCEE	Crankangle combustion and expansion period ends	[°CA]
8	CHCF11	Charge pressure for Pflaum's correlation	[psia]
	CHCF12	Coefficient for Pflaum's correlation	[psia]
	CRA12	Absorptivity of head	[-]
	CRA13	Absorptivity of sleeve	[-]
6	PRRP	Prandtl No. of gases in port systems	[-]
8	PTANK	Intake pressure for Flynn Correlation	[psia]
	CAINJ	Injection timing (360° CA TDC as reference angle) for Flynn Correlation	[°CA]
	EQRT	Overall equivalence ratio for Flynn Correlation	[-]
	The following 8 variables are thermal conductivities various parts of the engine.		
9	CØNDH1	Head	[Btu/hr-ft-°R]
	CØNDP	Piston	[Btu/hr-ft-°R]
	CØNDS	Sleeve	[Btu/hr-ft-°R]
	CØNDH2	Pre chamber wall	[Btu/hr-ft-°R]
10	CØNDIP	Intake port	[Btu/hr-ft-°R]
	CØNDEP	Exhaust port	[Btu/hr-ft-°R]
	CØNDIV	Intake valve	[Btu/hr-ft-°R]
	CØNDEV	Exhaust valve	[Btu/hr-ft-°R]
11	CØFRIC	The fraction of energy converted to heat and transmitted to sleeve through piston rings	[-]
	CBB	Multiplier for blow by mass flow rate around piston	[-]
	CWC1	Multiplier for coolant heat transfer coefficient	[-]
	CWC2	Muttiplier for coolant heat transfer coefficient	[-]

N1	N2	VARIABLE NAME	DESCRIPTION	UNITS
8	11	CWC3	Multiplier for coolant heat transfer coefficient	[-]
		DWCØLH	Coolant mass flow rate in head	[lb_m/min]
		DWCØLS	Coolant mass flow rate in sleeve.	[lb_m/min

The following 8 variables are multipliers for coolant heat transfer coefficient to adjust the rates for various parts

	12	CWCH1	Head	[-]
		CWCS	Sleeve	[-]
		CWCP	Piston	[-]
		CWCH2	Pre chamber	[-]
	13	CWCHIV	Intake valve	[-]
		CWCHEV	Exhaust valve	[-]
		CWCHIP	Intake port	[-]
		CWCHEP	Exhaust port	[-]

The following 9 variables are used in DYNIP Subroutine to solve one dimensional wave equation in intake port

9	1	NDYNIP	1 designates solution of wave equation in intake port 2 designates no solution and assumption of constant pressure in intake port	[-]
		ITDYN	Limit for no. of iterations to solve algebraic equation	[-]
		NX	Number of equal divisions in intake pipe	[-]
		NPX	Number of equal divisions in intake port	[-]
		NDIDBG	1 designates print output at the end of subroutine 2 designates no print output at the end of subroutine	[-]
	2	XLIP	Total length of intake pipe	[in.]
		ERRDYI	Relative error limit for solving algebraic equation	[-]
		DELZ	Relative increment in pressure ratio between System 1 and intake port used to solve algebraic equation in case of flow reversal	[-]
		TMAVI	Mass average temperature of gases through intake valve	[°R]

N1	N2	VARIABLE NAME	DESCRIPTION	UNITS

The following 4 variables are the multiplying factors for flow coefficients for various areas.

N1	N2	VARIABLE NAME	DESCRIPTION	UNITS
10	1	CØDDIV	Intake valve	[-]
		CØDEV	Exhaust valve	[-]
		CØDIM	Intake manifold for S.I. engine	[-]
		CØDPM	Throat for pre chamber engine	[-]
13	—	TEXT	Alphanumeric array to print any message at the top of print output (limit of 80 elements)	[-]

FROM PG49

N1	N2	VARIABLE NAME	DESCRIPTION	UNITS
5	1	T2	Temperature in System 2 *	[-]
		F2	Fuel air equivalence ratio in System 2	[-]
		DPIP	Pressure derivative in the intake port	[psia/°CA]
	2	PIP	Pressure in the intake port 2	[psia]
		TIP	Temperature in the intake port *	[°R]
		FIP	Fuel-air equivalence ratio in the intake port	[-]
		PEP	Pressure in the exhaust port *	[psia]
		TEP	Temperature in the exhaust port *	[°R]
		FEP	Fuel-air equivalence ratio in the exhaust port	[-]
		DPEP	Pressure derivative in exhaust port ?	[psia/°CA]

The following six weight fractions are used only for S.I. engine.

N1	N2	VARIABLE NAME	DESCRIPTION	UNITS
	3	WF1	Weight fraction of the products of combustion in System 1	[-]
		WFA1	Weight fraction of air in System 1	[-]
		WFV1	Weight fraction of fuel vapor in System 1	[-]
		WFIP	Weight fraction of the products of combustion in the intake port	[-]
		WFAIP	Weight fraction of air in the intake port	[-]
		WFVIP	Weight fraction of fuel vapor in the intake port	[-]

The following eight part temperatures are for the gas side surfaces.

N1	N2	VARIABLE NAME	DESCRIPTION	UNITS
	4	TWH1	Temperature of the head in System 1 *	[°R]
		TWS	Temperature of the sleeve *	[°R]
		TWP	Temperature of the piston *	[°R]
		TWIV	Temperature of the inlet valve *	[°R]

N1	N2	VARIABLE NAME	DESCRIPTION	UNITS
5	4	TWEV	Temperature of the exhaust valve *	[°R]
		TWIP	Temperature of the wall in the intake port *	[°R]
		TWEP	Temperature of the wall in the exhaust port *	[°R]
	5	TWH2	Temperature of the head in System 2 for pre chamber engine	[°R]
		TCHØ	Temperature of the cooling water around the head NO	[°R]
		TCSØ	Temperature of the cooling water around the sleeve NO	[°R]
		TØIL	Temperature of the oil for piston heat transfer NO	[°R]
		TFUEL	Temperature of the fuel NO	[°R]
		TADB	Adiabatic flame temperature of the fuel used in S.I. engine	[°R]
	6	PAMB	Ambient pressure NO	[psia]
		TAMB	Ambient temperature	[°R]
		PIM	Pressure in the intake manifold for S.I. engine	[psia]
		TIM	Temperature in the intake manifold for S.I. engine	[°R]
6	1	DCAL	1° crankangle increment	[-]
		DCAM	.1° crankangle	[-]
		DCAN	.01° crankangle increment (not used currently)	[-]
		FAS	Stoichiometric fuel air ratio	[-]
		HVF	Lower calorific value of fuel	[Btu/lb_m]
		RV	Gas constant for the fuel	[Btu/lb_m/°R]
7	1	NWEIBE	1 - for Weibe combustion model 2 - for Heat Release tabulated data	[-]
		CAHRS	Crankangle at which heat release starts	[°CA]
		CAHRE	Crankangle at which heat release ends	[°CA]

The following three array names are for the tabulated heat release input.

	2	CAF	? Array for crankangle (less than 200 elements)	[-]
		DWFF1	Array for fuel injection rate in System 1	[lb_m/°CA]
		DWFF2	Array for fuel injection rate in System 2 for pre chamber engine	[lb_m/°CA]

N1 N2

The following ten variables are used in the Weibe heat release function.

VARIABLE NAME	DESCRIPTION	UNITS
7 3 CAW1	Crankangle at which heat release ends	[°CA]
CAPHR1	Shape modulation factor (exponent) for System 1	[-]
WFCY1	Average fuel injection rate for System 1	[lb_m/°~~CA~~] CYCLE
WEIBE1	Shape modulation factor (multiplier) for System 1	[-]
YWF11	Total fuel injection rate per min. from experimental data for System 1	[lb_m/min]
4 CAW2	Same as above except for System 2 in case of pre chamber engine	[°CA]
CAPHR2		[°CA]
WFCY2		[lb_m/°CA]
WEIBE2		[-]
YWF21		[lb_m/min]

The following are multipliers of heat transfer coefficient used to adjust the calculated heat transfer coefficients.

VARIABLE NAME	DESCRIPTION	UNITS
8 1 CØHCH1	Convective heat transfer coefficient for the head and System 1 gases	[-]
CØHCP1	Convective heat transfer coefficient for the piston and System 1 gases	[-]
CØHCS	Convective heat transfer coefficient for the sleeve and System 1 gases	[-]
CHCIVF	Convective heat transfer coefficient for the inlet valve face and System 1 gases	[-]

```
@FOR,  I  SZ ENGINE.MS,.MR,.MS
C
C             MAIN PROGRAM
C             MATHEMATICAL SIMULATION OF THREE DIFFERENT TYPES OF INTERNAL
C             COMPUSTION ENGINES -
C             1) OPEN CHAMBER ENGINE
C             2)  PRE CHAMBER ENGINE
C             3) SPARK IGNITION ENGINE
C             ALL ENGINES ARE SINGLE CYLINDER AND FOUR STROKE TYPE.
              COMMON/DEBUG / NENG, NOUT1, NVLDBG, NARDBG, NEGDBG, NAVDBG,
     1                       NHTDBG, NDBFLO, NDBRT, NDBSOL
              COMMON/REV   / NRUN, RPM, DCATS, VEPM, VS, ICYCLE, IDVS,
     1                       ICA1, ICA2, CAS
              COMMON/MAIN1 / IPR1, IPR2, LCYCLE, JCYCLE
              COMMON/MAIN2 / NFL, NFLO1, NFLO2, NFLI1, TEXT, HTEXT
              COMMON/MAIN3 / NCYCLE
              COMMON/CA1   / CA, LERR
              DIMENSION  TEXT(80), HTEXT(15)
              DATA  TEXT / 80*6H        / HTEXT / 15*6H       /
              LOGICAL  LERR
              LOGICAL  LCYCLE
              LERR = .FALSE.
              NCYCLE = 0
C
C             READ THE INPUT DATA.
              CALL  INPUT
              CAS = ICA1
              IF( ICA2 .LE. 0 )  ICA2 = ICA1 + 719
              IPR1 = ICA1
              IPR2 = ICA2 + 1
C
C             INITIALIZE THE VARIABLES
              CALL  INTIAL
              CALL  INTLC
              NFLO1 = 6
              NFLO2 = 6
              CALL  OUTPUT
              CALL  OUT7
C
C             VARIABLES FOR FIRST STEP
       500    CA = CAS
              CALL  AREA
              CALL  RATE
              CALL  RATE4
              CALL  HEAT2
              IF ( LERR )  GO TO 2500
              CA = CAS - 1.0
        550   CALL  OUT1
        560   CONTINUE
              DO 1000  I = ICA1, ICA2
              CA = CA + 1.0
              IF ( CA . LE. 720.0 )  GO TO 510
              CA = CA - 720.0
        510   CALL  SOLVE
```

```
               IF ( LERR )  GO TO 2500
  700          CALL  OUT1
  1000         CONTINUE
               IF ( (ICA2-ICA1) .NE. 719 )  GO TO 2800
C
C              CALCULATE MEAN WALL TEMPERATURES.
               CALL  HEAT4
               CALL  HEAT3
C
C              CHECK FOR CYCLE CLOSING
               CALL  CYCLE1
               IF ( LCYCLE )  GO TO 1500
               NCYCLE = NCYCLE + 1
               IF ( NCYCLE .GT. ICYCLE )  GO TO 2000
C
C              CYCLE DOES NOT CLOSE.  START WITH DIFFERENT INITIAL VALUES.
               CALL  INTLC
               NFLO2 = 6
               CALL  OUT4
               GO TO 500
C
C              CYCLE CLOSES
  1500         NFLO2 = 6
               CALL  OUT8
               IF ( NOUT1 .EQ. 2 )  GO TO 1550
  1520         CALL  OUT2
               GO TO 1580
  1550         CALL  OUT9
  1580         CALL  OUT3
               GO TO 3000
C
C              CYCLE DOES NOT CLOSE IN ICYCLE NO. OF ITERATIONS.
  2000         CALL  INTLC
               NFLO2 = 6
               CALL  OUT5
               CALL  OUT4
               IF ( NOUT1 .EQ. 2 )  GO TO 2050
  2020         CALL  OUT2
               GO TO 2080
  2050         CALL  OUT9
  2080         CALL  OUT3
               GO TO 3000
C
C              ERROR
  2500         NFLO2 = 6
               CALL  OUT6
               IPR2  = 1
               IF ( NOUT1 .EQ. 2 )  GO TO 2650
  2600         CALL  OUT2
  2650         CONTINUE
               GO TO 3000
C
C              TABULAR OUTPUT IN CASE OF PART CYCLE CALCULATIONS
  2800         CONTINUE
```

```
            CALL  OUT9
 3000       STOP
            END
```

```
@FOR,  I  SZ ENGINE.S1,.R1,.S1
          SUBROUTINE  INPUT
C         THIS SUBROUTINE READS ALL THE INPUT DATA NEEDED FOR THE
C         SIMULATION PROGRAM
          COMMON/DEBUG / NENG, NOUT1, NVLDBG, NARDBG, NEGDBG, NAVDBG,
     1                   NHTDBG, NDBFLO, NDBRT, NDBSOL
          COMMON/REV   / NRUN, RPM, DCATS, VEPM, VS, ICYCLE, IDVS,
     1                   ICA1, ICA2, CAS
          COMMON/MAIN2 / NFL, NFLO1, NFLO2, NFLI1, TEXT, HTEXT
          COMMON/CON   / FAS, HVF, RA, RV, UAMB, HAMB, FIM, RIM, HIM, GAMIM
          COMMON/COND  / CONDM1, CONDM2, CONDP, CONDS, CONDIP, CONDEP,
     1                   CONDIV, CONDEV
          COMMON/CAD   / DCAL, DCAM, DCAN, DCA, DCA2, CAD, CA1, NIT, LCON
          COMMON/CAVALV/ CAEVOR, CAEVO, CAEVC, CAEVCR, CAIVOR, CAIVO,
     1                   CAIVC, CAIVCR
          COMMON/VALVE / YIVM, YEVM, YCIR, YCER, RALI, RALE, WIVT, WEVT,
     1                   SRSI, SRSE, SVTI, SVTE
          COMMON/GEOMC / BORE, STROKE, CONRD, SCL, VLPCL, VLVCL, VOLP2,
     1                   CONRT, SP, SRT
          COMMON/GEOM  / DMIP, DHEP, AIP, AEP, VIP, VEP, DIV, DEV, AIM,
     1                   APM, AH, AP
          COMMON/GEOMHG/ AH1, AH2, AP1, AP2, AS, AIVF, AEVF, AIVB, AEVB,
     1                   AIVP, AEVP
          COMMON/GEOMHC/ AH1C, AH2C, APC, APSC, ASC, ASBC, AIVC, AEVC,
     1                   AIPC, AEPC
          COMMON/GEOMHP/ XH1, XH2, XPG1, XPIS, XPIC, XSGC, XIP, XEP,
     1                   XIVO, XIVC, XEVO, XEVC
          COMMON/VAR   /  P1,  T1,  F1,  W1,  P2,  T2,  F2,  W2,
     1                   PIP, TIP, FIP, WIP, PEP, TEP, FEP, WEP, DPIP, DPEP
          COMMON/VARS  / WF1, WFA1, WFV1, WFIP, WFAIP, WFVIP
          COMMON/AMS   / PAMB, TAMB, PIM, TIM
          COMMON/ERROR1/  ERP1,  ERT1,  ERF1,  ERW1,  ERP2,  ERT2,  ERF2,
     1                    ERW2, ERPIP, ERTIP, ERFIP, ERWIP, ERPEP, ERTEP,
     2                   ERFEP, ERWEP
          COMMON/ERRORC/  ERP1C,  ERT1C,  ERF1C,  ERP2C,  ERT2C,  ERF2C,
     1                   ERPIPC, ERTIPC, ERFIPC, ERPEPC, ERTEPC, ERFEPC
          COMMON/ERRORT/ ERTWH1, ERTWH2, ERTWP, ERTWS, ERTWIV, ERTWEV,
     1                   ERTWIP, ERTWEP
          COMMON/MISC2 / CBB, COFRIC
          COMMON/HR1   / NWEIBE, NHROT, CAHRS, CAHRE
          COMMON/HR2   / CAF, DWFF1, DWFF2
          COMMON/HR3   / CAW1, CAPHR1, WFCY1, WEIBE1, YWF11,
     1                   CAW2, CAPHR2, WFCY2, WEIBE2, YWF21
          COMMON/SI1   / ERRVCL, TADB
          COMMON/HEAT1 / NHTC1, NHTCAW, NHTR1, NHT2, NHTC2, NHTR2, NHTP
          COMMON/HTCM1 / COHCM1, COHCP1, COHCS, CHCIVF, CHCEVF,
     1                   COHRM1, COHRP1, COHRS, CHRIVF, CHREVF
          COMMON/HTCM2 / COHCM2, COHCP2, COHRM2, COHRP2
          COMMON/HTCMV / CHCIVB, CHCIP, CHCEVB, CHCEP, CHCEIB, CHCEIP,
     1                   CHCEEB, CHCEEP
          COMMON/HTC1  / COVJ, COHCA1, COHCA2, THCNR, TRTHC, PRRA, VOLR,
     1                   PR, TR, CAWSS, CAWSE, CAWCS, CAWCEE
          COMMON/HTC2  / CHCF11, CHCF12, CRA12, CRA13, PTANK, CAINJ,
     1                   EQRT, PRRP
```

```
            COMMON/HTC   / DWCOLH, DACOLS, CWC1, CWC2, CWC3, CWCH1, CWCH2,
     1                     CWCS, CWCP, CWCHIV, CWCHEV, CWCHIP, CWCHEP
            COMMON/TEMP  / TWH1, TWH2, TWP, TWS, TWIV, TWEV, TWIP, TWEP,
     1                     TCHO, TCSO, TOIL, TFUEL
            COMMON/WAVE1 / XLIP, ERRDY1, DELZ
            COMMON/WAVE2 / ITDYN, NX, NPX, NOIDBG
            COMMON/SAVE3 / NOYNIP, LPASS, THAVI
            COMMON/FLOW  / LIV, LEV, AIV, AEV, CODIV, CODEV, CODIM, CODPM
            DIMENSION  TEXT(80), HTEXT(15)
            DIMENSION  A(10)
            DIMENSION  CAF(200), DWFF1(200), DWFF2(200)
            EQUIVALENCE  (NHROT, II)
            II = 0
 100        READ 110, NAME, N1, N2, (A(I), I= 1,7)
 110        FORMAT(A6,2I2,7E10.0)
            GO TO ( 500, 1000, 1500, 2000, 2500, 3000, 3500, 4000, 4500,
     1              5000, 5500, 6000, 6500, 7000 ),  N1
 500        GO TO ( 510, 520, 530, 540, 550, 560, 570, 580, 590, 600 ), N2
 510        CONTINUE
            NRUN   = A(1) + 0.1
            RPM    = A(2)
            BORE   = A(3)
            STROKE = A(4)
            CONRD  = A(5)
            GO TO 100
 520        CONTINUE
            SCL    = A(1)
            VLPCL  = A(2)
            VLVCL  = A(3)
            VOLP2  = A(4)
            APM    = A(5)
            AIM    = A(6)
            GO TO 100
 530        CONTINUE
            AH1    = A(1)
            AP     = A(2)
            AH2    = A(3)
            GO TO 100
 540        CONTINUE
            AH1C   = A(1)
            APC    = A(2)
            ASC    = A(3)
            APSC   = A(4)
            ASBC   = A(5)
            AH2C   = A(6)
            GO TO 100
 550        CONTINUE
            DIV    = A(1)
            DEV    = A(2)
            AIVF   = A(3)
            AEVF   = A(4)
            AIVB   = A(5)
            AEVB   = A(6)
            GO TO 100
```

```
560   CONTINUE
      AIVC   = A(1)
      AEVC   = A(2)
      GO TO 100
570   CONTINUE
      DMIP   = A(1)
      DMEP   = A(2)
      AIP    = A(3)
      AEP    = A(4)
      VIP    = A(5)
      VEP    = A(6)
      GO TO 100
580   CONTINUE
      AIVP   = A(1)
      AEVP   = A(2)
      AIPC   = A(3)
      AEPC   = A(4)
      GO TO 100
590   CONTINUE
      XH1    = A(1)
      XPGI   = A(2)
      XPIS   = A(3)
      XPIC   = A(4)
      XSGC   = A(5)
      XH2    = A(6)
      GO TO 100
600   CONTINUE
      XIP    = A(1)
      XEP    = A(2)
      XIVO   = A(3)
      XIVC   = A(4)
      XEVO   = A(5)
      XEVC   = A(6)
      GO TO 100
1000  GO TO ( 1010, 1020, 1030, 1040 ),  N2
1010  CONTINUE
      CAEVOR = A(1)
      CAEVO  = A(2)
      CAEVC  = A(3)
      CAEVCR = A(4)
      GO TO 100
1020  CONTINUE
      CAIVOR = A(1)
      CAIVO  = A(2)
      CAIVC  = A(3)
      CAIVCR = A(4)
      GO TO 100
1030  CONTINUE
      YIVM   = A(1)
      YEVM   = A(2)
      YCIR   = A(3)
      YCER   = A(4)
      RALI   = A(5)
      RALE   = A(6)
```

```
      GO TO 100
 1040 CONTINUE
      WIVT   = A(1)
      WEVT   = A(2)
      SRSI   = A(3)
      SRSE   = A(4)
      SVTI   = A(5)
      SVTE   = A(6)
      GO TO 100
 1500 GO TO ( 1510, 1520, 1530, 1540, 1550, 1560 ),  N2
 1510 CONTINUE
      ERP1   = A(1)
      ERT1   = A(2)
      ERF1   = A(3)
      ERW1   = A(4)
      ERP1C  = A(5)
      ERT1C  = A(6)
      ERF1C  = A(7)
      GO TO 100
 1520 CONTINUE
      ERP2   = A(1)
      ERT2   = A(2)
      ERF2   = A(3)
      ERW2   = A(4)
      ERP2C  = A(5)
      ERT2C  = A(6)
      ERF2C  = A(7)
      GO TO 100
 1530 CONTINUE
      ERPIP  = A(1)
      ERTIP  = A(2)
      ERFIP  = A(3)
      ERWIP  = A(4)
      ERPIPC = A(5)
      ERTIPC = A(6)
      ERFIPC = A(7)
      GO TO 100
 1540 CONTINUE
      ERPEP  = A(1)
      ERTEP  = A(2)
      ERFEP  = A(3)
      ERWEP  = A(4)
      ERPEPC = A(5)
      ERTEPC = A(6)
      ERFEPC = A(7)
      GO TO 100
 1550 CONTINUE
      ERTWHI = A(1)
      ERTWS  = A(2)
      ERTWP  = A(3)
      ERTWIV = A(4)
      ERTWEV = A(5)
      ERTWIP = A(6)
      ERTWEP = A(7)
```

```
              GO TO 100
 1560         CONTINUE
              ERTWH2 = A(1)
              ERRVOL = A(2)
              GO TO 100
 2000         GO TO ( 2010, 2020, 2030 ),  N2
 2010         CONTINUE
              NENG   = A(1) + 0.1
              NOUT1  = A(2) + 0.1
              NDBSOL = A(3) + 0.1
              NDBRT  = A(4) + 0.1
              NVLDBG = A(5) + 0.1
              NARDBG = A(6) + 0.1
              NEGDBG = A(7) + 0.1
              GO TO 100
 2020         CONTINUE
              NAVDBG = A(1) + 0.1
              NDBFLO = A(2) + 0.1
              NHTDBG = A(3) + 0.1
              ICYCLE = A(4) + 0.1
              IDVS   = A(5) + 0.1
              ICA1   = A(6) + 0.1
              ICA2   = A(7) + 0.1
              GO TO 100
 2030         CONTINUE
              NHTC1  = A(1) + 0.1
              NHTCAW = A(2) + 0.1
              NHTR1  = A(3) + 0.1
              NHT2   = A(4) + 0.1
              NHTC2  = A(5) + 0.1
              NHTR2  = A(6) + 0.1
              NHTP   = A(7) + 0.1
              GO TO 100
 2500         GO TO ( 2510, 2520, 2530, 2540, 2550, 2560 ),  N2
 2510         CONTINUE
              P1     = A(1)
              T1     = A(2)
              F1     = A(3)
              P2     = A(4)
              T2     = A(5)
              F2     = A(6)
              DP1P   = A(7)
              GO TO 100
 2520         CONTINUE
              P1P    = A(1)
              T1P    = A(2)
              F1P    = A(3)
              PEP    = A(4)
              TEP    = A(5)
              FEP    = A(6)
              DPEP   = A(7)
              GO TO 100
 2530         CONTINUE
              WF1    = A(1)
```

```
                WFA1    = A(2)
                WFV1    = A(3)
                WFIP    = A(4)
                WFAIP   = A(5)
                WFVIP   = A(6)
                GO TO 100
      2540      CONTINUE
                TAM1    = A(1)
                TAS     = A(2)
                TAP     = A(3)
                TWIV    = A(4)
                TAEV    = A(5)
                TWIP    = A(6)
                TAEP    = A(7)
                GO TO 100
      2550      CONTINUE
                TWH2    = A(1)
                TCHO    = A(2)
                TCSO    = A(3)
                TOIL    = A(4)
                TFUEL   = A(5)
                TADB    = A(6)
                GO TO 100
      2560      CONTINUE
                PAMB    = A(1)
                TAMB    = A(2)
                PIM     = A(3)
                TIM     = A(4)
                GO TO 100
      3000      GO TO ( 3010 ),  N2
      3010      CONTINUE
                DCAL    = A(1)
                DCAN    = A(2)
                DCAN    = A(3)
                FAS     = A(4)
                HVF     = A(5)
                RV      = A(6)
                GO TO 100
      3500      GO TO ( 3510, 3520, 3530, 3540 ),  N2
      3510      CONTINUE
                NWEIBE = A(1) + 0.1
                CAHRS  = A(2)
                CAHRE  = A(3)
                GO TO 100
      3520      CONTINUE
                II      = II + 1
                CAF(II)    = A(1)
                DWFF1(II) = A(2)
                DWFF2(II) = A(3)
                GO TO 100
      3530      CONTINUE
                CAW1    = A(1)
                CAPHR1 = A(2)
                WFCY1  = A(3)
```

```
            WEIBE1 = A(4)
            YMF11  = A(5)
            GO TO 100
 3540       CONTINUE
            CAM2   = A(1)
            CAPHR2 = A(2)
            WFCY2  = A(3)
            WEIBE2 = A(4)
            YMF21  = A(5)
            GO TO 100
 4000       GO TO ( 4010, 4020, 4030, 4040, 4050, 4060, 4070, 4080, 4090,
     1              4100, 4110, 4120, 4130 ),  N2
 4010       CONTINUE
            COHCH1 = A(1)
            COHCP1 = A(2)
            COHCS  = A(3)
            CHCIVF = A(4)
            CHCEVF = A(5)
            GO TO 100
 4020       CONTINUE
            COHRH1 = A(1)
            COHRP1 = A(2)
            COHRS  = A(3)
            CHRIVF = A(4)
            CHREVF = A(5)
            GO TO 100
 4030       CONTINUE
            COHCH2 = A(1)
            COHCP2 = A(2)
            COHRH2 = A(3)
            COHRP2 = A(4)
            GO TO 100
 4040       CONTINUE
            CHCIVB = A(1)
            CHCIP  = A(2)
            CHCEVB = A(3)
            CHCEP  = A(4)
            GO TO 100
 4050       CONTINUE
            CHCEIP = A(1)
            CHCEEP = A(2)
            CHCEIB = A(3)
            CHCEEB = A(4)
            GO TO 100
 4060       CONTINUE
            COVJ   = A(1)
            COHCA1 = A(2)
            COHCA2 = A(3)
            THCNR  = A(4)
            TRTHC  = A(5)
            PRRA   = A(6)
            PRRP   = A(7)
            GO TO 100
 4070       CONTINUE
```

```
          VOLR   = A(1)
          PR     = A(2)
          TR     = A(3)
          CAWSS  = A(4)
          CANSE  = A(5)
          CAWCS  = A(6)
          CANCEE = A(7)
          GO TO 100
 4080     CONTINUE
          CHCF11 = A(1)
          CHCF12 = A(2)
          CRA12  = A(3)
          CRA13  = A(4)
          PTANK  = A(5)
          CAINJ  = A(6)
          EQRT   = A(7)
          GO TO 100
 4090     CONTINUE
          CONDH1 = A(1)
          CONDP  = A(2)
          CONDS  = A(3)
          CONDH2 = A(4)
          GO TO 100
 4100     CONTINUE
          CONDIP = A(1)
          CONDEP = A(2)
          CONDIV = A(3)
          CONDEV = A(4)
          GO TO 100
 4110     CONTINUE
          COFRIC = A(1)
          CBB    = A(2)
          CWC1   = A(3)
          CWC2   = A(4)
          CWC3   = A(5)
          DWCOLH = A(6)
          DWCOLS = A(7)
          GO TO 100
 4120     CONTINUE
          CWCH1  = A(1)
          CWCS   = A(2)
          CWCP   = A(3)
          CWCH2  = A(4)
          GO TO 100
 4130     CONTINUE
          CWCHIV = A(1)
          CWCHEV = A(2)
          CWCHIP = A(3)
          CWCHEP = A(4)
          GO TO 100
 4500     GO TO ( 4510, 4520 ), N2
 4510     CONTINUE
          NDYNIP = A(1) + 0.1
          ITDYN  = A(2) + 0.1
```

```
              NX     = A(3) + 0.1
              NPX    = A(4) + 0.1
              NDIDBG = A(5) + 0.1
              GO TO 100
 4520         CONTINUE
              XLIP   = A(1)
              ERRDYI = A(2)
              DELZ   = A(3)
              TMAVI  = A(4)
              GO TO 100
 5000         GO TO ( 5010 ),  N2
 5010         CONTINUE
              CODIV  = A(1)
              CODEV  = A(2)
              CODIM  = A(3)
              CODPM  = A(4)
              GO TO 100
 5500         CONTINUE
              GO TO 100
 6000         CONTINUE
              GO TO 100
 6500         CONTINUE
              READ 6550,  (TEXT(I), I=1,80)
 6550         FORMAT(10A6/10A6)
              GO TO 100
 7000         CONTINUE
              RETURN
              END
```

```
@FOR, I  SZ ENGINE.S2,.R2,.S2
          SUBROUTINE  INTIAL
C         THIS SUBROUTINE INITIALIZES THE PARAMETERS.
          COMMON/DEBUG / NENG, NOUT1, NVLDBG, NARDBG, NEGDBG, NAVDBG,
     1                   NHTDBG, NDBFLO, NDBRT, NDBSOL
          COMMON/REV   / NRUN, RPM, DCATS, VEPM, VS, ICYCL, IDVS,
     1                   ICA1, ICA2, CAS
          COMMON/MAIN2 / NFL, NFLO1, NFLO2, NFLI1, TEXT, HTEXT
          COMMON/MAIN3 / NCYCLE
          COMMON/CON   / FAS, HVF, RA, RV, UAMB, HAMB, FIM, RIM, HIM, GAMIM
          COMMON/ENTYPE/ LOCD, LPCD, LSI
          COMMON/CA1   / CA, LERR
          COMMON/PROP  / CP1, RIS, R2
          COMMON/ENGY  / PE, TE, FE, UE, RE, DUPE, DUTE, DUFE, DRPE, DRTE,
     1                   DRFE, FAPC
          COMMON/AVGY  / TAV, UA, DUAT, UV, DUVT, HV, DHVT
          COMMON/VAR   /  P1,  T1,  F1,  W1,  P2,  T2,  F2,  W2,
     1                   PIP, TIP, FIP, WIP, PEP, TEP, FEP, WEP, DPIP, DPEP
          COMMON/VARS  / WF1, WFA1, WFV1, WFIP, WFAIP, WFVIP
          COMMON/VAR1  /  PI1,  TI1,  FI1,  P2I,  T2I,  F2I,
     1                   PIPI, TIPI, FIPI, PEPI, TEPI, FEPI
          COMMON/AMB   / PAMB, TAMB, PIM, TIM
          COMMON/VOLL  / LSIC, VOL, DVOL, VELPT, VOL1, VOL2, DVOL1, DVOL2
          COMMON/GEOMC / BORE, STROKE, CONRD, SCL, VLPCL, VLVCL, VOLP2,
     1                   COMRT, SP, SRT
          COMMON/GEOM  / DMIP, DMEP, AIP, AEP, VIP, VEP, DIV, DEV, AIM,
     1                   APM, AM, AP
          COMMON/GEOMHG/ AH1, AH2, AP1, AP2, AS, AIVF, AEVF, AIVB, AEVB,
     1                   AIVP, AEVP
          COMMON/TEMP. / TWH1, TWH2, TWP, TWS, TWIV, TWEV, TWIP, TWEP,
     1                   TCHO, TCSO, TOIL, TFUEL
          COMMON/TEMPP / TWH13, TWH23, TWP3, TWS3, TWIV3, TWEV3,
     1                   TWH14, TWH24, TWP4, TWS4, TWIV4, TWEV4
          COMMON/TEMPC / TWH1C, TWH2C, TWPC, TWSC, TWIVC, TWEVC, TWIPC,
     1                   TWEPC
          DATA  GC, XJ / 32.174, 778.16 /
          LOGICAL  LOCD, LPCD, LSI, LERR
          LERR  = .FALSE.
          TWH13 = TWH1 * TWH1 * TWH1
          TWS3  = TWS  * TWS  * TWS
          TWP3  = TWP  * TWP  * TWP
          TWIV3 = TWIV * TWIV * TWIV
          TWEV3 = TWEV * TWEV * TWEV
          TWH14 = TWH1 * TWH1 * TWH1* TWH1
          TWS4  = TWS  * TWS  * TWS  * TWS
          TWP4  = TWP  * TWP  * TWP  * TWP
          TWIV4 = TWIV * TWIV * TWIV * TWIV
          TWEV4 = TWEV * TWEV * TWEV * TWEV
C
C         ENGINE TYPE
          GO TO ( 500, 750, 1000 ),  NENG
C
C         OPEN CHAMBER DIESEL ENGINE.
  500     LOCD = .TRUE.
```

```
      LPCD = .FALSE.
      LSI  = .FALSE.
      ASSIGN 3100 TO MP1
      ASSIGN 3200 TO MP2
      ASSIGN 2000 TO MS1
C
C     INITIALIZE OUTPUT VARIABLES
      P2I   = 0.0
      T2I   = 0.0
      F2I   = 0.0
      TWH2C = 0.0
      GO TO 1500
C
C     PRE CHAMBER DIESEL ENGINE
  750 LPCD = .TRUE.
      LOCD = .FALSE.
      LSI  = .FALSE.
      FAPC = F2
      TWH23 = TWH2 * TWH2 * TWH2
      TWH24 = TWH2 * TWH2 * TWH2 * TWH2
      ASSIGN 3050 TO MP1
      ASSIGN 3150 TO MP2
      ASSIGN 2000 TO MS1
      GO TO 1500
C
C     SPARK IGNITION ENGINE
 1000 LSI  = .TRUE.
      LOCD = .FALSE.
      LPCD = .FALSE.
C
C     SET THE EQUIVALENCE RATIOS
      F2   = F1
      F1P  = F1
      F1M  = F1
      TWH2 = TWH1
      VOL2 = 0.0
      ASSIGN 3100 TO MP1
      ASSIGN 3200 TO MP2
      ASSIGN 1950 TO MS1
C
C     INITIALIZE OUTPUT VARIABLES
      P2I   = 0.0
      T2I   = 0.0
      F2I   = 0.0
C
C     INITIALIZE THE VARIOUS SUBROUTINES
 1500 CALL  IVLUME
      CALL  IAREA
      CALL  IDIFF
      CALL  IENRGY
      CALL  IAVRGY
      CALL  IHEAT
      CALL  IFLWCO
      CALL  ICOMB
```

```
      CALL  COMBSI
      CALL  ICYCLE
      CALL  IDYNIP
C
C     CALCULATE THE PROPERTIES OF AMBIENT AIR
      PE = PAMB
      TE = TAMB
      FE = 0.0
      CALL  ENERGY
      RA = RE
      UAMB = UE
      HAMB = UAMB + RA * TAMB
      CALL  IRATE
C
C     CALCULATE VOLUME AT STARTING CRANK ANGLE
      CA = CAS
      CALL  VOLUME
C
C     CALCULATE INITIAL MASSES FOR VARIOUS SYSTEMS
C     SYSTEM 1
      PE = PI
      TE = TI
      FE = FI
      CALL  ENERGY
      RI = RE
      GO TO ( 1650, 1650, 1610 ), NENG
C
C     SPARK IGNITION ENGINE
 1610 RI = WFI*RE + WFAI*RA + WFVI*RV
 1650 WI = PI * VOL / (12.0*XJ*RI*TI)
C
C     INTAKE PORT SYSTEM
      PE = PIP
      TE = TIP
      FE = FIP
      CALL  ENERGY
      RIP = RE
      GO TO ( 1710, 1710, 1680 ),  NENG
C
C     SPARK IGNITION ENGINE
 1680 RIP = WFIP*RE + WFAIP*RA + WFVIP*RV
 1710 WIP = PIP * VIP / (12.0*XJ*RIP*TIP)
C
C     EXHAUST PORT SYSTEM
      PE = PEP
      TE = TEP
      FE = FEP
      CALL  ENERGY
      REP = RE
      WEP = PEP * VEP / (12.0*XJ*REP*TEP)
      GO TO ( 1800, 1750, 1800 ),  NENG
C
C     SYSTEM 2 FOR PRE CHAMBER DIESEL ENGINE
 1750 PE = P2
```

```
                TE = T2
                FE = F2
                CALL  ENERGY
                R2 = RE
                W2 = P2 * VOLP2 / (12.0*XJ*R2*T2)
       1800     CONTINUE
                GO TO MS1
C
C               SPARK IGNITION ENGINE
C               CALCULATE THE PROPERTIES OF MANIFOLD MIXTURE
       1950     F      = FIM * FAS
                WFAIM = 1.0 / (1.0+F)
                WFVIM = 1.0 - WFAIM
                TAV    = TIM
                CALL  AVERGY
                HAIM   = UA + RA*TIM
                HIM    = WFAIM*HAIM + WFVIM*HV
                GAMAIM = 1.0 + RA/DUAT
                GAMVIM = 1.0 + RV/DUVT
                B1     = WFAIM*DUAT*GAMAIM + WFVIM*DUVT*GAMVIM
                B2     = WFAIM*DUAT + WFVIM*DUVT
                GAMIM  = B1 / B2
                RIM    = WFAIM*RA + WFVIM*RV
       2000     RETURN



                ENTRY  INTLC
C               INITIALIZES THE CYCLIC VARIABLES IN CASE CYCLE DOES NOT CLOSE.
C               SYSTEM VARIABLES
C               SYSTEM 1
                P11  = P1
                T11  = T1
                F11  = F1
C
C               INLET PORT SYSTEM
                PIP1 = PIP
                TIP1 = TIP
                FIP1 = FIP
C
C               EXHAUST PORT SYSTEM.
                PEP1 = PEP
                TEP1 = TEP
                FEP1 = FEP
                GO TO MP1
C
C               SYSTEM 2 FOR PRE CHAMBER DIESEL ENGINE.
       3050     P21  = P2
                T21  = T2
                F21  = F2
C
C               WALL TEMPERATURES
       3100     TWHIC = TWHI
                TWSC  = TWS
```

```
      TWPC  = TWP
      TWIVC = TWIV
      TWEVC = TWEV
      TWIPC = TWIP
      TWEPC = TWEP
      IF ( NENG .EQ. 3 )  TWH2C = TWHIC
      GO TO HP2
C
C     SYSTEM 2 FOR PRE CHAMBER DIESEL ENGINE.
 3150 TWH2C = TWH2
C
C     CALL SUBROUTINES TO BE INITIALIZED DURING EACH CYCLE
 3200 IF ( NCYCLE .GT. ICYCL )  GO TO 3400
      CALL  IAREAC
      CALL  IRATEC
      CALL  IHEATC
      CALL  ICOMRC
      CALL  IDYNIP
 3400 RETURN



      ENTRY  INTLOI
C     CYCLIC OUTPUT
      WRITE(NFL,9310)
 9310 FORMAT(18H SYSTEM PROPERTIES//30X,11X,8HPRESSURE,11X,10X,
     1       11HTEMPERATURE,9X,11X,9HEQ. RATIO/ 30X,14X,3HPSI,13X,
     2       14X,1HR)
      WRITE(NFL,9320)  PI1,  TI1,  FI1,  P2I,  T2I,  F2I,
     1                 PIPI, TIPI, FIPI, PEPI, TEPI, FEPI
 9320 FORMAT(20X,10HSYSTEM 1 =,        2(11X,F8.2,11X), 10X,F10.6 /
     1       20X,10HSYSTEM 2 =,        2(11X,F8.2,11X), 10X,F10.6 /
     2       17X,13HINTAKE PORT =,     2(11X,F8.2,11X), 10X,F10.6 /
     3       16X,14HEXHAUST PORT =,   2(11X,F8.2,11X), 10X,F10.6 )
      WRITE(NFL,9340)  TWHIC, TWSC, TWPC, TWH2C, TWIVC, TWEVC,
     1                 TWIPC, TWEPC
 9340 FORMAT(///18H WALL TEMPERATURES//6X,9HHEAD(1) =,F8.1,2H R,
     1       5X,7X,8HSLEEVE =,F8.1,2H R,5X,7X,8HPISTON =,F8.1,2H R,
     2       5X,6X,9HHEAD(2) =,F8.1,2H R/  8X,7HI. V. =,F8.1,2H R,5X,
     3       8X,7HE. V. =,F8.1,2H R,5X,8X,7HI. P. =,F8.1,2H R,5X,
     4       8X,7HE. P. =,F8.1,2H R)
      IF ( .NOT. LSI )  GO TO 9400
C
C     SPARK IGNITION ENGINE
      WRITE(NFL,9360)
 9360 FORMAT(///32H MASS FRACTIONS FOR S. I. ENGINE// 30X,13X,3HAIR,
     1       14X,10X,11HFUEL VAPOUR,9X,11X,8HPRODUCTS)
      WRITE(NFL,9380) WFA1, WFV1, WF1, WFAIP, WFVIP, WFIP
 9380 FORMAT(20X,10HSYSTEM 1 =,     3(10X,E11.5,9X) /
     1       17X,13HINTAKE PORT =,  3(10X,E11.5,9X) )
 9400 CONTINUE
      RETURN
      END
```

```
@FOR, I  SZ ENGINE.S3,.R3,.S3
              SUBROUTINE  SOLVE
              COMMON/CA1    / CA, LERR
              COMMON/CAD    / DCAL, DCAM, DCAN, DCA, DCA2, CADO, CA11, NIT, LCON
              COMMON/ENTYPE/ LOCD, LPCD, LSI
              COMMON/CAHP   / ICAHRS, ICAHRE, ICAHRT
              COMMON/VOLL   / LSIC, VOL, DVOL, VELPT, VOL1, VOL2, DVOL1, DVOL2
              COMMON/COMBSL/ LCONS2
              LOGICAL  LCONS2
              LOGICAL  LSI, LSIC
              LOGICAL  LCON, LERR
              LCONS2 = .TRUE.
              CAX = CA
              CADO = CA
              DCA = DCAL
              NIT = 0
              CALL  DIFF
              IF ( LCON )  GO TO 1300
C
C             DECREASE THE CRANK ANGLE INCREMENTAL TO 0.1 DEGREES.
              DCA = DCAM
              CA = CAX
              CALL  VOLUME
              CALL  AREA
              IF ( .NOT. LSI )  GO TO 800
C
C             SPARK IGNITION ENGINE
              ICA = CA + 0.1
              IF ( ICA .EQ. (ICAHRS-1))  GO TO 500
              IF ( ICA .EQ. ICAHRE )  GO TO 450
              IF ( LCONS2 )  GO TO 800
              LCONS2 = .TRUE.
C
C             HEAT RELEASE END
  450         CONTINUE
              LSIC = .TRUE.
              GO TO 750
C
C             HEAT RELEASE START
  500         LSIC = .FALSE.
  750         CALL  DIFF2
  800         CONTINUE
              CALL  RATE20
              DO 1200  I = 1,10
  950         CALL  DIFF
              IF ( LCON )  GO TO 1100
C
C             NO CONVERGENCE
              LERR = .TRUE.
              PRINT 1000
 1000         FORMAT(//23H ERROR   NO CONVERGENCE)
              GO TO 1500
 1100         CADO = CA11
              CALL  SUM
```

```
1200  CONTINUE
      GO TO 1500
1300  CALL  SUM
1500  CA = CAX
      RETURN
      END
```

```
@FOR,  I  SZ ENGINE.S4,.R4,.S4
          SUBROUTINE  IDIFF
          COMMON/DEBUG / NENG, NOUT1, NVLDBG, NARDBG, NEGDBG, NAVDBG,
        1                NMTDBG, NDBFLO, NDBRT, NDBSOL
          COMMON/CAD   / DCAL, DCAM, DCAN, DCA, DCA2, CADO, CAI1, NIT, LCON
          COMMON/CA1   / CAR, LERR
          COMMON/CONVS / LCONS
          COMMON/GEOM  / DMIP, DHEP, AIP, AEP, VIP, VEP, DIV, DEV, AIM,
        1                APM, AM, AP
          COMMON/ERROR1/  ERP1,  ERT1,  ERF1,  ERA1,  ERP2,  ERT2,  ERF2,
        1                 ERA2, ERPIP, ERTIP, ERFIP, ERWIP, ERPEP, ERTEP,
        2                ERFEP, ERWEP
          COMMON/VAR   /  P1,  T1,  F1,  W1,  P2,  T2,  F2,  W2,
        1                PIP, TIP, FIP, WIP, PEP, TEP, FEP, WEP, DPIP, DPEP
          COMMON/PROP  / CP1, RIS, R2
          COMMON/PROPIP/ RIPS
          COMMON/COMBSJ/ NJCOMB
          COMMON/VOLL  / LSIC, VOL, DVOL, VELPT, VOL1, VOL2, DVOL1, DVOL2
          COMMON/VARRAY/ NP, ARRAY, DARRAY, ARRAY1
          COMMON/AMB   / PAMB, TAMB, PIM, TIM
          COMMON/WAVE3 / NDYNIP, LPASS, THAV1
          DATA  GC, XJ / 32.174, 778.16 /
          LOGICAL  LCON, LERR, LSIC
          LOGICAL  LPASS
          LOGICAL  LCONS
          DIMENSION  ARRAY(2,4,4), DARRAY(2,4,4), ARRAY1(4,4), EARRAY(4,4)
          DIMENSION  EARRAW(4)
          XJ1 = 12.0 * XJ
          NJCOMB = 3
          EARRAY(1,1) = ERP1
          EARRAY(1,2) = ERT1
          EARRAY(1,3) = ERF1
          EARRAY(1,4) = ERA1
          EARRAY(2,1) = ERPIP
          EARRAY(2,2) = ERTIP
          EARRAY(2,3) = ERFIP
          EARRAY(2,4) = ERAIP
          EARRAY(3,2) = ERTEP
          EARRAY(3,3) = ERFEP
          EARRAY(3,4) = ERWEP
          EARRAW(1) = ERW1
          EARRAW(2) = ERWIP
          EARRAW(3) = ERWEP
C
C         GENERATE THE SWITCH VARIABLE FOR DEBUG
          GO TO ( 70, 80 ),  NDBSOL
  70      ASSIGN 3600 TO NDBSOL
          GO TO 90
  80      ASSIGN 3900 TO NDBSOL
  90      GO TO ( 100, 200, 300 ),  NENG
C
C         OPEN CHAMBER DIESEL ENGINE
 100      II = 3
          ASSIGN 2240 TO NS1
```

```
              ASSIGN 2300 TO MP1
              ASSIGN 2500 TO MP2
              ASSIGN 2700 TO MP3
              GO TO 400
C
C             PRE CHAMBER DIESEL ENGINE
  200         II = 4
              ASSIGN 2240 TO MS1
              ASSIGN 2250 TO MP1
              ASSIGN 2450 TO MP2
              ASSIGN 2650 TO MP3
              EARRAY(4,1) = ERP2
              EARRAY(4,2) = ERT2
              EARRAY(4,3) = ERF2
              EARRAY(4,4) = ERW2
              EARRAW(4) = ERW2
              GO TO 400
C
C             SPARK IGNITION ENGINE
  300         II = 3
              ASSIGN 2210 TO MS1
              ASSIGN 2270 TO MP1
              ASSIGN 2470 TO MP2
              ASSIGN 2700 TO MP3
              EARRAY(4,2) = ERT2
              EARRAY(4,4) = ERW2
  400         RETURN



              ENTRY  DIFF
C             SOLVE THE DIFFERENTIAL EQUATION BY PREDICTOR CORRECTOR METHOD.
              NP = 1
              CALL  RATE2
              CA11 = CA00 + DCA
              DCA2 = DCA / 2.0
              CAR = CA11
              CALL  VOLUME
              CALL  AREA
              LPASS = .TRUE.
              VOLX  = VOL
              DVOLX = DVOL
C
C             CALCULATE THE VALUES AT POINT 1 WITH SLOPES AT POINT 0 .
              DO 2200  I = 1,II
              DO 2200  J = 2,4
  2200        ARRAY1(I,J) = ARRAY(1,I,J) + DARRAY(1,I,J)*DCA
              GO TO MS1
C
C             SPARK IGNITION ENGINE
  2210        IF ( ARRAY1(1,3) .GT. 0.0 .AND. ARRAY1(1,4) .GT. 0.0) GO TO 2240
              ARRAY1(1,2) = ARRAY(1,1,2)
              ARRAY1(1,3) = ARRAY(1,1,3)
              ARRAY1(1,4) = ARRAY(1,1,4)
```

```
2240  CONTINUE
C
C     CALCULATE PRESSURE OF PORT SYSTEM FROM KNOWN DERIVATIVE
      ARRAY1(2,1) = ARRAY1(1,2,1) + DARRAY(1,2,1)*DCA
      ARRAY1(3,1) = ARRAY1(1,3,1) + DARRAY(1,3,1)*DCA
C
C     CALCULATE PRESSURE FROM  PV=MRT
C     SYSTEM 1
      ARRAY1(1,1) = ARRAY1(1,2) * ARRAY1(1,4) * R1S * XJ1 / VOL1
      GO TO MP1
C
C     SYSTEM 2 FOR PRE CHAMBER DIESEL ENGINE
2250  ARRAY1(4,1) = ARRAY1(4,2) * ARRAY1(4,4) * R2 * XJ1 / VOL2
      GO TO 2300
C
C     INTAKE PORT FOR S. I. ENGINE
2270  ARRAY1(2,1) = ARRAY1(2,2) * ARRAY1(2,4) * RIPS * XJ1 / VIP
2300  NP = 2
      DO 3000  I = 1,10
      CALL  RATE21
      CALL  RATE3
      CALL  RATE
      CALL  RATE2
      GO TO ( 2330, 2340, 2350 ),  NJCOMB
C
C     SPARK IGNITION ENGINE
C     COMBUSTION
2330  II = 4
      EARRAY(1,3)   = ERF1
      EARRAY(4,3)   = ERF2
      ARRAY(1,4,2) = T2
      ARRAY(1,4,3) = VOL2
      ARRAY(1,4,4) = W2
      ARRAY(1,1,3) = VOLX
      DARRAY(1,1,3) = DVOLX
      DARRAY(1,4,2) = 0.0
      DARRAY(1,4,3) = 0.0
      DARRAY(1,4,4) = 0.0
      NJCOMB = 3
      GO TO 2350
C
C     NO COMBUSTION
2340  II = 3
      EARRAY(1,3)   = 10.0
      ARRAY(1,1,2) = T1
      ARRAY(1,1,3) = F1
      ARRAY(1,1,4) = W1
      DARRAY(1,1,2) = 0.0
      DARRAY(1,1,3) = 0.0
      DARRAY(1,1,4) = 0.0
      NJCOMB = 3
2350  CONTINUE
C
C     CALCULATE THE MODIFIED EULER POINTS.
```

```
      DO 2400  J = 1,I1
      DO 2400  K = 2,4
 2400 ARRAY1(J,K) = ARRAY(1,J,K) + (DARRAY(1,J,K)+DARRAY(2,J,K))*DCA2
C
C     CALCULATE PRESSURE FROM  PV=MRT
C     SYSTEM 1
      ARRAY1(1,1) = ARRAY1(1,2) * ARRAY1(1,4) * R1S * XJ1 / VOL1
      GO TO MP2
C
C     SYSTEM 2 FOR PRE CHAMBER DIESEL ENGINE.
 2450 ARRAY1(4,1) = ARRAY1(4,2) * ARRAY1(4,4) * R2  * XJ1 / VOL2
      GO TO 2500
C
C     INTAKE PORT FOR S. I. ENGINE
 2470 ARRAY1(2,1) = ARRAY1(2,2) * ARRAY1(2,4) * RIPS * XJ1 / VIP
C
C     CONVERGENCE TEST
 2500 CONTINUE
      DO 2600  J = 1,I1
      EARRAY(J,4) = EARRAY(J) * ARRAY1(J,4)
      DO 2600  K = 2,4
      IF ( ABS(ARRAY1(J,K)-ARRAY(2,J,K)) .GT. EARRAY(J,K) )  GO TO 3000
 2600 CONTINUE
C
C     TEST FOR PRESSURE
C     SYSTEM 1
      EARRAY(1,1) = ERP1 + 0.01*ABS(ARRAY1(1,1)-PAMB)
      IF ( ABS(ARRAY1(1,1)-ARRAY(2,1,1)) .GT. EARRAY(1,1) )  GO TO 3000
      GO TO MP3
C
C     SYSTEM 2 FOR PRE CHAMBER DIESEL ENGINE.
 2650 CONTINUE
      EARRAY(4,1) = ERP2 + 0.01*ABS(ARRAY1(4,1)-PAMB)
      IF ( ABS(ARRAY1(4,1)-ARRAY(2,4,1)) .GT. EARRAY(4,1) )  GO TO 3000
C
C     CONVERGENCE TEST PASSED
 2700 LCON = .TRUE.
      LCONS = .TRUE.
      LPASS = .FALSE.
      GO TO 3500
 3000 CONTINUE
C
C     CONVERGENCE TEST FAILED.
      LCON = .FALSE.
      LCONS = .FALSE.
      GO TO 3900
 3500 CALL  RATE21
      CALL  RATE3
      NIT = NIT + 1
      GO TO MDBSOL
 3600 PRINT 3700,  NIT
 3700 FORMAT(/6H SOLVE,9X,36HNO. OF ITERATIONS FOR CONVERGENCE = ,I9)
 3900 RETURN
```

```
      ENTRY  DIFF1
C     GENERATE THE SWITCH VARIABLES FOR SPARK IGNITION ENGINE.
      IF ( LSIC )  GO TO 4100
C
C     NO COMBUSTION
      II = 3
      EARRAY(1,3) = 10.0
      GO TO 4200
C
C     COMBUSTION
 4100 II = 4
      EARRAY(1,3) = ERF1
      EARRAY(4,3) = ERF2
 4200 RETURN



      ENTRY  DIFF2
C     SPARK IGNITION ENGINE
      IF ( LSIC )  GO TO 5100
C
C     NO COMBUSTION
      II = 3
      EARRAY(1,3) = 10.0
      ARRAY(1,1,3) = F1
      DARRAY(1,1,3) = 0.0
      NJCOMB = 3
      GO TO 5150
C
C     COMBUSTION
 5100 II = 4
      EARRAY(1,3) = ERF1
      EARRAY(4,3) = ERF2
       ARRAY(1,1,3) =  VOL =  ARRAY(1,4,3)
      DARRAY(1,1,3) = DVOL = DARRAY(1,4,3)
      NJCOMB = 3
 5150 CALL  COMBSI
      RETURN



      ENTRY  SUM
C     CALCULATES THE SUMS AT THE END OF SUCCESSFUL CONVERGENCE
      CALL  RATE3
      CALL  HEAT1
C
C     STORE THE SUM
      CALL  RATE4
      CALL  HEAT2
      RETURN
      END
```

```
@FOR,  1  SZ ENGINE,S5,,R5,,S5
              SUBROUTINE  IRATE
      C       THIS PART OF THE SUBPROGRAM INITIALIZES VARIABLES FOR THE
      C       RATE SUBROUTINE.
              PARAMETER  NAR1=10,  NAR2=300
              COMMON/DEBUG / NENG, NOUT1, NVLDBG, NARDBG, NEGDBG, NAVDBG,
         1                   NHTDBG, NDRFLO, NDBRT, NDBSOL
              COMMON/REV   / NRUN, RPM, DCATS, VEPM, VS, ICYCLE, IDVS,
         1                   ICA1, ICA2, CAS
              COMMON/CON   / FAS, HVF, RA, RV, UAMB, HAMB, FIM, RIM, HIM, GAMIM
              COMMON/MAIN1 / IPR1, IPR2, LCYCLE, JCYCLE
              COMMON/MAIN2 / NFL, NFLO1, NFLO2, NFL11, TEXT, HTEXT
              COMMON/ENTYPE/ LOCO, LPCD, LSI
              COMMON/CA1   / CA, LERR
              COMMON/CAD   / DCAL, DCAM, DCAN, DCA, DCA2, CAD, CA1, NIT, LCON
              COMMON/CAHR  / ICAHRS, ICAHRE, ICAHRT
              COMMON/CONVS / LCONS
              COMMON/GEOMC / BORE, STROKE, CONRD, SCL, VLPCL, VLVCL, VOLP2,
         1                   COMRT, SP, SRT
              COMMON/GEOM  / DMIP, DMEP, AIP, AEP, VIP, VEP, DIV, DEV, AIM,
         1                   APM, AM, AP
              COMMON/PROP  / CPIS, RIS, R2
              COMMON/PROP2 /  UIS, HIS
              COMMON/PROPIP/ RIPS
              COMMON/ENGY  / PE, TE, FE, UE, RE, DUPE, DUTE, DUFE, DRPE, DRTE,
         1                   DRFE, FAPC
              COMMON/AVGY  / TAV, UA, DUAT, UV, DUVT, HV, DHVT
              COMMON/FLOW  / LIV, LEV, AIV, AEV, CODIV, CODEV, CODIM, CODPM
              COMMON/MASSI / PP1, TT1, FF1, RR1, GAMM1, HH1,
         1                   PP2, TT2, FF2, RR2, GAMM2, HH2, AREA
              COMMON/MASSO / I1, DW, HUS, FUS
              COMMON/MISC1 / DWIV, DWEV, DQ1, DQ2, DQIP, DQEP, YQ1, YQ2, YQIP,
         1                   YQEP, YQF, YWFF1, YWFF2, YTHAV1, YTAV1, YTHAVE,
         2                   YTAVE, DTCH, DTCS, DTC, DTAF, PMAX1, PMAX2,
         3                   TMAX1, TMAX2
              COMMON/MISC3 / SUMWS, WCX, WFIX, WFAIX, WFVIX
              COMMON/VOLL  / LSIC, VOL, DVOL, VELPT, VOL1, VOL2, DVOL1, DVOL2
              COMMON/FUELB / DWFI1, DWFI2, ID, DWD, DWA, DWB, DWC, ISC
              COMMON/COMBSI/ NICOMB
              COMMON/WAVE3 / NDYNIP, LPASS, THAVI
              COMMON/CAVALV/ CAEVOR, CAEVO, CAEVC, CAEVCR, CAIVOR, CAIVO,
         1                   CAIVC, CAIVCR
              COMMON/VAR   /  P1,  T1,  F1,  W1,  P2,  T2,  F2,  W2,
         1                   PIP, TIP, FIP, WIP, PEP, TEP, FEP, WEP, DPIP, DPEP
              COMMON/VARS  / WF1, WFA1, WFV1, WFIP, WFAIP, WFVIP
              COMMON/AMB   / PAMB, TAMB, PIM, TIM
              COMMON/MISC2 / CBB, COFRIC
              COMMON/VARRAY/ NP, ARRAY, DARRAY, ARRAY1
              COMMON/TEMP  / TWH1, TWH2, TWP, TWS, TWIV, TWEV, TWIP, TWEP,
         1                   TCHO, TCSO, TOIL, TFUEL
              COMMON/OUTAR1/ IPR, LOUT
              COMMON/OUTAR2/ ZOUT
              DATA  GC, XJ / 32.174, 778.16 /
              DATA NPR1, NPR2 / 20, 5/
```

```
      LOGICAL  LIV, LEV, LOCD, LPCD, LSI, LSIC
      LOGICAL  LCONS
      REAL  NIHP, IHP, NIMEP, IMEP, ISFC
      DIMENSION  ARRAY(2,4,4), DARRAY(2,4,4), ARRAY1(4,4)
      DIMENSION  LOUT(1,72)
      DIMENSION  ZOUT(NAR1,NAR2)
      DIMENSION  ARRAYF(2,2,3)
C
C     SET THE CONSTANTS.
      GCDXJ = GC / XJ
      XJ1    = XJ * 12.0
      CWFAV  = FI * FAS
      CWFAV1 = 1.0 + CWFAV
      CWFAVR = RA + CWFAV*RV
      CONS1  = 30.0 * RPM
      HF     = HVF - 19163.0 + 0.5*(TFUEL-537.0)
      CBR1   = CAR*5260.0*BORE*BORE*BORE*PAMB/(DCATS*0.491)
      NICOMB = 3
C
C     STORE PRESSURE DERIVATIVE OF VALVE SYSTEM IN ARRAY
      DARRAY(1,3,1) = DPEP
      DARRAY(2,3,1) = DPEP
C
C     GENERATE SWITCH VARIABLE FOR CA OUTPUT
      GO TO ( 10, 20 ),  NOUT1
   10 ASSIGN 5050 TO MOUT1
      GO TO 30
   20 ASSIGN 5110 TO MOUT1
   30 CONTINUE
C
C     GENERATE SWITCH VARIABLE FOR DYNIP SUBROUTINE
      GO TO ( 40, 50 ),  NDYNIP
   40 ASSIGN 1830 TO MDYNIP
      GO TO 60
   50 ASSIGN 1840 TO MDYNIP
   60 CONTINUE
C
C     GENERATE THE SWITCH VARIABLE FOR DEBUG
      GO TO ( 70, 80 ),  NDBRT
   70 ASSIGN 8000 TO MDBRT
      GO TO 90
   80 ASSIGN 9000 TO MDBRT
   90 GO TO ( 100, 100, 300 ),  NENG
C
C     DIESEL ENGINE
C     SYSTEM 1
C     GENERATE THE SWITCH VARIABLES.
  100 ASSIGN  820 TO MS1
      ASSIGN  840 TO MS2
      ASSIGN 1260 TO MS3
      ASSIGN 1900 TO MS5
      ASSIGN 2020 TO MS6
      ASSIGN 2500 TO MS7
      ASSIGN 2590 TO MS8
```

```
      ASSIGN 4510 TO MS12
      ASSIGN 4610 TO MS13
      ASSIGN 6000 TO MSCA1
      ASSIGN 5610 TO MCA1
      ASSIGN 9110 TO MSOT1
      ASSIGN 9140 TO MSOT2
      ASSIGN 1800 TO MSP1
      ASSIGN 3500 TO MSP2
      ASSIGN 4300 TO MSP3
      ASSIGN 4440 TO MSP21
      ASSIGN 9500 TO MSPO41
      ASSIGN 4600 TO MP1
      ASSIGN 4700 TO MF2
C
C     SET THE CONSTANT VARIABLES.
      DAI2  = 0.0
      DEFI2 = 0.0
      FI2   = 0.0
      DWFI  = 0.0
      DWFAI = 0.0
      DWFVI = 0.0
      WFI   = 1.0
      WFAI  = 0.0
      WFVI  = 0.0
      WFIP  = 1.0
      WFAIP = 0.0
      WFVIP = 0.0
      UAI   = 0.0
      UVI   = 0.0
      DUATI = 0.0
      DUVTI = 0.0
      YWAI2 = 0.0
      YWFI2 = 0.0
      YWI2  = 0.0
      YEFI2 = 0.0
      YWFF2 = 0.0
      YEFF2 = 0.0
      DWFI2 = 0.0
      DVOL2 = 0.0
C
C     INITIALIZE OUTPUT VARIABLES
      DT2   = 0.0
      DF2   = 0.0
      DW2   = 0.0
      IF ( LOCO )  GO TO 400
C
C     PRE CHAMBER ENGINE.
C     GENERATE THE SWITCH VARIABLES.
      ASSIGN 1240 TO MS4
      ASSIGN 4430 TO MS21
      ASSIGN 6000 TO MSCA1
      ASSIGN 5710 TO MCA1
      ASSIGN 1270 TO MSP1
      ASSIGN 3100 TO MSP2
```

```
      ASSIGN 4150 TO MSP3
      ASSIGN 4410 TO MSP21
      ASSIGN 9470 TO MSP041
      ASSIGN 4550 TO MP1
      ASSIGN 4650 TO MP2
      GO TO 400
C
C     SPARK IGNITION ENGINE.
C     GENERATE THE SWITCH VARIABLES.
 300  ASSIGN  810 TO MS1
      ASSIGN  830 TO MS2
      ASSIGN 1220 TO MS3
      ASSIGN 1800 TO MS4
      ASSIGN 1930 TO MS6
      ASSIGN 2520 TO MS7
      ASSIGN 2580 TO MS8
      ASSIGN 4570 TO MS12
      ASSIGN 4670 TO MS13
      ASSIGN 4450 TO MS21
      ASSIGN 5080 TO MSCA1
      ASSIGN 5810 TO MCA1
      ASSIGN 9120 TO MSOT1
      ASSIGN 9150 TO MSOT2
      ASSIGN 4600 TO MP1
      ASSIGN 4700 TO MP2
      ASSIGN 4500 TO MSP21
      ASSIGN 9470 TO MSP041
C
C     SET THE CONSTANT VARIABLES.
      DW12  = 0.0
      DEF12 = 0.0
      F12   = 0.0
      YWA12 = 0.0
      YAF12 = 0.0
      YAFF1  = 0.0
      YWFF2  = 0.0
      YEF12 = 0.0
      YEFF1 = 0.0
      YEFF2 = 0.0
      DFIP  = 0.0
      FA0   = F1 * FAS
      EQ0   = F1
 400  RETURN



      ENTRY  IRATEC
C
C     INITIALIZE THE CYCLIC VARIABLES
      IPR   = 0
      YWORK = 0.0
      YWORKP = 0.0
C
C     SYSTEM 1
```

```
C             MASS
              YWAIV  = 0.0
              YWFIV  = 0.0
              YWAEV  = 0.0
              YWFEV  = 0.0
              YWABI  = 0.0
              YWFBI  = 0.0
C
C             ENERGY
              YEFIV  = 0.0
              YEFEV  = 0.0
              YEFBBI = 0.0
C
C             INTAKE PORT SYSTEM
              YWAI   = 0.0
              YWFI   = 0.0
              YEFI   = 0.0
C
C             EXHAUST PORT SYSTEM
              YWAE   = 0.0
              YWFE   = 0.0
              YEFE   = 0.0
              GO TO ( 450, 450, 500 ),  NENG
C
C             DIESEL ENGINE
  450         CONTINUE
              YWAI2  = 0.0
              YWFI2  = 0.0
              YWFFI  = 0.0
              YFID   = WI / (1.0+FI*FAS)
              YFIN   = YFID * FI
              YFINO  = YFIN
              YFIDO  = YFID
              YEFFI  = 0.0
              YFIPD  = WIP / (1.0+FIP*FAS)
              YFIPN  = YFIPD * FIP
              YFIPNO = YFIPN
              YFIPDO = YFIPD
              YFEPD  = WEP / (1.0+FEP*FAS)
              YFEPN  = YFEPD * FEP
              YFEPNO = YFEPN
              YFEPDO = YFEPD
              IF ( LOCO )  GO TO 550
C
C             PRE CHAMBER DIESEL ENGINE
C             SYSTEM 2
              YWFF2  = 0.0
              YF2D   = W2 / (1.0+F2*FAS)
              YF2N   = YF2D * F2
              YF2DO  = YF2D
              YF2NO  = YF2N
              YEFI2  = 0.0
              YEFF2  = 0.0
              GO TO 550
```

```
C
C          SPARK IGNITION ENGINE
C          SYSTEM 1
  500      CONTINUE
           DWFC1  = 0.0
           DWFS1  = 0.0
           YWFS1  = 0.0
           YWFS10 = 0.0
           YWFC1  = 0.0
           YWFC10 = 0.0
           DWFES  = 0.0
           YWFES  = 0.0
           YWFESO = 0.0
           YWFIN  = WFI * W1
           YWFINO = YWFIN
C
C          INTAKE PORT SYSTEM
           YWFIP  = WFIP * WIP
           YWFIPO = YWFIP
C
C          EXHAUST PORT SYSTEM
           YFEPO  = WEP / (1.0+FEP+FAS)
           YFEPN  = YFEPO * FEP
           YFEPNO = YFEPN
           YFEPOO = YFEPO
C
C          OUTPUT VARIABLE
           P2     = 0.0
           T2     = 0.0
           F2     = 0.0
           W2     = 0.0
           VOL2   = 0.0
           DT2    = 0.0
           DF2    = 0.0
           DW2    = 0.0
           DVOL2  = 0.0
           DQ2    = 0.0
C
C          GENERATE SWITCH VARIABLES
           ASSIGN 1900 TO MS5
           ASSIGN 1800 TO MSP1
           ASSIGN 3500 TO MSP2
           ASSIGN 4300 TO MSP3
           ASSIGN 4500 TO MSP21
           ASSIGN 1960 TO MSC1
           DWFC10 = 0.0
           DWFC1  = 0.0
  550      RETURN



           ENTRY  RATE
C          CALL ENERGY SUBROUTINE FOR SYSTEM 1.
           PE     = P1
```

```
      TE    = TI
      FE    = FI
      CALL ENERGY
      UI    = UE
      DUPI  = DUPE
      DUTI  = DUTE
      DUFI  = DUFE
      RI    = RE
      DRPI  = DRPE
      DRTI  = DRTE
      DRFI  = DRFE
      HI    = UI + RI*TI
      GAMI  = 1.0 + RI / DUTI
      CPI   = GAMI * DUTI
      UIS   = UI
      RIS   = RI
      HIS   = HI
      GAMIS = GAMI
      CPIS  = CPI
      GO TO MSI
C
C     SPARK IGNITION ENGINE
  810 TAV   = TI
      CALL AVERGY
      UAI   = UA
      DUATI = DUAT
      HAI   = UA + RA*TI
      GAMAI = 1.0 + RA/DUATI
      UVI   = UV
      DUVTI = DUVT
      HVI   = HV
      GAMVI = 1.0 + RV/DUVTI
      UIS   = WFI*UI + WFAI*UA + WFVI*UV
      RIS   = WFI*RI + WFAI*CWFAVR
      HIS   = UIS + RIS*TI
      CPIS  = WFI*DUTI*GAMI + WFAI*DUATI*GAMAI + WFVI*DUVTI*GAMVI
      CVIS  = WFI*DUTI + WFAI*DUATI + WFVI*DUVTI
      GAMIS = CPIS / CVIS
C
C     CALL ENERGY SUBROUTINE FOR INLET VALVE SYSTEM.
  820 PE    = PIP
      TE    = TIP
      FE    = FIP
      CALL ENERGY
      UIP   = UE
      DUPIP = DUPE
      DUTIP = DUTE
      DUFIP = DUFE
      RIP   = RE
      DRPIP = DRPE
      DRTIP = DRTE
      DRFIP = DRFE
      HIP   = UIP + RIP*TIP
      GAMIP = 1.0 + RIP/DUTIP
```

```
      RIPS   = RIP
      UIPS   = UIP
      HIPS   = HIP
      GAMIPS = GAMIP
      GO TO MS2
C
C     SPARK IGNITION ENGINE
  830 TAV    = TIP
      CALL AVERGY
      UAIP   = UA
      DUATIP = DUAT
      HAIP   = UAIP + RA*TIP
      GAMAIP = 1.0 + RA/DUATIP
      UVIP   = UV
      DUVTIP = DUVT
      HVIP   = HV
      GAMVIP = 1.0 + RV / DUVTIP
      UIPS   = WFIP*UIP + WFAIP*UAIP + WFVIP*UVIP
      RIPS   = WFIP*RIP + WFAIP*CWFAVR
      HIPS   = UIPS + RIPS*TIP
      CPIPS  = WFIP*DUTIP*GAMIP + WFAIP*DUATIP*GAMAIP +
     1         WFVIP*DUVTIP*GAMVIP
      CVIPS  = WFIP*DUTIP + WFAIP*DUATIP + WFVIP*DUVTIP
      GAMIPS = CPIPS / CVIPS
C
C     CALL ENERGY SUBROUTINE FOR EXHAUST VALVE SYSTEM.
  840 PE     = PEP
      TE     = TEP
      FE     = FEP
      CALL ENERGY
      UEP    = UE
      DUPEP = DUPE
      DUTEP = DUTE
      DUFEP = DUFE
      REP    = RE
      DRPEP = DRPE
      DRTEP = DRTE
      DRFEP = DRFE
      HEP    = UEP + REP*TEP
      GAMEP = 1.0 + REP/DUTEP
C
C     CALCULATE MASS FLOW RATES.
C     MASS FLOW IS POSITIVE WHEN ENTERING SYSTEM 1 EITHER FROM I.V. ,
C     E.V. OR SYSTEM 2 FOR PRE-CHAMBER ENGINE.
C     MASS FLOW RATE OF FUEL INJECTION FOR DIESEL ENGINE OR MASS RATE
C     OF BURNING FOR SPARK IGNITION ENGINE.
      CALL  FUELRT
      GO TO ( 910, 960, 1000 ),  NICOMB
C
C     CALCULATE AIR MASS FRACTION LEFT AFTER COMBUSTION FOR S.I.ENGINE
  910 NICOMB = 3
      GO TO ( 920, 930 ),  ISC
C
C     NO AIR MASS FRACTION
```

```
920   DWFCID = 0.0
      DWFCI  = 0.0
      ASSIGN 1960 TO MSCI
      GO TO 1000
C
C     AIR MASS FRACTION LEFT
930   CONTINUE
      DWFAC  = (WCX * (WFAIX+WFVIX)) / ( CAIVOR-10.0-CA )
      YAFINX = YAFINO
      YAFINO = WI*WFI - (YWFIV+YWFES+YWFBI+YWFCI+YWFSI)
      ASSIGN 1950 TO MSCI
      GO TO 960
C
C     GENERATE SWITCH VARIABLES FOR S. I. ENGINE
960   NICOMB = 3
      IF ( LSIC )  GO TO 970
C
C     NO COMBUSTION.
      IF ( .NOT. LCONS )  GO TO 965
      YAFINX = YWFINO
      DWFSI = 0.0
      YAFINO = WI*WFI - (YWFIV+YWFES+YWFBI+YWFCI+YWFSI)
      GO TO 968
965   CONTINUE
      DWFSI  = 0.0
      DWFSIO = 0.0
      YWFSI  = 0.0
      YWFSIO = 0.0
968   CONTINUE
      P2     = 0.0
      T2     = 0.0
      F2     = 0.0
      W2     = 0.0
      VOL2   = 0.0
      DT2    = 0.0
      DF2    = 0.0
      DW2    = 0.0
      DVOL2  = 0.0
      DQ2    = 0.0
      ASSIGN 1900 TO MSS
      ASSIGN 1800 TO MSP1
      ASSIGN 3500 TO MSP2
      ASSIGN 4300 TO MSP3
      ASSIGN 4500 TO MSP21
      GO TO 1000
C
C     COMBUSTION.
970   CONTINUE
      IF ( LCONS )  GO TO 990
      YAFINO = YWFINX
990   CONTINUE
      ASSIGN 2050 TO MSS
      ASSIGN 1270 TO MSP1
      ASSIGN 3200 TO MSP2
```

```
      ASSIGN 4100 TO MSP3
      ASSIGN 4410 TO MSP21
 1000 CONTINUE
      DEFF1 = DWFI1 * HF
      DEFF2 = DWFI2 * HF
      CALL  FLOWCO
C
C     MASS FLOW RATE THROUGH INLET VALVE.
C     CHECK IF THE INLET VALVE IS OPEN =
 1010 IF ( LIV )  GO TO 1020
C
C     INLET VALVE CLOSED.
      DWIV = 0.0
      DEFIV = 0.0
      WFIVS = 0.0
      FI = 0.0
      GO TO 1110
C
C     INLET VALVE OPEN.
 1020 PP1 = PIP
      PP2 = PI
      TT1 = TIP
      TT2 = TI
      FF1 = FIP
      FF2 = FI
      RR1 = RIPS
      RR2 = RIS
      HH1 = HIPS
      HH2 = HIS
      GAMM1 = GAMIPS
      GAMM2 = GAMIS
      AREA = CODIV * AIV
      CALL  MASS
      DWIV  = DW
      DEFIV = DWIV * HUS
      WFIVS = (II+1)/2 * WFIP - (II-1)/2 * WFI
      FI = FUS
C
C     MASS FLOW RATE THROUGH EXHAUST VALVE.
C     CHECK IF EXHAUST VALVE IS OPEN,
 1110 IF ( LEV )  GO TO 1120
C
C     EXHAUST VALVE CLOSED.
      DWEV = 0.0
      DEFEV = 0.0
      WFEVS = 1.0
      FE = 0.0
      GO TO 1210
C
C     EXHAUST VALVE OPEN.
 1120 PP1 = PEP
      PP2 = PI
      TT1 = TEP
      TT2 = TI
```

```
              FF1 = FEP
              FF2 = FI
              RR1 = REP
              RR2 = RI
              HH1 = HEP
              HH2 = HI
              GAMM1 = GAMEP
              GAMM2 = GAMIS
              AREA = CODEV * AEV
              CALL  MASS
              DWEV  = DW
              DEFEV = DWEV * HUS
              WFEVS = 1.0
              FE    = FUS
 1210         GO TO MS3
C
C             MASS FLOW RATE BETWEEN INTAKE MANIFOLD AND INTAKE PORT FOR SPARK
C             IGNITION ENGINE.
 1220         PP1 = PIM
              PP2 = PIP
              TT1 = TIM
              TT2 = TIP
              FF1 = FIM
              FF2 = FIP
              RR1 = RIM
              RR2 = RIPS
              HH1 = HIM
              HH2 = HIPS
              GAMM1 = GAMIM
              GAMM2 = GAMIPS
              AREA = CODIM * AIM
              CALL  MASS
              DWI   = DW
              DEFI = DWI * HUS
 1260         GO TO MSP1
C
C             CALL ENERGY SUBROUTINE FOR SYSTEM 2.
 1270         PE    = P2
              TE    = T2
              FE    = F2
              CALL ENERGY
              U2    = UE
              DUP2 = DUPE
              DUT2 = DUTE
              DUF2 = DUFE
              R2    = RE
              DRP2 = DRPE
              DRT2 = DRTE
              DRF2 = DRFE
              H2    = U2 + R2*T2
              GAM2 = 1.0 + R2/DUT2
              GO TO MS4
C
C             MASS FLOW RATE BETWEEN PRE CHAMBER AND MAIN CHAMBER.
```

```
      1280   PP1 = P2
             PP2 = P1
             TT1 = T2
             TT2 = T1
             FF1 = F2
             FF2 = F1
             RR1 = R2
             RR2 = R1
             HH1 = H2
             HH2 = H1
             GAMM1 = GAM2
             GAMM2 = GAM1
             AREA = CODPM * APM
             CALL  MASS
             DW12  = CW
             DEF12 = DW12*HUS
             F12   = FUS
      1310   GO TO 1800
C
C            MASS FLOW RATE DUE TO BLOW BY THROUGH PISTON.
C            SYSTEM 1 --
      1800   DWBB1  = CBB1  * (1.0-P1/PAMB)
             DEFBB1 = DWBB1 * H1S
             CALL HEAT
C
C            CHECK TO CALL DYNIP SUBROUTINE
             GO TO MDYNIP
      1830   CALL  DYNIP
      1840   CONTINUE
             GO TO MS5
C
C            RATE OF CHANGE OF MASS FOR SYSTEM 1 FOR DIESEL ENGINE AND
C            SPARK IGNITION ENGINE DURING NO COMBUSTION.
      1900   DW1 = DW1V + DWEV + DWBB1 + DWF11 + DW12
             GO TO MS6
C
C            RATE OF CHANGE OF MASS FRACTIONS IN SYSTEM 1 FOR S. I. ENGINE.
      1930   CONTINUE
             DWF1V  = DW1V * WF1VS
             DWFES  = DWEV * WFEVS
             DWFBB1 = DWBB1* WF1
             DWA1V  = DW1V - DWF1V
             DWABB1 = DWBB1 - DWFBB1
             GO TO MSC1
C
C            MASS FRACTION LEFT AFTER COMBUSTION
      1950   CONTINUE
             DWFC1  = DWFAC
      1960   CONTINUE
             DWF1   = (W1*(DWF1V+DWFES+DWFBB1+DWFC1) - DW1*YWFIN) / (W1*W1)
             DWFA1  = -DWF1 / CWFAV1
             DWFV1  = CWFAV * DWFA1
C
C            RATE OF CHANGE OF EQUIVALENCE RATIO FOR SYSTEM 1.
```

```
      C           SPARK IGNITION ENGINE
       2010       DFI = 0.0
                  GO TO 2030
      C
      C           DIESEL ENGINE
       2020       DWAIV  = DWIV  / (1.0+FAS*FI )
                  DWAEV  = DWEV  / (1.0+FAS*FE )
                  DWABBI = DWBBI / (1.0+FAS*FI )
                  DWAI2  = DWI2  / (1.0+FAS*FI2)
                  DWFFI  = DWFII / FAS
                  DWFIV  = DWAIV * FI
                  DWFEV  = DWAEV * FE
                  DWFBBI = DWABBI* FI
                  DWFI2  = DWAI2 * FI2
                  DFI    = ((DWFIV+DWFEV+DWFBBI+DWFI2+DWFFI)*YFID -
           1              (DWAIV+DWAEV+DWABBI+DWAI2)*YFIN) / (YFID*YFID)
      C
      C           THE RATE OF CHANGE OF TEMPERATURE FOR SYSTEM I.
       2030       CONTINUE
                  BI = -RIS*TI*DVOL/VOL + (DQI+DEFIV+DEFEV+DEFBBI+DEFI2+DEFFI-
           1          UIS*DWI)/WI
                  B2 = DWFI*UI + DWFAI*UAI + DWFVI*UVI
                  B3 = WFI * DUFI * DFI
                  B4 = DWI/WI - DVOL/VOL + (DWFI*RI+DWFAI*CWFAVR+WFI*DRFI*DFI)/
           1          RIS
                  B5 = WFI*DUTI + WFAI*DUATI + WFVI*DUVTI
                  B6 = WFI * DUPI * PI * (1.0/TI+WFI*DRTI/RIS)
                  B7 = 1.0 - WFI*PI*DRPI/RIS
                  B8 = WFI * DUPI * PI * B4 / B7
                  DTI = (BI - B2 - B3 - B8) / (B5 + B6/B7)
      C
      C           RATE OF EXTERNAL WORK DONE
                  DWORK = PI * DVOL
      C
      C           RATE OF CHANGES OF MASS, EQUIVALENCE RATIO AND TEMPERATURE FOR
      C           VALVE SYSTEMS BY TRIAL AND ERROR METHOD.
      C           INLET VALVE SYSTEM--
       2050       GO TO MS7
      C
      C           DIESEL ENGINE
       2500       DTIP = 0.0
                  DO 2510  I = 1,IDVS
                  DWIP = WIP * (DPIP/PIP - DTIP/TIP)
                  DWI  = DWIP + DWIV
                  NN   = 1
                  IF ( DWI .LE. 0.0 )  NN = -1
                  FF   = (1-NN) / 2 * FIP
                  DWAI = DWI / (1.0+FAS*FF)
                  DWFI = DWAI * FF
                  DFIP = ((DWFI-DWFIV)*YFIPD - (DWAI-DWAIV)*YFIPN) / (YFIPD*YFIPD)
                  DEFI = ((1+NN)*HAMB + (1-NN)*HIPS) * DWI / 2.0
                  IF ( I .EQ. IDVS )  GO TO 2550
                  BI   = (DQIP - DEFIV + DEFI - UIP*DWIP) / WIP
       2510       DTIP = (BI - DUFIP*DFIP) / DUTIP
```

```
      GO TO 2550
C
C     SPARK IGNITION ENGINE
C     MASS BALANCE
 2520 DWIP  = DWI - DWIV
      NN = 1
      IF ( DWI .LE. 0.0 )  NN = -1
      FF = (1-NN) / 2 * WFIP
      DWFI  = DWI * FF
      DWAI  = DWI - DWFI
      DWFIP  = (WIP*(DWFI-DWFIV) - DWIP*YWFIPN) / (WIP*WIP)
      DWFAIP = -DWFIP / CWFAV1
      DWFVIP = CWFAV * DWFAIP
C
C     ENERGY BALANCE
      B1 = (DQIP + DEFI - DEFIV - UIPS*DWIP) / WIP
      B2 = DWFIP*UIP + DWFAIP*UAIP + DWFVIP*UVIP
      B3 = AFIP*DUTIP + WFAIP*DUATIP + WFVIP*DUVTIP
      DTIP = (B1 - B2) / B3
C
C     EXHAUST VALVE SYSTEM --
 2550 DTEP = 0.0
 2560 DO 2600  I = 1,IDVS
      DWEP = WEP * (DPEP/PEP - DTEP/TEP)
      DWE  = DWEP + DWEV
      NN   = 1
      IF ( DWE .LE. 0.0 )  NN = -1
      GO TO MS8
C
C     SPARK IGNITION ENGINE
 2580 CONTINUE
      B1 = DWEV * WFEVS / (1.0+FAS*FE)
      DWAEV = B1 + (1.0-WFEVS)*DWEV
      DWFEV = B1 * FE
 2590 CONTINUE
      FF   = (1-NN) / 2 * FEP
      DWAE = DWE / (1.0+FAS*FF)
      DWFE = DWAE * FF
      DFEP = ((DWFE-DWFEV)*YFEPD - (DWAE-DWAEV)*YFEPN) / (YFEPD*YFEPD)
      DEFE = ((1+NN)*HAMB + (1-NN)*HEP) * DWE / 2.0
      IF ( 1 .EQ. IDVS )  GO TO MSP2
      B1 = (DQEP - DEFEV + DEFE - UEP*DWEP) / WEP
      B2 = 1.0 + TEP*DRTEP/REP
      B3 = 1.0 - PEP*DRPEP/REP
      B4 = PEP * DUPEP * (DWEP/WEP + DRFEP*DFEP/REP)
      B5 = DUTEP + DUPEP*PEP*B2/(TEP*B3)
 2600 DTEP = (B1 - B4/B3 - DUFEP*DFEP) / B5
      GO TO MSP2
C
C     PRE CHAMBER DIESEL ENGINE
C     RATE OF CHANGE OF MASS FOR SYSTEM 2.
 3100 DW2 = DWFI2 - DWI2
C
C     RATE OF CHANGE OF EQUIVALENCE RATIO FOR SYSTEM 2.
```

```
                DWFF2 = DWFI2 / FAS
                DF2 = ((-DWFI2+DWFF2)*YF2D - (-DWAI2)*YF2N) / (YF2D*YF2D)
C
C               RATE OF CHANGE OF TEMPERATURE FOR SYSTEM 2.
                B1 = (DQ2-DEFI2+DEFF2-U2*DW2) / W2
                B2 = 1.0 + T2*DRT2/R2
                B3 = 1.0 - P2*DRP2/R2
                B4 = P2 * DUP2 * (DW2/W2+DRF2*DF2/R2)
                B5 = DUT2 + DUP2*P2*B2/(T2*B3)
                DT2 = (B1 - B4/B3 - DUF2*DF2) / B5
                GO TO 3500
C
C               TWO SYSTEMS DURING COMBUSTION PERIOD FOR S. I. ENGINE.
  3200          DW2   = DWFI2 + DWEV
                DW1   = DWBB1 - DWFI2
                DWF1  = 0.0
                DWFA1 = 0.0
                DWFV1 = 0.0
                DWFS1 = WF1 * DW1
                A1   = P1 / (R2-DRP2*P1)
                A2   = 1.0/T2 + DRT2/R2
                A3   = DQ1 + DW1*R1S*T1
                A4   = (DQ2 + DW2*(H1S-U2-R2*DUP2*A1)) / W2
                A5   = 1.0/VOL1 + 1.0/VOL2
                A6   = 1.0/T2 + DRP2*A1*A2 + DRT2/R2
                A7   = DUP2*R2*A1*A2 + DUT2
                A8   = A6 + (A1*DUP2*R2/VOL2-P1/(W2*9337.92)) -
         1             A7 * (A5*A1*DRP2/VOL2)
                A9   = DW1/W1 - DVOL/VOL1 - DW2*A1*R2/(W2*P1)
                A10 = (A3-P1*DVOL/9337.92)*A8 - (P1*A7*(DVOL/VOL1+DW2*(1.0/W1+
         1             1.0/W2+A1*DRP2/W2)) + P1*A6*A4) / 9337.92
                A11 = W1*CV1S*A8 - P1*A7/(T1*9337.92)
                DT1  = A10/A11
                DVOL2 = (A7*(DT1/T1-DVOL/VOL1-DW2*(1.0/W1+1.0/W2+A1*DRP2/W2)) -
         1             A6*A4) / A8
                DT2  = (DW1/W1 + DT1/T1 - DVOL/VOL1 + DVOL2*A5 - DW2/W2 -
         1             DRP2*A1*(DW2/W2-DVOL2/VOL2)) / A6
                DVOL1 = DVOL - DVOL2
                DWORK = P1 * DVOL
  3500          CONTINUE
                GO TO MDBRY
C
C               DEBUG
  8000          PRINT 8010, DWIV, DWEV, DWI, DWE, DWI2, DWFI1, DWFI2
  8010          FORMAT(/5H RATE,10X,7E15.5)
                PRINT 8020, P1, T1, F1, W1, DT1, DF1, DW1
                PRINT 8020, P1P, T1P, F1P, W1P, DT1P, DF1P, DW1P
                PRINT 8020, PEP, TEP, FEP, WEP, DTEP, DFEP, DWEP
                PRINT 8020, P2, T2, F2, W2, DT2, DF2, DW2
                PRINT 8020,  WF1,  WFA1,  WFV1,  WF1P,  WFA1P,  WFV1P
                PRINT 8020, DWF1, DWFA1, DWFV1, DWF1P, DWFA1P, DWFV1P
                PRINT 8020, VOL1, VOL2, DVOL1, DVOL2
  8020          FORMAT(15X,7E15.5)
  9000          RETURN
```

```
      ENTRY  RATE2
C     STORE RATE VARIABLES IN THREE DIMENSIONAL ARRAYS.
C     SYSTEM 1
       ARRAY(NP,1,1) = P1
       ARRAY(NP,1,2) = T1
       ARRAY(NP,1,3) = F1
       ARRAY(NP,1,4) = W1
      DARRAY(NP,1,2) = DT1
      DARRAY(NP,1,3) = DF1
      DARRAY(NP,1,4) = DW1
C
C     INLET PORT SYSTEM
       ARRAY(NP,2,1) = PIP
       ARRAY(NP,2,2) = TIP
       ARRAY(NP,2,3) = FIP
       ARRAY(NP,2,4) = WIP
      DARRAY(NP,2,1) = DPIP
      DARRAY(NP,2,2) = DTIP
      DARRAY(NP,2,3) = DFIP
      DARRAY(NP,2,4) = DWIP
C
C     EXHAUST PORT SYSTEM
       ARRAY(NP,3,1) = PEP
       ARRAY(NP,3,2) = TEP
       ARRAY(NP,3,3) = FEP
       ARRAY(NP,3,4) = WEP
      DARRAY(NP,3,2) = DTEP
      DARRAY(NP,3,3) = DFEP
      DARRAY(NP,3,4) = DWEP
      GO TO MSP3
C
C     SYSTEM 2
C     SPARK IGNITION ENGINE
 4100  ARRAY(NP,1,3) = VOL1
       ARRAY(NP,4,3) = VOL2
      DARRAY(NP,1,3) = DVOL1
      DARRAY(NP,4,3) = DVOL2
      ARRAYF(NP,1,1) = WF1
      ARRAYF(NP,1,2) = WFA1
      ARRAYF(NP,1,3) = WFV1
      ARRAYF(NP,2,1) = WFIP
      ARRAYF(NP,2,2) = WFAIP
      ARRAYF(NP,2,3) = WFVIP
      GO TO 4200
C
C     PRE CHAMBER ENGINE
 4150  ARRAY(NP,4,3) = F2
      DARRAY(NP,4,3) = DF2
 4200  ARRAY(NP,4,1) = P2
       ARRAY(NP,4,2) = T2
       ARRAY(NP,4,4) = W2
```

```
              DARRAY(NP,4,2) = DT2
              DARRAY(NP,4,4) = DW2
 4300         RETURN



              ENTRY  RATE2D
C             CONVERT THE VARIABLE NAMES FOR RATE2 IN CASE OF NO CONVERGENCE
              P1     =  APRAY(1,1,1)
              T1     =  ARRAY(1,1,2)
              W1     =  ARRAY(1,1,4)
              DT1    = DARRAY(1,1,2)
              DW1    = DARRAY(1,1,4)
              P1P    =  ARRAY(1,2,1)
              T1P    =  ARRAY(1,2,2)
              W1P    =  ARRAY(1,2,4)
              DT1P   = DARRAY(1,2,2)
              DW1P   = DARRAY(1,2,4)
              PEP    =  ARRAY(1,3,1)
              TEP    =  ARRAY(1,3,2)
              FEP    =  ARRAY(1,3,3)
              WEP    =  ARRAY(1,3,4)
              DTEP   = DARRAY(1,3,2)
              DFEP   = DARRAY(1,3,3)
              DWEP   = DARRAY(1,3,4)
              IF ( NENG .NE. 3 )  GO TO 4305
              WF1    = ARRAYF(1,1,1)
              WFA1   = ARRAYF(1,1,2)
              WFV1   = ARRAYF(1,1,3)
              WF1P   = ARRAYF(1,2,1)
              WFA1P  = ARRAYF(1,2,2)
              WFV1P  = ARRAYF(1,2,3)
 4305         CONTINUE
              GO TO ( 4340, 4320, 4310 ),  NENG
 4310         IF ( .NOT. LSIC )  GO TO 4400
 4320         P2     =  ARRAY(1,4,1)
              T2     =  ARRAY(1,4,2)
              W2     =  ARRAY(1,4,4)
              DT2    = DARRAY(1,4,2)
              DW2    = DARRAY(1,4,4)
              IF ( LSI )  GO TO 4350
 4330         F2     =  ARRAY(1,4,3)
              DF2    = DARRAY(1,4,3)
 4340         F1     =  ARRAY(1,1,3)
              F1P    =  ARRAY(1,2,3)
              DF1    = DARRAY(1,1,3)
              DF1P   = DARRAY(1,2,3)
              GO TO 4400
 4350         VOL1   =  ARRAY(1,1,3)
              VOL2   =  ARRAY(1,4,3)
              DVOL1  = DARRAY(1,1,3)
              DVOL2  = DARRAY(1,4,3)
              P2     = P1
 4400         RETURN
```

```
      ENTRY  RATE21
C     CONVERT THE VARIABLE NAMES FOR RATE SUBROUTINE
      P1    = ARRAY1(1,1)
      T1    = ARRAY1(1,2)
      W1    = ARRAY1(1,4)
      PIP   = ARRAY1(2,1)
      TIP   = ARRAY1(2,2)
      WIP   = ARRAY1(2,4)
      PEP   = ARRAY1(3,1)
      TEP   = ARRAY1(3,2)
      FEP   = ARRAY1(3,3)
      WEP   = ARRAY1(3,4)
      GO TO MSP21
 4410 P2    = ARRAY1(4,1)
      T2    = ARRAY1(4,2)
      W2    = ARRAY1(4,4)
 4420 GO TO MS21
 4430 F2    = ARRAY1(4,3)
 4440 F1    = ARRAY1(1,3)
      FIP   = ARRAY1(2,3)
      GO TO 4500
 4450 VOL1 = ARRAY1(1,3)
      VOL2 = ARRAY1(4,3)
      P2    = P1
 4500 RETURN


      ENTRY  RATE3
C     CALCULATE THE ACCUMULATED SUM
C     MASS
      YWAIV  = YWAIVO + (DWAIVO+DWAIV) * DCA2
      YWFIV  = YWFIVO + (DWFIVO+DWFIV ) * DCA2
      YWAEV  = YWAEVO + (DWAEVO+DWAEV ) * DCA2
      YWFEV  = YWFEVO + (DWFEVO+DWFEV ) * DCA2
      YWABI  = YWABIO + (DWABIO+DWABBI) * DCA2
      YWFBI  = YWFBIO + (DWFBIO+DWFBBI) * DCA2
      YWAI   = YWAIO  + (DWAIO+DWAI) * DCA2
      YWFI   = YWFIO  + (DWFIO+DWFI) * DCA2
      YWAE   = YWAEO  + (DWAEO+DWAE) * DCA2
      YWFE   = YWFEO  + (DWFEO+DWFE) * DCA2
C
C     ENERGY
      YEFIV  = YEFIVO + (DEFIVO+DEFIV ) * DCA2
      YEFEV  = YEFEVO + (DEFEVO+DEFEV ) * DCA2
      YEFBBI = YERBIO + (DEBBIO+DEFBBI) * DCA2
      YEFI   = YEFIO  + (DEFIO+DEFI) * DCA2
      YEFE   = YEFEO  + (DEFEO+DEFE) * DCA2
      GO TO MS12
C
C     DIESEL ENGINE
```

```
      4510 CONTINUE
           YWA12  = YWA120 + (DWA120+DWA12 ) * DCA2
           YWF12  = YWF120 + (DWF120+DWF12 ) * DCA2
           YWFF1  = YWFF10 + (DWFF10+DWFF1 ) * DCA2
           YFIN   = YFINO + YWFIV + YWFEV + YWFB1 + YWF12 + YWFF1
           YFID   = YFIDO + YWAIV + YWAEV + YWAB1 + YWA12
           YFIPN  = YFIPNO + YWFI - YWFIV
           YFIPD  = YFIPDO + YWAI - YWAIV
           YFEPN  = YFEPNO + YWFE - YWFEV
           YFEPD  = YFEPDO + YWAE - YWAEV
           YEFF1  = YEFF10 + (DEFF10+DEFF1 ) * DCA2
           GO TO MP1
     C
     C     PRE CHAMBER DIESEL ENGINE
      4550 YWFF2  = YWFF20 + (DWFF20+DWFF2) * DCA2
           YF2N   = YF2NO - YWF12 + YWFF2
           YF2D   = YF2DO - YWA12
           YEFF2  = YEFF20 + (DEFF20+DEFF2 ) * DCA2
           YEF12  = YEF120 + (DEF120+DEF12 ) * DCA2
           GO TO 4600
     C
     C     SPARK IGNITION ENGINE
     C     SYSTEM 1
      4570 CONTINUE
           YWFC1  = YWFC10 + (DWFC10+DWFC1 ) * DCA2
           YWFS1  = YWFS10 + (DWFS10+DWFS1) * DCA2
           YWFES  = YWFES0 + (DWFES0+DWFES) * DCA2
           YWFIN  = YWFINO + YWFIV + YWFES + YWFB1 + YWFC1 + YWFS1
           WF1    = YWFIN / WI
           IF ( WF1 .LT. 0.0 )  WF1 = 0.0
           IF ( WF1 .GT. 1.0 )  WF1 = 1.0
           WFA1   = (1.0-WF1) / CWFAV1
           WFV1   = CWFAV * WFA1
     C
     C     INTAKE PORT SYSTEM
           YWFIPN = YWFIPO - YWFIV + YWFI
           WFIP   = YWFIPN / WIP
           IF ( WFIP .LT. 0.0 )  WFIP = 0.0
           IF ( WFIP .GT. 1.0 )  WFIP = 1.0
           WFAIP  = (1.0-WFIP) / CWFAV1
           WFVIP  = CWFAV * WFAIP
     C
     C     EXHAUST PORT SYSTEM
           YFEPN  = YFEPNO + YWFE - YWFEV
           YFEPD  = YFEPDO + YWAE - YWAEV
     C
     C     TOTAL EXTERNAL WORK DONE
      4600 B = (DWORKO+DWORK) * DCA2
           YWORK  = YWORKO + B
     C
     C     PUMPING WORK
           IF ( CA .LE. 180.0 .OR. CA .GT. 540.0 ) YWORKP = YWOKPO + B
           RETURN
```

```
      ENTRY  RATE4
C     STORE VARIABLES FOR CALCULATING ACCUMULATED SUM
C     SYSTEM 1
C     MASS
      DWAIVO = DWAIV
      DWFIVO = DWFIV
      DWAEVO = DWAEV
      DWFEVO = DWFEV
      DWABIO = DWABBI
      DWFBIO = DWFBBI
      YWAIVO = YWAIV
      YWFIVO = YWFIV
      YWAEVO = YWAEV
      YWFEVO = YWFEV
      YWABIO = YWABI
      YWFBIO = YWFBI
C
C     ENERGY
      DEFIVO = DEFIV
      DEFEVO = DEFEV
      DEBBIO = DEFBBI
      YEFIVO = YEFIV
      YEFEVO = YEFEV
      YEBBIO = YEFBBI
C
C     INTAKE PORT SYSTEM
       DWAIO  = DWAI
       DWFIO  = DWFI
       YWAIO  = YWAI
       YWFIO  = YWFI
       DEFIO  = DEFI
       YEFIO  = YEFI
C
C     EXHAUST PORT SYSTEM
       DWAEO  = DWAE
       DWFEO  = DWFE
       YWAEO  = YWAE
       YWFEO  = YWFE
       DEFEO  = DEFE
       YEFEO  = YEFE
      GO TO MS13
C
C     DIESEL ENGINE
 4610 CONTINUE
      DWA12O = DWA12
      DWF12O = DWF12
      DWFFIO = DWFFI
      YWA12O = YWA12
      YWF12O = YWF12
      YWFFIO = YWFFI
      DEF12O = DEF12
      DEFFIO = DEFFI
```

```
      YEF120 = YEF12
      YEFF10 = YEFF1
      GO TO MP2
C
C     SYSTEM 2 FOR PRE CHAMBER ENGINE
 4650 DWFF20 = DWFF2
      YWFF20 = YWFF2
      DEFF20 = DEFF2
      YEFF20 = YEFF2
C
C     STORE THE OLD EQUIVALENCE RATIO
      FAPC   = F2
      GO TO 4700
C
C     SPARK IGNITION ENGINE
C     SYSTEM 1
 4670 CONTINUE
      DWFC10 = DWFC1
      YWFC10 = YWFC1
      DWFS10 = DWFS1
      YWFS10 = YWFS1
      DWFES0 = DWFES
      YWFES0 = YWFES
C
C     VARIABLES FOR WORK
 4700 DWORK0 = DWORK
      YWORK0 = YWORK
      YWOKP0 = YWORKP
      RETURN


      ENTRY  RATECA
C     STORE THE OUTPUT VARIABLES IN DIMENSIONED ARRAYS AT EACH CRANK
C     ANGLE
      GO TO MOUT1
 5050 CONTINUE
      LCA = CA + 0.1
      I = 1
      ZOUT(I,LCA) = CA
      I = I + 1
      ZOUT(I,LCA) = P1
      I = I + 1
      ZOUT(I,LCA) = T1
      I = I + 1
      ZOUT(I,LCA) = F1
      I = I + 1
      ZOUT(I,LCA) = W1
      I = I + 1
      ZOUT(I,LCA) = P2
      I = I + 1
      ZOUT(I,LCA) = T2
      I = I + 1
      ZOUT(I,LCA) = F2
```

```
      I = I + 1
      ZOUT(I,LCA) = W2
      I = I + 1
      ZOUT(I,LCA) = PIP
      I = I + 1
      ZOUT(I,LCA) = TIP
      I = I + 1
      ZOUT(I,LCA) = FIP
      I = I + 1
      ZOUT(I,LCA) = WIP
      I = I + 1
      ZOUT(I,LCA) = PEP
      I = I + 1
      ZOUT(I,LCA) = TEP
      I = I + 1
      ZOUT(I,LCA) = FEP
      I = I + 1
      ZOUT(I,LCA) = WEP
      I = I + 1
      ZOUT(I,LCA) = DWIV
      I = I + 1
      ZOUT(I,LCA) = DWEV
      I = I + 1
      ZOUT(I,LCA) = DW12
      I = I + 1
      ZOUT(I,LCA) = DWFI1
      I = I + 1
      ZOUT(I,LCA) = DWFI2
      I = I + 1
      ZOUT(I,LCA) = DWI
      I = I + 1
      ZOUT(I,LCA) = DWE
      I = I + 1
      ZOUT(I,LCA) = DTI
      I = I + 1
      ZOUT(I,LCA) = DFI
      I = I + 1
      ZOUT(I,LCA) = DWI
      I = I + 1
      ZOUT(I,LCA) = DT2
      I = I + 1
      ZOUT(I,LCA) = DF2
      I = I + 1
      ZOUT(I,LCA) = DW2
      I = I + 1
      ZOUT(I,LCA) = DTIP
      I = I + 1
      ZOUT(I,LCA) = DFIP
      I = I + 1
      ZOUT(I,LCA) = DWIP
      I = I + 1
      ZOUT(I,LCA) = DTEP
      I = I + 1
      ZOUT(I,LCA) = DFEP
```

```
      I = I + 1
      ZOUT(I,LCA) = DWEP
      I = I + 1
      ZOUT(I,LCA) = DQ1
      I = I + 1
      ZOUT(I,LCA) = DQ2
      I = I + 1
      ZOUT(I,LCA) = DQ1P
      I = I + 1
      ZOUT(I,LCA) = DQEP
      I = I + 1
      ZOUT(I,LCA) = DWORK
      LOUT( I,LCA) = NIT
      I = I + 1
      ZOUT(I,LCA) = VOL1
      I = I + 1
      ZOUT(I,LCA) = VOL2
      GO TO MSCA1
 5080 CONTINUE
      I = I + 1
      ZOUT(I,LCA) = WF1
      I = I + 1
      ZOUT(I,LCA) = WFA1
      I = I + 1
      ZOUT(I,LCA) = WFV1
      I = I + 1
      ZOUT(I,LCA) = WF1P
      I = I + 1
      ZOUT(I,LCA) = WFA1P
      I = I + 1
      ZOUT(I,LCA) = WFV1P
      I = I + 1
      ZOUT(I,LCA) = DVOL1
      I = I + 1
      ZOUT(I,LCA) = DVOL2
      GO TO 6000
 5110 CONTINUE
      LCA = CA + 0.1
      IF ( LCA - ICAHRS )  5210, 5410, 5310
 5210 IF ( LCA .NE. (LCA/NPR1*NPR1+1))  GO TO 6000
      WT   = W1
      WF   = 0.0
      VOLF = 0.0
      DQT  = DQ1
      GO TO 5510
 5310 IF ( LCA - ICAHRT )  5350, 5410, 5210
 5350 LL = LCA - ICAHRS
      IF ( LL .NE. (LL/NPR2*NPR2))  GO TO 6000
 5410 WT   = W1 + W2
      WF   = W2 / WT
      VOLF = VOL2 / VOL
      DQT  = DQ1 + DQ2
 5510 IPR = IPR + 1
      GO TO MCA1
```

```
C
C          OPEN CHAMBER DIESEL ENGINE
  5610     CONTINUE
           I = 1
           ZOUT(I,IPR) = CA
           I = I + 1
           ZOUT(I,IPR) = PI
           I = I + 1
           ZOUT(I,IPR) = TI
           I = I + 1
           ZOUT(I,IPR) = FI
           I = I + 1
           ZOUT(I,IPR) = WI
           I = I + 1
           ZOUT(I,IPR) = DWFII
           I = I + 1
           ZOUT(I,IPR) = DWORK / XJI
           I = I + 1
           ZOUT(I,IPR) = DQI
           I = I + 1
           ZOUT(I,IPR) = DWIV
           I = I + 1
           ZOUT(I,IPR) = DWEV
           GO TO 6000
C
C          PRE CHAMBER DIESEL ENGINE
  5710     CONTINUE
           GO TO 6000
C
C          SPARK IGNITION ENGINE
  5810     CONTINUE
           I = 1
           ZOUT(I,IPR) = CA
           I = I + 1
           ZOUT(I,IPR) = PI
           I = I + 1
           ZOUT(I,IPR) = TI
           I = I + 1
           ZOUT(I,IPR) = T2
           I = I + 1
           ZOUT(I,IPR) = WT
           I = I + 1
           ZOUT(I,IPR) = WF
           I = I + 1
           ZOUT(I,IPR) = VOLF
           I = I + 1
           ZOUT(I,IPR) = DQT
           I = I + 1
           ZOUT(I,IPR) = DWIV
           I = I + 1
           ZOUT(I,IPR) = DWEV
  6000     CONTINUE
           RETURN
```

```
      ENTRY  RATED1
C     OUTPUT AT EACH CRANK ANGLE
      XNIT = NIT
      WRITE(NFL,9510)  CA, P1, T1, F1, W1, P2, T2, F2, W2
 9510 FORMAT(2X,F6.1,2X,2(3X,F8.2,7X,F8.2,7X,F9.6,6X,E9.4,3X))
      WRITE(NFL,9510)  CA, PIP, TIP, FIP, WIP, PEP, TEP, FEP, WEP
      WRITE(NFL,9530)  CA, DWIV, DWEV, DW12, DWFI1, DWF12, DWI, DWE
 9530 FORMAT(2X,F6.1,2X,8(3X,E9.4,3X))
      WRITE(NFL,9550)  CA, DT1, DF1, DW1, DT2, DF2, DW2
 9550 FORMAT(2X,F6.1,2X,2(4X,F7.2,7X,E9.4,6X,E9.4,3X))
      WRITE(NFL,9550)  CA, DTIP, DFIP, DWIP, DTEP, DFEP, DWEP
      WRITE(NFL,9530)  CA, DQ1, DQ2, DQIP, DQEP, DWORK, XNIT,
     1                 VOL1,  VOL2
      WRITE(NFL,9530)  CA, WF1, WFA1, WFV1, WFIP, WFAIP, WFVIP,
     1                 DVOL1, DVOL2
      RETURN



      ENTRY  RATEOT
C     CALCULATE OUTPUT VARIABLES
C     MASS
      GO TO MSOT1
C
C     DIESEL ENGINE
 9110 CONTINUE
      YWFIV  = YWFIV  * FAS
      YWFB1  = YWFB1  * FAS
      YWF12  = YWF12  * FAS
      YWFI   = YWFI   * FAS
      YWFF1  = YWFF1  * FAS
      YWFF2  = YWFF2  * FAS
      YWFF   = YWFF1  + YWFF2
 9120 CONTINUE
      YWFEV  = YWFEV  * FAS
      YWFE   = YWFE   * FAS
      YWIV   = YWAIV + YWFIV
      YWEV   = YWAEV + YWFEV
      YWB1   = YWAB1 + YWFB1
      YW12   = YWA12 + YWF12
      YWI    = YWAI  + YWFI
      YWE    = YWAE  + YWFE
      YWIVH  = YWIV  * CONS1
      YWEVH  = YWEV  * CONS1
      YWB1H  = YWB1  * CONS1
      YW12H  = YW12  * CONS1
      YWIH   = YWI   * CONS1
      YWEH   = YWE   * CONS1
      YWFF1H = YWFF1 * CONS1
      YWFF2H = YWFF2 * CONS1
      GO TO MSOT2
C
```

```
C        DIESEL ENGINE
 9140    CONTINUE
         FAO    = YWFFI / YWIV
         EQO    = FAO   / FAS
         GO TO 9160
C
C        SPARK IGNITION ENGINE
 9150    CONTINUE
         EQO    = FI
         FAO    = FI * FAS
         YWFF   = YWAIV * CWFAV
 9160    CONTINUE
C
C        AVERAGE TEMPERATURES
         TMAVI  = YTMAVI / YWIV
         TAVI   =  YTAVI / 720.0
         TMAVE  = YTMAVE / YWEV
         TAVE   =  YTAVE / 720.0
C
C        MEAN EFFECTIVE PRESSURE AND HORSE POWER
         YWORKI = YWORK / (12.0*XJ)
         PMEP   = YWORKP / VS
         NIMEP  = YWORK  / VS
         IMEP   = NIMEP - PMEP
         RMEP   = 12.0 * XJ * YQF / VS
         RAMEP  = 10.0 + 0.0175*PMAXI + 0.01*RPM*STROKE/6.0
         BMEP   = NIMEP - RAMEP
         PHP    = YWORKP * RPM / (12.0*2.0*33000.0)
         NIHP   = PHP * NIMEP / PMEP
         IHP    = PHP *  IMEP / PMEP
         BHP    = PHP *  BMEP / PMEP
         RAHP   = PHP * RAMEP / PMEP
         XHP    = 100.0 * RAHP / BHP
         EFM    = 100.0 *  BHP / IHP
         EFV    = 100.0 * YWIV * 53.36 * 12.0 * TAMB / (PAMB*VS)
         EFITH  = 100.0 * IHP * 2.0 * 33000.0 / (YWFF*HVF*XJ*RPM)
         EFBTH  = EFITH * BHP / IHP
         ISFC   = YWFF * RPM * 30.0 / IHP
         BSFC   = ISFC * IHP / BHP
         RETURN



         ENTRY  RATEO2
C        OUTPUT AT THE END OF THE CYCLE(I)
         WRITE(NFL,9210)
 9210    FORMAT(15X,35HSUM OF MASS FLOW RATES DURING CYCLE//
     2          18X,3HAIR,3X,4X,3X,4HFUEL,2X,4X,8X,5HTOTAL/
     3          11X,3(4X,9HLBM/CYCLE),4X,2X,6HLBM/HR,1X,10X,
     4          9X,11HTEMPERATURE,9X,4X,5HDEG R/)
         WRITE(NFL,9220) YWAIV, YWFIV,  YWIV,  YWIVH,  TMAVI,
     2                   YWAEV, YWFEV,  YWEV,  YWEVH,   TAVI,
     3                   YWABI, YWFBI,  YWBI,  YWBIH,  TMAVE,
     4                   YWAI2, YWFI2,  YWI2,  YWI2H,   TAVE,
```

```
                 5                YWAI,  YWFI,   YWI,   YAIH,  DTCH,
                 6                YWAE,  YWFE,   YWE,   YWEH,  DTCS,
                 7                           YWFFI, YWFFI, YWFFIH,   D"C,
                 8                           YWFF2, YWFF2, YWFF2H,  DTAF
      9220       FORMAT(9H    I. V.,2X,    4(3X,E10.5),10X,
                 2      29H         MASS AVE  INTAKE TEMP,3X,F6.1/
                 3      9H    E. V.,2X,    4(3X,E10.5),10X,
                 4      29H              AVE  INTAKE TEMP,3X,F6.1/
                 5      9H   BLOWBY,2X,    4(3X,E10.5),10X,
                 6      29H         MASS AVE EXHAUST TEMP,3X,F6.1/
                 7      9H   THROAT,2X,    4(3X,E10.5),10X,
                 8      29H              AVE EXHAUST TEMP,3X,F6.1/
                 9      9H    I. P.,2X,    4(3X,E10.5),10X,
                 0      29HCOOLANT     TEMP RISE    HEAD,3X,F6.1/
                 1      9H    E. P.,2X,    4(3X,E10.5),10X,
                 2      29HCOOLANT     TEMP RISE  BARREL,3X,F6.1/
                 3      9H  FUEL(1),2X,13X,3(3X,E10.5),10X,
                 4      29HCOOLANT     TEMP RISE   TOTAL,3X,F6.1/
                 5      9H  FUEL(2),2X,13X,3(3X,E10.5),10X,
                 6      29HCOLING AIR TEMP RISE FRICTION,3X,F6.1)
                 RETURN



                 ENTRY  RATE03
C                OUTPUT AT THE END OF THE CYCLE(2)
                 WRITE(NFL,9310)
      9310       FORMAT(3X,29HSUM OF ENERGY FLOW RATES/20X,10H BTU/CYCLE/)
                 WRITE(NFL,9320) YEFIV, YEFEV, YEFBBI, YEFI2, YEFFI, YEFF2,
                 2                YEFI,  YEFE,YWORK)
      9320       FORMAT(15H    INLET VALVE,5X,E10.5/
                 2      15H  EXHAUST VALVE,5X,E10.5/
                 3      15H         BLOWBY,5X,E10.5/
                 4      15H         THROAT,5X,E10.5/
                 5      15H   FUEL INJ.(1),5X,E10.5/
                 6      15H   FUEL INJ.(2),5X,E10.5/
                 7      15H    INTAKE PORT,5X,E10.5/
                 8      15H   EXHAUST PORT,5X,E10.5/
                 9      15H     PISTON WORK,5X,E10.5)
                 RETURN



                 ENTRY  RATE04
C                OUTPUT AT THE END OF THE CYCLE(3)
                 WRITE(NFL,9410)
      9410       FORMAT(12X,11HHORSE POWER,11X,10X,7X,18HMEAN PRESSURE, PSI,7X,
                 2      12X,11X,12HEFFICIENCIES/)
                 WRITE(NFL,9420)  NIHP,   IHP, NIMEP,  IMEP,   EFM,   EFV,
                 2                BHP,   PHP,  BMEP,  PMEP, EFITH,  ISFC,
                 3                RAHP,   XHP, RAMEP,  RMEP, EFBTH,  BSFC
      9420       FORMAT(2X,8H    NIHP,3X,F5.2,10H       IHP,3X,F5.2,10X,
                 2      . 8H   NIMEP,2X,F6.2,8H    IMEP,2X,F6.2,12X,
                 3      10HMECHANICAL,3X,F5.2,12H  VOLUMETRIC,3X,F5.2/
```

```
     4          2X,8H      BHP,3X,F5.2,10H       PHP,3X,F5.2,10X,
     5            8H     BHEP,3X,F5.2,8H     PHEP,3X,F5.2,12X,
     6          10H I THERMAL,3X,F5.2,12H          ISFC,3X,F5.2/
     7          2X,8H     RAMP,3X,F5.2,10H  RAMP/BHP,3X,F5.2,10X,
     8            8H    RAMEP,3X,F5.2,8H     RMEP,3X,F5.2,12X,
     9          10H B THERMAL,3X,F5.2,12H          BSFC,3X,F5.2)
      WRITE(NFL,9440)
      WRITE(NFL,9440)
 9440 FORMAT(1H0)
      WRITE(NFL,9450) PMAX1, FA0, TMAX1, EQ0
 9450 FORMAT(18X,26HMAXIMUM     PRESSURE (1) = ,F8.2,4H PSI,12X,
     2          20H   FUEL/AIR RATIO = ,F7.5//26X,18HTEMPERATURE (1) = ,
     3          F8.2,2H R,14X,20HEQUIVALENCE RATIO = ,F7.5)
      GO TO MSP041
C
C     SYSTEM 2
 9470 WRITE(NFL,9480) PMAX2, TMAX2
 9480 FORMAT(/18X,26HMAXIMUM     PRESSURE (2) = ,F8.2,4H PSI//
     2          26X,18HTEMPERATURE (2) = ,F8.2,2H R)
 9500 CONTINUE
      RETURN



      ENTRY  RATE05
C     OUTPUT AT THE END OF THE CYCLE(4)
C     MASS AND ENERGY BALANCE
C     MASS
      YWI1    = YWIV + YWI2 + YWFF1
      YWO1    = -YWEV - YWB1
      DIW1    = YWI1 - YWO1
      YWI2    = YWFF2
      YWO2    = -YWI2
      DIW2    = YWI2 - YWO2
      YWIIP   = YWI
      YWOIP   = YWIV
      DIWIP   = YWIIP - YWOIP
      YWIEP   = -YWEV
      YWOEP   = -YWE
      DIWEP   = YWIEP - YWOEP
C
C     ENERGY
      GO TO ( 9740, 9740, 9720 ),  NENG
C
C     SPARK IGNITION ENGINE
 9720 YQ1     = YQ1 + YQ2
      YQ2     = 0.0
 9740 CONTINUE
      YEI1    = YEFIV + YEFI2 + YEFF1
      YEO1    = -YEFEV - YEFBB1 + YWORK1 - YQ1
      DIE1    = YEI1 - YEO1
      YEI2    = YEFF2
      YEO2    = -YEFI2 - YQ2
      DIE2    = YEI2 - YEO2
```

```
      YEIIP  = YEFI
      YEOIP  = YEFIV - YCIP
      DIEIP  = YEIIP - YEOIP
      YEIEP  = -YEFEV
      YEOEP  = -YEFE - YOEP
      DIEEP  = YEIEP - YEUEP
      WRITE(NFL,9760)  YWI1,  YWO1,  DIW1,  YEI1,  YEO1,  DIE1,
     1                 YWI2,  YWO2,  DIW2,  YEI2,  YEO2,  DIE2,
     2                 YWIIP, YWOIP, DIWIP, YEIIP, YEOIP, DIEIP,
     3                 YWIEP, YWOEP, DIWEP, YEIEP, YEOEP, DIEEP
 9760 FORMAT(20X,10HSYSTEM 1 -,        6(3X,E9.4,3X) /
     1       20X,10HSYSTEM 2 -,        6(3X,E9.4,3X) /
     3       16X,14HI. P. SYSTEM -,    6(3X,E9.4,3X) /
     3       16X,14HE. P. SYSTEM -,    6(3X,E9.4,3X) )
      RETURN
      END
```

```
@FOR,  I  SZ ENGINE.S6,.R6,.S6
                SUBROUTINE  MASS
                COMMON/REV   / NRUN, RPM, DCATS, VEPM, VS, ICYCLE, IDVS, ICA1,
          1                    ICA2, CAS
                COMMON/MASSI / PP1, TT1, FF1, RR1, GAMM1, HH1,
          1                    PP2, TT2, FF2, RR2, GAMM2, HH2, AREA
                COMMON/MASSO / II, DW, HUS, FUS
                DATA  GCDXJ / 0.04134625 /
C               MASS FLOW RATE CALCULATED FROM ORIFICE EQUATION.
C               CHECK THE DIRECTION OF FLOW.
 7510           IF ( PP1-PP2 )  7520, 7580, 7530
C
C               NEGATIVE MASS FLOW RATE.
 7520           PUS = PP2
                PDS = PP1
                TUS = TT2
                FUS = FF2
                RUS = RR2
                HUS = HH2
                GAMUS = GAMM2
                B = -1.0
                II = -1
                GO TO 7540
C
C               POSITIVE MASS FLOW RATE.
 7530           PUS = PP1
                PDS = PP2
                TUS = TT1
                FUS = FF1
                RUS = RR1
                HUS = HH1
                GAMUS = GAMM1
                B  = 1.0
                II =  1
 7540           B1 = PDS / PUS
                B2 = 1.0 / GAMUS
C
C               CHECK FOR CRITICAL FLOW.
                B3 = (2.0/(GAMUS+1.0)) ** (GAMUS/(GAMUS-1.0))
                IF ( B1 .GT. B3 )  GO TO 7550
C
C               CRITICAL FLOW
                B1 = B3
 7550           PHI = 2.0 / (1.0-B2) * (B1**(2.0*B2) - B1**(1.0+B2))
                DW = B * AREA * PUS * SQRT(PHI*GCDXJ/(RUS*TUS))/ DCATS
                GO TO 7600
C
C               ZERO MASS FLOW RATE.
 7580           DW  = 0.0
                HUS = 0.0
                FUS = 0.0
 7600           RETURN
                END
```

```
@FOR,  I  SZ ENGINE.S7,,R7,,S7
            SUBROUTINE  IVLUME
C           THIS PART OF THE SUBPROGRAM INITIALIZES THE VARIBLES.
C           GEOMETRICAL CONSTANTS
            COMMON/DEBUG / NENG, NOUT1, NVLDBG, NARDBG, NEGDBG, NAVDBG,
     1                     NHTDBG, NDRFLO, NDBRT, NDBSOL
            COMMON/REV   / NRUN, RPM, DCATS, VEPM, VSWEPT, ICYCLE, IDVS,
     1                     ICA1, ICA2, CAS
            COMMON/CA1   / CA, LERR
            COMMON/GEOMC / BORE, STROKE, CONRD, SCL, VLPCL, VLVCL, VOLP2,
     1                     COMRT, S, SRT
            COMMON/GEOM  / DMIP, DMEP, AIP, AEP, VIP, VEP, DIV, DEV, AIM,
     1                     APM, AH, AP
            COMMON/GEOMHG/ AH1, AH2, AP1, AP2, AS, AIVF, AEVF, AIVB, AEVB,
     1                     AIVP, AEVP
            COMMON/VOLL  / LSIC, VOL, DVOL, VELPT, VOL1, VOL2, DVOL1, DVOL2
            LOGICAL  LSIC
            AH     = AH1
            RADIUS = STROKE / 2.0
            SC     = 3.141592 * BORE
            OMEGA  = 6.283184 * RPM / 60.0
            ACCS   = SC * BORE / 4.0
            CNTRD  = CONRD / RADIUS
            VEPM   = RPM * STROKE / 30.0
            DCATS  = 6.0 * RPM
            VSWEPT = ACCS * STROKE
            VLSCL  = SCL * ACCS
            VOLCL  = VLPCL + VLVCL + VLSCL
C
C           COMPRESSION RATIO
            GO TO ( 100, 200, 300 ),  NENG
C
C           OPEN CHAMBER DIESEL ENGINE
  100       COMRT = (VSWEPT+VOLCL) / VOLCL
            ASSIGN 2050 TO MD1
            GO TO 900
C
C           PRE CHAMBER DIESEL ENGINE
  200       COMRT = (VSWEPT+VOLCL+VOL2) / (VOLCL+VOL2)
            ASSIGN 2050 TO MD1
            GO TO 900
C
C           SPARK IGNITION ENGINE
  300       COMRT = (VSWEPT+VOLCL) / VOLCL
            ASSIGN 2050 TO MD1
C
C           GENERATE THE SWITCH VARIABLES.
  900       GO TO ( 1000, 1010 ),  NVLDBG
  1000      ASSIGN 8000 TO MVLDBG
            GO TO 1050
  1010      ASSIGN 9000 TO MVLDBG
  1050      RETURN
```

```
              ENTRY  VOLUME
C             THIS SUBPROGRAM CALCULATES THE VOLUME OF TRAPPED GASES IN THE
C             ENGINE CYLINDER.
C             IT ALSO CALCULATES INSTANTANEOUS VELOCITY OF THE PISTON.
C             CONSTANT  PI         = 3.141592
C             CONSTANT  PI*2.0     = 6.283184
C             CONSTANT  PI/4.0     = 0.785398
C             CONSTANT  PI/180.0 = 0.0174532
              CAR = CA * 0.0174532
C
C             SR, CSR AND CS ARE DUMMY VARIABLES.
C             CNTRD STANDS FOR RATIO OF CONNECTING ROD TO CRANK RADIUS.
              SR  = SIN(CAR)
              CSR = COS(CAR)
              CS  = SQRT(1.0 - SR*SR/(CNTRD*CNTRD))
              S = RADIUS * (CNTRD*(1.0-CS) + 1.0 - CSR)
              B = SCL + S
              SRT = SCL / B
              DSCA = RADIUS * SR * (1.0+CSR/(CNTRD*CS)) * 0.0174532
              AS  = SC * S
              VOL = VOLCL + ACCS*S
              DVOL  = ACCS  * DSCA
              VELPT = DCATS * DSCA
              GO TO MDI
C
C             DIESEL ENGINE
       2050   VOL1  = VOL
              DVOL1 = DVOL
       2100   CONTINUE
              GO TO MVLDRG
C
C             DEBUG
       8000   PRINT 8010, CA, S, SRT, AS, VOL, DVOL, VELPT
       8010   FORMAT(/7H VOLUME,8X,7E15.5)
              PRINT 8020,  VOL1, VOL2, DVOL1, DVOL2
       8020   FORMAT(15X,7E15.5)
       9000   RETURN



              ENTRY  VOLS1
C             DIVIDE THE COMBUSTION CHAMBER IN TWO PARTS DURING COMBUSTION
C             IN S. I. ENGINE
              IF ( LSIC )  GO TO 4010
              ASSIGN 2050 TO MDI
              AP1 = AP
              AP2 = 0.0
              AH1 = AH
              AH2 = 0.0
              GO TO 4100
C
C             COMBUSTION
       4010   CONTINUE
```

```
      AH1 = AH * VOL1 / VOL
      AH2 = AH - AH1
      AP1 = AP * VOL1 / VOL
      AP2 = AP - AP1
      ASSIGN 2100 TO MD1
9100  RETURN
      END
```

```
@FOR,  I  SZ ENGINE.S8,.R8,.S8
              SUBROUTINE  IAREA
C             THIS PART OF THE SUBPROGRAM INITIALIZES THE VARIABLES FOR AREA
C             SUBROUTINE.
              COMMON/DEBUG / NENG, NOUTI, NVLDBG, NARDBG, NEGDBG, NAVDBG,
     1                       NHTDBG, NDBFLO, NDBRT, NDBSOL
              COMMON/REV   / NRUN, RPM, DCATS, VEPM, VS, ICYCLE, IDVS,
     1                       ICA1, ICA2, CAS
              COMMON/VALVE / YIVM, YEVM, YCIR, YCER, RALI, RALE, WIVT, WEVT,
     1                       SRSI, SRSE, SVTI, SVTE
              COMMON/CAI   / CA, LERR
              COMMON/CAVALV/ XAEVOR, XAEVO, XAEVC, XAEVCR, XAIVOR, XAIVO,
     1                       XAIVC, XAIVCR
              COMMON/FLOW  / LIV, LEV, AIV, AEV, CODIV, CODEV, CODIM, CODPM
              COMMON/TEMP  / TWH1, TAH2, TAP, TAS, TWIV, TWEV, TWIP, TWEP,
     1                       TCHO, TCSU, TOIL, TFUEL
              LOGICAL  LIV, LEV, LERR
C
C             CALCULATE THE CONSTANT PARAMETERS
              RPMC = RPM / 2.0
              SRI = 1.0 + SRSI / SVTI
              SRE = 1.0 + SRSE / SVTE
              PHIRI = 0.093 * WIVT * 1200.0 * 1200.0 / SVTI
              PHIRE = 0.093 * WEVT * 1200.0 * 1200.0 / SVTE
              PHIDI = 0.093 * WIVT *  RPMC  *  RPMC  / SVTI
              PHIDE = 0.093 * WEVT *  RPMC  *  RPMC  / SVTE
C
C             CHANGE THE ORIGIN OF CRANK ANGLE AXIS FOR THIS SUBROUTINE
              CAIVOR = XAIVOR - 360.0
              CAIVO  = XAIVO  - 360.0
              CAIVC  = XAIVC  + 360.0
              CAIVCR = XAIVCR + 360.0
              CAEVOR = XAEVOR - 360.0
              CAEVO  = XAEVO  - 360.0
              CAEVC  = XAEVC  + 360.0
              CAEVCR = XAEVCR + 360.0
C
C             GENERATE THE SWITCH VARIABLES.
              GO TO ( 5010, 5020 ),  NARDBG
 5010         ASSIGN 8000 TO MARDBG
              GO TO 5050
 5020         ASSIGN 9000 TO MARDBG
 5050         RETURN



              ENTRY  AREA
C             THIS SUBROUTINE CALCULATES THE EFFECTIVE FLOW AREA THROUGH
C             INTAKE AND EXHAUST VALVES .
C             REFERENCE - SS A SYMPOSIUM ON INTERNAL COMBUSTION ENGINE VALVESSS
C             THOMPSON PRODUCTS, INC.,  CHAPTER - SS POLYDYNE CAM DESIGN - IISS
C             PAGE 192 - 200 .
C             VALVE LIFT DATA ARE GIVEN AT ENGINE REFERENCE SPEED OF 2400 RPM.
C             THE PROGRAM FIRST FINDS THE CAM LIFT FROM GIVEN VALVE LIFT AT
```

```
C           REFERENCE SPEED AND THEN CALCULATES VALVE LIFT AT GIVEN SPEED.
C           ZERO CRANK ANGLE STARTS AT TDC OF EXPANSION STROKE.
C           Y IS ACTUAL LIFT OF VALVE.
C           YO IS EQUIVALENT CAM LIFT ON THE VALVE SIDE.
C           ZO IS ACTUAL CAM LIFT.
C           D2Y IS SECOND DERIVATIVE OF Y W. R. T. TIME.
C           INITIALIZE THE OUTPUT VARIABLES
            ZOI = 0.0
            ZOE = 0.0
            YI  = 0.0
            YE  = 0.0
            AIV = 0.0
            AEV = 0.0
            LIV = .FALSE.
            LEV = .FALSE.
C
C           CHANGE THE ORIGIN FOR CRANK ANGLE
            CAO = CA
            IF ( CA .GT. 360.0 )  GO TO 50
            CA = CAO + 360.0
            GO TO 80
 50         CA = CA - 360.0
 80         CONTINUE
            IF ( CA - CAEVOR )  7900, 220, 100
 100        IF ( CA - CAIVCR )  150, 520, 7900
 150        IF ( CA - CAEVO  )  220, 220, 180
 180        IF ( CA - (CAEVO+120.0) )  200, 200, 250
C
C           EXHAUST VALVE OPENING CAM LIFT
 200        CACEO = 1.0 - (CA-CAEVO) / 120.0
C
C           B IS DUMMY VARIABLE
            B = CACEO
            B2 = B * B
            B4 = B2*B2
            B6 = B2*B4
            B8 = B4*B4
            YRE = YEVM - 0.79072*B2 + B8*(0.395519 + B8*(-0.195219 + B8*
     1           (0.029582 - B8*0.002161)))
            D2Y = (-1.48144 + B6*(22.149064 + B8*(-34.852560 + B8*(16.329264
     1           - B8*2.142720)))) / 3600.0
            YOE = YCER + YRE*SRE + D2Y*PHIRE
            ZOE = YOE / RALE
            GO TO 240
C
C           EXHAUST VALVE OPENING RAMP
 220        ZOE = 0.00069 + (CA - CAEVOR)*0.0004
            YOE = ZOE * RALE
            D2Y = 0.0
C
C           EXHAUST VALVE OPENING LIFT , DYNAMIC
 240        YE = (YOE - YCED - PHIDE*D2Y) / SRE
C
C           EXHAUST VALVE OPENING EFFECTIVE AREA
```

```
      B = YE - 0.4575
      AEV = 1.18 - B*B*(((257.46*B + 253.05)*B + 86.741)*B + 17.009)
      LEV = .TRUE.
      IF ( AEV .GE. 0.0 )  GO TO 7900
      AEV = 0.0
      LEV = .FALSE.
      GO TO 7900
  250 IF ( CA - CAEVC )  300, 300, 270
  270 IF ( CA - CAEVCR ) 320, 320, 350
C
C     EXHAUST VALVE CLOSING CAM LIFT
  300 CACEC = (CA - CAEVO) / 120.0 - 1.0
C
C     B IS DUMMY VARIABLE
      B  = CACEC
      B2 = B * B
      B4 = B2*B2
      B6 = B2*B4
      B8 = B4*B4
      YRE = YEVM - 0.730081*B2 + B8*(0.387519 + B8*(-0.140077 + B8*
     1      (0.027400 - B4*0.001761)))
      D2Y =(-1.460162 + B6*(21.701064 + B8*(-33.618480 + B8*(15.124800
     1      - B8*1.7469121))) / 3600.0
      YOE = YCER + YRE*SRE + D2Y*PHIRE
      ZOE = YOE / RALE
      GO TO 340
C
C     EXHAUST VALE CLOSING RAMP
  320 ZOE = 0.00091 + (CAEVCR - CA) * 0.0004
      YOE = ZOE * RALE
      D2Y = 0.0
C
C     EXHAUST VALVE CLOSING LIFT , DYNAMIC
  340 YE = (YOE - YCED - PHIDE*D2Y) / SRE
C
C     EXHAUST VALVE CLOSING EFFECTIVE AREA
      B = YE - 0.4575
      AEV = 1.18 - B*B*(((257.46*B + 253.05)*B + 86.741)*B + 17.009)
      LEV = .TRUE.
      IF ( AEV .GE. 0.0 )  GO TO 350
      AEV = 0.0
      LEV = .FALSE.
  350 IF ( CA - CAIVOR )  7900, 420, 360
  360 IF ( CA - CAIVO  )  420, 420, 380
  380 IF ( CA - (CAIVO+120.0) )  400, 400, 450
C
C     INTAKE VALVE OPENING LIFT
  400 CACIO = 1.0 - (CA-CAIVO) / 120.0
C
C     B IS DUMMY VARIABLE
      B = CACIO
      B2 = B * B
      B4 = B2*B2
      B6 = B2*B4
```

```
      B8 = B4*B4
      YRI = YIVM - 0.753506*B2 + B8*(0.388047 + B8*(-0.128877 + B8*
     1      (0.019259 - B8*0.000076)))
      D2Y = (-1.507012 + B6*(21.730632 + B8*(-30.930480 + B8*(10.630968
     1      - B8*0.075392)))) / 3600.0
      YOI = YCIR + YRI*SPI + D2Y*PHIRI
      ZOI = YOI / RALI
      GO TO 440
C
C     INTAKE VALVE OPENING RAM
  420 ZOI = 0.0004575 + (CA-CAIVOR) * 0.0004575
      YOI = ZOI * RALI
      D2Y = 0.0
C
C     INTAKE VALVE OPENING LIFT , DYNAMIC
  440 YI = (YOI - YCID - PHIDI*D2Y) / SRI
C
C     INTAKE VALVE OPENING EFFECTIVE AREA
      B = YI - 0.475
      AIV = 1.30 + B*B*((((131.13*B + 165.68)*B + 63.162)*B + 0.91072)
      LIV = .TRUE.
      IF ( AIV .GE. 0.0 )  GO TO 7900
      AIV = 0.0
      LIV = .FALSE.
      GO TO 7900
  450 IF ( CA - CAIVC )  500, 500, 470
  470 IF ( CA - CAIVCR )  520, 520, 7500
C
C     INTAKE VALVE CLOSING CAM LIFT
  500 CACIC = (CA - CAIVO) / 120.0 - 1.0
C
C     B IS DUMMY VARIABLE
      B = CACIC
      B2 = B * B
      B4 = B2*B2
      B6 = B2*B4
      B8 = B4*B4
      YRI = YIVM - 0.739248*B2 + B8*(0.377103 + B8*(-0.121460 + B8*
     1      (0.015519 + B6*0.001086)))
      D2Y = (-1.478496 + B6*(21.117768 + B8*(-29.150400 + B8*(8.566488
     1      + B6*0.944820)))) / 3600.0
      YOI = YCIR + YRI*SRI + D2Y*PHIRI
      ZOI = YOI / RALI
      GO TO 540
C
C     INTAKE VALVE CLOSING RAMP
  520 ZOI = -0.0004575 + (CAIVCR-CA) * 0.0004575
      YOI = ZOI * RALI
      D2Y = 0.0
C
C     INTAKE VALVE CLOSING RAMP , DYNAMIC
  540 YI = (YOI - YCID - PHIDI * D2Y) / SRI
C
C     INTAKE VALVE CLOSING EFFECTIVE AREA
```

```
      B = YI - 0.475
      AIV = 1.30 + B*B*(((131.13*B + 165.68)*B + 63.162)*B + 0.91072)
      LIV = .TRUE.
      IF ( AIV .GE. 0.0 )  GO TO 7900
      AIV = 0.0
      LIV = .FALSE.
      GO TO 7900
C
C     ERROR
 7500 LERR = .TRUE.
      CA = CAO
      PRINT 7510,  CA
 7510 FORMAT(/5H AREA,10X,15HERROR IN LOGIC,,10X,5HCA = ,E15.5)
      GO TO 9000
 7900 CA = CAO
      GO TO HARDBG
C
C     DEBUG
 8000 PRINT 8110, CA, ZOI, YI, AIV, ZOE, YE, AEV
 8110 FORMAT(//5H AREA,10X,7E15.5)
 9000 RETURN



      ENTRY  IAREAC
C     INITIALIZE THE CYCLIC VARIABLES
      TEMP   = (TWIV+TWEV)/2.0 - 460.0
      VLASHI = (2700.0 - TEMP) / 20.0E4
      VLASHE = (2560.0 - TEMP) / 10.0E4
      YCID = 0.013 + VLASHI
      YCED = 0.020 + VLASHE
      RETURN
      END
```

```
@FOR, I  SZ ENGINE.S9,.R9,.S9
          SUBROUTINE  IENRGY
C         THIS PART OF THE SUBPROGRAM INITIALIZES THE SWITCH VARIABLE FOR
C         ENERGY SUBROUTINE.
          COMMON/DEBUG / NENG, NOUTI, NVLDBG, NARDBG, NEGDBG, NAVDBG,
     1                 NHTDBG, NDBFLO, NDBRT, NDBSOL
          COMMON/CON   / FAS, HVF, RA, RV, UAMB, HAMB, FIM, RIM, HIM, GAMIM
          COMMON/ENGY  / P, T, F, U, R, DUP, DUT, DUF, DRP, DRT, DRF, FAPC
          COMMON/CAI   / CA, LERR
          LOGICAL     LERR
C
C         GENERATE THE SWITCH VARIABLE.
          GO TO ( 5010, 5020 ), NEGDBG
 5010     ASSIGN 8000 TO NEGDBG
          GO TO 5050
 5020     ASSIGN 9000 TO NEGDBG
 5050     RETURN



          ENTRY  ENERGY
C        THIS SUBROUTINE CALCULATES THE PROPERTIES OF COMBUSTION MIXTURE ,
C        LEAN OR RICH.
C        UNITS
C        P (=) PSIA
C        T (=) R
C        U (=) BTU / LBM. MIXTURE
C        R (=) BTU / R LBM. MIXTURE
C        NOTE THAT REFERENCE TEMPERATURE IS 0 R
          J = 0
         IF ( F .LE. -1.0E-6)  GO TO 6000
          Z = 1.0 + FAS*F
         IF ( F - 1.0 )  100, 200, 250
C
C        PROPERTIES FOR LEAN MIXTURE
  100    IF ( T .LE. 2300.0 )  GO TO 130
C
C        U AND DU WITH DISSOCIATION FOR LEAN MIXTURE
         X=LOG(P)
         Y=1000./T                                                      DISC0005
         F2=F*F                                                         DISC0006
         F3=F2*F                                                        DISC0007
         A=(((6.3156E-17*T-9.3632E-13)*T+3.9016E-9)*T+5.1979E-6)*T      DISC0008
         A=(A+0.16528)*T                                                DISC0009
         B=1311.+(((-8.2022E-14*T+1.587E-9)*T-1.2605E-5)*T-1.3623E-2)*T DISC0010
         C1=10.41066+7.85125*F-3.71257*F3                               DISC0011
         C2=(-27.00107-28.5087*F+17.30375*F3)*Y                         DISC0012
         C3=(0.154226*F3-0.38656*F-0.10329+(.21289*F-.026574)*Y)*X      DISC0013
         DU=EXP(C1+C2+C3)                                               DISC0014
         U=(A-B*F+DU)/Z                                                 DISC0015
         DADT=(((3.1578E-16*T-3.74528E-12)*T+1.17048E-8)*T+1.03958E-5)*T DISC0016
         DADT=DADT+0.16528                                              DISC0017
         DBDT=-F*(((-3.28088E-13*T+4.761E-9)*T-2.521E-5)*T-.013623)     DISC0018
         DDUDT=-DU*(C2+X*Y*(.21289*F-.026574))/T                        DISC0019
```

```
      DUT=(DADT+DBDT+DDUDT)/Z                                          DISC0020
      DUP=DU*C3/(X*P*Z)                                                DISC0021
     0 DUDF=-B+DU*(7.85125+F2*(-11.13771+51.91125*Y+.462678*X)         DISC0022
     1 -(28.5387-.21289*X)*Y-.38656*X)                                 DISC0023
      DUF=(DUDF-.067623*U)/Z                                           DISC0024
      IF ( F .LE. 0.01 )  GO TO 130
C
C     R AND DR WITH DISSOCIATION AND F .GT. 0.01 FOR LEAN MIXTURE
      CR=F*(11.98-45.796*Y-.4354*X)+LOG(F)*0.2977
      DR=EXP(CR)/1000.                                                 DISC0027
      R=1.006+(.068146+.00476*F*DR)/Z                                  DISC0028
      DRT=46.0708*DR*F*Y/(T*Z)                                         DISC0029
      DRP=-.4380*DR*F/(P*Z)                                            DISC0030
      DDRF=DR*(11.98+0.2977/F-45.796*Y-.4354*X)                        DISC0031
      DRF=(1.006*(0.00476+DDRF)-R*.067623)/Z                           DISC0032
       GO TO 7900
C
C     R AND DR WITH NO DISSOCIATION AND DISSOCIATION WITH F .LE. 0.01
C     FOR LEAN MIXTURE
  130 R=(1.0685548+.004788*F)/Z
      DRT=0.0                                                          DISC0035
      DRP=0.0                                                          DISC0036
      DRF=(0.004788-.067623*R)/Z                                       DISC0037
       IF( T .GT. 2300.0 )  GO TO 7900
C
C     U AND DU WITH NO DISSOCIATION FOR LEAN MIXTURE
      A=(((6.3156E-17*T-9.3632E-13)*T+3.9016E-9)*T+5.1979E-6)*T        DI
      A=(A+0.16528)*T                                                  DISC0040
      B=1311.+(((-8.2022E-14*T+1.587E-9)*T-1.2605E-5)*T-1.3623E-2)*T   DISC0041
      U=(A-B*F)/Z                                                      DISC0042
      DADT=(((3.1578E-16*T-3.74528E-12)*T+1.17048E-8)*T+1.03958E-5)*T  DISC0043
      DADT=DADT+0.16528                                                DISC0044
      DBDT=-F*(((-3.28088E-13*T+4.761E-9)*T-2.521E-5)*T-.013623)       DISC0045
      DUT=(DADT+DBDT)/Z                                                DISC0046
      DUP=0.0                                                          DISC0047
      DUF=-(B+.067623*U)/Z                                             DISC0048
       GO TO 7900
C
C     PROPERTIES FOR STOICHIOMETRIC MIXTURE
C     CHECK FOR DUF TO BE CALCULATED FROM LEAN OR RICH SIDE.
  200 IF ( F .GE. FAPC )  GO TO 100
C
C     PROPERTIES FOR RICH MIXTURE
  250 IF ( F .GT. 1.2 )  GO TO 400
      IF ( T .GT. 2300.0 )  GO TO 320
C
C     PROPERTIES AT F = 1.0 WITH NO DISSOCIATION.
      X = LOG(P)
      Y = 1000./T
      FF  = F
      F   = 1.0
      F2  = 1.0
      F3 = 1.0
      A=(((6.3156E-17*T-9.3632E-13)*T+3.9016E-9)*T+5.1979E-6)*T        00013770
```

```
      A=(A+0.16528)*T
      B=1311.+(((-8.2022E-14*T+1.587E-9)*T-1.2605E-5)*T-1.3623E-2)*T
      C1=10.41066+7.85125*F-3.71257*F3
      C2=(-27.00107-28.5087*F+17.30375*F3)*Y
      C3=(0.154226*F3-0.38656*F-0.10329+(.21289*F-.026574)*Y)*X
      DU=EXP (C1+C2+C3)
      U10=(A-B*F+DU)/Z
      DADT=(((3.1578E-16*T-3.74528E-12)*T+1.17048E-8)*T+1.03958E-5)*T
      DADT=DADT+0.16528
      DBDT=-F*(((-3.28088E-13*T+4.761E-9)*T-2.521E-5)*T-.013623)
      DDUDT=-DU*(C2+X*Y*(.21289*F-.026574))/T
      DUT10=(DADT+DBDT+DDUDT)/Z
      DUP10=DU*C3/(X*P*Z)
      CR=F*(11.98-45.796*Y-.4354*X)+LOG (F)*0.2977
      DR=EXP (CR)/1000.
      R10=1.006*(.068146+.00476*F+DR)/Z
      DRT10=46.0708*DR*F*Y/(T*Z)
      DRP10=-.4380*DR*F/(P*Z)
      F = FF
      GO TO 330
C
C     PROPERTIES AT F = 1.0 WITH DISSOCIATION
  320 FBP = F
      F = 1.0
      R10=(.0685548+.004788*F)/Z
      DRT10=0.0
      DRP10=0.0
      A=(((6.3156E-17*T-9.3632E-13)*T+3.9016E-9)*T+5.1979E-6)*T
      A=(A+0.16528)*T
      B=1311.+(((-8.2022E-14*T+1.587E-9)*T-1.2605E-5)*T-1.3623E-2)*T
      U10=(A-B*F)/Z
      DADT=(((3.1578E-16*T-3.74528E-12)*T+1.17048E-8)*T+1.03958E-5)*T
      DADT=DADT+0.16528
      DBDT=-F*(((-3.28088E-13*T+4.761E-9)*T-2.521E-5)*T-.013623)
      DUT10=(DADT+DBDT)/Z
      DUP10=0.0
      F = FBP
  330 J = 1
      GO TO 440
  400 IF ( F .GT. 1.4 )  GO TO 420
      J = 2
      GO TO 440
  420 IF ( F .GT. 1.6 )  GO TO 6000
      J = 3
  440 IF ( T .GE. 3800.0 )  GO TO 1000
C
C     PROPERTIES FOR RICH MIXTURE WITH NO DISSOCIATION
      GO TO ( 510, 520, 600 ), J
C
C     CALCULATE NON DISSOCIATION PROPERTIES AT F = 1.1
  510 0 U11=((((.141725124E-14*T-.27466665E-10)*T+.2289123E-06)*T-.5660000
      1 33E-03)*T+12.605527)*T-33666.3123-.12199895*SQRT (T*T*T)+32266.359
      2 *(1./(1.+T/3000.))
      0 DUT11=(((.7086256E-14*T-.10986666E-9)*T+.68673693E-6)*T-.11320006E
```

```
            1  -02)*T+12.605527-.182998425*SQRT (T)-(32266.359/3000.)/(((1.+T/3000
            2  .)*(1.+T/3000.))
               DUP11=0.0
               R11=1.9869/(28.347   )
               DRT11=0.0
               DRP11=0.0
               U11=U11/Z
               DUT11=DUT11/Z
C
C              CALCULATE NON DISSOCIATION PROPERTIES AT F = 1.2
 520        0  U12=((((.803827123E-15*T-.155671825E-10)*T+.129282429E-6)*T-.2294
            1  98359E-03)*T+8.56112355)*T-22816.3174-.088101210*SQRT (T*T*T)+21475
            2  .1807*(1./(1.+T/3000.))
            0  DUT12=(((.40191356E-14*T-.62268732E-10)*T+.38784729E-6)*T-.4589967
            1  2E-3)*T+8.56112355-.132151815*SQRT (T)-21475.1807*(1./3000.)/(((1.+
            2  T/3000.)*(1.+T/3000.))
               DUP12=0.0
               R12=1.9869/(27.81838   )
               DRT12=0.0
               DRP12=0.0
               U12=U12/Z
               DUT12=DUT12/Z
               GO TO ( 530, 600, 6500) , J
 530           IF ( F .GT. 1.1 )  GO TO 550
C
C              LINEAR INTERPOLATION OF U AND DU BETWEEN 1.0 AND 1.1
 540           DF=F-1.0
               U=U10+(DF/.1)*(U11-U10)
               DUT=DUT10+(DF/.1)*(DUT11-DUT10)
               DUP=DUP10+(DF/.1)*(DUP11-DUP10)
               DUF = (U11 - U10 ) / 0.1
               GO TO 560
C
C              LINEAR INTERPOLATION OF U AND DU BETWEEN 1.1 AND 1.2
 550           DF=F-1.1
               U=U11+(DF/.1)*(U12-U11)
               DUT=DUT11+(DF/.1)*(DUT12-DUT11)
               DUP=0.0
               DUF = (U12 - U11) / 0.1
C
C              PARABOLIC INTERPOLATION OF R AND DR BETWEEN 1.0, 1.1 AND 1.2
 560        0  R=R10*(1.1-F)*(1.2-F)/.02+R11*(1.0-F)*(1.2-F)/(-.01)+R12*(1.0-F)*(
            1  1.1-F)/.02
            0  DRT=DRT10*(1.1-F)*(1.2-F)/.02+DRT11*(1.0-F)*(1.2-F)/(-.01)+DRT12*(
            1  1.0-F)*(1.1-F)/.02
            0  DRP=DRP10*(1.1-F)*(1.2-F)/.02+DRP11*(1.0-F)*(1.2-F)/(-.01)+DRP12*(
            1  1.0-F)*(1.1-F)/.02
               F2 = 2.0 * F
               DRF = R10 * (F2 - 2.3) / 0.02 + R11 * (F2 - 2.2) / (-0.01) +
            1  R12 * (F2 - 2.1) / 0.02
                GO TO 7900
C
C               CALCULATE NON DISSOCIATION PROPERTIES AT F = 1.4
 600        0  U14=((((.795724525E-15*T-.171752367E-10)*T+.15436898E-06)*T-.15855
```

```
          1  5481E-03)*T+12.6914415)*T-32997.4863-.13920633*SQRT (T*T*T)+31656.
          2  2603*(1./(1.+T/3000.))
          0  DUT14=(((.397862265E-14*T-.68700948E-10)*T+.4631697E-6)*T-.3171109
          1  6E-3)*T+12.6914415-.208809495*SQRT (T)-31656.2603*(1./3000.)/(((1.+
          2  T/3000.)*(1.+T/3000.))
             DUP14=0.0
             R14=1.9869/(26.8347775   )
             DRT14=0.0
             DRP14=0.0
             U14=U14/Z
             DUT14=DUT14/Z
             GO TO ( 6500, 610, 700 ), J
      C
      C      LINEAR INTERPOLATION OF PROPERTIES BETWEEN 1.2 AND 1.4
       610   DF=F-1.2
             U=U12+(DF/.2)*(U14-U12)
             DUT=DUT12+(DF/.2)*(DUT14-DUT12)
             DUP=0.0
             R=R12+(DF/.2)*(R14-R12)
             DRT=0.0
             DRP=0.0
             DUF = (U14 - U12) / 0.2
             DRF = (R14 - R12) / 0.2
              GO TO 7900
      C
      C      CALCULATE NON DISSOCIATION PROPERTIES AT F = 1.6
       700 0 U16=((((.676206952E-15*T-.156220752E-10)*T+.147422338E-06)*T-.7534
          1  29182E-04)*T+13.8039864)*T-35594.3825-.15522713*SQRT (T*T*T)+34292
          2  .2199*(1./(1.+T/3000.))
          0  DUT16=(((.338103475E-14*T-.624883E-10)*T+.44226702E-6)*T-.15068583
          1  6E-3)*T+13.8039864-.232840695*SQRT (T)-(34292.2199/3000.)/(((1.+T/3
          2  000.)*(1.+T/3000.))
             DUP16=0.0
             R16=1.9869/(25.940123   )
             DRT16=0.0
             DRP16=0.0
             U16=U16/Z
             DUT16=DUT16/Z
      C
      C      LINEAR INTERPOLATION OF PROPERTIES BETWEEN 1.4 AND 1.6
             DF=F-1.4
             U=U14+(DF/.2)*(U16-U14)
             DUT=DUT14+(DF/.2)*(DUT16-DUT14)
             DUP=0.0
             R=R14+(DF/.2)*(R16-R14)
             DRT=0.0
             DRP=0.0
             DUF = (U16 - U14) / 0.2
             DRF = (R16 - R14) / 0.2
              GO TO 7900
      C
      C      PROPERTIES FOR RICH MIXTURE WITH DISSOCIATION
      C
      1000   GO TO ( 1010, 1050, 1100 ), J
```

```
C
C           CALCULATE DISSOCIATION PROPERTIES AT F = 1.1
 1010  0    UB =((((.141725129E-14*T-.27466665E-10)*T+.2289123E-06)*T-.5660000
       1    33E-03)*T+12.605527)*T-33666.3123-.12199895*SQRT (T*T*T)+32266.359
       2    *(1./(1.+T/3000.))
            UA11 =((((6.6346E-10*T-3.1318E-8)*T-7.4922E-2)*T+3.6439E2)*T-
       1    4.0608E5)/(P**(1.0842-3.0849E-5*T))
            UC11=(((-2.1653E-6*T+6.7876E-3)*T+1.2846E2)*T-5.0418E5)/(P**((
       1    5.112E-9*T-1.7068E-4)*T+1.5636))
             U11 = (UA11 + UC11 + UB)/Z
       0    DUTB =(((.7086256E-14*T-.10986666E-9)*T+.68673693E-6)*T-.11320006E
       1    -02)*T+12.605527-.182998425*SQRT (T)-(32266.359/3000.)/((1.+T/3000
       2    .)*(1.+T/3000.))
            DUTA11 = (((2.65384E-9*T-9.3954E-8)*T-.149844)*T+3.6439E2)/(P**(
       1    1.0842-3.0849E-5*T))
            DUTC11  = ((-6.4959E-6*T+1.35752E-2)*T+1.2846E2)/(P**((5.112E-9*T-
       1    1.7068E-4)*T+1.5636))
            DUTB11 = 3.0849E-5*UA11*LOG (P)
            DUTD11  = -(1.0224E-6*T-1.7068E-4)*UC11*LOG (P)
            DUT11   = (DUTA11 + DUTB11 + DUTC11 + DUTD11 + DUTB)/Z
            DUP11   = -(UA11*(1.0842-3.0849E-5*T)+UC11*((5.112E-9*T-
       1    1.7068E-4)*T+1.5636))/(P*Z)
            WA11   = ((((1.2411E-11*T+1.4805E-7)*T-3.5636E-3)*T+16.990)*T-2.069
       1    7E4)/(P**(2.1345-1.9874E-4*T))
            WC11 = (((-4.6646E-8*T-3.0826E-6)*T+4.5919)*T-1.8074E4)/(P**((
       1    2.2661E-8*T-4.6987E-4)*T+2.8397))
            DWTA11 = (((4.9644E-11*T+4.4415E-7)*T-7.1272E-3)*T+16.990)/(P**(2.
       1    1345-1.9874E-4*T))
            DWTC11  = ((-1.39938E-7*T-6.1652E-6)*T+4.5919)/(P**((2.2661E-8*T
       1    -4.6987E-4)*T+2.8397))
            DWTB11  = 1.9874E-4*WA11*LOG (P)
            DWTD11 = -(4.5322E-8*T-4.6987E-4)*WC11*LOG (P)
            IF ( T .GT. 4200.0 )  GO TO 1030
            WB  = 28.347
            DWTB  = 0.
            GO TO 1040
 1030        WB = 26.6694-(9.513E-8*T-7.9898E-4)*T
             DWTB = -(1.9026E-7*T-7.9898E-4)
 1040        W11 = WB + WA11 + WC11
             R11 = 1.9698/W11
             DWT11 = DWTA11 + DWTB11 + DWTC11 + DWTD11 + DWTB
             DRT11 = -R11*DWT11/W11
             DRP11 = R11*(WA11*(2.1345-1.9874E-4*T)+WC11*((2.2661E-8*T-4.6987
       1    E-4)*T+2.8397))/(P*W11)
C
C           CALCULATE DISSOCIATION PROPERTIES AT F = 1.2
 1050  0    UB =((((.803827123E-15*T-.155671825E-10)*T+.129282429E-6)*T-.2294
       1    98359E-03)*T+8.56112355)*T-22816.3174-.08810121*SQRT (T*T*T)+21475
       2    .1807*(1./(1.+T/3000.))
             UA12 = ((((2.6823E-10*T+2.4449E-6)*T-6.9011E-2)*T+3.3230E2)*T-
       1    4.4494E5)/(P**(1.1101-1.7870E-5*T))
             UC12 = (((-9.7929E-7*T-2.1405E-5)*T+92.009)*T-3.1047E5)/(P**((
       1    -1.0530E-8*T-7.4656E-5)*T+1.5367))
             U12 = (UA12 + UC12 + UB)/Z
```

```
      0 DUTB =(((.40191356E-14*T-.62268732E-10)*T+.38784729E-6)*T-.4589967      12
      1 2E-3)*T+8.56112355-.132151815*SQRT (T)-21475.1807*(1./3000.)/(((1.+
      2 T/3000.)*(1.+T/3000.))
        DUTA12 = (((1.07292E-9*T+7.3347E-6)*T-.138022)*T+332.30)/(P**(
      1 1.1101-1.7870E-5*T))
        DUTC12 = ((-2.93787E-6*T-4.281E-5)*T+92.009)/(P**((-1.0530E-8*T-
      1 7.4656E-5)*T+1.5367))
        DUTB12 = 1.7870E-5*UA12*LOG (P)
        DUTD12 = (2.106E-8*T+7.4656E-5) * UC12*LOG (P)
        DUT12 = (DUTA12 + DUTB12 + DUTC12 + DUTD12 + DUTB)/Z
        DUP12 = -(UA12*(1.1101-1.787E-5*T) + UC12*((-1.053E-8*T-7.4656E-5
      1 )*T+1.5367))/(P*Z)
        WA12 = ((((1.4577E-11*T+1.4701E-7)*T-3.6044E-3)*T+16.804)*T-
      1 2.0232E4)/(P**(1.8252-1.2726E-4*T))
        WC12 = (((-5.0538E-8*T-1.6024E-5)*T+4.6218)*T-1.7161E4)/(P**((
      1 2.1759E-8*T-3.9490E-4)*T+2.5162))
        DWTA12 = (((5.8308E-11*T+4.4103E-7)*T-7.2088E-3)*T+16.804)/(P**(
      1 1.8252-1.2726E-4*T))
        DWTC12 = ((-1.51614E-7*T-3.2048E-5)*T+4.6218)/(P**((2.1759E-8*T
      1 -3.9490E-4)*T+2.5162))
        DWTB12 = 1.2726E-4*WA12*LOG (P)
        DWTD12 = -(4.3518E-8*T-3.9490E-4)*WC12 * LOG (P)
       IF( T .GT. 4000.0)  GO TO 1070
        WB = 27.81838
        DWTB = 0.
       GO TO 1080
 1070   WB = 31.1142-((4.0171E-11*T-5.207E-7)*T+2.264E-3)*T
        DWTB = -((1.20513E-10*T-1.0414E-6)*T+2.264E-3)
 1080   W12 = WB + WA12 + WC12
        R12 = 1.9698/W12
        DWT12 = DWTA12 + DWTB12 + DWTC12 + DWTD12 + DWTB
        DRT12 = -R12*DWT12/W12
        DRP12 = R12*(WA12*(1.8252-1.2726E-4*T)+WC12*((2.1759E-8*T-3.9490
      1 E-4)*T+2.5162))/(P*W12)
       GO TO ( 1090, 1100, 6500 ), J
C
C      PARABOLIC INTERPOLATION OF PROPERTIES BETWEEN 1.0, 1.1, 1.2
 1090  U = U10*(1.1-F)*(1.2-F)/.02+U11*(1.0-F)*(1.2-F)/(-.01)+U12*(1.0-F)
      1 *(1.1-F)/.02
       DUT = DUT10*(1.1-F)*(1.2-F)/.02+DUT11*(1.0-F)*(1.2-F)/(-.01)+DUT12
      1 *(1.0-F)*(1.1-F)/.02
       DUP = DUP10*(1.1-F)*(1.2-F)/.02+DUP11*(1.0-F)*(1.2-F)/(-.01)+DUP12
      1 *(1.0-F)*(1.1-F)/.02
       R = R10*(1.1-F)*(1.2-F)/.02+R11*(1.0-F)*(1.2-F)/(-.01)+R12*(1.0-F)
      1 *(1.1-F)/.02
       DRT = DRT10*(1.1-F)*(1.2-F)/.02+DRT11*(1.0-F)*(1.2-F)/(-.01)+DRT12
      1 *(1.0-F)*(1.1-F)/.02
       DRP = DRP10*(1.1-F)*(1.2-F)/.02+DRP11*(1.0-F)*(1.2-F)/(-.01)+DRP12
      1 *(1.0-F)*(1.1-F)/.02
       F2 = 2.0 * F
       DUF = U10 * (F2-2.3) /0.02 + U11 * (F2-2.2) / (-0.01) +
      1 U12 * (F2-2.1) / 0.02
       DRF = R10 * (F2-2.3) / 0.02 + R11 * (F2-2.2) / (-0.01) +
      1 R12 * (F2-2.1) / 0.02
```

```
              GO TO 7900
C
C             CALCULATE DISSOCIATION PROPERTIES AT F = 1.4
 1100  0      UB =((((.795724525E-15*T-.171752367E-10)*T+.15436898E-06)*T-.15855      14
       1      5481E-03)*T+12.6914415)*T-32997.4863-.13920633*SQRT (T*T*T)+31656.
       2      2603*(1./(1.+T/3000.))
               UA14 = ((((3.3249E-10*T+2.8381E-6)*T-7.1432E-2)*T+3.0542E2)*T
       1      -3.6229E5)/(P**(1.7999-1.2331E-4*T))
              UC14 = (((-9.5069E-7*T-7.4039E-4)*T+86.844)*T-2.5928E5)/(P**((
       1      -2.2418E-8*T-3.0134E-5)*T+1.7510))
               U14 = (UA14 + UC14 + UB)/Z
       0      DUTB =(((.397862265E-14*T-.68700948E-10)*T+.4631697E-6)*T-.3171109      14
       1      6E-3)*T+12.6914415-.208809495*SQRT (T)-31656.2603*(1./3000.)/(((1.+
       2      T/3000.)*(1.+T/3000.))
               DUTA14 = ((((1.32996E-9*T+8.5143E-6)*T-.142864)*T+3.0542E2)/(P**(
       1      1.7999-1.2331E-4*T))
               DUTC14 = ((-2.85207E-6*T-1.48078E-3)*T+86.844)  /(P**((-2.2418E-8
       1      *T-3.0134E-5)*T+1.7510))
               DUTB14 = 1.2331E-4*UA14*LOG (P)
               DUTD14 = (4.4836E-8*T+3.0134E-5)*UC14*LOG (P)
               DUT14 = (DUTA14 + DUTB14 + DUTC14 + DUTD14 + DUTB)/Z
               DUP14 = -(UA14*(1.7999-1.2331E-4*T)+UC14*((-2.2418E-8*T-3.0134E-5
       1      )*T+1.7510))/(P*Z)
               WA14 = (((((1.4714E-11*T+1.4428E-7)*T-3.6175E-3)*T+16.811)*T-2.000
       1      8E4)/(P**(1.8691-1.3785E-4*T))
               WC14 = (((-4.9096E-8*T-1.4143E-5)*T+4.6233)*T-1.7161E4)/(P**((
       1      2.1782E-8*T-4.0839E-4)*T+2.5668))
               DWTA14 = (((5.8856E-11*T+4.3284E-7)*T-7.2350E-3)*T+16.811)/(P**
       1      (1.8691-1.3785E-4*T))
               DWTC14 = ((-1.47288E-7*T-2.8286E-5)*T+4.6233)/(P**((2.1782E-8*T
       1      -4.0839E-4)*T+2.5668))
               DWTB14 = 1.3785E-4*WA14*LOG (P)
               DWTD14 = -(4.3564E-8*T-4.0839E-4)*WC14*LOG (P)
              IF ( T .GE. 4000.0 )  GO TO 1120
               WB = 26.8348
               DWTB = 0.
              GO TO 1130
 1120          WB = 26.4266-(2.3873E-8*T-1.9753E-4)*T
               DWTB = -(4.7746E-8*T-1.9753E-4)
 1130          W14 = WB + WA14 + WC14
               R14 = 1.9698/W14
               DWT14 = DWTA14 + DWTB14 + DWTC14 + DWTD14 + DWTB
               DRT14 = -R14*DWT14/W14
               DRP14 = R14*(WA14*(1.8691 - 1.3785E-4*T) + WC14*((2.1782E-8*T
       1      -4.0839E-4)*T+2.5668))/(P*W14)
              GO TO ( 6500, 1150, 1200 ), J
C
C             LINEAR INTERPOLATION OF PROPERTIES BETWEEN 1.2 AND 1.4
 1150         DF=F-1.2
              U=U12+(DF/.2)*(U14-U12)
              DUT=DUT12+(DF/.2)*(DUT14-DUT12)
              DUP=DUP12+(DF/.2)*(DUP14-DUP12)
              DRT=DRT12+(DF/.2)*(DRT14-DRT12)
              DRP=DRP12+(DF/.2)*(DRP14-DRP12)
```

```
      R=R12+(DF/.2)*(R14-R12)
      DUF = (U14 - U12) / 0.2
      DRF = (R14 - R12) / 0.2
       GO TO 7900
C
C     CALCULATE DISSOCIATION PROPERTIES AT F = 1.6
 1200 0 UB =((((.676206952E-15*T-.156220752E-10)*T+.147422338E-06)*T-.7534        16
     1 29182E-04)*T+13.8039864)*T-35594.3825-.15522713*SQRT (T*T*T)+34292
     2 .2199*(1./(1.+T/3000.))
       UA16 = ((((3.4285E-10*T+2.6522E-6)*T-7.1187E-2)*T+311.04)*T
     1 -3.7274E5)/ (P**(1.7916-1.2728E-4*T))
       UC16 = (((-8.8226E-7*T-8.0987E-4)*T+86.927)*T-2.6840E5)/(P**((
     1 -1.1712E-8*T-1.0942E-4)*T+1.8758))
       U16 = (UB + UA16 + UC16)/Z
     0 DUTB =(((.338103475E-14*T-.624883E-10)*T+.44226702E-6)*T-.15068583        16
     1 6E-3)*T+13.8039864-.232840695*SQRT (T)-(34292.2199/3000.)/(((1.+T/3
     2 000.)*(1.+T/3000.))
       DUTA16 = (((1.3714E-9*T+7.9566E-6)*T-0.142374)*T+311.04)/(P**(
     1 1.7916-1.2728E-4*T))
       DUTC16 = ((-2.64678E-6*T-1.61974E-3)*T+86.927)/(P**((-1.1712E-8*T
     1 -1.0942E-4)*T+1.8758))
       DUTB16 = 1.2728E-4*UA16*LOG (P)
       DUTD16 = (2.3424E-8*T+1.0942E-4)*UC16*LOG (P)
       DUT16 = (DUTA16+DUTB16 + DUTC16 + DUTD16 + DUTB)/Z
       DUP16 = -(UA16*(1.7916-1.2728E-4*T)+UC16*((-1.1712E-8*T-1.0942E-4
     1 )*T+1.8758))/(P*Z)
       WA16 = ((((1.4392E-11*T+1.4329E-7)*T-3.6177E-3)*T+16.846)*T-1.974
     1 3E4)/(P**(1.9931-1.5503E-4*T))
       WC16 = (((-4.7039E-8*T-1.3379E-5)*T+4.5915)*T-1.7328E4)/(P**((
     1 1.9631E-8*T-4.0518E-4)*T+2.6359))
       DWTA16 = (((5.7568E-11*T+4.2987E-7)*T-7.2354E-3)*T+16.846)/(P**(
     1 1.9931 - 1.5503E-4*T))
       DWTC16 = ((-1.41117E-7*T-2.6758E-5)*T+4.5915)/(P**((1.9631E-8*T
     1 -4.0518E-4)*T+2.6359))
       DWTB16 = 1.5503E-4*WA16*LOG (P)
       DWTD16 = -(3.9262E-8*T-4.0518E-4)*WC16*LOG (P)
      IF ( T .GE. 4200.0 )  GO TO 1220
       WB = 25.940123
       DWTB = 0.
      GO TO 1230
 1220  WB = 25.1063-((-4.5618E-12*T+8.6704E-8)*T-4.8221E-4)*T
       DWTB = -((-1.36854E-11*T+1.73408E-7)*T-4.8221E-4)
 1230  W16 = WB + WA16 + WC16
       R16 = 1.9698/W16
       DWT16 = DWTA16 + DWTC16 + DWTB16 + DWTD16 + DWTB
       DRT16 = -R16*DWT16/W16
       DRP16 = R16*(WA16*(1.9931-1.5503E-4*T)+WC16*((1.9631E-8*T-4.0518
     1 E-4)*T+2.6359))/(P*W16)
C
C      LINEAR INTERPOLATION OF PROPERTIES BETWEEN 1.4 AND 1.6
      DF=F-1.4
      U=U14+(DF/.2)*(U16-U14)
      DUT=DUT14+(DF/.2)*(DUT16-DUT14)
      DUP=DUP14+(DF/.2)*(DUP16-DUP14)
```

```
      R=R14+(DF/.2)*(R16-R14)
      DRT=DRT14+(DF/.2)*(DRT16-DRT14)
      DRP=DRP14+(DF/.2)*(DRP16-DRP14)
      DUF = (U16 - U14) / 0.2
      DRF = (R16 - R14) / 0.2
       GO TO 7900
C
C     ERROR
6000  PRINT 6010, F
6010   FORMAT(/7H ENERGY,8X,19HERROR IN EQ. RATIO.,7X,4HF = ,E15.5)
       LERR = .TRUE.
       GO TO 9000
6500  PRINT 6510, J
6510   FORMAT(/7H ENERGY,8X,15HERROR IN LOGIC.,11X,4HJ = ,I15)
       LERR = .TRUE.
       GO TO 9000
7900   GO TO MEGDRG
C
C     DEBUG
8000   PRINT 8010, J, P, T, F, U, R, DUP, DUT, DUF, DRP, DRT, DRF
8010   FORMAT(/7H ENERGY,8X,I15,5E15.5/15X,7E15.5)
9000   RETURN
       END
```

```
DFOR,  1  SZ ENGINE,SIO,,RIO,,SIO
           SUBROUTINE  IAVRGY
C          THIS PART OF THE SUBPROGRAM INITIALIZES THE VARIABLES.
           COMMON/DEBUG / NENG, NOUT1, NVLDBG, NARDBG, NEGDBG, NAVDBG,
     1                    NHTDBG, NDBFLO, NDBRT, NDBSOL
           COMMON/CON   / FAS, HVF, RA, RV, UAMB, HAMB, FIM, RIM, HIM, GAMIM
           COMMON/AVGY  / T, UA, DUAT, UV, DUVT, HV, DHVT
C
C          GENERATE THE SWITCH VARIABLES.
           GO TO ( 1000, 1010 ),  NAVDBG
 1000      ASSIGN 8000 TO MAVDBG
           GO TO 1050
 1010      ASSIGN 9000 TO MAVDBG
 1050      RETURN



           ENTRY  AVERGY
C          THIS SUBPROGRAM CALCULATES THE ABSOLUTE INTERNAL ENERGIES AND ITS
C          DERIVATIVE WITH TEMPERATURE FOR AIR AND FUEL VAPOR.
C          AIR--
           UA = ((((6.3156E-17*T - 9.3632E-13)*T + 3.9016E-9)*T + 5.1979E-6)
     1          *T + 0.16528)*T
           DUAT = (((3.15780E-16*T - 3.74528E-12)*T + 1.17048E-8)*T +
     1          1.03958E-5)*T + 0.16528
C
C          FUEL VAPOR --
C          ENTHALPY -
           HV = (((((2.4112E-15*T - 1.4220E-11)*T - 7.6185E-9)*T + 2.8321E-4)
     1          *T + 9.5767E-2)*T + 31.4188
           DHVT = ((((1.20560E-14*T - 5.6880E-11)*T - 2.28555E-8)*T +
     1          5.66420E-4)*T + 9.57670E-2
C
C          INTERNAL ENERGY -
           UV = HV - RV*T
           DUVT = DHVT - RV
           GO TO MAVDBG
C
C          DEBUG
 8000      PRINT 8010,  T, UA, DUAT, UV, DUVT, HV, DHVT
 8010      FORMAT(/7H AVERGY,8X,7E15.5)
 9000      RETURN
           END
```

```
 BFOR,  I  SZ ENGINE.SI1,.RI1,.SI1
            SUBROUTINE  IFLWCO
      C     THIS PART OF THE SUBPROGRAM INITIALIZES THE VARIABLES
      C     FOR SUBROUTINE FLOWCO.
            COMMON/DEBUG / NENG, NOUT1, NVLDBG, NARDBG, NEGDBG, NAVDBG,
     1                     NHTDBG, NDBFLO, NDBRT, NDBSOL
            COMMON/FLOW  / LIV, LEV, AIV, AEV, CODIV, CODEV, CODIM, CODPM
            COMMON/VAR   /  P1,  T1,  F1,  W1,  P2,  T2,  F2,  W2,
     1                     PIP, TIP, FIP, WIP, PEP, TEP, FEP, WEP, DPIP, DPEP
            CMIV = CODIV
            CMEV = CODEV
            CMIM = CODIM
            CMPM = CODPM
      C
      C     INITALIZE FOR OUTPUT
            CODIV = 0.0
            CODEV = 0.0
            CODIM = 0.0
            CODPM = 0.0
            GO TO ( 450, 500, 550 ),  NENG
      C
      C     OPEN CHAMBER ENGINE
       450  ASSIGN 4000 TO MSP1
            GO TO 600
      C
      C     PRE CHAMBER ENGINE
       500  ASSIGN 3000 TO MSP1
            GO TO 600
      C
      C     SPARK IGNITION ENGINE
       550  ASSIGN 2000 TO MSP1
      C
      C     DEBUG
       600  GO TO ( 900, 950 ),  NDBFLO
       900  ASSIGN 5100 TO MDBFLO
            GO TO 1000
       950  ASSIGN 6000 TO MDBFLO
      1000  RETURN



            ENTRY  FLOWCO
      C     FLOW COEFFICIENT FOR INLET VALVE
            CODIV = CMIV
      C
      C     FLOW COEFFICIENT FOR EXHAUST VALVE
            CODEV = CMEV
            GO TO MSP1
      C
      C     FLOW COEFFICIENT FOR INTAKE MANIFOLD ORIFICE
      2000  CODIM = CMIM
            GO TO 4000
      C
      C     FLOW COEFFICIENT FOR THROAT BETWEEN PRE CHAMBER AND MAIN CHAMBER
```

```
 3000 CODPM = CMPM
      X = ABS(P1-P2)
      CODPM = CMPM * (1.0 - EXP(-49.9*X)) ** 85587.0
 4000 GO TO MOBFLO
C
C     DEBUG
 5100 PRINT 5200,  CODIV, CODEV, CODIM, CODPM
 5200 FORMAT(/7H FLOWCO,8X,7E15.5)
 6000 RETURN
      END
```

```
@FOR,  I  SZ ENGINE.S12,.R12,.S12
          SUBROUTINE  IHEAT
C         THIS PART OF SUBPROGRAM INITIALIZES THE VALUES FOR HEAT TRANSFER
C         SUBROUTINE.
          COMMON/DEBUG / NENG, NOUT1, NVLDBG, NARDBG, NEGDBG, NAVDBG,
     1                   NHTDBG, NDRFLO, NDBRT, NDBSOL
          COMMON/REV   / NRUN, RPM, DCATS, VEPM, VS, ICYCLE, IDVS,
     1                   ICA1, ICA2, CAS
          COMMON/MAIN2 / NFL, NFLO1, NFLO2, NFLI1, TEXT, HTEXT
          COMMON/CON   / FAS, HVF, RA, RV, UAMB, HAMB, FIM, RIM, HIM, GAMIM
          COMMON/COND  / CONDH1, CONDH2, CONDP, CONDS, CONDIP, CONDEP,
     1                   CONDIV, CONDEV
          COMMON/CA1   / CA, LERR
          COMMON/CAD   / DCAL, DCAM, DCAN, DCA, DCA2, CAD, CAI, NIT, LCON
          COMMON/CAVALV/ CAEVOR, CAEVO, CAEVC, CAEVCR, CAIVOR, CAIVO,
     1                   CAIVC, CAIVCR
          COMMON/GEOMMP/ XM1, XM2, XPG1, XPIS, XPIC, XSGC, XIP, XEP,
     1                   XIVO, XIVC, XEVO, XEVC
          COMMON/GEOMC / BORE, STROKE, CONRD, SCL, VLPCL, VLVCL, VOLP2,
     1                   COMRT, S, SR
          COMMON/GEOM  / DMIP, DMEP, AIP, AEP, VIP, VEP, DIV, DEV, AIM,
     1                   APM, AH, AP
          COMMON/GEOMHG/ AH1, AH2, AP1, AP2, AS, AIVF, AEVF, AIVB, AEVB,
     1                   AIVP, AEVP
          COMMON/GEOMHC/ AH1C, AH2C, APC, APSC, ASC, ASBC, AIVC, AEVC,
     1                   AIPC, AEPC
          COMMON/VOLL  / LSIC, VOL, DVOL, VELPT, VOL1, VOL2, DVOL1, DVOL2
          COMMON/PROP  / CP1, R1S, R2
          COMMON/FLOW  / LIV, LEV, AIV, AEV, CODIV, CODEV, CODIM, CODPM
          COMMON/HR1   / NWEIBE, NHRDT, CAHRS, CAHRE
          COMMON/HR3   / CAW1, CAPHR1, WFCY1, WEIBE1, YWF11,
     1                   CAW2, CAPHR2, WFCY2, WEIBE2, YWF21
          COMMON/VAR   /  P1,  T1,  F1,  W1,  P2,  T2,  F2,  W2,
     1                   PIP, TIP, FIP, WIP, PEP, TEP, FEP, WEP, DPIP, DPEP
          COMMON/HEAT1 / NHTC1, NHTCAW, NHTR1, NHT2, NHTC2, NHTR2, NHTP
          COMMON/HTCM1 / COHCH1, COHCP1, COHCS, CHCIVF, CHCEVF,
     1                   COHRH1, COHRP1, COHRS, CHRIVF, CHREVF
          COMMON/HTCM2 / COHCH2, COHCP2, COHRH2, COHRP2
          COMMON/HTCMV / CHCIVB, CHCIP, CHCEVB, CHCEP, CHCEIB, CHCEIP,
     1                   CHCELB, CHCELP
          COMMON/HTC1  / COVJ, COHCA1, COHCA2, THCKR, TRTHC, PRRA, VOLR,
     1                   PR, TR, CAWSS, CAWSE, CAWCS, CAWCEE
          COMMON/HTC2  / CHCF11, CHCF12, CRA12, CRA13, PTANK, CAINJ,
     1                   EQRT, PRRP
          COMMON/HTC   / DWCOLM, DWCOLS, CWC1, CWC2, CWC3, CWCH1, CWCH2,
     1                   CWCS, CWCP, CWCHIV, CWCHEV, CWCHIP, CWCHEP
          COMMON/MISC1 / DWIV, DWEV, DQ1, DQ2, DQIP, DQEP, YQ1, YQ2, YQIP,
     1                   YQEP, YQFR, YWFF1, YWFF2, YTMAV1, YTAV1, YTMAVE,
     2                   YTAVE, DTCH, DTCS, DTC, DTAF, PMAX1, PMAX2,
     3                   TMAX1, TMAX2
          COMMON/MISC2 / CBB, COFRIC
          COMMON/TEMP  / TWH1, TWH2, TWP, TWS, TWIV, TWEV, TWIP, TWEP,
     1                   TCHO, TCSO, TOIL, TFUEL
          COMMON/TEMPP / TWH13, TWH23, TWP3, TWS3, TWIV3, TWEV3,
```

```
     1             TWH14, TWH24, TWP4, TWS4, TRIV4, TREV4
      DIMENSION  TEXT(80), HTEXT(15)
      LOGICAL  LIV, LEV, LFLOW, LSIC
      EQUIVALENCE ( YQF, YQFR )
      CONVER = 12.0 * 3600.0 * DCATS
C
C     CONSTANT FOR FRICTION
C     CONSTANT  9336.0 = 778.0 * 12.0
      COFR = COFRIC * VS / 9336.0
C
C     CONSTANT FOR COOLING WATER FLOW
      CODTH = RPM / (120.0*DWCOLH)
      CODTS = RPM / (120.0*DWCOLS)
C
C     CONSTANTS FOR COOLING HEAT TRANSFER COEFFICIENTS
      B      = RPM**0.6
      CWCOH = 0.514 * 0.157 * B * CWC1
      CWCOS = 0.514 * 0.270 * B * CWC2
      CWCOP = 0.0095 * B * CWC3
C
C     THERMAL RESISTANCES FOR WALL TEMPERATURES
C     UNITS OF RESISTANCES ARE  CA F / BTU
      R1   = CONVER * XH1  / (CONDH1*AH1C)
      R3   = CONVER * XPG1 / (CONDP *APC )
      R5   = CONVER * XP1C / (CONDP *APC )
      R6   = CONVER * XP1S / (CONDP *APSC)
      RP7H= CONVER * XSGC / (CONDS *ASC )
      R16 = CONVER * XIP  / (CONDIP*AIPC)
      R18 = CONVER * XEP  / (CONDEP*AEPC)
      R11 = (XIVO + (1.0-(CAIVC-CAIVO)/720.0)*XIVC) / DCATS
      R12 = (XEVO + (1.0-(CAEVC-CAEVO)/720.0)*XEVC) / DCATS
      R11    = 1.0 / R11
      R12    = 1.0 / R12
C
C     PISTON HEAT TRANSFER AREA
      AP1 = AP
      AP2 = 0.0
      GO TO ( 6410, 6420, 6430 ),  NENG
C
C     OPEN CHAMBER DIESEL ENGINE
 6410 CONTINUE
      ASSIGN 7430 TO MS31
      ASSIGN 7530 TO MS41
      ASSIGN 7300 TO MSP21
      ASSIGN 7330 TO MSP22
      ASSIGN 7400 TO MSP31
      ASSIGN 7450 TO MP41
      ASSIGN 7600 TO MP45
      GO TO 6500
C
C     PRE CHAMBER DIESEL ENGINE
 6420 CONTINUE
      ASSIGN 7430 TO MS31
      ASSIGN 7430 TO MS41
```

```
      ASSIGN 7240 TO MSP21
      ASSIGN 7320 TO MSP22
      ASSIGN 7300 TO MP21
      ASSIGN 7350 TO MSP31
      ASSIGN 7400 TO MP31
      ASSIGN 7410 TO MP41
      ASSIGN 7550 TO MP45
      R21 = CONVER * XH2  / (CONDH2*AH2C)
      GO TO 6500
C
C     SPARK IGNITION ENGINE
 6430 CONTINUE
      ASSIGN 7420 TO MS31
      ASSIGN 7520 TO MS41
      ASSIGN 7260 TO MP21
      ASSIGN 7380 TO MP31
      ASSIGN 7450 TO MP41
      ASSIGN 7600 TO MP45
C
C     GENERATE THE CONSTANTS AND SWITCH VARIABLES.
 6500 GO TO ( 6510, 6520, 6530, 6540 ),  NHTC1
C
C     ANNAND OR WOSCHNI CONVECTIVE CORRELATION
 6510 ASSIGN  100 TO MHTC1
      COVJ1 = COVJ * DCATS
      CHAW12 = (1.0-COHCA2) * 0.8
      CHAW13 = COHCA2
      CHAW11 = COHCA1 * (THCNR/(43200.0*BORE))**(1.0-COHCA2) /
     1 (DCATS * (TRTHC**CHAW12) * (PRRA**CHAW13) )
      GO TO 6600
C
C     EICHELBERG CONVECTIVE CORRELATION
 6520 ASSIGN  400 TO MHTC1
      CHCEC1 = CBRT(5.0*VEPM) / (3.6E7*DCATS)
      COCH1  = COHCH1 * CHCEC1
      COCS   = COHCS  * CHCEC1
      COCP1  = COHCP1 * CHCEC1
      COCIVF = CHCIVF * CHCEC1
      COCEVF = CHCEVF * CHCEC1
      HTEXT(1) = 6H  EICH
      HTEXT(2) = 6HELBERG
      GO TO 6650
C
C     PFLAUM CONVECTIVE CORRELATION
 6530 ASSIGN  500 TO MHTC1
      B  = (0.00254*VEPM)**2
      B1 = 6.2 - 5.2/(5.7**B) + 0.000635*B
      B2 = 0.322586E-3 * (CHCF11**0.25)
      B3 = 0.372742E-4 * (CHCF11**0.66)
      B4 = (CHCF12*6.06299/BORE) ** 0.25
      CHCF1  = B1 * B2 * B4 / (3600.0*DCATS)
      CHCF2  = B1 * B3 * B4 / (3600.0*DCATS)
      COCH1  * COHCH1 * CHCF1
      COCS   = COHCS  * CHCF2
```

```
      COCPI  = COHCPI * CHCFI
      COCIVF = CHCIVF * CHCFI
      COCEVF = CHCEVF * CHCFI
      HTEXT(1) = 6H  PFLA
      HTEXT(2) = 6HUM
      GO TO 6650
 6590 ASSIGN 1100 TO MHTCI
      GO TO 6650
 6600 GO TO ( 6610, 6620 ),  NHTCAW
C
C     ANNAND CONVECTIVE CORRELATION
 6610 ASSIGN  150 TO MHTCAW
      HTEXT(1) = 6H  ANNA
      HTEXT(2) = 6HND
      GO TO 6650
C
C     WOSCHNI CONVECTIVE CORRELATION
 6620 ASSIGN  180 TO MHTCAW
      CHCW11 = 6.18 * VEPM
      CHCW12 = 2.28 * VEPM
      CHCW13 = (3.24E-3*39.37/1.8) * (VS*TR/VOLR*PR)
      CHCW14 = PR * (VOLR**1.4)
      HTEXT(1) = 6H  WOSC
      HTEXT(2) = 6HHNI
 6650 GO TO ( 6660, 6670, 6680 ),  NHTRI
C
C     MODIFIED RADIATIVE CORRELATION
 6660 ASSIGN 1200 TO MHTRI
      CHRM11 = -4.0E4 * FAS
      CHRM12 = CRA12 * 0.1714 / (144.0*3.6E11*DCATS)
      CHRM13 = CHRM12 * CRA13 / CRA12
      HTEXT(7) = 6H  MODI
      HTEXT(8) = 6HFIED
      GO TO 6700
C
C     FLYNN RADIATIVE CORRELATION
 6670 ASSIGN 1300 TO MHTRI
      RRPM = RPM - 1995.0
      RPA = PTANK/0.491 - 59.8
      RINJ = -CAINJ - 20.0
      RF = EQRT - 0.459
      SQRAD = 27070.0 + 2.603*RRPM - 0.005893*RRPM*RRPM + 291.9*RPA -
     1        1.44*RPA*RPA + 401.1*RINJ + 4.620*RINJ*RINJ + 26270.0*RF-
     2        101200.0*RF*RF
      RAF = 0.3835 - 0.00008177*RRPM + 0.0000001592*RRPM*RRPM -
     1      0.002146*RPA + 0.0001565*RPA*RPA - 0.03017*RINJ +
     2      0.00009224*RINJ*RINJ - 0.5037*RF + 0.6062*RF*RF
      RBF = 21.54 - 0.01513*RRPM + 0.00003804*RRPM*RRPM - 0.8576*RPA +
     1      0.0454*RPA*RPA - 1.396*RINJ + 0.02164*RINJ*RINJ - 145.5*RF
     2      + 329.5*RF*RF
      RCAF = 349.7 + 0.004131*RRPM + 0.1992E-9*RRPM*RRPM - 0.1395*RPA +
     1       0.0001565*RPA*RPA - 0.5258*RINJ + 0.01022*RINJ*RINJ -
     2       8.309*RF + 3.345*RF*RF
      CHRF2 = RAF
```

```
            CHRF3 = RBF
            CHRF4 = RCAF
            CHRF5 = 1.0 + CHRF2
            CHRF1 = 2.0 * SQRAD * CHRF3 * CHRF5 / (144.0*60.0*RPM*360.0)
            HTEXT(7) = 6H FLYNN
            GO TO 6700
 6680       ASSIGN 2000 TO MHTR1
            HTEXT(7) = 6H  NONE
C
C           SYSTEM 2 FOR PRE CHAMBER DIESEL OR S. I. ENGINE
 6700       GO TO ( 6710, 6720 ),  NHT2
 6710       ASSIGN 2100 TO MHT2
            GO TO 6750
 6720       ASSIGN 4050 TO MHT2
            GO TO 6850
 6750       GO TO ( 6760, 6770 ),  NHTC2
C
C           EICHELBERG CONVECTIVE CORRELATION
 6760       ASSIGN 2150 TO MHTC2
            CHCEC1 = CBRT(5.0*VEPM) / (3.6E7*DCATS)
            COCH2 = COHCH2 * CHCEC1
            COCP2 = COHCP2 * CHCEC1
            GO TO 6800
 6770       ASSIGN 3050 TO MHTC2
 6800       GO TO ( 6810 ),  NHTR2
C
C           RADIATION HEAT TRANSFER FOR SYSTEM 2
 6810       ASSIGN 4000 TO MHTR2
 6850       GO TO ( 6860, 6870 ),  NHTP
C
C           PORT HEAT TRANSFER CALCULATIONS
 6860       ASSIGN 4100 TO MHTP
            CHCEC1 = CBRT(5.0*VEPM) / (3.6E7*DCATS)
            B      = 0.023 * 7.3 * (PRRP**0.4) / (DCATS**0.2)
            CHPFIB = B / (DIV**0.2)
            CHPFIP = B / ((DMIP**0.2) * (AIP**0.8))
            CHPFEB = B / (DEV**0.2)
            CHPFEP = B / ((DMEP**0.2) * (AEP**0.8))
            GO TO 6950
 6870       ASSIGN 6000 TO MHTP
 6950       GO TO ( 6960, 6970 ),  NHTDBG
 6960       ASSIGN 6100 TO MHTDBG
            GO TO 7000
 6970       ASSIGN 6200 TO MHTDBG
 7000       CONTINUE
            RETURN



            ENTRY  HEAT
C           THIS SUBPROGRAM CALCULATES INSTANTANEOUS VALUES OF HEAT TRANSFER
C           RATES AT A GIVEN CRANK ANGLE FOR VARIOUS BOUNDARY SURFACES.
C           HEAT TRANSFER RATES FOR SYSTEM 1 - OPEN COMBUSTION CHAMBER  OR
C           MAIN CHAMBER FOR PRE CHAMBER ENGINE  OR  UNBURNED PART FOR SPARK
```

```
C           IGNITION ENGINE,
C           HEAD, SLEEVE, PISTON, INLET VALVE FACE AND EXHAUST VALVE FACE.
C           CONVECTION PART =
            GO TO MHTC1
C
C           ANNAND OR WOSCHNI CORRELATION
C           CHECK IF THERE IS POSITIVE MASS FLOW FROM I. P. TO SYSTEM I
  100       IF ( DWIV .GT. 0.0 )  GO TO 110
C
C           NEGATIVE FLOW RATE
C           VEJI IS JET VELOCITY THROUGH INLET VALVE.
            VEJI = 0.0
            GO TO 120
C
C           POSITIVE FLOW RATE
  110       VEJI = COVJI * DWIV * SR * VOLI / (AIV*WI)
  120       GO TO MHTCAW
C
C           ANNAND CORRELATION
  150       VEAWI = VEJI + VEPM
            GO TO 280
C
C           WOSCHNI CORRELATION
  180       IF ( CA .GT. CAWSE  )  GO TO 190
C
C           SCAVENGING PERIOD
            BI = CHCWI1
            VECE = 0.0
            GO TO 250
  190       IF ( CA .GT. CAWCS  )  GO TO 200
C
C           BOUNDARY BETWEEN SCAVENGING AND COMPRESSION PERIODS.
            BI = CHCWI2 + (CHCWI1-CHCWI2) * (CAWCS -CA) / (CAWCS -CAWSE)
            VECE = 0.0
            GO TO 250
  200       IF( CA .GT. CAHRS )  GO TO 210
C
C           COMPRESSION PERIOD
            BI = CHCWI2
            VECE = 0.0
            GO TO 250
  210       IF ( CA .GT. CAWCEE )  GO TO 220
C
C           COMBUSTION AND EXPANSION PERIOD
            BI = CHCWI2
C
C           B IS DUMMY VARIABLE FOR ADIABATIC PRESSURE.
C           1.4 IS RATIO OF SPECIFIC HEATS FOR PURE AIR.
            B = CHCWI4 / (VOLI**1.4)
            VECE = CHCWI3 * (PI-B)
            GO TO 250
  220       IF ( CA .GT. CAWSS  )  GO TO 230
C
C           BOUNDARY BETWEEN EXPANSION AND SCAVENGING PERIODS.
```

```
      BI = CHCWI2 + (CHCWI1-CHCWI2) * (CA-CAWCEE) / (CAWSS-CAWCEE)
      VECE = 0.0
      GO TO 250
C
C     SCAVENGING PERIOD
  230 BI = CHCWI1
      VECE = 0.0
  250 VEAWI = BI + VECE + VEJI
  280 VEAWI = ABS(VEAWI)
      HCAWI = CHAWI1 * (TI**CHAWI2) * ((WI*CP)*VEAWI/VOLI))**CHAWI3)
      HCHI  = COHCHI * HCAWI
      HCS   = COHCS  * HCAWI
      HCPI  = COHCPI * HCAWI
      HCIVF = CHCIVF * HCAWI
      HCEVF = CHCEVF * HCAWI
      GO TO 1000
C
C     EICHELBERG CORRELATION
  400 B = SQRT(PI*TI)
      HCHI  = COCHI  * B
      HCS   = COCS   * B
      HCPI  = COCPI  * B
      HCIVF = COCIVF * B
      HCEVF = COCEVF * B
      GO TO 1000
C
C     PFLAUM CORRELATION
  500 B = SQRT(PI*TI)
      HCHI  = COCHI  * B
      HCS   = COCS   * B
      HCPI  = COCPI  * B
      HCIVF = COCIVF * B
      HCEVF = COCEVF * B
C
C     CALCULATE HEAT TRANSFER RATES OF EACH PART.
 1000 DQCHI  = HCHI  * AHI  * (TWHI-TI)
      DQCS   = HCS   * AS   * (TWS -TI)
      DQCPI  = HCPI  * API  * (TWP -TI)
      DQCIVF = HCIVF * AIVF * (TWIV-TI)
      DQCEVF = HCEVF * AEVF * (TWEV-TI)
 1100 GO TO MHTRI
C
C     RADIATION PART
C     MODIFIED CORRELATION
 1200 BI = CHRMI1 * WI * FI / VOLI
      B = CHRMI2 * (1.0-EXP(BI*(S+SCL)))
      HRHI  = COHRHI * B
      HRS   = COHRS  * CHRMI3 * (1.0-EXP(BI*BORE))
      HRPI  = COHRPI * B
      HRIVF = CHRIVF * B
      HREVF = CHREVF * B
C
C     GAS TEMPERATURE TAKEN AS POTENTIAL FOR RADIATION HEAT TRANSFER.
      B = TI * TI
```

```
      B = B  * B
      DQRHI  = HRHI  * AHI  * (TWHI4-B)
      DQRS   = HRS   * AS   * (TAS4 -B)
      DQRPI  = HRPI  * API  * (TWP4 -B)
      DQRIVF = HRIVF * AIVF * (TWIV4-B)
      DQREVF = HREVF * AEVF * (TWEV4-B)
      GO TO 2000
C
C     FLYNN CORRELATION
 1300 B1 = (CA-CHRF4) / 360.0
      B2 = 0.0
      IF ( B1 .LE. 0.0 )  GO TO 1320
      B2 = -CHRF1 * (B1**CHRF2) * EXP(-CHRF3*(B1**CHRF5))
 1320 B = T1 * T1
      B = B  * B
      HRHI   = COHRHI * B2 / (TWHI4-B)
      HRS    = COHRS  * B2 / (TWS4 -B)
      HRPI   = COHRPI * B2 / (TWP4 -B)
      HRIVF  = CHRIVF * B2 / (TWIV4-B)
      HREVF  = CHREVF * B2 / (TWEV4-B)
      DQRHI  = HRHI  * AHI  * (TWHI4-B)
      DQRS   = HRS   * AS   * (TWS4 -B)
      DQRPI  = HRPI  * API  * (TWP4 -B)
      DQRIVF = HRIVF * AIVF * (TWIV4-B)
      DQREVF = HREVF * AEVF * (TWEV4-B)
C
C     ADD CONVECTIVE AND RADIATIVE HEAT TRANSFER RATES FOR EACH PART.
 2000 DQHI  = DQCHI  + DQRHI
      DQS   = DQCS   + DQRS
      DQPI  = DQCPI  + DQRPI
      DQIVF = DQCIVF + DQRIVF
      DQEVF = DQCEVF + DQREVF
C
C     SUM THE HEAT TRANSFER RATES OF ALL THE INDIVIDUAL PARTS.
      DQC1 = DQCHI + DQCS + DQCPI + DQCIVF + DQCEVF
      DQR1 = DQRHI + DQRS + DQRPI + DQRIVF + DQREVF
      DQ1  = DQC1 + DQR1
      GO TO MHT2
C
C     HEAT TRANSFER RATES FOR SYSTEM2 - PRE CHAMBER FOR PRE CHAMBER
C     ENGINE  OR  BURNED PART FOR SPARK IGNITION.
C     PRE CHAMBER FOR PRE CHAMBER ENGINE  OR  HEAD AND PISTON FOR
C     SPARK IGNITION ENGINE.
C     CONVECTION PART
 2100 GO TO MHTC2
C
C     EICHELBERG CORRELATION.
 2150 B = SQRT(P2*T2)
      HCH2 = COCH2 * B
      HCP2 = COCP2 * B
      GO TO 3000
C
C     CALCULATE HEAT TRANSFER RATES OF EACH INDIVIDUAL PARTS.
 3000 DQCH2 = HCH2 * AH2 * (TWH2-T2)
```

```
           DQCP2 = HCP2 * AP2 * (TWP -T2)
      3050 GO TO MHTP2
C
C          RADIATION PART.
C
C          ADD CONVECTIVE AND RADIATIVE HEAT TRANSFER RATES FOR EACH PART.
      4000 DQH2 = DQCH2 + DQRH2
           DQP2 = DQCP2 + DQRP2
C
C          SUM THE HEAT TRANSFER RATES OF ALL INDIVIDUAL PARTS.
           DQ2 = DQH2 + DQP2
C
C          HEAT TRANSFER RATES FOR --  INTAKE PORT, EXHAUST PORT, INLET
C          VALVE BACK AND EXHAUST VALVE BACK  ---
      4050 GO TO MHTP
C
C          EICHELBERG AND PIPE FLOW CORRELATIONS
C          CALCULATE HEAT TRANSFER COEFFICIENT USING EICHELBERG CORRELATION
      4100 B  = TIP
           B3 = TEP
           HCECI = CHCECI * SQRT(PIP*B )
           HCECE = CHCECI * SQRT(PEP*B3)
           HCEIP = CHCEIP * HCECI
           HCEIB = CHCEIB * HCECI
           HCEEP = CHCEEP * HCECE
           HCEEB = CHCEEB * HCECE
C
C          CHECK THE DIRECTION OF FLOW IN THE INLET PORT.
           IF ( LIV ) GO TO 4110
C
C          INLET VALVE CLOSED
           HCIVB = HCEIB
           HCIP  = HCEIP
           B     = TIP
           TBIV  = TIP
           LFLOW = .TRUE.
           GO TO 4150
C
C          CALCULATE THE HEAT TRANSFER COEFFICIENT USING PIPE FLOW EQUATION
C          INLET VALVE OPEN
      4110 IF ( DWIV .GT. 0.0 )  GO TO 4130
      4120 B = TI
           TBIV = TI
           BI = -DWIV
           LFLOW = .TRUE.
           GO TO 4140
      4130 B  = TIP
           TBIV = TIP
           BI = DWIV
           LFLOW = .FALSE.
C
C          CALCULATE THE THERMAL CONDUCTIVITY , THCON, AND VISCOSITY,VIS.
      4140 THCON = 0.27324E-7 - (0.512E-13*B - 0.626E-9)*B
           VIS = 0.40277E-5 - (0.2032E-11*B - 0.172E-7)*B
```

```
      B2 = ((B1/VIS)**0.8) * THCON
      HCIVB = CHPFIB * B2 / (AIV**0.8)
      HCIP  = CHPFIP * B2
C
C     FIND THE GREATER HEAT TRANSFER COEFFICIENT OF THE TWO.
      IF( HCEIB .GT. HCIVB )  HCIVB = HCEIB
      IF( HCEIP .GT. HCIP  )  HCIP  = HCEIP
 4150 HCIVB = CHCIVB * HCIVB
      HCIP  = CHCIP  * HCIP
      DQIVB = HCIVB * AIVB * (TWIV-B  )
      DQIPA = HCIP  * AIVP * (TWIP-TIP)
      IF ( LFLOW )  GO TO 4155
      DQCI = DQCI - DQCIVF
      DQCIVF = HCIVF * AIVF * (TWIV-TIP)
      DQCI = DQCI + DQCIVF
      DQCI = DQCI + DQIVB
      DQI  = DQCI + DQRI
      DQIP = DQIPA
      GO TO 4160
 4155 DQIP = DQIPA + DQIVB
C
C     CHECK THE DIRECTION OF FLOW IN THE EXHAUST PORT.
 4160 CONTINUE
      IF ( LEV )  GO TO 4170
C
C     EXHAUST VALVE CLOSED
      HCEVB = HCEEB
      HCEP  = HCEEP
      B3    = TEP
      TBEV  = TEP
      LFLOW = .TRUE.
      GO TO 4210
C
C     CALCULATE THE HEAT TRANSFER COEFFICIENT USING PIPE FLOW EQUATION.
C     EXHAUST VALVE OPEN
 4170 IF ( DWEV .GT. 0.0 )  GO TO 4190
 4180 B3 = TI
      TBEV = TI
      B1 = -DWEV
      LFLOW = .TRUE.
      GO TO 4200
 4190 B3 = TEP
      TBEV = TEP
      B1 = DWEV
      LFLOW = .FALSE.
C
C     CALCULATE THERMAL CONDUCTIVITY , THCON, AND VISCOSITY, VIS.
 4200 THCON = 0.27324E-7 - (0.512E-13*B3 - 0.626E-9)*B3
      VIS = 0.40277E-5 * (0.2032E-11*B3 - 0.172E-7)*B3
      B2 = ((B1/VIS)**0.8) * THCON
      HCEVB = CHPFEB * B2 / (AEV**0.8)
      HCEP  = CHPFEP * B2
C
C     FIND THE GREATER HEAT TRANSFER COEFFICIENT OF THE TWO
```

```
       IF( HCEEB .GT. HCEVB )  HCEVB = HCEEB
       IF( HCEEP .GT. HCEP  )  HCEP  = HCEEP
 4210  HCEVB = CHCEVB * HCEVB
       HCEP  = CHCEP  * HCEP
       DQEVB = HCEVB * AEVB * (TWEV-B3 )
       DQEPW = HCEP  * AEVP * (TWEV-TEP)
       IF( LFLOW )  GO TO 5810
       DQCI = DQCI + DQEVB
       DQI  = DQCI + DQRI
       DQEP = DQEPW
       GO TO 6000
 5810  DQEP = DQEPW + DQEVB
 6000  CONTINUE
       GO TO MHTDRG
C
C      DEBUG
 6100  PRINT 6150, HCH1, HCS, HCP1, HCIVF, HCEVF, HCH2, HCP2,
     1                 HRH1, HRS, HRP1, HRIVF, HREVF, HRH2, HRP2
 6150  FORMAT(/5H HEAT,10X,7E15.5/15X,7E15.5)
       PRINT 6160, DQCH1, DQCS, DQCP1, DQCIVF, DQCEVF, DQCH2, DQCP2
       PRINT 6160, DQRH1, DQRS, DQRP1, DQRIVF, DQREVF, DQRH2, DQRP2
       PRINT 6160, DQH1, DQS, DQP1, DQIVF, DQEVF, DQH2, DQP2
       PRINT 6160, HCIVB, HCIP, HCEVB, HCEP
       PRINT 6160, DQIVB, DQIPW, DQEVB, DQEPW
       PRINT 6160, DQ1, DQ2, DQIP, DQEP
 6160  FORMAT(15X,7E15.5)
 6200  RETURN



       ENTRY  IHEATC
C      INITIALIZE THE OUTPUT VARIABLES.
       HCH1   = 0.0
       HCS    = 0.0
       HCP1   = 0.0
       HCIVF  = 0.0
       HCEVF  = 0.0
       HCH2   = 0.0
       HCP2   = 0.0
       HRH1   = 0.0
       HRS    = 0.0
       HRP1   = 0.0
       HRIVF  = 0.0
       HREVF  = 0.0
       HRH2   = 0.0
       HRP2   = 0.0
       DQCH1  = 0.0
       DQCS   = 0.0
       DQCP1  = 0.0
       DQCIVF = 0.0
       DQCEVF = 0.0
       DQCH2  = 0.0
       DQCP2  = 0.0
       DQRH1  = 0.0
```

```
      DQRS   = 0.0
      DQRP1  = 0.0
      DQRIVF = 0.0
      DQREVF = 0.0
      DQRH2  = 0.0
      DQRP2  = 0.0
      DQH1   = 0.0
      DQS    = 0.0
      DQP1   = 0.0
      DQIVF  = 0.0
      DQEVF  = 0.0
      DQH2   = 0.0
      DQP2   = 0.0
      HCIVB  = 0.0
      HCIP   = 0.0
      HCEVB  = 0.0
      HCEP   = 0.0
      DQIVB  = 0.0
      DQIPW  = 0.0
      DQEVB  = 0.0
      DQEPW  = 0.0
      DQC1   = 0.0
      DQR1   = 0.0
      DQ1    = 0.0
      DQ2    = 0.0
      DQIP   = 0.0
      DQEP   = 0.0
C
C     INITIALIZES THE CYCLIC VARIABLES
C     SYSTEM 1
      YQCH1  = 0.0
      YQCS   = 0.0
      YQCP1  = 0.0
      YQCIVF = 0.0
      YQCEVF = 0.0
      YQRH1  = 0.0
      YQRS   = 0.0
      YQRP1  = 0.0
      YQRIVF = 0.0
      YQREVF = 0.0
      YQC1   = 0.0
      YQR1   = 0.0
      YHTH1  = 0.0
      YHH1   = 0.0
      YHTS   = 0.0
      YHS    = 0.0
      YHTP1  = 0.0
      YHP1   = 0.0
      YHTIVF = 0.0
      YHIVF  = 0.0
      YHTEVF = 0.0
      YHEVF  = 0.0
      YQCP2  = 0.0
      YQRP2  = 0.0
```

```
                YQH2   = 0.0
      C
      C         INTAKE PORT SYSTEM
                YQIVB  = 0.0
                YQIPW  = 0.0
                YQIP   = 0.0
                YHTIVB = 0.0
                YHIVB  = 0.0
                YHTIPW = 0.0
                YHIPW  = 0.0
      C
      C         EXHAUST PORT SYSTEM
                YQEVB  = 0.0
                YQEPW  = 0.0
                YQEP   = 0.0
                YHTEVB = 0.0
                YHEVB  = 0.0
                YHTEPW = 0.0
                YHEPW  = 0.0
      C
      C         SYSTEM 2
       7050     YQCH2  = 0.0
                YQRH2  = 0.0
                YQCP2  = 0.0
                YQRP2  = 0.0
                YHTH2  = 0.0
                YHH2   = 0.0
                YHTP2  = 0.0
                YHP2   = 0.0
       7100     CONTINUE
                YTHAVI = 0.0
                YTAVI  = 0.0
                YTHAVE = 0.0
                YTAVE  = 0.0
                PMAX1  = 0.0
                TMAX1  = 0.0
                PMAX2  = 0.0
                TMAX2  = 0.0
                RETURN



                ENTRY  HEATSI
      C         COMBUSTION IN S. I. ENGINE
                IF ( LSIC )  GO TO 7150
      C
      C         NO COMBUSTION
                ASSIGN 4050 TO MHT2
                ASSIGN 7300 TO MSP21
                ASSIGN 7330 TO MSP22
                ASSIGN 7400 TO MSP31
                GO TO 7200
      C
      C         COMBUSTION
```

```
C           WALL TEMPERATURE CALCULATIONS
            HTIVB  = HCIVB * TBIV
            HIVB   = HCIVB
            HTIPW  = HCIP  * TIP
            HIPW   = HCIP
            YHTIVB = YHTIVB + (HTIVB+HTIVBO) * DCA2
            YHIVB  = YHIVB  + (HIVB +HIVBO ) * DCA2
            YHTIPW = YHTIPW + (HTIPW+HTIPWO) * DCA2
            YHIPW  = YHIPW  + (HIPW +HIPWO ) * DCA2
C
C           EXHAUST PORT SYSTEM
C           HEAT TRANSFER
            YQEVB  = YQEVB  + (DQEVBO+DQEVB ) * DCA2
            YQEPW  = YQEPW  + (DQEPWO+DQEPW ) * DCA2
            YQEP   = YQEP   + (DQEPO +DQEP  ) * DCA2
C
C           WALL TEMPERATURE CALCULATIONS
            HTEVB  = HCEVB * TBEV
            HEVB   = HCEVB
            HTEPW  = HCEP  * TEP
            HEPW   = HCEP
            YHTEVB = YHTEVB + (HTEVB+HTEVBO) * DCA2
            YHEVB  = YHEVB  + (HEVB +HEVBO ) * DCA2
            YHTEPW = YHTEPW + (HTEPW+HTEPWO) * DCA2
            YHEPW  = YHEPW  + (HEPW +HEPWO ) * DCA2
            GO TO MSP21
C
C           SYSTEM 2
C           PRE CHAMBER DIESEL ENGINE
C           HEAT TRANSFER
 7240       YQCH2  = YQCH2  + (DQCH2O+DQCH2 ) * DCA2
            YQRH2  = YQRH2  + (DQRH2O+DQRH2 ) * DCA2
C
C           WALL TEMPERATURE CALCULATIONS
            HTH2   = (HCH2+HRH2*T2*T2*T2) * T2 * AH2
            HH2    = (HCH2+HRH2*TWH23) * AH2
            YHTH2  = YHTH2 + (HTH2+HTH2O) * DCA2
            YHH2   = YHH2 + (HH2+HH2O) * DCA2
            GO TO MP21
C
C           SPARK IGNITION ENGINE
C           HEAT TRANSFER
 7260       CONTINUE
            YQCP2  = YQCP2  + (DQCP2O+DQCP2 ) * DCA2
            YQRP2  = YQRP2  + (DQRP2O+DQRP2 ) * DCA2
C
C           WALL TEMPERATURE CALCULATIONS
            HTP2   = (HCP2+HRP2*T2*T2*T2) * T2 * AP2
            HP2    = (HCP2+HRP2*TWP3) * AP2
            YHTP2  = YHTP2 + (HTP2+HTP2O) * DCA2
            YHP2   = YHP2 + (HP2+HP2O) * DCA2
C
C           AVERAGE TEMPERATURES
 7300       YTMAVI = YTMAVI + (DTMAIO+DWIV*TIP) * DCA2
```

```
 7150      ASSIGN 2100 TO MHT2
           ASSIGN 7240 TO MSP21
           ASSIGN 7320 TO MSP22
           ASSIGN 7350 TO MSP31
 7200      RETURN



           ENTRY  HEAT1
C          CALCULATE THE ACCUMULATED SUM.
C          SYSTEM 1
C          HEAT TRANSFER
           YQCH1  = YQCH1  + (DQCH1O+DQCH1 ) * DCA2
           YQCS   = YQCS   + (DQCSO +DQCS  ) * DCA2
           YQCP1  = YQCP1  + (DQCP1O+DQCP1 ) * DCA2
           YQCIVF = YQCIVF + (DQCIFO+DQCIVF) * DCA2
           YQCEVF = YQCEVF + (DQCEFO+DQCEVF) * DCA2
           YQRH1  = YQRH1  + (DQRH1O+DQRH1 ) * DCA2
           YQRS   = YQRS   + (DQRSO +DQRS  ) * DCA2
           YQRP1  = YQRP1  + (DQRP1O+DQRP1 ) * DCA2
           YQRIVF = YQRIVF + (DQRIFO+DQRIVF) * DCA2
           YQREVF = YQREVF + (DQREFO+DQREVF) * DCA2
           YQC1   = YQC1   + (DQC1O +DQC1  ) * DCA2
           YQR1   = YQR1   + (DQR1O +DQR1  ) * DCA2
C
C          WALL TEMPERATURE CALCULATIONS
           T13    = T1 * T1 * T1
           HTH1   = (HCH1+HRH1*T13) * T1 * AH1
           HH1    = (HCH1+HRH1*TWH13) * AH1
           HTS    = (HCS +HRS *T13) * T1 * AS
           HS     = (HCS +HRS *TWS3) * AS
           HTP1   = (HCP1+HRP1*T13) * T1 * AP1
           HP1    = (HCP1+HRP1*TWP3) * AP1
           HTIVF  = (HCIVF+HRIVF*T13) * T1
           HIVF   = (HCIVF+HRIVF*TWIV3)
           HTEVF  = (HCEVF+HREVF*T13) * T1
           HEVF   = (HCEVF+HREVF*TWEV3)
           YHTH1  = YHTH1 + (HTH1+HTH1O) * DCA2
           YHH1   = YHH1  + (HH1 +HH1O ) * DCA2
           YHTS   = YHTS  + (HTS +HTSO ) * DCA2
           YHS    = YHS   + (HS  +HSO  ) * DCA2
           YHTP1  = YHTP1 + (HTP1+HTP1O) * DCA2
           YHP1   = YHP1  + (HP1 +HP1O ) * DCA2
           YHTIVF = YHTIVF + (HTIVF+HTIVFO) * DCA2
           YHIVF  = YHIVF  + (HIVF +HIVFO ) * DCA2
           YHTEVF = YHTEVF + (HTEVF+HTEVFO) * DCA2
           YHEVF  = YHEVF  + (HEVF +HEVFO ) * DCA2
C
C          INTAKE PORT SYSTEM
C          HEAT TRANSFER
           YQIVB  = YQIVB  + (DQIVBO+DQIVB ) * DCA2
           YQIPW  = YQIPW  + (DQIPWO+DQIPW ) * DCA2
           YQIP   = YQIP   + (DQIPO +DQIP  ) * DCA2
C
```

```
      YTAVI  = YTAVI  + (TIPO  +TIP    ) * DCA2
      YTMAVE = YTMAVE + (DTMAEO+DMEV*TEP) * DCA2
      YTAVE  = YTAVE  + (TEPO  +TEP    ) * DCA2
C
C     CALCULATE MAXIMUM PRESSURE AND TEMPERATURE
C     SYSTEM 1
      IF ( P1 .GT. PMAX1 )  PMAX1 = P1
      IF ( T1 .GT. TMAX1 )  TMAX1 = T1
      GO TO MSP22
C
C     SYSTEM 2
 7120 IF ( P2 .GT. PMAX2 )  PMAX2 = P2
      IF ( T2 .GT. TMAX2 )  TMAX2 = T2
 7130 CONTINUE


      ENTRY  HEAT2
C     STORE THE VARIABLES FOR ACCUMULATED SUM.
C     SYSTEM 1
      DQCHIO = DQCHI
      DQCSO  = DQCS
      DQCPIO = DQCPI
      DQCIFO = DQCIVF
      DQCEFO = DQCEVF
      DQRHIO = DQRHI
      DQRSO  = DQRS
      DQRPIO = DQRPI
      DQRIFO = DQRIVF
      DQREFO = DQREVF
      DQCIO  = DQCI
      DQRIO  = DQRI
      HTHIO  = HTHI
      HHIO   = HHI
      HTSO   = HTS
      HSO    = HS
      HTPIO  = HTPI
      HPIO   = HPI
      HTIVFO = HTIVF
      HIVFO  = HIVF
      HTEVFO = HTEVF
      HEVFO  = HEVF
C
C     INTAKE PORT SYSTEM
      DQIVBO = DQIVB
      DQIPWO = DQIPW
      DQIPO  = DQIP
      TIPO   = TIP
      DTMAIO = DMIV * TIP
      HTIVBO = HTIVB
      HIVBO  = HIVB
      HTIPAO = HTIPW
      HIPWO  = HIPW
C
```

```
C             EXHAUST PORT SYSTEM
              DQEVBO = DQEVB
              DQEPWO = DQEPW
              DQEPO  = DQEP
              TEPO   = TEP
              DTMAEO = DWEV * TEP
              HTEVBO = HTEVB
              HEVBO  = HEVB
              HTEPWO = HTEPW
              HEPWO  = HEPW
              GO TO MSP31
C
C             SYSTEM 2
C             PRE CHAMBER DIESEL ENGINE
 7350         DQCH2O = DQCH2
              DQRH2O = DQRH2
              HTH2O  = HTH2
              HH2O   = HH2
              GO TO MP31
C
C             SPARK IGNITION ENGINE
 7380         DQCP2O = DQCP2
              DQRP2O = DQRP2
              HTP2O  = HTP2
              HP2O   = HP2
 7400         RETURN



              ENTRY  HEAT3
C             CALCULATE MEAN WALL TEMPERATURES AT THE END OF THE CYCLE.
              YHTIVF = YHTIVF * AIVF
              YHIVF  = YHIVF  * AIVF
              YHTEVF = YHTEVF * AEVF
              YHEVF  = YHEVF  * AEVF
              YHTIVB = YHTIVB * AIVB
              YHIVB  = YHIVB  * AIVB
              YHTIPW = YHTIPW * AIVP
              YHIPW  = YHIPW  * AIVP
              YHTEVB = YHTEVB * AEVB
              YHEVB  = YHEVB  * AEVB
              YHTEPW = YHTEPW * AEVP
              YHEPW  = YHEPW  * AEVP
              YHTP   = YHTP1 + YHTP2
              YHP    = YHP1  + YHP2
              GO TO MS31
C
C             ADD HEAD CONTRIBUTION FOR S. I. ENGINE
 7420         YHTH1  = YHTH1 + YHTH2
              YHH1   = YHH1  + YHH2
 7430         CONTINUE
              YHTH1  = YHTH1  / 720.0 * CWCH1
              YHH1   = YHH1   / 720.0 * CWCH1
              YHTP   = YHTP   / 720.0 * CWCP
```

```
      YHP    = YHP    / 720.0 * CWCP
      YHTS   = YHTS   / 720.0 * CWCS
      YHS    = YHS    / 720.0 * CWCS
      YHTIVF = YHTIVF / 720.0 * CWCHIV
      YHIVF  = YHIVF  / 720.0 * CWCHIV
      YHTEVF = YHTEVF / 720.0 * CWCHEV
      YHEVF  = YHEVF  / 720.0 * CWCHEV
      YHTIVB = YHTIVB / 720.0 * CWCHIV
      YHIVB  = YHIVB  / 720.0 * CWCHIV
      YHTEVB = YHTEVB / 720.0 * CWCHEV
      YHEVB  = YHEVB  / 720.0 * CWCHEV
      YHTIPW = YHTIPW / 720.0 * CWCHIP
      YHIPW  = YHIPW  / 720.0 * CWCHIP
      YHTEPW = YHTEPW / 720.0 * CWCHEP
      YHEPW  = YHEPW  / 720.0 * CWCHEP
      YQFR   = YQFR   / 720.0
      TWHI = (YHTHI+TCH/RP12) / (YHHI+1.0/RP12)
      B1 = (-R6-R3*(1.0+R6D45))*YHTP - R6D45*TOIL
      B2 = (1.0+R6D45)*(1.0+R3*YHP) + R6*YHP
      B3 = -YHTP*R3/R6 + YQFR + YHTS + TCS/RP789 + B1*(-1.0/R6-
     1     1.0/RP789-YHS)
      B4 = -(1.0+R3*YHP)/R6 - B2*(-1.0/R6-1.0/RP789-YHS)
      TWP  = B3 / B4
      TWS  = B1 + B2*TWP
      TWIV = (YHTIVF+YHTIVB+TCH/RP1113) / (YHIVF+YHIVB+1.0/RP1113)
      TWEV = (YHTEVF+YHTEVB+TCH/RP1214) / (YHEVF+YHEVB+1.0/RP1214)
      TWIP = (YHTIPW+TCH/RP1617) / (YHIPW+1.0/RP1617)
      TWEP = (YHTEPW+TCH/RP1819) / (YHEPW+1.0/RP1819)
      YQFR   = YQFR   * 720.0
      TWH13 = TWHI * TWHI * TWHI
      TWS3  = TWS  * TWS  * TWS
      TWP3  = TWP  * TWP  * TWP
      TWIV3 = TWIV * TWIV * TWIV
      TWEV3 = TWEV * TWEV * TWEV
      TWH14 = TWHI * TWHI * TWHI * TWHI
      TWP4  = TWP  * TWP  * TWP  * TWP
      TWS4  = TWS  * TWS  * TWS  *TWS
      TWIV4 = TWIV * TWIV * TWIV * TWIV
      TWEV4 = TWEV * TWEV * TWEV * TWEV
      GO TO MP41
C
C     PRE CHAMBER HEAD
 7410 YHTH2  = YHTH2  / 720.0
      YHH2   = YHH2   / 720.0 * CWCH2
      TWH2   = (YHTH2+TCH/RP2122) / (YHH2+1.0/RP2122)
      TWH23 = TWH2 * TWH2 * TWH2
      TWH24 = TWH2 * TWH2 * TWH2 * TWH2
 7450 RETURN



      ENTRY  HEAT4
C     CALCULATE WEIBE PARAMETR FOR HEAT RELEASE
      GO TO ( 7480, 7490 ), NWEIBE
```

```
 7480     WFCY1 = WFCY1 * YWF11 / (YWFF1*FAS*RPM*30.0)
          IF ( NENG .EQ. 2 )  WFCY2 = WFCY2 * YWF21 / (YWFF2*FAS*RPM*30.0)
 7490     CONTINUE
C
C         CALCULATE THE RESISTANCES OF VARIOUS PATHS FOR WALL TEMPERATURE
C         CALCULATIONS.
C         CALCULATE FRICTION ENERGY BETWEEN PISTON AND SLEEVE
          YQFR = COFR * (15.0 + 0.01*PMAX1)
C
C         HEAT TRANSFER COEFFICIENT ON COOLANT SIDE
          YQH1   = YQCH1 + YQRH1
          YQS    = YQCS  + YQRS
          YQP    = YQCP1 + YQRP1 + YQCP2 + YQRP2
          YQIV   = YQCIVF + YQRIVF + YQIVB
          YQEV   = YQCEVF + YQREVF + YQEVB
          GO TO MS41
C
C         S. I. ENGINE
 7520     YQH1   = YQH1 + YQCH2 + YQRH2
 7530     CONTINUE
C
C         HEAT TRANSFER TO COOLANT
          YQCOH  = -YQH1 - YQIPW - YQEPW - YQIV - YQEV - YQH2
          YQCOS  = -YQS + YQFR - YQP
          YQCOT  = YQCOH + YQCOS
C
C         TEMPERATURE RISE IN COOLANT
          DTCH = YQCOH * CODTH
          DTCS = YQCOS * CODTS
          TCH  = TCHO + DTCH/2.0
          TCS  = TCSO + DTCS/2.0
          DTC  = DTCH + DTCS
          DTAF = YQF * RPM / (28.8*DWCOLS)
C
C         UNITS OF HEAT TRANSFER COEFFICIENT ARE BTU / CYCLE SQ.IN. F
C         CONSTANT  60.0 = 12.0 * 3600.0 / 720.0
          B = (2.0 + 0.000012*YQCOH*60.0*DCATS/(CONDH1*AHIC)) /
     1        (3600.0*DCATS)
          HWCH1 = CWCOH * B
          HWCIP = CWCOH * B
          HWCEP = CWCOH * B
          HWCIV = CWCOH * B
          HWCEV = CWCOH * B
          HWCS  = CWCOS * (0.21 + 0.000012*YQCOS*60.0*DCATS/(CONDS*ASBC))/
     1        (3600.0*DCATS)
          HWCP  = CWCOP / (3600.0*DCATS)
C
C         UNITS OF RESISTANCES ARE CYCLE F / BTU
          R2     = 1.0 / (HWCH1*AHIC)
          R9     = 1.0 / (HWCS *ASC )
          R4     = 1.0 / (HWCP *APC )
          R13    = R2
          R14    = R2
          R17    = R2
```

```
      R19    = R2
      RP12   = R1 + R2
      R6045  = R6 / (R4+R5)
      RP789  = RP78 + R9
      RP1113 = R11 + R13
      RP1214 = R12 + R14
      RP1617 = R16 + R17
      RP1819 = R18 + R19
      GO TO MP45
C
C     PRE CHAMBER DIESEL ENGINE
 7550 YQH2   = YQCH2 + YQRH2
      HWCH2  = CWCOM * B
      R22    = 1.0 / (HWCH2*AH2C)
      RP2122 = R21 + R22
 7600 RETURN



      ENTRY  HEATOT
C     CALCULATE OUTPUT VARIABLES
C     TOTAL HEAT TRANSFER RATES
      YQH1  = YQCH1  + YQRH1
      YQH2  = YQCH2  + YQRH2
      YQS   = YQCS   + YQRS
      YQP1  = YQCP1  + YQRP1
      YQP2  = YQCP2  + YQRP2
      YQIVF = YQCIVF + YQRIVF
      YQEVF = YQCEVF + YQREVF
      YQ1   = YQC1   + YQR1
      GO TO ( 7620, 7630, 7640 ),  NENG
C
C     OPEN CHAMBER DIESEL ENGINE
 7620 YQC2  = 0.0
      YQR2  = 0.0
      YQ2   = 0.0
      GO TO 7650
C
C     PRE CHAMBER DIESEL ENGINE
 7630 YQC2  = YQCH2
      YQR2  = YQRH2
      YQ2   = YQC2 + YQR2
      GO TO 7650
C
C     SPARK IGNITION ENGINE
 7640 YQC2  = YQCH2 + YQCP2
      YQR2  = YQRH2 + YQRP2
      YQ2   = YQC2 + YQR2
 7650 CONTINUE
C
C     EFFECTIVE GAS TEMPERATURES
      TEGH1  = YHTH1  / YHH1
      IF ( NENG .EQ. 2 )  TEGH2 = YHTH2 / YHH2
      TEGS   = YHTS   / YHS
```

```
          TEGP   = YHTP   / YHP
          TEGIVF = YHTIVF / YHIVF
          TEGIVB = YHTIVB / YHIVB
          TEGEVF = YHTEVF / YHEVF
          TEGEVB = YHTEVB / YHEVB
          TEGIPW = YHTIPW / YHIPW
          TEGEPW = YHTEPW / YHEPW
          RETURN



          ENTRY  HEATO1
C         OUTPUT AT THE END OF THE CYCLE(I)
          WRITE(NFL,9210)
 9210     FORMAT(12X,26HCYCLIC HEAT TRANSFER RATES//
     2          15X,10HCONVECTION,3X,10H RADIATION,3X,3X,5HTOTAL,2X,5X,
     3          9HWALL TEMP,3X,12HEFF GAS TEMP/
     4          12X,3(3X,10H BTU/CYCLE),5X,9H  DEG R  ,3X,4X,5HDEG R/)
          WRITE(NFL,9220)  YQCH1,  YQRH1,  YQH1, TWH1,  TEGH1,
     2                     YQCH2,  YQRH2,  YQH2, TWH2,  TEGH2,
     3                      YQCS,   YQRS,   YQS,  TWS,   TEGS,
     4                     YQCP1,  YQRP1,  YQP1,  TWP,   TEGP,
     5                     YQCP2,  YQRP2,  YQP2
 9220     FORMAT(12H     HEAD(1),3X,E10.5,3X,E10.5,3X,E10.5,5X,2X,
     2                                            F6.1,1X,3X,3X,F6.1/
     3          12H     HEAD(2),3X,E10.5,3X,E10.5,3X,E10.5,5X,2X,
     4                                            F6.1,1X,3X,3X,F6.1/
     5          12H      SLEEVE,3X,E10.5,3X,E10.5,3X,E10.5,5X,2X,
     6                                            F6.1,1X,3X,3X,F6.1/
     7          12H   PISTON(1),3X,E10.5,3X,E10.5,3X,E10.5,5X,2X,
     8                                            F6.1,1X,3X,3X,F6.1/
     9          12H   PISTON(2),3X,E10.5,3X,E10.5,3X,E10.5,5X,2X,
     *                                                              )
          WRITE(NFL,9230) YQCIVF, YQRIVF, YQIVF, TWIV, TEGIVF,
     2                     YQIVB,          YQIVB,       TEGIVB,
     3                    YQCEVF, YQREVF, YQEVF, TWEV, TEGEVF,
     4                     YQEVB,          YQEVB,       TEGEVB,
     5                     YQIPW,          YQIPW, TWIP, TEGIPW
 9230     FORMAT(12H I. V. FRONT,3X,E10.5,3X,E10.5,3X,E10.5,5X,2X,
     2                                            F6.1,1X,3X,3X,F6.1/
     3          12H I. V.  BACK,3X,E10.5,     13X,3X,E10.5,5X,2X,
     4                                            6X,1X,3X,3X,F6.1/
     5          12H E. V. FRONT,3X,E10.5,3X,E10.5,3X,E10.5,5X,2X,
     6                                            F6.1,1X,3X,3X,F6.1/
     7          12H E. V.  BACK,3X,E10.5,     13X,3X,E10.5,5X,2X,
     8                                            6X,1X,3X,3X,F6.1/
     9          12H I. P.  WALL,3X,E10.5,     13X,3X,E10.5,5X,2X,
     *                                            F6.1,1X,3X,3X,F6.1)
          WRITE(NFL,9240)  YQEPW,          YQEPW, TWEP, TEGEPW,
     2                     YQC1,   YQR1,   YQ1,
     3                     YQC2,   YQR2,   YQ2,
     4                     YQIP,           YQIP,
     5                     YQEP,           YQEP
 9240     FORMAT(12H E. P.  WALL,3X,E10.5,     13X,3X,E10.5,5X,2X,
```

```
     2                                                   F6.1,1X,3X,3X,F6.1/
     3   12H  SYSTEM(1),3X,E10.5,3X,E10.5,3X,E10.5,5X,2X,
     4
     5   12H  SYSTEM(2),3X,E10.5,3X,E10.5,3X,E10.5,5X,2X,         /
     6
     7   12H    I. PORT,3X,E10.5,        13X,3X,E10.5,5X,2X,      /
     8
     9   12H    E. PURT,3X,E10.5,        13X,3X,E10.5,5X,2X,      /
     .
      RETURN                                                      )
      END
```

```
@FOR,  I  SZ ENGINE.S13,.R13,.S13
          SUBROUTINE  ICOMB
C         THIS PART OF THE SUBPROGRAM INITIALIZES VARIABLES FOR COMB SUB.
          COMMON/DEBUG / NENG, NOUT1, NVLDBG, NARDBG, NEGDBG, NAVDBG,
     1                   NHTDBG, NDBFLO, NDBRT, NDBSOL
          COMMON/PROP  / CP1, R1, R2
          COMMON/HR1   / NWEIBE, NHRDT, CAHRS, CAHRE
          COMMON/HR2   / CAF, DWFF1, DWFF2
          COMMON/HR3   / CAW1, CAPHR1, WFCY1, WEIBE1, YWF11,
     1                   CAW2, CAPHR2, WFCY2, WEIBE2, YWF21
          COMMON/CA1   / CA, LERR
          COMMON/CAHR  / ICAHRS, ICAHRE, ICAHRT
          COMMON/ENGY  / PE, TE, FE, UE, RE, DUPE, DUTE, DUFE, DRPE, DRTE,
     1                   DRFE, FAPC
          COMMON/CON   / FAS, HVF, RA, RV, UAMB, HAMB, FIM, RIM, HIM, GAMIM
          COMMON/PROP2 /  UIS, HIS
          COMMON/MISC3 / SUM1, WCX, WFIX, WFAIX, WFVIX
          COMMON/VOLL  / LSIC, VOL, DVOL, VELPT, VOL1, VOL2, DVOL1, DVOL2
          COMMON/VAR   /  P1,  T1,  F1,  W1,  P2,  T2,  F2,  W2,
     1                   PIP, TIP, FIP, WIP, PEP, TEP, FEP, WEP, DPIP, DPEP
          COMMON/VARS  / WF1, WFA1, WFV1, WFIP, WFAIP, WFVIP
          COMMON/FUELB / DWF1, DWF2, I1, DWO, DW1, DW2, DW, ISC
          COMMON/SI1   / ERRVOL, TADB
          COMMON/CAVALV/ CAEVOR, CAEVO, CAEVC, CAEVCR, CAIVOR, CAIVO,
     1                   CAIVC, CAIVCR
          COMMON/COMBSI/ NICOMB
          COMMON/COMBSJ/ NJCOMB
          COMMON/COMBSL/ LCONS2
          COMMON/ENTYPE/ LOCD, LPCD, LSI
          LOGICAL  LOCD, LPCD, LSI
          LOGICAL  LSIC
          LOGICAL  LCONS2
          LOGICAL  LSICS, LSICEA, LISC
          DIMENSION  CAF(200), DWFF1(200), DWFF2(200)
          LCONS2 = .TRUE.
          ICAHRS = CAHRS + 0.1
          ICAHRE = CAHRE + 0.1
          GO TO ( 900, 950, 970 ),  NENG
C
C         OPEN CHAMBER ENGINE
 900      ASSIGN 5100 TO MD1
          ASSIGN 6400 TO MD2
          ASSIGN 6500 TO MSP1
          ASSIGN 6500 TO MP1
          ASSIGN 1300 TO MS1
          ASSIGN 6320 TO MS2
          GO TO 1000
C
C         PRE CHAMBER DIESEL ENGINE
 950      ASSIGN 5100 TO MD1
          ASSIGN 6400 TO MD2
          ASSIGN 6450 TO MSP1
          ASSIGN 5550 TO MP1
          ASSIGN 1300 TO MS1
```

```
              ASSIGN 6320 TO MS2
              GO TO 1000
C
C             SPARK IGNITION ENGINE
  970         ASSIGN 1500 TO MD1
              ASSIGN 6480 TO MD2
              ASSIGN 1250 TO MS1
              ASSIGN 6480 TO MSP1
              ASSIGN 6330 TO MS2
 1000         CONTINUE
C
C             WEIBE SWITCH VARIABLE
              GO TO ( 1050, 1080 ),  NWEIBE
 1050         ASSIGN 5500 TO MWEIBE
              WEB1 = CAW1 - CAHRS
              WEB2 = CAW2 - CAHRS
              GO TO 1100
 1080         ASSIGN 6200 TO MWEIBE
 1100         CONTINUE
              RETURN



              ENTRY  ICOMBC
C             INITIALIZE THE CYCLIC VARIABLES
              GO TO MS1
C
C             SPARK IGNITION ENGINE
 1250         CONTINUE
              LSICS  = .FALSE.
              LSICEA = .FALSE.
              LISC   = .FALSE.
              LSIC   = .FALSE.
              ISC    = 1
              ICAHRT = ICAHRE
              CALL  DIFF1
              CALL  VOLS1
              CALL  HEATS1
              ASSIGN 6100 TO MCOMB
 1300         CONTINUE
              DWF1   = 0.0
              DWF2   = 0.0
              I1     = 1
              RETURN



              ENTRY  COMBS1
C             NORMALIZE THE HEAT RELEASE CURVE FOR S. I. ENGINE
              IF ( .NOT. LSI )  GO TO 1380
              SUMDWF = 0.0
              DO 1320  I = 1,NHRDT
              SUMDWF = SUMDWF + DWFF1(I)
 1320         CONTINUE
```

```
      DO 1340  I = 1,NHROT
      DAFF(I) = DWFF(I) / SUMDWF
 1340 CONTINUE
 1380 RETURN



      ENTRY  COMBSI
C     SPARK IGNITION ENGINE
      IF ( LSIC )  GO TO 1400
C
C     NO COMBUSTION
      NICOMB = 2
      LSICS  = .FALSE.
      LSICEA = .FALSE.
      LISC   = .FALSE.
      LSIC   = .FALSE.
      ISC    = 1
      CALL  VOLSI
      CALL  HEATSI
      ASSIGN 6100 TO MCOMB
      GO TO 1450
C
C     COMBUSTION
 1400 ISC    = 2
      NICOMB = 2
      NJCOMB = 3
      LSIC   = .TRUE.
      LSICEA = .TRUE.
      CALL  VOLSI
      CALL  HEATSI
      ASSIGN 6200 TO MCOMB
 1450 CONTINUE
      RETURN



      ENTRY  FUELRT
C     THIS PART OF THE SUBPROGRAM INTERPOLATES THE FUEL RATE INJECTION
C     FOR DIESEL ENGINE OR RATE OF BURNING FOR SPARK IGNITION ENGINE
C     BY LAGRANGIAN SCHEME.
      GO TO MD1.
C
C     SPARK IGNITION ENGINE
 1500 CONTINUE
      IF ( CA .LT. CAHRS )  GO TO 4500
      IF ( CA .GT. CAHRE )  GO TO 2500
      IF ( LISC )  GO TO 4500
      IF ( W2/(W1+W2) .GE. ERRVOL )  GO TO 2000
      IF ( VOL2/VOL .LT. ERRVOL )  GO TO 3000
C
C     COMBUSTION STOPS DUE TO COMPLETE BURNING
 2000 CONTINUE
      RX   = (R1*W1+R2*W2) / (W1+W2)
```

```
      W1    = SUM1
      VOL1  = VOL
      T1    = P1 * VOL1 / (RX*W1*12.0*778.16)
      WF1   = 1.0
      WFA1  = 0.0
      WFV1  = 0.0
      LSIC  = .FALSE.
      LISC    = .TRUE.
      LSICEA  = .TRUE.
      LCONS2  = .FALSE.
      ICAHRT  = CA + 0.1
      NICOMB  = 2
      NJCOMB  = 2
      ASSIGN 6100 TO MCOMB
      GO TO 4200
 2500 IF ( LSICEA )  GO TO 2800
C
C     COMBUSTION  STOPS AT CAHRE
      ISC    = 2
      NICOMB = 1
      NJCOMB = 2
      RX     = (R1*W1+R2*W2) / (W1+W2)
      WCX    = W1
      WF1X   = WF1
      WFA1X  = WFA1
      WFV1X  = WFV1
      WF1  = (WF1X*W1+W2) / SUM1
      WFA1 = (1.0-WF1) / (1.0+F1*FAS)
      WFV1 = WFA1 * (F1*FAS)
      W1     = SUM1
      VOL1   = VOL
      T1     = P1 * VOL1 / (RX*W1*12.0*778.16)
      LSIC = .FALSE.
      LSICEA = .TRUE.
      ASSIGN 6100 TO MCOMB
      GO TO 4200
 2800 CONTINUE
      IF ( LISC )  GO TO 4500
      IF ( CA .LT. (CAIVOR-10.0) )  GO TO 4500
      ISC    = 1
      NICOMB = 1
      LISC = .TRUE.
      GO TO 4500
C
C     COMBUSTION
 3000 CONTINUE
      IF ( LSICS )  GO TO 3500
C
C     COMBUSTION STARTS AT THIS POINT
      P2    = P1
      F2    = F1
      SUM1 = W1
      VOL2 = (1.0-ERRVOL) * VOL
      VOL1 = VOL - VOL2
```

```
             PE    = PI
             FE    = FI
       3100  TE    = TADB
             CALL  ENERGY
             HE    = UE + RE * TE
             TADBX = TADB - (HE-HIS)/(DUTE*RE)
             IF ( ABS(TADBX-TADB) .LE. 2.0 )  GO TO 3120
             TADB = TADBX
             GO TO 3100
       3120  T2    = TADBX
             R2    = RE
             W2    = P2 * VOL2 / (R2*T2*12.0*778.16)
             W1    = SUM1 - W2
             LSIC = .TRUE.
             LSICS = .TRUE.
             NICOMB = 2
             NJCOMB = 1
             ASSIGN 6200 TO MCOMB
             GO TO 4200
       3500  CALL  VOLS1
            P2 = P1
             GO TO 4500
       4200  CONTINUE
             CALL  VOLS1
             CALL  HEATS1
       4500  GO TO MCOMB
      C
      C      DIESEL ENGINE
       5100  CONTINUE
             IF ( CA .LT. CAHRS )  GO TO 6100
             IF ( CA .GT. CAHRE )  GO TO 6100
             GO TO MWEIBE
      C
      C      WEIBE EQUQTION FOR HEAT RELEASE
       5500  B   = (CA-CAHRS) / WEB1
             B1 = 1.0 + CAPHR1
             DWF1 = WEIBE1*B1*(B**CAPHR1)*WFCY1/WEB1*EXP(-WEIBE1*(B**B1))
             GO TO MP1
      C
      C      PRE CHAMBER DIESEL ENGINE
       5550  B   = (CA-CAHRS) / WEB2
             B1 = 1.0 + CAPHR2
             DWF2 = WEIBE2*B1*(B**CAPHR2)*WFCY2/WEB2*EXP(-WEIBE2*(B**B1))
             GO TO 6500
      C
      C      NO COMBUSTION
       6100  DWF1 = 0.0
             DWF2 = 0.0
             GO TO 6500
      C
      C      COMBUSTION
       6200  IF ( CA - CAF(I1))  6210, 6300, 6220
       6210  I1 = I1 - 1
             GO TO 6200
```

```
 6220     IF ( CA - CAF(II+1))  6350, 6280, 6230
 6230     II = II + 1
          GO TO 6220
C
C         SEARCH FUEL RATES AT INTEGER VALUES OF CRANK ANGLE.
 6280     II = II + 1
 6300     GO TO MS2
C
C         DIESEL ENGINE
 6320     DWF1 = DWFF1(II)
          DWF2 = DWFF2(II)
          GO TO 6500
C
C         SPARK IGNITION ENGINE
 6330     DWF2 = DWFF1(II)
          DWF2 = DWF2 + SUM1
          GO TO 6500
 6350     GO TO MD2
C
C         DIESEL ENGINE
 6400     DW0 = DWFF1(II)
          DW1 = DWFF1(II+1)
          DW2 = DWFF1(II+2)
          CALL  LAGINT
          DWF1 = DW
          GO TO MSP1
C
C         PRE CHAMBER DIESEL ENGINE
 6450     DW0 = DWFF2(II)
          DW1 = DWFF2(II+1)
          DW2 = DWFF2(II+2)
          CALL  LAGINT
          DWF2 = DW
          GO TO 6500
C
C         SPARK IGNITION ENGINE
 6480     DW0 = DWFF1(II)
          DW1 = DWFF1(II+1)
          DW2 = DWFF1(II+2)
          CALL LAGINT
          DWF2 = DW
          DWF2 = DWF2 + SUM1
 6500     RETURN
          END
```

```
@FOR, I  SZ ENGINE.S14,.R14,.S14
         SUBROUTINE  LAGINT
         COMMON/CA1   / CA, LERR
         COMMON/HR2   / CAF, DWFF1, DWFF2
         COMMON/FUELB / DWFI1, DWFI2, II, DW0, DW1, DW2, DW, ISC
         DIMENSION  CAF(200), DWFF1(200), DWFF2(200)
C
C        THIS SUBROUTINE INTERPOLATES ACCORDING TO LAGRANGIAN SCHEME.
         A0  = CAF(II)   - CA
         A1  = CAF(II+1) - CA
         A2  = CAF(II+2) - CA
         A10 = CAF(II+1) - CAF(II)
         A20 = CAF(II+2) - CAF(II)
         A21 = CAF(II+2) - CAF(II+1)
         DW  = DW0 * A1 * A2 / (A10*A20) - DW1 * A2 * A0 / (A21*A10) +
     1         DW2 * A0 * A1 / (A20*A21)
         RETURN
         END
```

```
@FOR,  I  S2 ENGINE.S15,.R15,.S15
            SUBROUTINE  IDYNIP
C           THIS PART OF THE SUBPROGRAM INITIALIZES THE VARIABLES FOR
C           DYINP SUBROUTINE.
            COMMON/REV   / NRUN, RPM, DCATS, VEPM, VS, ICYCLE, IDVS, ICA1,
      1                    ICA2, CAS
            COMMON/GEOM  / DMIP, DMEP, AIP, AEP, VIP, VEP, DIV, DEV, AIM,
      1                    APM, AM, AP
            COMMON/CAD   / DCAL, DCAM, DCAV, DCA, DCA2, CAO, CAA, NIT, LCON
            COMMON/CA1   / CA, LERR
            COMMON/VAR   / PCYL, T1, F1, W1, PCYL2, T2, F2, W2, PIP, TIP,
      1                    FIP, WIP, PEP, TEP, FEP, WEP, DPIP, DPEP
            COMMON/FLOW  / LIV, LEV, AIV, AEV, CODIV, CODEV, CODIM, CODPM
            COMMON/AMB   / PA, TAMB, PIM, TIM
            COMMON/WAVE1 / XLIP, ERRDYI, DELZ
            COMMON/WAVE2 / ITDYN, NA, NPX, NDIDBG
            COMMON/WAVE3 / NDYNIP, LPASS, THAVI
            DIMENSION  PO(15), PI(15), UO(15), UI(15), AO(15), AI(15)
            REAL        NCLS
            LOGICAL   LBFLOW, LB, LIV, LPASS, LERR
C
C           CALCULATE THE NORMALIZING FACTORS
            NCLS  = 98.0 * SQRT(THAVI) / (RPM*XLIP)
            DELX  = 1.0 / NX
            DAREA = SQRT(5.0) / AIP
            PLB   = -40.0
            PUB   =  40.0
C
C           INITIALIZATION
            LPASS = .TRUE.
            NXP1 = NX + 1
            DO 3650  I = 1,NXP1
            PU(I) = PIP / PA
            AO(I) = 1.0
            UO(I) = 0.0
 3650       CONTINUE
            PIPO  = PIP
C
C           GENERATE THE SWITCH VARIABLES.
            GO TO ( 4010, 4020 ),  NDIDBG
 4010       ASSIGN 8000 TO NDIDBG
            GO TO 4050
 4020       ASSIGN 9000 TO NDIDBG
 4050       RETURN



            ENTRY  DYNIP
C           THIS SUBROUTINE CALCULATES THE PRESSURE DISTRIBUTION IN THE
C           INTAKE PIPR BY SOLVING THE FINITE AMPLITUDE WAVE EQUATION.
C           IF K STANDS FOR RATIO OF SPECIFIC HEATS OF AIR, THEN -
C           0.142857 = (K-1)/(2*K)
C           0.2857   = (K-1)/K
C           0.7      = K/2
```

```
C          0.71428  = 1/K
C          0.857    = 3*(K-1)/K
C          1.4      = K
C          1.42857  = 2/K
C          1.714286 = (K+1)/K
C          2.5      = 1/(K-1)
C          2.8      = 2*K
C          5.0      = 2/(K-1)
           PCYLN = PCYL / PA
           LR = .FALSE.
           AR = AIV * DAREA
C
C          NCLS IS NORMALIZING FACTOR , BASED ON CA , FOR CHARACTERISTIC
C          LINE SLOPE.
           B = NCLS * DCA
C
C          DISPLACEMENT OF LEFT RUNNING CHARACTERISTIC AT NODE 1 .
           XL = B * (UO(1) - AO(1))
           PL = PO(1) - XL*(PO(2) - PO(1))/DELX
           UL = UO(1) - XL*(UO(2) - UO(1))/DELX
           B1 = 1.4 * (PO(1)**0.857)
C
C          USE B. C. AT PORT END TO CALCULATE PARAMETERS AT NODE 1.
C          CHECK IF INLET VALVE IS OPEN
           IF(LIV)  GO TO 200
C
C          INLET VALVE IS CLOSED
           U1(1) = 0.0
           P1(1) = PL - B1*UL
           A1(1) = P1(1)**0.142857
           GO TO 800
C
C          INLET VALVE IS OPEN
C          SOLVE THE EQUATION BY THE COMBINATION OF BISECTION METHOD AND
C          SECANT METHOD.
C          THE EQUATION TO BE SOLVED IS OF THE FORM -  P = F(P)  AT NODE 1.
C          FOR THIS PART OF THE SUBPROGRAM X STANDS FOR PRESSURE AT NODE 1
C          AND Y = F(P).
C          INITIAL GUESS OF THE ROOT BY LINEAR EXTRAPOLATION IN TIME SPACE.
      200  XO = PO(1) + DPIPN*DCA
           Z = XO / PCYLN
           IF( Z-1.0 )  210, 220, 230
      210  U = AR * (XO**0.142857) * SQRT(Z**1.42857 - Z**1.714286) / Z
           LBFLOW = .TRUE.
           GO TO 240
      220  U = 0.0
           GO TO 240
      230  Z = 1.0 / Z
           U = -AR * (XO**0.142857) * SQRT(Z**1.42857 - Z**1.714286)
           LBFLOW = .FALSE.
      240  YO = PL + B1 * (U - UL)
           X1 = YO
           I = 1
C
```

```
C             START ITERATION LOOP
  300         Z = XI / PCYLN
              IF( Z - 1.0 )  305, 460, 310
C
C             BACKFLOW TO PORT
  305         U = AR * (XI**0.142857) * SQRT(Z**1.42857 - Z**1.714286) / Z
              YI = PL + BI * (U-UL)
              IF ( LBFLOW )  GO TO 320
              GO TO 450
C
C             INFLOW TO CYLINDER
  310         Z = 1.0 / Z
              U = -AR * (XI**0.142857) * SQRT(Z**1.42857 - Z**1.714286)
              YI = PL + BI * (U-UL)
              IF ( LBFLOW )  GO TO 470
C
C             CHECK TO SEE IF THE ROOT SATISFIES THE EQUATION.
  320         ABXI = ABS(XI)
              B2 = ERRDYI
              IF( ABXI - 1.0 )  340, 340, 330
  330         B2 = B2 * ABXI
  340         IF( ABS(XI-XO) - B2 )  350, 350, 360
  350         IF( ABS(XI-YI) - 10.0*B2 )  700, 700, 360
  360         B2 = (XO-YO) / (XI-YI) - 1.0
              X2 = XI + (XI-XO) / B2
              XO = XI
              YO = YI
              XI = X2
              I = I + 1
              IF( I-ITDYN )  370, 2000, 2000
  370         IF (LB)  GO TO 400
              GO TO 300
  400         IF ( XI .GE. PLB .AND. XI .LE. PUB )  GO TO 300
              GO TO 2100
  450         GO TO 320
  470         GO TO 320
  460         U = 0.0
              YI = PL + BI * (U-UL)
              GO TO 320
C
C             EQUATION SOLVED SUCCESSFULLY
C             CALCULATE PARAMETERS AT NODE I
  700         PI(I) = XI
              UI(I) = (XI-PL)/BI + UL
              AI(I) = XI**0.142857
C
C             CHECK THE CRANK ANGLE CONVERGENCE
  800         IF ( LPASS )  GO TO 810
C
C             CONVERGENCE
              ND = NX
              GO TO 820
C
C             NO CONVERGENCE
```

```
  810   ND = NPX + 1
C
C       CALCULATE PARAMETERS AT VARIOUS NODES
  820   DO 850  I = 2, ND
        XR = B * (UO(I) + AO(I))
        XL = B * (UO(I) - AO(I))
        PR = PO(I) - XR * (PO(I)-PO(I-1)) / DELX
        PL = PO(I) - XL * (PO(I+1)-PO(I)) / DELX
        UR = UO(I) - XR * (UO(I)-UO(I-1)) / DELX
        UL = UO(I) - XL * (UO(I+1)-UO(I)) / DELX
        R = PO(I)**0.857
        PI(I) = (PR+PL)/2.0 + 0.7*R*(UR-UL)
        UI(I) = (UR+UL)/2.0 + (PR-PL)/(2.8*R)
        AI(I) = PI(I)**0.142857
  850   CONTINUE
        IF(LPASS)  GO TO 1000
C
C       SOLVE THE B. C. AT THE OPEN END OF INTAKE PIPE
        XR = B * (UO(NXPI)+AO(NXPI))
        PR = PO(NXPI) - XR * (PO(NXPI)-PO(NXPI-1)) / DELX
        UR = UO(NXPI) - XR * (UO(NXPI)-UO(NXPI-1)) / DELX
C
C       CHECK THE DIRECTION OF FLOW
        IF(UR)  910, 900, 900
C
C       FLOW TO SURGE TANK
  900   PI(NXPI) = 1.0
        UI(NXPI) = UR + (PR-1.0) / (1.4*PO(NXPI)**0.857)
        AI(NXPI) = 1.0
        GO TO 1000
C
C       FLOW TO THE INTAKE PIPE
C       SOLVE THE VELOCITY EQUATION  F(U)=0.  BY NEWTON-RAPHSON METHOD.
C       FOR THIS PART OF THE SUBPROGRAM, X STANDS FOR UI(NXPI) AND Y=F(U)
  910   BB  = 1.4 * (PO(NXPI)**0.857)
        XO  = UR + (PR-1.0)/BB
  920   BB1 = PR - BB*(XO-UR)
        Y   = 0.2*XO*XO - 1.0 + BB1**0.2857
        DY  = 0.4*XO - 0.2857*BB*(BB1**(-0.714285))
        X1 = XO - Y/DY
        IF ( ABS(X1-XO) .LE. ERRDY1 )  GO TO 960
  950   XO = X1
        I = I + 1
        IF(I - ITDYN)  920, 2500, 2500
C
C       EQUQTION SOLVED SUCCESSFULLY
  960   UI(NXPI) = X1
        PI(NXPI) = PR - (X1-UR)*BB
        AI(NXPI) = PI(NXPI)**0.142857
C
C       CALCULATE MEAN PORT PRESSURE
 1000   PIP = PI(1) + PI(NPX+1)
        DO 1010  I = 2, NPX
 1010   PIP = PIP + 2.0*PI(I)
```

```
                PIP = PIP / (2*NPX)
                PIP = PIP * PA
                IF( LPASS )  GO TO 7900
C
C               RESET ALL THE VARIABLES AND CALCULATE THE SLOPE AT NODE 1.
                DPIP = (PIP - PIPO) / DCA
                DPIPN = DPIP / PA
                DO 1050  I = 1,NXP1
                PO(I) = PI(I)
                AO(I) = AI(I)
 1050           UO(I) = UI(I)
                PIPO  = PIP
                GO TO 7900
C
C               ERROR MESSAGE
 2000           PRINT 2010, I
 2010           FORMAT(/6H DYNIP,9X,21HFAILS TO CONVERGE IN ,I2,
          1             22H ITERATIONS AT NODE 1.)
                PRINT 2020, LBFLOW, XO, YO, X1, Y1
 2020           FORMAT(15X,L15,6E15.5)
                LERR = .TRUE.
                GO TO 9000
 2100           PRINT 2110
 2110           FORMAT(/6H DYNIP,9X,40HTHE ROOT LIES OUTSIDE THE LIMITS SET BY ,
          1             17HBISECTION METHOD.)
                PRINT 2120,  LBFLOW, LB, PUB, PLB, XO, YO, X1, Y1
 2120           FORMAT(15X,2L15,4E15.5/15X,2E15.5/15X,7E15.5/15X,7E15.5)
                LERR = .TRUE.
                GO TO 9000
 2500           PRINT 2510,  I, XO, Y, DY, X1
 2510           FORMAT(/6H DYNIP,9X,21HFAILS TO CONVERGE IN , I2,
          1             29H ITERATIONS AT OPEN END NODE./15X,7E15.5)
                B2 = 0.0
                PO(NXP1) = B2
                UO(NXP1) = B2
                AO(NXP1) = B2
                LERR = .TRUE.
                GO TO 8120
 7900           GO TO MDIDBG
C
C               DEBUG
 8000           PRINT 8100,  LPASS, PIP, DPIP
 8100           FORMAT(/6H DYNIP,9X,L15,5E15.5)
 8120           PRINT 8150, (PO(I), UO(I), AO(I),  I=1,ND)
 8150           FORMAT(15X,3E15.5)
 9000           RETURN
                END
```

```
@FOR,  I  SZ ENGINE,S16,,R16,,S16
            SUBROUTINE  ICYCLE
C           THIS SUBPROGRAM IS CALLED AT THE END OF EACH CYCLE
            COMMON/DEBUG / NENG, NOUT1, NVLDBG, NARDBG, NEGDBG, NAVDBG,
       1                   NHTDBG, NDBFLO, NDBRT, NDBSOL
            COMMON/MAIN1 / IPR1, IPR2, LCYCLE, JCYCLE
            COMMON/ERRORC/  ERPIC,  ERTIC,  ERFIC,  ERP2C,  ERT2C,  ERF2C,
       1                   ERPIPC, ERTIPC, ERFIPC, ERPEPC, ERTEPC, ERFEPC
            COMMON/ERRORT/ ERTWH1, ERTWH2, ERTWP, ERTWS, ERTWIV, ERTWEV,
       1                   ERTWIP, ERTWEP
            COMMON/VAR   /  P1,  T1,  F1,  W1,  P2,  T2,  F2,  W2,
       1                   PIP, TIP, FIP, WIP, PEP, TEP, FEP, WEP, DPIP, DPEP
            COMMON/VAR1  /  P11,  T11,  F11,  P21,  T21,  F21,
       1                   PIP1, TIP1, FIP1, PEP1, TEP1, FEP1
            COMMON/TEMP  / TWH1, TWH2, TWP, TWS, TWIV, TWEV, TWIP, TWEP,
       1                   TCHO, TCSO, TOIL, TFUEL
            COMMON/TEMPC / TWH1C, TWH2C, TWPC, TWSC, TWIVC, TWEVC, TWIPC,
       1                   TWEPC
            LOGICAL  LCYCLE
            GO TO ( 100, 200, 100 ),  NENG
C
C           OPEN CHAMBER DIESEL ENGINE  OR  SPARK IGNITION ENGINE
 100        ASSIGN 2100 TO MP1
            ASSIGN 2200 TO MP2
            GO TO 300
C
C           OPEN CHAMBER DIESEL ENGINE
 200        ASSIGN 2050 TO MP1
            ASSIGN 2150 TO MP2
 300        RETURN



            ENTRY  CYCLE1
C           CHECK VARIABLES FOR CYCLE CLOSING.
C           SYSTEM PROPERTIES
C           SYSTEM 1
            IF ( ABS(P1 -P11 ) .GT. ERPIC  )  GO TO 2500
            IF ( ABS(T1 -T11 ) .GT. ERTIC  )  GO TO 2500
            IF ( ABS(F1 -F11 ) .GT. ERFIC  )  GO TO 2500
C
C           INLET PORT SYSTEM.
            IF ( ABS(PIP-PIP1) .GT. ERPIPC )  GO TO 2500
            IF ( ABS(TIP-TIP1) .GT. ERTIPC )  GO TO 2500
            IF ( ABS(FIP-FIP1) .GT. ERFIPC )  GO TO 2500
C
C           EXHAUST PORT SYSTEM.
            IF ( ABS(TEP-TEP1) .GT. ERTEPC )  GO TO 2500
            IF ( ABS(FEP-FEP1) .GT. ERFEPC )  GO TO 2500
            GO TO MP1
C
C           SYSTEM 2 FOR PRE CHAMBER DIESEL ENGINE.
 2050       IF ( ABS(P2 -P21 ) .GT. ERP2C )  GO TO 2500
            IF ( ABS(T2 -T21 ) .GT. ERT2C )  GO TO 2500
```

```
      IF ( ABS(F2 -F21 ) .GT. ERF2C )  GO TO 2500
C
C     SYSTEM PROPERTIES CLOSE AT THE END OF THE CYCLE.
C     CHECK FOR WALL TEMPERATURES.
 2100 IF ( ABS(TWHIC-TWHI) .GT. ERTWHI )  GO TO 2600
      IF ( ABS(TWSC -TWS ) .GT. ERTWS  )  GO TO 2600
      IF ( ABS(TWPC -TWP ) .GT. ERTWP  )  GO TO 2600
      IF ( ABS(TWIVC-TWIV) .GT. ERTWIV )  GO TO 2600
      IF ( ABS(TWEVC-TWEV) .GT. ERTWEV )  GO TO 2600
      IF ( ABS(TWIPC-TWIP) .GT. ERTWIP )  GO TO 2600
      IF ( ABS(TWEPC-TWEP) .GT. ERTWEP )  GO TO 2600
      GO TO MP2
C
C     SYSTEM 2 FOR PRE CHAMBER DIESEL ENGINE.
 2150 IF ( ABS(TWH2C-TWH2) .GT. ERTWH2 )  GO TO 2600
C
C     WALL TEMPERATURES CLOSE AT THE END OF THE CYCLE.
 2200 LCYCLE = .TRUE.
      GO TO 3000
C
C     SYSTEM PROPERTIES DO NOT CLOSE.
 2500 JCYCLE = 1
      LCYCLE = .FALSE.
      GO TO 3000
C
C     WALL TEMPERATURES DO NOT CLOSE.
 2600 JCYCLE = 2
      LCYCLE = .FALSE.
 3000 RETURN
      END
```

```
      @FOR,  I  SZ ENGINE.S17,.R17,.S17
            SUBROUTINE  OUTPUT
            PARAMETER  NAR1=10,  NAR2=300
            COMMON/DEBUG / NENG, NOUT1, NVLDBG, NARDBG, NEGDBG, NAVDBG,
     1                     NHTDBG, NDBFLO, NDHRT, NDBSOL
            COMMON/REV   / NRUN, RPM, DCATS, VEPM, VS, ICYCLE, IDVS,
     1                     ICA1, ICA2, CAS
            COMMON/MAIN1 / IPR1, IPR2, LCYCLE, JCYCLE
            COMMON/MAIN2 / NFL, N1, N3, N2, TEXT, HTEXT
            COMMON/CA1   / CA, LERR
            COMMON/CAVALV/ CAEVOR, CAEVO, CAEVC, CAEVCR, CAIVOR, CAIVO,
     1                     CAIVC, CAIVCR
            COMMON/GEOMC / BORE, STROKE, CONRD, SCL, VLPCL, VLVCL, VOLP2,
     1                     COMPT, SP, SRT
            COMMON/GEOM  / DMIP, DMEP, AIP, AEP, VIP, VEP, DIV, DEV, AIM,
     1                     APM, AM, AP
            COMMON/GEOMHG/ AH1, AH2, AP1, AP2, AS, AIVF, AEVF, AIVB, AEVB,
     1                     AIVP, AEVP
            COMMON/GEOMHC/ AH1C, AH2C, APC, APSC, ASC, ASBC, AIVC, AEVC,
     1                     AIPC, AEPC
            COMMON/ERROR1/  ERP1,  ERT1,  ERF1,  ERW1,  ERP2,  ERT2,  ERF2,
     1                      ERW2, ERPIP, ERTIP, ERFIP, ERWIP, ERPEP, ERTEP,
     2                     ERFEP, ERWEP
            COMMON/ERRORC/  ERP1C,  ERT1C,  ERF1C,  ERP2C,  ERT2C,  ERF2C,
     1                     ERPIPC, ERTIPC, ERFIPC, ERPEPC, ERTEPC, ERFEPC
            COMMON/ERRORT/ ERTWH1, ERTWH2, ERTWP, ERTWS, ERTWIV, ERTWEV,
     1                     ERTWIP, ERTWEP
            COMMON/HR1   / NWEIBE, NHRDT, CAHRS, CAHRE
            COMMON/HR2   / CAF, DWFF1, DWFF2
            COMMON/HR3   / CAA1, CAPHR1, WFCY1, WEIBE1, YWF11,
     1                     CAA2, CAPHR2, WFCY2, WEIBE2, YWF21
            COMMON/HTCM1 / COHCH1, COHCP1, COHCS, CHCIVF, CHCEVF,
     1                     COHRH1, COHRP1, COHRS, CHRIVF, CHREVF
            COMMON/HTCM2 / COHCH2, COHCP2, COHRH2, COHRP2
            COMMON/HTCMV / CHCIVB, CHCIP, CHCEVB, CHCEP, CHCEIB, CHCEIP,
     1                     CHCEEB, CHCEEP
            COMMON/WAVE1 / XLIP, ERRDY1, DELZ
            COMMON/WAVE2 / ITDYN, NX, NPX, NDIDBG
            COMMON/WAVE3 / NDYNIP, LPASS, THAV1
            COMMON/OUTAR1/ IPR, LOUT
            COMMON/OUTAR2/ ZOUT
            DIMENSION  LOUT(1,72))
            DIMENSION  ZOUT(NAR1,NAR2)
            DIMENSION  TEXT(80), HTEXT(15)
            DIMENSION  CAF(200), DWFF1(200), DWFF2(200)
            DIMENSION  A(2,3), B(3,5)
            LOGICAL  LCYCLE
            LOGICAL  LERR
      C
      C     GENERATE THE SWITCH VARIABLES
            GO TO ( 100, 200, 300 ),  NENG
      C
      C     OPEN CHAMBER DIESEL ENGINE
       100  ASSIGN 6700 TO MS02
```

```
                ASSIGN 9210 TO MCAI
                GO TO 400
      C
      C         PRE CHAMBER DIESEL ENGINE
       200      ASSIGN 6700 TO MS02
                ASSIGN 9310 TO MCAI
                GO TO 400
      C
      C         SPARK IGNITION ENGINE
       300      ASSIGN 6410 TO MS02
                ASSIGN 9410 TO MCAI
       400     CONTINUE
                A(1,1) = 6HSYSTEM
                A(1,2) = 6H PROPE
                A(1,3) = 6HRTIES.
                A(2,1) = 6HWALL T
                A(2,2) = 6HEMPERA
                A(2,3) = 6HTURES.
                B(1,1) = 6HOPEN
                B(1,2) = 6HCHAMBE
                B(1,3) = 6HR   DI
                B(1,4) = 6HESEL
                B(1,5) = 6HENGINE
                B(2,1) = 6HPRE
                B(2,2) = B(1,2)
                B(2,3) = B(1,3)
                B(2,4) = B(1,4)
                B(2,5) = B(1,5)
                B(3,1) = 6HSPARK
                B(3,2) = 6H IGNIT
                B(3,3) = 6HION
                B(3,4) = 6HENGINE
                B(3,5) = 6H
                WRITE(6,1050)
       1050     FORMAT(1H1)
                WRITE(NI,1100)
       1100     FORMAT(1H0)
                WRITE(NI,1200)  (B(NENG,J),  J=1,5)
       1200     FORMAT(38X,5H*****,2X,5A6,2X,5H*****//)
                WRITE(NI,1210)  (TEXT(J), J = 1,80)
       1210     FORMAT(20A6/)
                WRITE(NI,1100)
                WRITE(NI,1100)
                WRITE(NI,1250)
       1250     FORMAT(23H ENGINE GEOMETRY DATA =/)
                WRITE(NI,1300)  NRUN, RPM, COMRT, BORE, STROKE, DIV, CONRD,
               1                VOLP2, DEV
       1300     FORMAT(11X,9HRUN NO. =,I6,14X,15X,5HRPM =,F10.4,11X,
               1       19HCOMPRESSION RATIO =,F10.4/14X,6HBORE =,F10.4,4H IN.,
               2       6X,12X,8HSTROKE =,F10.4,4H IN.,6X,20HVALVE DIA.  INTAKE =,
               3       F10.4,4H IN./2X,18HCONN. ROD LENGTH =,F10.4,4H IN.,6X,4X,
               4       16HPRE CUP VOLUME =,F10.4,8H CU. IN.,2X,11X,9HEXHAUST =,
               5       F10.4,4H IN.)
                WRITE(NI,1350)  DMIP, AIP, VIP, DMEP, AEP, VEP
```

```
 1350     FORMAT(/16H PORT GEOMETRY -/ 12H HYD. DIA., , 8HINTAKE =, F10.4,
        1        4H IN.,6X,12H C.S. AREA, , 8HINTAKE =,F10.4,8H SQ. IN.,
        2        2X, 4X,8HVOLUME, , 8HINTAKE =,F10.4,8H CU. IN., 2X/
        3        11X,9HEXHAUST =,F10.4,4H IN.,6X,11X,9HEXHAUST =,F10.4,
        4        8H SQ. IN.,2X,11X,9HEXHAUST =,F10.4,8H CU. IN.)
          WRITE(NI,1100)
          WRITE(NI,1100)
          WRITE(NI,1400)
 1400     FORMAT(/35H HEAT TRANSFER AREA,     GAS SIDE -)
          WRITE(NI,1450)  AH1, AP, AH2, AIVF, AEVF, AIVB, AEVB, AIVP, AEVP
 1450     FORMAT(14X,6HHEAD =,F10.4,8H SQ. IN.,2X,12X,8HPISTON =,F10.4,
        1        8H SQ. IN.,2X,11X,9HPRE CUP =,F10.4,8H SQ. IN. /
        2        7X,13HI. V. FRONT =,F10.4,8H SQ. IN.,2X,
        3        7X,13HE. V. FRONT =,F10.4,8H SQ. IN.,2X/
        4        7X,13HI. V.  BACK =,F10.4,8H SQ. IN.,2X,
        5        7X,13HE. V.  BACK =,F10.4,8H SQ. IN.,2X/
        6        7X,13HINTAKE PORT =,F10.4,8H SQ. IN.,2X,
        7        6X,14HEXHAUST PORT =,F10.4,8H SQ. IN.)
          WRITE(NI,1100)
          WRITE(NI,1100)
          WRITE(NI,1500)
 1500     FORMAT(/35H HEAT TRANSFER AREA, COOLANT SIDE -)
          WRITE(NI,1550)  AH1C, APC, ASC, AH2C, AIVC, AEVC, AIPC, AEPC
 1550     FORMAT(14X,6HHEAD =,F10.4,8H SQ. IN.,2X,12X,8HPISTON =, F10.4,
        1        8H SQ. IN.,2X,12X,8HSLEEVE =,F10.4,8H SQ. IN.,2X/11X,
        2        9HPRE CUP =,F10.4,8H SQ. IN./ 6X,14HINTAKE VALVE =, F10.4,
        3        8H SQ. IN.,2X,5X,15HEXHAUST VALVE =,F10.4,8H SQ. IN.,
        4        2X/7X,13HINTAKE PORT =,F10.4,8H SQ. IN.,2X, 6X,
        5        14HEXHAUST PORT =,F10.4,8H SQ. IN.)
          WRITE(NI,1100)
          WRITE(NI,1100)
          WRITE(NI,1600)
 1600     FORMAT(/18H VALVE FLOW AREA -)
          WRITE(NI,1650)  CAIVOR, CAIVO, CAIVC, CAIVCR, CAEVOR, CAEVO,
        1                 CAEVC, CAEVCR
 1650     FORMAT(20X,5X,10HOPEN. RAMP,5X,7X,7HOPENING,6X,7X,7HCLOSING,6X,
        1        5X,10HCLOS. RAMP/  20X,4(9X,2HCA,9X)/
        2        8X,12HINTAKE VALVE,       4(7X,F6.1,7X) /
        3        7X,13HEXHAUST VALVE,      4(7X,F6.1,7X) )
          WRITE(NI,1050)
          WRITE(NI,1660)  NX, XLIP, NPX, ERRDYI
 1660     FORMAT(/19H INTAKE PIPE DATA -/
        2        5X,15HGRIDS IN PIPE =,I4,16X,4X,16HLENGTH OF PIPE =,F6.1,
        2        4H IN./
        3        5X,15HGRIDS IN PORT =,I4,16X2X,18HREL. ERROR LIMIT =,F6.3)
          IF ( NDYNIP .EQ. 2 )  GO TO 1680
          WRITE(NI,1670)
 1670     FORMAT(/41H **  INTAKE PIPE DYNAMICS IS INCLUDED  **//)
          GO TO 1695
 1680     WRITE(NI,1690)
 1690     FORMAT(/45H **  INTAKE PIPE DYNAMICS IS NOT INCLUDED  **//)
 1695     CONTINUE
          WRITE(NI,1700)
 1700     FORMAT(/15H ERROR LIMITS -)
```

```
      WRITE(NI,1750)  ERP1,  ERT1,  ERF1,  ER*1,
     1                ERP2,  ERT2,  ERF2,  ER*2,
     2                ERPIP, ERTIP, ERFIP, ER*IP,
     4                       ERTEP, ERFEP, ER*EP
1750  FORMAT(20X,6X,8HPRESSURE,6X,5X,11HTEMPERATURE,4X,6X,9HEQ. RATIO,
     1       5X,8X,4HMASS/  20X,9X,3HPSI,8X,11X,1HR,9X,20X,9X,3HLBM/
     2       16X, 4HMAIN,        3(6X,F8.5,6X),6X,E8.4 /
     3       17X,  3HPRE,        3(6X,F8.5,6X),6X,E8.4 /
     4       15X,5HI. P.,        3(6X,F8.5,6X),6X,E8.4 /
     5       15X,5HE. P.,20X,    2(6X,F8.5,6X),6X,E8.4 )
      WRITE(NI,1100)
      WRITE(NI,1100)
      WRITE(NI,1100)
      WRITE(NI,1100)
      WRITE(NI,1950)
1950  FORMAT(22H CYCLIC ERROR LIMITS -)
      WRITE(NI,2000)  ERP1C,  ERT1C,  ERF1C,  ERP2C,  ERT2C,  ERF2C,
     1                ERPIPC, ERTIPC, ERFIPC,         ERTEPC, ERFEPC
2000  FORMAT(20X,6X,8HPRESSURE,6X,5X,11HTEMPERATURE,4X,6X,9HEQ. RATIO/
     1       20X, 9X,3HPSI,8X,10X,1HR,5X/
     2       16X,4HMAIN,  3(6X,F8.5,6X) /
     3       17X,3HPRE,   3(6X,F8.5,6X) /
     4       15X,5HI. P., 3(6X,F8.5,6X) /
     5       15X,5HE. P.,20X,2(6X,F8.5,6X) )
      WRITE(NI,1100)
      WRITE(NI,1100)
      WRITE(NI,1100)
      WRITE(NI,2100)
2100  FORMAT(32H WALL TEMPERATURE ERROR LIMITS -)
      WRITE(NI,2150)  ERTWH1, ERTWS, ERTWP, ERTWH2, ERTWIV, ERTWEV,
     1                ERTWIP, ERTWEP
2150  FORMAT(20H MAIN CHAMBER HEAD =,F10.4,2H R,8X,12X,8HSLEEVE =,
     1       F10.4,2H R,8X,12X,8HPISTON =,F10.4,2H R,8X/11X,
     2       9HPRE CUP =,F10.4,2H R/  6X,14HINTAKE VALVE =,F10.4,2H R,
     3       8X,5X,15HEXHAUST VALVE =,F10.4,2H R,8X/7X,
     4       13HINTAKE PORT =,F10.4,2H R,8X,6X,14HEXHAUST PORT =,
     5       F10.4,2H R)
      WRITE(NI,1050)
      WRITE(NI,2200)
2200  FORMAT(57X,17HHEAT RELEASE DATA//)
      WRITE(NI,2250)  CAHRS, CAHRE
2250  FORMAT(/20H   COMB. STARTS AT =,F10.4,3H CA,7X,
     1       20H     COMB. ENDS AT =,F10.4,3H CA)
      GO TO ( 2380, 2280 ), NWEIBE
2280  CONTINUE
      WRITE(NI,2300)
2300  FORMAT(/21H HEAT RELEASE RATES -/6X,
     1       2(2HCA,18X,4HMAIN,18X,3HPRE,17X) / 25X, 6HLBM/CA, 15X,
     2       6HLBM/CA,35X,6HLBM/CA,15X,6HLBM/CA)
      NM = (2*NHRDT+3) / 4
      NN = NHRDT + 1
        CAF(NN) = 0.0
      DWFF1(NN) = 0.0
      DWFF2(NN) = 0.0
```

```
      WRITE(NI,2350)  ( CAF(J), DWFF1(J), DWFF2(J), CAF(J+NM),
     1                 DWFF1(J+NM), DWFF2(J+NM),  J = 1,NM )
 2350 FORMAT(2(4X,F6.1,12X,E10.5,12X,E10.5,8X))
       GO TO 2480
 2380 CONTINUE
      WRITE(NI,2390)
 2390 FORMAT(//30H WEIBE HEAT RELEASE PARAMETERS//18X,4HMAIN,17X,3HPRE)
      WRITE(NI,2400)  CAW1, CAW2, CAPHR1, CAPHR2, WFCY1, WFCY2,
     1                WEIBE1, WEIBE2, YWF11, YWF21
 2400 FORMAT(10H      CAW,5X,E10.4,10X,E10.4/
     1        10H    CAPHR,5X,E10.4,10X,E10.4/
     2        10H     WFCY,5X,E10.4,10X,E10.4/
     3        10H    WEIBE,5X,E10.4,10X,E10.4/
     4        10H      YWF,5X,E10.4,10X,E10.4)
 2480 CONTINUE
      WRITE(NI,1050)
      WRITE(NI,2500)  (HTEXT(J),  J = 1,12)
 2500 FORMAT(36H TYPE OF HEAT TRANSFER CORRELATION = /
     1        13H CONVECTION =,6A6 /
     2        13H  RADIATION =,6A6//)
      WRITE(NI,2550)
 2550 FORMAT(/48H HEAT TRANSFER COEFFICIENT MULTIPLYING FACTORS =)
      WRITE(NI,2600)
 2600 FORMAT(35H CONVECTION   =    MAIN(1) AND PRE(2))
      WRITE(NI,2650)  COHCH1, COHCS, COHCP1, CHCIVF, CHCEVF, COHCH2,
     1                COHCP2
 2650 FORMAT(11X,9HHEAD(1) =,F10.4,     12X,8HSLEEVE =,F10.4,
     1        9X,11HPISTON(1) =,F10.4/ 7X,13HI. V. FRONT =,F10.4,
     2        7X,13HE. V. FRONT =,F10.4,      12X,8HPRE(2) =,F10.4,
     3        9X,11HPISTON(2) =,F10.4)
      WRITE(NI,1100)
      WRITE(NI,1100)
      WRITE(NI,2700)
 2700 FORMAT(35H  RADIATION   =    MAIN(1) AND PRE(2))
      WRITE(NI,2650)  COHRH1, COHRS, COHRP1, CHRIVF, CHREVF, COHRH2,
     1                COHRP2
      WRITE(NI,1100)
      WRITE(NI,1100)
      WRITE(NI,1100)
      WRITE(NI,2750)  CHCIVB, CHCEVB, CHCIP, CHCEP
 2750 FORMAT(/14H PORT SYSTEM =/  8X,12HI. V. BACK =,F10.4,     8X,
     1        12HE. V. BACK =,F10.4,     7X,13HINTAKE PORT =,F10.4,
     2        6X,14HEXHAUST PORT =,F10.4)
      RETURN



      ENTRY  OUT1
C     OUTPUT AT EACH CRANK ANGLE
      CA = CA + 1.0
      CALL  RATECA
      CA = CA - 1.0
      RETURN
```

```
      ENTRY  OUT2
C     OUTPUT AT THE END OF SUCCESSFUL CYCLE.
C     VARIABLES AND THEIR RATES
      WRITE(N3,5050)
 5050 FORMAT(1H1)
      WRITE(N3,5100)
 5100 FORMAT(1H0)
      WRITE(N3,5200)
 5200 FORMAT(49X,35HMAIN(1) AND PRE(2) SYSTEM VARIABLES// 4X,2HCA,4X,
     1      2X,11HPRESSURE(1),2X,4X,8HTEMP.(1),3X,2X,12HEQ. RATIO(1),
     2      1X,4X,7HMASS(1),4X,2X,11HPRESSURE(2),2X,4X,8HTEMP.(2),3X,
     3      2X,12HEQ. RATIO(2),1X,4X,7HMASS(2)/  10X,
     4      2(6X,3HPSI,6X,7X,1HR,7X,15X,6X,3HLBM,6X))
      WRITE(N3,5100)
      WRITE(N3,5100)
      J1 = 1
      DO 5400  I = IPR1, IPR2
      WRITE(N3,5350)  ZOUT(J1,I), (ZOUT(J,I), J= 2, 9)
 5350 FORMAT(2X,F6.1,2X,2(3X,F8.2,7X,F8.2,7X,F9.6,6X,E9.4,3X))
 5400 CONTINUE
      WRITE(N3,5050)
      WRITE(N3,5450)
 5450 FORMAT(40X,51HINTAKE PORT(I) AND EXHAUST PORT(E) SYSTEM VARIABLES
     1      //  4X,2HCA,4X,2X,11HPRESSURE(I),2X,4X,8HTEMP.(I),3X,2X,
     2      12HEQ. RATIO(I),1X,4X,7HMASS(I),4X,2X,11HPRESSURE(E),2X,
     3      4X,8HTEMP.(E),3X,2X,12HEQ. RATIO(E),1X,4X,7HMASS(E)/ 10X,
     4      2(6X,3HPSI,6X,7X,1HR,7X,15X,6X,3HLBM,6X))
      WRITE(N3,5100)
      WRITE(N3,5100)
      DO 5600  I = IPR1, IPR2
      WRITE(N3,5550)  ZOUT(J1,I), (ZOUT(J,I), J=10,17)
 5550 FORMAT( 2X,F6.1,2X,2(3X,F8.2,7X,F8.2,7X,F9.6,6X,E9.4,3X))
 5600 CONTINUE
      WRITE(N3,5050)
      WRITE(N3,5650)
 5650 FORMAT(58X,17HRATE OF MASS FLOW//  4X,2HCA,4X,5X,4HI.V.,6X,5X,
     1      4HE.V.,6X,4X,6HTHROAT,5X,1X,12HFUEL INJ.(1),2X, 2X,
     2      12HFUEL INJ.(2),1X,5X,6HINTAKE,4X.4X,7HEXHAUST,4X,5X,
     3      4X/ 10X, 7(4X,6HLBM/CA,5X))
      WRITE(N3,5100)
      WRITE(N3,5100)
      DO 5800  I = IPR1, IPR2
      WRITE(N3,5750)  ZOUT(J1,I), (ZOUT(J,I), J=18,24)
 5750 FORMAT(   2X,F6.1,2X, 8(3X,E9.4,3X)     )
 5800 CONTINUE
      WRITE(N3,5050)
      WRITE(N3,5850)
 5850 FORMAT(46X,40HMAIN(1) AND PRE(2) SYSTEM RATE VARIABLES//
     1      4X,2HCA,4X,4X,8HTEMP.(1),3X,2X,12HEQ. RATIO(1),1X,4X,
     2      7HMASS(1),4X,4X,8HTEMP.(2),3X,2X,12HEQ. RATIO(2),1X,4X,
     3      7HMASS(2)/ 10X,2(6X,4HR/CA,5X,6X,3H/CA,6X,5X,6HLBM/CA,
     4      4X))
```

```
      WRITE(N3,5100)
      WRITE(N3,5100)
      DO 6000  I = IPR1, IPR2
      WRITE(N3,5950)  ZOUT(J1,I), (ZOUT(J,I), J=25,30)
 5950 FORMAT(    2X,F6.1,2X, 2(4X,F7.2,7X,E9.4,6X,E9.4,3X)     )
 6000 CONTINUE
      WRITE(N3,5050)
      WRITE(N3,6050)
 6050 FORMAT(38X,47HINTAKE PORT(I) AND EXHAUST PORT(E) SYSTEM RATE ,
     1       9HVARIABLES//  4X,2HCA,4X,4X,8HTEMP.(I),3X,2X,
     2       12HEQ. RATIO(I),1X,4X,7HMASS(I),4X,4X,8HTEMP.(E),3X,2X,
     3       12HEQ. RATIO(E),1X,4X,7HMASS(E)/ 10X, 2(6X,4HR/CA,5X,6X,
     4       3H/CA,6X,5X,6HLBM/CA,4X))
      WRITE(N3,5100)
      WRITE(N3,5100)
      DO 6200  I = IPR1, IPR2
      WRITE(N3,6150)  ZOUT(J1,I), (ZOUT(J,I), J=31,36)
 6150 FORMAT(     2X,F6.1,2X, 2(4X,F7.2,7X,E9.4,6X,E9.4,3X)    )
 6200 CONTINUE
      WRITE(N3,5050)
      WRITE(N3,6250)
 6250 FORMAT(56X,19HHEAT TRANSFER RATES//  4X, 2HCA, 4X,6X,4HMAIN,
     1       5X,6X,3HPRE,6X,5X,4HI.P.,6X,5X,4HE.P.,6X,3X,9HWORK DONE,
     2       3X,3X,10HITERATIONS,2X,6X,4HVOL1,5X,6X,4HVOL2,5X/
     3       10X,4(4X,6HBTU/CA,5X),2X,10HLBF. IN/CA,3X,3X,9HFOR CONV.,
     4       3X,2(4X,7HCU. IN.,4X))
      WRITE(N3,5100)
      WRITE(N3,5100)
      J42 = 42
      J43 = 43
      DO 6400  I = IPR1, IPR2
      WRITE(N3,6350)  ZOUT(J1,I), (ZOUT(J,I), J=37,41), LOUT(1,I),
     1                ZOUT(J42,I), ZOUT(J43,I)
 6350 FORMAT(     2X,F6.1,2X,5(3X,E9.4,3X) ,6X,I3,6X,2(3X,E9.4,3X))
 6400 CONTINUE
      GO TO MS02
 6410 WRITE(N3,5050)
      WRITE(N3,6450)
 6450 FORMAT(40X,45HMASS FRACTION FOR MAIN(I) AND INTAKE PORT(I) ,
     1       7HSYSTEMS/ 41X,33HAND VOLUME RATES FOR TWO SYSTEMS ,
     2       17HDURING COMBUSTION//  4X, 2HCA, 4X,2X,11HPRODUCTS(I),
     3       2X,4X,6HAIR(I),5X,1X,13HFUEL VAPOR(I),1X,2X,11HPRODUCTS(I)
     4       2X,4X,6HAIR(I),5X,1X,13HFUEL VAPOR(I),1X,4X,7HDVOL(1),
     5       4X,4X,7HDVOL(2)/ 100X,2(2X,10HCU. IN./CA,3X))
      WRITE(N3,5100)
      WRITE(N3,5100)
      DO 6600  I = IPR1, IPR2
      WRITE(N3,6550)  ZOUT(J1,I), (ZOUT(J,I), J=44,51)
 6550 FORMAT(      2X,F6.1,2X,8(3X,E9.4,3X))
 6600 CONTINUE
 6700 CONTINUE
      RETURN
```

```
      ENTRY  OUT3
C     OUTPUT AT THE END OF SUCCESSFUL CYCLE
C     SUM OF MASS AND ENERGY FLOW
C     MASS FLOW
      CALL  RATE0T
      NFL = 6
      WRITE(N3,5050)
      CALL  RATE02
      WRITE(N3,5100)
      WRITE(N3,5100)
      WRITE(N3,5100)
C
C     ENERGY FLOW
      CALL  RATE03
      WRITE(N3,5100)
      WRITE(N3,5100)
      CALL  HEATOT
      CALL  HEATO1
C
C     MASS AND ENERGY BALANCE
      WRITE(N3,5050)
      WRITE(N3,6830)
 6830 FORMAT(54X,23HMASS AND ENERGY BALANCE, // 30X,4X,7HMASS IN,4X,
     1        3X,8HMASS OUT,4X,5X,5HERROR,5X,3X,9HENERGY IN,3X,3X,
     2        10HENERGY OUT,2X,5X,5HERROR, / 30X,3(3X,9HLBM/CYCLE,3X),
     3        3(3X,9HBTU/CYCLE,3X)//)
      CALL  RATE05
C
C     POWER OUTPUT
      WRITE(N3,5100)
      WRITE(N3,5100)
      WRITE(N3,5100)
      WRITE(N3,5100)
      WRITE(N3,5100)
      CALL  RATE04
      RETURN



      ENTRY  OUT4
C     OUTPUT WHEN CYCLE DOES NOT CLOSE
      WRITE(N3,5050)
      WRITE(N3,7100)  (A(JCYCLE,I),  I = 1,3)
 7100 FORMAT(17X,28HCYCLE DOES NOT CLOSE DUE TO ,3A6,5X,
     1        35HSTART WITH DIFFERENT INITIAL VALUES///)
      NFL = 6
      CALL  INTLO1
      RETURN



      ENTRY  OUT5
C     OUTPUT FOR UNSUCCESSFUL CYCLE CLOSING AFTER NO. OF ITERATIONS
```

```
      WRITE(N3,5050)
      WRITE(N3,7510)  ICYCLE
 7510 FORMAT(53X,26H******  CYCLIC ERROR  *****///  5X,
     1      23HCYCLE DOES NOT CLOSE IN,I2,18H NO. OF ITERATIONS//)
      WRITE(N3,7520)
 7520 FORMAT(5X,43HFOLLOWING OUTPUT IS FOR LAST COMPUTED CYCLE//)
      RETURN



      ENTRY  OUT6
C     OUTPUT IN CASE OF ERROR
      LERR = .TRUE.
      N3 = 6
      CA = CA + 1.0
      WRITE(N3,5050)
      WRITE(N3,8100)  CA
 8100 FORMAT(46X,20H*****  ERROR AT CA =,F6.1,7H  *****///)
      NFL = 6
      CALL  RATEO1
      RETURN



      ENTRY  OUT7
C     INITIAL VALUES
      WRITE(N3,5050)
      WRITE(N3,8510)
 8510 FORMAT(53X,14HINITIAL VALUES///)
      NFL = 6
      CALL  INTLO1
      RETURN



      ENTRY  OUT8
C     FINAL VALUES AT THE END OF SUCCESSFUL CYCLE
      WRITE(N3,5050)
      WRITE(N3,9010)
 9010 FORMAT(49X,22H***  CYCLE CLOSES  ***//
     1      42X,36HFINAL VALUES AT THE END OF THE CYCLE//)
      NFL = 6
      CALL  INTLO1
      RETURN



      ENTRY  OUT9
C     TABULAR RESULTS
      WRITE(N3,5050)
      WRITE(N3,9150)
 9150 FORMAT(59X,14HTABULAR OUTPUT/)
      GO TO MCA1
C
```

```
C           OPEN CHAMBER DIESEL ENGINE
  9210      CONTINUE
            WRITE(N3,9250)
  9250      FORMAT(3X,2HCA,5X,2X,8HPRESSURE,2X,4X,5HTEMP.,3X,2X,9HEQ. RATIO,
         1        2X,5X,4HMASS,5X,5X,4HFUEL,5X,5X,4HWORK,5X,5X,4HHEAT,5X,
         2        2X,10HI. V. MASS,2X,2X,10HE. V. MASS/ 61X,2X,9HINJ. RATE,
         3        3X,5X,4HRATE,5X,1X,11HTRANS. RATE,2X,2(3X,9HFLOW RATE,2X))
            WRITE(N3,9260)
  9260      FORMAT(10X,5X,3HPSI,4X,5X,2HOR,5X,13X,5X,3HLBM,6X,4X,6HLBM/CA,
         1        4X,2(4X,6HBTU/CA,4X),2(4X,6HLBM/CA,4X)/)
            DO 9300  J = 1,IPR
            WRITE(N3,9280)  (ZOUT(I,J), I=1,10)
  9280      FORMAT(F7.1,3X,2(2X,F7.2,3X),3X,F6.5,4X,6(2X,E10.5,2X))
  9300      CONTINUE
            GO TO 9580
C
C           PRE CHAMBER DIESEL ENGINE
  9310      CONTINUE
            GO TO 9580
C
C           SPARK IGNITION ENGINE
  9410      CONTINUE
            WRITE(N3,9450)
  9450      FORMAT(3X,2HCA,5X,2X,8HPRESSURE,3X,2(4X,5HTEMP.,4X),5X,4HCYL.,
         1        5X,4X,4HMASS,5X,4X,6HVOLUME,3X,5X,4HHEAT,5X,2X,
         2        10HI. V. MASS,2X,2X,10HE. V. MASS/
         3        10X,13X,3X,7HUNBURNT,3X,4X,5HBURNT,4X,5X,4HMASS,5X,
         4        2(2X,8HFRACTION,3X),2X,11HTRANS. RATE,1X,2(3X,9HFLOW RATE,
         5        2X))
            WRITE(N3,9460)
  9460      FORMAT(10X,5X,3HPSI,5X,2(6X,2HOR,5X),6X,3HLBM,5X,13X,13X,4X,
         1        6HBTU/CA,4X,2(4X,6HLBM/CA,4X)/)
            DO 9500  J = 1,IPR
            WRITE(N3,9480)  (ZOUT(I,J), I=1,10)
  9480      FORMAT(F7.1,3X,3(3X,F7.2,3X ),3X,E9.5,3X,2(4X,F6.5,3X),
         1        3(2X,E10.5,2X))
  9500      CONTINUE
  9580      RETURN
            END
```

```
*****  OPEN  CHAMBER   DIESEL  ENGINE  *****


                         TOM LEFUEVRE RUN NO.  73

                         WEIBE HEAT RELEASE MODEL

                              21 JAN, 1972


ENGINE GEOMETRY DATA =

           RUN NO. =    110                       RPM = 2025.0000         COMPRESSION RATIO =   15.4000
              BORE =     4.5000 IN.            STROKE =    4.5000 IN.    VALVE DIA.  INTAKE =    2.0000 IN.
  CONN. ROD LENGTH =     9.0000 IN.   PRE CUP VOLUME =    1.4000 CU. IN.            EXHAUST =    1.7000 IN.

PORT GEOMETRY =
HYD. DIA.. INTAKE =     2.0000 IN.  C.S. AREA, INTAKE =    3.1400 SQ. IN.   VOLUME, INTAKE =   18.3700 CU. IN.
          EXHAUST =     1.7000 IN.            EXHAUST =    2.8900 SQ. IN.           EXHAUST =   13.3600 CU. IN.


HEAT TRANSFER AREA,    GAS SIDE =
             HEAD =  10.4900 SQ. IN.            PISTON =  20.5700 SQ. IN.           PRE CUP =    6.8685 SQ. IN.
       I. V. FRONT =  3.1400 SQ. IN.       E. V. FRONT =   2.2700 SQ. IN.
       I. V.  BACK =  6.9100 SQ. IN.       E. V.  BACK =   5.0000 SQ. IN.
       INTAKE PORT = 36.9100 SQ. IN.      EXHAUST PORT =  27.7300 SQ. IN.


HEAT TRANSFER AREA, COOLANT SIDE =
             HEAD =  10.4900 SQ. IN.            PISTON =  20.5700 SQ. IN.            SLEEVE =   67.8000 SQ. IN.
           PRE CUP =  6.8685 SQ. IN.
      INTAKE VALVE =  6.9100 SQ. IN.     EXHAUST VALVE =   5.0000 SQ. IN.
       INTAKE PORT = 36.9100 SQ. IN.      EXHAUST PORT =  27.7300 SQ. IN.


VALVE FLOW AREA =
                     OPEN. RAMP         OPENING          CLOSING         CLOS. RAMP
                         CA                CA               CA               CA
      INTAKE VALVE      676.0             700.0            220.0            256.0
     EXHAUST VALVE      446.0             490.0             10.0             62.0
```

```
INTAKE PIPE DATA =
    GRIDS IN PIPE =  12                LENGTH OF PIPE =  36.0 IN.
    GRIDS IN PORT =   2              REL. ERROR LIMIT =  .030

** INTAKE PIPE DYNAMICS IS INCLUDED **
```

ERROR LIMITS =

	PRESSURE PSI	TEMPERATURE R	EQ. RATIO	MASS LBM
MAIN	.50000	1.00000	.00100	.2000-01
PRE	.50000	1.00000	.00100	.2000-01
I. P.	.02000	3.00000	.05000	.2000-01
E. P.		3.00000	.05000	.2000-01

CYCLIC ERROR LIMITS =

	PRESSURE PSI	TEMPERATURE R	EQ. RATIO
MAIN	.50000	5.00000	.00500
PRE	.50000	5.00000	.00500
I. P.	.15000	5.00000	.00500
E. P.		25.00000	.00500

WALL TEMPERATURE ERROR LIMITS =

MAIN CHAMBER HEAD =	10.0000 R	SLEEVE =	10.0000 R	PISTON =	10.0000 R
PRE CUP =	10.0000 R				
INTAKE VALVE =	10.0000 R	EXHAUST VALVE =	10.0000 R		
INTAKE PORT =	10.0000 R	EXHAUST PORT =	10.0000 R		

HEAT RELEASE DATA

COMB. STARTS AT = 345.0000 CA   COMB. ENDS AT = 559.0000 CA

WEIBE HEAT RELEASE PARAMETERS

	MAIN	PRE
CAW	.4900+03	.4900+03
CAPHR	.7000+00	.7000+00
WFCY	.2500-03	.2500-03
WLIBE	.1100+02	.1100+02
YWF	.1504+02	.1504+02

```
TYPE OF HEAT TRANSFER CORRELATION =
CONVECTION = ANNAND
 RADIATION = MODIFIED


HEAT TRANSFER COEFFICIENT MULTIPLYING FACTORS =
CONVECTION  -  MAIN(1) AND PRE(2)
        HEAD(1) =    1.1000          SLEEVE =    .5000       PISTON(1) =    .7000
     I. V. FRONT =   1.1000     E. V. FRONT =   1.1000          PRE(2) =   1.0000      PISTON(2) =    1.0000


 RADIATION  -  MAIN(1) AND PRE(2)
        HEAD(1) =    1.1000          SLEEVE =    .5000       PISTON(1) =    .7000
     I. V. FRONT =   1.1000     E. V. FRONT =   1.1000          PRE(2) =   1.0000      PISTON(2) =    1.0000


PORT SYSTEM =
      I. V. BACK =   1.0000      E. V. BACK =   1.0000     INTAKE PORT =   1.0000   EXHAUST PORT =    1.0000
```

INITIAL VALUES

SYSTEM PROPERTIES

	PRESSURE PSI	TEMPERATURE R	EQ. RATIO
SYSTEM 1 =	31.56	1604.00	.708000
SYSTEM 2 =	.00	.00	.000000
INTAKE PORT =	29.99	692.00	.010000
EXHAUST PORT =	29.50	1534.00	.708000

WALL TEMPERATURES

HEAD(1) = 900.0 R	SLEEVE = 785.3 R	PISTON = 869.2 R	HEAD(2) = .0 R
I. V. = 1205.3 R	E. V. = 1683.7 R	I. P. = 648.3 R	E. P. = 787.6 R

CYCLE DOES NOT CLOSE DUE TO SYSTEM PROPERTIES.   START WITH DIFFERENT INITIAL VALUES

SYSTEM PROPERTIES

	PRESSURE PSI	TEMPERATURE R	EQ. RATIO
SYSTEM 1 =	31.83	1607.82	.696653
SYSTEM 2 =	.00	.00	.000000
INTAKE PORT =	30.14	680.92	.013360
EXHAUST PORT =	29.50	1678.18	.695634

WALL TEMPERATURES

HEAD(1) = 911.8 R	SLEEVE = 735.2 R	PISTON = 796.4 R	HEAD(2) = .0 R
I. V. = 1159.0 R	E. V. = 1796.3 R	I. P. = 646.6 R	E. P. = 856.8 R

CYCLE DOES NOT CLOSE DUE TO SYSTEM PROPERTIES.   START WITH DIFFERENT INITIAL VALUES

SYSTEM PROPERTIES

	PRESSURE PSI	TEMPERATURE R	EQ. RATIO
SYSTEM 1 =	31.95	1582.29	.682814
SYSTEM 2 =	.00	.00	.000000
INTAKE PORT =	30.29	675.00	.013193
EXHAUST PORT =	29.50	1671.23	.681673

WALL TEMPERATURES

HEAD(1) = 906.3 R	SLEEVE = 733.7 R	PISTON = 793.6 R	HEAD(2) = .0 R
I. V. = 1145.5 R	E. V. = 1762.8 R	I. P. = 646.0 R	E. P. = 871.9 R

CYCLE DOES NOT CLOSE DUE TO SYSTEM PROPERTIES.   START WITH DIFFERENT INITIAL VALUES

SYSTEM PROPERTIES

	PRESSURE PSI	TEMPERATURE R	EQ. RATIO
SYSTEM 1 =	32.05	1574.33	.677628
SYSTEM 2 =	.00	.00	.000000
INTAKE PORT =	30.49	673.21	.013023
EXHAUST PORT =	29.50	1667.54	.676526

WALL TEMPERATURES

HEAD(1) = 905.1 R	SLEEVE = 733.4 R	PISTON = 793.1 R	HEAD(2) = .0 R
I. V. = 1191.4 R	E. V. = 1761.1 R	I. P. = 645.8 R	E. P. = 872.6 R

CYCLE DOES NOT CLOSE DUE TO SYSTEM PROPERTIES. START WITH DIFFERENT INITIAL VALUES

SYSTEM PROPERTIES

	PRESSURE PSI	TEMPERATURE R	EQ. RATIO
SYSTEM 1 =	32.15	1569.02	.673709
SYSTEM 2 =	.00	.00	.000000
INTAKE PORT =	30.59	672.60	.012875
EXHAUST PORT =	29.50	1661.83	.672653

WALL TEMPERATURES

HEAD(1) = 904.5 R	SLEEVE = 733.2 R	PISTON = 792.8 R	HEAD(2) = .0 R
I. V. = 1138.8 R	E. V. = 1756.8 R	I. P. = 645.7 R	E. P. = 871.7 R

*** CYCLE CLOSES ***

FINAL VALUES AT THE END OF THE CYCLE

SYSTEM PROPERTIES

	PRESSURE PSI	TEMPERATURE R	EQ. RATIO
SYSTEM 1 =	32.15	1569.02	.673709
SYSTEM 2 =	.00	.00	.000000
INTAKE PORT =	30.59	672.60	.012875
EXHAUST PORT =	29.50	1661.83	.672653

WALL TEMPERATURES

HEAD(1) = 904.5 R	SLEEVE = 733.2 R	PISTON = 792.8 R	HEAD(2) = .0 R
I. V. = 1138.6 R	E. V. = 1756.8 R	I. P. = 695.7 R	E. P. = 871.7 R

TABULAR OUTPUT

CA	PRESSURE PSI	TEMP. OR	EQ. RATIO	MASS LBM	FUEL INJ. RATE LBM/CA	WORK RATE BTU/CA	HEAT TRANS. RATE BTU/CA	I. V. MASS FLOW RATE LBM/CA	E. V. MASS FLOW RATE LBM/CA
1.0	32.15	1569.02	.67371	.15906-03	.00000	.46725-04	-.97902-04	-.25108-05	-.28532-06
21.0	28.69	1092.34	.32182	.32423-03	.00000	.84564-03	.28011-04	.17710-04	.00000
41.0	28.23	816.79	.12710	.84653-03	.00000	.14745-02	.78576-04	.33591-04	.00000
61.0	27.75	717.30	.06838	.16234-02	.00000	.18245-02	.10730-03	.42947-04	.00000
81.0	27.41	671.29	.04470	.25245-02	.00000	.18834-02	.12591-03	.46367-04	.00000
101.0	27.58	648.69	.03287	.34507-02	.00000	.17217-02	.13640-03	.45609-04	.00000
121.0	28.27	638.62	.02621	.43229-02	.00000	.14073-02	.13957-03	.40950-04	.00000
141.0	29.26	635.53	.02233	.50584-02	.00000	.98922-03	.13538-03	.31710-04	.00000
161.0	30.13	635.98	.02027	.55558-02	.00000	.50042-03	.13574-03	.17393-04	.00000
181.0	30.72	638.83	.01957	.57485-02	.00000	-.26870-04	.13602-03	.15774-05	.00000
201.0	31.47	644.51	.01957	.57012-02	.00000	-.57758-03	.86915-04	-.26587-05	.00000
221.0	34.51	662.62	.01958	.56709-02	.00000	-.12247-02	.82216-04	-.87498-06	.00000
241.0	41.06	696.69	.01958	.56676-02	.00000	-.21034-02	.73193-04	.00000	.00000
261.0	53.70	751.69	.01958	.56676-02	.00000	-.34043-02	.56604-04	.00000	.00000
281.0	79.38	838.05	.01958	.56676-02	.00000	-.54679-02	.23468-04	.00000	.00000
301.0	137.84	974.45	.01958	.56676-02	.00000	-.89433-02	-.53834-04	.00000	.00000
321.0	293.69	1192.16	.01958	.56676-02	.00000	-.14793-01	-.27276-03	.00000	.00000
341.0	741.71	1511.72	.01958	.56676-02	.00000	-.19984-01	-.94220-03	.00000	.00000
345.0	882.16	1577.86	.01958	.56676-02	.00000	-.18971-01	-.11559-02	.00000	.00000
361.0	1879.57	2547.28	.16716	.57241-02	.52690-05	.27382-02	-.41951-02	.00000	.00000
381.0	1579.87	3347.83	.43537	.58267-02	.43020-05	.46738-01	-.55879-02	.00000	.00000
401.0	807.08	3352.04	.59352	.58873-02	.18507-05	.42192-01	-.40555-02	.00000	.00000
421.0	435.41	3087.37	.65000	.59089-02	.51883-06	.28634-01	-.27725-02	.00000	.00000
441.0	268.76	2805.89	.66376	.59141-02	.10217-06	.18471-01	-.20041-02	.00000	.00000
461.0	188.94	2588.70	.66618	.59151-02	.14707-07	.11794-01	-.15741-02	.00000	.00000
481.0	147.94	2436.56	.66649	.59152-02	.15879-08	.73634-02	-.13317-02	.00000	.00000
501.0	126.11	2339.93	.66652	.59137-02	.13096-09	.42640-02	-.11923-02	.00000	-.93593-06
521.0	109.59	2255.07	.66656	.56903-02	.83666-11	.18210-02	-.10582-02	.00000	-.28281-04
541.0	84.06	2112.92	.66674	.47500-02	.41871-12	-.73395-04	-.79868-03	.00000	-.59849-04
561.0	58.59	1935.60	.66703	.35292-02	.00000	-.10751-02	-.52609-03	.00000	-.58793-04
581.0	40.36	1766.28	.66738	.24846-02	.00000	-.14319-02	-.32924-03	.00000	-.43352-04
601.0	31.90	1663.01	.66767	.18423-02	.00000	-.16337-02	-.23146-03	.00000	-.21823-04
621.0	30.85	1641.71	.66788	.14887-02	.00000	-.19557-02	-.19657-03	.00000	-.16541-04
641.0	31.23	1637.71	.66814	.11394-02	.00000	-.21513-02	-.17375-03	.00000	-.18261-04
661.0	31.57	1631.76	.66852	.77426-03	.00000	-.20487-02	-.14773-03	.00000	-.17749-04
681.0	31.91	1622.09	.66905	.45192-03	.00000	-.16067-02	-.12450-03	.00000	-.13885-04
701.0	34.02	1624.09	.66967	.24164-03	.00000	-.91575-03	-.11483-03	.00000	-.66708-05
721.0	32.25	1564.98	.67007	.16001-03	.00000	.46807-04	-.97409-04	-.24465-05	-.28871-06

SUM OF MASS FLOW RATES DURING CYCLE

	AIR LBM/CYCLE	FUEL LBM/CYCLE	TOTAL LBM/CYCLE	TOTAL LBM/HR
I. V.	.54860-02	-.41899-07	.54859-02	.33327+03
E. V.	-.54850-02	-.24755-03	-.57326-02	-.34825+03
BLOWBY	.00000	.00000	.00000	.00000
THROAT	.00000	.00000	.00000	.00000
I. P.	.54867-02	-.53549-07	.54867-02	.33332+03
E. P.	-.54637-02	-.24758-03	-.57313-02	-.34818+03
FUEL(1)		.24760-03	.24760-03	.15042+02
FUEL(2)		.00000	.00000	.00000

TEMPERATURE		DEG R
	MASS AVE INTAKE TEMP	587.8
	AVE INTAKE TEMP	613.6
	MASS AVE EXHAUST TEMP	1882.1
	AVE EXHAUST TEMP	1744.0
COOLANT	TEMP RISE HEAD	2.8
COOLANT	TEMP RISE BARREL	5.9
COOLANT	TEMP RISE TOTAL	8.7
COLING AIR	TEMP RISE FRICTION	1.9

SUM OF ENERGY FLOW RATES

	BTU/CYCLE
INLET VALVE	.76031+00
EXHAUST VALVE	.19394+01
BLOWBY	.00000
THROAT	.00000
FUEL INJ.(1)	-.57940-01
FUEL INJ.(2)	.00000
INTAKE PORT	.72880+00
EXHAUST PORT	.19406+01
PISTON WORK	.21149+01

CYCLIC HEAT TRANSFER RATES

	CONVECTION BTU/CYCLE	RADIATION BTU/CYCLE	TOTAL BTU/CYCLE	WALL TEMP DEG R	EFF GAS TEMP DEG R
HEAD(1)	-.14442+00	-.14886-01	-.15931+00	903.9	2198.4
HEAD(2)	.00000	.00000	.00000	800.0	.0
SLEEVE	-.10559+00	-.61256-02	-.11172+00	733.1	1728.6
PISTON(1)	-.19735+00	-.18688-01	-.21604+00	792.5	2199.8
PISTON(2)	.00000	.00000	.00000		
I. V. FRONT	-.34029-01	-.43564-02	-.38386-01	1136.7	2194.1
I. V. BACK	.31277-01		.31277-01		650.6
E. V. FRONT	-.85897-02	-.25921-02	-.11182-01	1752.0	2171.3
E. V. BACK	-.47631-02		-.47631-02		1814.2
I. P. WALL	.10007-01		.10007-01	645.6	614.3
E. P. WALL	.40626-02		.40626-02	870.4	1746.6
SYSTEM(1)	-.46040+00	-.46648-01	-.52704+00		
SYSTEM(2)	.00000	.00000	.00000		
I. PORT	.31728-01		.31728-01		
E. PORT	-.73477-03		-.73477-03		

MASS AND ENERGY BALANCE

	MASS IN LBM/CYCLE	MASS OUT LBM/CYCLE	ERROR LBM/CYCLE	ENERGY IN BTU/CYCLE	ENERGY OUT BTU/CYCLE	ERROR BTU/CYCLE
SYSTEM 1 =	.5734-02	.5733-02	.9598-06	.7024+00	.7025+00	-.1594-03
SYSTEM 2 =	.0000	.0000	.0000	.0000	.0000	.0000
I. P. SYSTEM =	.5487-02	.5486-02	.7513-06	.7288+00	.7286+00	.2176-03
E. P. SYSTEM =	.5733-02	.5731-02	.1283-05	-.1939+01	-.1940+01	.4371-03

HORSE POWER

NIHP	50.49	IHP	51.58
BHP	39.41	PHP	-1.08
RAHP	11.09	RAHP/BHP	28.14

MEAN PRESSURE, PSI

NIMEP	275.94	IMEP	281.86
BMEP	*****	PMEP	-5.92
RAMEP	60.59	RMEP	3.52

EFFICIENCIES

MECHANICAL	76.40	VOLUMETRIC	91.81
I THERMAL	46.16	ISFC	.29
B THERMAL	35.27	BSFC	.38

MAXIMUM PRESSURE (1) = 2023.17 PSI   FUEL/AIR RATIO = .04513

TEMPERATURE (1) = 3409.37 R   EQUIVALENCE RATIO = .66744

APPENDIX II

A

Development and Evaluation of the Simulation of the Compression-Ignition Engine

K.J. McAulay, Tang Wu and Simon K. Chen
International Harvester Co.

G.I. Borman, P.S. Myers and O.A. Uyehara
Mechanical Engineering Dept.
University of Wisconsin

ABSTRACT

The first part of the paper deals with the mathematical model and computer program for simulating a compression-ignition engine. The various assumptions used and the effects of these assumptions on the results are discussed. The second part of the paper evaluates results of the engine simulation program by comparisons with experimental data and with other simplified cycle calculations. The comparisons with experimental data include motoring, part load, and full load data for a speed range of 1400-3200 rpm. The simulation results show good agreement with experimental pressure-volume diagrams. The computed trends of volumetric efficiency, heat rejection, and metal part temperatures show reasonable agreement with experimental data.

HISTORY

This paper represents work done at International Harvester Co. and at the University of Wisconsin. Because this study has covered a considerable period of time, it has inevitably involved a large number of people. Thus, while all of the six authors have made major contributions to the study, many other individuals have also made significant contributions, particularly in obtaining experimental data. It should also be recognized that this paper is the result of collaboration by all six authors although, for convenience, it is presented in two parts by the authors shown.

The work was originated at IH in 1960 with the objective of reducing design and development time of diesel engines. Personnel from the University of Wisconsin initially participated as consultants to IH. As the program developed, the Army Tank Automotive Center (ATAC) recognized that an engine simulation program would be useful to them in their development work. Consequently they began to support various phases of the program with the work being conducted at the University of Wisconsin through the cooperation of Continental Aviation and Engineering Company.

Although no attempt will be made to give credit to particular organizations for particular parts of the program, it should be mentioned that a large part of the comparison data were obtained by International Harvester Co., as part of its continuing combustion research.

Cooperative work in further development and refinement of the program is continuing through extensive programs at IH with its own funds, and studies at the University of Wisconsin financed primarily by ATAC. Thus, this paper represents a report on progress made to date.

PART I - DEVELOPMENT OF THE SIMULATION PROGRAM

K.J. McAulay, G.L. Borman, Tang Wu

Because of the complexity of physical phenomena encountered in engines, the design of engines has relied heavily on experience and "know how". As a result, extensive testing of prototypes has been a necessary prerequisite to all engine development. To obtain the best design from such testing is a task of considerable magnitude, and probably no engine has ever been truly optimized.

Development engineers have recognized that cycle analysis (engine simulation) is a useful tool for the following reasons:

1. Engine simulation necessitates and provides a better understanding of the variables involved and of their effect on engine performance.
2. Engine simulation systematizes knowledge obtained through expensive engine testing.
3. Engine simulation reduces the amount of required engine testing by narrowing the range of engine variables that must be studied experimentally.
4. Engine simulation provides a tool in optimizing an engine design for a particular application.
5. Engine simulation clearly delineates those areas in which our knowledge is deficient.

Air-standard cycle analysis is commonly used, but because of its simplicity, the preceding benefits can be only partially obtained. Air-standard cycle analysis can be only partially obtained. Air-standard cycle analysis can be improved by the introduction of more realistic expressions for thermodynamic properties of combustion gases and by the introduction of a prescribed amount of heat transfer during the various processes. More recently, the analysis of adiabatic constant-volume fuel-air cycles has been programmed for the digital computer (1)*. This type of analysis gives useful relationships between the performance parameters, compression ratio, fuel-air ratio, and type of fuel used.

The assumption of constant-volume combustion may be modified by assuming a constant-volume combustion followed by a constant-pressure combustion with the division between these two processes being arbitrary and usually chosen to limit the peak pressure. Reference 2 illustrates one way in which heat transfer and finite combustion rates may be included in the analysis.

With the availability of high-speed digital computers, a number of attempts to produce a realistic simulation model (cycle analysis) have been made. To date, Cook (3), Whitehouse (4), Patterson (5), and Huber (6) have published papers dealing with computer models for the internal combustion engine.

The work of Cook, begun in 1953 and first published in 1959 (3), is the first published analysis of engines going beyond the traditional fuel-air cycle assumptions. Unfortunately, Cook's papers deal primarily with the results of the analysis rather than with specific information concerning the assumptions incorporated in the program.

The model of Whitehouse, et al. (4) did not take into account heat transfer during the exhaust or intake processes, but did allow the heat transfer from the cylinder gas to the piston crown, head, and liner surfaces. The metal surface temperatures were calculated prior to the cycle analysis, and a single, constant, surface temperature for heat transfer was used to calculate the heat transfer at each crank angle. The flow through the valves was computed at each crank angle from the valve lift and the instantaneous pressure difference, assuming quasi-steady adiabatic flow. The properties of the combustion products were obtained from linear interpolation of the data of Keenan and Kaye and thus did not include the dissociation effects. Since these authors did not give extensive comparisons between calculated and experimental results, the utility of their program cannot be evaluated. It is not clear from their paper whether their assumptions for heat transfer during the intake process and for the metal surface temperatures will cause significant error in calculating volumetric efficiencies.

*Numbers in parentheses designate References at end of paper.

While simulation of spark-ignition engines is not directly applicable, there are enough similarities that simulation programs for these engines should be mentioned. Strange (2), and Patterson and Van Wylen (5) included the effects of dissociation in computing the properties of combustion products as well as heat transfer while assuming the intake and exhaust processes to be ideal, that is, instantaneous events and isentropic. The paper of Huber and Brown (6) is a fairly detailed simulation. They calculated the flow through the valves as a function of valve lift and pressure ratio. Instantaneous heat transfer was computed throughout the entire cycle. In addition, heat transfer to the intake and exhaust flows was taken into account. The effects of dissociation were neglected. Metal temperatures were assumed rather than calculated.

More or less simultaneously with the above mentioned studies, IH decided that a detailed simulation of compression-ignition engines should produce useful results. It was recognized that many of the assumptions would, by necessity, be simple and that in order to verify these assumptions, many comparisons would have to be made with experimental data. As will be pointed out later, the experimental data used for these comparisons must be extremely reliable and as complete as possible. The two sections of this paper will present the model used, assumptions made, results obtained, and a comparison of results with experimental and with other types of cycle analysis.

BASIC PROCEDURES USED

Mathematical simulation of an engine requires that:

1. We define all thermodynamic systems involved in the simulation.
2. Assumptions for each system be clearly stated.
3. The equations which apply to each system be written.
4. All required data be collected.
5. The resulting equations be solved.

In addition, in order to improve the assumptions and to gain confidence in the simulations, one would want to collect and compare computed and experimental results. Before starting to describe our detailed simulation, let us first review basic thermodynamics and simple cycle analysis.

Normally five kinds of equations are required to describe completely the behavior of a thermodynamic system. These equations are:

1. Conservation of energy.
2. Conservation of mass.
3. Conservation of momentum.
4. A relationship between pressure, volume, and temperature for the working fluid.
5. An expression for the internal energy of the working fluid in terms of temperature, pressure, and composition of the working fluid.

The energy equation may be written for the general case as

$$\dot{U} = (\dot{\overline{Mu}}) = -p\dot{V} + \Sigma\dot{Q}_i + \Sigma h_i\dot{M}_i \tag{1}$$

where:

Dot = Derivative with respect to time
M = Mass
u = Total internal energy per unit mass
h = Total enthalpy per unit mass
p = Pressure
V = Total volume
Q = Rate of heat transfer
Index i = Different surfaces at the boundaries of the system

The left-hand side is the rate of change of internal energy with time. The right-hand side consists of the rate of work due to piston motion, the sum of the heat transfer rates over the boundaries, and the sum of all energy flowing in or out of the system because of mass transfer.

Let us first "simulate" the familiar air-standard-cycle engine. The usual model (assumptions made) is an engine using the same working fluid (air) over and over again without mass transfer across the boundaries. With these assumptions, Eq. 1 simplifies to

$$\dot{U} = -p\dot{V} + \Sigma\dot{Q}_i \tag{2}$$

Equation 2 can be integrated for a closed cycle to give

$$\int p\dot{V}\,dt = \int \Sigma\dot{Q}_{Ai} - \int \Sigma\dot{Q}_{Ri} = Q_A - Q_R \tag{3}$$

where the left-hand side represents all the work done during the cycle and Q_A and Q_R represent the heat added and heat rejected respectively during one cycle. Thermal efficiency is defined as

$$E = \frac{\int p\dot{V}\,dt}{Q_A} = 1 - \frac{Q_R}{Q_A}$$

In the air-standard cycle, heat is added only when desired and by an arbitrarily specified process, that is, constant volume, constant pressure, and so on. Under these conditions the $\int p\dot{V}\,dt$ can be integrated since for these cases the paths are known. When applied to the constant-volume air-standard cycle, the expression for its efficiency is obtained as

$$E = 1 - 1/(CR)^{k-1} \tag{4}$$

where:

CR = Compression ratio
k = Ratio of specific heats

For the fuel-air cycle, the internal energy is considered to be a function of temperature and fuel-air ratio (and pressure when dissociation is present), but the same basic procedure is followed.

The above models are attractive because of their mathematical simplicity but can give only limited information because of the simplifying assumptions inherent in their development. In the real engine, mass transfer and heat transfer are a function of time. These complications must be included if the real engine is to be simulated.

The more complex and detailed model, which will be described below, gives such complicated equations that they cannot be integrated in closed form as was done for the air-standard cycle but must be integrated numerically. The model will yield information regarding volumetric efficiency, rates of heat transfer, pressure-time diagrams, metal temperatures, and such. The completeness and accuracy of the resulting computed data will depend upon the amount of detail included and our ability to express the phenomena that occur in an engine in mathematical terms.

SYSTEMS AND ASSUMPTIONS ... For present purposes, the analysis was restricted to a single-cylinder engine. The basic procedures would be the same, but more complicated, for a multicylinder engine. This single-cylinder engine was divided into four systems: the cylinder, intake port (and in some cases the intake manifold), exhaust port (and in some cases the exhaust manifold), and engine cooling system.

Cylinder - The model assumes five different heat transfer surfaces. Each of these heat transfer surfaces was assumed to have a uniform surface temperature over its entire area. The five heat transfer surfaces used were the intake valve, exhaust valve, remaining portions of the head, sleeve area exposed to the gases at any instant, and piston. The temperature of any one of these five surfaces undoubtedly varies slightly with time and with position on the surface, but it is felt that these assumptions were a reasonable compromise between accuracy and complexity. Neglecting the variation of the temperature with position does not cause a significant error in the cycle calculations but does mean that no information can be obtained as to the maximum temperature reached at a particular location. The variation of metal temperature with time (typically 30-40 F) could cause some error, particularly on the intake stroke where the temperature difference between the metal and incoming gases is small.

The model assumes no deposits on the inside surface of the cylinder walls. A recent idealized study (7) indicates that, due to the thermal characteristics of the deposits, small amounts of deposits may have detectable effects on heat transfer rates, thus influencing volumetric efficiencies and heat rejection rates.

The rate of heat transfer from the gases to the wall was calculated using an instantaneous heat transfer coefficient, $\bar{h}$, an instantaneous mass-averaged gas temperature, T, and a uniform metal surface temperature, T_i.

An equivalent, one-dimensional, metal path length for heat transfer was assigned to each metal part. At the end of a cycle calculation, the total heat transfer from the gas to the metal must equal the total heat transfer through the metal which must equal the total heat transfer to the coolant from that part. This condition gives equations from which the metal temperatures for each part can be calculated. Because there is friction between the piston and sleeve and because much of the heat transfer from the piston must go through the sleeve, a different passive network must be solved. Likewise, both the intake and the exhaust valves are in contact with port gases as well as cylinder gases. Again, a heat transfer network must be set up for these parts. The details are given in Appendix A.

During "combustion" a rate of heat release was specified. This rate was determined originally by analysis of an experimental pressure-time diagram from an engine of similar design. The fuel-air ratio, which is considered uniform throughout the cylinder at any one instant, increases as burning occurs. In general, the fuel-air ratio in the cylinder may be affected by mass flows in and out of the cylinder as well as by combustion, and appropriate corrections must be made.

Thermodynamic equilibrium was assumed at each instant of time for the calculation of the thermodynamic properties of the gases in the cylinder. In addition, the kinetic and potential energies of the cylinder gas were assumed to be zero. The pressure was, therefore, assumed uniform throughout the cylinder at any instant of time. The perfect gas relationship was assumed to hold at all times.

Equilibrium thermodynamic computations for the products of combustion for C_nH_{2n} were performed by E.S. Starkmand and H.K. Newhall of the University of California. These calculations gave tables of internal energy for different values of temperature, pressure, and fuel-air ratio. As a means of interpolating in these tables, mathematical expressions were developed to give internal energy as a function of pressure, temperature, and fuel-air ratio.

The molecular weight which appears in the equation of state is a function of pressure, temperature, and fuel-air ratio when dissociation occurs. Thus, an equation was also developed for the molecular weight as a function of the three variables.

Flow into or out of the cylinder can occur from any one of three places, that is, the two valves and blowby past the piston. Without any experimental basis for the assumption, the blowby past the piston was assumed to be proportional to the cylinder gage pressure. The proportionality constant was included as an arbitrarily specified constant and was assumed to be zero for the calculations reported herein.

An instantaneous flow rate through either valve was computed using conventional flow equations, the pressure in the port, and the pressure in the cylinder, together with a flow coefficient. The flow coefficient was obtained in steady-flow experiments. The valve life can be determined from engine geometry although it may be necessary to take into account valve dynamics and temperature effects.

Intake Port - The properties of the gases in the intake port were computed using the same relationship as those used for the gases in the cylinder. The fuel-air ratio in the intake port is not zero when flow from the cylinder to the intake port occurs. Although the extent of mixing is uncertain, this back-flow from the cylinder was assumed to mix instantaneously with the air throughout the entire port volume. For simplicity, the small amount of flow from the port to the atmosphere was assumed to be air only.

For calculation of heat transfer, two different surfaces were considered, that is, the port wall, and the back of the intake valve which was assumed to be at the same temperature as the face of the intake valve. An instantaneous heat transfer coefficient was used to describe the rate of heat transfer. When gas flowed from port to cylinder, the heat transferred from the back of the intake valve was added to the cylinder energy balance.

An assumption must be made regarding the variation of port pressure with time. The simplest assumption, but one seldom realized in practice, would be to assume port pressure constant and independent of time. The pressure at the port will vary with time for the usual single cylinder set up where the intake port is connected to a surge tank by a length of pipe. One procedure used was to determine experimentally the pressure in the port as a function of time and use these data as input to the program. Another procedure used was to construct an unsteady flow model with the same assumptions as Ref. 9, that is, one-dimensional, large amplitude waves, no heat transfer, and no friction. The details of the unsteady-flow analysis are shown. in Ref. 10. Data obtained from both of these procedures will be shown in Part II.

Exhaust Port - The properties of the gases in the exhaust port were computed from the equations for the properties of the products of combustion. Any gases flowing from cylinder to exhaust port were considered to be mixed instantaneously with the gases in the port. Any gases flowing out of the exhaust port had the composition of this mixture. Any gases flowing from exhaust port to cylinder were instantaneously mixed with the cylinder gases.

Heat transfer was handled in a manner analogous to that for the intake port.

The exhaust port pressure can be considered either constant or as a function of time. For some of the comparison runs presented in Part II, the exhaust port pressure was considered constant with time. In other runs experimental values of of exhaust port pressure versus time were used. An unsteady-flow analysis for the exhaust port has just been programmed for the computer. This analysis assumes one-dimensional unsteady flow, large amplitude waves, and includes the effect of both heat transfer and friction.

Engine Coolant - Two different cases have been considered -- air-cooling (10) and liquid-cooling -- although only the data for liquid-cooling are presented here. The coolant enters the engine at a specified temperature. The rate of heat transfer to the coolant was specified by a heat transfer coefficient which is a function of coolant properties and engine geometry. The geometry of the cooling system is quite complicated, and judgment is involved in determining the heat transfer coefficient.

BASIC EQUATIONS USED ... The basic equations used for each of the thermodynamic systems must be solved simultaneously and integrated numerically. It is convenient to express these equations in terms of the dependent variables, pressure, p; temperature, T; and equivalence ratio, F; (actual fuel-air ratio divided by stoichiometric fuel-air ratio).

Energy Equation - The time derivative of the internal energy (which includes both sensible and chemical energy) can be written as

$$\dot{u} = \frac{\partial u}{\partial T}\dot{T} + \frac{\partial u}{\partial p}\dot{p} + \frac{\partial u}{\partial F}\dot{F} \tag{5}$$

where the partial derivatives are known functions of the dependent variables.

Equation 5 and the equation of state ($pV=RT$) can be substituted into the energy equation (Eq. 1) and the resulting form of the energy equation rearranged to give

$$\dot{T} = \frac{A - \frac{p}{D}\frac{\partial u}{\partial p}\left[\frac{\dot{M}}{M} - \frac{\dot{V}}{V} + \frac{\dot{F}}{R}\frac{\partial R}{\partial F}\right] - \left[\frac{\partial u}{\partial F}\dot{F}\right]}{\frac{\partial u}{\partial T} + \frac{\partial u}{\partial p}\frac{p}{T}\frac{C}{D}} \tag{6}$$

where:

$$A = -RT\,\frac{\dot{V}}{V} + \frac{1}{M}\left[\Sigma\dot{Q}_i + \Sigma h_i\dot{M}_i - u\dot{M}\right] \tag{7}$$

$$C = 1 + \frac{T}{R}\,\frac{\partial R}{\partial T} \tag{8}$$

$$D = 1 - \frac{p}{R}\,\frac{\partial R}{\partial p} \tag{9}$$

For temperatures below about 3000 R, the term $\partial u/\partial p$ is zero, that is, dissociation is negligible. Under these conditions Eq. 6 simplifies to

$$\dot{T} = \left[A - \frac{\partial u}{\partial F}\,\dot{F}\right]\Big/\frac{\partial u}{\partial T} \tag{10}$$

The volume and rate of change of volume with time used in Eq. 7 were determined by standard relationship from engine geometry. The term $\dot{F}$ was obtained by differentiating the equation for F. The equation for the instantaneous value of equivalence ratio, F, for the cylinder is given by

$$F = \frac{\dfrac{M_oF_o}{1+f_o} + \displaystyle\int_o^t\left[\frac{\dot{M}_IF_I}{1+f_I} + \frac{\dot{M}_EF_E}{1+f_E} + \frac{\dot{M}_F}{f_s}\right]dt}{\dfrac{M_o}{1+f_o} + \displaystyle\int_o^t\left[\frac{\dot{M}_I}{1+f_I} + \frac{\dot{M}_E}{1+f_E}\right]dt} \tag{11}$$

where f is the fuel-air ratio and the subscripts o, I, E, F, s refer to the initial values in the cylinder, the value of the intake, the value for the exhaust, the fuel added, and stoichiometric, respectively.

The values f_I, F_I, f_E, F_E are the port values for flow into the cylinder and the cylinder values for flow out of the cylinder. Equation 11 assumes no blowby and complete mixing. Similar expressions were developed for the value of F in the intake and exhaust ports.

Mass Flow Rate - The value for the rate of mass flow, M, was computed from the steady flow relationship,

$$M = A_e p_1\sqrt{\phi_1 g_c/R_1T_1} \tag{12}$$

where:

A_e = Effective flow area

g_c = Dimensional constant

$$\phi_1 = \frac{2k}{k-1}\left[\left(\frac{p_2}{p_1}\right)^{2/k} - \left(\frac{p_2}{p_1}\right)^{(k+1)/k}\right] \tag{13}$$

Subscripts 1 and 2 denote upstream and effective area conditions respectively, and the pressure ratio is the critical value when sonic conditions prevail.

Heat Transfer Rate - The instantaneous rate of heat transfer, Q_i, for any surface was computed using a heat transfer coefficient $\tilde{h}_i$ by

$$Q_i = \tilde{h}_iA_i(T_i - T) \tag{14}$$

In order to compute the heat transfer through the metal wall readily, a time-average value of the product of the heat transfer coefficient and exposed area and an appropriately defined effective gas temperature were used. These values were used to give an equivalent steady heat transfer model for the gas, wall, and coolant film combination having a heat transfer rate equal to the average gas side rate. Using this equivalent model, the metal temperature at the gas-wall interface can be computed as well as the heat transfer through the wall and coolant film.

The model did not include unsteady state operation, that is, a warmup period, and thus the initial conditions for steady state had to be estimated and the correct values determined by successive iteration.

Intake System Gas Dynamics - For the unsteady airflow, a straight pipe of constant area with isentropic flow was assumed. For these conditions the equations used were

$$\begin{aligned} \frac{\partial v}{\partial t} + v\,\frac{\partial v}{\partial x} + \frac{c^2}{\rho}\,\frac{\partial \rho}{\partial x} &= 0 \\ \frac{\partial \rho}{\partial t} + v\,\frac{\partial \rho}{\partial x} + \rho\,\frac{\partial v}{\partial x} &= 0 \end{aligned} \qquad (15)$$

where:

v and ρ = local gas velocity and density

c = local velocity of sound

Two boundary conditions are specified: one at the open end of the intake system and one at the valve end. The solution is iterated until it becomes periodic.

The solution to these equations provides an average pressure for the intake port thermodynamic equations and the pressure at the valve which determines the mass flow. It is assumed that the heat transfer in the port has a negligible effect on the wave solution, but is important for determining the average temperature of the gases flowing into the cylinder. Details of the solution are shown in Ref. 10.

DETERMINATION OF INPUT DATA ... A complete physical description of the engine is required before the calculations can begin. Some of the data (bore, stroke, connecting rod length, compression ratio) are readily obtained from engine geometry, but judgments are involved in obtaining some of the other data such as heat transfer path lengths.

Fluid Flow - Flow data must be obtained for the coolant passages, the intake valve, and exhaust valve.

The determination of the hydraulic diameter and velocity of the cooling fluid (for a fixed pump rpm) involves a knowledge of the flow rate, inspection of the water passages, and judgment as to the Reynolds number to be used. The variation of fluid velocity with engine rpm can be determined from water pump test data or, in the absence of such data, assumed to vary linearly with engine rpm (this assumes a constant pump efficiency).

Flow through both the exhaust and intake valves is computed using steady compressible flow equations (Eq. 12) and an effective flow area which is determined experimentally for the particular port and valve combination by a steady flow bench test. The effective flow area should be determined for flow in both directions and and for a wide range of pressure drops, although tests, to date, have indicated that this area is not markedly dependent upon these variables. The measuring stations were the port flanges and the cylinder. Under these conditions, the flow was steady and adiabatic. An effective valve flow area as a function of valve lift was then computed, using isentropic flow relationships and the total pressures at the measuring stations. In the actual engine, heat transfer does occur, and the flow is intermittent. Stanitz (8) has concluded that the error in using effective areas, as determined by a steady flow bench, is a maximum of a few per cent when applied to engine conditions. Heat transfer could contribute to some of the discrepancy between computed and experimental results. Differences between actual and computed valve lifts, as a result of valve dynamics and temperature effects, could also contribute to this discrepancy.

Heat Transfer - As indicated previously, the heat transfer is assumed to be one-dimensional through the metal, and an equivalent one-dimensional heat transfer path length must be assigned to each engine part under consideration.

Equivalent one-dimensional path lengths for the sleeve can be determined by direct measurement from drawings of the engine, if the path is nearly one-dimensional.

The head geometry is very complicated. Thus judgment must be used in assigning equivalent one-dimensional path lengths.

The equivalent heat transfer path length for the valve is even harder to determine. When the valve is seated, the valve head is cooled by the valve seat as well as by conduction through the stem. The intake valve is also cooled by inlet air. The procedure used is to adjust the effective length to a value that gives reasonable valve temperatures. If gas heat transfer coefficients are reasonably well known, correct trends for valve temperature as a function of operating conditions should be obtained.

On the gas side in the cylinder, two basically different types of correlations are available, one by Eichelberg (11) and one by Annand (12).

Eichelberg's equation is

$$\tilde{h} = \text{constant } (c_m)^{1/3} (PT)^{1/2} \tag{16}$$

where c_m is mean piston speed.

In use the constant was adjusted to produce the desired total heat transfer.

Annand's pipe-flow type equation is

$$\tilde{h} = c_1 \frac{k}{B} \left(\text{Re}\right)^b + c_2 \frac{\left(T^4 - T_i\right)}{\left(T - T_i\right)} \tag{17}$$

where:

Re = Reynolds number

B = Bore

c_1 and c_2 = Constants, with c_2 taken as zero during the compression stroke

For present computations, b was assumed to be 0.7, gas properties were considered as functions of temperature, and c_1 was taken as 0.17. The radiation was calculated by replacing the constant c_2 with the variable value obtained from

$$c_2 = \sigma\alpha(1 - e^{-KL}) \tag{18}$$

where:

σ = Stefan-Boltzmann constant

α = 0.90 for head and piston

α = 0.25 for the sleeve

L = Bore for the sleeve, in.

L = Instantaneous distance between the head and piston, for the head, piston, and valve faces, in.

$K = 4 \times (10)^4 \rho_F$ and is a measure of the number of radiating carbon particles per unit path length.

ρ_F = Pounds of fuel burned per cu in. of cylinder volume.

Figure 1 shows the total heat flux for all cylinder surfaces as computed using the Annand and Eichelberg formulas. The proportionality constant in the Eichelberg coefficient was adjusted to give the same total heat transfer for the cycle shown as did the Annand coefficient. Figure 1 thus shows these two correlations give different rates of heat transfer at different times in the cycle. Based on computations performed and comparisons with experimental data, the authors are inclined to prefer the pipe-flow type of correlation with radiation included. Neither of these expressions include the effect of instantaneous air velocity either during the stroke or between different engine designs (13). In addition, there is evidence to indicate that the rate of change of pressure with time may affect rates of heat transfer (14). Our knowledge of heat transfer coefficients is limited. Under ATAC sponsorship, experimental studies being conducted at the University of Wisconsin are aimed at improving our understanding of this problem.

Referring to the intake and exhaust ports, heat transfer coefficients in unsteady-pipe-flow with waves are unknown. If free convection heat transfer is assumed during the approximately three-quarters of the cycle when the valve is closed, the values will be too small and will not reflect the disturbances caused by the flow during the valve open period. For present computations heat transfer coefficients were computed for both the Eichelberg and pipe-flow type expressions for intake port conditions and the expression giving the largest heat transfer coefficient at any instant was used. The Eichelberg expression was arbitrarily multiplied by a factor of three on the basis that waves in the manifold would probably increase the rate of heat transfer.

For the liquid coolant the heat transfer $\tilde{h}$ was computed by a combination of boiling and convection formulas, that is, by

$$\tilde{h} = \frac{k}{D}(\mathrm{Re})^{n}(\mathrm{Pr})^{m}\ a+b\ \frac{\dot{Q}}{A} \tag{19}$$

where:

k = Thermal conductivity of liquid

D = Hydraulic diameter

n = 0.6

m = 0.4

Pr = Prandtl number

a = 0.270

b = 0.00125 in.^{2}-hr/Btu

$\dot{Q}/A$ = Heat flux, Btu/in.^{2}-hr

Engine Friction - Various definitions and relations are needed and are presented below:

FMEP = RMEP + AMEP + PMEP = GIMEP - BMEP

where:

RMEP = Friction due to rubbing between mechanical parts

AMEP = Friction due to accessories, in this case the injection, water, and oil pumps

PMEP = Net work during exhaust and intake strokes

GIMEP = Net work during compression and expansion strokes

BMEP = Brake output

Other relations to be used are:

$$NIMEP = GIMEP - PMEP$$

$$MIMEP = BMEP + MMEP$$

where:

MMEP = Work needed to motor an engine

Determination of brake performance from the computed indicated performance involves an estimate of RMEP + AMEP, since PMEP is computed during the analysis. The best estimate of these values would be obtained from an engine similar or identical to the one being simulated. In the absence of such information, a general correlation such as that suggested by Bishop (15) can be used.

For present studies it was assumed that the RMEP varied linearly with the peak pressure (16) as well as with piston speed. The relationship used was

$$RAMEP = RMEP + AMEP = 17 + 0.01\ P_{max} + 0.012\ c_m$$

where:

P_{max} = Peak pressure, psia

c_m = Piston speed, fpm

The constants 17 and 0.012 can be obtained from indicator diagrams or from motoring data with the head removed. The constant of 0.01 can be obtained only from indicator diagrams.

Heat Release Rates - With present knowledge, heat release rates must either be arbitrarily estimated or estimated from experimental pressure-time diagrams on similar engines.

In determining heat release rates from experimental pressure-time diagrams, the energy equation (Eq. 1) is used but with p and $\dot{p}$ as input items determined from the experimental pressure-time diagram. Before Eq. 1 can be solved, estimates must be made of the trapped mass of gas in the cylinder and metal surface temperatures. Thus, the heat release rate curve must be arrived at by successive iterations. The procedure followed is to estimate metal temperatures and trapped volumetric efficiency. These values, together with the experimental pressure-time diagram and numerical integration of Eq. 1, enable a first estimate of the rate of heat release curve to be obtained. This estimate can then be used, together with the cycle analysis program, to obtain new estimates for the volumetric efficiency and metal temperatures. These new estimates, together with the same experimental pressure-time diagram can be used to obtain a second estimate of the heat release rate. In both estimates the area under the heat release curve should equal the quantity of fuel injected. Because of discrepancies in the data, this may not be true in practice.

Figure 2 presents the first and second estimates obtained as outlined above. For the first estimate, the ordinates of the curve were multiplied by the factor required to make the area under the curve equal to the fuel injected. The ordinates for the second curve were plotted as computed. The area under the second curve from CA = 159 to CA = 251 is 96% of the fuel injected. Because of this close agreement and because of small uncertainties in the data, additional iterations were not performed.

SOLUTIONS OF EQUATIONS ... The modified Euler method was used to integrate the equations numerically. The normal time interval used was one crank angle degree. If the iteration gave an oscillating difference larger than the predetermined limit for any variable, the time increment was reduced by a factor of 10 for 10 increments.

Flow Diagram - Figure 3 shows the flow diagram. There are four subroutines, the details of which are not shown. These subroutines calculate valve flow areas, internal energy and gas constant, intake port dynamics, and desired performance parameters at the end of the computations.

The program starts by reading in those conditions which determine the engine operation. There are 12 such numbers: engine speed, intake pipe air temperature, coolant input temperature, coolant mass flow, coolant pressure drop, ambient pressure at the intake pipe entrance, ambient pressure at the exhaust pipe exit, fuel rate, crank angle at which heat release starts, crank angle at which heat release ends, heating value of the fuel used, and the liquid fuel temperature. Next, estimates of the initial conditions are read in. These are the temperature, pressure, and equivalence ratio for each system at the starting crank angle. The last set of estimated numbers read in are the five metal temperatures of the gas-side surfaces of piston, sleeve, head, intake port, and exhaust port, as well as the two valve temperatures.

Next to be read in is the engine description, which is determined by its geometry and the materials from which it is constructed. Items such as the compression ratio, bore stroke, heat transfer areas, intake and exhaust system areas, volumes and lengths, and thermal conductivity of each different metal make up a list of about 50-60 input parameters.

Before the actual cycle calculations begins, the balance factors (accuracy of energy balance) for iteration at each increment, the error limit on wall temperatures, and the error limits which define cycle closing are specified.

The rest of the flow diagram should be self-explanatory with the exception of the crank angle CA_0 and CA_1. For any increment, CA_0 is the crank angle at the beginning of the increment while CA_1 is the crank angle at the end of the increment.

As can be seen from the flow diagram, when all conditions have been met, the program repeats the cycle one final time. During this final calculation the computer is asked to print out at each crank angle increment the computed values of pressure, temperature, equivalence ratio, mass flow, heat transfer rates, and the like. When the final cycle is completed, the program calls the output subroutine which computes and prints out the performance parameters and summary data. The program then stops.

Output Data - Table 1 shows a sample of the type of data printed out as a function of crank angle. The data shown in Table 1 were selected to illustrate the important events during the cycle. The actual output sheet lists values for at least every crank angle degree. Many additional variables are computed and could be presented if desired.

Table 2 shows the performance parameters which are computed and printed out for each run.

Computing Time - The program written in FORTRAN compiles in two minutes and takes about two minutes of computing time per cycle on the CDC 1604 computer. If the estimated initial values are close to the correct values, the program takes about 11 minutes of computer time. Very poor initial guesses may cause this time to increase to 30 minutes. Several calculations with different estimates of the initial conditions showed that the procedure converged to the same final value of initial values in each case.

SENSITIVITY OF RESULTS TO VARIATIONS IN MODEL PARAMETERS ... As indicated in previous sections, the simulation program has a multitude of input parameters. The values to be used for these parameters are reasonably well known in some cases and represent engineering judgment in other cases. It is desirable to determine the sensitivity of the results to variations in input parameters.

Table 3 presents selected parameters to show the results of computations for a single-cylinder engine whose physical dimensions are given in Table 4.

The results shown in Table 3 illustrate one of the major values of the simulation program: you can readily evaluate the effect of varying a single parameter. This is impossible experimentally.

Reference Runs - For reference purposes, computations labelled A in Table 3 were performed. For convenience Run A at 3200 rpm will be called A-3200 while at 1400 rpm it will be called A-1400. For the A computations inlet port dynamics and dissociation effects were included, and the pipe-flow form of the heat transfer coefficient was used. For subsequent computations labelled B, C, D, and so on, the

input parameter was varied as indicated in Table 3. In all cases the exhaust port pressure was considered constant with time.

At a fixed speed, the same pounds of fuel per cycle were introduced for all runs in Table 3. The quantity of fuel injected varied with speed to match experimental injection quantities. Thus, for any one speed, the indicated fuel economy is directly related to NIMEP plus PMEP.

Care must be exercised in interpreting the results since the relationship between the input parameters and the performance data is highly nonlinear. For example, if the effective intake valve flow area is reduced by 10%, a decrease in volumetric efficiency of 2.6% is found. This does not necessarily mean that a 20% reduction will cause a reduction of 5.2% in volumetric efficiency.

Heat Transfer Coefficients - There is considerable uncertainty as to the magnitude of the radiant heat transfer (17). The combustion model assumed a homogeneous air-fuel mixture, uniform in temperature throughout the combustion chamber. This results in a lower maximum gas temperature than if stratification were assumed. Since radiation is assumed proportional to the fourth power of the temperature, radiant heat transfer, computed using the homogeneous combustion model, could be low. In run B-3200 and B-2000, the radiation temperature was computed by arbitrarily multiplying the gas temperature by 1.3. As would be expected, this gave higher total heat transfer and higher metal temperatures. The decrease in NIMEP is primarily a result of heat losses since the volumetric efficiency decreased very little.

In runs C-3200 and C-2000, the intake port heat transfer coefficient was increased by five times. As a result, the volumetric efficiency, as well as the inlet valve temperature decreased. The volumetric efficiency decrease is caused by the increase in air temperature at intake valve closing.

Runs J-3200 and J-2000 show that a 30% increase in the heat transfer and a lower volumetric efficiency and NIMEP.

Runs M and A should first be compared at 2000 rpm where the constant in the Eichelberg equation was adjusted to give the same total heat transfer. Even though they had the same total heat transfer, the volumetric efficiency and NIMEP were higher for run M. This is due to the differences in rates of heat transfer at different parts of the cycle, as shown in Fig. 1. The difference is even more pronounced at 3200 rpm.

Figure 4 indicates that metal surface temperatures increase less rapidly with increased engine rpm when using the Eichelberg correlation. The "leveling off" of the exhaust and intake valve curves indicates that, at the higher engine rpm, they are approaching their effective gas temperatures.

Heat Transfer Path Length - In computing runs H-3200 and I-3200, it was realized that the temperatures of the metal parts (piston and intake valve) would change with a changed path length. The runs show that the effect was minor on other parameters, such as volumetric efficiency, NIMEP, and others.

Run K-3200 shows that inclusion of frictional heating at the piston-sleeve interface, that is, the piston rubbing friction (which was estimated at 10% of the total) dissipated to the sleeve, does not markedly affect the performance parameters at full load although the piston temperature is lowered. Other runs not shown indicate that there is a significant effect under motoring conditions.

Dissociation - Looking at run F-3200, it can be seen that, for the simplified combustion model assumed, dissociation computations are not necessary. However, dissociation could become significant as the stoichiometric F/A ratio is approached or exceeded. If a more detailed combustion model including stratification is developed, dissociation may need to be included, that is the internal energy would have to be considered pressure dependent.

Flow Parameters - Runs A-3200, D-3200, E-3200, and N-3200 illustrate the effects of valve flow area and timing. The reduction of flow area of the intake valve (Run D-3200) caused a significant change in volumetric efficiency, but varying the other parameters gave smaller effects.

It is necessary to show a range of speeds in order to indicate properly the effect of constant port pressure as opposed to including inlet dynamics. Consequently, some of the parameters for Runs A and G at different speeds are plotted in Fig. 5. The temperature when the inlet valve is just closed is lower in Run G as compared to Run A. Since the real engine volumetric efficiency trend follows more nearly the upper curve of Fig. 4, inlet dynamics must be included for this particular configuration.

Heat Release Rates - Runs A-3200 and L-3200 compare the effect of the shape of the heat release curve. The shape of the heat release curves is shown in Fig. 6. Run L has almost as high an NIMEP and a considerably lower peak pressure. Thus, in the practical engine, there is a possible "tradeoff" of significantly lower peak pressures for a very small decrease in indicated economy. Good knowledge of heat release rates is required to predict an accurate pressure-time diagram, but very accurate heat release rates are not required in predicting other performance factors such as NIMEP and metal temperatures.

Total Heat Rejection - While the data in Table 3 were prepared to show possible effects due to uncertainties in input data, the series of runs can also be looked upon as a series of different engines. For example, Run D can be considered as an engine with a smaller intake valve than the engine in Run A.

Following this line of reasoning, Fig. 7 presents computed metal temperatures (piston, head, and the like) and values of NIMEP versus computed heat rejection Btu/cycle at 3200 rpm. Except for special cases, there is a good correlation between metal temperatures and heat rejection except for the exhaust valve. For example, in Run H, the effective path length of the piston was varied and this point falls "off the curve" for the piston. In Run C, the intake port and back side of the valve heat transfer coefficient was changed markedly.

The effect on the intake valve is evident even though the effect on the other parts was small. Likewise, in Run I, the effective length of the intake valve was varied and, as a result, the point is "off the curve." Eliminating the piston friction (Run K) lowered the piston temperature.

CONCLUSION

The preceding sections have described the various equations, assumptions, correlations, and methods of solution used to simulate the complicated phenomena which make up the diesel engine cycle. Results of computations with different values of engine parameters showed moderate sensitivity to these parameter changes as well as reasonable trends.

Before the usefulness of the simulation is established, comparisons with experimental data and with other analytical techniques must be made. Part II of the paper is concerned with this evaluation.

PART II - ENGINEERING EVALUATION OF THE SIMULATION

Simon K. Chen, P.S. Myers, and O.A. Uyehara

Part I of this has described the assumptions made and the detail with which the real engine is approximated. There are four questions that must be answered from an engineering standpoint before the usefulness of the simulation is demonstrated, other than as a means of forcing the logical and precise thinking required in advancing engine design.

The four questions are:

1. How well does the behavior of the simulated model agree with the behavior of the real engine?
2. Could equivalent results have been obtained from a simpler simulation?
3. What areas of the program need improvement in order to better simulate the real engine?
4. What are the advantages and limitations of "running a test" on a "computer engine" as opposed to running the test experimentally?

These questions will be discussed in order.

COMPARISON OF EXPERIMENTAL AND COMPUTED RESULTS

In this section, comparisons between experimental and calculated results are presented. The test setup and equipment will be presented first, followed by general performance data, and ending with comparisons of indicator diagrams.

TEST STAND AND INSTRUMENTATION ... The single-cylinder engine test stand used to obtain experimental data is shown in Fig. 8. An Amplidyne G.E. cradle dynamometer was used for load determination and for motoring. A laminar flowmeter was used in conjunction with a surge tank to determine airflow. All indicator diagrams used for comparison were taken with a point-by-point balanced diaphragm indicator (16). Intake and exhaust pressures were measured by two Kistler transducers.

In studying time-dependent pressure, temperature, and flow characteristics, there is always concern whether:

1. The specified property is measured.
2. The measurement is sufficiently accurate.

Valid and meaningful comparisons between experimental and computed results cannot be made unless the same properties are compared and the accuracy of experimental data and the limitations of the computed data are considered.

GENERAL PERFORMANCE COMPARISON ... Figure 9 presents a comparison of computed and experimental performance data. Test data for 2000 and 3200 rpm are shown in solid lines.

Two different sets of computations were run. For the first set, called Computed Data 1, measured port pressures were fed into the computer programs as input. For the second set, called Computed Data 2, intake dynamics were computed as described previously. In general, the calculated GIMEP are a few psi larger than experimental values. This difference is attributed to possible errors in experimental indicator diagrams, insufficient heat transfer in the simulation, and possibly unburned fuel and blowby in the experimental engine.

In Fig. 10 experimental volumetric efficiency data are compared side by side with computed data. Both sets of computed data agree with the general trend of experimental data. The rather unfamiliar shape of the motoring volumetric efficiency is correctly predicted by both computer runs. When the engine is motored at high speed, considerable exhaust gas flows back to the intake port due to the high cylinder pressure at the end of the exhaust stroke. Because there is no exhaust blowdown, the entire mass must be pushed out by the piston during the entire exhaust period.

Comparing Computed Data 1 with the test data, the computed runs give 1-2% lower volumetric efficiency at 3200 rpm. This indicates that either the experimental port pressures used as input data were not sufficiently precise or some inaccurate assumptions were made.

Comparing Computed Data 2 with Computed Data 1, higher values are obtained for run 2. Some of the difference could stem from the lack of exhaust dynamics simulation and the oversimplified assumptions of a straight pipe connecting an infinite size surge tank for the engine intake system used.

Figure 11 shows a comparison of experimental and computed pumping loss. The agreement is well within experimental error. At 3200 rpm, the PMEP at full load is around 8 psi, while at motoring it is 10 psi. This is caused by the lack of blowdown at the motoring condition as explained previously. At lower speeds, the PMEP is not affected appreciably by load.

HEAT BALANCE ... Figure 12 shows the insulated enclosure built for the heat balance test setup. In addition to conventional heat balance measurements of coolant and exhaust, the ventilation airflow rate through the enclosure, its inlet and its exit temperatures were measured. These measurements provide information on how much heat was radiated and convected from the engine outside surfaces to the surrounding atmosphere.

Test data are shown in Fig. 13, plotted both versus engine speed and fuel-air ratio. The specific heat rejection of a single cylinder engine is generally higher than that of a full scale engine due to large mechanical and accessory friction. Radiation and convection loss from the engine outside surface is substantial, especially at part load conditions, and does not vary appreciably with engine speed. Even with all the precautions taken in this test, an "unaccounted for loss" is still significant. At low speed and load, it is as high as 20%. This "loss" can be attributed to: measurement technique such as exhaust temperature and coolant flow determinations; unaccounted for losses such as heat loss from the insulated enclosure to the atmosphere and heat conducted through the metallic dynamometer bed plate; and incomplete combustion.

Computed Data 1 are superimposed on this diagram as dots. These data generally show somewhat higher exhaust temperatures and, therefore, higher exhaust losses than that of experimental results. The inaccuracy of the exhaust temperature measurement could contribute to part of this discrepancy. Another explanation could be that the exhaust port heat transfer has not been adequately predicted.

Concerning measurement techniques, the conventional method of measuring exhaust temperature is by a bare-wire thermocouple. Depending on shape and location, this thermocouple reads some average local static gas temperature plus some velocity head and plus or minus some radiation and conduction losses. Afterburning may also be present. The cycle analysis provides two average static temperatures, that is, a time average and a mass average which must be used for a heat balance. Since the experimental thermocouple readings are typically lower than the mass average temperature (but higher than the time average), the experimental exhaust loss will tend to be lower than the computed exhaust loss.

SURFACE TEMPERATURE ... Figure 14 presents tests made on one piston of a 8-cyl engine. Eleven sets of four fusible plugs were embedded in the piston flush with the top surface to obtain an area-averaged piston temperature. Five test runs were made with varying engine conditions. A comparison of tests 1 and 2 shows the effect of adding a turbocharger wastegate, reducing the boost from 30 to 22 in. Hg. The measured reduction in average crown temperature was 21 F while the computed reduction was 18 F.

A comparison of tests 1 and 3 shows the effect of higher output. The engine speed was increased from 1800 to 2100 fpm and the intake manifold boost pressure from 30 to 42 in. Hg. The measured increase in average piston crown temperature was 60 F while the computed increase was 54 F.

A comparison of tests 3 and 4 shows the effect of changing turbochargers. The compressor in test 4 was operated at a lower pressure ratio than that in test 3, and its efficiency was lower. Measured data show a reduction of 2 F while computer data show an increase of 17 F. The computed increase in temperature seems more reasonable than the temperature reduction shown by the experimental data. The large steps (10-30 F) between melting points of the plugs used could contribute to the discrepancy.

A comparison of tests 4 and 5 shows the effect of adding an intercooler. The intake manifold temperature was reduced from 294 to 197 F and the intake manifold pressure from 31.85 to 28.50 in. Hg. The measured piston temperature drop was 6 F, compared to a computed drop of 53 F. Again, the computed results seem more reliable. The measured temperature could be high due to poor contact between the plugs and the piston base material.

This test illustrates the feasibility of using detailed analysis to predict "relative" surface temperature change due to design change. The last two comparisons also illustrate the need for improving the surface temperature measurement technique. Further tests are being planned using thermocouples in the piston.

INDICATOR DIAGRAM ... Figure 15 shows experimental p-t diagrams at part load and two engine speeds. Figure 16 shows full load and two engine speeds. Experimental needle lift curves are also displayed.

These p-t diagrams were used to obtain experimental heat release rates which were fed into the program along with other input data. These input heat release rates are shown in Figs. 15 and 16. The resulting computed p-t data are shown as dots for comparison. The agreement is good.

From these p-t data, log P - log V diagrams were plotted as shown in Figs. 17-19. Due to the log scale used, small differences in low pressure regions can be more readily compared. Figure 17 shows motoring data at 3200 and 2000 rpm. In the pumping loops, both sets of computed data check with experimental data within 1 to 1-1/2 psi, which is the same order as experimental error. During the compression stroke, both sets of computed data are high, with Computed Data 2 giving slightly higher pressures than computed Data 1, which is consistent with its higher volumetric efficiencies. Both sets of computed data give slightly larger HMEP loops (negative GIMEP) during motoring. The theoretical HMEP represents the net effect of heat transfer, blowby, and other flow irreversibilities during compression and exhaust stroke

In the full load runs shown in Fig. 18, both computed runs show 1-2 psi higher pressures at intake valve closing (IVC), resulting in higher compression pressures. In the pumping loop, Computed Data 2 shows lower cylinder pressure during the exhaust stroke. This is attributed to the assumption of constant exhaust back pressure which is lower than the actual dynamic exhaust back pressure.

In part load runs shown in Fig. 19, this discrepancy, due to lack of exhaust dynamic simulation, is reduced. This is expected because of the effect of dynamic exhaust pressure is reduced when the load is decreased.

The inaccurate simulation of pressure and temperatures at intake valve closing, IVC, is related to the lack of complete agreement in predicting absolute level of volumetric efficiency. When the IVC cylinder pressure is high (or the temperature is low), inlet density is high, resulting in higher volumetric efficiency. A difference of 1 psi pressure would result in a difference of 7% in volumetric efficiency. Even with a balanced diaphragm indicator, an accuracy of 1 psi at a particular volume is not easily obtained. Considering the limitations in test equipment, as well as the many assumptions made in cycle analysis, the overall agreement in these instantaneous pressure and volume data are considered quite encouraging.

These experimental log P - log V diagrams were replotted as P-V diagrams to obtain GIMEP, NIMEP, and PMEP values. RAMEP data shown previously were obtained by subtracting BMEP from NIMEP.

COMPARISONS WITH SIMPLER SIMULATIONS

CONSTANT VOLUME AND LIMITED PRESSURE CYCLES ... As discussed in Part I, the simplest possible model is the isentropic, constant volume, air-standard cycle. The results of this rudimentary cycle analysis are simple and well known; the efficiency is a function of the compression ratio and the ratio of specific heats of the working fluid, k. For the cold air cycle, k is a constant of 1.4. This cycle is sometimes used to predict the effect of compression ratio on efficiency.

The next step in complexity would be to use more realistic properties of the working fluid, that is, the adiabatic, constant volume, fuel-air cycle. Equations needed for this analysis can be programmed on a computer.

The effect of fuel-air ratio and compression ratio on efficiency, using this model, is shown in Fig. 20. A maximum imep of 195 psi is obtained with an isfc of 0.25 lb/ihp-hr for an engine with a compression ratio of 16:1 at a fuel-air ratio of 0.05. While similar data could have been obtained from the simpler pure air model, these figures are much more realistic as ideal goals.

In Fig. 20, peak pressure increases with increasing compression ratio and fuel-ratio. Inasmuch as engine structure often limits permissible peak pressure, a "dual" cycle with both constant volume and constant pressure combustion is an even more realistic model. In addition, such a model can more nearly approximate actual finite combustion rates. With this limited pressure model. efficiency of an engine is now a function of three variables: compression ratio, fuel-air ratio, and peak pressure.

As shown in Fig. 21, at a compression ratio of 15-17 and a peak pressure limit of 1000 psi, a maximum imep of 160 psi and an isfc of 0.29 are predicted for a fuel-air ratio of 0.05. Performance does not improve much when the compression ratio is further increased if the peak pressure is limited to 1000 psi. This model assumes a more realistic combustion rate and peak pressure.

SIMPLIFIED SIMULATED CYCLES ... All of the above models have neglected the time-dependent heat transfer and fluid flow losses. As an intermediate step to the very detailed model, these losses were represented by loss factors. This is called a "simplified" cycle analysis. In the same manner, pumping and mechanical losses, as well as turbo-charging and intercooling, can be considered.

Because of the increased number of variables, a single plot showing all results is no longer possible. For illustrative purposes, Fig. 22 presents computed data with the following assumptions:

Fraction of fuel burned at constant volume = 0.4
Fraction of fuel lost by heat transfer = 0.2
Intercooler effectiveness = 0.9
Compressor efficiency = 0.75
Turbine overall efficiency = 0.72

The results are plotted versus inlet air density (extent of turbocharging) as an independent variable. There are two sets of engine performance curves on this plot. The first engine has a compression ratio of 10:1; the second 16:1. On the indicated basis, a compression ratio of 10:1 would give significantly higher isfc, but when compared on the brake basis, differences in bsfc will be narrowed. High mechanical friction is typically associated with high compression ratio engines.

Isfc also improves slightly as inlet density ratio (extent of turbocharging) increases. The effect of low compression ratio on peak pressure at the same output level is quite dramatic. For example, for an engine of 400 imep, the peak pressure for a 16:1 compression ratio engine would be around 3400 psi at a fuel-air ratio of of 0.05. The same output can be obtained with only 2200 psi peak pressure when the compression ratio is lowered to 10:1. The decrease in thermal load, not plotted here, is equally dramatic. This trend has been predicted by other researchers using similar analytical techniques.

Inclusion of mechanical friction and heat transfer in our model permits prediction of an optimum compression ratio. The result is shown in Fig. 23 where two engines are assumed; one whose friction varies little with peak pressure and one whose friction varies significantly with peak pressure. An optimum compression ratio of 19:1 is predicted for the low friction engine and 16:1 for the high friction engine.

This enables us to study the trend of engine performance with basically different cycles such as turbocharging, supercharging, and intercooling. However, due to the many simple assumptions involved, this type of analysis cannot be used to study detailed engine design changes in order to optimize the performance of a specific design. In other words, these simplified analyses cannot be used to "develop" a specific engine as can the detailed analysis.

FUTURE STUDIES

The preceding part of this paper has presented the simulation of the engine and compared the computed results both with experimental and other simpler analyses. The comparison between computed and experimental results is quite promising. The additional information given by the detailed simulation, beyond that given by simpler analyses, has been helpful in engine development. A detailed evaluation of the simulation at this stage of development, as well as improvements needed, will be considered next.

IMPROVEMENTS TO THE SIMULATION ...

Flow Model - An accurate description of the flow model is important because of its effect on volumetric efficiency, heat transfer, and combustion.

As discussed previously, the port and valve are calibrated in a bench test providing steady, adiabatic flow, but the test results are applied to an engine having unsteady, nonadiabatic flow. The validity of this procedure should be determined.

When improved accuracy in simulation is needed, dynamic valve lift must be described more precisely. At higher rotational speeds, actual valve lifts may depart from static lift. Operating temperature also affects valve lift and timing, especially if valve lifters are not used.

Different engine designs would have different air motions in the cylinder. These air motions have not yet been described in mathematical terms. Semenov (18), using a pressure-compensated hot wire anemometer, has found considerable variation in turbulence throughout the chamber and cycle. Further investigation and correlation, as well as reliable instrumentation, are needed.

As illustrated by Fig. 5, fluctuations in port pressure affect engine performance. These fluctuations occur because of simple emptying and filling processes and wave effects. In most high speed single-cylinder engine test setups, the intake and exhaust pipes are long enough that wave effects must be taken into account. Figure 24 shows a comparison of measured and computed pressure fluctuations. The general trend is predicted, but the computed pressure waves damp out more rapidly than the experimental ones. In order to check the calculated damping, tests were run at room temperature on a pipe closed at one end. These tests showed good agreement between experimental and computed damping, indicating good simulation when a simple adiabatic model is used. Additional analytical as well as experimental studies in this area are needed.

Exhaust dynamics are currently being added to the program. No comparison between computed and experimental data are as yet available.

To improve predictions of volumetric efficiencies, the intake port flow model must be refined. Figure 25 is a composite of the pressures in the cylinder and ports and illustrates the complexity of predicting volumetric efficiency. Instantaneous mass flows through the intake and exhaust valves are also shown. During blowdown, the exhaust port pressure increases, but drops during the exhaust stroke. When the intake valve first opens, cylinder pressure is high because of recompression and high exhaust port pressures. As a result, exhaust gases flow into the intake as well as the exhaust ports. After piston motion is reversed and the exhaust valve closes, cylinder pressure drops below the intake port pressure. Exhaust gases left in the intake port, as well as fresh air, now enter the cylinder. During the start of compression, cylinder gas flows back into the intake port before the valve closes. The plot of instantaneous mass flow rate (Fig. 25) illustrates these effects. Heat transfer from the intake port, intake valve, and combustion chamber also affect these flows and, thus, the volumetric efficiency.

Heat Transfer - There are uncertainties in simulating engine heat transfer. The treatment of combustion radiation must be improved. The use of pipe-flow-type correlations for engine heat transfer has never been justified in detail. Runs A-2000 and M-2000 shown in Table 3, for example, have the same total heat transfer but differ by more than 1% in volumetric efficiency as a result of different values of heat transfer rate at different times in the cycle. There are also difficulties in obtaining test data for checking these correlations. Usual overall heat transfer measurements cannot be used to give the instantaneous rates of heat transfer needed for detailed engine simulation.

The model used for heat transfer in the port has not been confirmed. Measurements of instantaneous heat transfer rates in the ports are needed to improve the model.

Due to the complexity of the engine structure, more studies are needed to establish the equivalent one-dimensional path length for the various components considered. In addition, heat losses from the exterior of some engines are not negligible (Fig. 13) and must be included in a complete simulation.

To provide information on instantaneous heat transfer rates, studies are now in progress at Wisconsin under ATAC sponsorship.

Rate of Heat Release - Rates of heat release, determined from similar engines, are now an input item. The determination of heat release rate by combustion system design variables is preferable, but not presently feasible. This requires simulation of the injection system first (19), and then a correlation between injection and heat release rate of different engines. Lyn (20) has suggested a correlation for open chamber engines which does not include details of air motion and mixing. Further confirmation of this correlation, as well as a correlation for other types of combustion chambers, is needed.

Studies aimed at providing a semi-empirical correlation between rates of injection and rates of heat release have been started at Wisconsin under ATAC sponsorship.

Friction - For most single cylinder combustion work, indicated performance is used to compare with other single-cylinder and multicylinder engine data. Due to the dependency between mechanical friction and engine loads, an engine with optimum indicated performance does not necessarily provide optimum brake performance. This is especially true for a multicylinder engine where engine rubbing friction varies substantially with engine load or peak pressure (16).

Bishop (15) predicts engine friction from engine design variables and cylinder pressure conditions. It has been applied with reasonable success on multicylinder engines, but not on single-cylinder engines.

Figure 26 shows motoring friction compared to friction determined from experimental P-V diagrams. The curve labeled MMEP was obtained by standard motoring techniques. FMEP and RAMEP were determined by P-V diagrams as follows:

$$\mathrm{FMEP} = \mathrm{GIMEP} - \mathrm{BMEP}$$

$$= \mathrm{RAMEP} + \mathrm{PMEP}$$

$$\mathrm{RAMEP} = \mathrm{FMEP} - \mathrm{PMEP}$$

FMEP of a firing engine is in better agreement with the usual measured motoring friction, MMEP, which is the summation of RAMEP, PMEP, and HMEP (representing heat transfer and blowby losses) at the motoring condition.

Figure 27 is a plot of rubbing friction against peak pressure. The equation used for computing friction is based on this experimental correlation. As mentioned before, theoretical prediction of single-cylinder engine friction is not yet perfected.

Figure 28 shows a comparison between Bishop's formula and multicylinder engine data for AMEP. There is reasonable agreement at the higher rpm. However, experimental data do not seem to go through zero as do Bishop's correlations. Again, Bishop's prediction of AMEP does not apply to single-cylinder engines. Further study of friction is needed to extend Bishop's type of correlation for engine simulation.

EXTENSIONS OF SIMULATION ...

Multicylinder Engines - The extension of the program to multicylinder engines is simple in concept, but complicated in practice, because of manifold branching, and variations in heat transfer and fuel injection between cylinders. This will require increased computer storage, and running time.

Turbocharging - The addition of a turbocharger introduces many additional variables. These additional variables make optimization of the engine-turbocharger combination more complex in practice. Simulation, when developed, could be substantial help in developing turbocharged engines. Inclusion of the turbocharger in the simulation is now in progress.

Gasoline Engines - The basic techniques are applicable to spark ignition engines. However, there are definite differences and problems in intake processes and in combustion. Work on simulating a two stroke cycle spark ignition engine has been started at the University of Wisconsin.

ADVANTAGES AND LIMITATIONS

In the preceding, a critical evaluation of the engine simulation was made and areas of improvement indicated. From this evaluation, the limitations and advantages of the simulation can now be summarized in this section.

LIMITATIONS ...

Simple Assumptions - The simulation is as accurate as its assumptions. In constructing the model, compromises were made between reality and simplicity. Due to this quest for rather simple mathematical methods and, at times, the lack of information, the accuracy, though adequate for some purposes, might not be sufficient for others.

Simplest Possible Configuration Required - The simulation, as presently programmed, is applicable only to an open chamber single cylinder engine with comparatively straight pipes in the inlet and exhaust.

Certain Input Data Required - Input items such as heat release rates, valve flow coefficients, and friction characteristics are required and require, to varying degrees, prior experience.

What - But Not How - The simulations will predict engine performance with a particular heat release rate, but will give no information on the combination of nozzle characteristics and air motion required to achieve this rate. The same statement is true with regard to heat losses, friction, flow coefficients, and others.

ADVANTAGES

Scientific Thinking - When computed results and experience gained from the engine simulation program are utilized in planning tests and interpreting test data, the number of trial and error tests can be reduced significantly.

Rapid Results Possible - It is not necessary to wait a month for a new camshaft or two months for a casting! The entire set of tests presented in Table 3 were run on a computer during a period of about two weeks. For some preliminary work, it might not immediately predict precisely the optimum engine design, but it will at least show the area in which experimental studies can be more fruitfully conducted.

Complete Set of Test Data - Much valuable information such as surface temperature and instantaneous mass flow rate cannot be readily obtained on a test stand due to experimental difficulties. This information is automatically obtained by a simulation program. In addition, test conditions can be precisely controlled in the simulation.

Single Variable Studied - One variable can be changed at a time to see its effect. For example, the simulation can tell if an effort to achieve a particular heat release curve is justified. Changing one variable at a time is difficult to do on a test stand.

Systematizes and Preserves Experience - This is exactly what engine simulation attempts to achieve--systematization of engine knowhow. Experience obtained is expressed in mathematical and logical terms and retained for future use.

EXAMPLES OF UTILITY OF SIMULATION

This closing section will present two examples of the utility of this simulation. The first one illustrates the use of simulation to optimize engine components; the second one to provide information as to which areas of engine performance most gain can be made.

ENGINE DEVELOPMENT ... As part of an engine development program, the relationship between valve sizes and volumetric efficiency was studied. Figure 29 presents computed data of volumetric efficiency of an engine using a range of exhaust valve sizes. The intake valve size was fixed. For this computer engine, a large exhaust

valve would increase volumetric efficiency and reduce pumping loss. However, in a real engine, the size of the exhaust valve is limited by space. These data provide the information on the optimized exhaust and intake valve sizes in the space allotted for valves. The trend shown in this figure has been confirmed experimentally.

ANALYSIS OF LOSSES ... Procedures for improving efficiency involve a careful analysis of losses. These losses must be identified and defined before specific gains can be made. A detailed study of losses provides information on the practicability and feasibility of making an improvement as well as the amount of improvement possible, thus avoiding time consuming trial and error in areas where little gain is possible. Figure 30 shows a detailed breakdown of engine losses.

Basic Cycle Loss - This thermodynamic loss represents the difference between MEP_{fuel}, the fuel input, and $IMEP_{isent}$, the maximum indicated work possible with a cold air cycle. This is the minimum exhaust loss for any adiabatic engine and can be predicted from simple cycle analysis (air cycle, Fig. 20).

Real Gas Property Loss - This is the loss involved from the use of a fuel-air mixture instead of cold air as a working medium. The higher the fuel-air ratio, the larger this loss becomes, as predicted from simple cycle analysis. This loss is a function of pressure when dissociation is considered.

Volumetric Loss - This is the loss involved by not having the maximum mass of air in the cylinder for given ambient conditions. This cannot be predicted by simple cycle analysis. The detailed cycle analysis can be used to determine optimum design for obtaining maximum feasible volumetric efficiency at a specified operating condition. An example of this work has been shown in Fig. 29.

Heat Transfer Loss - For structural reasons, a practical engine needs to be cooled. This results in a power loss. Generally speaking, to obtain maximum performance, the minimum tolerable amount of coolant should be used. For example, at part load, engine performance can be enhanced if coolant flow is reduced, maintaining a tolerable structural temperature. At high BMEP regions the engine should be designed such that thermal load limits are not exceeded. Detailed cycle analysis can be used to determine these limits (surface temperature, heat flux, and the like) and the magnitude of heat transfer losses at different conditions.

Late Combustion Loss - Late combustion loss is caused by having a practical heat release rate which deviates from constant volume combustion. This loss is generally proportionally reduced at high speed, as rate of pressure rise is typically increased at higher speeds. Figure 30 shows that only limited gain can be made as the late combustion loss is a small percentage of total loss. In Fig. 31, the performance of two seemingly identical combustion systems, engine A and engine B, are compared. The comparison is based on combustion efficiency, E_{comb}.. This parameter defines the combined heat transfer and combustion loss. This figure indicates further improvement can be made for engine B to at least attain the performance level of engine A. A more careful analysis also indicates that the gain will probably come from reducing heat transfer loss rather than from late combustion loss.

Pumping Loss - As presented previously, pumping loss can be simulated very well by detailed analysis. Therefore, the detailed analysis is capable of providing design criteria for minimizing this loss. Figure 29 has shown that an improvement in exhaust valve size could effect a substantial reduction in pumping loss with only a slight gain in volumetric efficiency.

Rubbing Loss - Rubbing loss is a function of engine design, engine load, and reliability requirements. Reducing rubbing loss requires meticulous sizing of bearings, gears, and structural parts, without sacrificing engine life or reliability for a specific application. As pistons and rings contribute a large percentage to this loss, study in this area could lead to the most fruitful results. Detailed cycle analysis shows how this loss varies with operating conditions.

Accessory Loss - Accessory loss of an engine is another area in which some gain can be made. Due to the complexity of modern vehicles, accessory load is increasing. Careful matching be accessory requirements to engine characteristics should be productive.

The above breakdown of engine losses, made possible by detailed analysis, provides the clues to where experimental tests should be conducted.

CONCLUSION

The detailed cycle analysis requires much more effort than the simplified analysis. While the simple analysis is useful in some general areas, the detailed analysis must be used to provide detailed design criteria for engine development. It is now feasible to simulate a single cylinder diesel engine in significant detail. The computed data agrees reasonably well with test data.

Efforts in developing this detailed analysis can be justified by:

1. Its potential for developing advanced engines.
2. Its systematization of engine knowhow.

The simulation program in its present form includes some simplified assumptions, only applicable to a single cylinder engine. Considerable effort is required to develop fundamental data needed for improvements. This is a challenging task. Additional cooperative work among industry and universities will certainly be beneficial to this program.

ACKNOWLEDGMENTS

Many people have contributed to the program. At International Harvester Co., L.D. Evans initiated this work; Carl Meile and Keith Blackwood have been providing most needed support and encouragement. ATAC has provided, in part through Continental Aviation, funds for the research work done at Wisconsin and continuing encouragement from Floyd Lux has been most helpful.

REFERENCES

1. M.H. Edson, "The Influence of Compression Ratio and Dissociation on the Ideal Otto Cycle Efficiency." SAE Progress in Technology, Vol. 7, "Digital Calculations of Engine Cycles," p. 49.
2. F.M. Strange, "An Analysis of Ideal Otto Cycle, Including the Effects of Heat Transfer, Finite Combustion Rates Chemical Dissociation and Mechanical Losses." SAE Progress in Technology, Vol. 7, "Digital Calculations of Engine Cycles," p. 92.
3. H.A. Cook, "Digital Computer Analysis and Interpretation of Turbocharged Diesel Engine Performance." SAE Transactions, Vol. 67, (1959), 532-544.
4. N.D. Whitehouse, A Stotter, G.D. Goudie, and B.W. Prentice, "Method of Predicting Some Aspects of Performance of a Diesel Engine Using a Digital Computer." Proceedings of the Institution of Mechanical Engineers, Vol. 176, (1962), 195-217.
5. D.J. Patterson and G. Van Wylen, "A Digital Computer Simulation for Spark-Ignited Engine Cycles." SAE Progress in Technology, Vol. 7, "Digital Calculations of Engine Cycles," p. 82.
6. P. Huber and J.R. Brown. "Computation of Instantaneous Air Flow and Volumetric Efficiency." SAE Transactions, Vol. 73, (1965).
7. J.P. Bradish, "Instantaneous Deposit Surface Temperatures and Heat Flow Rates in an Internal Combustion Engine." PhD Thesis, Mechanical Engineering Dept., University of Wisconsin, 1965.
8. J.R. Stanitz, et al, "Steady and Intermittent Heat Coefficients of Poppet Intake Valves." NACA TN 1035 (1946).
9. D.H. Tsai, "A Study of the Dynamics in the Inlet System of a Four-Stroke, Single-Cylinder Engine With Inlet Pipes of Different Lengths and Diameters." ScD Thesis, Course XVI, Massachusetts Institute of Technology, 1952.
10. G.L. Borman, "Mathematical Simulation of Internal Combustion Engine Processes and Performance Including Comparisons with Experiment." PhD Thesis, Mechanical Engineering Dept., University of Wisconsin, 1964.
11. G. Eichelberg, "Some New Investigations on Old Combustion Engine Problems." Engineering, London, Vol. 148, (1939), 603.
12. W.J.D. Annand, "Heat Transfer in The Cylinders of Reciprocating Internal Combustion Engines." Institution of Mechanical Engineers, 1962.

13. N.A. Heinen, "Instantaneous Heat Transfer Rates and Coefficients between the Gas and Combustion Chamber of a Diesel Engine." Paper 969B presented at SAE 1965 International Congress, Detroit.

14. V.D. Overbye, J.E. Bennethum, O.A. Uyehara, and P.S. Myers, "Unsteady Heat Transfer in Engines." SAE Transactions, Vol. 69, (1961), 461-493.

15. I.N. Bishop, "An Analysis of Engine Friction and Economy." SAE Transactions, Vol. 73, (1965).

16. R.E. Gish, J.D. McCullough, J.B. Retzlaff, and H.T. Mueller, "Determination of True Engine Friction." SAE Paper 117, 1957.

17. G.D. Eversole, P.S. Myers, and O.A. Uyehara, "The Radiant and Convective Components of Diesel Engine Heat Transfer." Paper 701C presented at SAE International Summer Meeting, June 1963, Montreal.

18. E.S. Semenov, "Studies of Turbulent Gas Flow in Piston Engines," in "Combustion in Turbulent Flow," L.N. Klutrin, Editor. Proceedings of the Moscow Seminar on Combustion, Translated by NSF from the Russian.

19. B.E. Knight, "Fuel Injection System Calculations." Institution of Mechanical Engineers, Proceedings of the Automotive Division, 1960-1961, No. 1, pp 25-33.

20. W.T. Lyn, "Calculations of the Effect of Rate of Heat Release on the Shape of Cylinder-Pressure Diagrams and Cycle Efficiency." Institution of Mechanical Engineers, Proceedings of the Automotive Division, 1960-1961, No. 1, pp 34-46.

∇∆∇∆∇∆∇∆∇∆∇

APPENDIX A

CONDUCTION HEAT TRANSFER MODEL

An equivalent one-dimensional metal path was assigned to each of the seven metal parts. At the end of each cycle calculation, the total heat transfer to each part surface must equal the total heat transfer to the coolant for that part. These conditions give the equations from which the metal temperatures for each part can be calculated.

For the gas-side heat transfer an integration over the entire cycle gives

$$\oint \dot{Q}_i dt = \oint \tilde{h}_i A_i [T_i - T_{eg}] dt$$

where T_{eg} is the effective gas temperature defined by

$$T_{eg} = \frac{\oint \tilde{h}_i A_i T dt}{\oint \tilde{h}_i A_i dt}$$

Model for Cylinder Head - The temperature of the head may vary by as much as 50 F from maximum to minimum temperature location. The one-dimensional model thus gives only some average temperature, and the variation about the average could amount to ±10%. The resistance network consists of the gas side resistance, the head resistance, and the coolant side resistance. The heat transfer from the valves and ports was added to the total load on the head coolant.

Model for Piston - The most severe extension of the one-dimensional model is in its application to piston cooling. The top (or crown) surface of the piston may vary by 100 F or more. Correlation of the piston temperature depends on the piston shape and amount of oil cooling. The effect of oil cooling can be estimated from tests run with different rates of oil cooling.

If the piston temperature is measured by hardness tests or other direct means, the heat flux to the piston can be calculated from the cycle analysis. If the coolant passage metal temperatures are also measured, the effective overall heat transfer path length for the piston can be calculated. This path length includes the sleeve resistance. The path length calculated in this way will have a maximum length for the case of no oil cooling. This maximum length has been found to be about equal to the radius of the piston. When oil cooling is present, the effective path length will decrease roughly in proportion to the oil flow per cycle. If the effective path length to the coolant with oil flow is divided by the effective path length with no oil flow, the resulting ratio is also the fraction of total piston heat transfer going directly to the coolant. The heat transfer resistance path network should contain a path to the oil as well as to the coolant.

Model for Sleeve - The sleeve receives a heat flux which can be divided into three parts: heat flux from the cylinder gas, heat flux from the piston, and heat flux from friction generated at the interface between sleeve and piston. The upper diagram of Fig. A-1 shows the resistance network for the case of a piston with negligible oil cooling. The effective gas temperatures for the sleeve and piston are different because the sleeve area exposed to heat transfer from the gas is a function of crank angle while the exposed piston area is constant. The temperature T_3 is the gas-side (that is, crown surface) piston temperature. The resistance R_4 is the total resistance between the sleeve and piston crown. The resistance R_2 is the sleeve resistance. T_2 and T_1 are the sleeve temperatures on the gas-side and coolant side respectively. The friction heat flux is added at the piston sleeve interface. If oil cooling of the piston is present, an addition path to the oil, branching off from T_3, should be added to the diagram.

If the experimental method for obtaining the piston resistance gives the total resistance $R_2 + R_4 = R_T$, then R_4 can be replaced by $R_T - R_2$. The resistance R_2 is calculated from the thickness of the sleeve and the sleeve conductivity. The error in treating the sleeve as an equivalent flat surface is negligible for most cases because the bore is so much larger than the sleeve thickness. The temperatures T_1 T_2, and T_3 can be obtained in terms of the resistances, the effective gas temperatures, and the friction heat flux.

At the end of each calculated cycle, the effective gas temperatures and friction heat flux are computed. The resistances are available from the values read into the program. Thus the piston and sleeve temperatures can be calculated. Obviously the temperatures could also be calculated from the total heat transfer based on the assumed wall temperatures used during the cycle, but this procedure is not necessarily stable. The effective gas temperatures are relatively insensitive to the assumed wall temperatures and thus the calculated wall temperatures converge rapidly to the balanced values. The equations for the temperatures T_3 and T_2 are

$$T_3 = [\dot{Q} + T_C/(R_1+R_2) + T_{egs}/R_3 + T_{eg}X]/[1/(R_1+R_2) + 1/R_3 + X]$$

where:

$$X = 1/R_5 + R_4/R_5[1/(R_1+R_2) + 1/R_3]$$

$$T_2 = T_3 - (R_4/R_5)(T_{eg}-T_3)$$

The effect of frictional heating is felt by both the sleeve and piston. The evaluation of frictional heating is closely tied to the piston ring design and can be divided into three contributing factors: friction caused by ring tension, viscous friction, and the effect of the gas pressure behind the rings. Bishop (15) has shown that friction caused by ring tension is proportional to the piston speed, while viscous heating is proportional to the square of the piston speed. If no direct data are available, Bishop's formulas for friction can be used to estimate the frictional loss, $\dot{Q}$. If direct engine data are available, it is probably better to adjust Bishop's formulas to fit these data.

The sleeve temperature varies considerably from the top to the bottom of piston travel. The position on the sleeve, represented by the average sleeve temperature, can be estimated from the calculated values of effective gas temperature. For most calculations of fired cycles, the effective gas temperature for the sleeve corresponds to the gas temperature at about 30 crank degrees before top center on compression. This fact and comparisons with other data indicate that the average calculated temperature corresponds to points on the sleeve somewhat above the center of piston travel.

Model for Valve and Ports - The lower diagram of Fig. A-1 shows the resistance network for the valves. The heat transfer from the valves, ports, and head are all added to the load on the head coolant. The ports exchange heat between the port gas and the coolant, and thus have a simple series network. The port wall resistance is estimated from the port wall thickness and conductivity. The valve exchanges heat with the cylinder gas, the port gas, the head through the valve seat, and the coolant through the valve stem. The temperature T_2 in the diagram represents the entire valve temperature. From a practical standpoint, the maximum valve head temperature is of most interest. However, the model is so crude that only trends in average valve temperature can be estimated from the calculations. Comparisons with experimental data indicate that the computed temperatures correspond most closely to the valve face temperature. The resistance R_2 is the sum of the resistances for the stem and seat paths. The resistance for the stem is straight forward, but estimation of the seat to valve resistance is difficult. The resistance network gives the valve temperature as

$$T_2 = \frac{T_C + (R_1+R_2)(T_{egf}/R_3+T_{egp}/R_4)}{1 + (R_1+R_2)(1/R_3+1/R_4)}$$

DISCUSSION

FRANK J. PEKAR
Mack Trucks, Inc.

The scope and attention to detail incorporated in the paper is awesome. Anyone who has ever attempted even a small portion of the authors' undertaking can appreciate the tremendous amount of work involved in reaching the desired goal. As the authors clearly pointed out, previous SAE papers on diesel engine simulation stopped at comparing computed with test results, giving no clue to the extent of the necessary simplifications, or to the methods and equations used. "Development and Evaluation of the Simulation of the Compression-Ignition Engine" has gone a long way in providing many of the previous missing stepping stones. However, after closely studying the paper, one still cannot help wondering why a few additional detailed equations could not have been included without betraying the proprietary nature of the work. Regardless of some of its drawbacks, this paper is still one of the most informative and useful SAE papers ever presented. Due to the wide range of the paper, I will restrict my comments to the area of direct parallel experience -- the inlet cycle simulation.

Referring to the basic equation section of the paper, intake system gas dynamics are briefly treated by presenting the fundamental unsteady flow equations (Eq. 15) along with their governing assumptions. Unfortunately, since a copy of Ref. 1* was not available, the exact mathematical mechanics used to calculate intake system dynamics could not be discerned.

However, there are only two possible solutions to the fundamental unsteady flow equations (Eq. 15). A simplified solution can be obtained by assuming small perturbations which results in a convenient linearized method, similar to the solution for vibrations of a string, or a rod, or to the propagation of sound. A second and more accurate general solution for large amplitude waves can be obtained by discarding small perturbations resulting in a distinctly nonlinear method often called one dimensional characteristics. Which method to use depends on the problem. It would seem that, to be as general as possible, a digital engine program should incorporate the second nonlinear method to handle large amplitude waves encountered at high engine speeds or within long inlet ducts.

A digital simulation of intake cycles only (2) will be used as a basis of comparison to evaluate the subject paper.

The objectives of the intake cycle program were somewhat different from those of the authors. It was desired to obtain only a relative, not an absolute, comparison of volumetric efficiency for inlet system variables such as duct length and diameter, effective valve flow area, valve timing, and so forth. Simplification to a relative comparison minimizes the need to include heat transfer, so that with the removal of heat transfer from further consideration, many difficult and dubious assumptions could be eliminated.

Since the general nonlinear one dimensional characteristic method was used in Ref. 2, consideration had to be given regarding the inclusion or omission of frictional effects. Based on the experience of others, it was decided to neglect friction--a bad decision as will be illustrated later. It should be noted that the authors also neglected friction in their intake cycle calculations.

Experimental volumetric efficiencies for the 4-7/8 by 6 in. 6-cyl diesel engine were obtained using standard engine laboratory techniques. Located at each of the six inlet ports were straight tuned inlet pipes joined at the open end by a large diameter header pipe running parallel to the engine. A large header pipe facilitated air flow measurements without introducing multi-cylinder disturbances into the inlet pipe flow dynamics.

An IBM 1410 digital computer in conjunction with a FORTRAN program that follows the nonlinear analytical method was used to obtain the calculated results. Angle increments were progressively reduced until further reductions exhibited negligible effect on the calculated results. A negligible effect in this case was defined as one resulting in less than a 0.5% change in volumetric efficiency for subsequent decreases in angle increment.

*Numbers in parentheses designate References at end of authors' closure.

Returning to the authors' paper, Fig. 24 in particular, a comparison of calculated and experimental inlet pressures, illustrates the very rapid attenuation of calculated inlet pressure after closing of the inlet valve. Reference is made in the text to auxiliary bench tests, the results of which imply that the nonadiabatic inlet process is somehow responsible for the difference. Their closely controlled auxiliary adiabatic test was reported to give almost identical test and computed results. Although for entirely different engine conditions, Fig. A shows calculated inlet pressure for one inlet cycle. The decay of pressure after the inlet valve closes has the same order of magnitude as the authors' experimental decay. Unfortunately test port pressures corresponding to Fig. A do not exist. (Since the method used to generate Fig. A assumes adiabatic inlet conditions and, based on the authors' auxiliary tests, it would seem that perhaps a reevaluation of heat addition modes during the inlet cycle of the authors' program is in order.) Because the calculation of heat transfer in the inlet port and cylinder is somewhat arbitrary, a practical solution to the authors' inlet discrepancy may be to increase the heat transfer rate in the cylinder and decrease it in the inlet port. If properly done, the same absolute volumetric efficiency should result without the exaggerated wave damping after inlet valve closure; that is, if including heat transfer is actually responsible for the computed wave decay. A statement made early in the authors' paper, indicating that heat addition during the inlet cycle has very little effect on computed wave dynamics, seems to have been contradicted.

Even if the authors' method of adding heat has some faults, heat transfer can not be neglected if absolute volumetric efficiencies are desired. Figure B clearly illustrates the importance of heat transfer. The main difference between motoring and full load data is the reduced importance of heat transfer under motoring conditions. Both the motoring and full load curves are plotted for steady state conditions with the full load curve corresponding to a fuel-air ratio of 0.045. At low speeds motoring volumetric efficiencies were greater by 10%, but at the governed speed the spread was reduced to 0.5%. Realizing that at high speeds considerable frictional heat is available to raise metallic part temperature and influence volumetric efficiency under steady state conditions, a very rapid measurement was made at 2100 rpm after soaking the engine at room temperature for an entire weekend. Even with these precautions the 2100 rpm motoring volumetric efficiency was only 2.5% greater than the full load value, the cross in Fig. B. Based on these tests, it was concluded that if absolute volumetric efficiencies were desired, the addition of heat transfer effects would close the calculated and experimental gap at low speeds, but could not explain the high speed differential.

At this point, the findings of others with respect to the necessity of including friction had to be questioned. Fortunately, experimental data for a wide range of duct lengths were available and similar computed data were obtained. The results of this parallel investigation are shown in Table A. At 1000 rpm, regardless of pipe length, the spread between calculated and experimental volumetric efficiencies remained the same. However, at 2100 rpm the differential increased with increasing pipe length. The necessary conclusion drawn from this comparison is that friction cannot be neglected if absolute volumetric efficiencies or relative volumetric efficiencies for a wide range of pipe lengths are desired. The inlet cycle program (2) is presently being expanded to include friction.

Possibly the authors should consider the addition of friction to their analysis. They indicated that in the near future they plan to include a program for the computation of exhaust dynamics including both heat transfer and friction. Certainly, with slight rearrangement, this more generalized approach could replace the present inlet cycle analysis.

Some of the proposed future additions to the authors' present program should go a long way in enhancing its usefulness. Anyone who has ever experimentally followed the high speed valve motion divergence from the ideal has to concur with the desirability of including actual instead of theoretical valve motions. At the critical low lifts encountered during the beginning and end of the valve event, deviations from the theoretical valve motion can easily change the effective flow area as much as 50%.

As combustion and injection simulation proceed, it will be necessary to include a representation of swirl for many direct injection engines. A very good reference along these lines is a paper by Fitzgeorge and Allison (3). The basic swirl approach is similar to flow calculations that combine a steady flow coefficient with unsteady pressures. For swirl calculations the flow coefficient is replaced by a swirl coefficient and air momentum instead of air volume is integrated with respect to time. Unfortunately, Messrs. Fitzgeorge and Allison do not offer a validification of their method with experimental results.

Expanding the program to include multi-cylinders will be very difficult. Correlation of experimental and computed data would be impossible if the experimental engine is equipped with manifolds of poor aerodynamic design. All inlet and exhaust gas dynamic calculations are one dimensional and cannot account for flow separation in sharp bends or unstreamlined entrances. Manifolds with substantial change in cross-sectional area with length are also very difficult to handle analytically. Therefore, as far as multicylinder conditions are concerned, the extent of simulation success will depend as much on the designer of the manifolds as on the analyst trying to simulate the manifolds mathematically. A quick survey of the present production manifolds, of most diesel engine manufacturers, would reveal many examples requiring improved flow paths.

The paper is certainly very enlighting technically. However, to launch once and for all the diesel engine industry into the computer age, an additional paper is still required: a paper that will demonstrate to engineering management the money and development time savings that could result when the digital engine is fully integrated into standard development programs, and is no longer looked at as just an interesting curiosity.

Table A - Difference between Claculated and Full Load Test Volumetric Efficiencies for Speed Extremes

Pipe Length, in.	1000 rpm, %	2100 rpm, %
21	15.0	11.3
45	14.9	14.7
53	15.0	15.0
67	14.9	16.6

WILLIAM L. BROWN, JR.
Caterpillar Tractor Co.

Although there is little to add to the authors' paper, there are several matters that did puzzle me.

Figures 30 and 31 of the paper represent an extremely important result from this study. As mentioned in the paper, Fig. 30 shows where effort can best be applied to improve the engine, which could be an extremely valuable tool. The very low amount of late combustion losses is extremely surprising to me and I find it hard to believe. If the combustion in the engine used for the data is this good, then it is close to the ultimate in combustion efficiency. Could the authors give any information as to how close the integral of the heat release rate approaches the lower heating value for the amount of fuel actually injected into the cylinder for Fig. 31?

There are several factors that could contribute to the more rapid decay of the computed intake port pressure waves shown in Fig. 24. One factor could be the use of an orifice coefficient for the entrance to the intake port, mentioned in Prof. Borman's thesis (1). Another factor could be the surge tank and flow meter on the test engine shown in Fig. 8, which could reduce the losses to the ambient air. There may even be an energy addition at the intake valve due to heat transfer that could keep the waves going. I have seen glass tubes that will develop self-excited vibrations when heated at the closed end. Would the authors comment on these possibilities?

AUTHORS' CLOSURE TO DISCUSSION

In reply to Mr. Pekar, the method used in solving the intake unsteady flow was based on the hybrid method of Courant, Issaacson, and Rees (Commun. Pure Appl. Math. 5, 243 (1952)). This method solves the nonlinear flow equations along approximated characteristic lines. A fixed finite difference mesh is used throughout for the distance coordinate. The time increments are dictated by the cycle program and generally correspond to one crank angle. The effects of friction and heat transfer on the pressure waves were neglected. The unsteady flow equations thus supply pressure and rate-of-change-of-pressure data. The cycle program then uses these data to compute port gas temperatures. In this way the effects of port and value heat transfer on volumetric efficiency are included, but their influence on the shapes of the pressure waves is zero during the valve closed period and only indirect during the valve open period. Increasing the cylinder heat transfer during the intake stroke can decrease the volumetric efficiency considerably without significantly changing the total heat load (1). While this may well provide a key to lowering the calculated volumetric efficiency, it would not change the calculated damping of the intake pipe waves during the intake valve closed period. At any rate damping of these waves is only indicative of some general discrepancy between the calculations and the experiments. From the viewpoint of the effect on the overall cycle the difference between calculated and experimental port pressures just prior to valve closing is much more important than the damping rate.

It is interesting to note that in Ref. 1, as well as the present paper, the calculated values of volumetric efficiency were always too high by an almost constant amount for all speeds and fixed load. Mr. Pekar's data show a similar trend. It may well be that heat transfer and friction effects in the intake cannot be neglected, but the authors tend to believe that the heat transfer in the cylinder during intake may be equally or even more important. In this regard they agree that the addition of the effects of swirl and other cylinder air motion should be included in the cycle calculations.

Mr. Pekar's remarks concerning further work both in extending the model and in showing its economic utility are certainly in agreement with the thinking of the authors. It must be remembered however, that if the program is too complex the cost of the additional information or accuracy gained may not be warranted.

Table 1 - Cycle Analysis of Single-Cylinder 4 Stroke Diesel Engine

Fired Prob 1

Engine	ER-1	INT	OP	529.0	CADEG	Speed	3200.0 rpm	INT	T	552.0 R	CAGRS	165
Bore	4.125	INT	CL	59.0	CADEG	Coolant Temp	635.5 R	INT	P	14.08 psia	CAPHR	180
Stroke	4.313	EXH	OP	295.0	CADEG	Coolant Flow	1.3390 lb/sec	EXH	P	14.08 psia	CAHRE	260
Comp Ratio	16.000	EXH	CL	549.0	CADEG	Fuel	10.67 lb/hr	0. CADEG = BDC				

Crank Angle	Pres Cyl psia	Temp Cyl R	Mass Cyl 10^6 lbm	Equiv. Ratio	Temp Int. Port R	Flow IV lbm /hr	Temp EP R	Flow EV lbm /hr	Tot. Ht. Tr. Cyl 10^4 B/CA	Tot. Ht. Tr. IP 10^4 B/CA	Tot. Ht. Tr. EP 10^3 B/CA	Pres. Int. Port Ot. Port psia	Vol. in.^{3}
529.	19.39	1865.	73.	0.849	647.		1717.	-90.	-0.669	0.1747	-0.1714	14.11	4.52
547.	15.40	1713.	58.	0.849	662.	-39.	1659.	-1.	-0.454	-0.2303	-0.1500	14.42	4.12
549.	14.26	1678.	57.	0.849	663.	-9.	1653.		-0.405	-0.2187	-0.1458	14.22	4.29
550.	13.81	1660.	57.	0.844	663.	36.	1650.		-0.110	-0.0716	-0.1449	14.00	4.40
560.	11.11	1355.	77.	0.617	653.	239.	1619.		0.129	-0.0491	-0.1361	13.09	6.05
580.	9.32	920.	193.	0.247	621.	531.	1567.		0.437	0.0146	-0.1212	11.54	12.23
600.	8.79	774.	377.	0.130	601.	740.	1522.		0.608	0.0503	-0.1090	11.57	21.24
620.	9.05	720.	619.	0.081	594.	917.	1484.		0.755	0.0664	-0.0987	12.75	31.53
650.	10.05	694.	1042.	0.049	581.	999.	1436.		0.915	0.0919	-0.0861	13.63	46.04
710.	13.17	701.	1796.	0.029	571.	658.	1363.		1.056	0.1149	-0.0675	14.58	61.16
20.	15.37	724.	1997.	0.026	577.	223.	1334.		1.081	0.1065	-0.0604	15.84	60.20
30.	16.19	735.	2016.	0.026	581.	43.	1326.		1.078	0.1014	-0.0583	16.24	56.61
40.	17.08	748.	2011.	0.026	585.	-65.	1317.		0.807	0.2752	-0.0563	18.21	56.38
59.	19.91	783.	2002.	0.026	577.		1303.		0.767	0.3296	-0.0528	14.49	50.43
80.	26.16	848.	2002.	0.026	564.		1288.		0.688	0.3348	-0.0493	12.77	41.53
110.	49.22	1011.	2002.	0.026	578.		1269.		0.395	0.3191	-0.4448	13.77	26.33
140.	139.91	1336.	2002.	0.026	596.		1252.		-0.917	0.2976	-0.0409	15.12	12.23
170.	546.69	1876.	2002.	0.027	590.		1237.		-7.662	0.2959	-0.0375	13.87	4.40
186.	1202.45	3686.	2053.	0.407	589.		1230.		-40.240	0.2942	-0.0358	13.37	4.04
200.	836.31	3797.	2074.	0.558	592.		1224.		-34.300	0.2887	-0.0344	13.49	6.05
230.	287.79	3517.	2101.	0.760	606.		1212.		-17.890	0.2702	-0.0317	14.50	16.48
260.	138.47	3221.	2113.	0.849	609.		1201.		-11.600	0.2607	-0.0293	14.31	31.53
296.	78.79	2821.	2113.	0.849	610.		1188.	-9.	-7.455	0.2534	-0.1807	13.71	48.52
310.	68.58	2725.	2100.	0.849	614.		1230.	-152.	-6.672	0.2471	-0.1714	13.90	53.52
330.	65.71	2588.	1967.	0.849	620.		1973.	-842.	-5.496	0.2370	-0.3198	14.27	58.61
360.	36.30	2335.	1490.	0.849	624.		2300.	-1161.	-3.422	0.2270	-0.3744	14.23	61.47
390.	23.60	2103.	1026.	0.849	626.		2083.	-949.	-1.985	0.2201	-0.2850	13.89	58.61
420.	17.10	1937.	689.	0.849	632.		1912.	-599.	-1.214	0.2089	-0.2264	14.06	50.06
480.	16.26	1873.	288.	0.849	640.		1784.	-433.	-0.774	0.1903	-0.1891	14.03	21.34
520.	17.88	1855.	91.	0.849	646.		1738.	-183.	-0.638	0.1780	-0.1762	14.06	6.05

Table 2 - Cycle Analysis of a Single-Cylinder 4 Stroke Diesel Engine — Prob No. 1.0

Performance Data Fired at 3200 rpm with a Fuel/Air Ratio of 0.0576 = 0.85 Eq Ratio

Horsepower				Mean Pressure, psi			
NIHP	31.62	IHP	33.35	NIMEP	135.77	GIMEP	143.20
BHP	18.08	PHP	-1.73	BMEP	77.64	PMEP	-7.43
RAHP	13.54	RAHP/BHP	0.75	RAMEP	58.13	RMEP	-27.00

Flow Rates	Lb/cycle	Lb/hr	Temperatures, F		Efficiencies	
Intake	0.0019375	186.003	Mass ave int temp	127.4	Volumetric	82.8%
Exhaust	0.0020486	196.670	Mass ave exh temp	1966.5	Mechanical	54.2%
Blowby	-0.0000000	0.000	Time ave exh temp	1060.1	I Thermal	43.3%
Fuel	0.0001111	10.670	Peak temp	3340.2	B Thermal	23.5%
			Peak press	1202.0 psi	ISFC	0.3200
					BSFC	0.5901

Energy Balance	Btu/cycle		Wall Temp (Gas Side) F	Heat Transfer (Gas to Wall) Btu/Cycle	Effective Gas Temp, F
Net work on piston	0.838	Piston	686.7	0.1478348	1995.9
Heat transfer sum	0.360	Cyl head	509.6	0.0664871	1995.9
Blowby	0.000	Cyl sleeve	616.4	0.0480521	1531.4
Net intake and exhaust	-1.283	Int valve	803.8	0.0190501 (face)	1977.5
				-0.0157012 (back)	198.3
Fuel total enthalpy	0.086	Int port	168.6	-0.0031827	146.6
Balance error	-0.001	Ex valve	1369.0	0.0080898 (face)	1995.9
Sum				-0.0021407 (back)	1307.1
HHV fuel input	2.041	Ex port	435.8	0.0914701	1092.6

Energy Distribution		Coolant Temperature Rise		
% Brake work	23.4	Head	3.3 F	1.3390 lb/sec
% Heat transfer	16.8	Barrel	4.2 F	1.3390 lb/sec
% Exhaust	42.3	Friction	1.4 F out of 4.2	
% Friction and Acces.	17.5	Total	7.5 F	

Table 3 - Selected Parameters Showing Results of Computations for Single-Cylinder Engine

Run	Volumetric Efficiency	NIMEP	PMEP	Mass Average Int. Temp., F	Mass Average Exh. Temp., F	Time Average Exh. Temp., F	Peak Temp., F	Peak Pressure, psia	Piston Temp., F	Cylinder Head Temp., F	Cylinder Sleeve Temp., F	Intake Valve Temp., F	Exhaust Valve Temp., F	At Intake Valve Closing		At 160 deg Crank Angle		Total Heat Transfer, q (Btu/cycle)
														P psia	T °F	P psia	T °F	
3200 rpm, 0.0001111 lb fuel/cycle, coolant flow = 1.339 lb/sec																		
A	82.8	135.8	-7.43	127	1567	1060	3347	1202	688	510	616	804	1369	19.91	323	359	1233	0.360
B	82.1	133.9	-7.32	129	1536	1047	3372	1202	740	555	659	884	1396	19.94	331	360	1253	0.396
C	79.6	133.9	-7.07	144	1621	1091	3455	1189	703	522	630	437	1412	19.97	359	357	1293	0.368
D	80.2	134.6	-7.66	128	1602	1081	3407	1184	694	513	623	811	1395	19.44	329	350	1295	0.368
E	82.5	135.7	-7.40	128	1570	1061	3353	1199	687	510	617	799	1370	20.93	335	357	1232	0.361
F	82.9	136.5	-7.44	127	1565	1059	3369	1205	681	505	612	795	1364	19.90	322	359	1231	0.356
G	77.1	136.3	-5.89	131	1632	1098	3437	1145	691	509	620	814	1406	17.94	298	326	1190	0.370
H	82.7	135.9	-7.42	127	1572	1063	3356	1203	737	511	609	807	1373	19.91	325	359	1239	0.357
I	83.0	135.8	-7.45	127	1563	1058	3341	1203	686	508	615	769	1366	19.90	321	359	1229	0.360
J	81.2	131.7	-7.21	129	1542	1047	3385	1197	763	575	679	908	1398	20.08	395	362	1281	0.414
K	82.9	135.8	-7.44	127	1562	1057	3341	1202	663	508	593	801	1365	19.88	321	358	1228	0.362
L	82.9	135.7	-7.45	127	1574	1063	3350	1069	677	501	609	788	1362	19.89	322	358	1229	0.355
M	84.2	139.2	-7.58	125	1555	1049	3322	1210	653	468	593	738	1349	19.70	362	356	1191	0.334
N	82.3	134.4	-8.64	129	1579	1075	3359	1201	691	512	621	813	1386	19.91	327	359	1239	0.366
O	82.2	133.4	-7.27	129	1499	1020	3365	1204	781	574	698	912	1392	19.91	328	360	1249	0.422
2600 rpm, 0.0001128 lb fuel/cycle, coolant flow = 1.165 lb/sec																		
A	84.6	139.7	-4.77	128	1620	997	3300	1206	637	476	576	753	1307	19.58	301	354	1188	0.382
G	78.5	139.5	-3.72	131	1590	1039	3417	1149	644	478	582	769	1353	17.70	281	323	1156	0.395
2000 rpm, 0.0001068 lb fuel/cycle, coolant flow = 1.09 lb/sec																		
A	83.3	135.2	-2.65	130	1398	906	3266	1149	573	434	525	670	1190	18.69	273	338	1132	0.388
B	82.4	132.7	-2.62	132	1362	891	3290	1148	623	475	567	746	1212	18.71	282	339	1153	0.433
C	78.0	132.5	-2.47	153	1473	947	3422	1125	592	448	541	400	1246	18.51	315	331	1203	0.402
G	79.7	135.2	-2.12	132	1435	927	3327	1117	576	435	528	678	1212	17.63	262	320	1113	0.395
J	81.2	130.7	-2.58	133	1374	894	3299	1138	636	486	579	758	1213	18.74	293	339	1174	0.447
M	84.5	136.9	-2.69	131	1367	886	3247	1158	579	428	533	662	1181	18.65	261	339	1110	0.388
O	81.4	129.2	-2.58	134	1308	850	3293	1144	694	521	630	821	1223	18.71	289	340	1174	0.495
1400 rpm, 0.000959 lb fuel/cycle, coolant flow = 0.625 lb/sec																		
A	80.0	124.7	-1.28	129	1223	803	3055	942	529	405	498	553	1026	17.96	243	326	1071	0.366
G	79.7	125.0	-1.06	129	1225	804	3058	940	529	405	498	553	1028	17.87	242	325	1069	0.365

A. With intake dynamics and dissociation.
B. Radiation temperature increased 30%, that is, $T = 1.3\ Tg$.
C. Intake valve and port heat transfer coefficient increased by factor of 5.
D. Intake effective valve flow area reduced by 10%.
E. Intake valve opens and closes 5 crank angle degrees later.
F. Without dissociation.
G. With constant port pressure.
H. Piston metal heat transfer path 50% longer.
I. Intake valve metal heat transfer path 67% of original length.
J. Cylinder gas-side heat transfer coefficient increased by 30%.
K. No frictional heating at sleeve-piston interface.
L. Shape of heat release curve changed.
M. Eichelberg heat transfer coefficient : q same at 2000 as Run A-2000.
N. Exhaust effective valve flow area reduced by 10%.
O. Eichelberg heat transfer coefficient : q nearly same at 3200 as Run J-3200.

Table 4 - IH Test Engine Parameters

Bore	4.125
Stroke	4.3125
Compression ratio	16.
Port diameters	1.8
Port length	6.0
Intake pipe length	12.9
Intake valve diameter	1.900
Exhaust valve diameter	1.693
Maximum intake flow area, effect.	1.032 $in.^2$
Maximum exhaust flow area, effect.	1.042 $in.^2$
Intake opens 16 btdc, closes 64 abdc	
Exhaust opens 70 bbdc, closes 14 atdc	

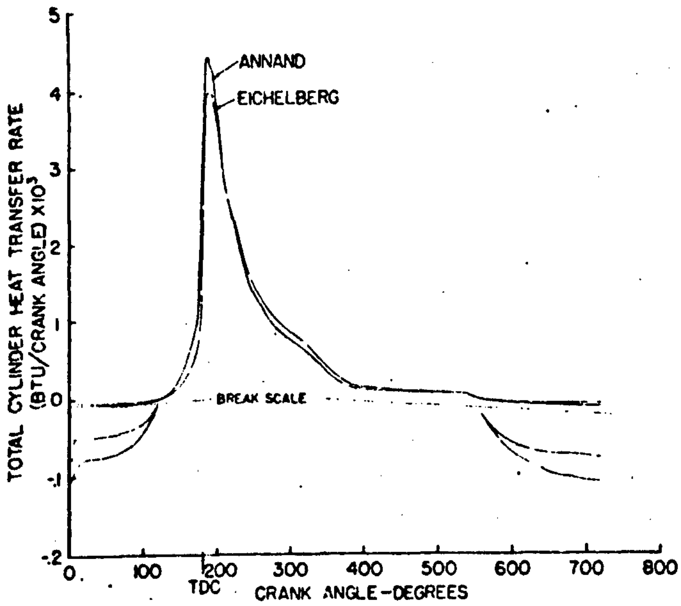

Fig. 1 Heat transfer rate comparison, Eichelberg versus Annand.

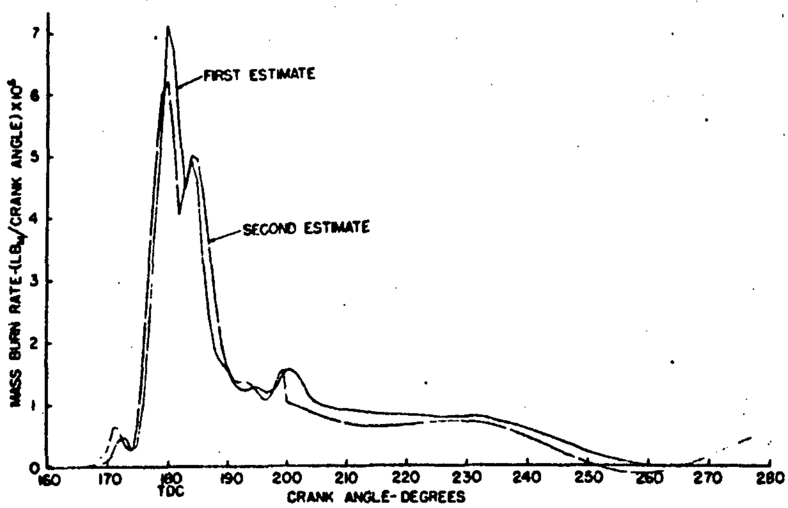

Fig. 2 Heat release rate iteration.

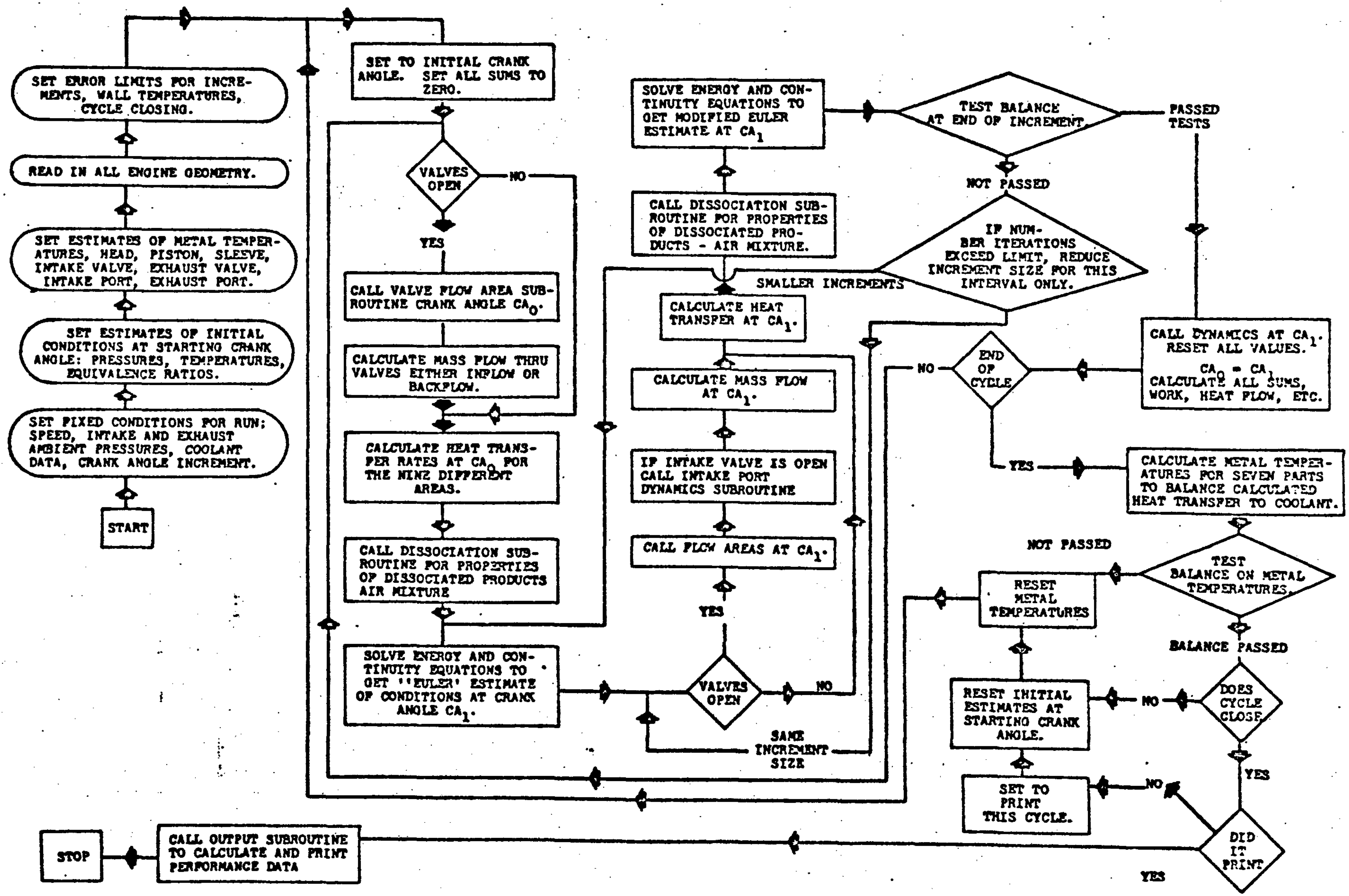

Fig. 3 - Computer flow diagram

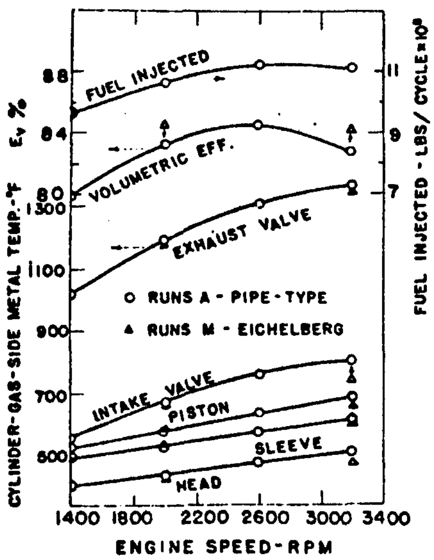

Fig. 4 - Computed data as affected by heat transfer correlations

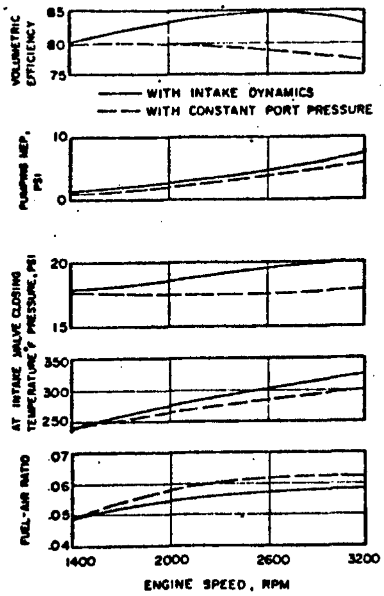

Fig. 4 Computed data as affected by heat transfer correlations

Fig. 5 Computed volumetric efficiency data as affected by intake dynamics.

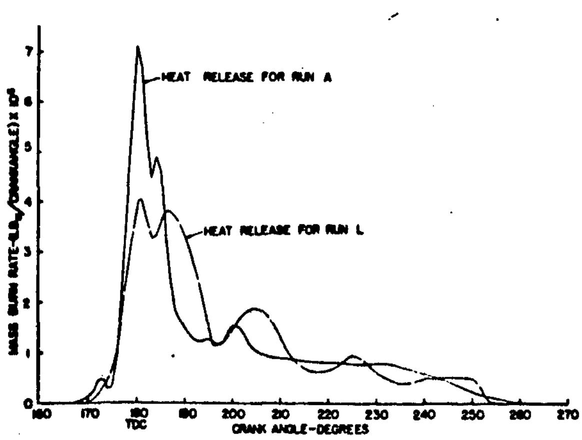

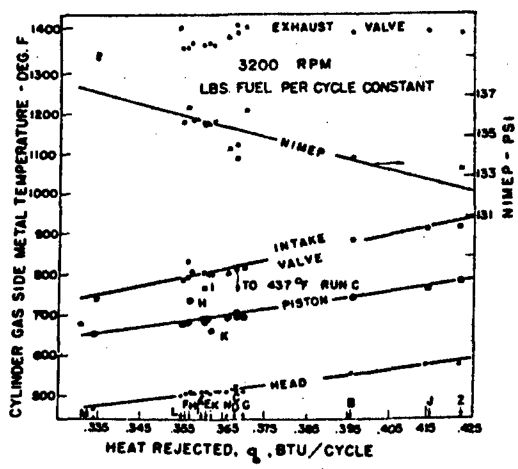

Fig. 6 Heat release input data.

Fig. 7 Effect of heat rejection on computed results.

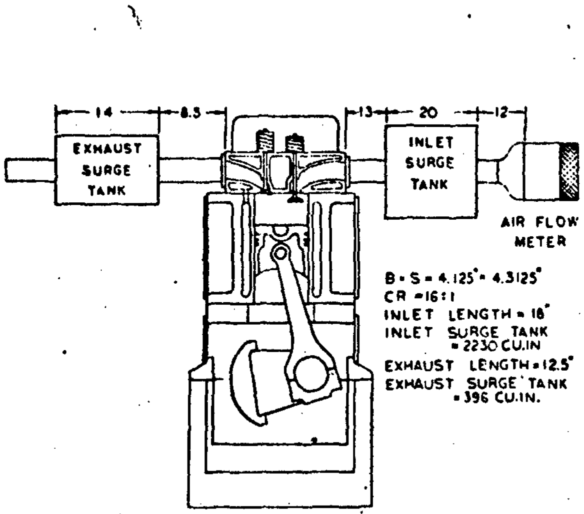

Fig. 8 Single cylinder engine test stand, ER-1-1A.

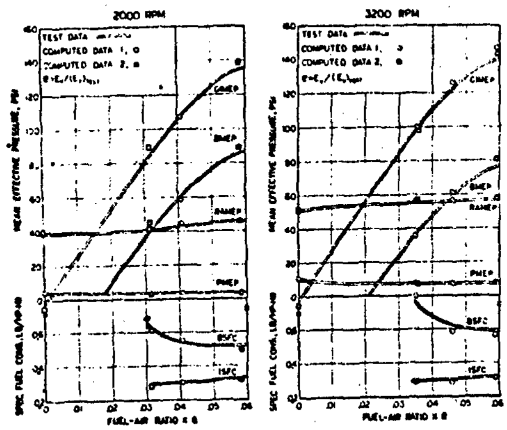

Fig. 9 General performance - computed versus test data.

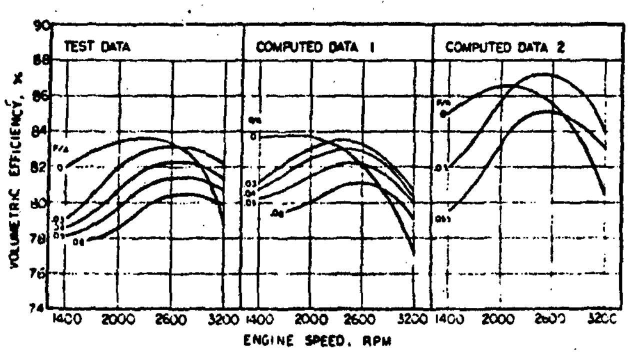

Fig. 10 Volumetric efficiency trends, ER-1-1A.

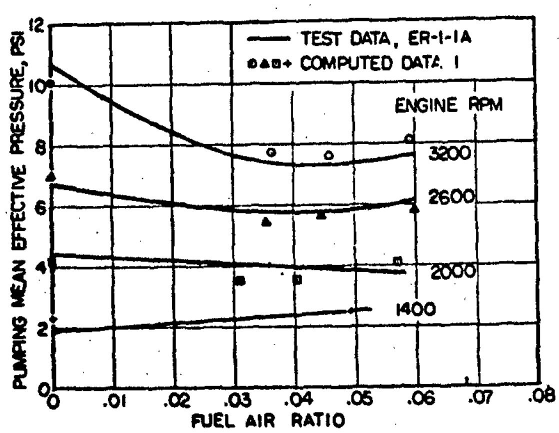

Fig. 11 Pumping MEP.

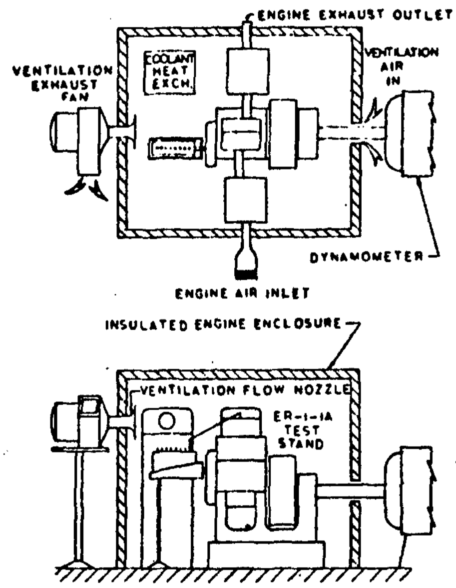

Fig. 12 Heat balance test setup.

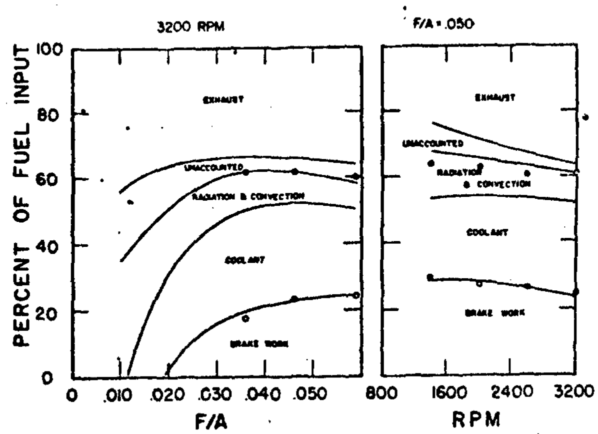

Fig. 13 Heat balance data, ER-1-1A.

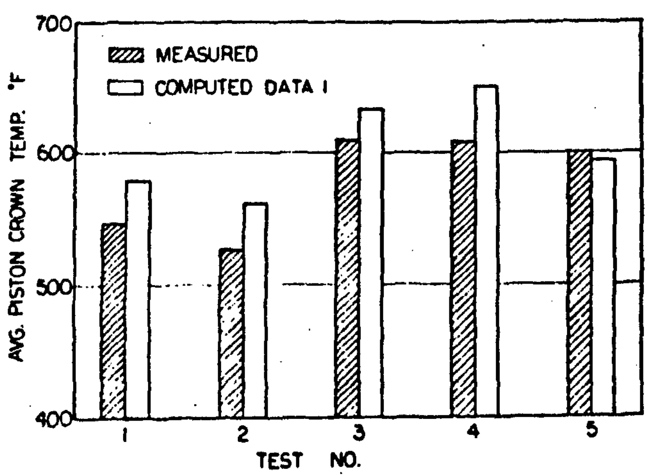

Fig. 14 Piston crown temperature.

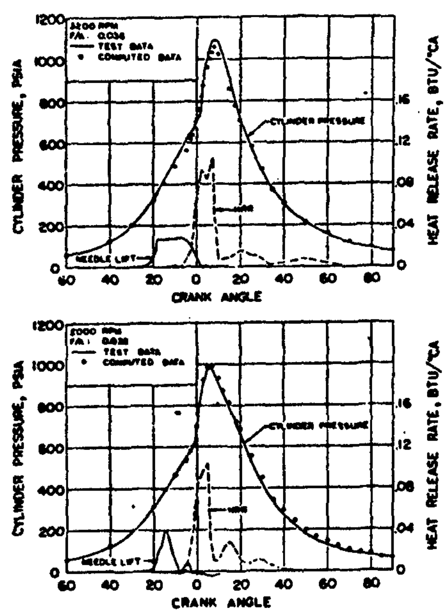

Fig. 15 P-T diagrams - part load.

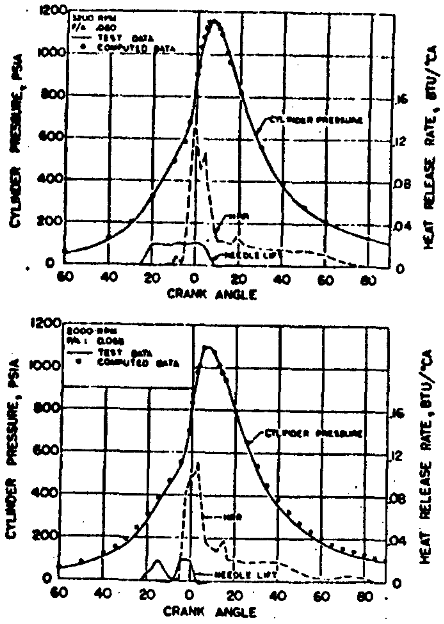

Fig. 16 P-T diagrams - full load

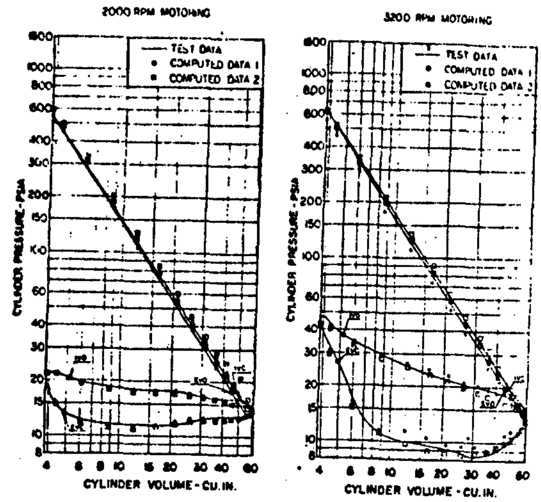

Fig. 17 Log P - Log V diagram, motoring.

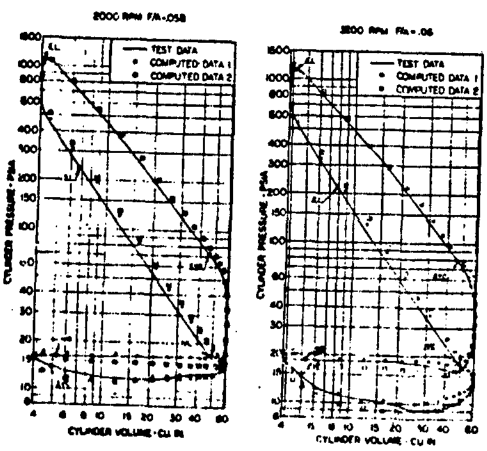

Fig. 18 Log P - Log V diagram, full load.

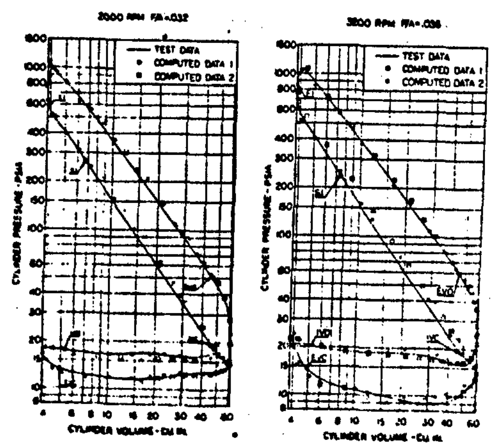

Fig. 19 Log P - Log V diagram, half load.

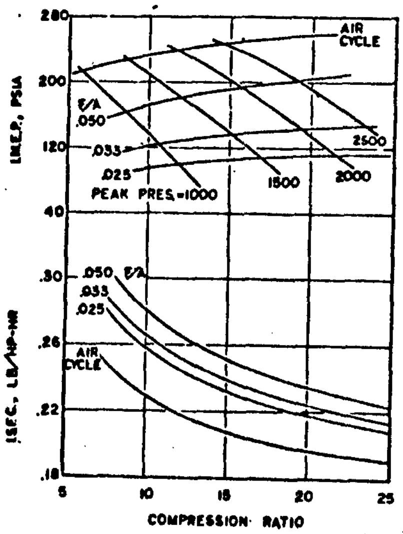

Fig. 20 Constant volume cycles.

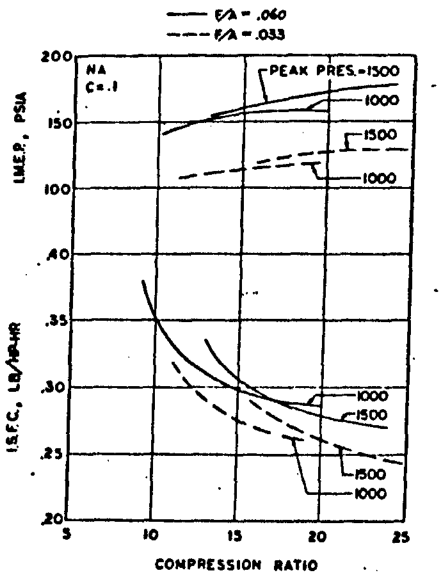

Fig. 21 Limited pressure cycle.

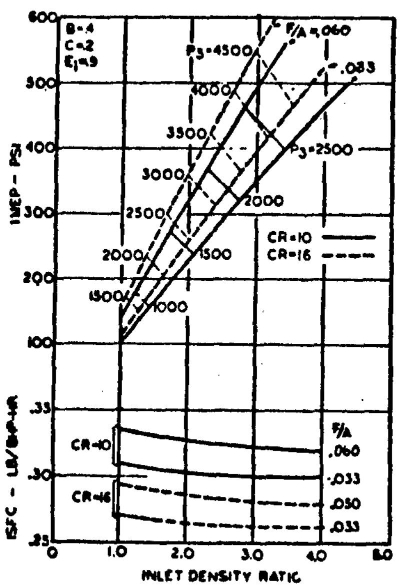

Fig. 22 Simplified simulated cycle.

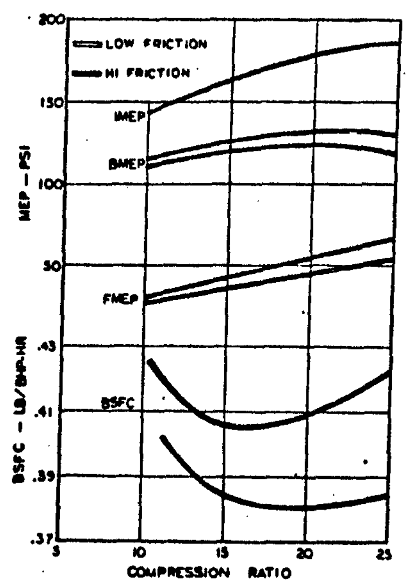

Fig. 23 Optimum compression ratio as affected by friction.

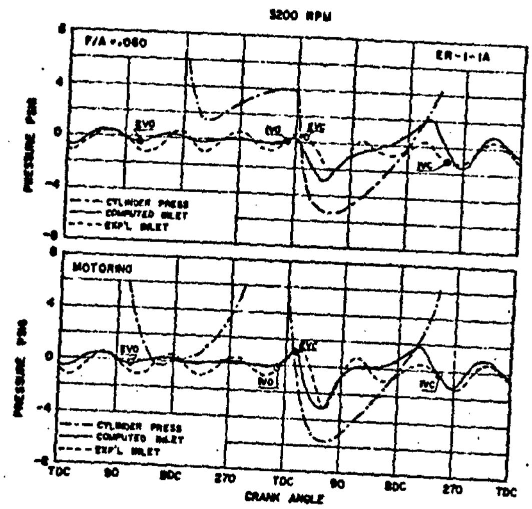

Fig. 24 Experimental and computed inlet port pressures.

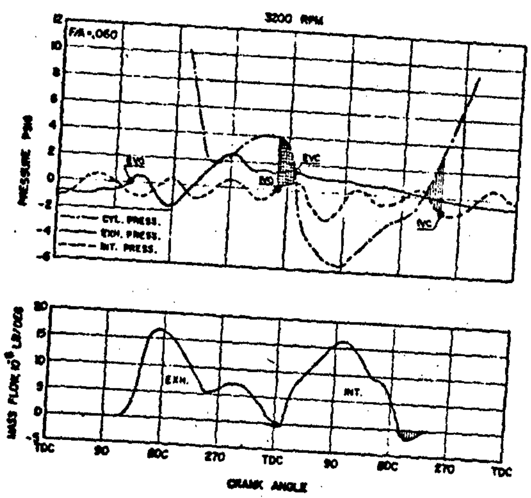

Fig. 25. Instantaneous flow rate and port pressures.

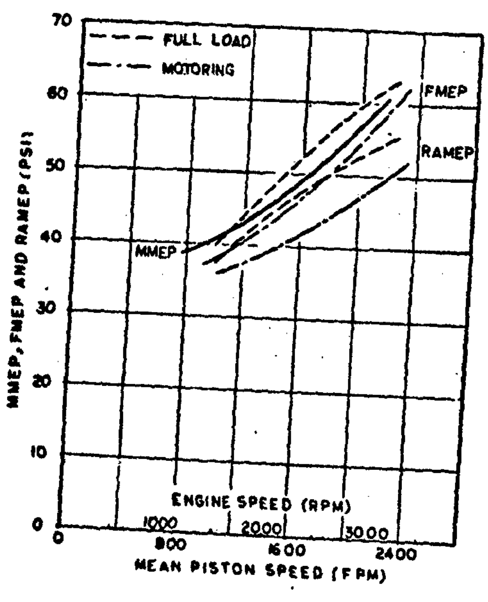

Fig. 26 MMEP, FMEP, and RAMEP, ER-1-1A

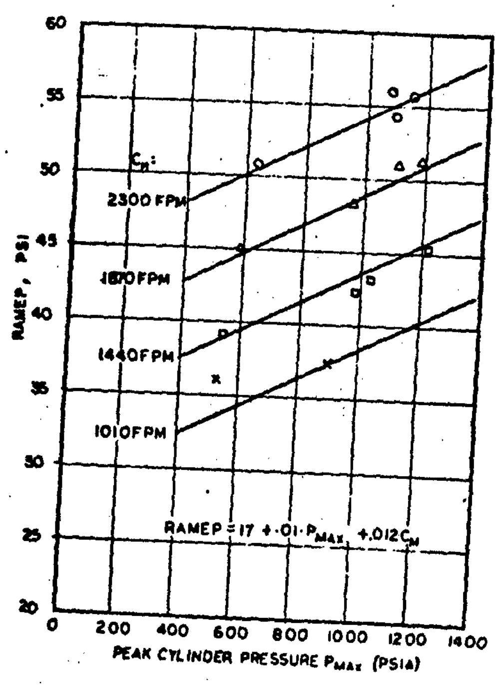

Fig. 27 RAMEP as affected by peak cylinder pressure.

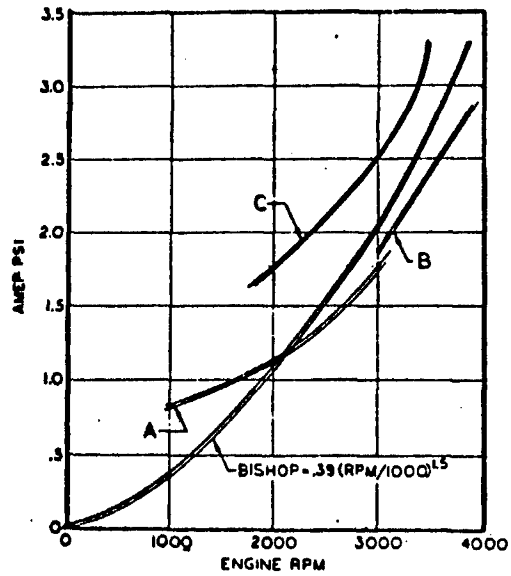

Fig. 28 Oil and water pump power consumption.

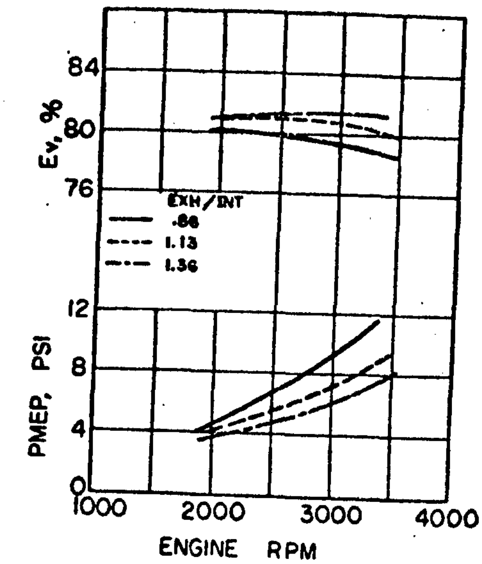

Fig. 29 Exhaust valve flow capacity and volumetric efficiency (full load).

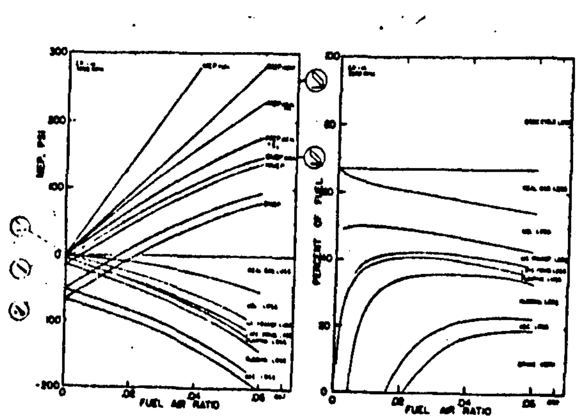

Fig. 30 Engine performance and losses, computed data.

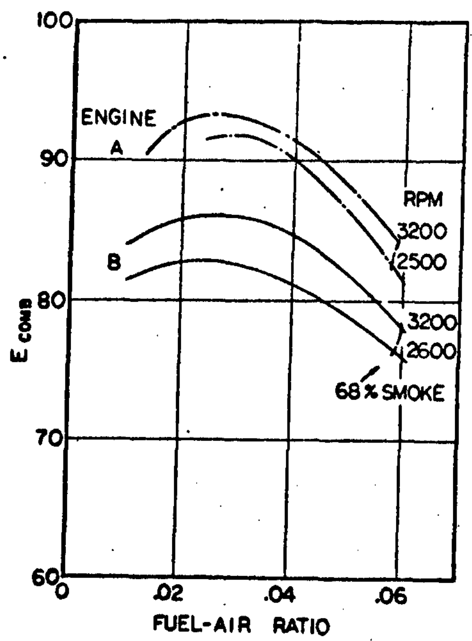

Fig. 31 Combustion efficiency, E_{Comb}.

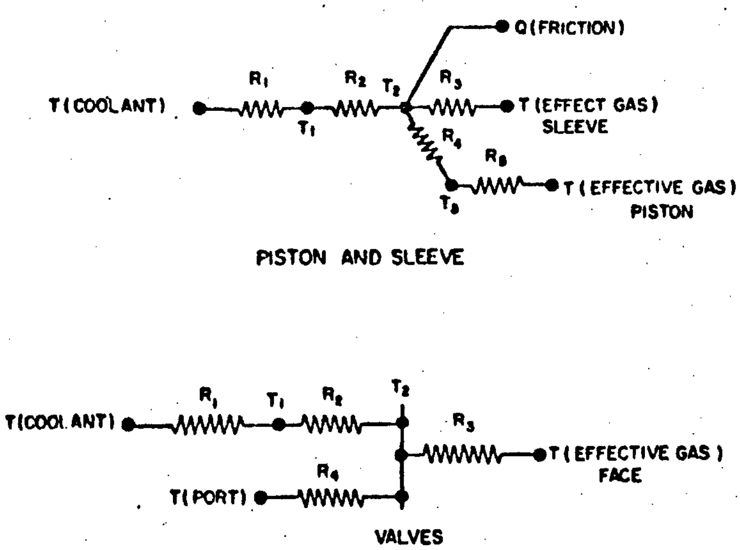

Fig. A-1 Resistance network.

APPENDIX III

Parametric Studies Using a Mathematically Simulated Diesel Engine Cycle

Harold G. Weber and Gary L. Borman
Mechanical Engineering Dept.
University of Wisconsin

ABSTRACT

A detailed mathematical simulation of a single cylinder, open chamber, naturally aspirated diesel engine was used to predict changes in performance caused by changing various engine design parameters. The computations have, in some cases, been used to obtain the parameter values which give optimum performance.

Among the parameters studied are: bore-stroke ratio, valve timing, intake and exhaust valve size, heat release patterns, compression ratio, and atmospheric temperature and pressure. The results are discussed and evaluated in terms of the assumptions used in the calculations.

INTRODUCTION

This investigation is a study of the effects produced by changing some of the design parameters in a computer simulation model of a four cycle compression ignition engine. The particular parameters varied were: bore-stroke ratio, valve diameters, valve timing, heat release rate, and atmospheric conditions. The results should prove useful in two ways.

1. They should help to give a better understanding of the casual relationships between the design changes and the resulting changes in performance.
2. They should provide a further illustration of the use of the computer simulation as a design tool.

References 1 and 2 give a detailed explanation of the simulation model used in this study. These references also contain an evaluation of the program based on comparisons with experimental data. Because data were not available for the many engine configurations considered here, this paper is restricted to a study of the calculated results. Thus, since the model contains many assumptions, the reader should be careful in interpreting the results and, in general, should consider only the significant trends rather than the absolute values.

SIMULATION MODEL

Only the major assumptions used in the program are listed here. The reader is referred to Ref. 2 for a detailed description of the program. The basic engine specifications were taken from a single cylinder test engine currently being used for research purposes at the University of Wisconsin. These specifications are listed in Appendix A. The following discussion of the assumptions is grouped according to the models used for heat transfer, mass flow, combustion, and friction.

The heat transfer in the cylinder is assumed to take place between the gas and five metal surfaces each of which are assigned a constant uniform temperature. The five surfaces are: the piston, the head, the intake valve face, the exhaust valve face, and the exposed sleeve area. The instantaneous heat transfer to each surface is computed using the instantaneous gas temperature and the coefficient of Annand (3)* with the radiation term modified as explained in Ref. 2. The heat transfer in each port is assumed to take place between the gas and the surface of the back of

*Numbers in parentheses designate References at end of paper.

the valve and the port wall. The temperature of the back of each valve is assumed to be the same as the valve face temperature. The heat transfer coefficient used when flow is taking place is of the type used in pipe flow. When the valve is closed, the Eichelberg (4) coefficient is used. The surface temperatures of the seven metal areas are computed from a steady state heat balance between the net heat flow per cycle from the gas and the heat flow to the coolant.

The mass flow rates through the valves are calculated using instantaneous values of effective flow area and the instantaneous cylinder gas pressure. The port pressures were assumed to be constant. This assumption was used in order to avoid the effects of manifold tuning which might cloud the effects of other variables.

The combustion process is simulated by specifying the rate of conversion of fuel mass to combustion products as a function of crankangle. These mass rate of burning or heat release curves were obtained from an analysis of experimental pressure diagrams following the procedures given in Ref. 5. Since pressure diagrams for the various engine designs considered were not available, the heat release patterns were assumed to be the same for all designs. Thus the effects of design parameter variations on combustion are not included here. A study was made, however, of the effects of arbitrary changes in the mass rate of burning patterns.

The simulation program basically calculates indicated values of performance. In order to obtain brake values, data on engine friction must be obtained from experimental data. The brake mean effect pressure is defined by

$$\text{BMEP} = \text{GIMEP} - \text{PMEP} - \text{RAMEP}$$

where:

GIMEP = Net work during the compression and expansion strokes
PMEP = Net work during the exhaust and intake strokes
RAMEP = Friction due to rubbing between the mechanical parts plus the friction due to accessories such as the injector, water pump, and oil pump.

For the present study the RAMEP was computed from Ref. 6

$$\text{RAMEP} = A + B \cdot P_{max} + C \cdot S_m$$

where

P_{max} = Peak cylinder pressure
S_m = Mean piston speed
A, B, C = Experimentally determined constants

The simulation program incorporates the above models and assumptions into the equations of energy and mass continuity for the cylinder, intake port, and exhaust port systems. These equations are solved numerically to obtain pressures, gas temperatures, and flow rates as functions of crankangle. In addition the program calculates cycle performance factors such as volumetric efficiency, heat transfer sums, GIMEP, BMEP, and metal temperatures. The simulation program with constant port pressures compiles in less than one minute and calculates at the rate of one minute per 720 crank degrees on the CDC 1604 computer. The number of 720 deg cycle calculations needed to obtain the final balanced cycle depends on the accuracy with which the initial conditions are estimated. The conditions which must be estimated are the metal temperatures and system gas temperatures and pressures at the starting crankangle. The average computer time required to obtain the results for one set of operating conditions was six minutes.

EFFECTS OF VALVE DIAMETER AND VALVE TIMING ON PERFORMANCE

This section of the investigation deals with the effects of several parameter changes on engine performance. The combined effects of several simultaneous parameter changes will be investigated. Unlike many laboratory studies in which each variable is changed while holding others constant, this method allows one to determine the interactions among the independent variables. Both the combined and independent effects of engine speed, valve diameters, and valve timings will be investigated. In addition to showing the effects of these parameters on performance, a method will be proposed and tried from which an optimum setting of the independent parameters may be found.

The quantities held constant in this section are the functional relationship between mass rate of burning and crankangle, the fuel per cycle ($1.305 \cdot 10^{-4} lb_m$/cycle, that is, full load), the atmospheric pressure (14.08 psia), the atmospheric temperature (95F), and all engine geometry except as noted below.

The fundamental parameters which are varied in this section are the valve diameters and the valve timing. In order to minimize the number of variables, the shape of the valve lift curves was held constant. With this assumption, if a valve opens 5 deg earlier, it also closes 5 deg earlier. In addition, the sum of the two valve diameters was held constant at 3.7 in. Thus, when the diameter of the intake valve was increased, the exhaust valve diameter was made proportionately smaller. Changing the valve diameter must be accompanied by appropriate changes in the port areas, port volumes, valve surface areas, head surface area, and valve flow areas. The surface areas of the ports and the flow areas of the valves at each crankangle were assumed to vary linearly with valve diameter. The port volume, the valve face area and the valve back surface area were assumed to vary as the square of the valve diameter for each valve. The heat transfer surface area of the head was computed by subtracting the face areas of the valves from the total head area.

For those computations where engine speed was varied it was assumed that the cooling water flow rate varied linearly with engine speed.

In order to study the effects of changing several parameters in a complex system, Box(7) introduced the techniques of response surface methodology. Briefly, the technique consists of picking data points in such a way that the minimum number of points will give maximum information. Having obtained the data at the selected points, a mathematical function is fit to the data by the least-squares method. The function can then be used to predict the data at other desired points. Obviously, the function cannot be extrapolated very far out of the range of the original data points. The function can, however, be used to locate maximum or minimum points within the range studied.

The methods of response surface methodology will be applied here to study various performance parameters as functions of intake valve diameter, timing, and engine speed. Since the method is more easily visualized for the case of three independent variables, we will begin the discussion by holding speed constant at 2000 rpm. To illustrate the method, volumetric efficiency was chosen as the performance parameter to be maximized. As we shall see, this point of maximum volumetric efficiency will not be the point of maximum power output at this speed.

Figure 1 shows the values of volumetric efficiency calculated at seven selected data points. The independent variables are intake valve diameter, exhaust valve opening crankangle, and intake valve opening crankangle. These three values fix the engine design since the sum of the valve diameters is constant and the valve durations are constant. The numerical values of the parameters corresponding to the points shown in Fig. 1 are given in Table 1. From the values shown in Fig. 1, it can be seen that volumetric efficiency increases in the direction of decreasing intake valve diameter, retarded exhaust valve timing, and advanced intake valve timing It is also observed that the changes in volumetric efficiency are small. Thus we are near the maximum value which should lie in the front-lower-left-hand region of the space shown in Fig. 1. In order to determine the maximum point, an additional set of 13 calculations was made. Data for all of these runs are given in Table 1 and some of the additional points are shown in Fig. 2. From Figs. 1 and 2, it appears that the maximum point is contained within the region defined by the data points.

To find the parameter values which give maximum volumetric efficiency, the data points should be fit to an appropriate function. A second degree polynomial in the three variables was chosen as the simplest equation which could fit the data and predict a maximum value. A third degree equation could be fit with the 20 data points available, but would be justified only if it gave an improved fit. The second degree equation is given by

$$VE = A1 + A2 \cdot X + A3 \cdot X^2 + A4 \cdot Y + A5 \cdot Y^2 + A6 \cdot Z + A7 \cdot Z^2 + A8 \cdot X \cdot Y + A9 \cdot X \cdot Z + A10 \cdot Y \cdot Z \tag{1}$$

where:

VE = Volumetric efficiency
$A1,\ldots,A10$ = Constants to be determined
X = Intake valve diameter
Y = Intake valve opening crankangle
Z = Exhaust valve opening crankangle

There were 10 constants to be determined and Table 1 shows that there were 20 data points available. To fit Eq. 1 to the data, a computer program for least square curve fitting was used(8). The results are shown in Appendix B. With the exception of points 24, 52, and 53, the equation fits the data well. If these points are reasonably far away from the predicted maximum, the prediction of the maximum point should be accurate.

With an equation describing the behavior of volumetric efficiency in terms of the three variables, the maximum could be calculated. Since the slope of the surface will be zero at the maximum point, Eq. 1 was differentiated with respect to each variable and each resulting equation was set equal to zero;

$$0 = A2 + 2 \cdot A3 \cdot X + A8 \cdot Y + A9 \cdot Z \tag{2}$$

$$0 = A4 + 2 \cdot A5 \cdot Y + A8 \cdot X + A10 \cdot Z \tag{3}$$

$$0 = A6 + 2 \cdot A7 \cdot Z + A9 \cdot X + A10 \cdot Y \tag{4}$$

This resulting set of three equations and three unknowns was solved to yield:

Intake valve diameter = 1.963 in.

Intake valve opens = 513.54 deg.

Exhaust valve opens = 321.68 deg.

These values represent the predicted point of maximum volumetric efficiency. It is sufficiently far away from the points which did not fit the equation, so the point should be predicted accurately.

By substituting the above values back into Eq. 1, the value of the predicted volumetric efficiency was found to be 84.578%. This point was checked by using the predicted values of diameter and timing in the simulation program. The simulation yielded a volumetric efficiency of 84.56%--very close to the predicted value.

This point has been found while holding engine speed constant. Without many more tests, there is no way of telling how the optimum values of these three variables would change if speed were varied. Figure 3 compares the original and the optimum engines on the basis of volumetric efficiency. Volumetric efficiency is clearly up at all speeds, so the investigation has yielded a better engine on the basis of volumetric efficiency.

In order to evaluate the effect of engine speed, one could follow the same procedure used here for 2000 rpm at other engine speeds. The point of optimum design will clearly be a function of the speed. The designer is thus faced with the problem of either optimizing at a given speed or designing to obtain the best average value over a range of speeds. One way of obtaining such a compromise design would be to construct curves such as given in Fig. 3 for various fixed speed optimums and then by judgment pick the desired design.

The results of this investigation show that it is possible to use engine simulation to study the effects of parameter changes. Equally important, the results show that mathematical analysis can be combined with engine simulation to yield at least a region where any performance quantity is optimum. Of course, the three variables studied here are only a fraction of the total number which influence performance. However, as the number of independent variables increases, the number of data points necessary also increases. For example, the minimum number of tests

needed to investigate the effects of 10 independent variables would be 1045. These studies are possible, but they become quite long and involved.

DISCUSSION OF RESULTS ... With the exception of the effects of valve diameter, the trends predicted here could have easily been predicted by tests on actual engines. However, the use of engine simulation allows one to go a step further. With engine simulation, the specific causes of each effect can be determined. Although these effects are interrelated, the effect of each variable will be discussed separately to clarify the discussion.

Figure 4 summarizes the effects of intake valve timing on volumetric efficiency when the other variables are held constant. The cylinder pressures at intake valve closing go up as the intake valve timing is retarded. This means that the intake valve is closing too late in the compression stroke, allowing a significant amount of backflow.

The volumetric efficiency also drops when intake timing is advanced. Because the valve opens earlier, there is more time for backflow into the intake port to occur before induction begins. This backflow heats up the intake valve and port. In addition, the backflow is again pulled in upon induction. The combination of these effects raise the mass averaged intake temperature. Higher temperatures expand the air, causing less mass to be inducted.

The effects of exhaust valve timing on volumetric efficiency are shown in Fig. 5. As with the discussion on intake timing, all other variables were held constant. Volumetric efficiency drops off very quickly as exhaust timing is advanced. The cylinder pressure at exhaust valve closing rises very quickly with advanced exhaust timing. This pressure rise is caused by the blowdown process being cut off prematurely. This high pressure causes backflow into the intake port, raising the mass averaged intake temperature as shown.

Volumetric efficiency also drops if exhaust timing is retarded sufficiently. The exhaust blowdown has been delayed and, as a result, more heat is transferred to the combustion chamber walls, raising their temperatures. This fact is shown by the increase in the cylinder gas temperature when the intake valve closes. The higher metal temperatures result in increased heat transfer to the fresh charge.

These results for valve timing have been obtained by holding the shapes of the valve lift curves constant. If the shapes of these lift curves were also changed, different results would be obtained, but the analysis would be more complicated because the crankangle at which each valve closed would have to be specified.

Figures 6 and 7 show the effects of varying the valve diameters. As in the previous discussions, all other variables were held constant. An increase in the intake valve diameter also means a decrease in exhaust valve diameter since their sum was held constant. The port surface areas and volumes were also changed with valve diameters.

For increasing intake valve diameter (also decreasing exhaust valve diameter), intake inflow is more efficient as shown by the drop in cylinder pressure at intake valve closing. In addition, the total heat transfer is lower because the total area of both valves is increasing. However, these gains are offset by the smaller diameter of the exhaust valve. Since the exhaust flow is more restricted, more exhaust gas remains in the cylinder and the pressure at intake valve opening is increased. This results in more backflow through the intake valve, raising the mass average intake temperature. In addition, the combustion chamber wall temperatures increase, so more heat is transferred to the fresh charge.

If the intake valve diameter is decreased (increasing exhaust valve diameter), exhaust flow leaves more readily, as shown by the drop in cylinder pressure at exhaust valve closing and at intake valve opening. However, the intake flow is now restricted, as evidenced by the drop in cylinder pressure at intake valve closing.

It is interesting to note that the simulation program predicts that volumetric efficiency will fall off more rapidly as the intake valve diameter increases than when exhaust valve diameter increases. In addition, Fig. 6 shows that for best volumetric efficiency for this engine, the ratio of intake to exhaust valve diameter

should be about 1.0. At this ratio, the total heat transfer area of the valve faces will be a minimum.

OPTIMIZATION ... Figures 4-7 predict an optimum setting for each parameter that was varied. However, these settings are not the same as those predicted by the analysis when all three parameters were varied simultaneously. This is because of the interaction of the parameters upon each other.

The simplest way to show the total effect of the optimization on the engine cycle is by Fig. 8. This figure shows the cylinder pressure through the pumping loop as it exists for both original and optimum engines. The major effects of the optimization have been to:

1. Remove the sharp cylinder pressure increase at top dead center of the intake stroke.
2. Decrease cylinder pressure during most of the intake stroke.
3. Increase cylinder pressure both entering and leaving the pumping loop.

The effects of optimization on engine performance are shown in Table 2. For comparison purposes the optimized engine was first run at the same fuel-air ratio as the original engine and then at the same fuel rate. On the basis of indicated performance, the optimized engine shows improvement over the original engine. This improvement is slight, however, and was obtained under the assumption that the shape of the heat release curve was constant.

The simulation predicts that the cylinder pressure and temperature at the start of injection show practically no changes for the three runs in Table 2. In addition, the only change in the geometry of the combustion chamber has been the use of slightly different valve diameters. But since the change in indicated performance is also small, it is difficult to say whether the use of the correct heat release shape would support or nullify the predicted changes.

On the basis of brake performance, the increased pumping and friction horsepowers caused the brake figures to rise slightly for constant fuel-air ratio and to drop slightly for constant fuel rate. Before any conclusions can be drawn on the effect of variable changes on brake performance, two things must be noted.

First, for a constant engine speed, the simulation calculates friction work as a constant plus a linear function of peak pressure. The data in Ref. 2 show that changes in heat release shape will alter the calculated peak pressure significantly while barely affecting the indicated performance. In addition, the constants for the friction expression were determined from motoring data. Reference 9 points out a few of the errors that this will cause. Therefore even if the expression for friction is correct, the correct value of friction work will not be obtained unless the heat release shape is correct.

Second, the pumping work was calculated by defining pumping work as the net work during the intake and exhaust strokes(2). Figure 9 shows the pumping loops for both the original and optimum engine at constant fuel rate. The areas inside the loops are very nearly the same for both engines.

Again it should be pointed out that the trends rather than the absolute increases in performance should be considered. Engine simulation does offer a valuable method of studying these trends and their causes. The search for optimum performance was conducted only to determine whether the simulation program would predict reasonable trends. Due to the very small variations in performance near the optimum point, the best that can be said is that this point is in the region of optimum performance. Slight variations in performance will be caused by factors which are not considered in this simulation. Experimental work would have to be done to find the best point in this region.

If more precise values of performance are desired from the simulation program, heat release curves will have to be predicted very accurately. The next section of this investigation points out some of the trends which are obtained when heat release shape is varied.

EFFECTS OF HEAT RELEASE SHAPE AND COMPRESSION RATIO ON ENGINE PERFORMANCE

At present, the simulation will not predict combustion--it is assumed that the combustion heat release shape is already known. However, the simulation will predict the effects of different combustion heat releases on engine performance. This part of the investigation was made to study the effect of a few heat release shapes and compression ratio changes on performance. Two different heat release shapes were used, and the compression ratio was varied from 16 to 18.2.

ASSUMPTIONS ... In the other sections of this investigation, it is assumed that the changes made do not affect the heat release curve significantly. Because the purpose of this section is to study the performance which can be obtained with different heat release shapes and compression ratios; the heat release shape will be assumed to be an independent variable. The results will show the performance which will be obtained if these heat release shapes can be obtained.

RESULTS ... The simulation was run with a rate of heat release curve obtained at 3200 rpm from Ref. 2. The curve is shown in Fig. 10. In order to simplify the curve, it was approximated by two triangular sections. The area under the approximate curve was made the same as that under the original curve. This simplified curve is also shown in Fig. 10. The simulation program was then run using this curve. The results of the two tests are shown in columns one and two of Table 3. Use of the simplified curve resulted in a slightly higher imep and slightly lower peak pressure. The higher output is caused mainly by the greater amount of heat released near top dead center and the lower peak pressure is caused by the smaller amount of heat released directly before top dead center.

It is doubtful that the simplified curve can be obtained in practice. However, the result does point out some of the benefits which can be obtained by accurately controlling the rate of heat release.

The simplified curve in Fig. 10 was modified so that the peak heat release would be 75% of the value of the curves in Fig. 10. This curve is shown in Fig. 11 where the simplified curve is again shown to point out the changes. This modified curve is typical of that found in M.A.N. type engines (10). The slope of the line leading to the peak is less steep. This means that the rate of pressure rise per degree should be less. In addition, more fuel will be burned later in the cycle. This should cause lower pressures and therefore less output from the engine. This modified curve was run in the simulation program to study the results.

Columns two and three of Table 3 show the results obtained from the simplified heat release curve compared with those from the modified curve. The simulation does predict that a lower rate of pressure rise and peak pressure will exist. This reduction in pressure lowers the heat transfer.

Another way to increase the output is to advance the modified curve so that the modified curve so that the heat release will occur earlier in the cycle. Figure 12 shows the modified curve advanced so that both the simplified and the modified curve release 50% of their total heat at the same crank angle. This curve was also run in the simulation program and the results are shown in column four of Table 3. Column four shows the effect of a lower peak heat release and a 7 deg advance. The output is nearly the same as that for the simplified heat release case but the maximum rate of pressure rise has been reduced.

Increasing the compression ratio of the engine should also increase the output. Thus the compression ratio was raised until the peak pressure reached the same value as was obtained using the simplified heat release curve. This compression ratio was found to be 18.19 compared to the compression ratio of 16 used with the simplified curve.

The results of the calculations using the lower peak heat release at the higher compression ratio are shown in column five of Table 3. This calculation reveals that the performance has again increased. Although the increase was not quite as much as that obtained by advancing the curve, the maximum rate of pressure rise is significantly lower. Both the peak cylinder pressure and the maximum rate of pressure rise were found to increase linearly over the range of compression ratios studied. These results were obtained by using the modified heat release curve with 75% of the peak heat release of the original curve.

DISCUSSION OF RESULTS ... The results show that there may be ways to obtain increased performance without resorting to higher peak pressures or rates of pressure rises. There probably exists an ideal rate of heat release curve which will give optimum performance. However, it must be remembered that the heat release curve was assumed to be an independent variable for this section of the investigation. In the real engine, the heat release curve is dependent on many factors and cannot be changed without changing these factors. In order to perform future investigations on combustion using engine simulation, a good relation will be needed between the rate of injection of the fuel and the rate of heat release. However, even if this correlation were known, it would probably only apply for a particular fuel and for a particular engine configuration.

EFFECTS OF ATMOSPHERIC CONDITIONS ON ENGINE PERFORMANCE

Since few laboratories have means to control the temperatures and pressures of the environment in which their engines are tested, it has been customary to correct performance to some standard atmospheric conditions. The formulas used for these corrections are numerous but they all contain several assumptions. The simulation program may also be used to predict performance at various atmospheric conditions. While the simulation also has many assumptions, they are different from those made when using performance correction formulas.

This section of the investigation is a study of simulated engine performance over a range of atmospheric conditions. The results found point out some of the reasons for difficulties encountered when performance correction formulas are used.

All of the calculations made for this section of the investigation were at engine speeds for which heat release data had been obtained (2). In addition, all of the tests were made at a constant fuel-air ratio. Despite these precautions, the shape of the combustion heat release curve will probably change as the atmospheric temperature and pressure are varied. For this investigation, the changes in combustion were assumed to be small enough that the use of the same heat release curve would not significantly affect the results.

As in all sections of this investigation, the intake and exhaust port pressures were held constant over the cycle. The effects of wave dynamics will change the results, but these effects are highly dependent on the port and manifold designs. Similarly, the assumption of no heating in the intake manifold will affect the results, but the degree of heating is also dependent on the particular manifold design.

RESULTS ... The atmospheric pressure was varied from 15 to 9 psia and the atmospheric temperature was held constant at 85 F. The decreasing pressure caused a linear decrease in the mass of air inducted as shown in Fig. 13. Consequently, the fuel injected per cycle decreased in order to maintain a constant fuel-air ratio. The heat transfer to the walls decreased, lowering all wall temperatures except the intake port. The piston and head temperatures decreased about 70 F as shown in Fig. 13. The most significant temperature decrease was found to occur at the exhaust valve. This was because of less heat transfer to the valve during combustion and less mass flow past the valve during exhaust. The intake and exhaust valve temperatures are shown in Fig. 14.

The effects of pressure changes on engine breathing were found to be small. The results showed that both the intake port temperature and the mass averaged intake temperature stayed constant. As a result, the volumetric efficiency remained constant. However, the pumping work did decrease with atmospheric pressure.

The effects of pressure changes on performance are shown in Figs. 14 and 15. As the atmospheric pressure decreased, the peak cylinder pressure decreased because there was less fuel burned. The indicated power decreased linearly with decreasing atmospheric pressure. The friction and pumping work was also found to decrease linearly. As a result, the brake horsepower also decreased linearly, but not at the same rate as the indicated horsepower.

The next set of calculations was made holding the atmospheric pressure constant at 14.19 psia. The atmospheric temperature was varied 30-110 F. The mass of air inducted per cycle decreased linearly with increasing temperature. The fuel rate was proportionately lowered to maintain a constant fuel-air ratio. The piston,

head, and sleeve temperatures, and the total heat transfer remained nearly constant. The port and valve temperatures were found to increase slightly with increased temperature. Over the 80 F range studied, the intake valve and port temperatures rose 25 F. The exhaust valve temperature rose 13 F and the exhaust port temperature rose 4 F. These temperature increases were due to the gas temperature increase throughout the cycle. The reason that the heat transfer stayed essentially constant was because the heat transfer coefficient depends on cylinder pressure, which decreased as atmospheric temperature increased.

The increase in atmospheric temperature was found to improve engine breathing slightly. The volumetric efficiency increased about 3% as shown in Fig. 16. This occurred because the heat transfer from the intake port (Fig. 16) and the back of the intake valve decreased as the atmospheric temperature increased. The mass averaged intake temperature was found to increase at the same rate as the atmospheric temperature.

The effects of temperature changes on performance are shown in Fig. 17. The indicated horsepower decreased linearly with increased temperature. The pumping and friction horsepower also decreased linearly but not at the same rate as the indicated horsepower.

DISCUSSION OF RESULTS ... The simulation predicts that changes in atmospheric pressure and temperature will cause the indicated and brake horsepowers to vary linearly. As was mentioned, there will be differences in the slope of the indicated and brake horsepower lines because of the changes in friction and pumping horsepower. The friction horsepower was taken to vary proportionally with peak pressure (6,9) and the pumping horsepower was taken as the net work during the intake and exhaust strokes. The results of the two sets of tests can be combined to yield the following correction formula for indicated horsepower:

$$\frac{IHP}{IHP_0} = \left(\frac{P}{P_0}\right)^{1.03}\left(\frac{T_0}{T}\right)^{0.855} \tag{5}$$

Equation 5 has exponents which are different from those obtained from other studies. It is likely that the exponents will vary depending on the particular engine studied.

In order to determine how much of an effect heat loss has on the temperature exponent of Eq. 5, all heat transfers were reduced to zero in the simulation program. The results obtained are compared to a run with heat transfer in Table 4. This table shows that even though the heat loss has been reduced to zero, the mass averaged intake temperature is still higher than atmospheric. This is caused by the backflow of the hot cylinder gas. Although the volumetric efficiency has increased significantly, it is still not 100% because of the backflow, the internal energy increase caused by the filling process, and the residual exhaust gases trapped in the cylinder.

Although these results do represent a highly idealized engine, they show that heat loss has a significant effect on power. The use of the simulation with no heat transfer for a few runs at varying atmospheric temperatures yielded the following correction formula:

$$\frac{IHP}{IHP_0} = \left(\frac{T_0}{T}\right)^{1.04} \tag{6}$$

The exponent in Eq. 6 is considerably higher than that of Eq. 5. This shows that among other things, the heat loss inherent in an engine design will change the performance correction formula.

A few more tests were made to determine the effect of engine geometry on the exponents of the correction formula. For these tests, the engine speed was increased to 3200 rpm and an experimentally determined heat release curve for this speed was used (2). Both a 4.5 and a 5.0 in. bore engine of equal displacement were simulated. The fuel-air ratio was held constant for both engines at a value of 0.0569. The results of these tests yielded Eq. 7 for the 5.0 in. bore and Eq. 8 for the 4.5 in. bore:

$$\frac{IHP}{IHP_0} = \left(\frac{P}{P_0}\right)^{1.032}\left(\frac{T_0}{T}\right)^{0.818} \tag{7}$$

$$\frac{IHP}{IHP_0} = \left(\frac{P}{P_0}\right)^{1.029}\left(\frac{T_0}{T}\right)^{0.794} \tag{8}$$

From Eqs. 5-8, it is seen that the pressure exponent stays essentially constant. However, the temperature exponent does vary depending upon the particular engine conditions. Each of these equations was determined by holding engine speed, engine geometry, and fuel-air ratio constant. In addition, for each of the equations, it was assumed that the shape of the heat release curve would not vary as atmospheric temperature and pressure were varied. Provided that this assumption does not introduce much error, Eqs. 5-8 show that different values will be obtained for the temperature exponent, depending upon the design and operating conditions of the particular engine studied.

EFFECTS OF BORE-STROKE RATIO ON ENGINE PERFORMANCE

This final section of the investigation deals with the effects of bore-stroke ratio. Increasing bore-stroke ratio allows the use of larger valves but also increases the surface area of the combustion chamber. At a fixed engine speed, the piston speed decreases as the bore-stroke ratio is increased. In addition, the relationship between displacement volume and crankangle will be different unless the connecting-rod-crank ratio is held constant as bore-stroke ratio is varied. All of these related phenomena are, of course, accounted for in the simulation program.

The quantities held constant in this section are heat release shape, fuel per cycle, atmospheric temperature and pressure, engine displacement, compression ratio, and all geometric factors except as noted below.

For a given bore, the stroke was computed to give the same constant displacement. The heat transfer path length for the piston metal was assumed to be proportional to the bore, but the path length for the head metal was assumed to be constant. The valve diameters where assumed proportional to the bore using the same assumptions regarding area and volume changes as were made in the section on valve diameter variations. The connecting rod length was held constant for nearly all of the calculations so that the connecting rod-crank ratio was not constant, but increased with increasing bore. In practice, the ratio should probably decrease slightly with bore. However, comparing 4.5 and 5.0 in. bore engines with the same displacements and same rod lengths, the volume curves differ by a maximum of only 3.5% at about 50 crank degrees from tdc. A comparison of calculations with constant connecting rod length and calculations with constant connecting rod to crank ratio showed that the two cases give essentially the same results.

The expression for engine friction at a fixed speed and fuel rate was used without changing the experimental constants A, B, C. The calculated friction horsepower versus bore-stroke ratio curve was then compared with data given in Ref. 11. It was found that adding 4 hp to the data of Ref. 11 made the two curves agree to within 3% over the range of 0.7-1.35 bore-stroke ratio. It was thus concluded that the calculations used here gave a reasonable estimated of the variation of friction horsepower with bore-stroke ratio.

It is important to recognize that large changes in borestroke ratio imply changes in combustion chamber geometry which may significantly change the shape of the heat release curve. As shown previously here and in Refs. 2 and 12, the cycle is not very sensitive to such changes. Nevertheless such small changes could be determining in those cases where only small changes in performance with borestroke ratio are predicted. In addition to changing the shape of the heat release, the effect of larger bores may be to increase the volume of air which is not utilized in the combustion process resulting in a change in effective fuel-air ratio.

RESULTS OF BORE-STROKE VARIATION CALCULATIONS ... It was found that if the piston speed is held constant, the values of pmep, fmep, and volumetric efficiency will be essentially constant as the bore is varied from 4 to 5 in. A very slight increase in imep was found to occur as the bore was increased in size. This was attributed to the decrease in total heat transfer per cycle. Figure 18 shows total heat transfer, Q, plotted versus engine speed and versus piston speed for lines of constant

bore. At a fixed piston speed the larger bore values correspond to higher engine speeds. Thus if the average time rate of heat transfer is the same for the same piston speed and two different bores, the total heat transfer per cycle will be smaller for the larger bore since the time for one cycle is shorter for the larger bore. It should be noted that the product of convective heat transfer coefficient and piston area is proportional to the 1.75 power of bore at a constant piston speed when using the Annand coefficient. Since the effective gas and metal temperatures are constant for a constant piston speed and changing bore, the heat transfer rate through the piston will increase as $B^{1.75}$. The total heat transfer per cycle to the piston will be proportional to $1/B^{1/4}$, that is, decreased with increasing B. It is interesting that the Eichelberg coefficient (4) would predict a constant total heat transfer per cycle under these conditions. Figure 18 also shows that at a constant engine speed the total heat transfer decreases with increasing bore.

Figure 19 shows the effect of bore-stroke ratio on brake horsepower. Since the larger bore engine is running at a higher speed for the same piston speed, the brake horsepower is higher. Figure 20 shows brake horsepower versus engine speed. It should be remembered when looking at these graphs that bmep is essentially constant at a constant piston speed. Figure 21 shows the effect of bore on friction horsepower. Figure 22 shows volumetric efficiency as a function of engine speed. Lines of constant piston speed would be nearly horizontal on this graph.

DISCUSSION OF BORE-STROKE RATIO RESULTS ... In considering the results given above, it should be remembered that the effects of engine geometry on combustion are not included. It is also important to note that the different bore engines were not optimized for valve size and timing. Within these limitations, the trends should be correct. Since engines are normally designed for essentially the same piston speed regardless of bore, the analysis indicates that bmep values will not be affected, but that bhp will be slightly higher at the higher bore stroke ratios because of the higher engine speed with its higher fuel rate per hour.

CONCLUSIONS

This investigation has shown further evidence of the value of engine simulation programs as an aid to engine design. The greatest weakness of the program is in its inability to simulate the combustion process in detail. To be really useful, the simulation should be able to predict changes in combustion performance and aid the designer in selecting the proper combination of injector, injector nozzle, and chamber geometry. Thus, the authors believe that the main thrust of research on engine simulation should be in the area of simulating the combustion phenomena.

Within the confines of its ability to predict combustion, the simulation has predicted trends which appear to be reasonable. The technique of engine optimization furthermore seems to be a promising method of reducing the required amount of testing during the development stages of engine design. In this sense, the value of the simulation in contrast to experiments lies in the fact that it is cheaper and more instructive. Experiments tell us what will happen precisely, but the causes may not be evident. The simulation is less precise in telling us what will happen, but clearly points out the causes.

Although there are numerous areas in which the simulation can be improved, more detailed models may increase the cost to the point of diminishing returns. Care must be taken, therefore, that is seeking more accurate results we also carefully evaluate their worth in terms of the cost.

ACKNOWLEDGMENTS

This activity was conducted under contract to and with the technical assistance of the Systems Propulsion Laboratory of the U.S. Army Tank and Automotive Command.

The authors wish to express their appreciation to W.A.R.F. and N.S.F. for their support in making available the CDC 1604 computer facilities. The authors would also like to thank Prof. P.S. Myers, Prof. O.A. Uyehara, and Dr. J.H. Johnson for their many helpful suggestions.

REFERENCES

1. G.L. Borman, "Mathematical Simulation of Internal Combustion Processes and Performance Including Comparison with Experiment," PhD Thesis, University of Wisconsin, 1964.
2. K.J. McAulay, Tang Wu, S.K. Chen, G.L. Borman, P.S. Myers, O.A. Uyehara, "Development and Evaluation of the Simulation of the Compression Ignition Engine " SAE Transaction, 1966.
3. W.J.D. Annand, "Heat Transfer in the Cylinders of Reciprocating Internal Combustion Engines," Institution of Mechanical Engineers, 1962.
4. G. Eichelberg, "Some New Investigation on Old Combustion Engine Problems," Engineering, London, Vol. 148, 1939, p. 603.
5. R. Krieger and G.L. Borman, "The Computation of Apparent Heat Release for Internal Combustion Engines," Proc. Diesel Gas Power, ASME, 1967.
6. S.K. Chen and P.F. Flynn, "Combustion Effects at High BMEP are Demonstrated with Single Cylinder Research Engine," SAE Journal, Vol. 74, No. 6, p. 52.
7. G.E.P. Box, "Mathematics Research Center Advanced Statistical Seminar," University of Wisconsin, January 1961.
8. B. Morrison, "Least Square Program for the CDC 1604 Computer," November 1962. Co-op Identification: GZ WISC LSTSQ. University of Wisconsin Computing Center.
9. R.E. Gish, J.D. McCullough, J.B. Retzloff, and H.T. Mueller, "Determination of True Engine Friction," SAE Paper 117, 1957.
10. G.D. Goudie, "A Preliminary Study of Heat Release in the M-Engine Combustion System," Eleventh International Combustion Symposium, August 1966.
11. L.W. Blair, "A Mathematical Model to Simulate Cylinder Friction," Midwestern Simulation Council Meeting, NASA Lewis Research Center, March 1965.
12. W.T. Lyn, "Calculations of the Effects of Rate of Heat Release on the Shape of Cylinder Pressure Diagrams and Cycle Efficiency," Institution of Mechanical Engineers, Proceedings of the Automotive Division, 1960-1961, No. 1, pp. 34-46.

APPENDIX A

SPECIFICATIONS OF EXPERIMENTAL ENGINE FROM WHICH SIMULATION PROGRAM WAS WRITTEN

Crankcase	Labeco Mod. CLR
Cylinder Heat	International Harvester
Cylinder Sleeve	International Harvester
Piston	International Harvester
Connecting Rod	International Harvester
Camshaft	International Harvester
Injection	Direct (4 hole nozzle)

Cylinder head, sleeve, piston, rod, and camshaft are from International Harvester Model DT 429 6 cyl. engine. Where necessary, these parts have been modified to fit the Labeco crankcase.

Cylinder bore	4.5 in.
Stroke	4.5 in.
Compression ratio	16.0
Displacement	71.57 $in.^3$
Intake valve timing	520-50
Exhaust valve timing (zero degrees is bdc of intake stroke)	310-560

$$RAMEP = 10.0 + 0.0175\, P_{max} + 0.01\, S_m$$

APPENDIX B

COEFFICIENTS OBTAINED FROM LEAST SQUARE FIT OF VOLUMETRIC EFFICIENCY DATA TO EQ. 1

Coefficient	
A1	-3905.8500
A2	2.2808
A3	-0.0014
A4	20.2586
A5	-0.0338
A6	14.4999
A7	-0.0399
A8	-0.0080
A9	-0.0022
A10	-0.0081

For the least square fit, the independent variable values were defined as follows:

X = Intake valve diameter time 100

Y = Intake valve timing/2

Z = Exhaust valve timing/2

The valve timing was taken as the crankangle when the valves opened.

DISCUSSION

WILLIAM L. BROWN
Caterpillar Tractor Co.

I want to congratulate Mr. Weber and Prof. Borman on a very interesting and informative paper. It is studies of this type that will give the greatest benefit from computer analysis of engine cycles. I will confine my discussion to the problem of finding the optimum combination of several variables and to the presentation of results from some valve timing studies of our own.

This paper shows how a computer simulation can be used to select the optimum valve timing. One of the major problems in reciprocating engine development is the many significant variables that must be optimized to obtain the best engine for a given application. This problem is so big that no engine even comes close to the optimum. The success of an engine depends very heavily on the success of the manufacturer in selecting the best combination of the many design variables.

Some simple mathematics will show how big this problem is. I have a list of 28 variables that are known to affect the fuel consumption of diesel engines with one type of combustion system. There is not time to go over the list and discuss each one, but if anyone has any doubts about the number, they can look at the list. Testing all possible combinations with ten different values of each variable would require 10^{28} separate tests.

No one is attempting to run a test of this magnitude. We all have our own schemes for beating the odds. Some are quite scientific, but others are pure conjecture. Nothing vary radical is tried because we fast lose our feel for what will happen, and then there is very little chance for any success.

The computer and the systematic study of the fundamental processes of reciprocating engines offers the best hope of overcoming this problem, but even the perfect program will not completely solve the problem. A computer program takes as long to run as a test on the engine, but it is much cheaper and easier to change the design of the engine in the computer than to redesign the engine and set up the test. This paper presents one method of reducing the number of tests or computer runs required to find the closest peak in engine performance. It is important to remember that it is only the closest peak. There could be many other peaks that would remain hidden.

The only way that we are likely to discover all the peaks is to learn the interrelationship between the variables, because then we greatly reduce the number of combinations required. It is also a big help in predicting results in areas far removed from the region being tested.

Dimensionless numbers and other parameters have traditionally been used in transport processes and fluid machine analysis to reduce the number of variables, and the reciprocating engine can be analyzed in a similar way. Taylor in his book, "The Internal Combustion Engine in Theory and Practice," makes a point of using dimensionless ratios in the analysis of engine performance. It might be interesting to see what basis for these ratios can be found in the equations used in the mathematically simulated engine. We have made a study of this type using a computer program of our own and found it extremely revealing. Not only are the general trends verified, but under certain conditions the numbers repeat exactly down to the eighth digit.

We have made good use of dimensionless ratios and a flow parameter on a series of calculations to study valve timing. Similar assumptions to those of Bormann and Weber were made, except that all walls were made adiabatic and the intake valve duration was varied while holding the intake opening at a fixed crankangle. The walls were made adiabatic because not enough is known about heat transfer on the intake stroke to get correct answers and because many turbocharged and aftercooled engines have nearly adiabatic walls on the intake stroke. In order to have realistic valve lift curves, the valve acceleration was kept constant except for duration and the seating velocity was kept the same for all cams. Figure A shows the family of valve lift curves plotted in dimensionless numbers and labeled according to the intake closing angle abdc. The earliest cam seats at 1 deg abdc and the latest seats at 81 deg abdc. Figure B shows the volumetric efficiency versus an engine speed

parameter. The only difference between Taylor's Mach number and our parameter is the omission of the average flow coefficient and the substitution of the square root of the inlet air temperature, T_i, for the velocity of sound. "n" is the number of intake valves, "d" is the intake valve diameter, capital "D" is the cylinder bore, and "S" is the piston speed. The flow coefficient was made a fixed function of the valve lift to diameter ratio, and the ratio of exhaust to intake valve area was also kept constant. With this study we are able to obtain optimum intake valve closing for a given application in the few minutes that it takes to calculate a flow parameter. Valve timing can be optimized at high speed or low speed, depending on the need. Effect on starting and cylinder pressures can also be estimated.

In the study on effects of bore-stroke ratio presented by Borman and Weber, the predicted heat rejection was shown to vary inversely with the 3/4 power of the bore at a constant piston speed. This is a direct consequence of the assumed correlation function for heat transfer. As long as the borestroke ratio does not change, the Reynold's number-Nusselt number correlation should give a good indication of the influence of speed and size on heat rejection, but once geometric similarity is lost the correlation is questionable. Not enough is known about engine heat transfer, friction, or combustion to predict the changes in engine performance that occur when the bore-stroke ratio is changed.

Parametric studies of the type made by Borman and Weber not only reveal ways of improving engines based on the best understanding of the individual processes available, but they also show where more research is needed to make the correlations more general. At the rate that the Wisconsin group is going, they should improve their simulation greatly within the next few years. Ten years from now use of the computer to design engines may be absolutely imperative to remain competitive.

N.J. BECK
White Motor Corp.

The authors are to be complimented on their scholarly treatment of the computerized diesel engine simulator. The simulator offers a very powerful tool in analyzing causes and effects, comparing analytical and experimental results, and for generating clues on how to optimize engine design. The clear and concise presentation of data was excellent. The authors exhibit a thorough understanding of the problems by pointing out the weaknesses of their simulator.

I believe the authors can be accused of being overly modest by their repeated warnings that the simulator data should be questioned because of the uncertainty in some of the assumptions. I think that the data and conclusions are really better than inferred by some of the comments in the paper.

Of particular note are the effects of detailed changes on volumetric efficiency. I am sure that there are several factors that affect volumetric efficiency which can be more accurately calculated than they can be measured experimentally. The engine simulator offers an opportunity to refute some of the unwarranted erroneous reliance on experimental data. The evaluation of a multitude of factors, each with a fractional effect but all acting simulaaneously, is difficult, if not impossible, to attain experimentally but quite practical to attain analytically with the use of the computer.

It would seem that some elaboration on the effect of valve sizing on volumetric efficiency and engine performance is in order.

The oversimplified simulation of combustion seems somewhat disappointing and I wonder why a treatment, such as that described by Harvey Cook in his earlier paper on the subject, is not used.

The authors have covered much of the same ground as previous treatments. I would like to suggest that it is probably time to review the state-of-the-simulator-art to see if it is not now more important to explain some of the more practical applications of the program rather than the details of how it was developed. In other words, we have the computer, we have the software, now let us use it to optimize engines and not just for comparing calculated data with experimental results.

In conclusion, I wholeheartedly agree with the authors in the comment that experimental data can tell us what will happen precisely, but the causes may not be evident. On the other hand, the simulator, even if sometimes less precise in telling us what will happen, can more clearly point out the causes. Since the age of the internal combustion engine is approaching the century mark the engineering task becomes more one of evolutionary refinement rather than revolutionary innovation, and we obtain our improvement from many small and even minute effects rather than a few large ones. It is here where an engine simulator may have great potential. Perhaps further refinements of the simulator will enable us to further expand our ability to predict results and trends more accurately than we can with experimental data. We look forward to future developments which will encourage us to use the diesel engine simulator routinely as a research and development tool, and this paper is another milestone in progressing toward this goal.

AUTHORS' CLOSURE TO DISCUSSION

The authors would first like to thank the discussors for their comments and encouraging remarks concerning the usefulness of cycle simulation calculations.

The reduction of data to dimensionless plots can result in a considerable saving in computation time if the number of dimensionless groups is small, but in the case of a large number of groups the saving may be less significant. It is important to recognize that in Mr. Brown's Fig. B many parameters have been held constant such a valve design parameters, intake opening crankangle, ratio of intake to exhaust valve diameter, exhaust valve timing, and so forth. In addition, although it is true that heat transfer during intake is poorly understood, it is not necessarily true that its effect can be neglected. The single additional parameter of heat transfer would make a compact presentation of volumetric efficiency in terms of dimensionless groups much more difficult.

We tend to agree with Mr. Brown's comments concerning bore-stroke ratio calculations; however, the calculations performed in the paper do show the effects under a given set of assumptions. Again, as stated in both the paper and discussion, such calculations point to the need for further research into the areas of engine combustion, heat transfer, and friction.

Although Mr. Brown and the authors have both used optimization examples involving a single performance parameter, actual design optimizations must use a weighted optimization based on a number of performance parameters. This simply points out how complex a problem a true optimization is and how much more work is required to make engine design a quantitative mathematical procedure.

Table 1 - Calculation Results for Variation of Valve Diameters and Timing

All runs at 2000 rpm and 1.305 10^{-4} lb_m/cycle of fuel.

Atmospheric temperature 95 F and pressure 14.08 psia.

Run	Intake Valve Diameter, in.	CAIVO, deg	CAEVO, deg	Volumetric Efficiency	IMEP, psi	PMEP, psi	Mass Averaged Intake Temp, R	Peak Temperature, R	Peak Pressure, psia	Total Heat Transfer, Btu/cycle	Piston Temp, R	Head Temp, R	Intake Valve Temp, R	Exhaust Valve Temp, R	At CAIVO		At CAIVC		At CAEVO		At ·CAEVC	
															P psia	T °R	P psia	T °R	P psia	T °R	P psia	T °R
19	2.15	520	310	82.4	138.36	3.86	596.2	3714	1136	0.451	1039	907	1174	1628	17.63	1623	16.69	704	60.58	2516	13.58	1347
20	1.85	520	310	83.8	138.82	2.75	584.3	3686	1142	0.461	1031	899	1138	1622	15.92	1672	16.78	699	60.81	2493	13.25	1342
21	2.00	530	310	81.7	138.29	3.18	587.8	3726	1126	0.460	1036	904	1152	1635	18.01	1715	17.98	713	60.25	2528	12.78	1460
22	2.00	510	310	83.5	138.63	2.93	592.1	3691	1145	0.454	1034	903	1160	1621	15.57	1683	15.75	689	61.31	2500	13.82	1322
23	2.00	520	320	84.2	139.13	3.88	584.9	3679	1142	0.452	1036	904	1148	1604	14.70	1635	16.61	694	57.43	2449	13.18	1092
24	2.00	520	300	79.4	136.97	2.87	608.4	3768	1129	0.472	1041	907	1194	1670	23.85	1881	16.72	721	65.56	2613	18.23	1703
25	2.00	520	310	83.3	138.69	3.02	589.7	3694	1140	0.455	1034	902	1155	1622	16.59	1691	16.74	700	60.72	2500	13.43	1343
41	2.00	500	310	82.0	138.20	2.84	598.2	3717	1138	0.460	1037	904	1171	1630	15.17	1708	14.81	682	61.08	2521	13.95	1335
42	2.00	500	330	83.3	138.80	5.19	591.2	3697	1142	0.460	1043	908	1173	1610	14.58	1678	14.81	676	55.09	2431	13.56	951
43	2.00	520	330	83.9	139.08	5.28	584.2	3684	1142	0.456	1040	906	1153	1600	14.33	1627	16.75	697	55.08	2422	13.08	942
44	1.70	500	330	80.1	138.06	4.08	582.3	3763	1117	0.487	1045	905	1148	1642	14.33	1719	14.13	672	54.47	2439	13.07	933
45	1.70	500	310	79.5	137.58	2.61	587.4	3773	1115	0.485	1038	900	1145	1659	14.61	1734	14.12	676	60.24	2571	13.82	1356
46	1.70	520	330	83.4	138.83	4.34	577.1	3701	1141	0.476	1040	903	1121	1615	14.20	1638	16.78	703	55.06	2434	12.33	947
47	1.70	520	310	83.6	138.69	2.88	579.7	3695	1147	0.470	1030	897	1121	1629	15.46	1667	16.78	701	61.19	2505	13.05	1350
48	1.85	510	320	84.5	139.12	3.31	582.5	3675	1147	0.460	1034	901	1143	1606	14.52	1648	15.71	684	57.58	2445	13.42	1061
49	2.00	510	320	84.5	139.08	3.82	587.1	3765	1148	0.452	1036	904	1157	1603	14.72	1652	15.66	684	57.60	2444	13.61	1084
50	1.86	520	316	84.4	139.11	3.10	581.7	3676	1143	0.459	1032	900	1134	1609	14.83	1639	16.79	696	58.69	2461	13.04	1187
51	1.70	510	320	83.3	138.82	3.24	578.6	3701	1138	0.473	1035	900	1130	1623	14.40	1664	15.51	684	57.59	2469	13.19	1068
52	2.15	510	320	84.1	138.92	4.97	592.3	3685	1146	0.447	1040	908	1171	1605	15.05	1665	15.75	687	57.55	2451	13.72	1068
53	1.85	530	320	82.7	138.69	3.65	581.3	3713	1131	0.467	1037	902	1129	1622	14.38	1622	17.88	714	57.34	2480	11.48	1160

Table 2 - Comparison of Original and Proposed Optimum Engine Performance

	Original	Optimum w/cons. F/A Ratio	Optimum w/cons. Fuel Rate
Performance			
Imep, psi	138.69	140.95	139.16
Ind. thermal efficiency, %	0.4437	0.4443	0.4452
Isfc, lb/bhp-hr	0.3124	0.3120	0.3114
Mass avg. int. temp, F	129.70	124.70	124.50
Vol. eff., %	83.30	84.56	84.58
Pumping mep, psi	-3.02	-3.91	-3.89
Friction mep, psi	-44.94	-45.20	-45.06
Brake mep, psi	90.72	91.84	90.20
Pcyl at st. inj., psi	229.98	232.38	232.29
Tcyl at st. inj., R	1428.00	1428.00	1426.00
Engine Conditions			
Speed, rpm	2000.00	2000.00	2000.00
Fuel air ratio	0.0540	0.0540	0.0531
Fuel rate, lb/hr	7.831	7.948	7.831
Caivo, deg	520.00	514.00	514.00
Caivc, deg	50.00	44.00	44.00
Caevo, deg	310.00	322.00	322.00
Caevc, deg	560.00	572.00	572.00
Int. valve dia., in.	2.00	1.962	1.962
Exh. valve dia., in.	1.70	1.738	1.738
P atm, psi	14.08	14.08	14.08
T atm, F	95.00	95.00	95.00

Table 3 - Effects of Heat Release Shape and Compression Ratio

Compression Ratio	16.00	16.00	16.00	16.00	18.19
Peak cyl. temp., R	3737.1	3750.5	3758.7	3764.1	3550.5
Peak cyl. pressure, psi	1130.0	1110.0	966.0	1112.0	1110.0
Max. pressure rise, psi/deg	88.38	81.03	50.82	70.64	56.19
Imep, psi	137.85	138.92	135.32	138.56	137.98
Heat transfer sum, Btu/cycle	0.423	0.421	0.413	0.432	0.415

Column	Heat Release Curve
1	Original (Fig. 10)
2	Simplified (Fig. 10)
3	Modified, 75% peak (Fig. 11)
4	Modified, w/7 deg advance (Fig. 12)
5	Modified, 75% peak (Fig. 11)

Table 4 - Effect of No Heat Transfer on Engine Performance

	With Heat Transfer	Without Heat Transfer
Engine speed, rpm	2000.0	2000.0
Fuel-air ratio	0.0497	0.0497
Atm. temp., F	30.0	30.0
Atm. press., psia	14.19	14.19
Mass Avg. int. T, F	71.8	36.8
Volumetric efficiency, %	83.0	92.5
Peak pressure, psia	1185.0	1286.0
Indicated horsepower	26.32	32.47
Pumping horsepower	0.62	0.76
Friction horsepower	8.27	8.59
Brake horsepower	17.44	23.12

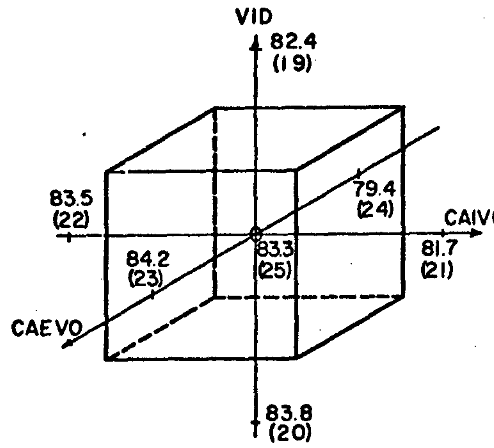

Fig. 1 Volumetric efficiency at 2000 rpm for various values of valve diameter and valve timing.

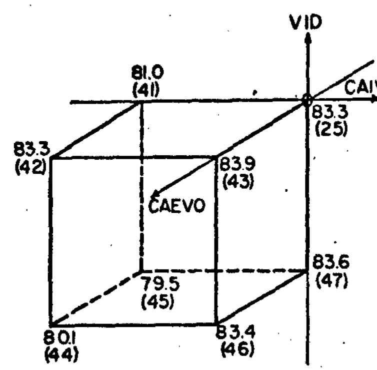

Fig. 2 Additional values of volumetric efficiency at 2000 rpm for various values of valve diameter and timing.

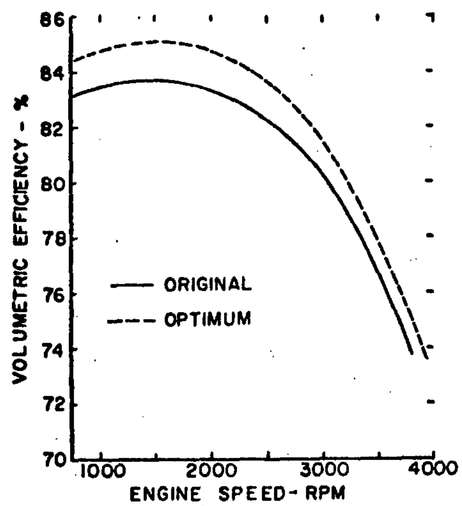

Fig. 3 Comparison of original and predicted optimum volumetric efficiency versus engine speed.

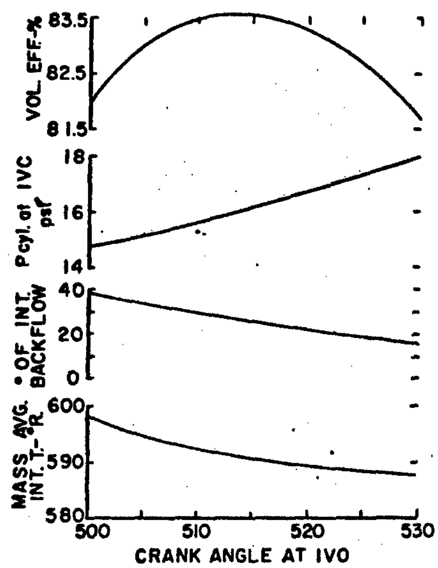

Fig. 4 Various computed values versus crankangle when intake valve opens.

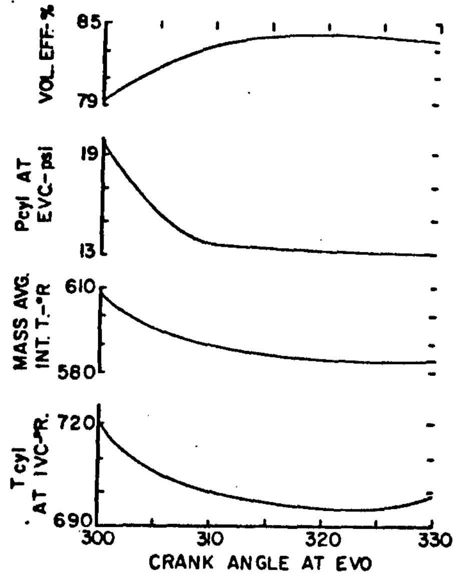

Fig. 5 Various computed values versus crankangle when exhaust valve opens.

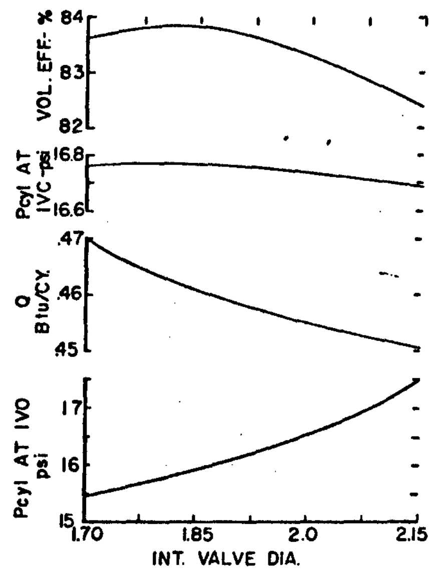

Fig. 6 Various computed properties versus intake valve diameter.

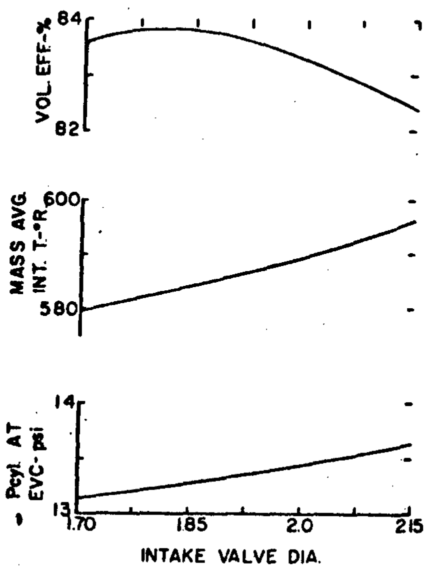

Fig. 7 Various computed properties versus intake valve diameter.

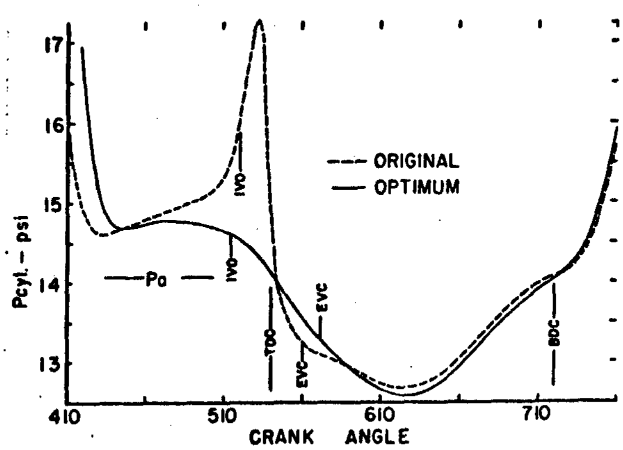

Fig. 8 Cylinder pressure versus crank-angle for original and predicted optimum engines.

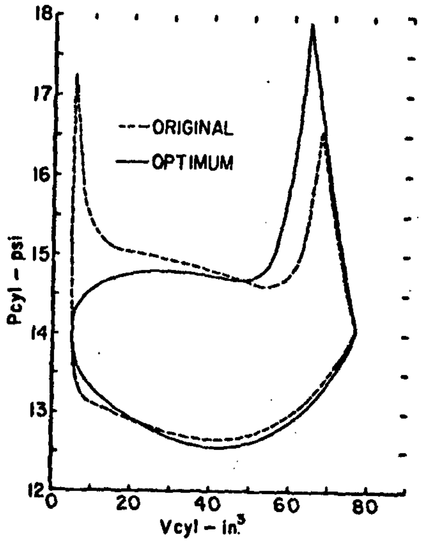

Fig. 9 Pumping loop for original and predicted optimum engines.

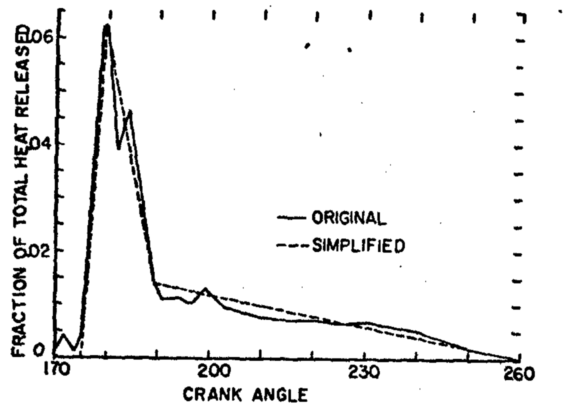

Fig. 10 Original experimental and simplified heat release versus crankangle at an engine speed of 3200 rpm.

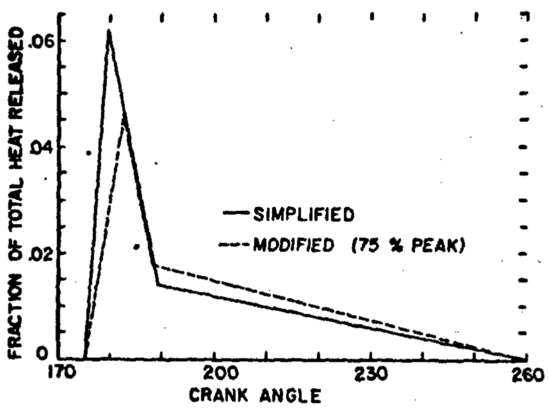

Fig. 11 Simplified heat release shape and modified heat release shape with 75% of simplified peak.

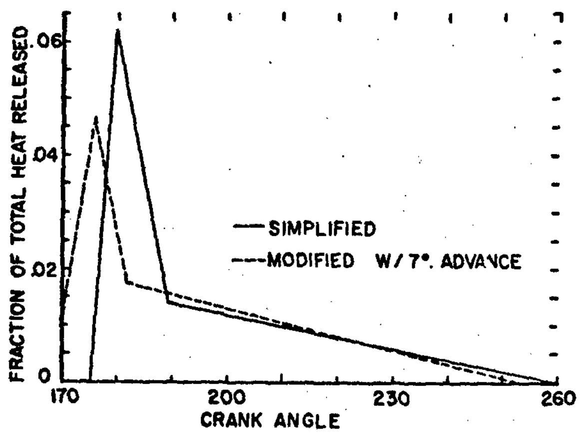

Fig. 12 Modified heat release shape and modified heat release shape advanced 7 deg.

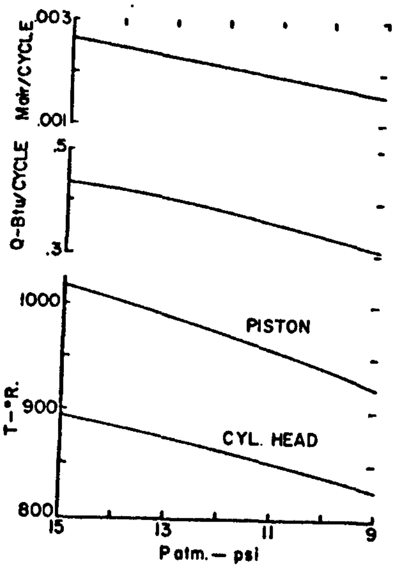

Fig. 13 Engine performance versus atmospheric pressure with constant fuel air ratio and an engine speed of 2000 rpm.

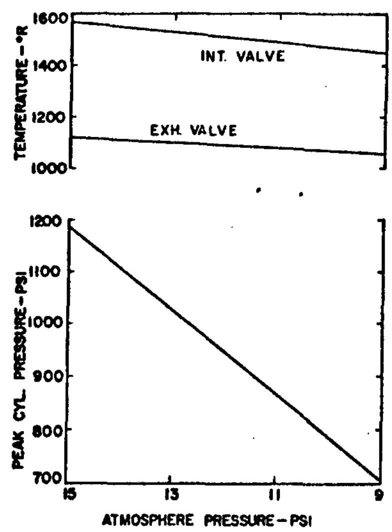

Fig. 14 Engine performance versus atmospheric pressure with constant fuel air ratio and an engine speed of 2000 rpm.

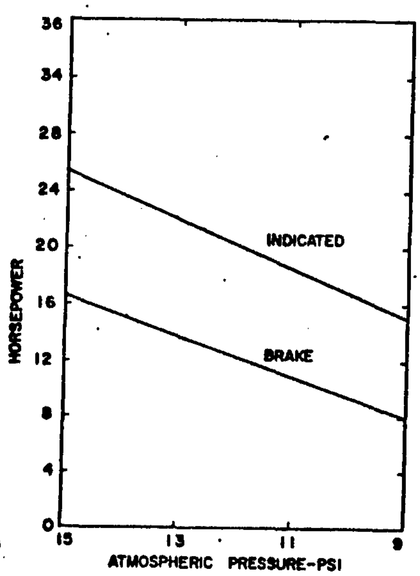

Fig. 15 Engine performance versus atmospheric pressure with constant fuel-air ratio and an engine speed of 2000 rpm.

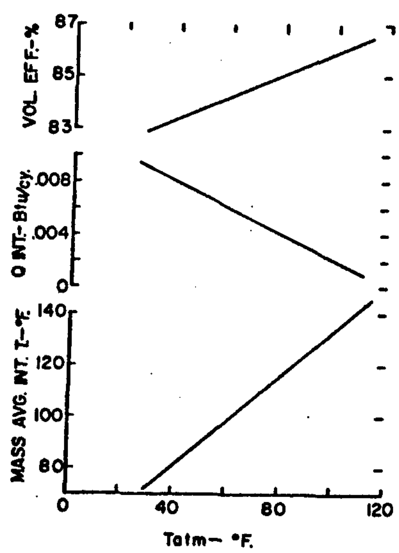

Fig. 16 Engine performance versus atmospheric temperature with constant fuel-air ràtio and an engine speed of 2000 rpm.

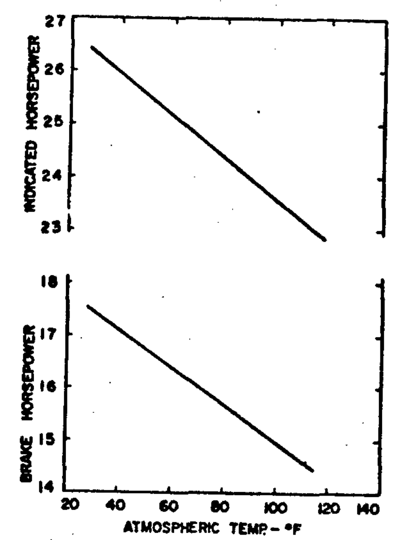

Fig. 17 Engine performance versus atmospheric temperature with constant fuel-air ratio and an engine speed of 2000 rpm.

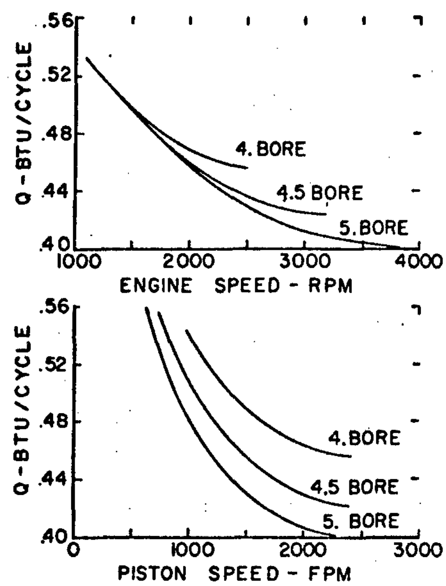

FIGURE 9
TOTAL Q PER CYCLE VS ENGINE AND PISTON SPEED

Fig. 18 Total heat transfer per cycle versus engine and piston speed for various bore-stroke ratios.

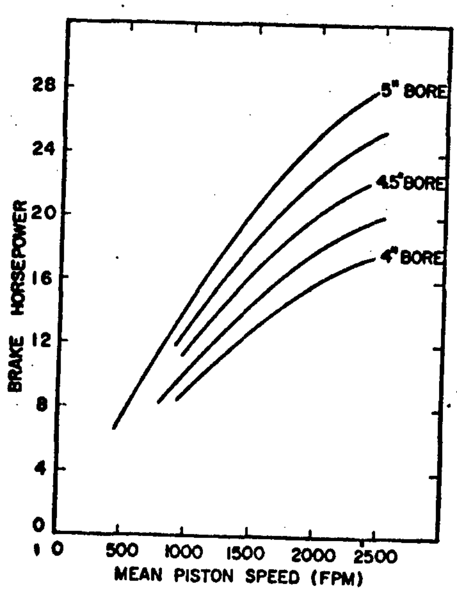

Fig. 19 Brake horsepower versus piston speed for various cylinder bores.

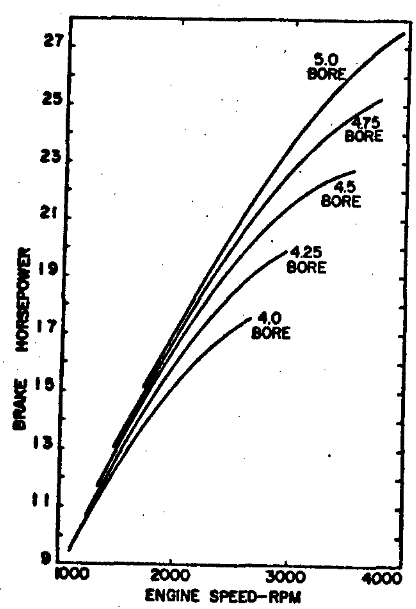

Fig. 20 Brake horsepower versus engine speed for various cylinder bores.

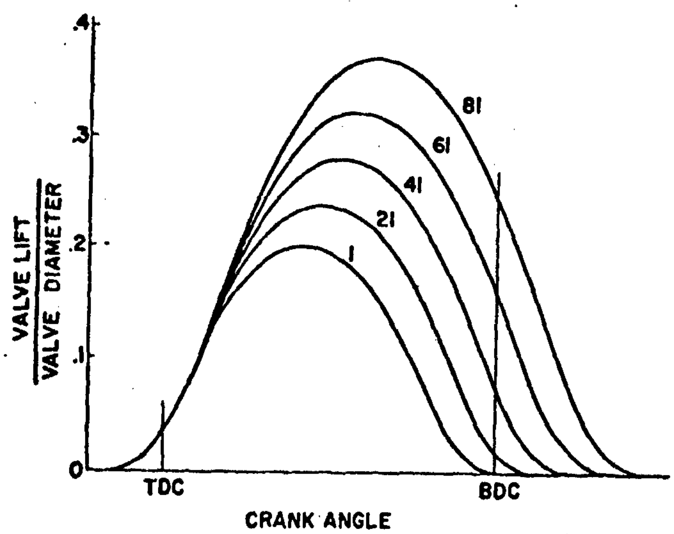

Fig. A Family of valve lift curves.

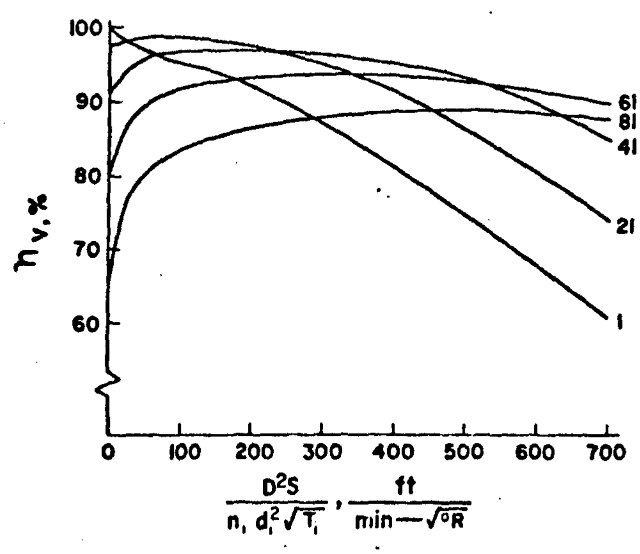

Fig. B Volumetric efficiency versus engine speed parameter.

APPENDIX IV

A

A Tape Recording and Computer Processing System for Instantaneous Engine Data

T. Le Feuvre, J.H. Shipinski, P.S. Myers, and O.A. Uyehara
Mechanical Engineering Dept.
University of Wisconsin

ABSTRACT

The development of a high speed, multichannel data acquisition system is described. A precision magnetic tape recorder is used to record analog data from highly transient phenomena. Analog-to-digital data conversion is performed on a hybrid computer and the digitized data is processed using large, high speed digital computers.

A detailed example of the application of the system to the measurement of rates-of-irjection, rates-of-heat release, and instantaneous rates-of-heat transfer from the cylinder gases to the cylinder walls in a high speed open-chamber diesel engine is presented.

CONCEPTUAL SYSTEM

The research activities at the College of Engineering of the University of Wisconsin have more than doubled from 1961 to 1966.(1)* In order to keep pace with this growth of research activity, data acquisition and processing systems have had to be continually improved.

In addition to the growth in amount of research done, the nature of the instrumentation that is both commerically available and that is developed in the laboratory has changed. Thus in less than a generation, we have seen the change from slow speed, mechanical indicators to electronic devices with response times of a microsecond. Data recording techniques have had to change accordingly. Indicator cards, chart recorders, ultra violet oscillograms, and the drum camera and oscilloscope are some of the recording devices used previously. The significant drawback to most of the above methods is that manual processing, which usually includes time-consuming and irreproducible hand scaling, is required. For example, the minimum time required to hand scale one pressure-time (p-t) diagram from an engine is on the order of magnitude of one hour. By utilizing modern analog-to-digital converters, with conversion rates of several kHz, one would hope to reduce this time by several orders of magnitude. Other significant disadvantages of previously used recording devices include the difficulty in simultaneously obtaining high frequency response and more than 4-8 channel recording capability. In other words, chart recorders can be obtained with eight or more channels, but high frequency response is poor and Y-axis (dependent variable) resolution is limited. Most oscilloscopes have good high frequency response but are restricted in number of channels.

The availability of high speed, digital computers permits the rapid processing of large amounts of data. The data must be supplied in digital form to the digital computer. The automatic conversion from analog to digital form is a sine qua non if the data processing abilities of the digital computer are to be utilized.

Current research areas in the Mechanical Engineering Department, which would benefit from a high performance data acquisition system, include:

1. Diesel engine combustion phenomena.
2. Oscillatory combustion.

*Numbers in parentheses designate References at end of paper.

3. Welding heat transfer.
4. Human body member motion studies.
5. Knock phenomena in spark ignition engines.
6. Automobile driver research.

The specific objectives of two of the authors were to obtain data from a single cylinder diesel engine for the computation of rate-of-injection (ROI), rate-of-heat-release (ROHR), and instantaneous rate-of-heat-transfer (ROHT). Thus, much of the latter part of the paper, which illustrates the use of the instrumentation, is devoted to the implementation of the system for the particular problems incurred in obtaining these data.

Summarizing then, a data acquisition system which would meet the very general current and future needs for research in the Department of Mechanical Engineering was required.

OVERALL SYSTEM REQUIREMENTS ... A high speed tape recorder in combination with some kind of analog-to-digital converter was judged to fit the needs of the department. Such an arrangement is shown conceptually in Fig. 1. Having decided on the approach to the problem, the factors affecting the equipment selection must be considered. In view of the phenomena to be studied, we can note the characteristics which the overall system should have:

1. Wide frequency response - The entire system must have a frequency response from d-c to greater than the highest frequency of interest.
2. Good signal-to-noise ratio - Many transducers have outputs in the milli- or even micro-volt range where noise problems become severe.
3. Multichannel capability - Even in studies where only one response is being measured, a timing record is necessary. Thus, the minimum number of channels is two. Moreover the interaction of variables may demand that many effects be measured simultaneously in order to draw significant conclusions. Thus, a large number of channels is desirable.
4. Automatic scaling - If significant quantities of data are to be processed, some form of automatic scaling or analog-to-digital (A/D) conversion process is necessary. Not only does this speed up the total acquisition system, but it ensures consistent and accurate scaling.
5. Flexible operation - Any combination of recorder and digitizer should be as flexible as possible to serve the needs of the department as a whole. Since any tape recorder having maximum accuracy and frequency response and a large number of channels is not a readily portable machine, there should be some way to operate the machine remotely. Some of the studies for which the system is being used do not require the high frequency response that others do. Since the high frequency cutoff point of a tape recorder is proportional to the tape speed and tape economy is important, several recording speeds are desirable. The speeds used on playback depend on the frequencies originally recorded as well as the medium being used for display, that is, direct reproducing recorders such as a Brush recorder, a Visicorder, an oscilloscope, or a hybrid computer.
6. Visual observation of data before and after recording - Display of the data just prior to recording ensures that the desired data are to be recorded. Observation after recording and before digitizing is helpful in observing trends and avoids digitizing is helpful in observing trends and avoids digitizing data judged not to be of interest.

SPECIFIC SYSTEM DEVELOPED

GENERAL CHARACTERISTICS ... On the basis of the above mentioned factors, the Mechanical Engineering Department, University of Wisconsin, purchased a tape recorder, Sangamo, model 4784 as the initial step in realizing the conceptual system shown in Fig. 1. Some of the specifications of the machine are included in Appendix A. Briefly, the machine is a completely transistorized, multichannel, multispeed machine with modular electronics. The particular machine which was purchased has electronics for eleven frequency modulation (fm) record channels and three direct record (dr) channels. Because of lack of funds only four fm and one dr playback modules were purchased. The limited number of playback modules has not been a drawback to the authors since only three signals, two timing and one analog data, were simultaneously required for digitizing. Data from all channels can be digitized by repeated playing of the tape.

For purposes of standardization, the recorder input sensitivities were set so that a 2v peak-to-peak signal, centered about ground, gave the maximum signal-to-noise ratio.

The availability of the tape recorder solved the data recording and storage problem and also served to emphasize the need for some form of automatic scaling. The authors wished to handle large amounts of data (on the order of 10^7 data points) and electronic scaling appeared to be the only reasonable solution. Fortunately, the College of Engineering was in the process of establishing a hybrid computing facility which would incorporate an analog-to-digital (A/D) converter. Thus, hardware was available to perform the tasks outlined in concept in Fig. 1, and the authors' attention was devoted to incorporating these facilities into a workable data recording and processing system.

The specific system developed and used by the authors is outlined in the block diagram of Fig. 2. Several blocks of the complete system are general and are to be used for other studies. The block diagram is more of an information flow chart than a description of the physical system. Details of the hardware and software used by the authors for their specific objectives are given in this section.

The phenomena of interest to the authors, namely rate-of-fuel injection, heat release, and heat transfer, were occurring in the cylinder of a high speed, supercharged diesel engine. Several transducers sensed the pressure, temperatures, and displacements related to the phenomena of interest. Thus the lines of information flow shown in Fig. 2 actually represent several parallel paths. All of the transducer output signals needed conditioning to ensure maximum signal-to-noise ratio when recorded on magnetic tape.

The tape recorder is in a central location with the various research areas connected to it via coaxial lines. This influenced the design of the conditioning equipment used. The Hybrid Computer Laboratory (HCL) is in the Electrical Engineering Building, which necessitated stringing coaxial transmission lines through existing underground tunnels for a distance of some 700 ft. The equipment at the HCL includes a large iterative analog computer, a hybrid interface, and a small high speed, general purpose digital computer. Digital output is available in printed form or via magnetic tape.

The University of Wisconsin Computing Center (USCC) has a number of large, high speed digital computers along with a large library of subroutines and functions, several of which were used extensively by the authors as given in detail in the section on Data Processing.

SYSTEM UTILIZATION ...

Engine Operation - The engine, engine installation, and performance instrumentation are described elsewhere.(2) Briefly, the engine was a single cylinder, four stroke cycle open chamber diesel engine having a 4.5 in. bore and stroke and similar to the ER-2 described by Chen.(3) The transducers, amplifiers, and signal conditioning equipment are described below.

Measurements - Transducers and Conditioning Equipment -

1. Time Base - Crank position provides a convenient time reference. A uniformly slotted flywheel and electromagnetic pickup were used to trigger a Schmitt trigger circuit at each crank angle (CA). An emitter follower amplifier provided impedance matching to the transmission line and the tape recorder. The combination of trigger circuit and amplifier had a frequency response of greater than 100 kHz and a phase shift of less than 0.01 CA at 3000 rpm. The resultant uniform height pulses were recorded on one channel of the tape recorder, while a second channel was used to record a TDC pulse.

2. Surface Temperature - A total of eight surface thermocouples were installed in the cylinder walls, three in the head, and five in the cylinder sleeve. These thermocouples were of the plated junction design of Bendersky (4) as used previously at the University of Wisconsin, (5,6). Both iron-nickel and iron-constantan thermocouples were used. The thermocouples were installed in areas of the head and sleeve where the heat transfer through the walls to the coolant was approximately one-dimensional. Since the surface thermocouple junction was located only one micron below the surface, the thermocouple output was considered to represent

the actual surface temperature. The temperature of the cylinder wall at the coolant interface was obtained by forming a second thermocouple junction at the interface, as shown schematically in Fig. 3A.

The arrangement for a surface temperature measurement is outlined in the block diagram of Fig. 3B. Since there were eight surface thermocouples, there are eight units in many of the blocks shown in the block diagram.

The temperature of the wall-coolant interface was constant and recorded by the multipoint recorder 1. (Numbers in circles refer to components shown in the block diagram, Fig. 3b). The average value of the temperature difference through the wall was measured by a light-beam galvanometer 2. The fixed-gain amplifiers had to be capable of high gain, wide bandwidth, low noise operation. A compromise was necessarily reached on the degree to which any one amplifier could meet these requirements. The amplifiers used, 3, Astrodata model 885, feature calibrated gains in steps to 1000, a bandwidth of d-c to 10 kHz, output noise of 2 mv rms at a gain of 1000, and a linear phase-frequency relationship of approximately 19°/kHz. It was desired to modulate the tape recorder with only the oscillatory component of the surface temperature. Thus the average value was biased out 4. The variable gain amplifiers permitted optimum modulation of the tape recorder 5. A calibration signal was recorded on tape so that the entire system, including the tape recorder and the hybrid computer, was calibrated for each run.

3. Cylinder Pressure Measurement - A technique for relating instantaneous heat release and cylinder pressure is outlined in Appendix E. The requirements and errors of cylinder pressure measurement in piston engines have been presented in the literature.(7-9). The authors used a Kistler, model 601H, piezo-electric pressure transducer in conjunction with a Kistler charge amplifier to obtain an electrical representation of the cylinder pressure. The sensitivity of the transducer to transient heating was minimized by the use of an RTV coating on the transducer diaphragm. Flame chopper and flashbulb tests confirmed the effectiveness of the RTV coating for this purpose. The transducer and amplifier combination had a frequency response of greater than 35 kHz. The output from the change amplifier was amplified (or attenuated if necessary) by a variable gain amplifier, incorporating suitable calibration, as used for the surface temperature measurements.

4. Needle Life and Injection Pressure - A nozzle holder was instrumented CAV Ltd. for needle lift and injection pressure. The needle lift transducer was a variable inductance device and functioned as the external arm in Tektronix Q unit bridge having a 26 kHz carrier frequency. The injection pressure was sensed by a strain tube pressure transducer in conjunction with a d-c bridge circuit.(10)

Tape Recorder Operation - The cylinder pressure and wall temperature data were always recorded at the highest tape speed, 120 in. per sec (ips) since frequency response is proportional to tape speed. Two d-c voltages, measured with digital voltmeters accurate to 0.1%, were recorded at the start of each recording period for calibration purposes. Approximately 200 consecutive cycles of engine data was recorded per engine run. All data were recorded on f.m. channels. The linear phase amplifiers in the tape recorder ensured no relative phase shift between signals. The injection nozzle pressure and needle lift were recorded by Polaroid pictures of the screen of a Tektronix 565 four trace oscilloscope. Adequate time resolution was possible on the oscilloscope screen, since the injection period is only about 1/6 of the complete cycle.

Digital Conversion of Taped Data - The data, having been recorded on magnetic tape, was inspected by playback into an oscilloscope or a Brush recorder. Then it was played back at 7.5 ips, that is, 1/16 record speed, to the hybrid computer via the coaxial lines mentioned previously. It should be noted that noise pickup during this transmission was not a problem as long as only one end of the system was grounded. The facilities available at the HCL have already been mentioned. These facilities were not used at full capacity for the authors' purposes, but it should be noted that a portion of each of the three basic units, analog, interface, and digital, was needed. The iterative analog equipment was used for conditioning and control purposes, the interface for the A/D function, and the digital computer for storage, calculation, control, and output. The analog-to-digital converter by itself is essentially useless since it possesses no memory in which to retain either a set of operating instructions or the digitized data. It functions as a slave of the digital computer.

The authors wrote a FORTRAN language program incorporating a library subroutine, IGATHER, of the HCL. With this program, and suitable analog and logic circuitry, (as shown in Appendix C) the following operations can be performed at the HCL:

1. Individual cycles of engine data may be identified and sampled at each crank angle degree.
2. A number of engine cycles can be identified, sampled, and averaged.
3. The results from either item 1 or 2 can be converted to meaningful units of pressure and temperature, and can be presented in listed form and/or written on magnetic tape for later use in various data reduction and computation programs.

The technique which was used for digitizing data for N consecutive engine cycles is listed briefly below:

1. The analog, CA, and TDC signals were transmitted through f.m. playback units and through the underground cables to the hybrid computer.
2. The signals were amplified by operational amplifiers. The maximum input to the analog-to-digital converter was plus or minus 100v.
3. The logic circuit (Appendix C) counted any desired number of cycles and then triggered the command-to-sample at the next following TDC mark.
4. The A/D converter sampled the analog signal at each CA degree.
5. Each digitized sample was stored in core in a memory location assigned to the discrete CA.
6. The process continued through the cycle and for a total of N cycles, each time adding the digitized value to the core location corresponding to the CA.
7. At the end of N cycles, the sum of the digitized samples for each CA was divided by N, and a print out of the averaged values for each CA of the cycle was obtained.
8. If desired, the listed results could be in units of pressure or temperature by incorporating suitable calibration and sensitivity factors into the digital computer program.

The A/D converter was a successive approximation device as mentioned in Appendix B. The conversion time, 30 μ sec, represented about 1/40 the time between CA's when playback was at 8.5 ips. If the playback speed had been considerably faster, say 120 ips, then the time necessary for the successive approximation analog-to-digital conversion would represent approximately 1/2 of the time between CA pulses. Depending on the rate-of-change of the analog signal being digitized, the latter situation could lead to errors.

The averaging of a number of engine cycles served two purposes. First, cycle-to-cycle variation was eliminated to arrive at an average pressure-time or temperature-time curve. Secondly, random noise introduced by the various electronic components, was attenuated by the factor $1/\sqrt{N}$, where N is the number of cycles averaged.(11) This was particularly critical for the heat release studies as outlined in Shipinski.(2)

The injection nozzle needle lift and injection pressure traces were scaled by hand from the Polaroid prints. These data were added to the cylinder pressure-CA listing obtained from the A/D converter and punched on IBM cards for use as input to the program which computed rate-of-injection, apparent heat release, and the fitted heat release function.

Hand punching on IBM cards was originally necessary, since at the time part of this work was carried out, there was no tape transport or machine punch available at the HCL. Subsequently, a tape transport with IBM compatible tape has been installed at the HCL and the digitized data has been written directly on the tape. The process of punching did not involve any human judgment or smoothing, contrary to the case of scaling photographs or oscillograms. The data was simply transferred from a printer listing to cards. It was, however, difficult to eliminate keypunch errors, and the HRR program with its graphing routines was nearly always able to "find" punching errors which human inspection could not find.

Computer Processing for Heat Release - The digitized pressure-CA and injection data, together with the engine operating conditions and estimates of the wall temperatures, are used as input to the program which calculates the ROI and HRR

(heat release rate). A brief description of the basic equations used is presented in Appendices D and E.

In addition to the computation of apparent heat release (12,13) and ROI, the program includes a least sum of squares fit of the smoothing function (14) to the HRR. A subroutine (called GAUSHAUS) which is available on call from the function library of both the CDC 1604 and 3600 computers at the UWCC is used for the fitting. The purpose of GAUSHAUS is to obtain a least squares estimate of parameters entering nonlinearly into a mathematical model, or to solve a system of N nonlinear equations in N unknowns. An iterative technique is used in the subroutine; the estimates at each iteration are obtained by a method which combines the Gauss (Taylor series) method and the method of steepest descent. According to UWCC documentation, this algorithm should share with the gradient or steepest descent method the ability to converge from a region far from the minimum, and like the method of Gauss, should converge rapidly once the vicinity of the minimum is reached. Program GAUSHAUS can be misleading, however. For example:

1. If the initial estimates are not in the neighborhood of the least sum of squares, a convergence to a local minimum in some other region may be obtained from GAUSHAUS.
2. GAUSHAUS puts equal weight on each data point unless otherwise specified. Thus if many data points for one region are fitted, the result will be biased in favor of that region.
3. The technique of minimizing the sum of squares puts significantly greater weight on data points which deviate markedly from the mean of a plot.

A detailed description of the equations, technique, and use of GAUSHAUS is contained in UWCC documentation.

The apparent heat release rate curves, the computed rates-of-injection, and the fitting obtained by the Wiebe smoothing function are programmed into a single computer program. The program has been set up to process the data for more than one run on each job submission. This proves to be a quite attractive economical procedure as the compile time for the program is spread over many runs. For example, Table 1 gives the actual results obtained on the CDC 1604 computer. The cost for computer time per "production" run is less than one-half that per individual run.

The graphs which are part of the output of the data recording and processing system appear in Figs. 4-6. These have been plotted by the Calcomp plotter, which is the last item in the block diagram of the system shown in Fig. 2. In order to maintain a one-to-one compatibility with the cycle simulation, 0 crank angle deg is at BDC on compression and thus 180 crank angle deg corresponds to TDC fired. The "X s" appearing in Fig. 4 are the pressures averaged from 50 engine cycles. The thin line connecting the X's is the curve fit by the computer program through the averaged experimental points; the dashed line is the computed mass averaged gas temperature times the given scale factor.

Table 1 Actual Results from CDC 1604 Computer

Job	Number of Runs	Total Time	Time/Run
0651	1	4 min 9 sec	4 min 9 sec
1099	11	20 min 8 sec	1 min 51 sec

In Fig. 5, the irregular solid light line is the apparent heat release (HRR) as computed and plotted by the system. The fine dotted line is the rate-of-injection (ROI) as computed by the system and converted to a rate of heat addition by multiplication by the heating value of the fuel. The rate-of-heat addition (or rate-of-injection) is multiplied by a scale factor of 0.5 to facilitate plotting. The rate of-heat transfer, computed by Borman's (12) formula is plotted times a scale factor of 10. It is seen that the rate of heat transfer computed by Borman's formula is small relative to the maximum rate-of-heat release.

If the spikes and dips in the apparent HRR curve are considered to be due to some extraneous cause, then a curve can be faired through the mean of the apparent HRR. The heavy dashed line is one such possible curve; it is perhaps the best simple curve which can be faired through the oscillations.

Figure 6 shows the ROI and a curve fit to the apparent heat release of Fig. 5 by program GAUSHAUS, using Wiebe's function as the model for the curve. This is the same curve which has been faired through the apparent HRR in Fig. 5.

Computer Processing for Heat Transfer - From the HCL the cyclic temperature-time history for several positions on the cylinder wall corresponding to a particular operating condition was obtained. From these data the cyclic heat flux can be calculated as described below.

Recall that the thermocouples were installed in regions of the head and sleeve where the heat transfer can be considered as one dimensional. Note that since the coolant-wall interface temperature is constant, the wall behaves as a semi-infinte solid to the cyclic variations in the gas-wall interface temperature $T(0,\theta)$. The governing differential equation for the temperature distribution in a one dimensional slab is:

$$\frac{\partial T(x,\theta)}{\partial \theta} = \alpha \frac{\partial^2 T(x,\theta)}{\partial x^2} \tag{1}$$

where: θ = Time
x = Distance from gas-wall interface
$T(x,\theta)$ = Temperature at position x and time θ
α = Thermal diffusivity of the slab material

Carslaw (15) outlines a method of solution for this equation if the surface temperature variation, $T(0,\theta)$ is expressed as a trigonometric series. Overby (5) used a technique proposed by Sokolnikoff and Sokolnikoff (16) to express $T(0,\theta)$ as a Fourier series. The authors found this technique to be unnecessarily time consuming when programmed on the computer, and therefore have developed a faster and more flexible technique which is outlines in the Appendix F. Having obtained a Fourier series representation of $T(0,\theta)$, the solution for $T(x,\theta)$ and $\dot{Q}(0,\theta)$, the wall surface heat flux, is straightforward and is presented by Carslaw (15) and Overbye (5). Lanczos sigma factors (17) were used in the computation of $\dot{Q}(0,\theta)$ to correct for the familiar Gibbs, or overshoot, phenomenon encountered in the summation of a Fourier series. The solution was carried out by digital computer. A plotting subroutine is available at the UWCC which provides a graphical output to complement the usual printed output.

Figure 7 is a typical plot of the average temperature-time history for three positions on the cylinder wall for a particular operating condition. The operating condition is not the same as that associated with Figs. 1-6. The instantaneous heat fluxes shown in Fig. 8 are computed from the temperature-time histories of Fig. 7 by the method outlined above.

Summary of Characteristics of Specific System - This section has outlined a specific configuration of the system shown in concept in Fig. 1. It should be emphasized that one could develop many other specific systems from Fig. 1, for tasks both similar and dissimilar to that of the authors'. The characteristics of each system would be different. However, we feel that a short discussion of the performance of the specific system detailed above may prove helpful to others who wish to develop data systems based on the concepts shown in Fig. 1.

The more important characteristics of any instrumentation system include: frequency response and phase shift; signal to noise ratio; accuracy; and time for calibrating, recording, and processing data. The performance of the system in any one of these areas is generally governed by the weakest link.

1. Frequency response and phase shift - This work involved the handling of two different types of signals. The time base was represented by a series of pulses and attenuation was relatively unimportant. The critical feature for the timing signals was phase shift relative to the data, or analog, signals.

Attentuation, or distortion, of the analog signals was, of course, unacceptable. The Astrodata amplifiers which were used on the wall temperature signals had a frequency-phase relationship which was linear. This meant that each component frequency in the analog signal within the amplifier bandwidth was delayed by the same time interval upon passage through these amplifiers. That is, there was no wave distortion, only time delay, in the amplifier. Such a delay introduces no error if either of two conditions is met: every signal was delayed by the same amount, or the delay time was negligible. For the temperature signals, the latter condition applied since a phase difference between temperature and timing signals of about 0.8 crankangles was considered to be a negligible error. However, a phase difference between the cylinder pressure and timing signals would lead to an error in heat release. Since insufficient amplifiers were available to handle the two timing signals, the cylinder pressure signal, and all eight thermocouple signals, only thermocouple signals were passed through the Astrodata amplifiers. Phase shift of the pressure signal in the variable gain amplifiers relative to the timing signals, which bypassed the variable gain amplifiers was about 0.002 CA deg. As mentioned previously, the linear phase characteristic of the f.m. record/reproduce amplifiers ensured no relative phase shift during the recording/reproducing process.

A limitation on frequency response is applied by the sampling, or digitizing, process. According to Shannon (18), if the sampling frequency is N, one can gather information only on frequencies up to N/2. In fact, if components of frequency higher than N are present, they are reflected back into the spectrum below N/2, thereby causing errors. This is the process of "aliasing".(19) For example, the authors sampled at every crankangle, or 720 samples per period. Therefore, by Shannon, we could not deduce information on harmonics above the 360-th.

2. Signal to noise ratio (S/N) - The Astrodata amplifiers were characterized by very low noise, as mentioned previously. The tape recorder possessed inherent noise in the high frequency spectrum, 1% of full scale at 40% modulation. The theoretically lowest overall S/N from the transducer output to the A/D converter input was approximately 28 db. Experimentally, the actual S/N was measured at 32 db. Since 50 cycles of engine data were generally averaged in the conversion process, the actual overall S/N was improved by $1/\sqrt{50}$ to 49 db. If one were interested in studying individual engine cycles, low pass filtering prior to digitizing would be advisable.

3. Accuracy - The pressure calibration values which were recorded on magnetic tape were measured with an accuracy of at least ±0.2%. The temperature calibration values were determined accurately to ±1%. The accuracy of the final results is also dependent on the time and amplitude accuracy of the digitizing process. The A/D converter had an amplitude accuracy specification of ±0.01% for full scale. The authors found it convenient to work over half the full scale range, resulting in a conversion accuracy of about ±0.02%. The time accuracy is affected by any phase relation between the timing pulses and the signal being sampled. Where time accuracy was critical, in the digitizing of the cylinder pressure data, the time accuracy was judged to be ±0.15 CA from the transducer through to the digitized results. This does not include error due to crankshaft windup, conservatively estimated at less than 0.2 CA deg.(20)

4. Speed - Automatic recording equipment was used wherever feasible in the complete system. For example, a multipoint chart recorder was used to record the thermocouple outputs indicative of the temperatures on the coolant side of the combustion chamber. However, due to the complexity of the program and the large quantity of data being taken simultaneously, two operators were necessary both during the recording phase and during the digitizing phase. During the recording phase, the limiting factor was the time necessary to attain operating equilibrium of the engine. Time per run was on the order of 15 minutes. The data recording process, including setting levels and gains, took 5-10 minutes. The use of the A/D converter instead of human operator scaling greatly increased the scaling speed. The time necessary for digitizing was governed by the time required to set levels and gains at the hybrid computer. The time to digitize the pressure and temperature data for 50 cycles from one engine operating condition was about 30 minutes.

CONCLUSION

Three factors which are important in any engineering study are: the quantity of information obtained during the study, the quality of that information, and the cost of the information. The instrumentation system developed from the conceptual scheme shown in Fig. 1 is a tool which the authors have used in an attempt to optimize these three factors. The amount of data which could be recorded has been increased over previous studies using oscilloscope, cameras, and chart recorders by the use of a high speed, multichannel tape recorder. By incorporating an analog-to digital converter in the system, the conversion of this increased quantity of data into a digital form for computer processing was fast and consistent. The judicious choice of instrumentation hardware, including the tape recorder, has ensured that the uncertainties in the data be kept at a minimum. The increase in processed data output per time obviously has an effect on the cost per unit of processed data. Another important cost feature is the flexibility of the two high cost components, namely the tape recorder and the hybrid computer. The use of these two relatively high cost items by many projects decreases the cost per project and unit of processed data.

ACKNOWLEDGMENTS

The authors thank the United States Army Tank and Automotive Command for research support during the development of this data acquisition system. The scholarship support from General Motors Corp., Cummins Engine Co., and Caterpillar Tractor Co. is appreciated. A portion of the funds for purchase of the tape recorder was supplied by the National Science Foundation.

REFERENCES

1. W.R. Marshall, "Annual Report, Engineering Experiment Station." Univ. of Wisconsin, 1965-66.

2. J.H. Shipinski, "Relationships Between Rates-of-Injection and Rates-of-Heat Release in Diesel Engines." PhD Thesis, Mech. Engr. Dept., Univ. of Wisc., 1967.

3. S.K. Chen and P. Flynn, "IH-LABECO High BMEP Single Cylinder Research Engine." SAE Paper presented at Cleveland, Oct. 1965.

4. D. Bendersky, "A Special Thermocouple for Measuring Transient Temperatures." Mechanical Engineering, Vol. 75, 1953, p. 117.

5. V.D. Overbye, J.E. Bennethum, O.A. Uyehara, and P.S. Myers, "Unsteady Heat Transfer in Engines." Trans. SAE, Vol. 69, 1961, p. 461.

6. G.D. Ebersole, P.S. Myers, and O.A. Uyehara, "The Radiant and Convective Components of Diesel Engine Heat Transfer." SAE Paper 701C, 1963.

7. J.D. McCullough, "Engine Cylinder Pressure Measurements." SAE Trans. Vol. 61, 1953, pp. 557-573.

8. J. Hempson, "Instrumentation Problems of Internal Combustion Engine Development." Proc. Inst. Mech. Engr. (AS), Vol. 3, 1961-62, p. 81.

9. J. Alyea, "The Development and Application of an Electric Indicated Horsepower Meter." PhD Thesis, Mechanical Engineering, Univ. of Wisconsin, 1968.

10. A.E.W. Austen and W.T. Lyn, "Relation Between Fuel Injection and Heat Release in a Direct-Injection Engine." Proc. Inst. Mech. Engr., 1960-61, pp. 47-62.

11. C.A. Bennett and N.L. Franklin, "Statistical Analysis in Chemistry and the Chemical Industry." New York: Wiley, 1954.

12. G.L. Borman, "Mathematical Simulation of Internal Combustion Engine Processes and Performance Including Comparisons with Experiment." PhD Thesis, Mech. Engr. Dept., Univ. of Wis., 1964, reprinted as CAE Report No. 954 submitted to Detroit Arsenal, August 1964.

13. R.B. Krieger, and G.L. Borman, "Computation of Apparent Heat Release for Internal Combustion Engines." ASME Paper 66-WA/DGP4 presented at Annual Winter Meeting, Nov. 1966.

14. I. Wiebe, "Halbempirische Formel fur die Verbrennungsgeschwindigkeit." Moskau: Verlag der Akademie der Wissenschaften der VdSSR, 1956.

15. H.S. Carslaw and J.C. Jaeger, "Conduction of Heat in Solids." Second Ed., Oxford: Clarendon Press, 1959.

16. I.S. Sokolnikoff and E.S. Sokolnikoff, "Higher Mathematics for Engineers and Physicists." New York: McGraw-Hill, 1941, pp. 545-548.

17. R.W. Hamming, "Numerical Methods for Scientists and Engineers." New York: McGraw-Hill, 1962.

18. C.E. Shannon, "Communications in the Presence of Noise," Proc. IRE, Vol. 37, Jan 1949, pp. 10-21.

19. R.B. Blackman and J.W. Tukey, "The Measurement of Power Spectra." New York: Dover, 1959.

20. P. Flynn, Private Communication, 1967.

21. J. McLeod, Ed., Simulation, Vol. 6, March, 1966, pp. 138-140.

22. B.E. Knight, "Communication on the Performance of a Type of Swirl Atomizer." Proc. Inst. of Mech. Engr., 1955, pp. 104-105.

23. Y. Wakuir, M. Fujii, T. Amitani, and R. Tsuneya, "Studies of the Penetration of Fuel Spray in a Diesel Engine." Bulletin of J.S.M.E. Vol. 3, No. 9, 1960, p. 123.

24. K.J. McAulay, T. Wu, S.K. Chen, G.L. Borman, P.S. Myers, and O.A. Uyehara, "Development and Evaluation of the Simulation of the Compression-Ignition Engine." SAE Paper No. 650451 presented at Chicago, May, 1965.

25. O.A. Uyehara and P.S. Myers, "Diesel Combustion Temperatures - Influence of Fuel of Selected Composition." SAE Trans., 1949.

APPENDIX A

TAPE RECORDER SPECIFICATIONS

Sangamo Model 4784	
Drive	Eddy current clutch ensures smooth and accurate tape handling.
	Reel to reel, reel to bin and loop operation selectable.
	Eight speeds, electrically selectable.
	Capstan speed ±0.01%
IRIG compatible magnetic heads	
Direct Record/Reproduce	Variable input sensitivity
	20,000 Ω input impedance
	50 Ω output impedance

	Frequency response	Signal/Noise
at 120 ips	500 Hz ⟶ 600 kHz	28 db
at 15/16 ips	100 Hz ⟶ 4.7 kHz	24 db

Frequency Modulation Record/Reproduce	Variable input sensitivity
	20,000 Ω input impedance
	50 Ω output impedance

	Frequency response	Signal/Noise
at 120 ips	d-c ⟶ 40 kHz ± 0.5 db	45 db
at 15/16 ips	d-c ⟶ 0.312 kHz ± 0.5 db	34 db

APPENDIX B

HYBRID COMPUTER SPECIFICATIONS

Operational amplifiers	Solid state: chopper-stabilized; Bandwidth: d-c to 75 kHz; Noise less than 15 mv p-p
Logic elements	Change of state times 1 or 2 μ sec
Analog to digital converter	Successive approximation; Resolution: one part in 2^{15}; Accuracy: ±0.01%; Maximum sample rate: 30.9 kHz
Digital computer	High speed, general purpose; 8 K word storage; Memory cycle time 1.75 μ sec; FORTRAN II included in software

APPENDIX C

LOGIC CIRCUITRY FOR A/D CONVERSION

Figure C-1 shows the analog and logic circuitry used in the A/D process as described in the second section of this paper. The figure is included for the benefit of those interested in developing digitizing systems similar to that of the authors'. The symbolism used is standard.(21) The interrupt line defines the beginning and end of a period of the signal on the ADC line. Once the beginning of the period has been signified by a change of state of the interrupt line, the A/D converter samples the signal on the ADC line on command from the input flag.

APPENDIX D

COMPUTATION OF RATE-OF-INJECTION FROM EXPERIMENTAL DATA

The injection nozzle tip needle valve lift is measured by a variable inductance transducer, and the injection pressure is measured by a strain gage transducer installed in the nozzle body. In addition to these time-dependent quantities, the physical measurements of the nozzle tip are known. The calculation is programmed into the heat release rate program. Briefly, the flow area of the needle valve is calculated, then the effective area of the nozzle is computed, this being a function of the needle flow area and the orifice's hole area in series. Then the flow rate is computed using Bernoulli's equation and the instantaneous experimental measurements of injection pressure and cylinder pressure. This calculation is repeated at each crankangle that the effective flow area is non-zero. At the end of the injection period, the computed cumulative flow is compared against the experimentally measured flow rate. A coefficient of mass flow discharge is defined as the ratio of the actual measured flow to the computed (ideal) flow. Then the computed flow rate is adjusted by this coefficient of flow, so that the flow rate at each crank angle is reduced by the same coefficient and the cumulative flow computed now corresponds to the experimentally observed flow.

A computation of the surface mean diameter or Sauter's mean diameter (SMD) is also programmed into the rate of injection routine. The following form of Knight's equation (22) is used:

$$\mathrm{SMD}[\mu] = 220.(\Delta P)^{-0.458}(\dot{Q})^{0.209}(\nu)^{0.215}\left(\frac{A(t)_{eff}}{A_{orf}}\right)^{-0.916} \tag{2}$$

where:

μ = micron
ΔP = Pressure drop across nozzle, psi
$\dot{Q}$ = Instantaneous flow rate, $\mathrm{lb_m/hr}$
ν = Kinematic viscosity of fuel, centistokes
$A\ t_{eff}$ = Instantaneous effective nozzle flow area, $\mathrm{in.}^2$
A_{orf} = Orifice area, $\mathrm{in.}^2$

SMD is computed at each crankangle during the injection period.

A computation of the penetration of the spray is also done. A momentum balance on the spray (23) is made. The resulting equation after some simplification is:

$$S[\text{inches}] = \left(\frac{2\cdot\Delta P}{\rho_A}\right)^{0.25}\left(\frac{1.67\cdot D_{orf}}{\tan\ \mathrm{RPM}}\right)^{0.5}(12)(32.2) \tag{3}$$

where:

S = Penetration
P = Pressure drop across nozzle, psi
A = Density of combustion chamber air, $\mathrm{lb_m/ft^3}$
D_{orf} = Diameter of injection nozzle orifice, in.
θ = Half angle of spray cone
RPM = Engine speed, revolutions/min

and the numbers 12 and 32.2 are unit conversion factors.

This expression gives the penetration of the spray during a ten CA period following the injection of each increment of fuel, and is independent of vaporization, droplet size, and so forth. It should be emphasized that the selection of 10 CA deg as the time period for the penetration calculation is fairly arbitrary. The calculation is made simply to give a relative estimate of the spray penetration for the quite different experimental injection conditions which were obtained by varying the injection system components on the engine.

APPENDIX E

COMPUTATION OF HEAT RELEASE FROM EXPERIMENTAL DATA

The calculation technique for obtaining heat release rates is basically that used by Borman (12) and reported upon by Krieger.(13) A thermodynamic system was defined; the system is the mixture in the cylinder at any instant and this is assumed to have the properties of air and combustion products only. The boundaries of the system are the cylinder walls, the cylinder head (including valves), and the top of the piston (which is moving up or down). Work is added or taken from the system by the motion of the piston, heat is transferred to or from the system through any and all of the surface boundaries, and energy is added to the system through the heat release process.

For the heat release computations, the heat transfer coefficient as used in the cycle simulation (12) is used for the computation of instantaneous heat transfer from the cylinder gases. The metal temperatures are obtained from experiment and from the cycle simulation. The cycle simulation predicts metal temperatures corresponding to those reported by McAulay (24) for the engine. The cycle simulation is used in conjunction with the experimental data to determine trapped mass, residual facction, and port pressures.

The equations have been programmed for numerical solution by a digital computer. The result obtained is dm/dt, the rate of conversion of liquid fuel to products of combustion, that is, the rate at which fuel is burned and becomes part of the defined system. The rate of heat release is then obtained by multiplying the above by the heating value of the fuel.

The result of this computation has been called the "apparent" heat release rate (AROHR) by Borman. The term apparent is used because of the probable differences between this computed result and the actual complex processes during the heat release in an engine. Even the actual heat release for the combustion chamber as a whole differs from this AROHR because of:

1. The approximation of the internal energy of the mixture in the cylinder by an expression which is an approximation for the internal energy of an equilibrium mixture of the products of combustion of C_nH_{2n} and air.
2. The assumption of homogeneity of mass, temperature, and pressure in the cylinder and the approximation of the internal energy of the mixture of liquid fuel, fuel vapor, air, and products of combustion by an expression for a homogeneous mixture.
3. The difference between the computed heat transfer and the actual temporal heat transfer.
4. The difference between the actual mass in the cylinder and that computed and used by the program on the basis of the heat release.
5. The neglecting of changes in kinetic energy and potential energy.

The equations might be said to correspond to a homogeneous combustion or uniform heat source model. One of the consequences of the assumption of homogeneity of temperature is the prediction by the computations of very little dissociation, since the computed mass averaged temperatures are not much greater than 2300 R. Borman (12) has found dissociation to be negligible below 2300R. However, Uyehara and Myers (25) have measured true flame temperatures of nearly 5000 R in diesel combustion. The effect of dissociation on internal energy is quite significant at these temperatures. The model is using an incorrect value for internal energy then, and this is one of the things which makes it yield an "apparent" heat release.

The items discussed above are a significant consideration in a detailed study of the combustion process. However, for purposes of simulation of an engine, they may not be so significant.

APPENDIX F

FOURIER SERIES ANALYSIS OF WALL TEMPERATURE FUNCTION

Sokolnikoff (16) outlines a method for getting the Fourier series representation of a curve represented by a set of ordinate values. The ordinate values must be uniformly spaced along the abscissa. If one wishes to use small time (abscissa) increments, the computation time becomes prohibitive. One of the authors has developed

One of the authors has developed a technique to obtain a Fourier series representation of a periodic function which permits variable abscissa spacing between the ordinate values. This is particularly useful since the surface temperature function is characterized by a high rate of change over only about one quarter of its period. The key step in the technique involves making a piecewise linear approximation to the temperature function. This is accomplished on a digital computer. The temperature data is stored in memory as a 720 number array, one number corresponding to each crank angle value. The machine determines the equation of a straight line which passes through two ordinate values separated by 10 crankangle deg. The sum of squares of the error between this line and each data point in the 10 crankangle deg interval is then determined and compared to an allowable error. If the comparison test is passed, the machine stores the equation of the linear segment and proceeds to the next 10 crankangle deg segment. If the comparison test is failed, the machine tries a 5 crank angle deg increment, and if necessary a 2 crankangle deg increment. The allowable error is a function of the peak-to-peak amplitude of the temperature curve. When the temperature function has been broken down into a number of linear segments covering a complete period, the Fourier coefficients may be found. Recall that the Fourier coefficients A_n and B_n are defined as:

$$A_n = \frac{1}{\pi} \int_0^{2\pi} f(\theta) \cos (n\theta) \, d\theta \tag{4}$$

$$B_n = \frac{1}{\pi} \int_0^{2\pi} f(\theta) \sin (n\theta) \, d\theta \tag{5}$$

Using the piecewise linear representation of $f(\theta)$, the above integrations can be carried out exactly.

DISCUSSION

G.E. FERRE
Caterpillar Tractor Co.

I want to congratulate Messrs. Le Feuvre and Shipinski; and Professors Myers and Uyehara on a very worthy contribution to the area of data acquisition applications. It is apparent from the papers presented here and the literature published over a period of years that the hardware for automated data reduction is available, and will continue to improve. The challenge ahead is for the users, test engineers, field engineers and applied mathematicians to find the areas of applications where automatic data reduction can be used most profitably and to educate themselves in these areas. Automatic data reduction can be profitable in several different ways:

1. It reduces the amount of time used by high priced labor to perform repetitive calculations, and in so doing makes more time for creative engineering by the individual.

2. It can eliminate the tying up of valuable facilities. It does this by providing a test engineer with the calculated results of a particular test so he can go on with ensuing tests or turn the test facility over to another project. Since large scale tests are expensive to set up, it is not economical to dismantle it until the engineer is sure he has all the information he needs to make an engineering judgment.

3. It is a way of getting urgent information from the test to the designers in a relatively short time. Project engineers and designers will have more information with which to make engineering decisions earlier in their programs. This should enable them to turn out a better product. Designers many times must go ahead without the complete results from tests because of tightening schedules.

4. It is a way of getting information not practically available by any other means. Information on random signals such as cumulative damage, power-spectral-density, correlation theory and others cannot be economically obtained except with the aid of computers.

With all of the benefits readily apparent in automated data reduction, however, it is not a "cure-all" for all engineers and all facilities. The test procedure must be sufficiently organized and the test engineer must thoroughly understand the assumptions and limitations of the computer programs for the profitability in automated data reduction to be realized.

I would like to mention two instances where data reduction is easily paying for itself at Caterpillar Tractor Co. In the first instance, an on-site analog computer is being used on vehicle transmission tests. The analog converts measured signals such as torques, pressures, and speeds to such variables as horsepower, energy, and friction coefficients which are necessary to make intelligent engineering decisions. Previously, hand calculations took as much as two weeks on a series of these tests, while an off-site digital took as much as two days because of transit time and job-stack delays. Today this on-site computation provides answers as fast as the engineer can read them. There have been considerable savings in facilities using this system since more tests can be run.

The second example was on the calculation of cumulative damage information from stresses recorded on an earthmoving cycle. On one study, we wanted to analyze 33 cycles, each about 10 minutes long. There were six channels or variables to analyze on each cycle. Before we used automated data reduction on this work, we edited the basic data manually and keypunched it for the digital computer. Had we used this manual method on this study, it would have taken nearly one year to get the proper data to the digital computer. Instead we went to an automated system involving an FM tape recorder and analog-to-digital converter; using this system, it took only one day including setup.

The kind of savings illustrated in these examples is typical when automated data acquisition and reduction are used intelligently. If used indiscriminately, however, this automation may produce some disappointing results.

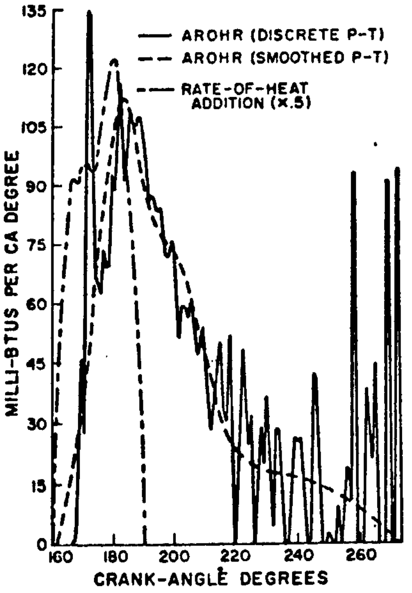

Fig. 1 Comparison of AROHR computed from discrete (unsmoothed) p-t diagram and AROHR computed from smoothed (curve-fitted) p-t diagram.

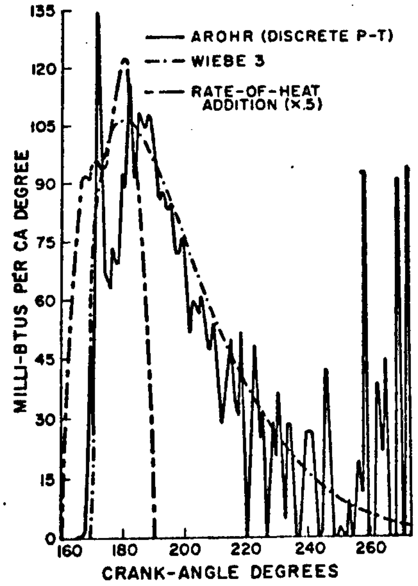

Fig. 2 AROHR computed from discrete p-t diagram and smooth curve fitted to AROHR using three Wiebe parameters.

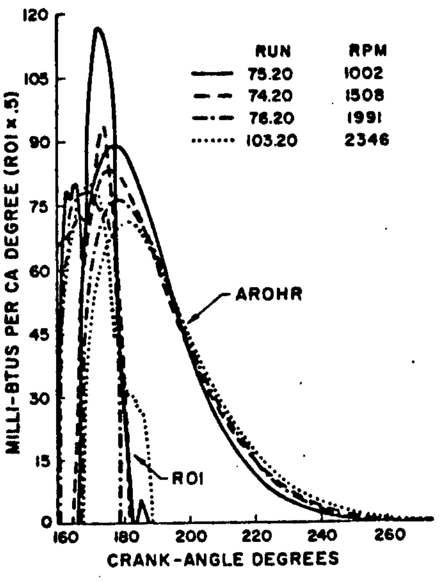

Fig. 3 Effect of speed on ROI and AROHR.

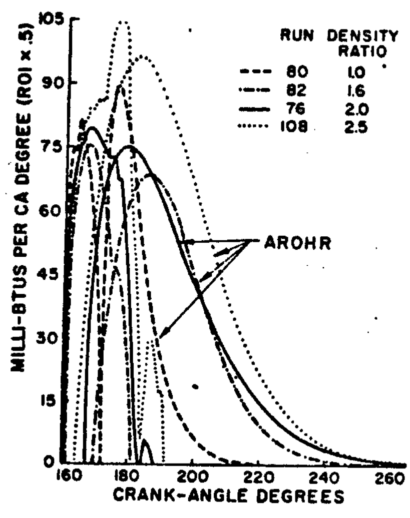

Fig. 4 Effect of inlet manifold density ratio on ROI and AROHR at 2000 rpm and 0.5 equivalence ratio.

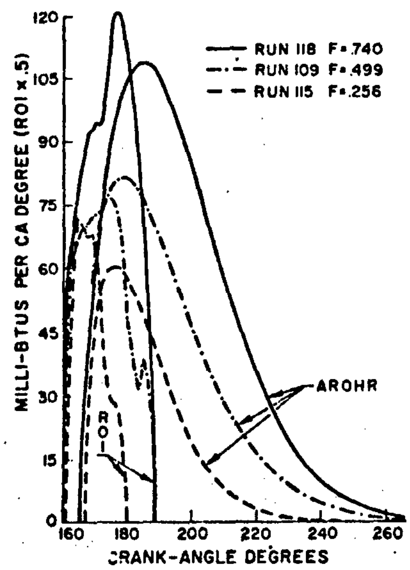

Fig. 5 Effect of ER on ROI and AROHR at 2000 rpm and 2.0 DR

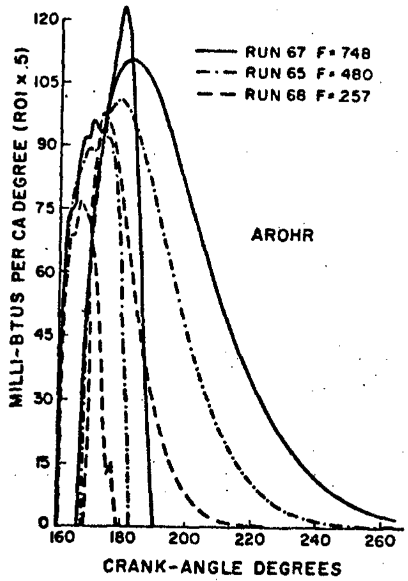

Fig. 6 Effect of ER on ROI and AROHR at 2000 rpm and 2.0 DR with CIE fuel.

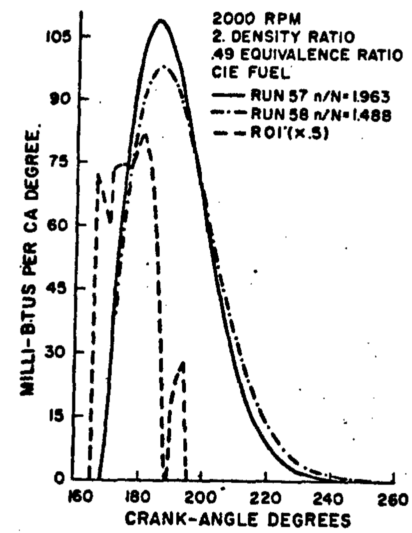

Fig. 7 Effect of swirl ratio on AROHR with CIE fuel. (ROI is the same for both runs since swirl did not affect ROI).

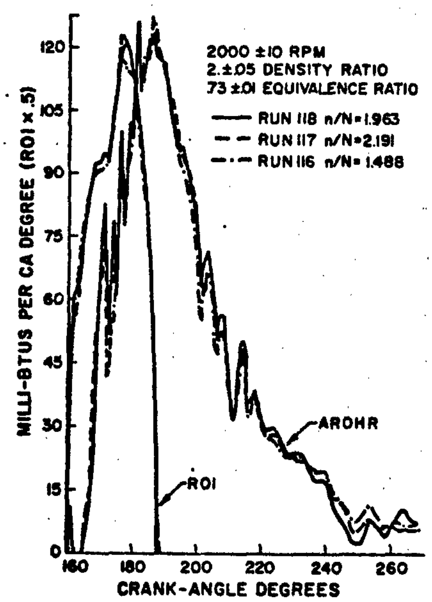

Fig. 8 Lack of effect of swirl on AROHR with SRF.

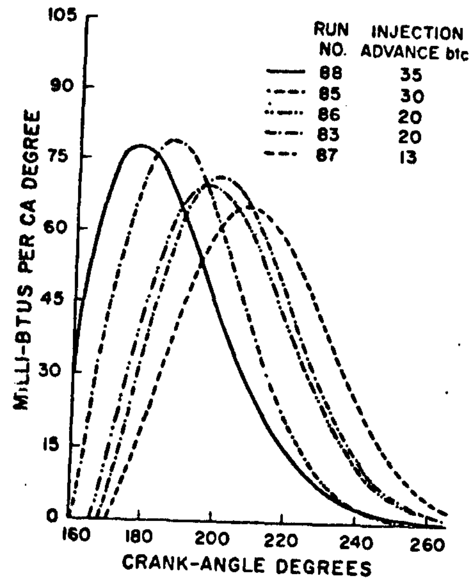

Fig. 9 Effect of injection timing on AROHR with low ROI system giving pilot-injection effect.

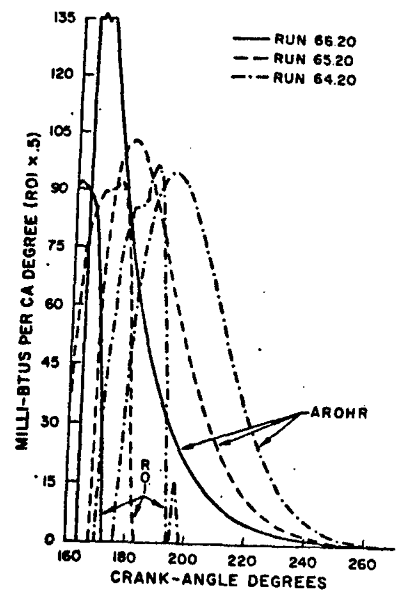

Fig. 10 Effect of INJ timing on AROHR with CIE fuel.

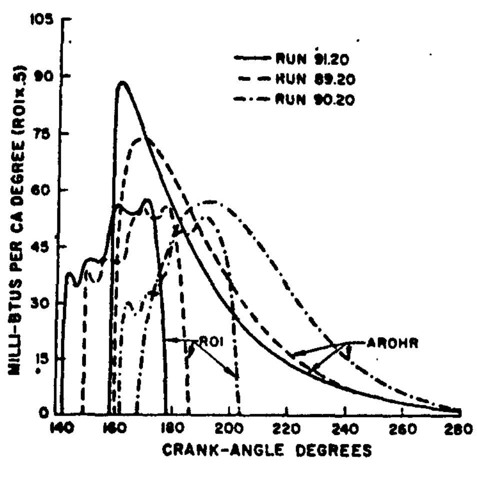

Fig. 11 Effect of INJ timing on AROHR with small (0.0118) nozzle tip and low ROI.

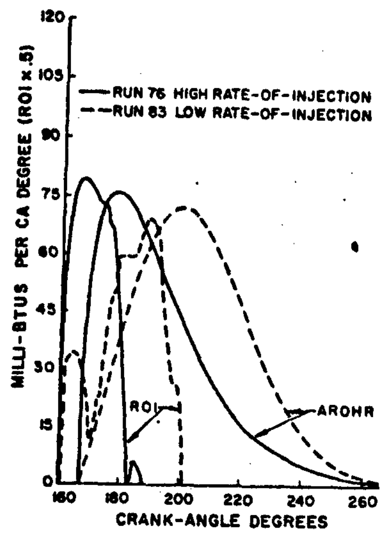

Fig. 12 Comparison of AROHR for high ROI and low ROI.

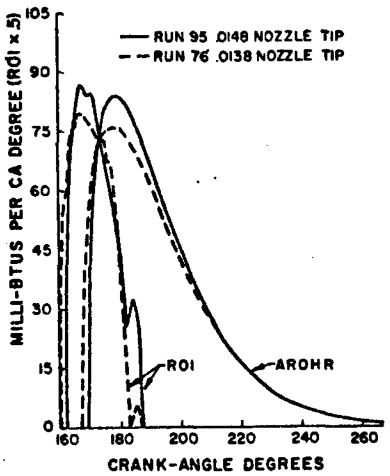

Fig. 13 Effect of size of nozzle-tip hole on ROI and AROHR.

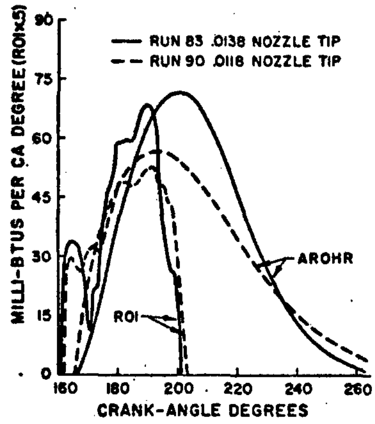

Fig. 14 Effect of size of nozzle-tip orifice on ROI and AROHR with low ROI pump.

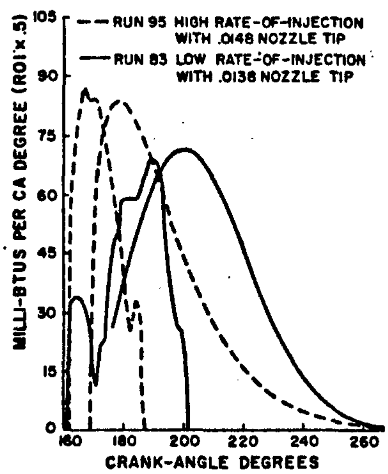

Fig. 15 Comparison of AROHR obtained with two different rates of INJ.

Table 6 Observed Engine Operating Conditions, Combustion Performance, and Wiebe Parameters

Run[a]	C1[b]	C2[b]	C3[b]	Pibi[c]	Pbtc[d]	CN[e]	RPM[f]	A/F[g]	Rho[h]	INJ[i]	Z[j]	IMEP[k]	ISFC[ℓ]
063	.4050	19.96	172.	.555	100.	38.5	1002	23.6	.88	166	1.00	110.	.309
064	.7810	16.22	176.	.142	33.4	38.5	2000	30.1	2.1	172	.332	210.	.286
065	.4783	14.77	168.	.305	94.9	38.5	2008	30.8	2.1	162	.498	216.	.267
066	.1536	13.32	163.	.622	100.	38.5	2005	30.4	2.1	151	1.00	210.	.275
067	.4850	9.200	167.	.174	71.6	38.5	2002	19.8	2.1	162	.417	270.	.325
073	.5189	13.11	167.	.272	100.	47.1	2025	33.3	2.0	162	.412	202.	.260
074	.3895	9.802	166.	.295	97.5	47.1	1508	32.4	2.0	160	.664	203.	.267
075	.5094	14.56	165.	.180	100.	47.1	1002	31.9	2.0	162	.500	198.	.278
076	.4159	10.63	167.	.310	94.6	47.1	1991	33.6	2.0	161	.503	200.	.257
079	.4685	8.079	168.	.214	71.3	47.1	1999	21.2	2.0	162	.500	262.	.306
082	.7064	18.74	170.	.550	99.2	47.1	1997	32.9	2.0	162	.666	155.	.257
083	1.170	14.14	168.	.125	36.5	47.1	2005	28.8	2.0	162	.499	199.	.306
085	.9870	17.02	161.	.139	72.1	47.1	2011	28.7	2.0	152	.745	211.	.287
086	1.088	13.26	166.	.091	38.3	47.1	2009	28.6	2.0	162	.332	200.	.305
087	1.300	12.00	170.	.050	21.2	47.1	2016	29.0	2.0	168	.165	188.	.324
088	.6575	12.72	158.	.143	93.8	47.1	2008	28.8	2.0	147	.913	215.	.278
089	.3486	8.380	160.	.256	88.4	47.1	2004	30.3	2.0	150	.832	198.	.291
091	.0661	5.656	159.	.417	100.	47.1	2001	29.7	2.0	143	1.34	192.	.302
095	.4892	13.13	168.	.293	86.7	47.1	1998	33.2	2.0	163	.417	196.	.267
096	.4568	10.28	168.	.298	84.3	47.1	2506	32.8	2.0	162	.400	192.	.266
097	.4873	8.738	168.	.212	73.5	47.1	2495	23.5	2.0	162	.401	240.	.297
099	.4516	14.31	167.	.347	100.	47.1	0997	18.2	.76	161	1.00	124.	.354
100	.4360	13.61	167.	.439	100.	47.1	1002	19.2	.95	160	1.16	131.	.354
102	.3718	6.565	166.	.203	91.0	47.1	2005	30.0	2.0	161	.416	212.	.273
103	.5306	11.70	167.	.238	83.5	47.1	2546	30.9	2.0	161	.393	208.	.256
104	.5503	8.979	166.	.135	78.5	47.1	2498	20.0	2.0	162	.267	191.	.317
106	.5766	10.64	167.	.195	85.4	47.1	2563	30.9	2.5	162	.325	253.	.264
107	.5321	7.492	166.	.141	64.9	47.1	2508	20.8	2.5	159	.466	322.	.317
108	.6636	13.22	164.	.136	85.3	47.1	1999	29.7	2.5	160	.332	261.	.278
109	.4384	10.38	166.	.206	81.7	47.1	1998	29.6	2.0	161	.417	218.	.268
110	.6470	8.887	163.	.083	71.5	47.1	2013	20.1	2.5	159	.331	332.	.322
111	.3824	15.83	167.	.457	100.	47.1	2002	50.9	2.0	161	.500	116.	.299
112	.7698	18.46	165.	.157	90.0	47.1	2016	24.3	2.0	161	.331	226.	.322
113	.6518	10.53	164.	.126	79.5	47.1	2007	18.8	2.0	160	.332	275.	.340
114	.3937	16.27	168.	.637	100.	47.1	2012	58.1	2.0	160	.663	113.	.269
116	.6777	11.00	165.	.127	75.3	47.1	2005	20.6	2.0	161	.333	270.	.321
117	.7023	11.53	165.	.116	75.0	47.1	2006	20.4	2.0	161	.332	272.	.322
118	.6820	11.36	165.	.145	76.0	47.1	1996	20.0	2.0	161	.334	275.	.318
120	.7369	8.641	164.	.106	83.4	47.1	2011	25.0	2.5	160	.331	305.	.284
121	.5917	8.641	164.	.110	73.6	47.1	2013	20.0	2.5	159	.414	337	.318

[a] Identifying number

[b] Wiebe parameters

[c] Fuel percentage injected before ignition

[d] Fuel percentage injected before tdc

[e] Cetane number

[f] Engine speed

[g] Air-fuel ratio

[h] Inlet manifold density divided by standard atmospheric density

[i] CA at which injection starts

[j] Ignition delay in milliseconds

[k] Motored indicated mep (psi)

[ℓ] Motored indicated specific fuel consumption (lb/ihphr)

APPENDIX V

A

The Effect of Heat Transfer on the Steady Flow Through a Poppet Valve

D.N. Kapadia and G.L. Borman
Mechanical Engineering Dept.
University of Wisconsin

ABSTRACT

A study was made to determine the effect of heat transfer from the backface of a poppet intake valve on the flow rate through the valve. All tests were made under steady flow conditions.

The results show that for the same lift and same pressure drop across the valve, the flow rate through a hot valve is less than through a cold valve. This effect increases almost linearly with the heat transfer rate and decreases rapidly with lift. The results also show that the effective flow area is independent of pressure drop through the valve.

A correlation of heat transfer from the back of the valve surface to the flowing air shows that the Nusselt number varies as the 1.27 power of the Reynolds number.

INTRODUCTION

The detailed mathematical simulation of engine cycles requires the computation of instantaneous flow rates through the engine valves. Typically, these mass flows have been computed by applying steady flow formulas at each instant even though the actual flow is unsteady (1,2).* The flow coefficients which are needed in order to apply such formulas can be obtained by measuring the pressure drop and mass flow through the valve for steady flow at various fixed valve lifts. Such measurements are normally made by using a laboratory apparatus which incorporates the actual valve and port, but simulates the cylinder with a section of pipe. The valve is at the ambient temperature for such tests and the flow is caused by either providing pressurized air upstream of the port or by reducing the pressure in the downstream pipe by means of a blower or ejector.

In measurements of the kind described above, the pressures measured are the stagnation pressures before the port and after the valve respectively. In simulation analysis on the other hand, the static pressure in the port close to the valve is either measured or calculated and the pressure downstream is the calculated cylinder stagnation pressure. In general, the mass flow through the valve can be shown (3) to be given by

$$\dot{M} = CA_V A_F p_i F_i \qquad (1)$$

where:

C = Flow coefficient

A_V = Valve flow area

$A_F = [1 - (A_V/A_p)^2 (p_i/p_V)^{2/k}]^{-\frac{1}{2}}$

A_p = Area of the upstream section where pressure and temperature are measured

*Numbers in parentheses designate References at end of paper.

p_i = Static pressure at A_p

p_V = Static pressure at A_V

$$F_i = \left[\frac{2kg_c}{RT_j(k-1)}\left[(p_i/p_V)^{2/k} - (p_i/p_V)^{\frac{k+1}{k}}\right]\right]^{\frac{1}{2}}$$

k = Ratio of specific heats

R = Specific gas constant

g_c = Dimensional constant

T_i = Static temperature at A_p

Because it is difficult to measure p_V, the stagnation pressure downstream of the valve, p is used in place of p_V. Similarly, the area A_V is unknown so it is more convenient to use an effective flow area, A_e, which is equal to the product CA_V. In calculating A_F it is then necessary to use the approximation $A_V/A_p \approx A_e/A_p$. For the experimental measurements where the upstream pressure is the ambient pressure prior to the port, $A_F = 1$.

It should be noted that the formulation of the problem in this way does not follow conventional practice. All dissipation terms which appear in the steady-state macroscopic mechanical energy balance equation are first neglected and the equation is integrated assuming isentropic flow. Then the correction for the dissipation terms is made by the inclusion of the coefficient C. This coefficient thus includes all dissipation effects; that is, the sudden contraction entrance effect, the friction losses in the straight pipe, the losses in the port bend, the valve contraction and friction losses, and the sudden enlargement losses. The engine system may thus have a slightly different coefficient since the sudden enlargement dissipation may be different for the cylinder-piston geometry than for the large pipe used in the tests.

The flow coefficient in Eq. 1 to be most useful should be only a function of valve lift and thus the effective flow area A_e should be constant for a given lift and various pressure differences across the valve. This has generally been found to be true within the limits of the experimental accuracy.

In applying steady flow formulas and data to the cycle simulation, it was found that the resulting computed volumetric efficiencies were a few per cent too high at all speeds (1,2). A number of causes can be given for such differences, among these being inaccurate calculation of heat transfer in the cylinder during the intake process, the use of the quasi-steady flow approximation, inaccurate expressions for valve lift as a function of crankangle, and the effects of heat transfer from the valve and seat on the valve flow coefficients. Although any or all of these effects may be important, only the last named is taken up in this paper.

TEST APPARATUS

The basic concept of the experiment was to run conventional steady flow tests on a given poppet valve and to then run the same tests but with the valve held at an elevated temperature.

Figure 1 shows the schematic diagram for the flow system. A Jet-Vac 3 in. suction size single-stage steam ejector was used to draw air through the system at rates up to 900 lb_m/hr. The intake system consisting of the seat insert, the valve and stem, and the port was mounted on a base plate which was attached to a 4 in. pipe which simulated the engine cylinder. The port opened directly to the room. Figure 2 shows a schematic of this intake system. The seat insert and 2 in. diameter 1.52 in. long valve head were machined from mild steel according to specifications provided by the International Harvester Co. The seat insert was press fitted into a 1/2 in. transite plate. The valve head was further machined so that an electrical heater could be attached to its lower surface by two small screws.

As is shown in Fig. 3, the heater consisted of two identical units: a valve heater directly beneath the valve face and a guard heater separated from the valve heater by a layer of transite. The dimensions of the heater assembly were such that after its installation, the overall dimensions of the original valve were closely maintained. The valve head was screwed onto a hollow steel stem. A 1 in. long transite section incorporated between the stem and head minimized heat conduction from the head to the stem. The intake port was simulated by a 90 deg copper elbow having a centerline radius of 2-5/16 in. and an inside diameter of 1-5/8 in.

The valve lift was set by a fine-thread screw positioned above the stem by a rectangular supporting frame. The motion of the screw was transmitted to the stem by means of a link. A dial indicator was used to measure the link position.

INSTRUMENTATION

The valve lift, mass flow rate, pressure drop across the valve and port, heat transfer from the backsurface of the valve, and the valve temperature at the center of the face were measured for each data point.

The ambient pressure was measured with a laboratory cistern manometer. The downstream static pressure was measured at a point in the 4 in. pipe 4 in. below the seat. The pressure was read on a 60 in. manometer graduated in 0.1 in. with a fluid of specific gravity 1.00. It was found that for even the highest flow rates (900 lb_m/hr) the static and stagnation pressure at this point differed by only 1/2%.

The pressure drop across the orifice meters was measured with an inclined manometer having a range of 10 in. graduated in 0.01 in. The temperature ahead of the orifice was measured with an iron-constantan thermocouple. Flow rates up to 150 lb_m/hr were measured with a 1.05 in. bore flange-type orifice plate mounted in a 1.5 in. pipe. Flow rates between 150 and 400 lb_m/hr were measured with a 1.65 in. bore orifice in a 3 in. pipe and flow rates between 400 and 900 lb_m/hr were measured with a 2.10 in. bore orifice also in the 3 in. pipe.

The temperature difference across the transite layer between the valve and guard heater was measured with a pair of calibrated iron-constantan thermocouples fabricated from B&S No. 30 wires. The junctions were installed in fine grooves on opposite sides of the transite. Each junction was about 1-1/4 in. long to insure that the temperatures did not correspond to a point. The temperature difference was monitored on a recording potentiometer but a Rubicon portable potentiometer was used to measure the e.m.f. while nullifying the temperature drop across the transite layer. The valve and guard heater power inputs were measured with a Weston Model 310 wattmeter.

TEST PROCEDURES

First, a cold run was made. The lift was set by means of the fine adjustment screw and the flow rate through the valve adjusted by means of the bleed valve (Fig. 1) so that a predetermined pressure drop through the valve, ΔP, was obtained. The flow was channeled through either the 1-1/2 in. pipe or the 3 in. pipe depending on the flow rate.

Next, hot runs were made. Without disturbing the lift set for the cold run, the valve was heated by passing current through the valve heater. The energy input was brought to a desired level by the fine adjustment rheostat in the valve heater circuit. Current was then passed through the guard heater circuit. By means of adjustments made in this circuit only, the temperature drop across the guard transite was nullified. The flow rate was adjusted meanwhile so that ΔP was maintained constant. Readings were taken only when the steady state conditions remained unchanged for at least five minutes.

The procedure described above for a cold run and a series of hot runs was repeated in that sequence for two more values of ΔP for this setting of the valve lift.

The entire procedure was then repeated for a number of lifts. From the data thus obtained, the change in the effective flow area could be plotted as a function of the rate of heat transfer from the back of the valve, the pressure drop through the valve, and the valve lift.

ERRORS AND ASSUMPTIONS

It was assumed that under steady state conditions the rate of heat transfer from the backface of the valve was equal to the power supplied to the valve heater when the temperature gradient in the guard transite was zero. However, there were radiation losses to the seat and to a portion of the port, conduction losses up the stem, and conduction losses down the heater wires.

Radiation losses from the backface of the valve to the seat and the port could be significant for high valve temperatures coupled with high flow rates; for under these conditions the seat and port would be coolest and the temperature difference between them and the valve surface the highest. To estimate the maximum loss, a black body sphere (emissivity = 1) at 700 F was considered enclosed in a black sphere at room temperature (77 F). The surface area of the inner sphere was considered to be equal to the radiating surface, estimated to be 4 sq. in. The inside area of the enclosing sphere was made equal to the area of the port and seat estimated to be "seeing" the valve surface. It was found that for this case, the radiation loss was 7.6% of the power supplied to the valve heater. In the actual case, the valve head had oxidized after a few hot runs so that its emissivity was more likely to be about 0.5. Further, the port and seat temperatures were about 30 F higher than the room temperature under steady state conditions and the temperature at the valve surface was probably about 100 F less than the temperature indicated by the plug in the valve head. Changing the numbers accordingly, the calculated loss fell to 1.74% of the power supplied to the heater. This loss was considered negligible for these tests.

Conduction losses up the stem could not be estimated with reasonable accuracy since no data regarding temperature gradient in the stem were taken. In an attempt to minimize this loss, a transite section was included in the stem. The thermal conductivity of transite is smaller than that of mild steel by a factor of 100. Further, the stem was hollow. On the basis of the above, the conduction loss up the stem was not considered significant.

The eight wires leading away from the heater assembly were each about 0.010 in. diameter. Each wire was insulated for a distance of 2 in. below the valve by alumina fish scales or single bore alumina tubes. The total heat conduction along these wires was estimated to be about 0.1% of the power supplied to the valve heater.

It was concluded from the above that the assumption that the rate of heat transfer from the back of the valve equaled the rate of energy input to the valve heater was quite good.

It was found that the power required in the guard heater was generally 30% of the power supplied to the valve heater. Some of this energy entered the flow by heat transfer from the circular "wall" around the guard heater. The rest was carried into the flow by heat transfer from the lid of the heater assembly, that is, the lower flat surface of the valve. There probably was considerable swirling and turbulence under the valve, so that reasonable estimates of the relative magnitudes of the heat transfer coefficients on these surfaces could not be made. However, the valve head with both the backface and the lower surface at elevated temperatures simulated actual engine conditions; and if the change in the effective flow area is correlated in terms of the measured heat transfer rate from the back of the valve, then the results are usable when this particular quantity is known or calculated as in the simulation model.

The linear expansion of the valve head and stem was calculated to be about 0.003-0.010 in. for the temperature ranges encountered in the tests. This linear expansion was not indicated on the dial indicator because the valve was effectively clamped at the upper end of the stem. The expansion therefore caused the actual lift for hot runs to be greater than the lift of the corresponding cold runs. The expansion of the head and stem from the top of the transite section to the valve face was thus measured directly in a separate bench test. The test was run with air flowing over the valve and the heat supplied by the valve heater. The coefficient of linear expansion was found to be 10.3×10^{-6} in./in./F.

DISCUSSION OF RESULTS

The effective flow area for each cold run was calculated from Eq. 1 with $A_F = 1$. For ΔP ranging 20-40 in. of water, the effective flow area without heat transfer was found to be independent of ΔP.

The values of the effective flow areas for the flows with valve heating were calculated also using Eq. 1. Thus the heat transfer effects were lumped along with frictional effects into the effective area values. The hot and cold effective areas were then compared after correcting the hot lift values for linear expansion. Figure 4 shows that the per cent change in flow area caused by heating was essentially independent of ΔP at a given lift and power input. Figure 5 shows the per cent change in effective area caused by heat transfer. Figure 6 is a replot of Figure 5 with lines of constant lift. The lines of constant lift are almost linear so that

$$\frac{A_{ec} - A_{eh}}{A_{ec}} \approx Qf(x) \tag{2}$$

where

A_{ec} = Effective cold flow area

A_{eh} = Effective hot valve flow area

x = A_{ec} divided by the value of A_{ec} at maximum lift

Q = Heat transfer rate from the back of valve, Btu/sec

Although the experiment was designed to give data on flow rates, it also can be used to obtain some crude estimates of convective heat transfer coefficients for the back of the valve. Unfortunately, the valve surface temperature distribution was unknown as was the local gas temperature. However, some estimates may be obtained using a lumped parameter resistance for the valve and taking the valve surface temperature, the gas temperature, and the convective heat transfer coefficient each to be an average constant value. An energy balance then gives

$$\dot{Q} = \bar{h}A_s \; \bar{T}_s - \bar{T}_g$$

$$= (K_v A_s / L_v)(T_{vc} - \bar{T}_s) \tag{3}$$

where:

$\bar{h}$ = Average heat transfer coefficient

A_s = Area of the backface of the valve

$\bar{T}_s$ = Average temperature of the surface area A_s

$\bar{T}_g$ = Bulk gas temperature

K_v = Thermal conductivity of the valve

L_v = Average conduction path between surface and valve face center where temperature was measured to be T_{vc}

The bulk gas temperature is given by

$$\bar{T}_g = T_0 + \dot{Q}/(2\dot{M}c_p) \tag{4}$$

where:

T_0 = Gas temperature upstream of the heated section

Solving for $\bar{h}$ and eliminating $\bar{T}_s$ we obtain the Nusselt number,

$$Nu = \frac{\bar{h}D_H}{K_g} = \frac{\dot{Q}D_H/K_g}{A_s(T_{vc}-\bar{T}_g) + \dot{Q}L_v/K_v} \qquad (5)$$

where:

K_g = Thermal conductivity of the air evaluated at the bulk gas temperature

$D_H = D_s - D_1$

$D_1 = \sqrt{D_s^2 - 4A_{eh}/\pi}$

D_s = Diameter of seat insert at the entrance

A Reynolds number for the flow may be defined as

$$Re = \dot{M}D_H/\mu A_{eh} \qquad (6)$$

where:

μ = Viscosity of the air evaluated at the bulk gas temperature

Figure 7 is a log-log plot of Nu versus Re. The data fall on a straight line which was least square fit to give

$$Nu = 1.012 \times 10^{-4}(Re)^{1.27} \qquad (7)$$

This result is unusual in that for most cases of turbulent flow over heated objects, Nu is proportional to the 0.8 power of Re. The reasons for this difference may be attributed to the fact that the flow is accelerated as it passes over the back surface of the valve and that the hydraulic diameter used here is smaller than an average hydraulic diameter for the flow region. The data used for the correlation are given in the Appendix.

Turning now to the cycle simulation, Eq. 2 was fit to the data and used in the simulation program described in Ref. 1. A comparison of calculated volumetric efficiencies with and without the reduced effective flow area showed that the volumetric efficiency was not changed by the reduction of flow area caused by heat transfer. The pumping mean effective pressure was about 1% higher when the valve area correction given by Eq. 2 was used.

The cylinder pressure was reduced slightly during the first portion (about 40 engine crankangles) of the inflow but this effect was overcome during the rest of the inflow because the correction factor is unity for large lifts. One should also note that the effect of backflow through the valve plays an important part in determining the effect of the correction factor. The correction factor is most important during the low lift portion of the flow, but if backflow occurs during this time the effect is negated since it was assumed that valve heat transfer had no effect on backflow. For the case studied this was particularly true for the valve closing period. The backflow started just slightly after the correction factor began to deviate from unity so that the correction had essentially no effect on the flow during valve closing.

In the cycle calculation which was run the valve lift was corrected for dynamic and thermal expansion effects. In particular the thermal expansion effects can be most important in that they change the effective valve timing at least for overhead valve engines. In the experiments conducted on the bench rig the expansion effects were large enough to more than compensate for the effect of the heat transfer to the air.

While the above results would tend to indicate that the effects of valve heating on the flow are small, one must not make this hasty conclusion. The intake valve for the particular engine simulated is somewhat oversized so that a reduction in flow area had only a small effect. For an engine with a smaller than ideal valve, the effect could be important.

REFERENCES

1. K.J. McAulay, T. Wu, S.K. Chen, G.L. Borman, P.S. Myers, and O.A. Uyehara, "Development and Evaluation of the Simulation of the Compression-Ignition Engine," SAE Transactions, 1966.

2. G.L. Borman, "Mathematical Simulation of Internal Combustion Engine Processes and Performance Including Comparisons with Experiment," PhD Thesis, University of Wisconsin, 1964.

3. D.N. Kapadia, "An Experimental Study of the Effect of Heat Transfer on Steady Flow through a Poppet Intake Valve," MS Thesis, University of Wisconsin, 1966.

ACKNOWLEDGMENTS

This activity was conducted under contract to and with the technical assistance of the Systems Propulsion Laboratory of the U.S. Army Tank and Automotive Command. The authors wish to thank Prof. P.S. Myers and O.A. Uyehara for their many helpful suggestion.

APPENDIX

DATA USED FOR HEAT TRANSFER CORRELATION

A_s = 6.0 in.^{2}

c_p = 0.240 Btu/lb_m,F

D_s = 1.625 in.

k_g = 0.0154 Btu/hr ft, F

k_v = 25 Btu/hr ft, F

T_0 = 77 F

μ = 0.04624 lb_m/ft hr

L_v = Average length from valve center to valve backface, estimated from the design drawing to be 0.5 in.

Run	$\dot{M}_m$ lb_m/hr	A_h in.^{2}	$\dot{Q}$ watts	T_{vc} F	Nu	R_{DH}
8.10	63.6	0.084	100	316	6.9	6530
8.22	98.1	0.130	100	305	11.1	10100
8.31	116.3	0.176	200	552	14.3	12080
9.02	132	0.175	100	301	15.2	13700
9.08	187.8	0.342	300	727	31.1	19900
9.11	224.9	0.339	200	471	34.1	23900
11.02	311	0.566	300	256	65.1	34200
11.07	374	0.563	200	397	73	41000
12.04	423	0.560	100	530	77.3	46300
13.15	420	0.760	100	245	96.9	47550
13.12	500	0.753	200	380	106.6	56500
13.09	569	0.754	300	477	123	64320
13.27	660	1.199	100	230	182.5	81300
13.24	800	1.193	200	337	219.3	98500
13.33	780	1.415	300	478	263.8	101400

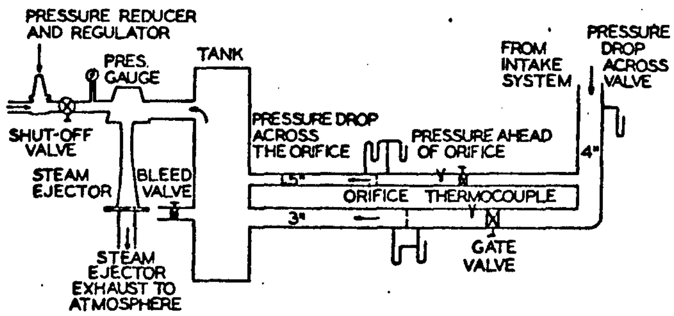

Fig. 1 Schematic representation of flow system apparatus.

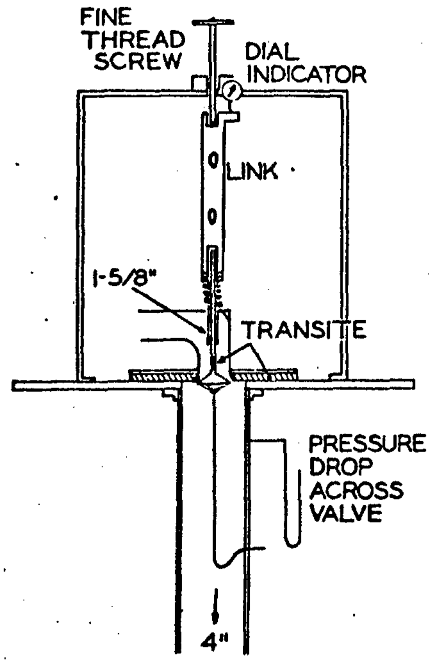

Fig. 2 Schematic of intake system showing valve linkage and valve heater.

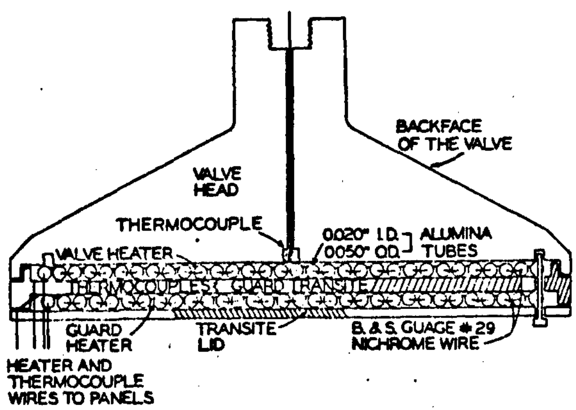

Fig. 3 Diagram of valve head and heater assembly.

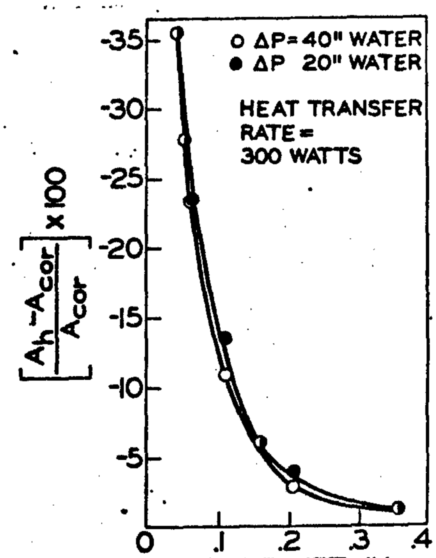

Fig. 4 Percentage change in effective flow area caused by constant rate of heat transfer as function of lift. Lift was corrected for linear expansion of valve stem and head.

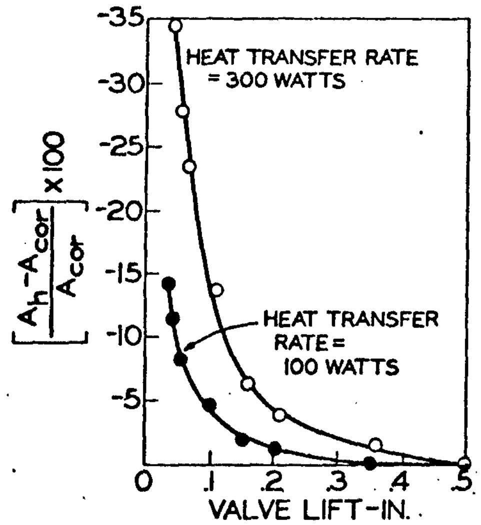

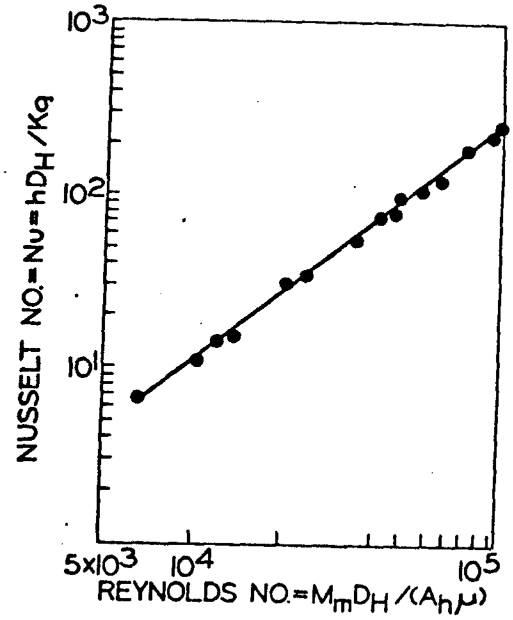

Fig. 5 Percentage change in effective flow area for two different heat transfer rates. Lift was corrected for linear expansion.

Fig. 6 Percentage change in effective flow area as function of heat transfer rate. Lines of constant lift with lift values corrected for expansion.

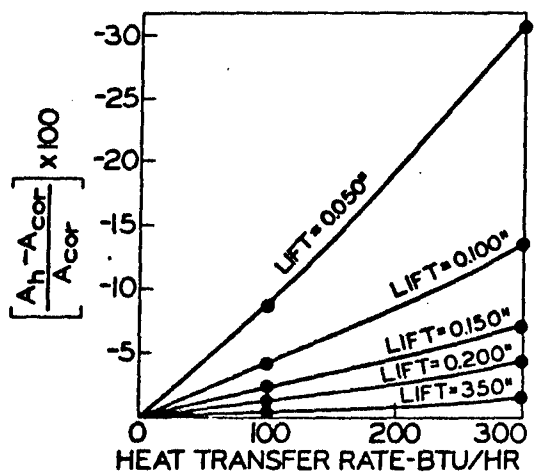

Fig. 7 Nusselt number as function of Reynolds number for valve heat transfer.

APPENDIX V

B

Experimental Instantaneous Heat Fluxes in a Diesel Engine and Their Correlation

T. LeFeuvre, P.S. Myers and O.A. Uyehara
Mechanical Engineering Dept.
University of Wisconsin

ABSTRACT

By the use of surface thermocouples to measure instantaneous temperatures, the instantaneous heat fluxes are calculated at several positions on the cylinder head and sleeve of a direct injection diesel engine for both motored and fired operation. Existing correlations are shown to be unable to predict these data.

An analysis of convective heat transfer in the engine leads to a boundary layer model which adequately correlates the data for motored operation. The extension of this motored correlation to fired operation demonstrates the need for instantaneous local gas velocity and temperature data.

INTRODUCTION

The design of internal combustion engines is necessarily becoming more scientific as the standards of performance, economy, and pollution control are increased. One manifestation of this trend is the increasing use of mathematical simulation as a design and development tool. However, an engine design based on a mathematical model is no better than the assumptions in the model. Both Borman (1)* and McAulay (2) noted that, along with other information, a knowledge of the instantaneous heat transfer to the cylinder surface is necessary in order to formulate an accurate model of engine processes.

The instantaneous heat fluxes at the surface of the cylinder wall (either head, valve face, piston face, or cylinder sleeve) have historically been expressed with the use of surface heat transfer coefficients, that is.

$$\dot{q}(t) = h(t) \cdot \left(T_g(t) - T_w(t)\right) \tag{1}$$

where

t = time

$\dot{q}(t)$ = wall surface heat flux

$h(t)$ = heat transfer coefficient

$T_g(t)$ = mass-averaged gas temperature

$T_w(t)$ = wall surface temperature

It should be noted that for a clean metal wall $T_w(t)$ is relatively constant with time and, therefore, is often considered constant. For simplicity the modifier (t) will be dropped for all of the quantities.

Nusselt (3), Eichelberg (4), Pflaum (5), Annand (6), Woschini (7), and numerous other authors' have presented expressions which can be used to determine $h(t)$ in Eq. (1). In general, these expressions, or correlations, have been ones which related the surface heat transfer coefficient, h to the properties of the working fluid (that is, p_g, T_g, k_g, etc.).

*Numbers in parentheses designate References at end of paper.

The majority of the correlations proposed to date are not based on instantaneous data, either at a point or averaged over an area, but on time-averaged data often obtained from an energy balance on the engine. Eichelberg did have access to Hug's (8) data which was obtained using subsurface thermocouples from a large, low speed, naturally aspirated diesel engine.

Nusselt showed that the pressure-temperature term in his correlation was a free convection relationship. Eichelberg, Pflaum, and others have used modifications of this free convection form to describe the forced, convection heat transfer in an engine cylinder. The analyses of Annand and Woschini are examples of several attempts to characterize engine heat transfer by dimensionless parameters. However, the lack of experimental data has precluded the construction of conceptual models of instantaneous heat transfer in engines.

In light of the previous discussion and as part of a continuing program of research on the phenomena occurring in internal combustion engines, the authors have conducted a study of the instantaneous surface-heat transfer in a direct injection diesel engine. Since there was a severe lack of experimental data, instantaneous heat fluxes were obtained at several positions on the cylinder head and sleeve under both motored and fired operation. Part 1 of this paper summarizes the experimental program and the data obtained.

The next logical step in the program was to compare the experimental data with already proposed correlations. This phase of the program is covered in Part 2 of the paper. Since the agreement found in Part 2 was not satisfactory, a detailed theoretical investigation of the mechanisms of surface heat transfer was conducted with the experimental data serving as a guide and comparison.

Part 3 of the paper reviews the theoretical considerations involved in correlating surface heat transfer in diesel engines and emphasizes the areas where further study and data are needed.

EXPERIMENTAL PROGRAM AND RESULTS

The engine, instrumentation, and processing techniques used in this study have been described in detail by LeFeuvre (9). Two other publications, Shipinski (10,11) describe the results of a study of engine heat release run concurrently and employing the same instrumentation system. A brief review of this system is given in the following paragraphs.

EXPERIMENTAL APPARATUS AND PROCEDURES ... Instantaneous wall temperatures were measured using a Bendersky (12) type surface thermocouple. The instantaneous surface fluxes were then calculated using the measured instantaneous temperatures, Because of the spacial, temporal (during one engine cycle), and cycle-to-cycle variations in surface temperature (and hence surface heat flux), it was felt that a large quantity of data (over 10^6 points) had to be examined if meaningful and significant results were to be obtained. Thus a high speed, multichannel, data recording, reduction, and processing system was developed. The block diagram of this system is shown in Fig. 1, while LeFeuvre (13) gives complete specifications.

The engine was a 4-stroke, direction-injection, single-cylinder diesel engine with a 4.5 in. bore and stroke. Shipinski describes the engine, dynamometer, and systems for obtaining performance data such as speed, power, air and fuel consumption, heat balance, intake and exhaust temperatures and pressures, etc.

The primary transducers for the determination of surface heat flux are the surface thermocouples as illustrated in Fig. 2. The thermocouples are of the plated junction design used by Overbye (14,15), Bennethum (16), and Ebersole (17). The thermocouples used were in the form of a 2-56 screw. Since the major portion of the thermocouple probe was iron, the disturbance to the heat transfer pattern was kept to a minimum. When flush mounted, the thermocouple junction temperature was considered to be the true surface temperature.

During the course of the work, thermocouples were installed in a total of nine locations in the engine head deck and sleeve. These locations are shown in Fig. 3. For all of these locations, except at TC-9, the heat flux in the cylinder wall could with good accuracy, be considered to be one-dimensional. A schematic of a thermocouple circuit used is shown in Fig. 4. Since data from up to eight thermocouples were recorded simultaneously, there are eight units in many of the blocks of Fig. 4.

The temperature of the wall-coolant interface was constant during each test and recorded by the multipoint recorder ①.* The time-averaged value of the instantaneous temperature difference through the wall was measured by a light beam galvameter ②.

The conditioning step of Fig. 1 consists primarily of amplification and biasing. The fixed gain amplifiers ③ had low noise, wideband high-gain amplification. It was desired to modulate the tape recorder with only the oscillatory component of the surface temperature. Thus the average value was biased out ④. The variable gain amplifiers ⑤ permitted optimum modulation of the tape recorder. A d-c calibration signal was recorded at the start of each data recording.

The magnetic tape recorder was a fully transistorized, 14-channel, 8-speed, high-performance machine of modular design and capable of frequency modulated (fm) or direct (dr) record/reproduce operation with a maximum tape speed of 120 in./sec. The data recorded during an engine run included cylinder pressure, crank angle (CA) indication at every degree of crank rotation, a pulse indicating piston top-dead-center (TDC), and eight surface thermocouple signals.

In most previous data handling systems it was necessary to manually scale the analog data. This drawback was overcome in the authors' system by using the analog-to-digital (A/D) conversion capability of a hybrid computer.

The analog signal representing pressure or temperature was played back from the tape recorder at 1/16 record speed to the hybrid computer and digitized at every CA for 50 cycles. An average cycle of pressure or temperature variation was then determined and written onto magnetic tape in digital form for subsequent processing. The averaging of a number of engine cycles served two purposes. First, cycle-to-cycle variation was eliminated to arrive at an average pressure-time or temperature-time curve. Second, random noise, introduced by the various electronic components, was attenuated by the factor $1/\sqrt{N}$, where N is the number of cycles averaged from Bennett (18). This was particularly critical for the heat release studies as outlined in Shipinski (10).

Since the heat transfer in the cylinder wall at the thermocouple locations was one-dimensional, the instantaneous heat flux was calculated as outlined by Carslaw (19) and Overbye (15). The method involves the representation of the surface temperature by a Fourier series and the use of this series in a superposition solution of the partial differential equation governing heat conduction through the cylinder wall. This solution was carried out on the digital computer and the results obtained in both tabular and graphical form.

EXPERIMENTAL RESULTS ... The following paragraphs contain a discussion of the experimental data. Some results are presented graphically in this section, typically with data from TC-1. However the data are quite extensive and space makes it impractical to put all the data in this paper. Table 1 shows the conditions studied. Mass-averaged temperature-time data have been computed for the runs marked with an asterisk (*). Copies of these digitized data, including instantaneous gas pressure and temperature and heat fluxes at five thermocouple positions, may be obtained by writing to the authors at the University of Wisconsin and paying a nominal reproduction fee.

One engine operating condition (Table 2) was defined as the standard operating condition (SOC) and repeated several times during the course of the experiments. For all subsequent figures, any variable whose value is not specified may be assumed to be at the value shown in Table 2. A comparison of the data obtained during these repeated SOC runs gives an indication of the reproducibility of the data. This is illustrated in Fig. 5, which shows instantaneous surface heat flux at one position on the cylinder head for five different engine tests at the same operating conditions. In general, the reproducibility of the data was very good on the cylinder head, whereas data from the cylinder sleeve indicated moderate scatter.

Figure 6 shows the surface temperature-time curves for five different thermocouples for SOC operation. Note that the temperature axis is broken at several places to permit inclusion of all five curves on the one graph at a uniform scale, namely 10 F/div. The temperatures at TC's 3, 4, and 8 at CA = 0 are in parentheses. The surface heat flux histories corresponding to the temperature histories of Fig. 6 are shown in Fig. 7. Note that the peak instantaneous heat fluxes to the cylinder

*Numbers in circles designate components shown in blockdiagrams, Fig. 4.

head can be 10 times the time-averaged values. The peak instantaneous flux at TC-1 was typically twice that at TC-2 for fired operation. With the exception of the time-averaged data from TC-3, the instantaneous and time-averaged heat fluxes decrease at lower positions on the sleeve for fired operation. The exception at TC-3 is attributed to the ineffectiveness of an improvised coolant passage near TC-3.

It is evident from Fig. 6 that the passage of the piston rings over TC's 4 and 8 cause rapid temperature rises. This effect was particularly interesting at TC-4 as shown in Fig. 8. Note that five spikes are generated during the compression-expansion process compared to six spikes during the exhaust-intake process. Theoretically the third piston ring should cover, but not go above, TC-4 at TDC. Six spikes occurred during the compression-expansion process only when the intake density ratio (ρ/ρ_0) was reduced to unity, either for motored or fired operation.

The effects of four operating parameters on the surface heat flux were investigated, where applicable, under both motored and fired operation. These parameters are speed, equivalence ratio, injection advance, and intake density ratio. The authors do not wish to imply that surface heat flux depends only on the levels of these four parameters. These parameters were selected on the basis of the physical capabilities of the equipment available. The variations of surface heat flux with changes in each of the four parameters are discussed in subsequent paragraphs.

Over the speed range of 1000-2500 rpm, both motored and fired, the instantaneous and time-averaged surface heat fluxes generally showed an increase with increasing speed. This trend is most evident near TDC during the compression and expansion processes, as shown in Fig. 9. Note in Fig. 9 that the peak heat flux at TC-1 is higher at 1000 rpm than at 1500 rpm. This is an exception to the above generalization on the heat flux-speed trend. This exception occurred for both motored and fired operation but only at TC-1. The question as to whether this exception is physically significant, or whether it is due to experimental error, could not be answered.

The effect of equivalence ratio on the instantaneous heat flux at TC-1 is shown in Fig. 10. Both instantaneous and time-averaged heat fluxes were increased by an increase in equivalence ratio.

The cylinder head thermocouples indicated increased heat flux at TDC with increasing injection advance, as shown in Fig. 11. However, the heat flux at about 20 deg CA ATDC decreased with increased injection advance, even though the mass-averaged temperature and pressure increased. The effect of injection advance on surface heat flux was shown to be small for the sleeve thermocouples. Most of the thermocouples indicated an increased time-averaged heat flux as injection advance was increased.

In general, an increased density ratio resulted in increased heat fluxes, as shown in Fig. 12. This generality applied for both instantaneous and time-averaged values at all thermocouples for several density ratios, with one interesting exception. At naturally aspirated ($\rho/\rho_0=1$) operation, the instantaneous heat flux values at both TC-1 and TC-2 on the cylinder head were higher near TDC than those at higher density ratios (see Fig. 13). Yet the time-averaged values followed the above-mentioned general trend. Apparent pressure oscillations (Fig. 14), which may have been gas pressure oscillations, could account for the increased heat transfer, but the origin of the apparent pressure oscillations could not be proven.

OBSERVATIONS ON THE EXPERIMENTAL RESULTS ... For fired operation the heat flux was greater at TC-1 than at TC-2. However, as shown in Fig. 15, this situation was reversed for motored operation. Notice that the thermocouple at the larger radius, TC-2 at r = 0.9 B/2, indicated a higher heat flux than TC-1 for motored operation. The existence of the relatively higher heat flux at TC-2 for motored operation is shown in Part 3 to be compatible with a swirl-initiated-boundary-layer model of cylinder head heat transfer.

Since the gas temperature and pressure histories on a CA basis are not significantly affected by a variation of engine speed, the increase in heat transfer with speed must be attributed to velocity and rate effects. Certainly the average gas velocity would be higher at increased engine speed. Moreover, the rate of compression of the thermal boundary layer is higher at the engine speeds. Since both of these factors contribute to surface heat trnasfer, one would expect higher fluxes a the higher speeds.

One would expect that, during the intake stroke when the bulk-gas temperature is less than the cylinder wall temperature, the direction of heat transfer would be from the wall to the gas, or, negative heat transfer. Generally the thermocouples on the sleeve show this effect. However, the cylinder head thermocouples show positive heat transfer throughout the cycle for fired operation. This indicates that the mass-averaged gas temperature may not be representative of the gas temperature for heat transfer calculations over at least part of the cycle during fixed operation.

PREVIOUSLY PROPOSED CORRELATIONS

As noted before, many previously proposed correlations were based on time-averaged data. The extent to which these correlations can be used to predict the instantaneous heat fluxes in a modern, high-speed, supercharged engine as used in this study is certainly of interest.

The cylinder head and piston surfaces are exposed to the cylinder gases throughout the complete cycle. During the compression and expansion processes, particularly near TDC, the cylinder sleeve is shielded from the high temperature gases by the piston. Thus the heat fluxes on the sleeve surface are expected to be less than those on the head and piston surfaces. This is confirmed by Fig. 7, which shows that the heat fluxes are generally higher on the cylinder head than on the cylinder sleeve. The correlations for surface heat transfer already proposed have considered cylinder head heat transfer almost exclusively. Thus the experimental data from the cylinder head thermocouples, that is T.C.'s 1 and 2, are used in evaluating presently used correlations.

Annand gives a very good review of proposed correlations for surface heat transfer in engines. The extent to which several previously proposed correlations predict the authors' experimental data is shown in Figs. 16-19. The exact forms of the correlations used are given in Appendix A. Obviously it would be impractical to compare the experimental data with every correlation proposed heretofore. Those presented were thought to be the most popular ones.

Note that the existing correlations predict a single heat flux-time curve for the whole head area. The experimental data from TC-1 and TC-2 show that there is indeed considerable variation in the surface heat flux over the heat area. Figure 19 shows that the Eichelberg's empirical relationship does a poor job of predicting motored heat transfer.

In general, none of the correlations used in Figs. 16-19 provides a good fit of the data from either of the thermocouples installed in the cylinder head. It is interesting to note that all of the correlations presented give a peak in the heat flux-time curve at about 190 deg CA for fired operation. The experimental data, particularly TC-1, show a heat flux peak around 200 deg CA, over a wide range of operating conditions as seen in the figures of Part 1.

ANALYSIS OF ENGINE HEAT TRANSFER AND DATA CORRELATION

Since none of the previously proposed correlations adequately predicted the experimental data, it was decided to next conduct a detailed, theoretical, study of heat transfer in an engine. At the least, such a study should delineate additional information needed and conceivably could lead to a new and better correlation.

Heat transfer in an engine is a complicated problem. Ebersole (17) presents data to show that radiant heat transfer is important, while Woschini (7) argues that it is negligible. Semenov (20) has experimentally demonstrated the existence of a boundary layer on the cylinder heat but the relationship between this boundary layer and ordered and random gas velocities has not been established. Appendix B contains a discussion of ordered gas velocities in a motored engine and categorizes the velocities as either intake or piston related. The boundary layer has thermal capacity and in addition is compressed and expanded by the piston and the combustion processes with a consequent effect on heat transfer, Wendland (21).

An experimental investigation aimed at evaluating instantaneous radiant heat transfer in a diesel engine is currently in progress at the University of Wisconsin. Because of this and because of the disagreement as to the importance of radiant transfer, this study concentrated on the conductive aspects of heat transfer in an engine.

The heat transfer for motored operation is relatively simple compared to the situation for fired operation. For motored operation, where there is no combustion, the radiant component is negligible and gas motions caused by combustion are not present. Thus the first step in correlating the experimental data is to formulate a correlation of the motored heat transfer. If this motored correlation can be expressed in a correct fundamental form, it should be adaptable to fired operation.

As already noted, Fig. 7 shows that the heat fluxes measured on the cylinder head are larger than those on the sleeve. In fact the time-averaged fluxes on the cylinder head are generally four times the time averaged values on the sleeve even though there is friction heating of the sleeve by the piston rings. The convective heat fluxes to the piston should behave similarly to those on the cylinder head. Thus in the following discussion, heat transfer to the cylinder head will be considered almost exclusively. Comparisons between theory and experiment will utilize the experimental data from the thermocouples in the cylinder head, that is, TC's 1 and 2.

CONDUCTION-COMPRESSION MODEL OF HEAT TRANSFER IN THE MOTORED ENGINE ... In an attempt to delineate the significance of the various factors, the authors used a one-dimensional conductive-compressive heat transfer model, called the Adiabatic Plane model by Wendland, are:

1. The system is one-dimensional.
2. The gas is ideal.
3. The cylinder pressure is a function only of time and not of position.
4. A plane midway between the piston and the cylinder head is an adiabatic plane.

The gas mass between the head (or the piston) and the adiabatic plane is divided into a number of constant mass elements. Energy transfer between adjacent elements is by work or conduction heat transfer. A system of energy balances, one for each element, is solved to yield the temperatures of all the elements at some point in time when the temperatures were known at the previous point in time.

A gas temperature profile was assumed at the intake valve closure (50 deg CA). This assumed profile, in conjunction with the known trapped mass, and the experimentally determined cylinder pressure were submitted to a computer program containing the governing equations of the Wendland model. The choice of any reasonable initial temperature profile was found to have a negligible effect on the resultant heat flux at the gas-wall interface.

The results of using the conduction-compression model to predict surface heat flux in the authors' engine are summarized in Fig. 20. The use of pure conduction energy transfer between adjacent mass elements resulted in approximately 20-25% of the peak experimental valve.

It was expected that in the engine the effect of free stream turbulence was to increase the effective conductivity of the gas through eddy conductivity, from Bird (22). The temperature gradient would be very low, not just at one plane (the adiabatic plane in Wendland's analysis) but over a region in the center of the gas. Thus the "adiabatic plane" could be considered to be closer to the wall than in the molecular conduction case. In an attempt to simulate free stream turbulence, the gas conductivity was increased by a factor of five everywhere but at the gas-wall interface. This resulted in a prediction of a peak flux 35-50% of the experimental value.

The conduction-compression model does not provide a good fit of the motored experimental data as seen in Fig. 20. Apart from the fact that the predicted heat fluxes are considerably lower than the experimental values, the model does not provide any means of predicting the different heat fluxes at TC's 1 and 2. Gas velocities parallel to the cylinder head surface are expected in the engine used in this study. Moreover, these velocities may not be the same at the two thermocouple

positions. Thus it is felt that the weak point in the application of this model to the authors' engine is the ignoring of these gas velocities parallel to the head and piston surfaces. The model does incorporate the effects of pressure work and variable density in the boundary layer, but the thickness of the boundary layer is not controlled by a gas flow parallel to the surface as in the engine. Figure 20 shows that the conduction-compression model does predict the rapid decrease in surface heat flux early in the expansion stroke which is evident at TC-2. Negative heat flux early in the expansion process (30 deg ATDC) was measured experimentally by Wendland, and the conduction-compression model is the only one which predicts negative flux when the mass-averaged gas temperature is higher than the wall temperature.

Although the conduction-compression model predicted 50-75% of the experimentally measured heat flux in Wendland's study, an essentially identical model predicted almost 100% of the experimental value in a study by Goluba (23). Goluba measured the instantaneous surface heat flux at the stagnation point of a flow experiencing high-amplitude pressure oscillations. Using the same first three assumptions mentioned above, Goluba formulated the model in a different mathematical expression and achieved excellent agreement with his experimental data.

BOUNDARY LAYER MODEL OF HEAT TRANSFER IN MOTORED ENGINE ... The concept of a boundary layer existing between the free stream fluid flow and some relatively stationary object was introduced by Prandtl in 1904. This concept has proven to be an extremely useful one for the study of both laminar and turbulant convective heat transfer. However, in general, the problems considered have been steady state ones, that is, where the boundary layer thickness at a point is constant with time. In the present case, the boundary layer thickness is expected to change throughout the engine cycle. Thus, the first point to be considered is whether or not this steady state type of model is applicable to the unsteady heat transfer in engines.

Moore (24) shows that the time for a change in the freestream conditions to diffuse through a laminar boundary layer is approximately equal to δ^2/ν, where δ is the boundary layer thickness, and ν the momentum diffusivity in the boundary layer. If this diffusion time is small, relative to other significant times in the problem, the boundary layer may be considered quasi-steady. That is, at any instant of time the boundary layer would be that associated with the conditions existing outside the boundary at that instant. For the present purpose, if this time is shown to be about 1 deg CA, the boundary layer was considered to be quasi-steady.

In Appendix B it is shown that the gas flow parallel to the head and piston surfaces is generally turbulent. Also, it is shown that the most significant gas velocity is probably a swirling one whereby the bulk of the cylinder gas can be considered to be in solid body rotation. Using this model, an analysis of Hartnett (25) may be applied to determine the turbulent boundary layer thickness. This calculation yields a turbulent boundary layer thickness on the head and piston of approximately 0.01 in. near TDC during the compression and expansion process. The thickness, which is representative of δ for this turbulent boundary layer, is determined by assuming a 1/7 power law velocity distribution and that the velocity achieves 50% of its maximum value in the region of the boundary layer which presents the greatest resistance to diffusion. Both of these assumptions are approximations, of course, but suffice for present purposes. Having determined this effective value of δ, the diffusion time is found to be approximately 0.5 deg CA at the SOC.

Alternatively, the conduction-compression model could be applied to furnish an estimate of the boundary layer thickness. From this model one obtains an estimate of the diffusion time of 10 deg CA at 2000 rpm. Since the model predicts less than 50% of the experimental heat flux, a reasonable estimate of the actual diffusion time from the conduction-compression model would be about 2.5 deg CA if the model predicted 100% of the experimental value.

On the basis of the above two estimates of the diffusion time, the authors feel that the assumption of a quasi-steady boundary layer is justified.

Either the partial differential energy equation or the Buckingham Pi theorem may be used to generate the significant dimensionless parameters to be used in a correlation for the surface heat transfer. The details of the former approach are given by LeFeuvre (13). Both approaches give rise to rate dependent parameters which distinguish the unsteady situation in the engine from the classical steady-state situations. However, as shown above, the unsteady heat transfer in the engine

from the classical steady-state situations. However, as shown above, the unsteady heat transfer in the engine may be considered to be quasi-steady. Thus as a first approximation, the rate dependent, dimensionless parameters are not included and a correlation of the standard form,

$$Nu = f(Re, Pr) \tag{2}$$

is appropriate.

From Eq. (2) it is seen that if a correlation containing some special variation is to be developed, the significant velocities and/or significant distances must be spacially dependent. The other significant quantities involved are essentially all functions of the gas temperature which must be determined from the cylinder pressure and density which we have assumed to be spacially independent.

For motored operation the instantaneous heat fluxes at TC-2 are higher than those at TC-1 (see Fig. 15). On the basis of a boundary layer concept this difference in heat fluxes could result from different boundary layer thicknesses since significant gas temperature gradients parallel to the cylinder head and piston surface are not expected in a motored engine. Thus, different boundary layer thickness resulting from different velocities appear to be the only reasonable explanation of the differences in the heat fluxes between TC-1 and TC-2.

A detailed discussion of the significant distances and velocities to be used Eq. (2) in the correlation of the motored data is given in Appendix B. Briefly, for an open-chamber engine with moderate swirl, the significant distance for any position on the cylinder head (or piston) is taken to be the radial distance from the center of the bore. Also the significant velocity is considered equal to $r\omega$, where ω represents the angular velocity resulting from intake-induced swirl. The assumption of a constant value for ω throughout the cycle is discussed in Appendix B. The Reynolds number in Eq. (2) is the same as that used in the correlation of friction factors and heat transfer coefficients in rotating flow systems, namely:

$$Re = \frac{r^2\omega}{\nu} \tag{3}$$

where:

r = radius, here measured from the cylinder bore axis,

ω = angular velocity of the cylinder gases, and

ν = kinematic viscosity

For rotating systems, Dorfman (26) has shown that

$$Nu = a\ Re^{.8} Pr^{.33} \tag{4}$$

Equation (4) may be rearranged to determine the film cooefficient h which may then be substituted into Eq. (1) to calculate the surface heat flux as:

$$q(t) = a\ \frac{k(t)}{r}\ Re(t)^{.8}\ Pr(t)^{.33}\left(T_g(t)-T_w(t)\right) \tag{5}$$

A least-squared error fit of the data from the motored engine using Eq. (5) predicted a value of 0.047 for "a". The fit was made at the SOC (motored) and the results are shown in Figs. 21 and 22. The gas properties were calculated at the average boundary layer temperature, the significant gas velocity was the swirl velocity, and the significant distance was the radius to the thermocouple position from the bore axis.

The agreement between the experimental data and the prediction from the correlation, Eq. (5), is quite good during the compression and expansion processes, although there is a small phase difference near TDC as indicated in Fig. 22. However, the fit is considered adequate since the motored correlation is not an end in itself, that is, the object in correlating the motored data is to describe the convective portion of the surface heat flux and then to apply this correlation to fired data.

The correctness of the speed dependency, $(r,\omega)^{0.8}$, of Eq. (5) is evident from Fig. 23 where the predicted and experimental fluxes are shown for four engine speeds for four engine speeds for TC-1. The agreement between the model and the experimental data is better at TC-2 as the 1000 rpm singularity (Fig. 9) was not evident at TC-2.

The mass-averaged gas temperature-time history is essentially independent of ρ/ρ_0. Thus at any instant for two different values of ρ/ρ_0, the ratio of the two heat fluxes predicted by Eq. (5) is the same as the ratio of the two values of ρ/ρ_0 to the 0.8 power. Figure 24 shows the experimental and calculated (Eq. (5)) heat fluxes at TC-1 for four different intake density ratios. The calculated values at $\rho/\rho_0 = 1$, 1.5 and 2.5 were found from the values at $\rho/\rho_0 = 2$ by using the ratios of intake densities to the 0.8 power.

EXTENSION OF THE MOTORED BOUNDARY LAYER CORRELATION TO FIRED OPERATION ... The correlation in Eq. (5) is shown to predict the motored data with moderate success. Gas velocities arising from combustion and radiation effects are expected to augment the predicted heat flux in the fired case. The correlation is for convective heat transfer and thus would not be expected to predict the total heat flux under fired operation. However, as an aid in furthering our understanding of heat transfer in the fired engine, the motored correlation, Eq. (5), was used to predict the fired heat transfer at TC's 1 and 2, and the results are presented in Figs. 25 and 26. The agreement between the correlation and the data is fair at TC-1 and poor at TC-2. The correlation predicts a convective flux greater than the total experimental heat flux for portions of the cycle, particularly at TC-2.

Note that the heat flux predicted by Eq. (5) is larger than the experimental value in Fig. 25 from 15 deg CA BTDC to 15 deg CA ATDC. Recall that many of the previous correlations reviewed (Figs. 16-19) show a similar tendency. From Fig. 27 it is seen that the motored and fired heat fluxes at TC-1 are approximately equal for CA < 185 deg. Note, however, that the mass-averaged gas temperature and pressure for fired operation, are significantly different than the motored values for CA > 170 deg. Thus the correlation, Eq. (5), as based on the mass-average gas properties, could not be expected to predict the apparent lag between the surface flux and the mass-averaged gas properties. These remarks apply equally to the flux at at TC-2 the flux prediction from Eq. (5) shows a greater error at TC-2 than at TC-1.

The combustion in the engine originates somewhere in the combustion chamber raising the temperature locally and the pressure uniformly throughout the cylinder. This is in line with the assumption of uniform pressure in the cylinder which is valid for most operating conditions. The assumption of uniform gas temperature throughout the cylinder and the use of this mass-averaged temperature as the source temperature for heat flux to the cylinder walls is questionable. In fact, until the flame actually reaches the boundary layer, the boundary layer temperature history is probably close to the temperature history under motored operation. However, the temperature gradient at the wall in the fired case would be greater than in the motored case because of the increased compression due to combustion.

In order to test this theory, the correlation from Eq. (5) was used to predict the surface heat flux for fired operation but the gas temperature used was that for motored operation. The results are shown in Figs. 28 and 29. Poor agreement will be noted for TC-1 and fair agreement for TC-2.

Due to the offset position of the combustion chamber and to the valve cutouts in the piston, there should be considerable motion of the flame and unburned fuel into the area between TC-1 and the No. 2 pressure pickup hole (see Fig. 3). This, no doubt, produces appreciable gas velocities near TC-1. Figure 3 shows that TC-1 and TC-2 are approximately equidistant from the combustion chamber formed by the cavity in the piston. While the flame is concentrated in the cavity both TC's should receive equal heat flux by radiation. However, later burning is more likely to be symmetrical about the bore axis and TC-1 should receive a greater radiant flux than TC-2. Thus both radiation effects and gas velocity effects contribute to the higher peak flux at TC-1 at about 20 deg CA ATDC.

To be able to predict the total experimental heat flux for any position on the cylinder head or piston, it apparently is necessary to use the actual gas velocities and gas temperatures in Eq. (5). Furthermore, a separate term may be necessary to account for radiation. At present the necessary data are just not available to make

any more than the roughest estimate of these influences and thereby achieve a fit of the data. A current study at the University of Wisconsin should provide the first experimental data on instantaneous radiant heat transfer in the engine. With this data one of the two presently unknown combustion related terms, that is gas velocity and radiation, would be known. Then a more logical estimate of the gas velocity term should be possible.

CONCLUSIONS

The comparisons between the experimental data presented in this paper and the heat fluxes calculated using present correlations have shown that these correlations provide at best only an approximation to the data. The use of average piston speed, cylinder bore, and mass-averaged gas temperature in correlations for the instantaneous surface heat fluxes precludes the prediction of the spacial variation shown by the experimental data.

A study of the spacial and temporal variations in gas temperature and velocity (both motored and fired) is necessary if one wishes to improve on the boundary layer models proposed by Sitkei (27), Annand, Woschni, and the present authors. Given the results of such a study, the authors suggest that this information should be incorporated into a boundary layer model as proposed in this paper. With an allowance for radiation (hopefully forthcoming from a current study at the University of Wisconsin) this improved correlation should furnish a better prediction of the data presented in Part 1 than is possible at present.

As mentioned in Part 3 the boundary layer models essentially ignore the effects of compression work in the boundary layer. Thus even an improved correlation incorporating instantaneous local gas velocities and temperatures cannot be expected to provide a complete picture. It may be necessary to combine the features of the conduction-compression and the boundary layer models. Some of the data of Part 1 suggest this combination.

Recall that the conduction-compression model predicted a rapid decrease of surface heat flux early in the expansion stroke as seen in Fig. 20. Note from Fig. 11 that the flux at 20 deg ATDC is much lower for the 30 deg injection advance run than for the 10 deg advance run, even though the gas temperature and pressure are higher at this point for the 30 deg advance run, LeFeuvre (1968-b). At 20 deg ATDC the 30 deg advance run has already experienced 35% of its pressure decrease (expansion) compared to 15% for the 10 deg advance case. Hence, by application of the conduction-compression model a lower heat flux might be expected.

The above reasoning follows from a conceptual combination of the conduction-compression and boundary layer models. Analytical work leading to a mathematical expression of this combination should prove to be interesting and profitable.

ACKNOWLEDGMENTS

The authors thank the United States Army Tank and Automotive Command for their continued interest in, and support of, diesel engine research. The scholarship support from General Motors Corp., Cummins Engine Co., and Caterpillar Tractor Co. is appreciated. The National Science Foundation provided financial support for the tape recorder, the hybrid computers at the U.W.C.C.

REFERENCES

1. G.L. Borman, "Mathematical Simulation of Internal Combustion Engine Processes and Performance Including Comparisons With Experiment." PhD Thesis, Mech. Engr. Dept., University of Wisconsin, 1964.

2. K.J. McAulay, T. Wu, S.K. Chen, G.L. Borman, P.S. Myers and O.A. Uyehara, "Development and Evaluation of the simulation of the Compression-Ignition Engine." Paper 650451 presented at SAE Mid-Year Meeting, Chicago, May 1965.

3. W. Nusselt, "Der Warmeubergang in der Verbrennungskraftmaschine." VDI Forschungshaft, No. 264, 1923.

4. G. Eichelberg, "Investigations on Combustion-Engine Problems." Engineering, Vol. 148, 1939, pp. 463, 547, 603, 682.

5. W. Pflaum, "Heat Transfer in Internal Combustion Engines." Presented at La Conferenze Internazionale di Termotecnia, Milan, November 1962.
6. W.J.D. Annand, "Heat Transfer in the Cylinders of Reciprocating Internal Combustion Engines." Proc. Inst. Mech. Engrs., Vol. 177, No. 36, 1963, p. 973.
7. G. Woschni, "A Universally Applicable Equation for the Instantaneous Heat Transfer Coefficient in the Internal Combustion Engine." Paper 670931 presented at SAE Combined National Meetings, Pittsburgh, October 1967.
8. K. Hug, "Messung and Berechnung von Kolbentemperaturen in Dieselmotoren." Mitt. Inst. Thermodyn, Zurich, No. 1, 1937.
9. T. LeFeuvre, P.S. Myers, O.A. Uyehara, and J.S. Shipinski, "A Tape Recording and Computer Processing System for Instantaneous Engine Data." Paper 680133, presented at SAE Automotive Engineering Congress, Detroit, January 1968.
10. J.H. Shipinski, "Relationships Between Rates-of-Injection and Rates-of-Heat Release in Diesel Engines." PhD Thesis, Mech. Engr. Dept., University of Wisconsin, 1967.
11. J.H. Shipinski, P.S. Myers, and O.A. Uyehara, "An Experimental Correlation Between Rate of Injection and Rate of Heat Release in a Diesel Engine." ASME Paper 68 DGP-11, to be published in ASME Diesel and Gas Power Proc., 1968.
12. D. Bendersky, "A Special Thermocouple for Measuring Transient Temperatures." Mechanical Engineering, Vol. 75, 1953, p. 117.
13. T. LeFeuvre, "Instantaneous Metal Temperatures and Heat Fluxes in a Diesel Engine." PhD Thesis, Mech. Engr. Dept., University of Wisconsin, 1968.
14. V.D. Overbye, "Variation of Instantaneous Wall Temperature, Heat Transfer, and Heat Transfer Coefficients in a Spark Ignition Engine." PhD Thesis, Mech. Engr. Dept., University of Wisconsin, 1960.
15. V.D. Overbye, J.E. Bennethun, P.S. Myers, and O.A. Uyehara, "Unsteady Heat Transfer in Engines, SAE Transactions, Vol. 69 (1961), p. 461.
16. J.E. Bennethum, "Heat Transfer and Combustion Chamber Deposits in a Spark Ignition Engine." PhD Thesis, Mech. Engr. Dept., University of Wisconsin, 1960.
17. G.D. Ebersole, P.S. Myers, and O.A. Uyehara, "The Radiant and Convective Components of Diesel Engine Heat Transfer." Paper 701C presented at SAE International Summer Meeting, Montreal, June 1963.
18. C.A. Bennett and N.L. Franklin, "Statistical Analysis in Chemistry and the Chemical Industry." New York: John Wiley & Sons, 1954.
19. H.S. Carslaw and J.C. Jaeger, "Conduction of Heat in Solids." Oxford: Clarendon Press, 1959.
20. E.S. Semenov. "Studies of Turbulent Flow." ed. L.N. Khitrin, 1959. Translated from Russian by Israel Program for Scientific Translations, 1963.
21. D.W. Wendland, "The Effect of Pressure and Temperature Fluctuations on Unsteady Heat Transfer in a Closed System." PhD Thesis, Mech. Engr. Dept., University of Wisconsin, 1968.
22. R.B. Bird, W.E. Stewart and E.N. Lightfoot, "Transport Phenomena." New York: John Wiley & Sons, 1960.
23. R.W. Goluba, "The Effect of Periodic Shock-Fronted Pressure Waves on the Instantaneous Heat Flux at the End-wall of a Tube." PhD Thesis, Mech. Engr. Dept., University of Wisconsin, 1968.
24. F.K. Moore, "Unsteady Laminar Boundary-Layer Flow." NACA TN2471, September 1951.
25. J.P. Hartnett, S.H. Tsai, and H.N. Jantscher, "Heat Transfer to a Nonisothermal Rotating Disk with a Turbulent Boundary Layer." Trans. ASME, Vol. 78, Series C, No. 3, August 1965, p. 363.
26. L.A. Dorfmann, "Hydrodynamic Resistance and the Heat Loss of Rotating Solids." Translated by N. Kemmer. Edinburgh: Oliver and Boyd, 1963.
27. G. Sitkei, "Beitrag zur Theorie des Warmeuberganges im Motor." Konstruktion, 14, 1962, p. 67.
28. A. Stambuleanu, "Contribution to the Study of the Distribution of Heat Transfer Coefficients during the Phase of the Working Cycle of an Internal Combustion Engine." Third International Heat Transfer Conference, Chicago, 1966.
29. K. Lohner, E. Dohring, and G. Chore, "Temperaturschwingungen an der Innenwand von Verbrennungskraftmaschinen." MTZ, Vol. 17, No. 12, December 1956, p. 413-418.
30. W. Pflaum, "Warmeubergang bei Dieselmaschinen mit und ohne Aufladung." MTZ, Vol. 22, No. 3, March 1961; Translated in the Engineers Digest, Vol. 22, No. 7, July 1961.
31. N.A. Henein, "Instantaneous Heat Transfer Rates and Coefficients Between the Gas and Combustion Chamber of a Diesel Engine. Paper 969B presented at SAE Automotive Engineering Congress, Detroit, January 1965.

32. C.F. Taylor, "Heat Transmission in Internal-Combustion Engines." Proc., General Discussion on Heat Transfer, Inst. Mech. Engrs., London, 1951, p. 397.
33. C.F. Taylor and T.Y. Toong, "Heat Transfer in Internal-Combustion Engines." ASME Paper No. 57-HT-17, 1957.
34. A. Nagel, "Heat Transfer in Reciprocating Engines." Engineering, Vol. 127, 1929, pp. 59, 179, 279, 466, 626.
35. K. Elser, "Der Instationaire Warmeubergang in Dieselmotoren." Mitt. Inst. Thermodyn, No. 15, Zurich, 1954.
36. B. Loeffler, "Development of an Improved Automotive Diesel Combustion System." SAE Transactions, Vol. 62, (1954), p. 243.
37. D. Fitzgeorge and J.L. Allison, "Air Swirl in a Road-Vehicle Diesel Engine." Proc. Inst. Mech. Engrs. (A.D.), No. 4, 1962-1963, p. 151.
38. J.F. Alcock and W.M. Scott, "Some More Light on Diesel Combustion." Proc. Inst. Mech. Engrs. (A.D.), No. 5, 1962-1963, p. 179.
39. T. Okaya and M. Hasegawa, "On the Friction to the Disk Rotating in a Cylinder." Jap. Journal of Physics, Vol. 13, 1939.
40. S.L. Soo, "Laminar Flow Over an Enclosed Rotating Disk." Trans. ASME, Col. 80, (1958), p. 287.
41. J.W. Daily and R.D. Nece, "Chamber Dimension Effects on Induced Flow and Frictional Resistance of Enclosed Rotating Disks." Trans. ASME, Vol. 82, Series D, March 1960, p. 217.

APPENDIX A

PREVIOUSLY PROPOSED CORRELATIONS

Many different expression have been proposed to correlate the surface heat fluxes in diesel engines. Attention is focused on three correlations upon which most other correlations have been based. The three correlations which are considered in some detail are those of Nusselt, Eichelberg, and correlations based on the Reynolds' analogy boundary layer theory. The modifications to these three basic forms which have been suggested by various authors are also considered. All the correlations discussed employ the mass-averaged gas temperature, $T_g(t)$, to represent the gas temperature.

NUSSELT'S CORRELATION ... Nusselt's work was based on measurements of the heat loss from the combustion of quiescent, homogeneous mixtures in spherical bombs. He determined the influence of radiation by using gold-plated or blackened, inside-surface coatings on the bombs.

By incorporating a term to account for forced convection due to piston motion, Nusselt adapted results from the bomb experiments to the situation in an engine, and proposed that the surface heat transfer coefficient be expressed as:

$$h(t) = 0.0278(1+0.38V_p)[P(t)^2T_g(t)]^{1/3} + 1.275 \times 10^{-10} \frac{[T_g(t)^4-T_w(t)^4]}{[T_g(t)-T_w(t)]} \tag{A-1}$$

where:

$P(t)$ = instantaneous cylinder gas pressure in psia,

$T_g(t)$ = instantaneous cylinder gas pressure in R, and

V_p = mean piston speed in ft/sec.

The first term on the right of Eq. (A-1) represents convective transfer and the second term gives the radiative portion. The choice of 2/3 for the exponent of $P(t)$ was actually an average of several values ranging from 0.5-0.8. Jaklitsch quoted by Stambuleanu (28) suggested values ranging from 0.44-0.90. Lohner (29) presents a linear temperature function for this exponent.

Brilling changed the piston speed term of Eq. (A-1) from $(1+0.38V_p)$ to $(2.45 + 0.056V_p)$ on the basis of tests on stationary Diesel engines. Figure 16 shows the heat fluxes computed using the formulae of Nusselt and Brilling along with the experimental results from the cylinder head thermocouples.

EICHELBERG'S CORRELATION ... Although Eichelberg's correlation is actually a modification of Nusselt's, it merits special consideration because of its wide usage and because of the related experimental work carried out by Eichelberg and his associates. Eichelberg summarized several years of research using subsurface thermocouples to study the instantaneous surface heat flux in large, low-speed diesel engines under NA operation. He proposed the correlation:

$$h(t) = 0.0565\, V_p^{1/3}\left(P(t)T_g(t)\right)^{1/2} \tag{A-2}$$

for the surface heat transfer coefficient.

Eichelberg stated that he expected a small heat flux due to radiation. Yet he gave a relatively greater significance than Nusselt to gas temperature to account for radiation and increased gas velocity during the intake stroke. Eichelberg preferred to omit the separate radiation term and to express the influence of speed by the cube root of the mean piston speed, V_p.

Pflaum (30), on the basis of time-averaged heat flux data, has proposed modification of Eq. (A-2) to account for the effects of higher engine speeds and supercharged operation. His most recent proposal is to replace Eq. (A-2) by the expression:

$$h(t) = f_1[P(t),T_g(t)] \cdot f_2(V_p) \cdot f_3(P_1) \tag{A-3}$$

where:

$$f_1[P(t),T(t)] = 0.0399\left(P(t) \cdot T_g(t)\right)^{1/2} \tag{A-4}$$

$$f_2(V_p) = 6.2 - 5.2(5.7)^{-(0.0305V_p)^2} + 0.00762\ V_p \tag{A-5}$$

$$f_3(P_1) = 1.175(P_1)^{1/4} \text{ for the cylinder head} \tag{A-6}$$

where P_1 is the intake pressure in psia. Note that at a fixed speed and intake pressure, the Pflaum correlation reduces to the same form as the Eichelberg correlation reduces to the same form as the Eichelberg correlation but with a different constant term.

Henein (31) obtained poor results in applying Eichelberg's correlation to a prechamber engine when the mean piston speed was used for V_p. When he substituted estimates of the swirl and squish velocities for V_p he obtained reasonable agreement between the experiment and the correlation for the compression stroke but not for the expansion stroke.

Figure 17 shows the degree to which the Eichelberg and Pflaum correlations fit the authors' experimental results from the SOC.

CORRELATIONS BASED REYNOLD'S ANALOGY OF BOUNDARY LAYER THEORY ... A number of authors have used the Nusselt number-Reynolds number relationships of steady state systems to correlate engine heat transfer data. Professor C.F. Taylor (32,33) advocated the use of dimensionless quantities such as Nu and Re in correlating time-averaged heat fluxes from several engines. However, apart from one brief reference, Herzfeld in Nagel (34), it is only recently that correlations of instantaneous surface heat transfer based on a Nu-Re relationship have been put forth in the literature.

Annand gave a rather extensive review of several correlations for $h(t)$ and used dimensional analysis to arrive at the relation:

$$\text{Nu} = (\text{constant}) \cdot \text{Re}^n \tag{A-7}$$

to correlate the convective heat flux. He suggested that the radiant heat flux be expressed by:

$$\dot{q}_r(t) = c\left(T_g(t)^4 - T_w(t)^4\right) \tag{A-8}$$

where "c" is a constant.

From a reanalysis of Elser's (35) data from a low-speed, 4 stroke diesel engine, Annand formulated the relation

$$q(t) = a\,\frac{k(t)}{D}(\text{Re})^b\left(T_g(t) - T_w(t)\right) + c\left(T_g(t)^4 - T_w(t)^4\right) \tag{A-9}$$

for the instantaneous surface heat flux.
where:

$k(t)$ - gas conductivity, $\dfrac{\text{Btu}}{\text{hr ft deg R}}$

D = bore diameter, ft

a = 0.49

b = 0.7

$c = (1.03 \pm 0.37)10^{-9}\ \dfrac{\text{Btu}}{\text{hr ft}^2\text{deg R}}$

Annand chose to select the bore diameter and the average piston speed as the significant distance and velocity to be used in Re of Eq. (A-7).

Woschni repeated some of the bomb experiments of Nussels and concluded that the results of such experiments are not suitable for application to engine heat transfer. Woschni proceeded to formulate a correlation for the heat transfer coefficient using the well-known correlation of turbulent heat transfer in pipes, $Nu \propto Re^{.8}$ as his starting point. He chose bore diameter and mean piston speed as significant quantities in the Reynolds number but applied multiplying constants to the mean piston speed. Woschni's correlation may be summarized as:

$$Nu = 0.035\ Re^{.8} \tag{A-10}$$

with cylinder bore as the characteristic length and the following expression for the gas velocity in Re:

$$V_g = 6.18\ c_m \quad \text{scavenging}$$

$$V_g = 2.28\ c_m \quad \text{compression}$$

$$V_g = 2.28\ c_m + (3.24)10^{-3}\ \frac{V_s T_1}{P_1 V_1}(P_g - P_{g0})$$

combustion and expansion

where:

c_m = average piston speed in m/sec

V_s = total cylinder displacement

T_1, P_1 and V_1 = cylinder gas temperature, pressure and volume at some convenient reference state

$(P_g - P_{g0})$ = instantaneous pressure difference between the fired and motored cycles.

Woschni determined the constants in the expression for V_g by fitting the time-averaged results of his correlation to heat balance data from the engine.

Figure 18 shows experimental data for the SOC compared to the heat fluxes calculated by Eq. (1) when the Annand and Woschni correlations are used for $h(t)$. The term which Annand attributed to radiation is shown and seen to be quite small.

APPENDIX B

SIGNIFICANT VELOCITIES AND DISTANCES TO BE USED IN REYNOLDS NUMBER

To fix the functional relationship of Eq. (2) the significant quantities, particularly gas velocity and distance, are considered. The choice of a significant velocity and distance, are considered. The choices of a significant velocity and a significant distance are not independent, as pointed out in the following discussion.

SIGNIFICANT OR CHARACTERISTIC VELOCITY ... The gas velocities in the motored engine are classified as being piston related or intake related.

Piston Related - The piston motion generates several gas velocities. One is a velocity perpendicular to the cylinder head and piston which creates a stagnation type heat transfer situation if the piston and head areas are flat and parallel. This is the gas velocity which is incorporated into the conduction-compression model. In reality, the piston and head surfaces are not flat but quite irregular due to protruding valves, valve cutouts in the piston, and a combustion cavity in the piston.

Due to the presence of a combustion cavity in the piston (see Fig. 3), the piston motion introduces radial velocities parallel to the head and piston surfaces. During compression the flow is radially inward and during expansion it is radially outward. These velocities, termed squish velocities in the engine literature, have been considered by a number of authors, for example, Loeffler (36) and Fitzgeorge (37). Fitzgeorge shows the magnitude of the squish velocities to be highly dependent on the head-to-piston clearance at TDC. The authors have calculated a peak squish velocity in the engine at TC-1 of about 50 ft/sec based on a radial flow into the combustion cavity from the lip area. However, the actual squish velocity is significantly less than this value due to squish flow into the valve cutouts in the piston. Moreover, as reported by Alcock (38), several attempts to determine experimental evidence of squish in a motored engine have yielded inconclusive results. On this basis the authors consider squish velocities to be relatively insignificant in the motored engine.

Intake Related -- During the intake process the intake port and valve combination can introduce significant gas velocities. In many engines, part of the design intent is to impart a swirling gas motion about the bore axis. Shipinski (10) has determined the mean angular velocity of the swirl motion in the engine used in this study to be approximately twice the angular velocity of the crankshaft. Strictly speaking, this swirl ratio, that is, swirl angular velocity divided by crankshaft angular velocity, applies only at the closing of the intake valve.

At intake valve closure (50 deg CA) the gas is swirling about the axis of the cylinder with diameter equal to the bore B. At TDC the major portion (about 80%) of the gas is in the combustion chamber which has a diameter of approximately 0.55 B. The axis of the combustion chamber is 0.5 in., or 0.11 B, from the bore axis. Thus, there is a movement of the center of mass of the swirling gas during compression and expansion. Because of the conservation of angular momentum, the angular velocity in the combustion chamber near TDC is approximately four times its value at BDC in the presence of negligible viscous dissipation.

Okaya (39) presents a method whereby the swirl deceleration due to viscous effects may be calculated. Using these results the authors have determined changes in swirl velocity during one engine revolution of approximately 10% and 20% of the value at intake valve closure for the BDC and TDC cases mentioned above.

The changes in the angular velocities in the lip area at TC-1 and TC-2 are influenced by the motion of the center of mass, the acceleration or deceleration due to the conservation of angular momentum, and the deceleration due to viscous effects. The viscous effects in the lip area near TDC are higher than in the combustion chamber but are counteracted by the acceleration necessary to conserve the angular momentum. As a first approximation the authors consider the swirl velocity to be constant throughout the engine cycle.

Semenov has published the only experimental results known to the authors on turbulence in engines. He used an 8 micron resistance wire in a 3.25 × 4.50 in. CFR engine under motored operation. The engine was an open chamber one with a flat piston and head. Semenov's results included: during intake considerable temporal and

spacial variations in the gas velocity exist with peak values being as much as 10 times the mean piston speed; significant gas velocity gradients are found within 2-3 mm of the cylinder head; and the fluctuating component of the gas velocity decreases rapidly after intake valve closure. The turbulence which exists throughout the compression stroke is essentially isotropic.

Semenov indicates that he did not use a shrouded intake valve and gives no indication of determining a swirl velocity. Since Semenov's engine was so dissimilar to the engine used in this project, many of the trends in Semenov's results may not be applicable in the present instance.

From the above discussion on gas velocities in the motored engine it is apparent that both squish and swirl velocities would be expected to vary with position in the cylinder. It is concluded that squish velocities are relatively insignificant in the motored engine. Moreover, the calculated squish velocity at TC-1 is greater than that at TC-2. This is opposite to the trend expected from the motored heat flux results. Thus the local squish velocity is not a good choice for the significant or characteristic velocity.

Thus swirl velocities are considered as the predominant velocities in the motored engine during compression and expansion. Certainly there are gas velocities related to the intake process, often referred to as jet velocities, which are significant for that portion of the cycle. However, for present purposes attention is focused on the velocities during the compression and expansion process.

SIGNIFICANT OR CHARACTERISTIC DISTANCE ... Accepting the significant velocity as the swirl velocity, the selection of the significant distance must be compatible. The gas flow pattern due to swirl flow can be looked upon as having many similarities to the flow near rotating discs. An excellent review of the fluid flow and heat transfer problems associated with rotating systems is found in Dorfman. The flow pattern close to the cylinder head and piston would resemble that near a casing which encloses a rotating disc, if the effects of the irregularities in the engine cylinder surfaces are considered small. That is, the tangential velocity increases with the radius and a secondary radially inward flow exists on the head and piston. This secondary flow is radially outward in the bulk gas in the engine whereas it is radially outward near the disc for the enclosed rotating disc. Soo (40) and Daily (41) present extensive studies of this type of flow. In general the flow Reynolds number characterizing the flow in rotating systems is defined as:

$$Re = \frac{r^2 \omega}{\nu} \tag{B-1}$$

As a result of the success achieved in correlating friction factors and heat transfer coefficients with this definition of the Reynolds number in rotating systems, the authors consider the local radius to be the significant distance in Eq. (2).

Using Eq. (B-1) flow Reynolds numbers are found to be in the range 10^5 to 6×10^5. Dorfman gives $Re = 3 \times 10^5$ as a transition Re for rotating systems. Due to the irregularities in the cylinder head and piston surfaces and the turbulent nature of the intake process, the flow is taken to be turbulent.

DISCUSSION

J.F. ALCOCK
Ricardo & Co. Engineers (1927) Ltd.

This extremely interesting paper contributes much to our understanding of the heat-transfer process in engines. There are some points on which I should like to comment.

1. *Squish*: In his Appendix B he mentions that Mr. Scott and myself could not find any squish in a motored engine. As regards inward squish during compression this is correct, but our paper (Authors' Ref. 38) showed, in our Fig. 9, a strong outward "unsquish" on the expansion stroke even when motoring. In a firing engine this "unsquish" would be even greater, due to the pressure rise in the bowl where combustion starts. From the photographs in Fig. 3 of our paper the radial "unsquish" velocity appears to be of the same order of magnitude as the tangential swirl velocity appears to be of the same order of magnitude as the tangential swirl velocity. In a firing engine this "unsquish" gas is hot, and its radial velocity must increase the heat transfer. This may account for some of the flux difference between couples 1 and 2.

2. *Swirl*: The authors say "Also the significant velocity is considered equal to $r\omega$, where ω is the angular velocity" and r is the radius, in other words a forced vortex. In near spherical prechambers we have found a "semifree" vortex, with linear velocity independent of radius. We have also found much the same relationship in other types of chamber.

Allowance for this would reduce the calculated heat-transfer at TC2, and thus the discrepancy between theory and experiment shown in Fig. 26.

AUTHORS' CLOSURE TO DISCUSSION

We appreciate Mr. Alcock's kind remarks and comments on our paper. Regarding our interpretation of his studies, Ref. 38 of the paper, our statement was that the results were inconclusive for the motored engine. Mr. Alcock's remarks above essentially enforce this statement since it is difficult to rationalize the existence, in the motored engine, of outward squish without the presence of inward squish.

Figures 21 and 22 of the paper show that the heat fluxes measured in the motoring engine are essentially symmetrical about TDC at TC-1 and peak about 3-5 deg BTDC at TC-2. During motoring, one would not expect appreciable instantaneous property differences of the gas from one position to the other. Thus, the different heat flux-time curves may well be due to different gas velocities at these two points. The symmetry of the flux-time curve at TC-1 may not result from a constant gas velocity, $r\omega$, as assumed in the authors' model, but rather from a combination of velocities, one of which is the squish velocity. The experimental evidence gathered by Alcock and Scott (Ref. 38) on the predominance of outward squish over inward squish might then explain the difference in motored fluxes between TC-1 and TC-2, since squish velocities would be higher at TC-1 than at TC-2. The authors do not feel that the experimental data currently available on instantaneous gas velocities in a motored engine warrant the use of this complex model of the gas motion.

The increased outward radial velocity in a firing engine (termed unsquished by Alcock) is certainly expected to contribute to the different heat fluxes measured at TC-1 and TC-2. However, Appendix B pertains to the selection of a significant velocity gas velocity for the motoring engine.

The authors' have some difficulty understanding the term "semifree" vortex in a spherical prechamber. Thus, we are unable to speculate on its usefulness in a conceptual model of surface heat transfer in a motoring engine.

Table 1 - Summary of Operating Conditions

Run No.	Motored-M or Fired-F	Nominal Speed, rpm	Nominal Equivalence Ratio f	Nominal Injection Advance (deg CA BTDC)	Intake Density Ratio ρ/ρ_o
142*	M	1000.	---	--	2.0
141*	M	1500.	---	--	2.0
140*	M	2000.	---	--	2.0
139*	M	2500.	---	--	2.0
136*	F	1000.	0.45	20.	2.0
137*	F	1500.	0.45	20.	2.0
135*	F(SOC)	2000.	0.45	20.	2.0
138*	F	2500.	0.45	20.	2.0
144	F	2000.	0.22	20.	2.0
134	F	2000.	0.37	20.	2.0
143	F(SOC)	2000.	0.44	20.	2.0
133	F	2000.	0.53	20.	2.0
145*	F	2000.	0.72	20.	2.0
150*	F	2000.	0.45	10.	2.0
148	F(SOC)	2000.	0.45	20.	2.0
151*	F	2000.	0.45	30.	2.0
157*	M	2000.	---	--	1.0
147*	M	2000.	---	--	1.5
146*	M	2000.	---	--	2.5
152	F	2000.	0.45	20.	1.0
153*	F	2000.	0.45	20.	1.5
156	F(SOC)	2000.	0.45	20.	2.0
132	F(SOC)	2000.	0.45	20.	2.0
154*	F	2000.	0.45	20.	2.5
155	F	2000.	0.72	20.	2.5

Table 2 - Operating Conditions Defined as Standard Operating Conditions (SOC)

Compression	15.4:1
Speed	2000 ± 20 rpm
Dynamic Injection Timing	20 ± 1 deg CA BTDC
Intake Temperature	100 ± 3 deg F
Intake Tank Pressure	60 ± 1 in Hg abs
Exhaust Tank Pressure	60 ± 2 in Hg abs
Intake Valve Opens	520 deg CA
Intake Valve Closes	50 deg CA
Exhaust Valve Opens	310 deg CA
Exhaust Valve Closes	560 deg CA
Coolant Inlet Temperature	190 ± 10 deg F
Fuel	50 - 50 blend U-9 and T-16 ASTM Secondary Cetane Reference Fuels
Equivalence Ratio	0.45
Fuel Flow	9.6 lb/hr

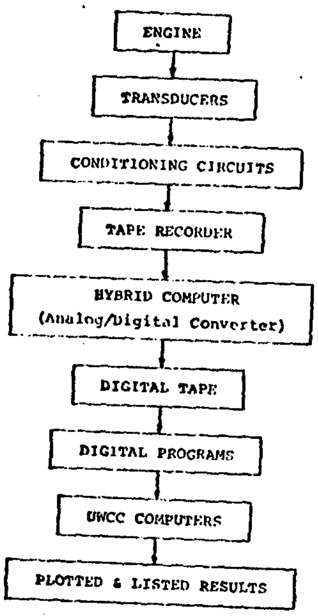

Fig. 1 Block diagram of experimental system.

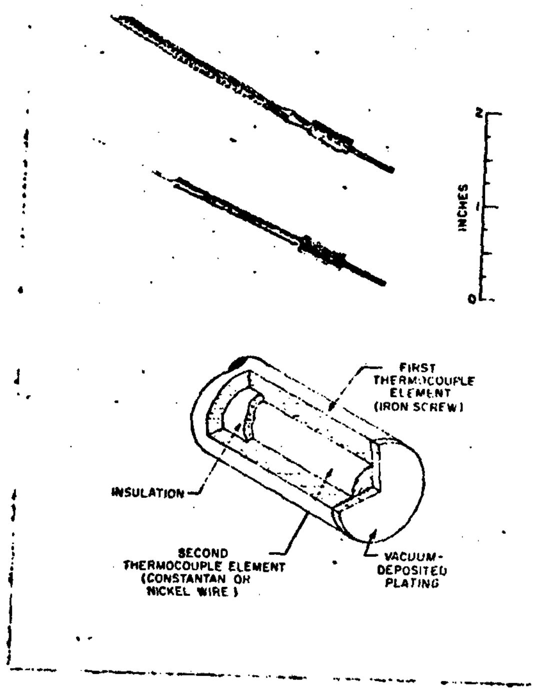

Fig. 2 Surface thermocouple.

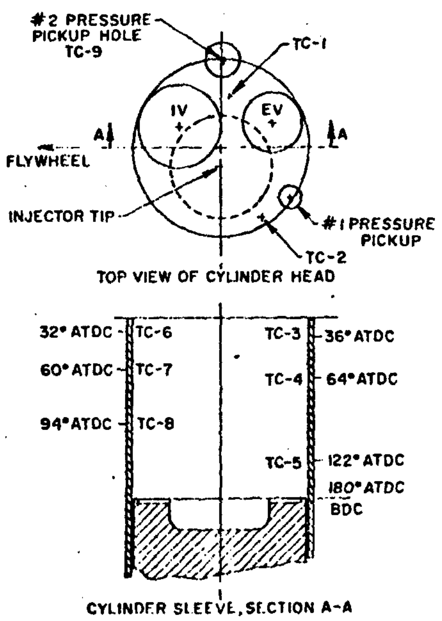

Fig. 3 Cylinder head and sleeve geometry showing thermocouple locations.

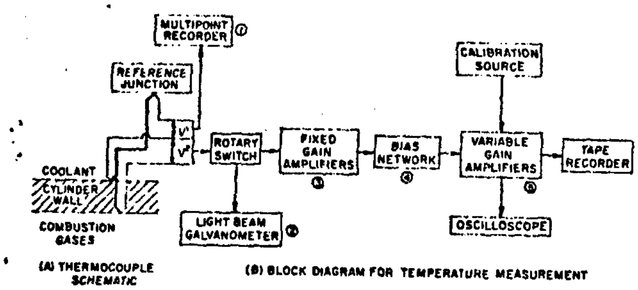

Fig. 4 Thermocouple schematic and instrumentation for surface temperature measurement.

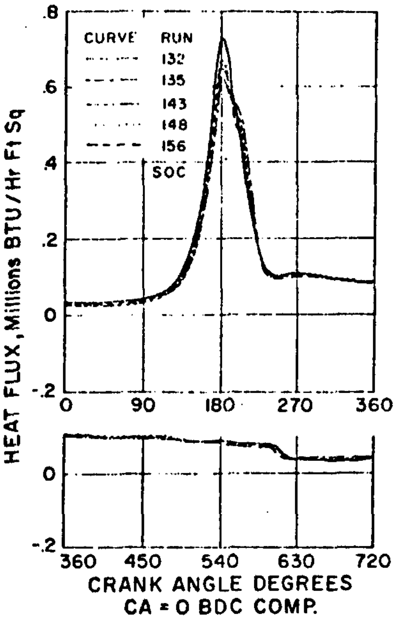

Fig. 5 Cyclic surface heat flux at TC-2 for several engine runs at the standard operating conditions.

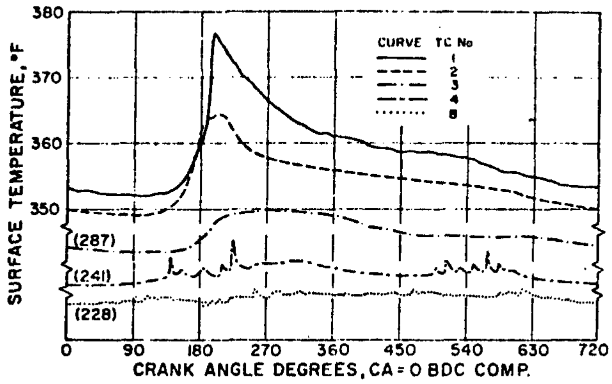

Fig. 6 Cyclic surface temperature at five locations in cylinder for SOC operation.

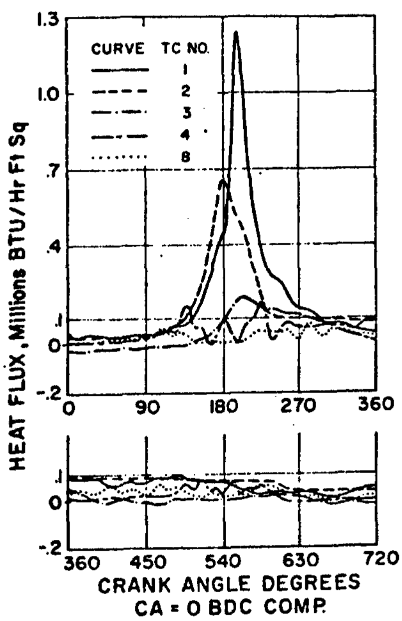

Fig. 7 Cyclic surface heat flux at five locations in cylinder for SOC operation.

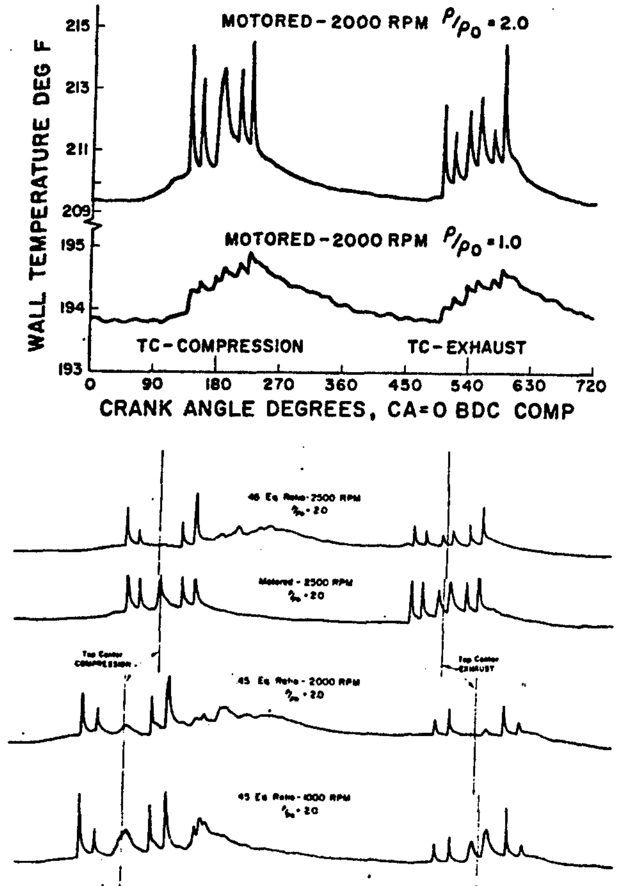

Fig. 8 Cyclic surface temperature-time records from TC-4 on cylinder sleeve.

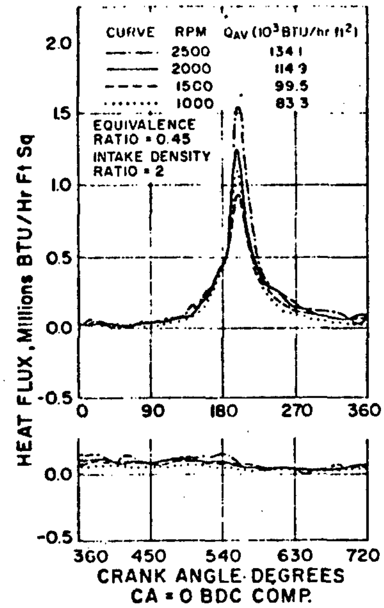

Fig. 9 Cyclic surface heat flux at TC-1 for fired operation at several engine speeds.

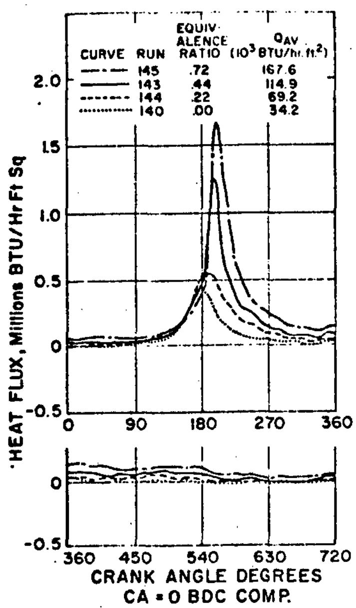

Fig. 10 Cyclic surface heat flux at TC-1 for fired operation at several equivalence ratios.

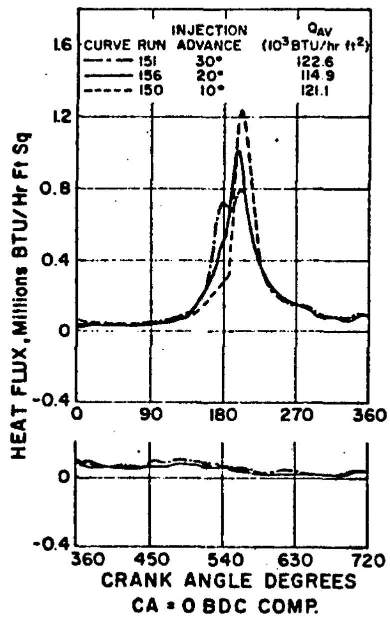

Fig. 11 Cyclic surface heat flux at TC-1 for fired operation at several injection timings.

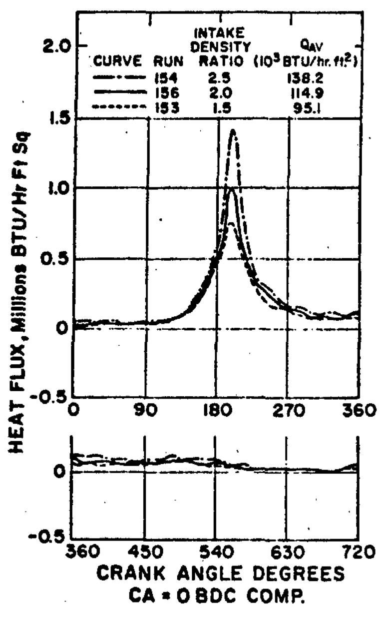

Fig. 12 Cyclic surface heat flux at TC-1 for fired operation at several intake density ratios.

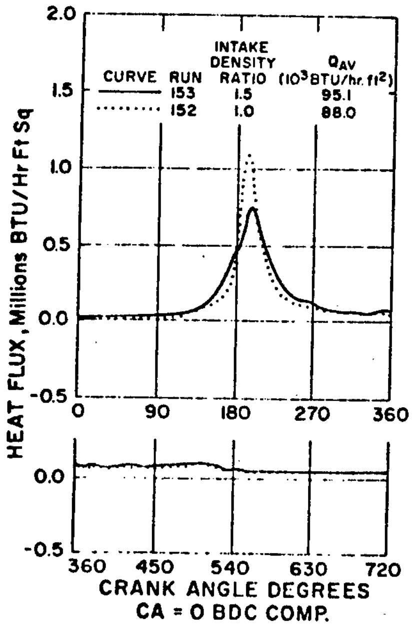

Fig. 13 Cyclic surface heat flux at TC-1 for fired operation at intake density ratios of 1.5 and 1.0 (that is, N.A.).

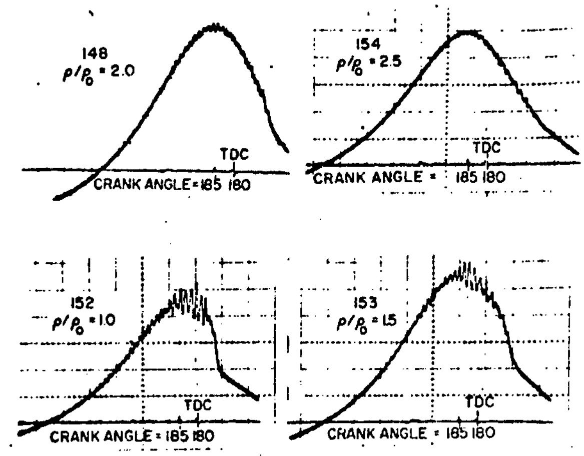

Fig. 14 Cylinder pressure-time diagrams for several intake density ratios. Note that crank angle increases from right to left for each photograph.

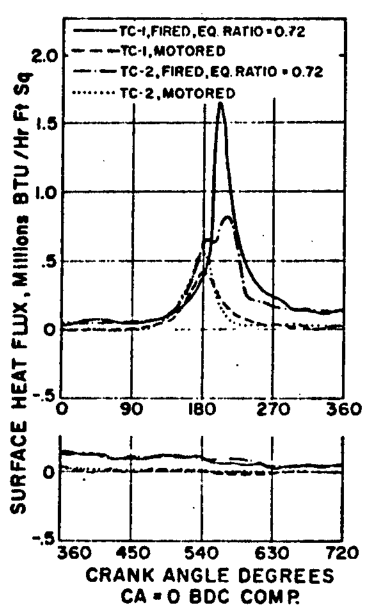

Fig. 15 Cyclic surface heat flux at TC's 1 and 2 for motored and fired operation.

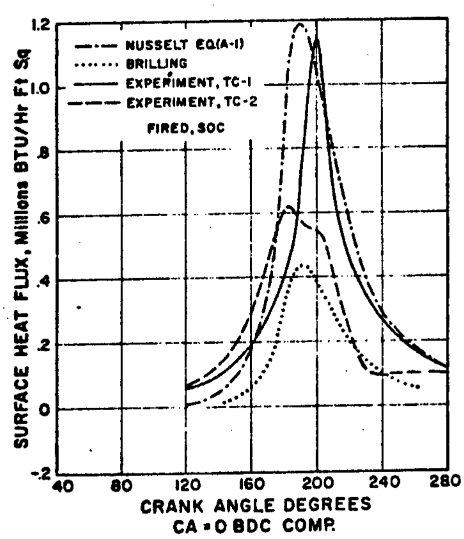

Fig. 16 Comparison of predictions of Nusselt and Brilling with experimental data from cylinder head for fired operation.

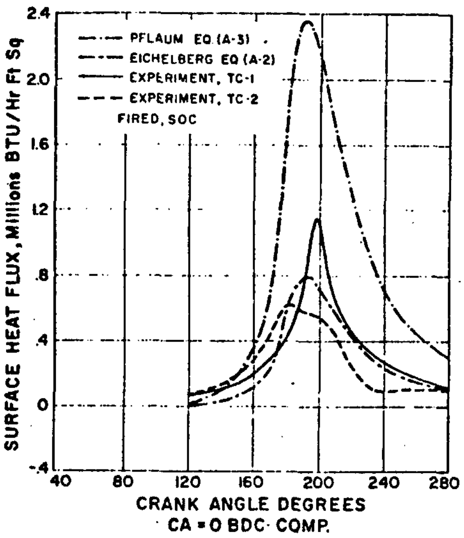

Fig. 17 Comparison of predictions of Eichelberg and Pflaum with the experimental data from cylinder head for fired operation.

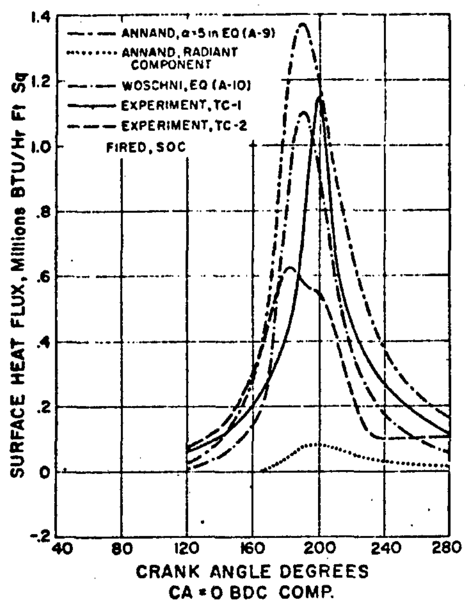

Fig. 18 Comparisons of predictions of Annand and Woschni with experimental data from cylinder head for fired operation.

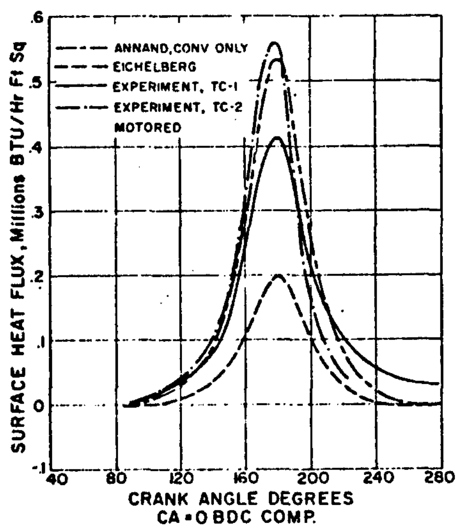

Fig. 19 Comparisons of predictions of Annand and Eichelberg with experimental data from cylinder head for motored operation.

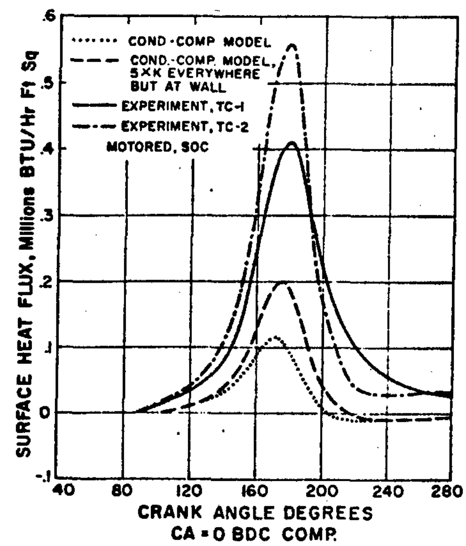

Fig. 20 Comparisons of the results from the conduction-compression model with experimental data for motored operation.

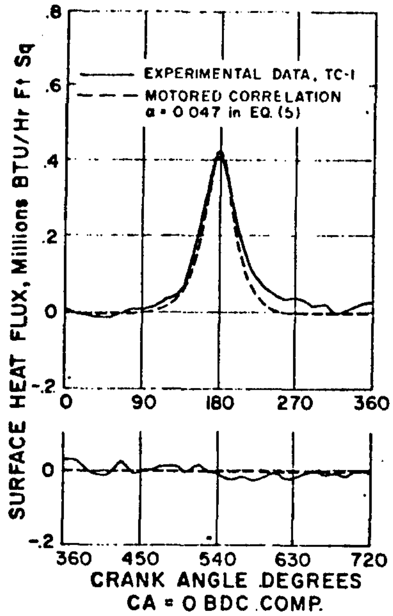

Fig. 21 Boundary layer model fit of motored (SOC) data at TC-1.

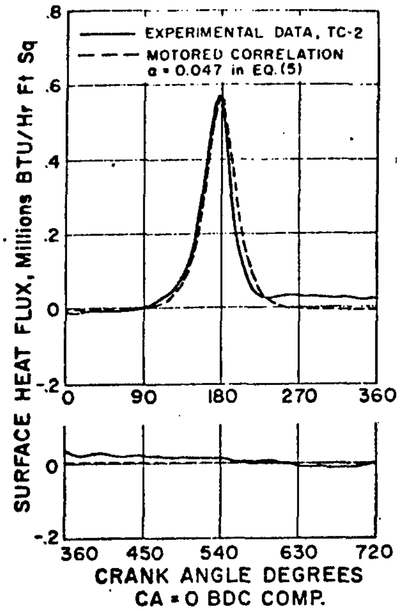

Fig. 22 Boundary layer model fit of motored (SOC) data at TC-2.

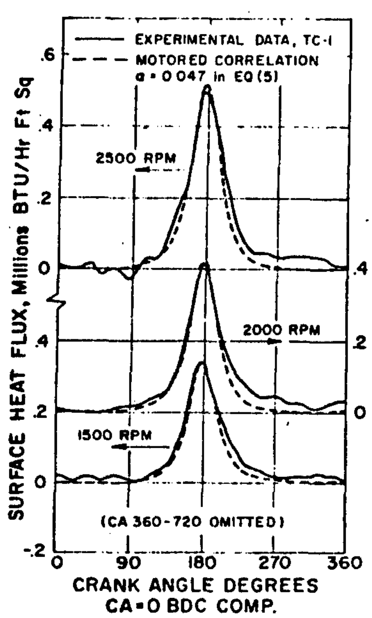

Fig. 23 Cyclic surface heat flux variation with speed for motored operation, comparison between experiment and boundary layer model of Eq. (5).

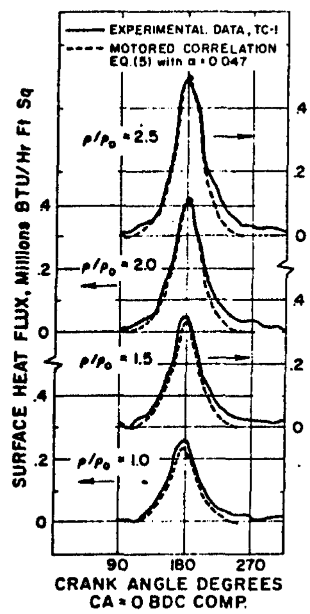

Fig. 24 Cyclic surface heat flux variation with intake density ratio for motored operation, comparisons between experiment and boundary layer model.

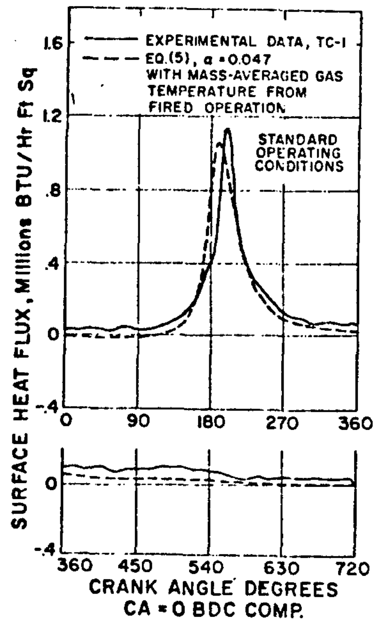

Fig. 25 Extension of motored correlation to fired operation (SOC), at TC-1.

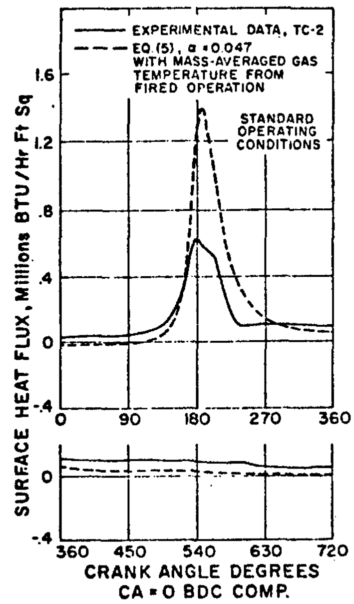

Fig. 26 Extension of motored correlation to fired operation (SOC), at TC-2.

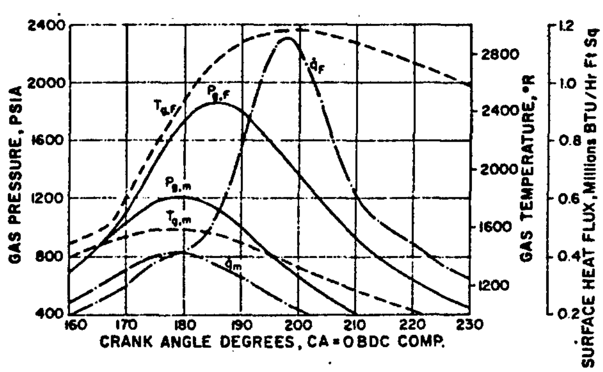

Fig. 27 Gas temperature and pressure, and heat flux at TC-1, for motored and fired operation.

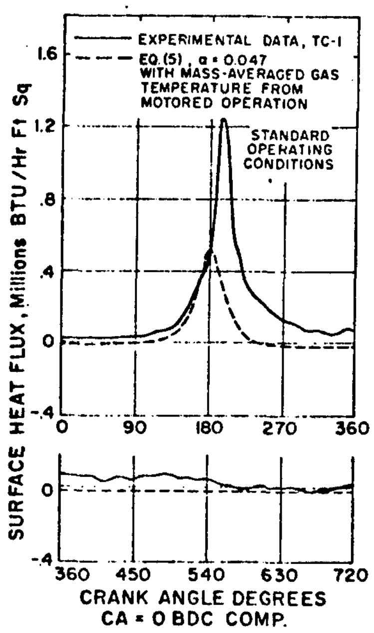

Fig. 28 Extension of motored correlation to fired operation (SOC) at TC-1 but with use of motored gas temperature.

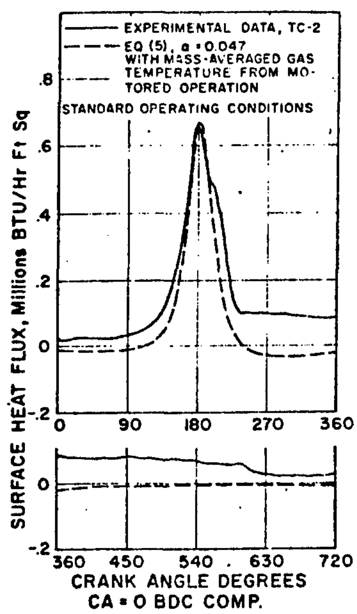

Fig. 29 Extension of motored correlation to fired operation (SOC) at TC-2 with use of motored gas temperature.

APPENDIX V

C

An Experimental Determination of the Instantaneous Potential Radiant Heat Transfer Within an Operating Diesel Engine

P. Flynn, Masatake Mizusawa, O.A. Uyehara and P.S. Myers
Mechanical Engineering Dept.
University of Wisconsin

ABSTRACT

An instrument was developed to measure absolute monochromatic infrared emission rates within an operating diesel engine. The instrument and data reduction system were developed for use in obtaining potential instantaneous rates of radiant heat transfer within an operating engine. Data are presented for variations of: engine speed, fuel-air ratio, fuel injection timing, intake air pressure, fuel injector nozzle spray patterns, fuel cetane numbers, fuel family, and fuel additives (tetra-eythl lead and amyl nitrate).

Also presented is an empirical correlation for instantaneous radiant heat transfer rates and some conclusions regarding radiant emission sources within the engine and their relationships to combustion processes.

INTRODUCTION

If designers are to increase engine performance while, at the same time, satisfying the needs of society for low air pollution and noise requirements, innovative forms of today's powerplant systems must be developed. Cycle simulations are playing an important role in such developments. However, if simulations are to predict engine characteristics accurately at conditions remote from those in a present-day engine system, the simulation must be based on widely applicable fundamental formulations of the basic thermodynamic and gas dynamic process involved.

With this goal in mind, the University of Wisconsin in cooperation with United States Army Tank-Automotive Command (USATAC) has carried out a research program to investigate basic phenomena which operate within a running engine. The subject of this presentation, radiation heat transfer, is one of many such studies (1-10).*

The information presented herein is the result of a three-phase program to study radiative heat transfer phenomena operating inside diesel combustion chambers. The first phase, involving the design of the experimental setup and the development of the system and technique for data analysis, was the responsibility of P.F. Flynn (11). The equipment and data reduction system was subsequently used by P.F. Flynn (11) and M. Mizusawa (12) to analyze the radiant emissions. Flynn focused upon the effect of engine operating variables, while Mizusawa dealt with the effect of fuel variables.

Heat transfer in engines has been investigated by many researchers. Eichelberg (13) and Pflaum (14) presented correlations for diesel engines which were based on engine thermocouple measurements. Neither author allowed for the effect of radiation except in an implicit manner. Correlations with explicit terms for radiant heat transfer were presented by Nusselt (15), Sitkei (16), Annand (17), and Woschni (18). These correlations, except in the case of Ref. 16, used the same mass-average gas temperature to correlate both radiant and convective heat transfer. Sitkei (16) used both a flame temperature and a gas temperature for his correlation for radiant transfer.

*Numbers in parentheses designate References at end of paper.

Ebersole (19) in the only published measurement of the apparent steady-state radiant contribution to total engine heat transfer, estimated that up to 40% of the heat transfer was by the radiation mechanism. Myers and Uyehara (20) and Lyn (21) demonstrated by optical means the existence of radiant temperatures much higher than the mean gas temperature within the engine. Myers and Uyehara (29) reported a study of flame temperature measured with an optical pyrometer when using different fuels.

Thus, previous experimental work presented no clear cut picture of the radiative heat transfer mechanism as it operates within a diesel engine. Recent data by LeFeuvre (6) have shown total instantaneous heat transfer rates within an operating engine. With these two facts in mind, the authors set out to obtain quantitative data on instantaneous radiant heat transfer rates in a diesel engine similar to the one used by LeFeuvre. It was hoped that this information, combined with LeFeuvre's results, would explain more clearly the relative importance of the radiative and convective heat transfer modes in a diesel engine. The data of LeFeuvre will be discussed in later comparisons with the data obtained in this study.

In summary, the authors undertook a study to fulfill the following goals:

1. Design and develop to a reliable state, a system for the determination of the potential rates of instantaneous radiant heat transfer* with a sensitivity high enough to determine the relative importance of the radiant heat transfer mode.

2. Obtain experimental data on potential instantaneous radiant heat transfer rates on a realistic diesel combustion system over a wide range of engine loads, speeds, and inlet manifold pressures for comparison with previously obtained data on total rates of heat transfer.

3. Determine the effect of variations in fuel structure, cetane rating, additive concentration, and additive type on the infrared emission within the combustion chamber.

4. Correlate the experimental data with pertinent engine parameters so that it might be used for analysis and predictions on other diesel combustion systems.

EXPERIMENTAL SETUP

RADIANT EMISSION MEASURING APPARATUS ... A complete description of the test engine and its associated instrumentation will be found in Ref. 11.

After a survey of the different methods of obtaining data on radiant heat transfer, a photodetector and infrared monochromator were chosen for intensity measurement and wavelength identification. The photoconductor sensor was chosen for its high frequency response and sensitivity. The choice of a photon counting device for a sensor necessitated the incorporation of the monochromator in the system to provide wavelength identification. Figures 1 and 2 show the modifications made to the engine and the layout of the optical system used.

Many attempts were made to develop a window viewing system which would remain clear of sooty combustion chamber deposits. After all attempts failed, the system shown in Fig. 1 was designed. Its unique feature is that it circumvented the need for keeping the combustion chamber window completely clean by the ability to change the combustion chamber window while the engine was operating at a loaded condition. This feature allowed the removal of the window from the engine and calibration of the transmissivity of the window and deposits.

---

*NOTE: The phrases potential rates of instantaneous radiant heat transfer and radiant emission rates are used interchangeably throughout this paper. The emission by the combustion chamber walls at a maximum temperature of 450 F (6), was insignificant compared to the combustion products emissions. Because of this fact, the portion of the radiant transport equations involving the wall emission has been dropped in all analysis presented. Potential radiant heat transfer rates are obtained by assuming emission of the intensity measured is input to the surface over the full hemispherical field of view available for any surface element.

Many attempts were made to develop a window viewing system which would remain clear of sooty combustion chamber deposits. After all attempts failed, the system shown in Fig. 1 was designed. Its unique feature is that is circumvented the need for keeping the combustion chamber window completely clean by the ability to change the combustion chamber window while the engine was operating at a loaded condition. This feature allowed the removal of the window from the engine and calibration of the transmissivity of the window and deposits.

Figure 2 shows the optical system that served as both a radiation detection system and a window transmission calibration system.

The movable mirror allowed the selection of radiation from either the engine or the calibration source. Also included in the system was a variable diameter iris to attenuate the radiant input to the monochromator. The optical system was designed such that the reduced images of the radiation viewing holes were imaged entirely between the edges of the entrance slit opening of the monochromator. This allowed clearance between the OD of the image and the edge of the entrance slit and rendered the system relatively insensitive to minor vibrations.

The wide ribbon tungsten filament lamp was calibrated for emission intensity versus wavelength against a black body radiation source. The emission from the lamp was modulated with a light chopper to supply the recurring zero level signal required for accurate calibration. Figure 3 illustrates the detector and cathode follower electronics used in the detection system. It also shows how a precision thermocouple potentiometer was connected to supply a stepping voltage of a precise known magnitude for use in measuring the amplitude of the chopper generated calibration lamp output.

A lead selenide photoconductor operating at room temperature was the active element in a half-bridge detection circuit. This element was sensitive over the 1-4 μm wavelength range investigated.

In order to obtain the instantaneous monochromatic emission intensity within the engine combustion chamber, the optical bench was set to view the combustion chamber emission at the desired wavelength. The signal from the photo-detector circuit was set at approximately 200 mV peak-to-peak by attenuating the image intensity with the variable diameter iris. Using these settings, approximately 250 consecutive cycles of the engine emissions were recorded together with a zero level input and a known voltage level for later data scaling purposes. When the recording process was completed, the petcock was immediately closed and a new window rotated into place. The window which had been used for data recording was then placed in the window which had been used for data recording was then placed in the window calibration block. Thus, the photodetector's response to the calibration lamp emission after passing through the window and deposits was measured without changing the monochromator or iris setting. The value of the absolute emission intensity at any time was then obtained by the following formula:

$$\text{Monochromatic emission intensity} = \frac{\text{detector response to engine signal}}{\text{detector response to lamp}} \text{(lamp intensity)}$$

DATA RECORDING AND REDUCTION ... The tape recorder and hybrid computer data scaling system used to record data were developed by LeFeuvre (6) but modified to meet the special needs of this project. Figure 4 shows the entire data acquisition and reduction system in block diagram form. The system may be logically divided into three subsystems which functioned independently of one another and used analog and digital data tape as data storage devices for interfacing the system.

The signal conditioning and recording system includes engine sensors to obtain signals for instantaneous emission intensity, cylinder pressure, crankshaft rotation, and crank top dead center (tdc) position. The signals from all of these sensors were conditioned so as to be compatible with the permissible ± 1 V d-c input to the FM tape recorder. Cylinder pressure was measured with a piezoelectric transducer and charge amplifier system. Crank rotation was sensed with a magnetic pickup responding to marks on the flywheel periphery every degree of crank rotation. The magnetic pickup output was conditioned with a high-frequency Schmidt trigger circuit which converted the output to a square wave pulse train with each rise separated by

1 deg of crank rotation. This square wave provided a more definite logic pulse for use in data sampling. The tdc position was sensed with a magnetic pickup whose response was recorded directly All signals were recorded using a Sangamo 4784 tape recorder at a tape speed of 120 in/s.

When scaling the data, the tape was played back at 7-1/2 in/s to a hybrid computer. Digital values were scaled at each degree of engine crankshaft rotation. Individual digital values were stored in 720 individual registers of the digital section of the hybrid computer (a description of this device, its accuracy, and the required analog and logic circuiting for scaling the data has been presented in Ref. 6). This scaling process continued for 50 consecutive cycles with the value at each crank angle being added to the appropriate accumulating register. After accumulating values for 50 cycles, the totals were divided by 50 to obtain average values at each time during the cycle. This digital listing was then printed and written on a digital magnetic tape for further analysis on a large-scale digital computer. The need for such a scaling and averaging technique is illustrated by Fig. 5, which shows approximately nine consecutive cycles of radiant emission versus crank rotation at 1 and 3 μm wavelengths.

In order to define the spectral emission envelope, seven wavelength values, (1, 1.5, 2, 2.5, 3, 3.5 and 4 μm) at each engine operating condition were chosen for data recording. These emission data plus pressure data were recorded in a consecutive manner on the digital data tape.

Emissivity - Wavelengths Models - To reduce the emission data further, it was necessary to develop a means of determining the total radiant energy represented by these seven distinct measurements. To illustrate the problem, Fig. 6 represents experimental values of average monochromatic emission intensity for three different crank positions during the cycle.

Since the emission was a continuous function of wavelength, integration over all wavelengths was required to obtain the entire energy under the spectral emission envelope. Thus, it was necessary to develop a means of interpolating between and extrapolating beyond the range of the data points. To accomplish this, various emission models were postulated and fit to the data.

The first model tested was a grey-body model. The fit to this and all subsequent models was made using a nonlinear least squares subroutine. This routine allowed the specification of the form of the emission model and then extracted by an iterative technique the parameters which provided the best fit to the experimental data. The attempt to fit a grey body emission model to the data provided a fitted curve with a consistent skew with regard to the data. Furthermore, the statistical output from the subroutine indicated an unreliable result.

Data by Hottel (22) and Liebert (23) indicate that emission from very small particles obey an emissivity variation described by:

$$\varepsilon_\lambda = 1 - e^{-kL/\lambda^{0.95}} \tag{1}$$

Attempts to fit an emission model incorporating the above wavelength variation of emissivity provided very good fits of the model to the experimental data as shown in Fig. 6. Also shown in Fig. 6 is the variation in monochromatic emissivity with wavelength for the fitted model.

The resulting parameters were the apparent radiant temperature (T_R) and the apparent optical thickness (KL) of the radiating medium. Thus, the information contained in seven monochromatic emission values at any given time was reduced to two parameters which could be used to represent the emission.

It is worthy to note that the data so obtained represent a temperature and optical thickness typical of average emission values and not a temperature and optical thickness which was the average of individual cycle temperatures and optical thicknesses. There may be differences between values obtained by these two types of averaging techniques; but since it was impossible to obtain data to accomplish averages in the latter manner, the difference could not be determined.

The above described technique was used to obtain an analytical representation of the emission as a function of wavelength. However, to evaluate the power represented by such an emission envelope, it was necessary to integrate this model over all wavelengths. Several unsuccessful attempts were made to obtain a closed form solution for the integral of this emission model. Consequently, the total heat transfer and the pseudo grey-body emissivity were evaluated using the following expression:

$$\varepsilon_a = \frac{\displaystyle\int_{0.5}^{10} \left(1-e^{-kL/\lambda^{0.95}}\right)\left(\frac{c_1}{\lambda^5\left(e^{c_2/\lambda T_R}-1\right)}\right)d\lambda}{\displaystyle\int_{0.5}^{10}\left(\frac{c_1}{\lambda^5\left(e^{c_2/\lambda T_R}-1\right)}\right)d\lambda} \tag{2}$$

and:

$$\dot{q}_R = \varepsilon_a \sigma T_R^{\,4} \tag{3}$$

The evaluation of the pseudo grey-body emissivity (ε_a) was accomplished numerically.

In summary, the data analysis technique allowed the extraction of an apparent radiant temperature, an apparent optical thickness, a pseudo grey-body emissivity, and a total potential radiant heat transfer rate at each crankangle during the cycle. These data, together with apparent heat release rate computed by the method of Kreiger (2), are presented in the following section for the engine conditions studies.

EXPERIMENTAL RESULTS

This section presents the time variation of selected parameters within the engine cycle when selected engine operating parameters were varied. The operating parameters varied for this group of tests included speed, fuel-air ratio, manifold pressure, injection timing, injection nozzle hole pattern, and fuels.

In the study of the effects of engine operating conditions, an attempt was made to vary each of the parameters one at a time while holding all others constant. For example, the tests at different speeds were run at approximately the same fuel-air ratio, nominal injection timing, and manifold pressure. All tests were run in groups containing a standard operating condition as a common point of reference. This standard operating condition (SOC) had 60 in Hg absolute manifold pressure, an equivalence ratio of 0.459, a 20 deg btdc nominal injection timing, and a 2000 rpm engine speed. Table 1 presents an abbreviated summary of the independent variables changed during the tests plus the estimate cetane rating for the fuel.

In the studies to determine the effect of fuel variations, tests were run with all engine operating conditions held constant and only the fuel characteristics varied. Table 2 summarizes the operating conditions and the fuel variations for those tests designed to determine the effect of fuel characteristics. The cetane numbers shown are estimated values.

REPEATABILITY OF DATA ... In order to establish the repeatability of the experimental data and the radiation heat release parameters determined from the analysis of the experimental data, two identical test runs (118 and 140) were made at SOC using a secondary reference fuel blend. Data from these two runs are presented in Fig. 7 showing that instantaneous potential heat transfer rates varied only slightly between the two runs. The time average potential radiant heat flux was also nearly identical for the two runs at about 25,850 Btu/h-ft^2. This time average rate is evaluated by integrating the area under the heat flux curve and then solving for the steady heat flux which, when applied over all 720 deg of crank rotation for an engine cycle, would yield the same integrated value.

Heat release rates are presented together with the radiation data, since it was felt that the information was significant in the presentation of the experimental data.

Note in Fig. 7 that the apparent potential radiant heat transfer rate has approximately the same shape and time span as the engine apparent heat release rate.

The peak magnitude of the radiant heat flux, 0.42 million Btu/h-ft^2, was a significant fraction of the total engine heat flux previously reported by LeFeuvre (6) which ranged from 0.9 million to 1.25 million Btu/h-ft^2. The radiant emission reached this high value through the combination of an apparent temperature of approximately 4100 R and an emissivity of approximately 0.86. The radiant temperature was 1.71 times higher than the calculated mean gas temperature of 2400 R.

In order to obtain data exhibiting the repeatability shown in Fig. 7, it was necessary to observe the following precautions:

1. The engine operating conditions must be maintained at a stable state during the entire data collection process. It was found that those data collected from runs when the engine was stopped or any other operating condition was varied between the collection of data at the various wavelengths, would not give repeatable or consistent results. However, data from runs where stable conditions were maintained showed the reproducibility and consistency of the data in Fig. 7.

2. The deposit thickness on the observation window could not be allowed to increase to a point where its transmittance was much below 0.7. If the transmittance of the window and deposit are allowed to deteriorate, radiation from outside the field of view normally accepted by the window can be reflected and diffracted by the window deposits into the instrument's field of view. This phenomena inflates the value of inferred in-cylinder radiant intensity. This relatively high overall transmittance requirement presented no particular problem, as the deposit buildup rate under all conditions tested was very slow after the engine operating conditions had stabilized. A more complete discussion of the above affects can be found in Refs. 11 and 12.

EFFECT OF SPEED ... Data shown in Fig. 8 present the radiation heat release parameter variation observed when the speed was varied holding all other factors constant. Note that the heat flux and heat release occur later as the speed increased. Also, a delay of between 4 and 6 deg CA occurred between the start of heat release and the start of significant emission. This same phase lag was noted between the peak heat release and the peak emission values.

The values of apparent temperature and optical thickness built up very rapidly. The maximum apparent temperature attained was again of the order of 4100 R except for the 2500 rpm run. Some of the variation in peak temperature and optical thickness values may have occurred because the 1000 rpm test (run 54) was inadvertently run with a equivalence ratio approximately 15% below the other three runs. The decay of the radiant heat flux rate, on a crankangle basis, was slower as speed was increased. This effect would be expected if one associated a more or less fixed time interval for combustion and carbon particle formation and destruction processes.

Two phases of radiant emission seemed to exist in Figs. 7 and 8 as well as in similar plots. The first phase, where relatively high emission values were attained, appeared to be associated with events pertaining to or caused by the rapid heat release rate combustion reactions. The second phase, occurring later in the expansion stroke, seemed associated with the portion of the combustion process occurring after most of the heat release had been completed.

The first phase of emission was characterized by relatively large constant values for the apparent flame optical thickness and high values of apparent temperature. One might speculate that the events controlling these values are the reaction kinetics and temperatures existing around the individual fuel droplets as they burned on in a very dense spray. It is believed that carbon particle production and destruction reactions would both be occurring at this time and that the emission noted would then be the result of some combination of these effects plus the corresponding reaction zone temperatures.

The second phase of emission occurred later in the cycle and was accompanied by an apparent increase in the net carbon particle concentration. To illustrate this, Fig. 9 presents a family of curves that indicates how the observed optical

thickness parameter varies as the piston changes position assuming a fixed mass of carbon particles of fixed size. Figure 9 assumes a fixed physical path length, that is, sighting across the bore.

When comparing the shape of the curve from run 84 with the family of plots in Fig. 9, it appears that the optical thickness was increasing during the initial portion of the second phase emission (390-440 CA). When the multislab model (which is described later) was used, it was concluded that this result could have been caused by at least two factors; an actual increase in the mass of carbon particles caused by net carbon particle formation, and a change in the relative temperatures of the carbon particles in the field of view in such a way as to cause a change in the apparent optical thickness.

Figure 8 shows large values for the apparent optical thickness and apparent emissivity at 540 deg atdc exhaust. These large values were caused by the relative instability of the model fitting technique at very low emission rates. When emission was low, a small amount of noise on any one of the monochromatic emission values caused a large percentage change in the residual sum of squares which results in relatively large shifts in the optical thickness and emissivity. This instability was exhibited only at very low emission rates and thus did not present a serious problem in the data analysis. This type of variation also appeared in the data for the equivalence ratio variation tests, and in the initial portion of some of the tests on fuel variables.

During the second phase of emission, the apparent temperature of the carbon particles was maintained at values that would infer some net energy addition to the particles as noted by comparing the temperature curve from run 84 with the family of temperature curves in Fig. 10. The family of temperature curves in Fig. 10 represents the temperature that should be observed if the combustion products were being adiabatically expanded, and the carbon particles being viewed were following that adiabatic expansion temperature. As can be noted by comparing the curves, the apparent radiant temperature decreased at a rate slower than that expected from from adiabatic expansion. This trend usually existed during the period between 390-450 CA.

The time-average heat flux rate increased as speed increased, but this rate of increase was not proportional to speed. This means that radiation losses should have a larger effect on engine efficiency at lower speeds, but that its effect would not be as the inverse relationship with speed that has been suggested.

EFFECT OF FUEL-AIR RATIO (FA) ... Plots of the radiation heat release parameter variations for different equivalence ratios are shown in Fig. 11. Note that the highest peak emission values were recorded during the lowest equivalence ratio run and the minimum peak emission values during the high equivalence ratio run. This result was entirely unexpected. If the apparent heat release rates for the runs are compared, it will be found that the peak heat release rates observed were almost directly proportional to the equivalence ratio. The combination of these two results was difficult to reconcile. From Fig. 11 one sees that the apparent radiating temperature was significantly lower for the high F/A run. One possible explanation is that there was an actual decrease in reaction zone temperatures caused by the higher overall F/A. A second possible explanation could have been the passage of carbon particles through the reaction zone in significant numbers followed by a subsequent cooling of the particles. These particles would then have masked the view of the hotter particles in the reaction zone. However, the apparent temperature for the high F/A run was lower even in the early part of the emission before one could justify the buildup of a cold carbon particle layer.

A third possibility for the lower emission at the high F/A is penetration of the fuel into the viewing access passage. Fuel droplets burning in this passage are relatively unaffected by the vigorous air swirl present in the main combustion chamber and might burn in a different rate or manner than those in the main chamber and thus have different heat losses.

The apparent time averaged radiant heat flux rate as a function of F/A appeared to increase with increasing F/A until some maximum value was reached, and then decreased sharply as the F/A was increased further.

There seemed to be little consistency in the optical thickness observed in the high emission portion of the curves. Although the values observed for each run were relatively constant during this phase, the level of the values could not be correlated with the overall F/A. The values of apparent optical thickness observed later in the cycle did seem to be directly related to the overall F/A, with runs having a higher F/A exhibiting a higher value for the apparent optical thickness. The same trends noted for the optical thickness were also noted in the apparent emissivity.

The same trends regarding the apparent buildup of carbon particles, and addition of heat to the carbon particles during the period between 390-450 deg CA were noted in these runs as they were in runs 54, 62, 70, and 84, with the possible exception of the low A/F run. During the low A/F run the observed rate of temperature decrease followed quite closely that which would have been expected with an adiabatic expansion. The apparent optical thickness also followed quite closely the trend that would have been predicted with a fixed mass basis carbon particle concentration.

The results of this series of tests indicated that there was no obvious direct correlation between the rate of radiant heat transfer and the rate of heat release. However, the previously noted trends with regard to the timing of the start of significant emission and the peak emission in comparison with the start of heat release and the peak heat release rate seemed to hold for these tests.

The high F/A run also produced a great deal of exhaust smoke. Whether this smoke production is directly related to the lower radiant emission values is unknown.

EFFECT OF MANIFOLD PRESSURE ... Figure 12 presents data where the inlet and exhaust manifold pressure were varied from 30-75 in Hg abs with the F/A, injection timing, engine speed, and inlet air temperatures all maintained constant. The characteristic shape of the heat release rate curve changed drastically in Fig. 12, as would have been expected when the manifold pressure was increased. The low manifold pressure run exhibited a heat release rate that started late as a result of a long ignition delay. The long delay period was followed by a high heat release rate which is normally associated with the combustion of the fuel and air mixture premixed during the delay period. However, this rapid heat release rate did not cause a significant amount of radiant emission. As Fig. 12 shows, the emission during the low manifold pressure run builds up at a rate only slightly faster than that noted for the runs at higher manifold pressure where much less premixed-type combustion occurs. This lack of radiant emission from the premixed portion of the combustion products is judged to be associated to the decreased tendency for carbon particle formation in premixed flames. Thus, even though very high local temperatures would have been expected in these premixed burning regions, they contributed little to the radiant heat transfer.

The two runs at the higher manifold pressure were characterized by heat release rates showing little or no premixed fast burning and subsequently followed the same trends noted in the earlier runs.

The peak radiation temperature for all three runs was again between 4000-4100 R. For the low manifold pressure run, the apparent temperature during the expansion stroke followed quite closely the trend which would be expected from expansion of the products of combustion. For the two runs at higher manifold pressures, the temperature again showed the effect of apparent heat addition to particles between 390 and 450 deg CA. The run at 75 in Hg manifold pressure indicated a larger amount of this late heat addition effect.

The data on apparent flame thickness indicated the same trend for an apparent increase in mass basis carbon particle concentration during the period between 390 and 450 deg CA for the 60 and 75 in Hg manifold pressure runs. Part of the differences in concentration level may have been associated with the variation in cylinder gas densities caused by changing the manifold pressures.

A comparison of the time average radiant heat transfer rate showed the rate at this F/A to be almost directly proportional to the manifold pressure with the value ranging from 14,893 Btu/h-ft^2 for run 98 to 28,441 Btu/h-ft^2 for run 91.

EFFECT OF INJECTION TIMING ... Data are presented in Fig. 13 for a series of tests in which all variables except fuel injection timing were held constant. The start of fuel injection ranged 10-30 deg btdc.

These variable injection advance runs were made using a blend of secondary reference fuels, and a nozzle with the hole pattern rotated 36 deg in the plan view, relative to the combustion chamber axis. However, the tssts run to ascertain the effects of manifold pressure, engine speed, and F/A were run using No. 2 diesel fuel and a nozzle having one hole which sprayed directly to the radiation viewing hole. It was felt that the change in injection nozzle and fuel for these tests should in no way invalidate them in terms of their comparison with each other, but caution is required when drawing comparisons between these runs and those runs in which the original nozzle (No. 1) and the No. 2 diesel fuel were used. The effect of the change in injection nozzle hole pattern is illustrated in the next section. The differences observed between runs using No. 2 diesel fuel and the secondary reference fuel are also reported in a following section.

The heat release rates shown in Fig. 13 illustrate that as the injection timing was increased beyond 20 deg btdc there was an accompnaying increase in ignition delay with a changed mode of combustion. The 30 deg btdc injection timing test was characterized by a significant amount of premixed combustion similar to that observed at low manifold pressure conditions. The radiant emission from this premixed flame portion of the heat release was negligible as it had been in run 98.

Comparison of the apparent temperature values showed that as the injection advance was increased the peak apparent temperature increased significantly. A peak temperature difference of approximately 600 R was observed between the 10 and 30 deg btdc injection timing runs. These temperature differences were originally thought to be explained by the difference in preflame gas temperature caused by the higher combustion pressure observed as injection was advanced. However, this explanation proved inadequate, as the predicted differences in preflame temperatures were only of the order of 300 R. An additional analysis was made to estimate the potential temperature variation in the products of combustion. The calculated variation in this temperature more nearly equaled the 600 R temperature differences observed. Because of the fourth power effect of temperature the peak emission rate for 30 deg injection timing was approximately 1.65 times the peak emission rate for 10 deg injection timing.

A comparison of time-average radiant heat transfer rates showed that the time-average radiant heat transfer rate increased from 23,498 to 31,466 Btu/h-ft^2 as the beginning of injection was advanced from 10 to 30 deg btdc.

The large changes in apparent temperature and apparent optical thickness between 360-400 deg CA for the 30 deg btdc injection timing is also of note. The authors feel that these apparent temperature decreases and optical thickness increases were the result of a portion of the fuel-air charge being trapped in the area of the piston that was removed to allow viewing access to the combustion chamber. It was thought that the fuel-air mixture trapped in this area was likely to burn at a slower rate and thus effectively block the instrument's view of the emission from the main portion of the combustion chamber. This effect would have been most pronounced during the time shortly after 360 deg CA for the 30 deg btdc injection timing run because the major portion of the combustion induced air motion had already taken place and the low piston velocity existing near tdc would not have been contributing to mixing of the air and fuel.

EFFECT OF NOZZLE HOLE PATTERN ROTATION ... Inspection of the carbon deposits on the piston after initial test runs indicated that one of the nozzle spray holes was pointed directly toward the passage which had been machined in the piston to gain viewing access to the combustion chamber. In order to determine the effect of this specific position of the nozzle spray pattern relative to the radiation viewing hole, a second nozzle with the hole pattern rotated 36 deg in the plan view was obtained. This second nozzle sprayed fuel such that the spray impinged on the combustion bowl on both sides of the viewing access hole. Figure 14 shows the relative positions of the nozzle spray patterns and the viewing hole for the nozzles used in these tests.

The data obtained from engine tests with these two nozzles are plotted in Fig. 15. As shown by Fig. 15 the fuel rate for the tests using the No. 1 nozzle was approximately 5% higher than that for the No. 2 nozzle.

The apparent temperatures observed were virtually equal for both nozzles, while the apparent optical thickness of the flame was slightly increased with the No. 2 nozzle. This difference in thickness was most important during the early portion of the emission where it caused an increase in the flame emissivity and a corresponding increase in potential radiant heat transfer.

Also of note was the relatively smaller increase in tha apparent optical thickness during the period between 390-430 deg CA when using the No. 2 nozzle. This change might have been associated with the fuel placed in the cavity formed by the viewing access hole, especially if that portion of the fuel was not completely burned and was left to participate in the carbon formation or combustion processes late in the burning period.

The observed difference in the time average radiant heat transfer rate was significant. The time average emission value obtained with the No. 2 nozzle was 27,531 Btu/h-ft^2 compared to a value of 22,957 Btu/h-ft^2 for the No. 1 nozzle. This difference represented a 20% increase in apparent radiant heat transfer for the case when the viewing hole looked between the sprays, compared to a 5% difference in fuel input rates.

EFFECT OF FUELS USED BY PREVIOUS INVESTIGATORS ... To obtain preliminary data on the effect of fuel structure and to enable comparisons to be made with other investigators who used different fuels, tests were run at the standard operating condition with three different fuels. The three fuels tested were:

1. Commercial No. 2 diesel fuel.
2. A blend of equal volumes of U9 and T16 secondary reference diesel test fuels.
3. Commercial grade normal heptane.

This combination of fuels was chosen because the authors felt that the most generally used commercial diesel fuel (No. 2 diesel) would yield results with the broadest practical application. At the same time a combination of the secondary reference fuels was chosen so that a comparison might be drawn between these data data and the data formerly obtained by LeFeuvre (6) when using secondary reference fuels. The third fuel, normal heptane, was chosen so that results from a fuel which could be duplicated at any time would be obtained and also to supply a correlation with results obtained by Ebersole (19) using normal heptane.

The data from these three fuels are presented in Fig. 16. Figure 16 shows that the heat release rate for the runs using the No. 2 fuel and the secondary reference fuel were nearly identical in shape. The heat release curve for the normal heptane differed slightly from the other two fuels in that it exhibited a slightly longer ignition delay and a very small amount of premixed burning associated with the fuel prepared to burn during the delay period. This increased ignition delay was interesting in light of the fact that the cetane number for normal heptane is 55, while the cetane ratings for the No. 2 diesel fuel and the secondary reference fuel were approximately 40 and 44, respectively.

As in previously reported results where an ignition delay was encountered, there was also a subsequent delay in the beginning of radiant emission. This late start, coupled with a temperature slightly below that observed for the No. 2 fuel and the secondary reference fuel, yielded a lower time averaged radiant heat transfer rate from the normal heptane.

The time average radiant heat transfer rate for the normal heptane run was 23,072 Btu/h-ft^2 compared to 27,531 Btu/h-ft^2 for the No. 2 diesel fuel. This result is in agreement with the result previously reported by Ebersole (19). He reported lower time average radiant heat transfer rates when using normal heptane as a fuel compared to those obtained using No. 2 diesel fuel.

EFFECT OF CETANE NUMBER VARIATION USING SECONDARY REFERENCE FUELS ... Data for this series and other series of runs in which fuel composition variables were studied are summarized in Table 2.

The effect of cetane number variation (for cetane numbers of 30, 40, and 50) on infrared emissions was measured under naturally aspirated and simulated turbocharged conditions at a speed of 2000 rpm, a beginning of fuel injection at 20 deg btdc, and an equivalence ratio of approximately 0.459.

The data for the runs made under naturally aspirated condition (Fig. 17) show there is an increase in ignition delay with decreasing cetane number. A significant decrease in peak radiant heat transfer rate was observed as the cetane number decreased. The peak rate for the 50 cetane fuel was 0.468 million Btu/h-ft^2 compared to 0.399 million Btu/h-ft^2 for the 40 cetane fuel, and 0.346 million Btu/h-ft^2 for the 30 cetane fuel.

Also of note is the tendency for larger values of kL as the cetane number increased and diffusion burning became more important. The magnitude of the differences in the kL parameters are larger than the percentage differences of heat transfer rates because of the nonlinear way in which kL enters the emission model. When the value kL goes above 4.0, further increase in kL becomes relatively unimportant because the overall emissivity has already begun to approach unity.

Again, the lack of any significant contribution to radiant heat transfer by the portion of the fuel that burns in a premixed mode is observed.

The peak cylinder pressures observed during the runs show a lower peak cylinder pressure at higher cetane number. This again indicates the lack of a relationship between the precombustion gas temperature and the final observed radiant temperature.

The time average radiant heat transfer rates followed the trends of the peak radiant heat transfer rates with the values ranging from 14,288 Btu/h-ft^2 for the 30 cetane fuel to 19,474 for the 50 cetane fuel.

Figure 18 presents data from a series of test runs at simulated turbocharged conditions. Note that the effect of the cetane number variations on the shape and timing of the heat release rate distribution is not nearly as significant as during the naturally aspirated runs. A smaller effect of cetane number differences on ignition delay under simulated turbocharged conditions was also noted in Fig. 16. The data indicate a higher peak radiant heat transfer rate for both the 30 cetane and 50 cetane fuel than the 40 cetane fuel (0.470, 0.479 and 0.430 million Btu/h-ft^2, respectively). Thus, cetane number variation by varying the relative percentage of the two secondary reference fuels used shows the lowest emission from fuel of mid-range.

EFFECT OF CETANE NUMBER VARIATION USING PARAFFIN FUELS ... Since the cetane number variation with the secondary reference fuels was obtained by changing the relative concentration of fuel components, an attempt was made to determine the effect of cetane number variation while keeping fuel character variations to a minimum. To accomplish this task, isooctane and normal heptane were chosen as the fuel constituents. Thus, the fuel cetane number was varied between 30 and 50 while maintaining the overall carbon to hydrogen atom ratio between 0.438-0.442. However, some of the physical characteristics of these fuels, such as viscosity and density, are quite different from those of normal diesel fuels. The effects of these variables on such significant parameters as fuel droplet size, spray penetration, and injection duration were beyond the scope of this study.

As Fig. 19 indicates, all runs for this group of paraffinic fuels showed a greater portion of the heat release occurring in the premixed flame mode than occurred with the blends of secondary reference fuels. The runs for the fuel of 40 and 50 cetane rating produced quite similar radiant heat transfer rate curves, while the run from the 30 cetane produced considerably lower values. The parameters which produced the same overall heat transfer rates for the 40 and 50 cetane runs were a higher temperature and lower kL value for one run and the converse for the other run. Also of note is the variation in kL value during the early portion of radiant emission; this is likely the result of signal nosie associated with low level signals as discussed with reference to Fig. 8.

EFFECTS OF FUEL FAMILY VARIATION AT FIXED CETANE NUMBER ...In order to determine the effect of fuel family characteristics at a given cetane number, three fuels were chosen, an aromatic, a paraffin, and an olefin.

Toluene was chosen as an aromatic fuel, isooctane as a paraffinic fuel, and isooctane as an olefinic fuel. To obtain a cetane number of 40, each of these fuels was modified by the addition of 50-58.7% by volume of normal heptane. Thus, these tests compare fuels having a common constitutent, normal heptane, with additions of the other hydrocarbon (HC) families. The carbon-to-hydrogen ratio for this series of fuels varied from 0.442 for the octane-heptane mixture to 0.608 for the toluene-heptane mixture.

Figure 20 portrays the results obtained from this series of runs. Some differences may be noted in the shape of the heat release curves and the ignition delay, even though an attempt was made to match cetane rating for the fuels. It is obvious that, although cetane rating as defined by a naturally aspirated engine test may be equal, the ignition delay can vary significantly under simulated turbocharged conditions. These variations in ignition delay may be part of the explanation for the lower radiant heat transfer rate of the isooctane-normal heptane blend. The increased ignition delay changes the entire pressure-time history encountered in the engine.

There was also a significantly higher heat transfer rate for the toluene-normal heptane combination as compared to the other two fuels. Since the observed radiant temperature histories were similar for the octane and toluene tests, the reasons for these differences can be associated with the larger value of kL obtained from the toluene-normal heptane fuel run. One explanation is that there is a significant increase in carbon particle concentration within the reaction zone as a result of the high carbon-to-hydrogen atom ratio of this fuel.

Aromatic fuels produce increased amounts of exhaust smoke in diesels. This observation agrees with the above conclusion and also with the fact the exhaust smoke values were measured to be higher with the toluene fuels.

EFFECT OF ADDITIVES CHOSEN TO GIVE SAME CETANE RATING ... Since tetraeythyl lead (TEL) and amyl nitrate are widely used additives for modifying the ignition character of fuels, a series of tests were run to determine their effect of radiant emission. To try to maintain constant overall combustion characteristics, secondary reference fuel blends were used with the addivites to give the same cetane numbers. Test data are shown in Fig. 18 for the undoped 30 and 50 cetane numbers blends in which the additives were used.

TEL was added to the 50 cetane blend to reduce its cetane rating to 40. Amyl nitrate was added to the 30 cetane blend to increase its cetane rating to 40.

Figure 21 shows the result of the radiant emission measurements. As the heat release rate curves indicate, the rate of burning for all three fuels was nearly identical. Thus, the variations in emission that were noted are likely the result of modifications of the reaction zone processes.

When comparing the data in Fig. 21 with that in Fig. 18, one notes that the addition of the amyl nitrate to the low cetane fuels brought about an increase in radiant transfer over that previously observed with the 30 cetane fuel. This increase was larger than the increase expected from a simple increase in cetane rating. Also, the addition of the TEL brought about a large decrease in the radiant heat transfer rate. This decrease in radiant heat transfer rate was also larger than that which would have been expected from the comparison of the 40 and 50 cetane curves in Fig. 18. Thus, it appears that the carbon and radiant emission aspects of the flame reaction are not directly controlled by the overall heat release rate.

COMPARISONS WITH OTHER INVESTIGATORS RESULTS

The tests in the first phase of this program were run at engine test conditions similar to those by LeFeuvre during his determination of total instantaneous heat transfer rates at various positions in the cylinder head and sleeve. Table 3 presents a summary of the results obtained by LeFeuvre and results obtained at the same conditions by the present authors.

Although the operating conditions used by LeFeuvre were maintained during these authors' tests, additional factors must be considered when comparing the results of the two sets of tests. Although the same engine was used, the combustion chamber bowl used for the radiation tests was considerably larger in diameter than that used for LeFeuvre's tests. Also the thermocouples used by LeFeuvre were all mounted in locations such that their view of the combustion chamber was completely obstructed during the period close to tdc when high values of radiant emission would have been expected. Since the hot running piston-to-head clearance for this engine was of the order of thousandths of an inch, LeFeuvre's data might not include a significant amount of the potential radiant heat transfer but they might, on the other hand, contain inflated values for the convective portion of the heat transfer.

Even with the above-mentioned difficulties, some interesting conclusions can be drawn from data comparisons. Under all operating conditions, the peak values for the radiant heat transfer were significant compared to the peak values of total heat transfer measured by LeFeuvre. The time-average values for the radiant heat transfer amounted to approximately 20% of the integrated time average values reported by LeFeuvre.

An additional interesting comparison with the data of LeFeuvre can be made by further analysis of the data for injection timing variations. Figure 22 presents data from LeFeuvre in which total heat transfer rates were measured as the injection timing was varied. The data have been replotted to the same scale used in Fig. 13 for the radiant emission data. When the corresponding curves for the various injection timings are compared, it appears that there is indication of a possible additive combination of radiative and conduction heat transfer effects. To depict this possibility more clearly, Fig. 23 presents a plot of the difference between the observed total heat flux of LeFeuvre and the potential radiant heat flux measured in this study, that is, if the data were directly comparable, the convective heat transfer. Note that during the high heat transfer rate portion of the curves there does appear a tendency towards a similar convective heat transfer rate. The major deviations occur during the time between 370 and 390 deg for the 30 deg btdc timing runs. As explained earlier, it is expected that the values of radiant heat transfer rate during this time period might have been attenuated by the viewing access passage. Thus, inflated values in the difference curve might be expected during this time.

The values obtained by this study appear at first not to substantiate the results obtained by Ebersole (19). Ebersole reported that radiant heat transfer should account for up to 40% of total diesel engine heat transfer at high F/A while this study yielded values for time average radiant heat transfer rates equivalent to approximately 20% of LeFeuvre's total heat transfer rates. Part of this difference might be explained by the differences in the combustion chambers employed by LeFeuvre and Ebersole, as well as their specific observation points in the combustion chamber. Ebersole's measurements were taken over the combustion bowl of a low-air-swirl, wide-bowl diesel combustion chamber. As a result of its placement, the sensor had full view of the combustion chamber during the period of the cycle in which high radiant emission would have been expected. Also because of the sensor's placement over the bowl, one would suspect that it was not subject to large combustion-induced gas velocities parallel to the head deck surface. This factor could have reduced the convective portion of the total heat transfer resulting in a higher percentage of the total heat transfer being caused by radiation. On the other hand, the placement of LeFeuvre's surface thermocouples was such that they were out of view of the bowl during the high emission period and they were subject to very high combustion-induced gas velocities parallel to the surface where the heat transfer was measured. Since the two factors mentioned regarding LeFeuvre's thermocouple placement caused opposing effects on the assessment of what portion of the total heat transfer was caused by radiation, no definite conclusion may be drawn with regard to this point.

ANALYSIS OF DATA

INTEGRATED EMISSION MODEL ..., As stated earlier, attempts to obtain a closed form solution for the integral of the emission model used proved unsuccessful. However, the analysis did suggest the following approximate function for ε_a which yields a closed form solution and pointed out the parameters to be used in an approximate evaluation. Changing the power to which λ was raised in the monochromatic emissivity expression to unity rather than 0.95 the following approximate expression for ε_a was obtained:

$$\varepsilon_a \approx 1 - \frac{c_1}{\sigma T_R^4} \int_0^\infty \frac{(e^{-kL/\lambda})\,d\lambda}{\lambda^5 (e^{c_2/\lambda T_R} - 1)} \tag{4}$$

Substituting

$$x = c_2/\lambda T_R \tag{5}$$

$$\beta = \frac{T_R kL}{c_2} \tag{6}$$

$$\varepsilon_a \approx 1 - \frac{1}{\sigma c_2^4} \int_0^\infty \frac{x^3 e^{-Bx}}{1 - e^{-x}}\,dx \tag{7}$$

Jolley (24) presented a solution to the above integral as follows:

$$\int_0^\infty \frac{x^3 e^{-\beta x}}{1 - e^{-x}}\,dx = \Gamma(4)\zeta(4,\beta) \tag{8}$$

Since $\Gamma(4)$ is equal to 6:

$$\varepsilon_a \approx 1 - \frac{6}{\sigma c_2^4}\,\zeta(4,\beta) \tag{9}$$

Therefore to a good approximation, emissivity is a unique function of the $T_R kL$ product. To check this result on the actual formula for ε_a used in the analysis, a numerical integration of the model was performed over the range of 0.5-10 μm. Values of temperatures between 2000-5000 R were used in conjunction with values of kL between 0.1 and 6.4. The data points plotted in Fig. 24 indicate that the actual ε_a of the model was essentially also a unique function of the $T_R kL$ product. Plotted along with the integrated data points is a function obtained with a least squares curve fit to the data points. The function was:

$$\begin{aligned}\varepsilon_a = -10.04 &+ 6.092\ln(T_R kL) - 1.360(\ln(T_R kL))^2 \\ &+ 0.1315(\ln(T_R kL))^3 - 0.004546(\ln(T_R kL))^4\end{aligned} \tag{10}$$

As can be noted in Fig. 26, this formula accurately describes the apparent grey-body emissivity of the model over the range of $T_R kL$ between 200 and 32,000.

Using the approximate solution for ε_a, the potential radiant heat transfer can be evaluated directly knowing values of T_R and kL.

POTENTIAL EMISSION SOURCES ... The experimental data obtained by this and other studies indicate very large variations in temperature must exist at times in the combustion chamber of a diesel engine due to stratification. Since the apparent temperature of the carbon particles was on the order of 4000 R while the mean (mass average) gas temperature was less than 3000 R, an analysis was made to determine whether the observed temperature and monochromatic emissivity variations could be used to infer a specific temperature and spatial distribution of the carbon particles.

Lyn (21) and Liebert (23) have presented data showing that the size of carbon particles in diffusion flames are of the order of magnitude of hundreds of angstroms in diameter. Analysis of particles of this size indicates that they would equilibrate thermally with the surroundings in less than 0.1 ms.

To test for any restraints the observed data might put upon the spatial carbon particle distributions, a 20 slab monodirectional flux* emission model was mechanized for solution on a digital computer. This model allowed the assignment of any arbitrary temperature and carbon particle distribution to the individual slabs and solved for the emitted monochromatic monodirectional fluxes. After analyzing several temperature and carbon particle distributions within the 20 slabs, it became evident that a great number of combinations of temperature and carbon particle distributions could be used to obtain the monochromatic intensity distribution emitted by the engine.

The analysis of the multislab model did indicate, however, that the range of combinations of T_R and kL values that were observed during the engine tests could be produced only by a grouping of the carbon particles in such a manner as to have an increasing temperature and a decreasing carbon particle concentration as one moved toward the observation point. This fact would indicate that the carbon must be formed on the cool fuel-rich side of the reaction zone and be consumed as it moves into the reaction zone with no significant concentrations of particles passing through the zone to the much cooler gases outside. This situation has been observed in laboratory diffusion flames (25).

Another point of interest was that the radiation emitted was of a continuous wavelength distribution with no absorption minima in the region of the 3.4 µm C-H stretching bond frequencies. Data presented by Lyn (21) also show this phenomena. This observation, combined with the slab analysis, indicates that during the high heat release diffusion burning period the radiant emission viewed by the instrument is that generated within one reaction zone thickness. Thus, the observations must represent events in the reaction zone interface between the fuel rich and oxidant rich portion of the combustion chamber space. This means that the radiating mass of burning fuel can be treated as a surface with the emission characterics measured by the instrument.

If this interface burning is the controlling factor in combustion chambers of turbocharged diesel engines, it appears that some rethinking and reanalysis of combustion processes and pollutant fixation processes must be done on the basis of diffusion reaction zone type models. Work by Tuteja (26) indicates a highly localized nitrogen fixation region in such diffusion flames.

If no accumulation of carbon particles occurs during the rapid heat release portion of the burning around the exterior of the burning fuel mass, one is forced to conclude that the carbon appearing in the engine exhaust as smoke must be associated with a leftover unburned fraction that has been trapped during the expansion stroke and thus not allowed to react before the temperatures become so low as to prohibit completion of combustion. Breaking of the flame surface could also result in unburned carbon particles.

A correlation between exhaust smoke and kL values occurring late in the expansion stroke seems logical and was observed in preliminary data. However, exhaust opacity levels and combustion chamber radiation signal levels were both relatively low. Thus, no detailed analysis was attempted.

TIME VARIATION OF APPARENT RADIATING TEMPERATURE ... The variation of the apparent radiant temperature with crank rotation is plotted in Fig. 25. Along with this plot are two other curves. One curve indicates the adiabatic compression temperature assuming compression of pure air from the engine manifold condition. It is apparent that the observed variations in the radiant temperature are of a larger magnitude than the variation expected due to the pre-reaction compression of the combustion air. The second curve was obtained by multiplying the adiabatic compression temperature value by a constant such that a value equivalent to the apparent radiant temperature was obtained at 360 deg crank position. This curve represents the potential temperature variation of a fictitious packet of the products of combustion with

*Even though this attenuated monodirection flux method was not exact in terms of actual heat flux calculations, it does represent closely the situation as observed in the engine. This agreement was caused by the fact that the engine instrumentation accepted only a monodirectional beam with a small divergence. Thus, the off-normal-incidence radiation which causes the errors in the overall heat flux calculation was not present in either the engine measurements or the analysis.

subsequent adiabatic compression and expansion caused by the combustion chamber pressure variations. This variation more nearly describes the instantaneous variation in apparent radiant temperature.

Since an extensive analysis of the data uncovered no basic method for obtaining values of apparent radiant temperature and optical thicknesses as a function of time during the engine cycle, the authors were forced to resort to an empirical correlation of the observed data with the engine operating variables.

EMPIRICAL DATA CORRELATION ... As stated earlier, the potential radiant heat transfer rate as a function of time during the engine cycle exhibited a shape and duration similar to that noted for heat release distributions. With this fact in mind the authors chose to use the Wiebe function (27,28) for a correlation function to describe the potential radiant heat transfer rate as a function of time.

This Weibe function takes the form:

$$\dot{q}_R = \frac{(\bar{q}_R)(720)}{\Delta t} (b)(a+1)\left(\frac{t-t_1}{\Delta t}\right)^a \exp\left[-b\left(\frac{t-t_1}{\Delta t}\right)^{a+1}\right] \tag{11}$$

Several of the terms in Eq. 11 which had previously been assigned a physical significance in the heat release analysis no longer have such a physical significance. The Weibe function as used here serves only as a distribution function with the shape desired for correlation. The combination of t_1, Δt, and t serve to yield a normalized time function within the duration of the radiant heat transfer. The a and b parameters, which previously had been associated with the combustion efficiency and shape of heat release curves, have become arbitrary shape factors. The product of ($\bar{q}_R$ x 720) was equivalent to the area under the curve representing $\dot{q}_R$ as a function of crankangle. Thus, it established the size of the area block that was to be distributed by the Weibe function. For heat release analysis, this area corresponded to the total fuel energy input per cycle, but it has no such physical significance in the heat transfer correlation.

To fit the Weibe function, it was necessary to correlate five parameters ($\bar{q}_R, a, b, t_1, \Delta t$) with engine operating variables. The correlation of $\bar{q}_R$ had already been obtained from an analysis of the instantaneous heat transfer rate data. To obtain the other parameters, the nonlinear least squares model fitting technique was again used. The emission versus crank rotation curves were represented by 39 equally spaced ordinate points located at 5 deg intervals from 15 deg btdc to bdc. Initial attempts extracted the four remaining parameters from the data, but the statistical output from the subroutine indicated that only two parameters were needed for the correlation. To utilize only two parameters, the start of emission was fixed at the experimental start of emission and correlated outside the fitting subroutine. The duration (Δt) was also fixed at 360 deg as it was shown to be the least important of the model parameters and the experimental data had shown no cases in which the duration of emission was more than 360 deg of crank rotation.

An additional problem with a unified data representation was the fact that there had been a change in nozzle hole pattern between runs. Since this change yielded higher emission rates for the later runs, it was necessary to multiply the values of $\bar{q}_R$ for the runs in which intake manifold pressure and A/F were varied by a factor of 1.11 to bring them into relative agreement with the later runs.

After doing this, the parameter values from all runs were fit with an interpolation formula including first and second order terms in each of the independent variables used in the test runs. The formulas so obtained are:

$$\begin{aligned}\bar{q}_R = {} & 27070 + 2.603(S_R-1995) - 0.005893(S_R-1995)^2 + 291.9(p_m-59.8) \\ & - 1.44(p_m-59.8)^2 + 401.1(t_{in}-20) + 4.620(t_{in}-20)^2 \\ & + 26270(F-0.459) - 101200(F-0.459)^2 + f(r_c) + f(T_m)\end{aligned} \tag{12}$$

$$a = 0.3835 - 0.00008177(S_R-1995)(+ 0.000000592(S_R-1995)^2$$
$$- 0.002146(p_m-59.8) + 0.0001565(p_m-59.8)^2 -$$
$$- 0.03017(t_{in}-20) + 0.00009224(t_{in}-20)^2$$
$$- 0.5037(F-0.459) + 0.6062(F-0.459)^2$$
$$+ f(r_c) + f(T_m) \tag{13}$$

$$b = 21.54 - 0.01513(S_R-1995) + 0.00003804(S_R-1995)^2 - 0.8576(p_m-59.8)$$
$$+ 0.0454(p_m-59.8)^2 - 1.396(t_{in}-20) + 0.0216(t_{in}-20)^2$$
$$- 145.5(F-0.459) + 328.5(F-0.459)^2 + f(r_c) + f(T_m) \tag{14}$$

$$t_1 = 349.7 + 0.004131(S_R-1995) + 0.0000000001992(S_R-1995)^2$$
$$- 0.1395(p_m-59.8) + 0.0001565(p_m-59.8)^2$$
$$- 0.5258(t_{in}-20) + 0.01022(t_{in}-20)^2$$
$$- 8.309(F-0.459) + 3.345(F-0.459)^2$$
$$+ f(r_c) + f(T_m) \tag{15}$$

Combining these parameters:

$$\dot{q}_R = (2\bar{q}_R)(b)(a+1)\left(\frac{t-t_1}{360}\right)^a \exp\left[-b\left(\frac{t-t_1}{360}\right)^{a+1}\right] \tag{16}$$

Thus the interpolation formulas and the correlation function allow the generation of an approximate potential radiant heat transfer rate as a function of time during the cycle.

Figures 26-29 show the correlation function generated by using the test conditions as independent variables in the interpolation formulas. A comparison of these figures with the corresponding figures for the experimentally measured data indicate that the correlation does indeed present a function with trends similar to that exhibited by the experimental data. The major deviance of the correlations from the experimental curves occurs when experimental curves possessed two humps. Since the correlation function was incapable of generating this shape, these characteristics are shown only implicitly in the overall shape and width of the correlation function. This was judged to be adequate since there was no assurance that this intermediate dip was not caused by the changes in the system introduced for viewing access, and the incorporation of enough parameters to generate such a two-humped curve would have made the correlation function very cumbersome.

To obtain an estimate for the radiant heat losses from the products of combustion, one need only to estimate the size and location of the flame as a function of time during the cycle and assign values for the area and absorptivity to each of the parts of the combustion chamber structure.

Figure 30 shows the results of a sample calculation using the correlation formulas. Plotted are the rate of radiant heat transfer to the cylinder head surface, the piston surface, and the cylinder sleeve.

To generate these values the flame was assumed to extend throughout the combustion chamber. The absorptivity of the head and piston top were assumed to be 0.85, and the absorptivity of the sleeve to be 0.2. The effective area of the cylinder head was assumed to be the plan area of the engine bore. The effective piston area was assumed to be 115% of cylinder head area and the sleeve area was considered to be that area exposed above the piston top at any instant. Note the very low values of radiative heat transfer for the sleeve caused by the fact that little sleeve area is exposed during period of high emission.

One will note that the correlation functions include terms for changes caused by intake air temperature changes and compression ratio changes. Although the test setup used would not allow the variation of these two parameters, it appeared from a review of the results that these two parameters could have significant effects on the radiant emission. Thus, they were included as a warning.

SUMMARY AND CONCLUSIONS

This study has demonstrated the capability of the infrared detection system developed. The system was used to obtain a large amount of data on an operating engine. Approximately 15 million data points were collected by the system and used in subsequent scaling, digital averaging, and analysis.

Analysis of the data obtained indicated that the radiant emission from the combustion chamber of a diesel engine was well described by a small particle model.

Engine data were collected over a wide range of engine loads, speeds, intake air pressures, and fuel injection timings. Data were also obtained with different fuels and fuel additives.

The engine observations show radiant emission from the combustion process within a diesel engine to be significant. Radiant temperatures as high as 4311 R were observed. The optical thickness kL during the period of high emission rate was observed to rise to near 6.0, yielding an emission nearly equivalent to that of a black body at the radiant temperature. These combinations of high radiant temperature and large optical thickness yielded peak emission rates up to 0.52 million Btu/h-ft^2. The apparent time-averaged radiant heat transfer rate was found to increase with increased inlet manifold air pressure at a fixed F/A. This increase was at a rate nearly directly proportional to the manifold pressure. Data taken from runs where injection timing was varied showed a large increase in emission rates as the injection timing was advanced. This increase in radiant emission appeared to be associated with corresponding changes in the engine cycle temperature history.

Data from runs in which engine speed was varied yielded increasing apparent time-averaged rates of radiant heat transfer as the engine speed was increased up to 2000 rpm. Above this speed the emission rate ceased to increase. Tests varying the F/A while holding other variables constant indicated a sharp rise in emission as the F/A was increased to an equivalence ratio of 0.514. At an equivalence ratio above 0.514 the emission rate was observed to drop sharply. Tests with No. 2 diesel fuel and a 50/50 blend of secondary reference diesel fuels yielded nearly equivalent emission rates, while a test run with normal heptane produced lower emission rates, as had been previously shown by Ebersole (19).

Rotation of the nozzle hole pattern relative to the viewing access port indicated that observed emission rates were higher when no fuel was deliberately directed into the viewing port hole. Tests in which significant portions of the fuel injected was burned after a sizeable ignition delay (presumably in a partially premixed mode) demonstrated the lack of carbon particle formation in such flames and the corresponding lack of carbon particle formation in such flames and the corresponding lack of infrared emission from such flames.

Fuel cetane number variations using secondary reference fuels were found to yield the expected trends in ignition delay under naturally aspirated conditions with these effects being attenuated to a great degree at simualted turbocharged conditions. Radiant heat transfer rates were found to decrease with decreasing cetane number under naturally aspirated conditions. This same trend was not evident under simulated turbocharged conditions.

Changes in cetane rating by variation of the percentage of isooctane and normal heptane in a fuel mixture yielded similar radiant emission rates for the 40 and 50 cetane blends and lower emission rates for a 30 cetane blend.

Tests run at the same cetane rating with fuel containing blends of toluene, isooctane, and isooctene with normal heptane showed larger radiant emission rates from the toluene blend as well as increases in exhaust smoke opacity. These tests also showed a considerable variation in ignition delay with fuel of the same nominal cetane rating.

The addition of amyl nitrate to a secondary reference fuel blend caused an increase in the radiant heat transfer rate beyond that expected from the change in fuel cetane rating. Addition of TEL caused larger decreases in radiant heat transfer rate than would have been expected with simple cetane number changes resulting from variation of secondary reference fuel blends.

An empirical function for the instantaneous radiant emission was fitted to the engine observations using a form similar to the Wiebe function used for heat release rate correlation. The correlation function was as follows:

$$\dot{q}_R = (2\bar{q}_R)(b)(a+1)\left(\frac{t-t_1}{360}\right)^{a} \exp\left[\left(\frac{t-t_1}{360}\right)^{a+1}\right]$$

The values for the $\bar{q}_R$, a, b, and t_1 parameters were fitted to second order interpolation functions in the test parameter spaces. Parameters which were included in the interpolation formulas included: engine speed, inlet manifold pressure, fuel-air equivalence ratio, and fuel injection timing. Also included in the formulas for the sake of completeness were terms for inlet air temperature and engine compression ratio since the analysis of the data indicated the potential singificance of these two terms even though the engine test hardware would not allow the explicit evaluation of their effects.

NOMENCLATURE

ε_λ = monochromatic emissivity

k = absorption coefficient/unit path length

L = path length

λ = wavelength

T_R = radiant temperature, R

ε_a = pseudo grey-body emissivity as defined by Eq. 2

C_1, C_2 = constants in Planck's radiation equation

σ = Stefan-Boltzman constant

$\dot{q}_R$ = radiant heat flux, Btu/h-ft^2

$\Gamma(4)$ = gamma function

$\zeta(4,\beta)$ = compound zeta function

$\bar{q}_R$ = time average radiant heat transfer, Btu/h-ft^2

b = shape modulation factor

a = shape modulation factor

t = time during cycle for which $\dot{q}_R$ is being calculated expressed as crankangle degrees

t_1 = time of start of radiant heat transfer, crankangle deg

Δt = duration of radiant heat transfer, crankangle deg

$\exp^{[\,]} = e^{[\,]}$

S_R = engine speed, rpm

p_m = manifold pressure, in Hg abs

t_{in} = beginning of fuel injection, crankangle deg btdc

F = fuel-air equivalence ratio, actual fuel-air/stoichiometric fuel-air

$f(r_c)$ = unevaluated function of compression ratio

$f(T_m)$ = unevaluated function of inlet air temperature

ACKNOWLEDGMENT

The authors would like to acknowledge the support of the U.S. Army Tank-Automotive Command throughout this work. Additional thanks go to Cummins Engine Co., Caterpillar Tractor Co., Komatsu, Ltd., and International Harvester Co. for the contribution of financial aid and supplies contributing to the completion of this study.

REFERENCES

1. K.J. McAulay, Tang Wu, Simon K. Chen, G.L. Borman, P.S. Myers and O.A. Uyehara, "Development and Evaluation of the Simulation of the Compression-Ignition Engine." SAE Transactions, Vol. 74 (1966) paper 650451.

2. R.E. Krieger and G.L. Borman, "The Computation of Apparent Heat Release for Internal Combustion Engines." ASME Publication 66-SA/DGP-4, 1966.

3. H.G. Weber and G.L. Borman, "Parametric Studies Using a Mathematically Simulated Diesel Engine Cycle." SAE Transactions, Vol. 76, paper 670480.

4. M. Goyal, Glen Scharpf, and G. Borman, "The Simulation of Single Cylinder Intake and Exhaust Systems." SAE Transactions, Vol. 76, paper 670478.

5. D.N. Kapadia and G.L. Borman, "The Effect of Heat Transfer on the Steady Flow Through a Poppet Valve." SAE Transactions, Vol. 76, paper 670479.

6. T. LeFeuvre, "Instantaneous Metal Temperatures and Heat Fluxes in a Diesel Engine." PhD thesis, Mechanical Engineering Department, University of Wisconsin, 1967.

7. John Shipinski, O.A. Uyehara, and P.S. Myers, "Experimental Correlation Between Rate-of-Injection and Rate-of-Heat-Release in a Diesel Engine." ASME Publication 68-DGP-11, 1968.

8. T. LeFeuvre, P.S. Myers, and O.A. Uyehara, "A Tape Recording and Computer Processing System for Instataneous Engine Data." SAE Transactions, Vol. 77 (1968) paper 680133.

9. J. Shipinski, P.S. Myers, and O.A. Uyehara, "A Spray-Droplet Model for Diesel Combustion." Proceedings of the Institution of Mechanical Engineers, 1969.

10. Bruce D. Peters and Gary L. Borman, "Cyclic Variations and Average Burning Rates in a S.I. Engine." Paper 700064 presented at SAE Automotive Engineering Congress, Detroit, January 1970.

11. P.F. Flynn, "An Experimental Determination of the Instantaneous Potential Radiant Heat Transfer Within an Operating Diesel Engine." PhD thesis, Mechanical Engineering Dept., University of Wisconsin, 1971.

12. M. Mizusawa, "Relationship Between Cetane Numbers of Fuel and Radiant Heat Transfer in a Diesel Engine." MS thesis, Mechanical Engineering, University of Wisconsin, 1972.

13. G. Eichelberg, "Some New Investigations on Old Combustion-Engine Problem." Engineering, Vol. 148, (1959), p. 139.

14. W. Pflaum, "Heat Transfer in Internal Combustion Engines." Paper presented at Conferenzia Internazionale di Termolernica, Milan, Italy, November 1962.

15. W. Nusselt, "Die Warmeubergang in Der Verbrennungskraftmaschine." V.D.I. Forschungshaft, No. 264 (1923).

16. G. Sitkei, "Contribution to the Theory of Heat Transfer in the Internal Combustion Engine." Translated from Konstruktion, Vol. 14 (1962), pp. 67-71.
17. W.J.D. Annand, "Heat Transfer in the Cylinders of Reciprocating Internal Combustion Engines." Proceedings Institute of Mechanical Engineers, Vol. 177, No. 36 (1963), p. 973.
18.. G. Woschni, "A Universally Applicable Equation for the Instantaneous Heat Transfer Coefficient in the Internal Combustion Engine." SAE Transactions, Vol. 76 paper 670931.
19. G.D. Ebersole, P.S. Myers, and O.A. Uyehara, "The Radiant and Convective Components of Diesel Engine Heat Transfer." Paper 701C presented at SAE Summer Meeting, Montreal, June 1963.
20. P.S. Myers, O.A. Uyehara, L.A. Wilson, and K.M. Watson, "Flame Temperature Measurements in Internal Combustion Engines." ASME Transaction, Vol. 68 (1946) pp. 17-30.
21. W.T. Lyn, "Diesel Combustion Study by Infra-Red Emission Spectroscopy." J. of the Institute of Petroleum. Vol. 43 (1957), pp. 25-46.
22. H.C. Hottel and F.P. Broughton, "Determination of True Flame Temperature and Total Radiation From Luminous Gas Flames." Industrial and Engineering Chemistry Analytical Edition, Vol. 41932, pp. 166-175.
23. C.H. Liebert and R.R. Hibbard, "Spectral Emittance of Soot." NASA Technical Note, NASA TN D-5647, 1970.
24. L.B.W. Jolley, "Summation of Series." New York: Dover Publication Inc., 1961, pp. 212-213.
25. R.S. Brokaw and M. Genstien, "Basic Considerations in Combustion of Hydrocarbon Fuels With Air." NACA Report 1300, 1959, p. 211.
26. A.D. Tuteja, H.K. Newhall, "Nitric Oxide Formation in Laminar Flames." General Motors Research Laboratories Symposium, September 1971.
27. J.H. Shipinski, "Relationships Between Rate-of Injection and Rate-of-Heat Release in Diesel Engines." PhD thesis, Mechanical Engineering Department, University of Wisconsin, 1967.
28. E. Streit, "Mathematical Simulation of a Large Pulse-Turbocharged Two-Cycle Diesel Engine." PhD thesis, Mechanical Engineering Department, University of Wisconsin, 1970.
29. P.S. Myers and O.A. Uyehara, "Diesel Combustion Temperature Influence of Fuels of Selected Composition." SAE Transactions, Vol. 48 (1949) pp. 178-187.

Table 1 - Summary of Engine Parameters when Operating Variables were Studied

Run	Rpm	Manifold Pressure, in Hg abs	Equivalence Ratio	Injection Advance deg CA btdc	Fuel	Nozzle	Cetane No.
20	2000	59.8	0.514	20	No. 2D	No. 1**	40
27	2010	60.2	0.230	20	No. 2D	No. 1	40.
54	1010	60.7	0.398	20	No. 2D	No. 1	40
62	1505	59.9	0.469	20	No. 2D	No. 1	40
70	2490	60.0	0.463	20	No. 2D	No. 1	40
77	2000	59.6	0.749	20	No. 2D	No. 1	40
84	1995	59.8	0.459	20	No. 2D	No. 1	40
91	2005	75.4	0.469	20	No. 2D	No. 1	40
98	1995	30.1	0.438	20	No. 2D	No. 1	40
111	2005	60.2	0.455	20	No. 2D	No. 2	40
118	2005	59.7	0.439	20	50/50 SRF*	No. 2	44
125	1995	59.9	0.455	30	50/50 SRF	No. 2	44
132	1995	59.9	0.457	10	50/50 SRF	No. 2	44
140	1980	60.4	0.434	20	50/50 SRF	No. 2	44
148	2000	60.3	0.445	20	N-Heptane	No. 2	55

*50/50 SRF specifies equal volumes of U9 and T16 secondary reference diesel.
**Refer to Fig. 14 for difference between No. 1 and No. 2 nozzle spray patterns.
NOTE: Intake manifold air temperature was maintained at 100 F for all runs reported in this study.

Table 2 - Engine Parameters and Fuel Specification

Run No.	Inlet Pressure, in Hg abs	Fuel	Cetane No.	Volume, %	Equivalent Formula
M26 M130	60.6 30.5	SRF (T16 + U9)	30	18.2 (T16)	C_nH_{2n}
M119 M159	60.2 30.2	SRF (T16 + U9)	40	38.2 (T16)	C_nH_{2n}
M34 M137	60.2 30.1	SRF (T16 + U9)	50	58.2 (T16)	C_nH_{2n}
M73	60.8	isooctane + n-heptane	30	75 (octane)	$C_{7.73}H_{17.5}$
M53	60.6	isooctane + n-heptane	40	50 (octane)	$C_{7.47}H_{16.9}$
M65	60.6	isooctane + n-heptane	50	20 (octane)	$C_{7.18}H_{16.4}$
M42	60.2	toluene + n-heptane	40	41.3 (toluene)	$C_7H_{11.5}$
M87	60.6	isooctane (DIB) + n-heptane	40	50.8 (octene)	$C_{7.49}H_{16}$
M94	60.6	SRF + amyl nitrate	40	CN30 SRF + 0.5% vol.	Amyl nitrate
M106	60.5	SRF + TEL	40	CN50 SRF + 3 gr/gal	TEL

Engine speed - 2000 rpm
Nominal injection timing - 20 deg btdc
Nozzle - No. 2

Table 3 - Comparison of Radiant to Overall Heat Transfer Rates

Radiant Heat Transfer			Total Heat Transfer*		
Run No.	Instantaneous Peak Rate**	Average Rate**	Run No.	Instantaneous Peak Rate**	Average Rate**
20	388000	27297	133	N.A.	137950
27	391155	14729	144	560000	69190
54	337435	15009	136	1080000	83250
62	414507	23362	137	930000	99460
70	334663	24747	138	1540000	134060
77	214531	23254	145	1650000	167570
84	366360	22957	132	1270000	119790
91	416445	28442	154	1420000	138170
98	407392	14893	152	1100000	88000
125	524143	31467	151	780000	122060
132	306001	23498	150	1250000	121090

*Data from the work of LeFeuvre. Information from runs at engine conditions similar to those of this author. Data presented represents LeFeuvre's data for thermocouple 1 located in the cylinder head deck.

**Btu/h-ft^2.

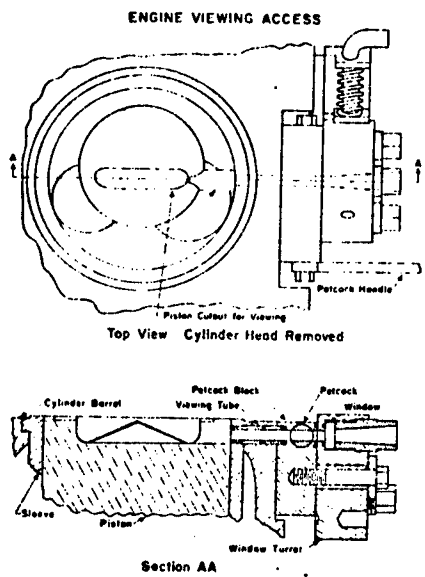

Fig. 1 Engine modifications for observing radiant emissions.

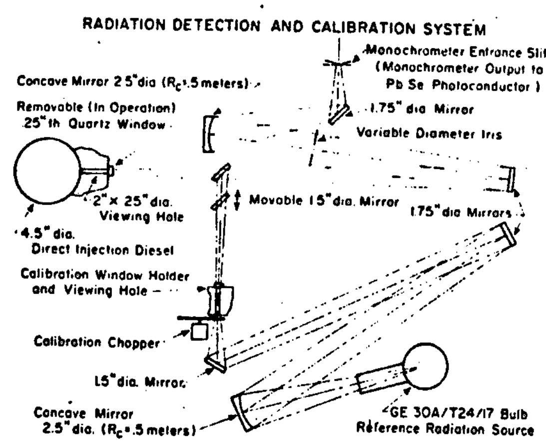

Fig. 2 Schematic diagram of detection and window transmission calibration system.

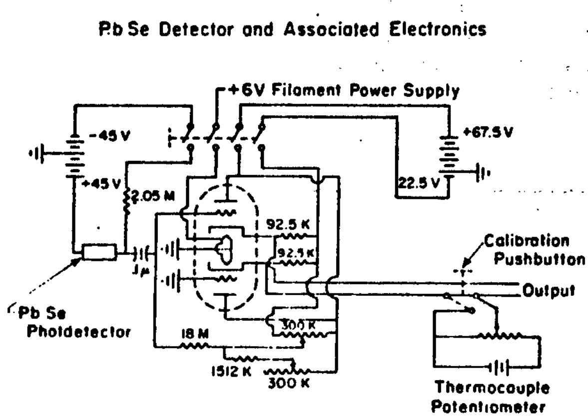

Fig. 3 Schematic diagram of radiation detection electronics.

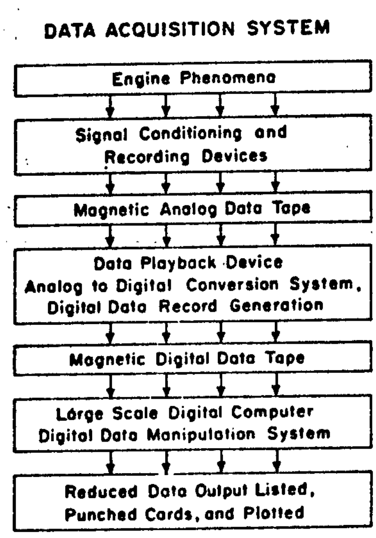

Fig. 4 Block diagram of data acquisition and reduction system.

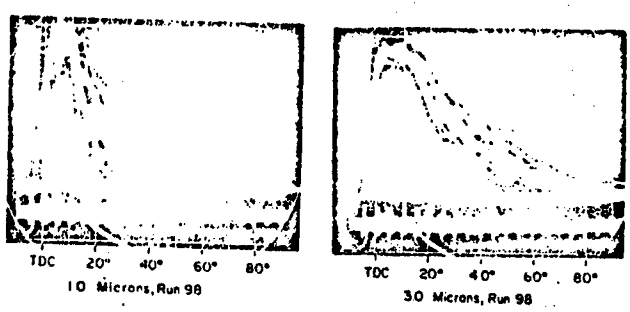

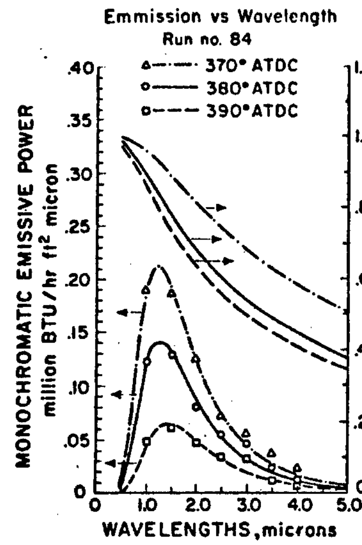

Fig. 5 Oscillograms showing cyclic irregularity of radiation at 1.0 and 3.0 μm wavelength.

Fig. 6 Variations in monochromatic emissive power and emissivity at three different crankangles, run 84.

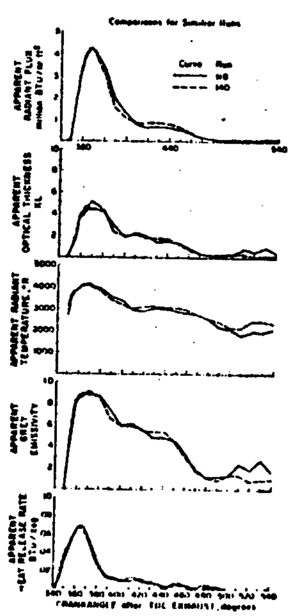

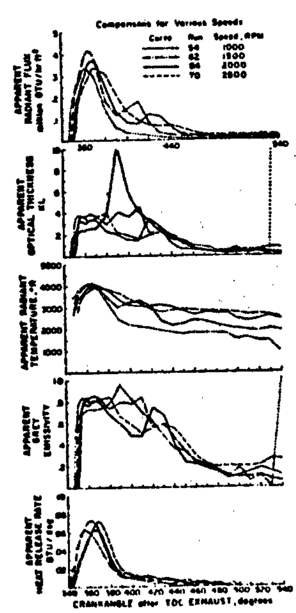

Fig. 7 Reproducibility of radiant heat flux from engine.

Fig. 8 Radiant emissions and heat release rates when engine speed is varied.

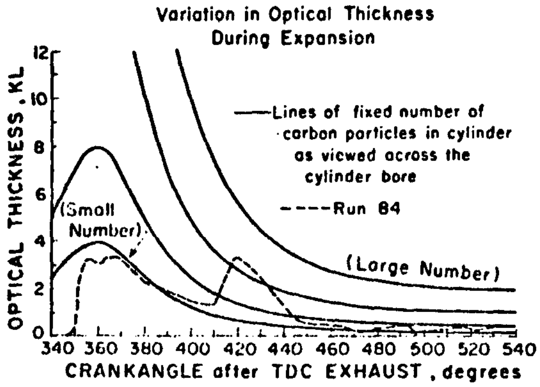

Fig. 9 Plot showing the variation in optical thickness for different particle concentrations during expansion.

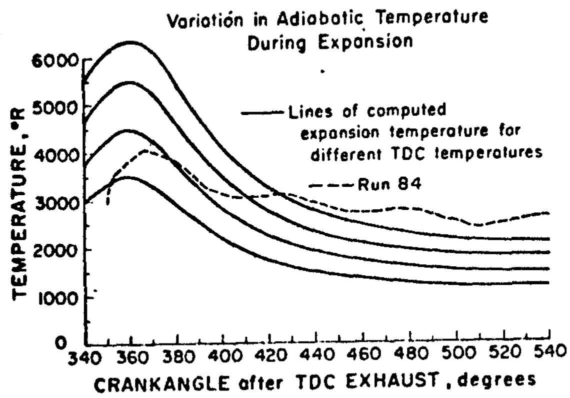

Fig. 10 Plot showing the variation in adiabatic gas temperature during expansion for different tdc temperatures.

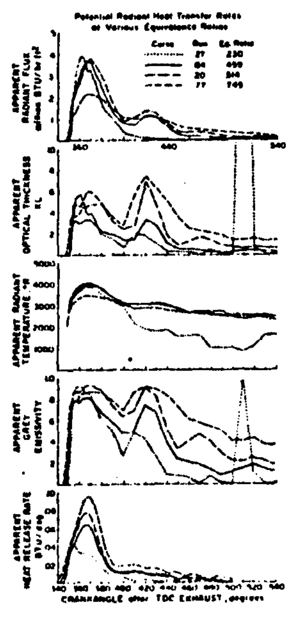

Fig. 11 Radiant emissions and heat release rates when equivalence ratio is varied.

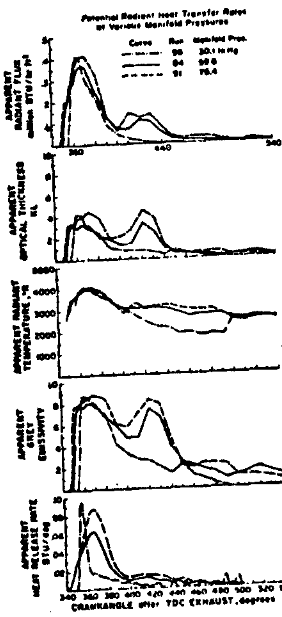

Fig. 12 Radiant emissions and heat release rates when inlet manifold pressure is varied.

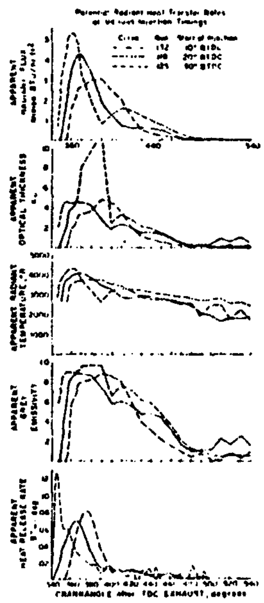

Fig. 13 Radiant emissions and heat release rates when injection timing is varied.

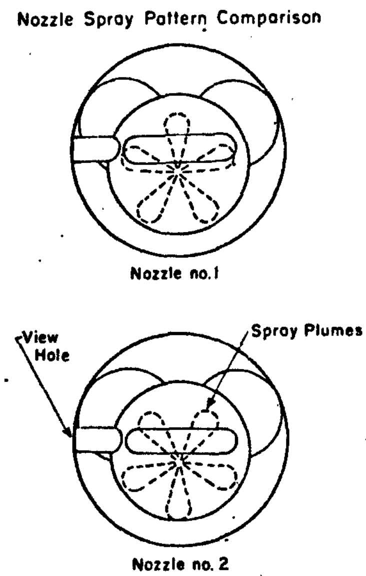

Fig. 14 Plan view of spray patterns of nozzles 1 and 2.

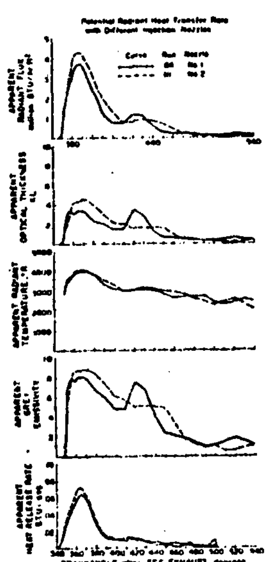

Fig. 15 Radiant emissions and heat release rate when nozzles 1 and 2 were used.

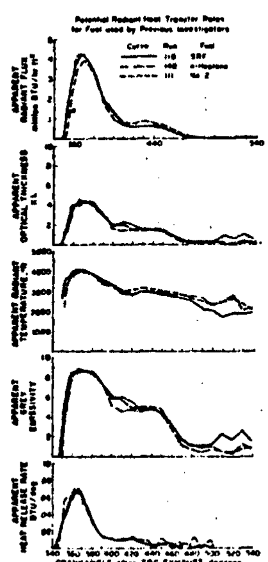

Fig. 16 Radiant emissions and heat release rates for fuels used by previous investigators.

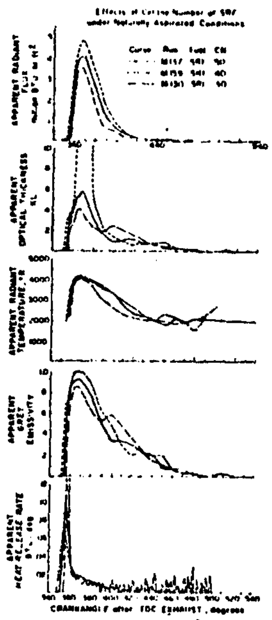

Fig. 17 Radiant emissions and heat release rates for various cetane number fuels under naturally aspirated conditions.

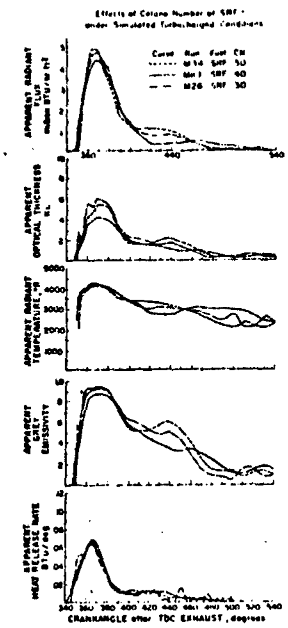

Fig. 18 Radiant emissions and heat release rates for various cetane number fuels under simulated turbo-charged conditions.

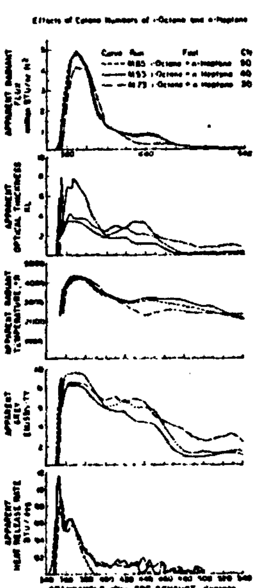

Fig. 19 Radiant emissions and heat release rates for various cetane number paraffinic fuels.

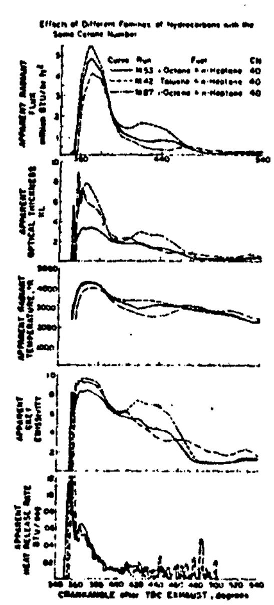

Fig. 20 Radiant emissions and heat release rates for different fuel families and fixed cetane number.

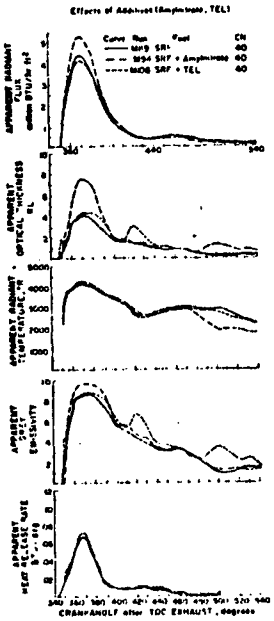

Fig. 21 Radiant emissions and heat release rates for different additives and fixed cetane number.

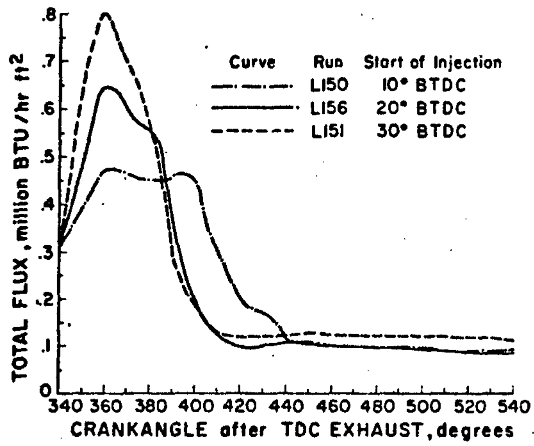

Fig. 22 Total heat flux for various injection timings as reported by LeFeuvre.

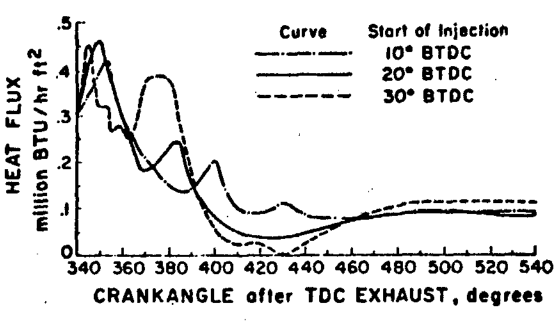

Fig. 23 Convective heat flux portion of LeFeuvre's total heat flux.

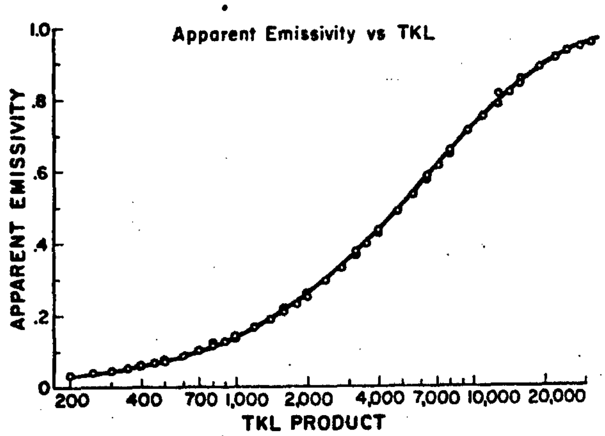

Fig. 24 Plot of apparent emissivity versus TKL product.

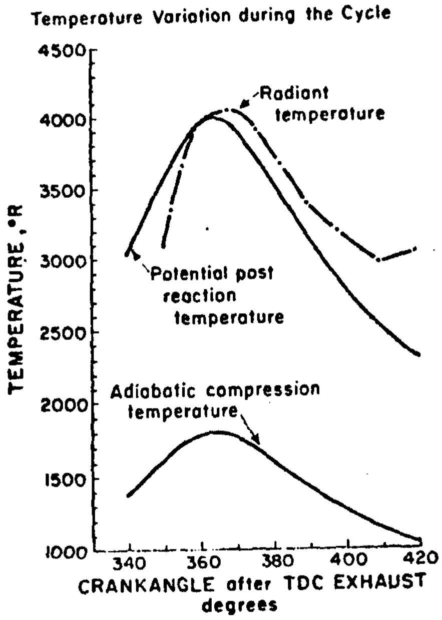

Fig. 25 Variation of apparent radiation temperature with crank rotation.

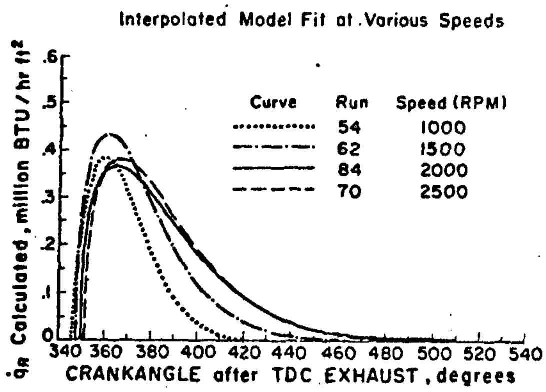

Fig. 26 Representation of Eq. 16 for runs of Fig. 8.

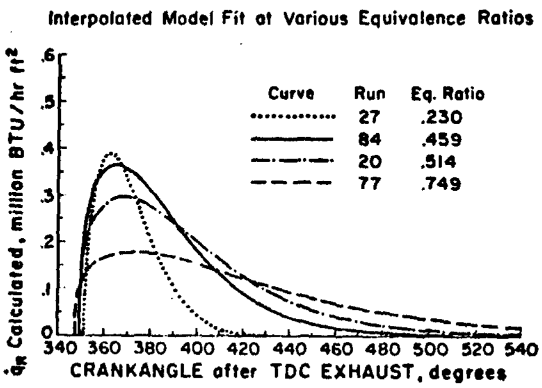

Fig. 27 Representation of Eq. 16 for runs of Fig. 11.

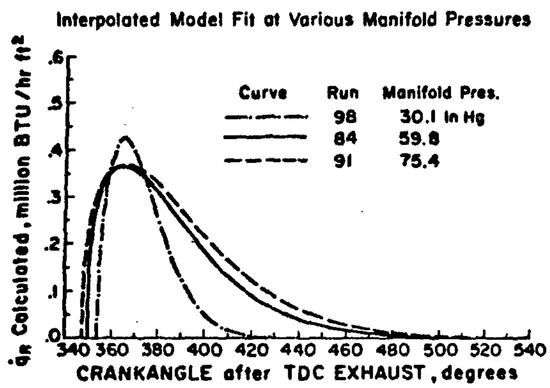

Fig. 28 Representation of Eq. 16 for runs of Fig.

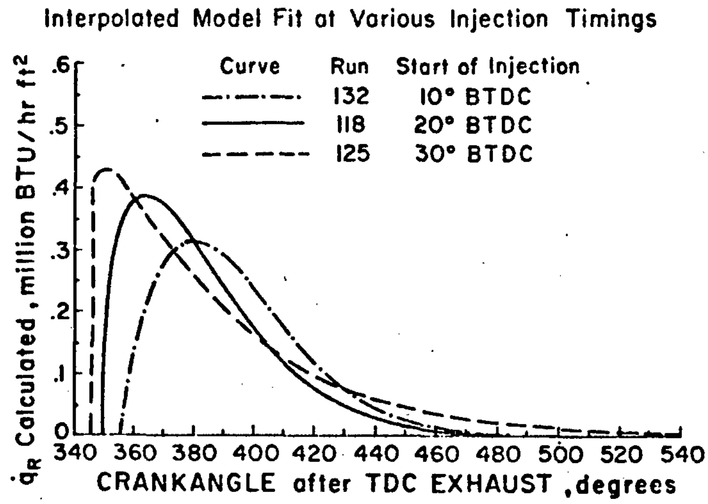

Fig. 29 Representation of Eq. 16 for runs of Fig. 13.

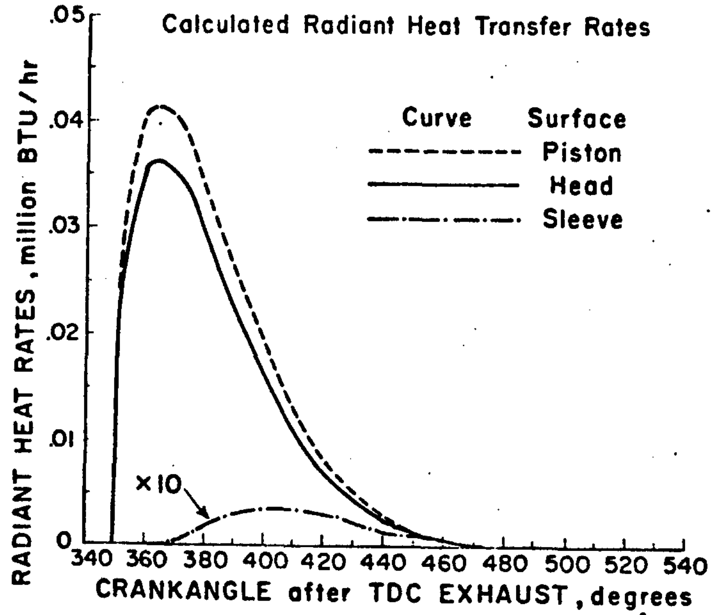

Fig. 30 Calculated radiant heat transfer rates.

APPENDIX VI

A

The Computation of Apparent Heat Release for Internal Combustion Engines

R.B. Krieger and G.L. Borman
Mechanical Engineering Dept.
University of Wisconsin

ABSTRACT

The equilibrium thermodynamic properties of the products of combustion of C_nH_{2n} and air as calculated by Newhall and Starkman are used to obtain mathematical expressions for the internal energy and gas constant as functions of temperature, pressure, and equivalence ratio. The lean side formulation is in terms of a single equation for internal energy which covers the region of normal interest in diesel engine practice. The rich side formulation is in terms of a single equation for each of a selected number of equivalence ratios. The equations for the properties are combined with thermodynamic analysis to predict heat release rates from experimentally obtained engine pressure diagrams. The models and computer methods used for these computations for both compression and spark ignition engines are given. Both models for heat release include the effects of instantaneous heat transfer. A homogeneous mixture with instantaneous burning of incremental fuel masses is assumed in the diesel computations. The spark ignition model utilizes a division of the combustion chamber into a burned and an unburned portion. The heat transfer from each of these two gas systems is computed independently. The computation gives a volume, temperature, and mass of the burned portion as a function of crankangle. Calculation results for different input data are discussed and compared. The various assumptions incorporated in the models are discussed in relation to the actual physical processes and to the use of the calculations in cycle simulation programs.

INTRODUCTION

The mathematical detailed simulation of engine cycles has been the subject of numerous investigations during the past ten years (1-9)[1]. In such detailed treatments, the equations of change for a fluid are applied to the engine cycle and solved step-by-step on a computer to give calculated pressures, temperatures, compositions, heat-transfer rates, mass flow rates, and so on as a function of engine crankangle. Comparisons of these calculated values with experimental data (1) have shown that it is feasible to simulate an engine in detail and that the computer results may be used to help design engines. Unfortunately these simulation cycles are least detailed in their description of the combustion process and thus give a minimum of information concerning the combustion aspects of the design problem. Furthermore, the basic models needed to simulate the nonhomogeneous diesel combustion process and the homogeneous spark-ignition combustion process are quite different.

In the case of diesel combustion, some effort (10,11) has been expended in trying to relate the fuel-injector diagram to the heat-release curve on a quasi-empirical basis. More fundamental studies (12,13) of the droplet vaporization and combustion mechanism do not seem to be far enough advanced to allow their use in calculating the burning rates. Until these more detailed approaches are successful, it is thus necessary to obtain the heat-release curves from an analysis of experimentally obtained pressure diagrams. This paper proposes such a method of calculation which includes both the effects of heat transfer and the dissociation of the products of combustion. While the model does not shed much light on the details of the combustion phenomena, it does give some quantitative information on the overall process. From a practical viewpoint, it also allows one to fit the combustion process into a detailed cycle simulation.

---

[1]Numbers in parentheses refer to References at end of paper.

TABLE 1

Pressure-Temperature Range for Lean-Side Fit

p, psia	T deg R maximum
10	4200
20	4400
30	4600
40	4800
60	5000
100	5200
200	5400
300	5600
400	5600
600	5800
1000	5800
2000	6000
3000	6000
5000	6000

TABLE 2

Coefficients for Equation(16)

F	1.1	1.2	1.4	1.6
a_1	-3.3958312+4*	-2.2215317+4	-3.2937435+4	-3.359-332+4
a_2	1.2505527+1	9.5611235	1.2591442+1	1.2322355+1
a_3	-5.6520223-4	-2.2943938-4	-1.5855548-4	-7.5342313-5
a_4	2.283123 -7	1.2923243-7	1.5435638-7	1.471234-7
a_5	-2.7455555-11	-1.5557133-11	-1.7175237-11	-1.5522075-11
a_6	1.4172512-15	8.0382712-16	7.3572453-16	6.7620535-16
a_7	-1.2199335	-8.810121 -2	-1.3920533-1	1.5522713-1
a_8	3.2258353+4	2.1475191+4	3.1655250+4	3.4292220+4

*Signed number following each table entry refers to associated power of ten.

TABLE 4

Coefficients for Equations (18) and (19)

F	1.1	1.2	1.4	1.6
c_1	9.513 -8		2.3873-2	
c_2	-7.3339-4		-1.9753-5	
d_1		4.0171-11		-4.5518-12
d_2		-5.207 -7		8.5704-3
d_3		2.254 -3		-4.8221-4
	for T ≤ 4200°R	for T ≤ 4000°R	for T ≤ 4000°R	for T ≤ 4200°R
$\tilde{M}(F)$	28.347	27.81828	26.8348	25.9401
	for T > 4200°R	for T > 4000°R	for T > 4000°R	for T > 4200°R
	26.6594	31.1142	25.4255	25.1053

TABLE 3

Coefficients for Equation(17)

F	1.1	1.2	1.4	1.6
b_1	-4.0523-5	-4.4434+5	-3.6229+5	-3.7274+5
b_2	3.5433+2	3.3230+2	3.0542+2	3.1104+2
b_3	-7.4922-2	-6.9011-2	-7.1432-2	-7.1137-2
b_4	-3.1313-8	2.4449-6	2.8381-6	2.5522-6
b_5	5.8345-10	2.6823-10	3.3249-10	3.4235-10
b_6	1.0842	1.1101	1.7999	1.7315
b_7	-3.0349-5	-1.7970-5	-1.2331-4	-1.2723-4
b_8	-5.0418+5	-3.1047+5	-2.5928+5	-2.8840+5
b_9	1.2946+2	9.2009+1	8.6844+1	8.6927+1
b_{10}	6.7875-3	-2.2405-5	-7.4039-4	-8.0937-4
b_{11}	-2.1653-6	-9.7929-7	-9.5069-7	-8.8226-7
b_{12}	1.5535	1.5367	1.7510	1.8753
b_{13}	-1.7263-4	-7.4656-5	-3.0134-5	-1.0942-4
b_{14}	5.1123-3	-1.0530-8	-2.2418-8	-1.1712-9

TABLE 5

Coefficients for ΔM in form of Equation(17)

F	1.1	1.2	1.4	1.6
b_1	-2.0697+4	-2.0232+4	-2.0003+4	-1.9743+4
b_2	1.6990+1	1.6834+1	1.6811+1	1.6845+1
b_3	-3.5635-3	-3.5044-3	-3.5175-3	-3.6177-3
b_4	1.4805-7	1.4701-7	1.4429-7	1.4329-7
b_5	1.2411-11	1.4577-11	1.4714-11	1.4392-11
b_6	2.1345	1.8252	1.8591	1.9931
b_7	-1.9874-4	-1.2725-4	-1.3785-4	-1.5503-4
b_8	-1.8074+4	-1.7161+4	-1.7151+4	-1.7329+4
b_9	4.5919	4.6218	4.6233	4.5915
b_{10}	-3.0825-5	-1.6024-5	-1.4143-5	-1.3379-5
b_{11}	-4.6546-8	-5.0538-8	-4.9335-8	-4.7039-8
b_{12}	2.8397	2.5162	2.5558	2.6359
b_{13}	-4.5987-4	-3.9490-4	-4.0339-4	-4.0519-4
b_{14}	2.2651-8	2.1759-8	2.1792-3	1.9631-8

In the case of homogeneous spark-ignition combustion, the phenomena seem more amenable to analysis and various theoretical models have been proposed (14-16). Patterson (8) applied the laminar flame-velocity theory of Semenov (17) with a correction factor for turbulence effects. Generally the factor for turbulence is not known and its value must be estimated from an experimental pressure-time diagram. Because of the many unknown factors caused by chamber shape, spark-plug location, quench, turbulence, and so on, Huber and Brown (9) have suggested that a highly simplified mass-burned curve be used with empirical adjustment based on the unpublished data of Mosher, Robison, and Ojala. Since both of these methods ultimately rely on experimental data, it would seem reasonable to obtain the burning rates directly from experimentally obtained pressure-time diagrams without recourse to any theories of flame velocity.

As is well known (18), the spark-ignition engine-pressure diagrams vary considerably from cycle to cycle. Thus if the ultimate simulation cycle is to represent a time-averaged cycle, an appropriate time-averaged pressure diagram must be used in the burning rate calculations. This paper proposes such a method of calculation which includes both the effects of heat transfer and dissociations of the products of combustion. The model does not account for prereactions in the end gas although such reactions may be quite significant (19).

Both heat-release models proposed here are similar in that they require:

1. An experimental pressure-time diagram.
2. Expressions for the internal energy and gas constant of the products and unburned mixture.
3. A correlation for gas-side heat-transfer coefficient.
4. An estimate of metal temperatures for the exposed cylinder surfaces.
5. An estimate of the initial composition and mass of the gas in the cylinder just prior to combustion
6. Data which describe the geometric design parameters of the engine.

Both models are also similar in that their main utility is their use in conjunction with a detailed cycle simulation. The results of heat-release calculations may, however, also prove useful in obtaining empirical correlations between various design parameters and the heat-release shape.

Because both heat-release models require expressions for the thermodynamic properties of the combustion gases, the first part of this paper gives mathematical equations for the dissociated products of combustion of C_nH_{2n} and air. The rest of the paper then discusses the combustion models and some results obtained from calculations based on these models.

INTERNAL ENERGY OF PRODUCTS OF COMBUSTION

The equilibrium thermodynamic properties of the products of combustion of C_nH_{2n} and air were calculated by Newhall and Starkman (20,21) using the data from the JANAF tables (22). The reference temperature used for these calculations was 298 deg K which is the reference used in the JANAF tables. For purposes of the computer program and in order to check against the calculations of reference (23), these values were converted to 0 deg R reference temperature.

The internal energy of the combustion products as used here is the absolute internal energy. The absolute internal energy is the sum of the sensible energy (at T deg R above that at 0 deg R) and the heat of formation (at T = 0 deg R from elements in their standard reference states at T = 0 deg R). For a fixed hydrogen-carbon ratio, the internal energy will be a function of temperature, pressure, and fuel-air ratio. The correction to 0 deg R reference was accomplished by use of the formula

$$\delta u = u_{(0°K)} - u_{(298°K)} \tag{1}$$

$$\delta u = 1800 \sum_i \tilde{x}_i \left[\left(H_{s(298)} - H_{s(0)}\right)_i - \left(H_{f(298)} - H_{f(0)}\right)_i\right] / \sum_i \tilde{x}_i \tilde{M}_i \tag{2}$$

The mole fractions, $\tilde{x}_i$, were frozen at the 1600 deg R values computed by Newhall and Starkman.

The internal energy per pound of original air for undissociated products is a linear function of equivalence ratio. Thus at a particular pressure, lines of constant temperature are straight lines on a plot of internal energy versus fuel-air ratio below 2600 deg R where the effects of dissociation are negligible. The effect of dissociation on such a diagram is to shift the lines upward at higher temperatures and to cause some deviation from straight lines near the equivalence ratio of $F = 1$. In general, the effects of dissociation are largest at low pressures, high temperatures, and equivalence ratios near unity. It should be noted that the derivative $\partial u/\partial F$ changes sign from negative to positive as F increases from less than one to greater than one. For no dissociation, the first partial of u with respect to F has a finite discontinuity at the value $F = 1$.

EQUATIONS FOR LEAN-SIDE INTERNAL ENERGY AND GAS CONSTANT

The internal energy of C_nH_{2n} as calculated by Newhall and Starkman is in the form of tables or graphs. A great saving of computer time can be achieved by having the data in the form of equations. The internal energy and gas constant were thus fit as a function of T, p, and F. For $F \leq 1$, the following procedure was used.

The first step was to compute the internal energy and gas constant assuming no dissociation

$$u^* = A(T) - B(T)\cdot F \qquad \text{BTU/lb original air} \tag{3}$$

where

$$A = 0.16528\,T + 5.1979(10)^{-6}T^2 + 3.9016(10)^{-9}T^3 - 9.3632(10)^{-13}T^4 + 6.3156(10)^{-17}T^5 \tag{4}$$

$$B = 1311. - 1.3623(10)^{-2}T - 1.2605(10)^{-5}T^2 + 1.587(10)^{-9}T^3 - 8.2022(10)^{-14}T^4 \tag{5}$$

$$R^* = .0685548 + .004788\,F \qquad \text{BTU/°R-lb}_m \text{ original air} \tag{6}$$

The second step was to limit the range of T and p to those values encountered in combustion engines. The ranges are listed in Table 1. The values of pressure listed correspond to those pressures for which Newhall calculated points.

The third step was to fit the deviations, $u - u^*$, from the nondissociated values as a function of T, p, and F using a least-squares routine. Graphs of the deviations at constant pressure versus $1/T$ on a semi-log plot give essentially straight lines. The final equation for the internal energy was thus found to be given by

$$u = u^* + \exp(C_1+C_2+C_3)$$

$$C_1 = 10.41066 + 7.85125\,F - 3.71257\,F^3$$

$$C_2 = (-27.00107-28.5087\,F+17.30375\,F^3)(1000/T)$$

$$C_3 = [0.154226\,F^3 - 0.38656\,F - 0.10329 + (.21289\,F - .026574)(1000/T)\,\ln(p)$$

$$\text{BTU/lb}_m \text{ original air} \tag{7}$$

The model first assumes thermodynamic equilibrium at each instant. As part of this assumption, it is thus assumed that the entire cylinder contains a homogeneous mixture of air and combustion products at each instant. Phenomena such as temperature gradients, pressure waves, nonequilibrium compositions, fuel vaporization, mixing, and so on are thus ignored in this model.

The burning is assumed to take place incrementally as a homogeneous combustion and thus acts as a uniform heat source. With these assumptions, the equation of energy becomes

$$\frac{d}{dt} Mu = -p \frac{dV}{dt} + \sum_i \dot{Q}_i + h_f \frac{dM}{dt} \tag{9}$$

In order to use this equation, it is convenient to write

$$\frac{du}{dt} = \frac{\partial u}{\partial T}\frac{dT}{dt} + \frac{\partial u}{\partial p}\frac{dp}{dt} + \frac{\partial u}{\partial F}\frac{dF}{dt} \tag{10}$$

$$\frac{dR}{dt} = \frac{\partial R}{\partial R}\frac{dT}{dt} + \frac{\partial R}{\partial p}\frac{dp}{dt} + \frac{\partial R}{\partial F}\frac{dF}{dt} \tag{11}$$

Using the functional forms of u and R given by equations (3) to (8), the partial derivatives can be written explicitly in terms of T, p, and F. The time derivative of the equation of state, $pV = MRT$, gives an expression for dT/dt which can be used to eliminate that quantity from the energy equation. The equivalence ratio at any instant is given by

$$F = F_0 + \left(\frac{M}{M_0} - 1\right)\left(\frac{1 + f_0}{f_s}\right) \tag{12}$$

$$\frac{dF}{dt} = \frac{1 + f_0}{f_s M_0}\frac{dM}{dt} \tag{13}$$

The equation of energy can thus be solved for $\dot{M}$, the mass burning rate

$$\frac{1}{M}\frac{dM}{dt} = \frac{\frac{-RT}{V}\frac{dV}{dt} - \frac{\partial u}{\partial p}\frac{dp}{dt} + \frac{1}{M}\sum_i \dot{Q}_i - C[B]}{u - h_f + D\frac{\partial u}{\partial F} - C\left(1 + \frac{D}{R}\frac{\partial R}{\partial F}\right)} \tag{14}$$

where

$$B = \frac{1}{p}\frac{dp}{dt} - \frac{1}{R}\frac{\partial R}{\partial p}\frac{dp}{dt} + \frac{1}{V}\frac{dV}{dt}\Big)$$

$$C = T\frac{\partial u}{\partial T} \Big/ \left(1 + \frac{T}{R}\frac{\partial R}{\partial T}\right)$$

$$D = \frac{(1+f_0)M}{f_s M_0}$$

These equations can be solved numerically to obtain $\dot{M}$ as a function of time (or crankangle) provided that the initial values of mass in the cylinder and equivalence ratio are specified with p and $\dot{p}$ supplied from experimental data.

Obtaining the pressure derivatives from pressure data is not a particularly accurate process since a good deal of smoothing of the pressure data is necessary in order to obtain reasonably smooth pressure-derivative curves. In most cases, naturally aspirated engines give pressure diagrams which contain high-frequency components of considerable magnitude. While some of the oscillations are introduced spuriously by the instrumentation, most of the waves are actually produced by the combustion

process. It is reasonable to expect, however, that these pressure oscillations are local pressure changes (waves) and that the mass average pressure is a smooth curve. Supercharged engines (or single-cylinder engines run with boosted tank pressures) on the other hand, normally give fairly smooth pressure-time diagrams so that little or no smoothing is required.

The instantaneous heat transfer from the gas was computed from the Annand (24) correlation. Five metal-surface areas representing the head, piston, sleeve, and valves were each assigned a different constant temperature. These surface temperatures must be either estimated from experimental data, or computed by use of a cycle analysis program (1,2).

The equations of energy and mass continuity together with the equations of state, internal energy, and gas constant are integrated using the modified Euler technique to obtain the mass of fuel burned during each crankangle increment. A running integral of the mass rate gives the total mass of fuel added up to any given crankangle. The pressure values which are needed at each step are calculated from a smoothed pressure-crankangle table by using a second-degree Lagrangian interpolation formula. Thus it is not necessary to tabulate the pressures at equal intervals. The values of the pressure derivative are computed from the differentiated form of the interpolation formula. Considerable care must be exercised in handling the data if the derivative curves are to be reasonably smooth. Spurious derivative values may cause the mass rate of burning curve to oscillate and even go negative for short intervals. Such oscillations are particularly apt to occur near the extremes of the burning period when the values of the burning rate are very small. Some "negative burning" should, of course, be expected if the calculation is started during the portion of the cycle when significant fuel vaporization but no combustion is occurring. The causes of "negative burning" near the end of the combustion period are more difficult to explain. In either case, however, negative mass rates cannot be allowed as they cause the following positive rates to start at invalid conditions.

The total CDC 1604 compile and computation time for one heat-release diagram using an increment size of one crank degree is less than 2 min.

RESULTS OF DIESEL HEAT-RELEASE CALCULATIONS

Calculations of apparent heat-release rate have been carried out using pressure-crankangle data supplied by International Harvester (1) and Continental Aviation Engineering (2). IH obtained their data from an open-chamber liquid-cooled single-cylinder research engine and CAE from a single-cylinder air-cooled engine. Calculation results shown here are based on the IH data although similar trends and qualitative behavior were found to hold for the CAE data. A description of the IH engine and its performance are to be found in reference (1).

All IH data were taken with a point-by-point balanced diaphragm indicator (28). While the balanced diaphragm method gives very accurate pressure readings, it also necessitates an undesirable sampling technique. Ideally, the heat release should be calculated from a pressure trace which results from averaging a large number of individual cycle pressure diagrams. The balanced diaphragm method, on the other hand, samples individual points from various cycles. Furthermore, since the method is tedious, it is difficult to obtain a large number of points.

Figure 3 shows the cylinder pressure and rate of change of pressure for 3200 rpm full load as obtained by IH. Figure 4 shows the resulting mass rate of burning curve obtained from the data of Fig. 3. The first peak in the burning curve corresponds to the peak in the pressure derivative. The flat portion of the derivative at about 183 CA° causes the downward dip in the burning curve. The second peak in the burning curve was exhibited in all data studied for both the CAE and IH data. It is interesting to note that small waves in the derivative such as that shown at about 200 CA° are greatly magnified in the burning curve. Thus, any erratic behavior in $\dot{p}$ causes large oscillations in the calculated $\dot{M}$ curve. The solid line in Fig. 5 shows the same curve as in Fig. 4 but expanded to show the behavior at larger crankangles. The burning rate, $\dot{M}$, goes negative at 250 CA° (70 CA° ATDC) and then goes positive again. The exhaust valve opens at 290 CA° so that some burning might still be going on at that time. The negative and then positive late burning has also been calculated by Lyn and others at CAE. Typically for purposes of cycle simulation, the burning rate curve would be terminated at the point of first negative

$\dot{M}$, i.e., at 251 CA° in Fig. 5. At 251 CA° the total fuel burned was calculated to be 3 percent less than the experimental value of fuel burned per cycle. At 280 CA° the calculated fuel burned equaled 100 percent of the experimental value and the calculation was stopped. About 60 percent of the fuel was burned during the first 1/3 of the heat-release period.

In order to study the effects of various parameter changes, a number of calculations were carried out using the 3200 rpm, full-load data. The first effect investigated was that of translating the pressure curve backward or forward with respect to crankangle. Such shifting may be inherent in the data because of experimental error. Shifting the pressure curve (and its derivative) by ± 2 CA° caused the heat-release curve to be shifted by about the same amount in the same direction. The magnitude of the curve was also changed by such shifting, but the general shape did not change. Figure 5 shows the three heat-release curves calculated in this way. The two ± 2 CA° pressure-shifted curves have been translated by ∓ 2 CA° in Fig. 5 so that the effect on shape can be more clearly seen. The higher dashed curve corresponds to the case of shifting the pressure curve forward, i.e., so that peak pressure was at 189.5 CA° instead of 187.5 CA°. The lower curve corresponds to shifting the curve back 2 CA°. Thus shifting the pressure forward causes the calculation to show more fuel burned and shifting backward, less fuel burned. Shifting forward corresponds to a delay in the balanced diaphragm response.

The second effect investigated was that of translating the pressure curve up or down by 5 psi. Such a shift does not change the derivative curve. The effects of the ± 5 psi shifts on the heat-release curve were negligible for the portion prior to 190 CA°. Comparing the amount of fuel burned up to the first negative burning rate, the shifted-pressure calculation showed 3.5 percent more fuel burned than the unshifted pressure. All of this extra fuel was burned between 190 and 254 CA°. In other words, the pressure shift caused a slight upward shift in the late burning portion of the heat-release curve.

Another parameter considered was the effect of the heat-transfer rate. Two calculations were made, one with the heat-transfer coefficient reduced by 50 percent and the other with it increased by 50 percent. The shape of the mass rate of burning curve was unchanged except for a slight change in the height of the peaks and the magnitude of the late burning portion. The total fuel burned at the point of first negative burning was 4.8 percent less for the reduced heat transfer and 4.8 percent greater for the increased heat transfer. Again the largest change was in the portion of the curve after 190 CA°.

One of the important factors in the process of iterating between the heat release and cycle simulation programs is the choice of initial conditions. Since the calculated mass in the cylinder and thus, the calculated pressure at the start of the heat release are primarily dependent on the intake and exhaust processes, these values do not necessarily agree with the experimental data. In order to determine the magnitude of this effect, the heat-release program was run with the initial mass changed from that estimated from the experimental air-flow data. As would be expected, increasing the initial mass decreases the final temperature, fuel-air ratio, and mass of fuel burned. The final temperature was reduced by 4.5 percent, the final fuel-air ratio by 6.24 percent, the total mass of fuel burned by 1.8 percent, and the peak of the rate of burning curve by 1.73 percent when the initial mass was increased by 5 percent. Thus, the two burning rate curves are simply proportional, the proportionality factor being given approximately by the ratio of the total fuel mass burned for the two cases. The fact that the heat-release calculation is not sensitive to changes in initial mass is significant since the iteration process might otherwise be unstable.

The effect of dissociation of the products was found to be negligible. If equation (3) is used instead of equation (7) to represent the internal energy, the effect is to reduce the calculated total fuel burned for 3200 rpm, full load by 1 percent. The peak of the $\dot{M}$ curve is not changed. Dissociation in this case caused only a 10 deg F reduction in peak temperature.

One further concluding observation may be made concerning the late burning portion of the heat-release curves. In all cases for the parameters varied, the rate curves showed a shallow dip starting at about 250 CA°. In most cases, this dip caused negative values of $\dot{M}$, but even when $\dot{M}$ did not go negative, the burning continued at a low level out to the time of exhaust valve opening. One can

speculate that the existence of nonequilibrium in the chemistry may be the cause of this apparent energy absorption and the continued release of energy which is calculated at late crankangles. The existence of "negative burning" is, at any rate, a signal that the model is failing to represent the actual physical process.

No attempt was made in this study to correlate heat release with basic combustion phenomena. Calculations for various speeds at full load showed the same characteristic heat-release shape. Figure 6 shows the effect of speed on the percent mass-burned curves. The percent mass burned is calculated from

$$M(\theta) = 100. \int_{\theta_0}^{\theta} (dm/d\theta)\, d\theta \Big/ \int_{\theta_0}^{\theta_f} (dm/d\theta)\, d\theta \tag{15}$$

Similar curves calculated from the CAE data are given in reference (2). No easily recognized pattern is discernible.

EQUATIONS FOR RICH-SIDE INTERNAL ENERGY AND GAS CONSTANT

For $F > 1$, the internal energy and molecular weight were fit as functions of T and p for various values of F. The gas constant was then calculated from the universal gas constant and the molecular weight. To do this, the internal energy was first fit versus temperature for each of the four F values: $F = 1.1$, $F = 1.2$, $F = 1.4$, $F = 1.6$ at a pressure of 8000 psi. A fifth-degree polynomial with two additional terms was used for this purpose. The resulting form was

$$u^* = a_1 + a_2T + a_3T^2 + a_4T^3 + a_5T^4 + a_6T^5 + a_7T^{3/2} + \frac{a_8}{1 + T/3000} \tag{16}$$

where u^* was an intermediate variable equivalent to the nondissociated internal energy. A set of constant coefficients a_i was obtained for each F value using a least-squares computer program and the tabulated data of Newhall and Starkman.

At lower pressures, this form of equation fit the tabulated data up to 3800 deg R where the effects of dissociation began to set in causing a deviation between the least-squares fit and the tabulated data. The deviation increased with increasing temperature. The deviations between the tabulated values and u^* were calculated and fit for pressures between 100 and 1000 psia and temperatures between 3800 and 6000 deg R. The form of the equations used to fit these data was

$$\Delta u = u - u^* = \frac{A(T)}{p^{B(T)}} + \frac{C(T)}{p^{D(T)}} \tag{17}$$

where

$$A = b_1 + b_2T + b_3T^2 + b_4T^3 + b_5T^4$$

$$B = b_6 + b_7T$$

$$C = b_8 + b_9T + b_{10}T^2 + b_{11}T^3$$

$$D = b_{12} + b_{13}T + b_{14}T^2$$

A set of b_i values was obtained for each of the four values of F by use of a computer program which performed a nonlinear least-squares estimation of parameters by the method of steepest descent (29). The values of the a_i and b_i coefficients are given in the Appendix.

The molecular weight was fit in much the same manner as the internal energy. Below 3800 deg R, the molecular weight did not vary with temperature and the base values were constant for each F value. Above 3800 deg R the effects of dissociation became important. To get base values for the entire range of temperatures and pressures, the differences between the tabulated molecular weights at 8000 psia and the constant molecular weights below 3800 deg R were fit using either a second or third-degree polynomial. The second-degree polynomial was more accurate for $F = 1.2$

and 1.6 and the third degree was more accurate for F = 1.1 and 1.4. The resulting form of the base or intermediate values was

$$\tilde{M}^* = \tilde{M}(F)_{\substack{\text{constant}\\ \text{below 3800}}} - \begin{cases} c_1T^2 + c_2T & [F=1.1,1.4] \quad (18) \\ d_1T^3 + d_2T^2 + d_3T & [F=1.2,1.6] \quad (19) \end{cases}$$

At lower pressures the deviation associated with dissociation was calculated using the relation

$$\Delta\tilde{M} = \tilde{M}^* - \tilde{M}_{\text{table}} \qquad (20)$$

This final deviation was then fit using the same form as that used for the internal-energy-deviation fit. The coefficient values are given in the Appendix.

To obtain the properties for values of equivalence ratio intermediate to those fit, interpolation was used. For values of equivalence ratio between F = 1.0 and F = 1.2, a second-degree Lagrangian interpolation formula was used. For values of equivalence ratio between F = 1.2 and F = 1.6, linear interpolation was used.

The resultant fitting equations are accurate to within 2 percent of the tabulated internal-energy values for temperatures below 3800 deg R for all equivalence ratios which were fit. Above 3800 deg R the internal-energy fit is within 2 percent of the tabulated values for internal-energy values greater than or equal to 100 BTU/lb_m and has an absolute error of less than 3 BTU/lb_m for internal-energy values less than 100 BTU/lb_m.

The fitting equations for the gas constant are all within 2½ percent of the tabulated values.

EQUATIONS FOR FUEL VAPOR-AIR MIXTURE INTERNAL ENERGY AND GAS CONSTANT

The fuel vapor-air mixture absolute internal energy may be connected to the absolute internal energy of the products of combustion with a hypothetical constant-volume combustion process. Dissociation does not occur in the reactants and therefore, the reactants are a function of only temperature and equivalence ratio. The internal energy of the reactants is given by the following equation:

$$u_{\substack{\text{air-vapor}\\ \text{0°R ref.}}}(T,F) = u_{\text{products}}(537°\text{R},F) + fQ_{\text{reaction}} + \Delta u_{\substack{\text{sensible}\\ \text{air-vapor}}}\Bigg]_{T=537°\text{R}}^{T°\text{R}} \quad \text{BTU/lb}_m\text{-air} \qquad (21)$$

Note that all internal-energy terms in this equation are based on 0 deg R reference. To use measured heats of reaction, a temperature of 537 deg R was chosen for the combustion process.

The first term on the right in equation (21) was obtained from the Newhall-Starkman tables. No dissociation occurs at 537 deg R and therefore, this absolute internal energy of the products at 537 deg R is a function of equivalence ratio only. This function is

$$u_{\text{products}}(537°\text{R},F) = -1208.4949 + (F-1.) \cdot 299.61685 \qquad (22)$$

As is customary in internal-combustion engine work, the lower heating value of the fuel at 77 deg F was used for Q_{reaction}. The third term in the right side of equation (21) which is the change in sensible internal energy of the air-vapor mixture was obtained by combining the changes in the sensible internal energies of the air and fuel vapor using ideal mixture rules. The change in sensible internal energy of the air was obtained from the lean-side fit equations for an equivalence ratio of

zero. The change in sensible internal energy of the fuel vapor was obtained from a fit of data obtained from Rossini (30). The particular fuel chosen as being representative of gasoline fuel was 1-octane, C_8H_{16}. The equation representing this fit is

$$u_{vapor}(T) = (15.791+3.4765(10)^{-2}T + 3.6285(10)^{-4}T^2 - 4.5032(10)^{-8}T^3 - 5.4331(10)^{-12}T^4 + 1.5757(10)^{-15}T^5)f \quad \text{BTU/lb}_m\text{-air} \tag{23}$$

The final expression for the absolute internal energy of the air-vapor mixture as a function of temperature and equivalence ratio is obtained by calculating the sensible u for the air-vapor mixture at 537 and T deg R using equations (4) and (23) and then substituting these values and the appropriate value from equation (22) into equation (21). The units for temperature are deg R and for u, BTU/lb_m air. Again, division by $1 + (0.067623)F$ is necessary to convert to units of BTU/lb_m air-vapor mixture.

The reactants also contain residual combustion products from the previous cycle. To obtain the absolute internal energy of the complete air vapor, residual mixture, the ideal mixture rule gives

$$u_{\substack{\text{reactants}\\ \text{total}}}(T,F) = m_{f_{\text{air vapor}}} u_{\text{air vapor}}(T,F) + m_{f_{\text{residual}}} u_{\text{residual}}(T,F) \quad \text{BTU/lb}_m \text{ mixture} \tag{24}$$

where the m_f are the appropriate mass fractions.

The gas constant for the total reactants mixture was also obtained from the mixture rule and the known molecular weights of the three constituents.

MODEL FOR SPARK-IGNITION HEAT RELEASE

One of the basic problems in determining the heat-release diagram for spark-ignition engines is the determination of the shape of the flame front and burned volume. This problem can be alleviated by formulating the model in such a way as to reduce the importance of the shape of the combustion products volume. In the model proposed here, the exact shapes of the burned and unburned mixture volumes is only important insofar as these shapes determine the heat transfer from the gases to the metal surfaces of the combustion chamber and the heat transfer across the flame front from the burned to the unburned mixture.

The model assumes that at any instant during combustion, the chamber volume can be divided into a burned and unburned volume separated by an infinitesimally thin flame front. Each volume is assumed to be in thermodynamic equilibrium and both systems are assumed to be at the same pressure at any instant. The subscript u is used to indicate the unburned system consisting of fuel vapor, air, and residual products. The subscript b is used to indicate the burned system consisting of the products of combustion.

The total volume, V, is defined by the geometry and speed of the engine as a function of the crankangle θ. Thus

$$V = V_b + V_u \tag{25}$$

The total mass can be assumed constant if blowby and valve leakage are neglected, thus giving

$$M = M_b + M_u \tag{26}$$

or

$$\dot{M}_b = -\dot{M}_u \tag{27}$$

Since the pressure is assumed uniform, the equation of state, assuming ideal gases, gives

$$p = JM_bR_bT_b/V_b = JM_uR_uT_u/V_u \tag{28}$$

Differentiation of equation (28) with respect to crankangle gives

$$\frac{\dot{p}}{p} = \frac{\dot{M}_b}{M_b} + \frac{\dot{R}_b}{R_b} + \frac{\dot{T}_b}{T_b} - \frac{\dot{V}_b}{V_b} \tag{29}$$

$$= \frac{\dot{M}_u}{M_u} + \frac{\dot{R}_u}{R_u} + \frac{\dot{T}_u}{T_u} - \frac{\dot{V}_u}{V_u} \tag{30}$$

If engine pressure data are available, the left-hand sides of equations (28), (29) and (30) are known functions.

We turn next to the energy equations for the two systems. By assuming thermodynamic equilibrium, we have neglected the thermal gradients in the two systems and may thus write

$$\dot{\overline{M_u u_u}} = \frac{-p\dot{V}_u}{J} + \sum_{i=1}^{n} \dot{Q}_{ui} + h_u\dot{M}_u \tag{31}$$

$$\dot{\overline{M_b u_b}} = \frac{-p\dot{V}_b}{J} + \sum_{i=1}^{m} \dot{Q}_{bi} + h_u\dot{M}_b \tag{32}$$

The heat-transfer terms are summed over the heat-exchanging surfaces. For the gas to metal heat-transfer surfaces, we write

$$\dot{Q}_{ui} = \tilde{h}_u A_{ui}(T_{wi}-T_u) \tag{33}$$

for the unburned system and a similar expression for the burned system. The heat-transfer coefficients, $\tilde{h}_b$ and $\tilde{h}_u$ are calculated using the Eichelberg (31) formula. The metal-surface temperatures, T_{wi}, are assumed constant over each of five surfaces; the head, piston crown, exposed sleeve area, intake valve, and exhaust valve. The temperatures assigned to each of these areas must be obtained from experimental data or from a detailed cycle simulation. The difficulty in calculating the heat transfer comes in selecting the fraction of each area which is exposed to the burned system. In order to determine that fraction, some burned volume shape must be assumed. It can be seen from examination of the equations that fortunately, this is the only part of the calculation which requires a knowledge of this shape. In order to simplify the calculations, it was arbitrarily assumed that the fraction of the piston area exposed to the burned gas is equal to the volume fraction, V_b/V. The exposed sleeve area was considered to be exposed to the unburned gases for the entire period of burning. For most of the calculations, the heat transfer across the flame front was neglected.

The system of equations can be solved for $\dot{T}_u$, assuming that $\dot{R}_u$ is constant, to give

$$\dot{T}_u = \left(T_u\,\dot{p}/p + \sum_i \dot{Q}_{ui}/(M_uR_u)\right) \Big/ \left(\frac{1}{R_u}\frac{\partial u_u}{\partial T_u} + 1\right) \tag{34}$$

Similarly, we may solve for $\dot{M}_b$. We first assume that $\partial R_b/\partial T_b$ and $\partial R_b/\partial p$ are negligible as can be supported by numerical investigation. Thus

$$\dot{M}_b = \frac{\left(M_uR_u\dot{T}_u - \frac{p\dot{V}}{J}\right)\left(\frac{1}{R_b}\frac{\partial u_b}{\partial T_b} + 1\right) - \frac{\dot{p}V}{J}\left(\frac{1}{R_b}\frac{\partial u_b}{\partial T_b} + \frac{M_bJ}{V}\frac{\partial u_b}{\partial p} + \frac{V_u}{V}\right) + \sum_i \dot{Q}_{bi}}{(u_b-u_u) + \left(\frac{R_uT_u}{R_b} - T_b\right)\frac{\partial u_b}{\partial T_b}} \tag{35}$$

Having calculated $\dot{T}_u$ and then $\dot{M}_b$, the rate of change of burned volume can be obtained from

$$\dot{V}_b = V_u[\dot{M}_b/M_u - \dot{T}_u/T_u + \dot{p}/p] + \dot{V} \tag{36}$$

The initial temperature of the burned gas is taken to be the adiabatic flame temperature obtained from solving

$$h_b(T_b) = h_u(T_u) \tag{37}$$

for T_b. The initial crankangle is set at the spark crankangle.

Equations (34), (35) and (36) were solved using the Runge-Kutta third-order formulas with a one CA° increment size. Calculation time for one set of data was about 1 min on the CDC 1604 computer using a precomplied binary program.

It was found that the third-order Runge-Kutta method gave oscillations in the burned gas temperature for about the first ten crankangle degrees. This was remedied by iterating at the center of each interval using a modified Euler formula to obtain the slope at this center point. This procedure gave smooth burned gas temperatures without changing the values of the other computed quantities as compared with the standard Runge-Kutta calculation results.

RESULTS OF SPARK-IGNITION HEAT-RELEASE CALCULATIONS

The experimental pressure diagrams given in reference (32) were used to calculate mass burning rates. These data were obtained on a Waukesha RDH Engine. All data used were for an engine speed of approximately 1830 rpm with a fuel rate of 5.08 lb_m/hr. The compression ratios ranged from 7:1 to 12:1. In each case the equivalence ratio was 1.2 and the residual fraction was estimated to be 0.05. The RDH engine has a bore of $3^{13}/16$ in. and a stroke of $3^5/8$ in. The lower heating value of the fuel was 18600 BTU/lb.

Figure 7 shows the pressure and pressure-derivative data for the 7:1 compression ratio. The calculated mass rate of burning is also shown in Fig. 7. As in the compression ignition calculations, small ripples in the pressure derivative caused similar amplified ripples in the burning rate. For example, the small wave in $dp/d\theta$ at 183 CA° showed up as a similar wave in $dM_b/d\theta$.

Figure 8 shows the computed values of T_b, T_u, and V_b/V as a function of crankangle as obtained from the 12:1 compression ratio data. The burned temperature reaches a peak several crankangle degrees before the unburned temperature does. The shapes and general magnitude of the temperatures agree with the experimental data given in reference (33).

Figure 9 is a compilation of the computed mass-burned fraction curves for the various data investigated. The rather odd shape of the 9.7:1 compression ratio curve was compared to data given in reference (33). Examination of Fig. 18 of reference (33) shows that when experimental pressures and temperatures were used to calculate the mass-burned fraction, curves similar to that shown for 9.7:1 were sometimes obtained. The 12:1 compression ratio calculation did not reach the 100 percent burned point because "negative burning" was predicted at 200 CA° (about 5 CA° after peak pressure). Examination of the pressure curve showed that a rather rapid decrease in pressure occurred at this point. Similar decreases in pressure are sometimes observed in combustion bomb data where they are usually attributed to the increased heat transfer which occurs when the burned gas comes into contact with the bomb walls.

One of the standard plots used in spark-ignition heat-release work is a plot of mass fraction burned versus volume fraction burned. It has been found (34) that this curve is essentially universal in that data for various operating conditions and various engines all fall on this curve. Figure 10 shows such a curve as obtained from the computer calculations. All compression ratio data fell within the band shown. The computed curve agrees with the "universal curve" as obtained from analysis of flame pictures.

Various calculations were performed to investigate the effects of charge-mass changes, pressure magnitude shifts, heat-transfer magnitude changes, and shifting the pressure data with respect to crankangle. Increasing the charge mass by 5 percent caused the burning rate to decrease and thus prolonged the burning period. Thus the mass of the charge must be known accurately if duration of burning is to be predicted accurately. Shifting the pressure curve upward by 5 psia did not cause any significant changes in the burning rate. Increasing the heat-transfer coefficient by 50 percent caused the burning rate to increase slightly so that the duration of burning was decreased very slightly. The general effect was negligible however. Shifting the pressure curve to the right or left by 2 CA° caused a change in burning rate. Figure 11 shows the mass fraction burned curves again shifted back in the opposite direction in the same manner as was described for Fig. 5. Figure 11 shows that the first 70 percent of burning was essentially unchanged except that the curves were shifted about 2 CA° in the same direction as were the pressure curves. The duration of burning, nevertheless, was unaffected by these shifts because of the change in burning rate during the last 30 percent of burning. When the pressure was shifted to the right, the burning was completed 2 CA° before peak pressure which is clearly impossible. When the pressure was shifted to the left, burning continued for 2 CA° beyond peak pressure. It should be remarked in this regard that for all but the 7:1 compression ratio, the unshifted "basic" calculations showed burning beyond peak pressure. For example, 93 percent of the mass had burned at peak pressure for the 8:1 compression ratio, 86 percent for the 9.7:1 data, and only 80 percent for the 12:1 data. Returning to the data of Fig. 11, it was found that these data also fell on the plot of Fig. 10 but that the data for the right shifted pressure fell slightly below the band shown. The curve of Fig. 10 was insensitive to all of the various changes in the calculations.

CONCLUSIONS AND SUGGESTIONS FOR FUTURE STUDIES

The methods presented here for calculating rates of heat release are particularly useful when applied to complete cycle simulations. They allow for the simulation of combustion without requiring a detailed knowledge of the phenomena, but are particularly sensitive to the pressure-derivative data and thus require excellent quality pressure diagrams. The methods are also limited further by the rather severe assumption of thermodynamic equilibrium. They should nevertheless provide a basis for more detailed studies of engine combustion-chamber design. Since one of the most promising uses of cycle simulation programs is to predict performance for engines not yet built, it is imperative that a considerable effort be made to either replace the programs given here with more basic models which do not require pressure input data, or to correlate various design and operating variables with the heat-release curves as predicted by the present models. In fact, a great deal of practical knowledge might be obtained by using the heat-release and cycle programs in conjunction with a comprehensive experimental study of the effects of design variations.

ACKNOWLEDGMENTS

The authors wish to thank Dr. Chen, Dr. Wu and Mr. McAulay all of the International Harvester Company; Mr. Basiletti and the staff of Continental Engineering Corporation; the research staff of Ethyl Corporation; and Dr. Patterson of General Motors Engineering Staff for their cooperation in supplying data for this project. The authors also wish to extend special thanks to Dr. H. Newhall who supplied the thermodynamic property data, Mr. G. Ebersole who helped in processing the property data, and Professors Myers and Uyehara who supplied continuous encouragement and advice.

The authors extend their gratitude to the Army Tank Automotive Command for its financial support and to NSF and WARF for their support in making available the CDC 1604 computer.

NOMENCLATURE

A_i = area of surface i, sq in.
CA° = crankangle degrees
f = fuel-air ratio
f_0 = initial fuel-air ratio prior to fuel addition
f_s = stoichiometric fuel-air ratio
F = f/f_s, equivalence ratio
h_b = enthalpy of products, BTU/lb_m
h_f = enthalpy of fuel, BTU/lb_m
h_u = enthalpy of reactants, BTU/lb_m
$\mathcal{H}$ = heat-transfer coefficient, BTU/sq in-deg R-sec
$H_{f(T)})_i$ = enthalpy of formation at T deg R for species i, kcal/mole
$H_{s(T)})_i$ = sensible enthalpy T deg R reference for species i, kcal/mole
J = conversion factor, 9337.44 in-lb/BTU
$\tilde{M}_i$ = molecular weight of species i
M = mass, lb_m
m_f = mass fraction
p = pressure, psia
$\dot{Q}_i$ = heat transfer to surface i, BTU/sec
R = gas constant, BTU/lb_m-deg R
R^* = gas constant for undissociated products, BTU/lb_m-deg R
t = time, sec
T = temperature, deg R
T_w = surface temperature, deg R
u = internal energy, BTU/lb_m
u^* = undissociated internal energy, BTU/lb_m-air
δu = correction to 0 deg R reference, BTU/lb_m-air
Δu = deviation caused by dissociation, BTU/lb_m-air
V = volume, cu in.
$\tilde{x}_i$ = mole fraction of species
μ = viscosity coefficient
θ = engine, crankangle, deg

SUPERSCRIPT

• = derivative, d/dt

SUBSCRIPTS

u = value for unburned mixture
b = value for burned mixture

REFERENCES

1. K.J. McAulay, G.L. Borman and T. Wu, "Development and Evaluation of the Simulation of the Compression Ignition Engine." Part 1, Part 2, by S.K. Chen, P.S. Myers and O.A. Uyehara, SAE Paper No. 650451, May 1965.

2. G.L. Borman, "Mathematical Simulation of Internal Combustion Engine Processes and Performance Including Comparisons with Experiment." PhD thesis, ME Dept. University of Wisconsin, Madison, Wis., 1964.

3. H.A. Cook, "Digital Computer Analysis and Interpretation of Turbocharged Diesel Engine Performance." SAE Transactions, Vol. 67, 1959, pp. 532-544.

4. H.A. Cook, "Appraisal of Effects of Operating Conditions and Engine Design on Combustion in Reciprocating Engines by Engine Cycle Calculations." SAE Paper No. 633C, 1963.

5. N.D. Whitehouse, A. Stotter, G.D. Goudie and B.W. Prentice, "Method of Predicting Some Aspects of Performance of a Diesel Engine Using a Digital Computer." Proceedings, Institution of Mechanical Engineers, Vol. 176, No. 9, 1962.

6. F.M. Strange, "An Analysis of Ideal Otto Cycle." SAE Paper No. 633D, 1963.

7. D.J. Patterson and G. Van Wylen, "A Digital Computer Simulation of Spark-Ignited Engine Cycles." SAE Paper No. 633F, 1963.

8. D.J. Patterson, "A Comprehensive Cycle Analysis and Digital Computer Simulation for Spark-Ignited Engines." PhD thesis, Dept. of Mechanical Engineering, University of Michigan, Ann Arbor, Mich., 1962.

9. P. Huber and J.R. Brown, "Computation of Instantaneous Air Flow and Volumetric Efficiency." SAE Paper No. 812B, 1964.

10. W.T. Lyn, "Study of Burning Rate and Nature of Combustion in Diesel Engines." Ninth International Symposium on Combustion, Academic Press, New York, N.Y., 1962, pp. 1069-1082.

11. A.E.W. Austen and W.T. Lyn, "The Application of Heat Release Analysis to Engine Combustion Study." CIMAC Conference, Copenhagen, Denmark, 1962, pp. 1067-1099.

12. M.M. El-Wakil, P.S. Myers and O.A. Uyehara, "Fuel Vaporization and Ignition Lag in Diesel Combustion." SAE Transactions, Vol. 64, 1956, pp. 712-729.

13. G. Borman and J. Johnson, "Unsteady Vaporization Histories and Trajectories of Fuel Drops Injected into Swirling Air." SAE Paper No. 598C, 1962.

14. M.H. Edson, "A Mathematical Model for Combustion." Industrial and Engineering Chemistry, Vol. 52, No. 12, December 1960, pp. 1007-1014.

15. G. Walker, "Effect of the Rate of Combustion on Gasoline Engine Performance." Journal of the Institution of Fuel, June 1964, pp. 228-233.

16. "Basic Considerations in the Combustion of Hydrocarbon Fuels with Air." Propulsion Chemistry Division, Lewis Laboratory, NACA, Report 1300, 1959.

17. N.N. Semnov, "Thermal Theory of Combustion and Explosion - Theory of Normal Flame Propagation," NACA TM 1026, September 1942.

18. D.J. Patterson, "Cylinder Pressure Variations, A Fundamental Combustion Problem." SAE Paper No. 660129, January 1966.

19. J.H. Johnson, "End-Gas Temperatures, Pressures, and Reaction Rates." PhD thesis, Dept. of Mechanical Engineering, Univessity of Wisconsin, Madison, Wis., 1964.

20. H.K. Newhall and E.S. Starkman, "Thermodynamic Properties of Octane and Air for Engine Performance Calculations." SAE Paper No. 633G, 1963.

21. H.K. Newhall, private communication, 1963.

22. "JANAF Interim Thermodynamical Data Tables," Dow Chemical Corporation, Midland, Mich., 1960.

23. H.N. Powell, "Applications of an Enthalpy-Fuel/Air Ratio Diagram to 'First Law' Combustion Problems." Trans. ASME, Vol. 79, December 1957, pp. 1129-1142.

24. W.J.D. Annand, "Heat Transfer in the Cylinders of Reciprocating Internal Combustion Engines." Institution of Mechanical Engineers, Vol. 177, No. 36, 1963, pp. 973-996.

25. C.R. Wilke, "A Viscosity Equation for Gas Mixtures." Journal of Chemical Physics, Vol. 18, 1950, p. 517.

26. J. Hilsenrath, "Tables of Thermodynamic and Transport Properties." Pergamon Press, London, England, 1960; also NBS Circular 564, November 1955.

27. A.L. Linsay and L.A. Bromley, "Thermal Conductivity of Gas Mixtures." Industrial Engineering Chemistry, Vol. 42, 1950, p. 1508.

28. R.E. Gish, J.D. McCullough, J.B. Retzlaff and H.T. Mueller, "Determination of True Engine Friction." SAE Paper No. 117, 1957

29. D.W. Marquardt, "An Algorithm for Least Squares Estimation of Non-linear Parameters." Journal of the Society of Industrial and Applied Mathematics, Vol. 2, No. 2, June 1963, pp. 431-441.

30. F.D. Rossini, "Selected Values of Physical and Thermodynamic Properties of Hydrocarbons and Related Compounds." Carnegie Press, Pittsburgh, Pa., 1953.

31. G. Eichelberg, "Some New Investigations on Old Combustion Engine Problems." Engineer, London, England, Vol. 148, 1939, p. 603.

32. R.V. Kerley and K.W. Thurston, "The Indicated Performance of Otto-Cycle Engine." National Fuels and Lubricants Meeting, Houston, Tex., November 1961.

33. G.H. Millar, O.A. Uyehara and P.S. Myers, "Practical Application of Engine Flame Temperature Measurements." SAE Transactions, Vol. 62, 1954, pp. 514-522.

34. E.F. Obert, "Internal Combustion Engines." International Textbook Company Scranton, Pa., 1950, pp. 449-455.

APPENDIX

RICH-SIDE INTERNAL-ENERGY AND GAS-CONSTANT EQUATIONS

The quantity u^* is calculated from equation (16) using the coefficients given in Table 2. The quantity Δu is calculated from equation (17) using the coefficients given in Table 3. The internal energy in units of BTU per pound of mixture is then given by

$$u = u^*/(1. + .067623\ F) \qquad T < 3800\ °R \tag{38}$$

$$u = (u^* + \Delta u)/(1. + .067623\ F) \qquad T \geq 3800\ °R \tag{39}$$

The quantity $\tilde{M}^*$ is calculated from equation (18) or (19) using the coefficients given in Table 4. The quantity $\Delta\tilde{M}$ is calculated from an equation of the same form as equation (17). The coefficients are given in Table 5. The gas constant for the products of combustion in units of BTU/deg R per pound of mixture is given by

$$R_b = 1.9698/\tilde{M}^* = 1.9698/\tilde{M}(F) \qquad T < 3800\ °R \tag{40}$$

$$R_b = 1.9698/(\tilde{M}^* + \Delta\tilde{M}) \qquad T \geq 3800\ °R \tag{41}$$

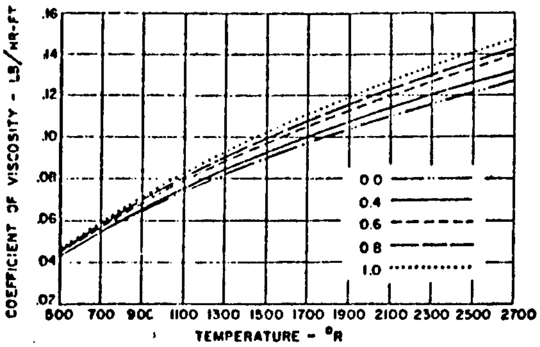

Fig. 1 Viscosity of products of combustion of C_nH_{2n} and air calculated using data of NBS 564 and equations of Wilke for equivalence ratios of 0.4, 0.6, 0.8, 1.0.

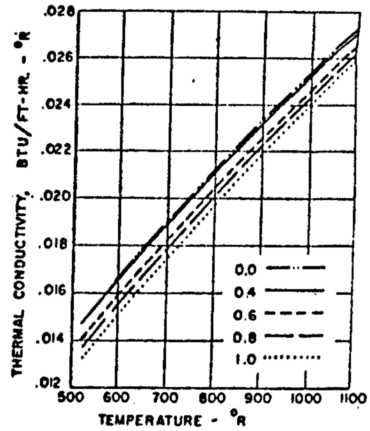

Fig. 2 Thermal conductivities of products of combustion of air and C_nH_{2n} for equivalence ratios of 0, 0.4, 0.6, 0.8, 1.0.

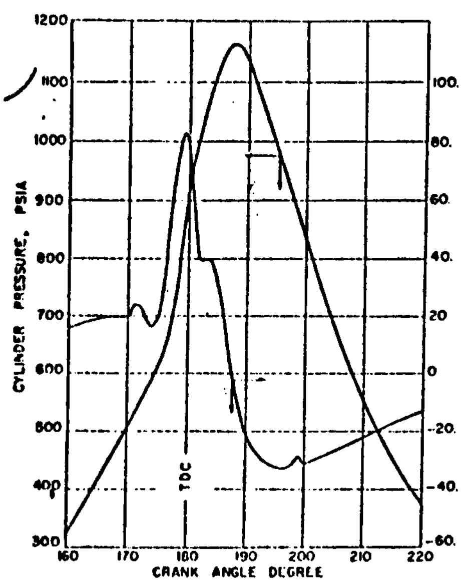

Fig. 3 Experimental pressure and pressure-derivative diagram, 3200 rpm, full load.

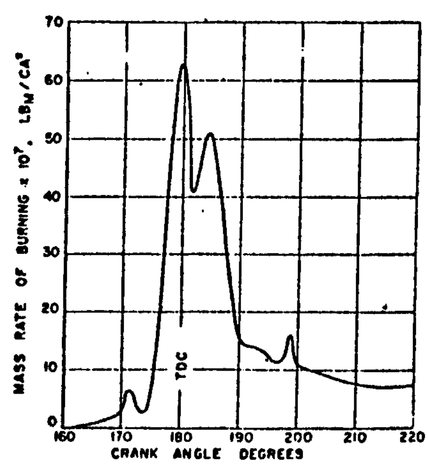

Fig. 4 Computed mass burning rate calculated from data of Fig. 3.

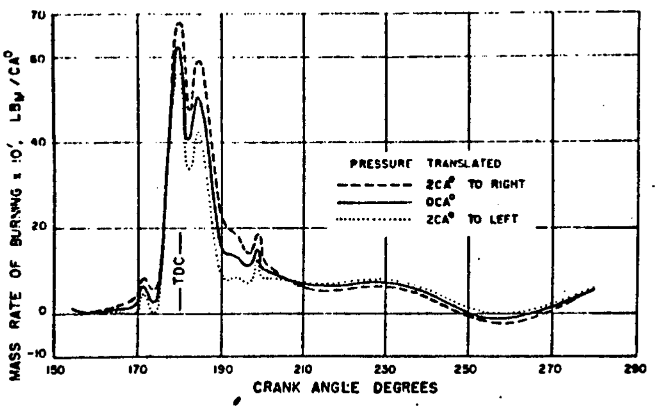

Fig. 5 Mass burning rate curves calculated with pressure shifted ± 2 CA°. Burning rates shifted ∓ 2 CA° to show shape change.

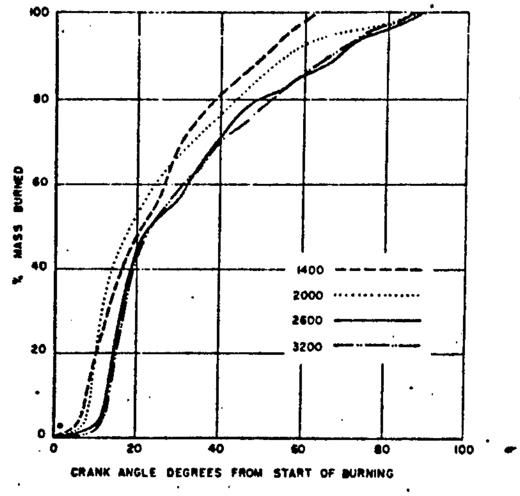

Fig. 6 Percent mass-burned curves for various engine speeds.

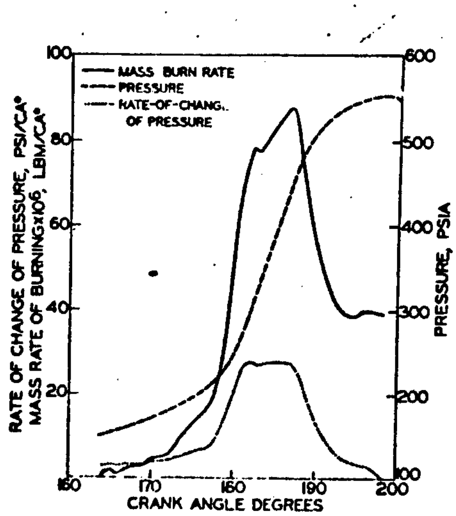

Fig. 7 $\dot{M}_b, P, \dot{P}$, for compression ratio 7:1, speed 1825 rpm.

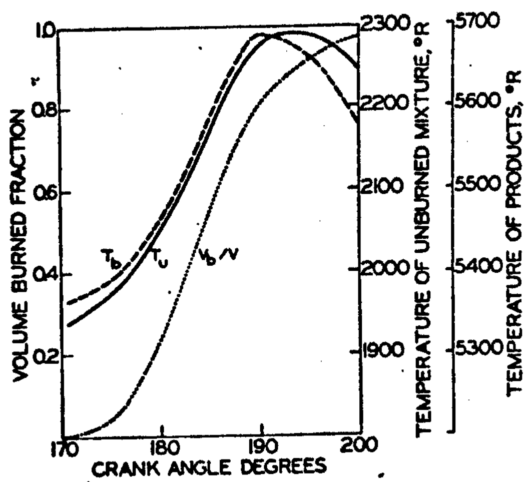

Fig. 8 Gas temperatures and fraction of volume burned for 12:1 compression ratio and 1830 rpm.

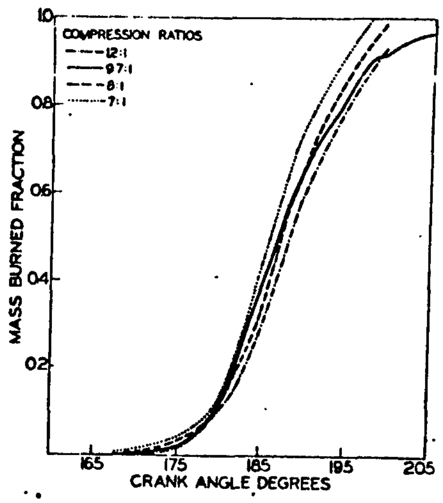

Fig. 9 Mass-burned fraction curves for various compression ratios.

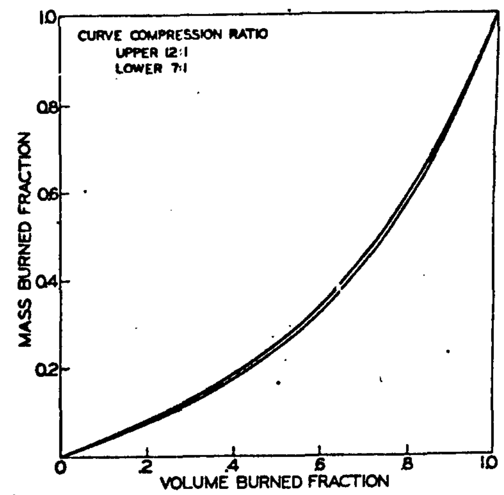

Fig. 10 "Universal" mass versus volume burned curve.

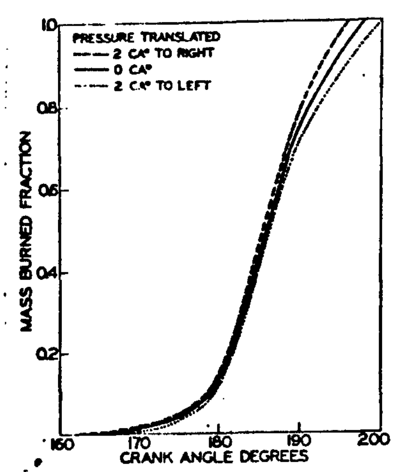

Fig. 11 Mass fraction burned calculated with pressure shifted ± 2 CA°. Burned fraction curves shifted ∓ 2 CA° to show shape change.

APPENDIX VI

B

Cyclic Variation and Average Burning Rates in a S.I. Engine

B.D. Peters and G.L. Borman
Mechanical Engineering Dept.
University of Wisconsin

ABSTRACT

A method of calculating mass burning rates for a single cylinder spark-ignition combustion engine based on experimentally obtained pressure-time diagrams was used to analyze the effects of fuel-air ratio, engine speed, spark timing, load, and cyclic cylinder pressure variations on mass burning rates and engine output.

A study of the effects on mass burning rates by cyclic pressure changes showed the low pressure cycles were initially slow burning cycles. Although large cyclic cylinder pressure variations existed in the data the cyclic variations in imep were relatively small.

INTRODUCTION

In an attempt to simulate analytically a spark ignition engine, the problem of handling the combustion process became obvious. Consequently, a study was initiated to determine a method of representing the combustion process. This problem is especially difficult since several factors alter the way the mixture burns. These effects include the amount of bulk mixture motion in the combustion chamber, temperature gradients in the burned and unburned gases, prereactions in the end gas, cyclic burning rate changes, magnitudes of the heat transfer rates, and the final burned gas composition.

Previous investigations have shed some light on how to handle some of the combustion model problems while others remain unsolved. Combustion pictures (1)* have shown that the flame propagates across the combustion chamber with a turbulent flame front. Also, it is generally believed (2) that prereactions in the unburned gas are oxidation reactions that result in autoignition as the necessary pressures and temperatures are reached. Instantaneous heat transfer rates are not well understood and thus the correlations by Nusselt and Eichelburg are frequently used to calculate instantaneous heat transfer (3). The burned gas is often assumed to be composed of equilibrium concentrations of about ten species. Cyclic combustion rate variations, and hence pressure variations, are believed to be primarily caused by differences in mixture motion in the chamber (4,5). However, the mixture motion in a combustion chamber is currently not well understood. As a consequence cyclic combustion rate changes can not be predicted. Also, burned gas temperature variations appear to be not too important when computing burned gas energy (6). Thus as one reviews the problems and current knowledge about them it can be seen that it is difficult to predict accurately energy release rates without resorting to empirical data for correction factors.

Although many unsolved problems exist in forming an accurate combustion model, the need for such a description has led several investigators to develop models which incorporate various simplifying assumptions. The models that have been developed can be divided into six categories. The first group includes constant volume combustion models. Obert (7), Bonamy (8), and Goodwine and Pickett (9) furnish examples of this type. The second method uses combustion pictures similar to those of Rassweiler and Withrow (1) to determine approximate mass burning rates. A third technique uses experimentally obtained pressure-time data to calculate mass burning rates.

*Numbers in parentheses designate References at end of paper.

Examples of this general procedure have been furnished by Rassweiler and Withrow (1), Krieger and Borman (10), Schweitzer (11), Bascunana (12), and Millar, Uyehara, and Myers (13). The fourth procedure uses an arbitrary relationship between mass burned and time to describe the combustion rate. Walker (14), Edson (15), and Huber and Brown (16) have used this method. A fifth procedure is to assume a flame velocity and a flame shape and use this information to calculate a mass burning rate; Strange (17) has used this approach. The sixth technique is to use a flame propagation theory to determine the rate of energy release of the fuel. This procedure has been used by Patterson (18).

Since all these models eventually resort to experimental data to obtain values of assumed coefficients, etc., (some to a larger extent then others) it was decided to use a combustion representation for this study that relies upon empirical pressure-time data. In this way it was hoped that an accurate set of mass burned fraction versus crankangle curves could be obtained for different engine operating conditions. An available model of this type is one developed by Krieger and Borman (10). This model divides the combustion chamber into burned and unburned sections. Energy rate equations are written for each system which include instantaneous heat transfer. Mass is assumed to go from the unburned to the burned state instantaneously with the burned gas assumed to be at equilibrium and to dissociate above burned temperatures of 3800 R. The dissociated species are assumed to be O, H, N, OH, NO, H_2, CO, N_2, O_2, CO_2, and H_2O. The unburned gas is taken to be a fuel-air mixture plus a residual from the previous cycle. Prereactions in the unburned gas are neglected. Both systems are assumed to be at uniform but different temperatures and at the same uniform pressure. Heat transfer to the combustion chamber walls is calculated using the Eichelburg heat transfer coefficient with the instantaneous area fractions exposed to the burned gas equal to the instantaneous volume burned fraction. The wall temperatures were estimated with the sleeve, piston, head, and valves, each at a different assigned temperature. The perfect gas law is assumed valid for both the burned and unburned gases. By numerically solving the equations based on the above assumptions, a mass burning rate as a function of burned and unburned thermodynamic gas properties and pressure-time data was determined.

This model was then used in conjunction with a set of experimentally obtained pressure-time traces for engine runs of various engine operating conditions. The results are a set of mass burned fraction versus crankangle plots for runs in which the fuel-air ratio, engine speed, ignition timing, and engine load were changed.

EXPERIMENTAL APPARATUS

For this investigation, pressure-time data were generated by a Department of the Army model M151 engine. It is a four cylinder, inline, overhead valve gasoline unit with a cylinder displacement of 35.375 cu in. For this project it was converted to one cylinder operation. The fuel-air inlet system included critical flow nozzles to measure the air flow rate, a bellows displacement type gas meter to measure the gaseous fuel rate, a gas mixer to mix the fuel and air, a surge tank and an intake pipe with a flame arrester. Isobutylene was used as the fuel. Crankshaft position was determined by using two channels of phototransistors along with a 2 ft diameter slotted disc mounted on the front end of the crankshaft. Cylinder pressure was obtained using a Kistler model 601L quartz pressure transducer covered with G.E. RTV 106 silicon adhesive. The pressure time data was then recorded at 120 ips on magnetic tape using a Sangamo Electric model 4784 tape recorder described in Ref. 19.

DATA REDUCTION

The cylinder pressure and crankshaft position data were reduced by playing the tape recorded data back at 7 1/2 ips and analyzing the data on a hybrid computer. The hybrid computer was composed of an Applied, Dynamics model 256 analog computer and a Scientific Data Systems model 930 digital computer. Three different operations were performed on the data using this computer. First a program was used that reads the cylinder pressure at a specified crankangle for a given number of cycles and calculates the average pressure and standard deviation at that crankangle. Second, a program was used that reads the cylinder pressure from 179 BTDC to 180 ATDC on the compression-expansion portion of the cycle. This program computes an average pressure trace formed by taking the average pressure at each crankangle for 300 cycles. It also saves the cycles with the maximum peak pressure, minimum peak pressure, and

a randomly selected cycle. The third program calculates the mean effective pressure for 720 deg of each cycle using Simpson's rule and calculates the average mep and the standard deviation. This program also saves the peak pressure for each cycle and the crankangle at which it occurred. The output from these three programs was obtained in printed form.

EXPERIMENTAL ERROR

The accuracy of the piezoelectric pressure measurements was dependent on the accuracy of the pressure transducer, charge amplifier, the tape recorder, and the hybrid computer. Based on the study of pressure transducer accuracy of Ref. 20 and on tape recorder and hybrid computer capabilities it is estimated that a maximum error of about 5% is possible in the cylinder pressure measurements. The crankangle marks are believed to be accurate to within 0.25 crankangle when the samples are taken on the hybrid computer. The fuel and air flow rates are believed to have errors of 0.3%. Thus the fuel-air ratio and inlet flow rate could have errors up to about 6%.

EFFECTS OF ERRORS AND ASSUMPTIONS ON COMPUTED BURNING RATES

Since errors in measured data and any invalid combustion model assumptions would affect the magnitudes of calculated mass burning rates it was necessary to determine these effects. Experimental errors could be introduced by inaccurate pressure data, fuel flow rates and air flow rates.

It was found that the pressure trace would have to be shifted about 1 deg before the effect of a phase shift caused more than about a 1% change in the amount of mass calculated to have been consumed. The mass burned fraction versus crankangle curves were essentially the same. It was also found that an addition of 5 psi to all pressures had a negligible effect on the mass burned fraction versus crankangle curve. However, a 2% increase in all pressures increased the amount of mass calculated to be consumed by about 2%.

Figure 1 shows the effect of altering the fuel and air flow rates by 10% for a given pressure-time diagram. It can be seen that it is quite important to measure flow rates accurately.

Two semiempirical quantities that could introduce errors were the amount of residual from the previous cycle and the amount of trapped mass in the cylinder. The amount of residual was determined by estimating the mass contained in the cylinder at TDC on the exhaust-intake stroke based on the clearance volume, the cylinder pressure, and an assumed temperature. It was found that one could completely eliminate a 7% residual with only a negligible effect on the mass burned fraction versus crankangle curve.

Figure 2 shows the effect of changing the trapped mass in the cylinder for a given pressure-time diagram. The normal value was determined by multiplying the input fuel-air flow rate by the time for one cycle. For all three of these runs the amount of mass calculated to have burned was nearly constant.

Three combustion model assumptions were examined. These were the effect of changing the heat transfer coefficient, the effect of burned gas dissociation, and the effect of the assumption of a uniform burned gas temperature. The effects of nonequilibrium states in the burned gas and the effects or wall quenching were not examined. Krieger and Borman (10) tested the effect of increasing the Eichelburg heat transfer coefficient by 50% and found that the overall effect was negligible. Their calculations, however, were based on a combustion period of only about 40 deg. The results of this study show that, initiating with the spark, the combustion period is approximately 80 deg. With this longer duration of burning it was found that a 50% increase in the heat transfer coefficient increased the final mass burned fraction; for example, for data run no. 1 the final mass burned fraction was increased by 4.8% with the major portion of this increase coming after the 80% mass burned point. Thus if combustion takes place over a long period the accuracy of the heat transfer coefficient becomes more important. The effect of dissociation of the products can be seen on Fig. 3. This figure shows that dissociation has only a small effect on the mass burned fraction versus crankangle plot. The other combustion

model assumption that was studied was the effect of a nonuniform burned gas temperature. To investigate this effect the final mass of the burned gas was divided into eleven equal units with temperatures in 100 R increments from 500 F below to 500 R above the calculated final mass average burned gas temperature. It was found that the internal energy changed only about 1% with a 1000 R temperature differential. Consequently, this effect was assumed negligible.

The results of these studies indicate that several sources of error exist in the combustion model and in the experimental data. Errors in the amount of mixture burned caused by each of the combustion model assumptions investigated except heat transfer would be about 1% each. Roughly, a 10% increase in heat transfer would increase the mass burned by about 1%. However, the accuracy of the Eichelburg coefficient is unknown. Errors of up to a maximum of 4-5% could be caused by inaccurate fuel-air mixture flow rates and by incorrect cylinder pressure values. Also, an unknown error could be caused by mixture loss due to piston blowby and valve overlap.

EXPERIMENTAL RESULTS ON CYCLIC VARIATIONS

A large cyclic cylinder pressure variation was found in the data from the 17 different data runs. An example of the variations can be seen from Fig. 4 in which the cycles with the maximum and minimum peak pressures and the average pressure trace based on 300 individual cycles are shown. These curves are for data run no. 1:2000 rpm, 23 BTDC ignition timing, 0.96 equivalence ration and wide open throttle. Figure 5 shows a frequency plot of data taken at 9 ATDC for the above mentioned run. The 9 ATDC crankangle was selected to be in the region of largest cyclic pressure variation. An analysis of the data of Fig. 5 shows the cyclic pressure distribution is essentially a normal distribution. The average pressure at 9 ATDC based on 300 cycles was 360 psia with a standard deviation of 53.3 psi. The average and standard deviation at this crankangle were calculated for the first 50 cycles, 100, etc., up to 400 cycles. It was found that after 300 cycles were included these values varied less than 1%.

The cyclic variation in work was also investigated. Initially pressure-time traces for the cycles with the maximum and minimum peak pressures and the average cycle were used with Simpson's rule to calculate the imep from 180 BTDC to 180 ATDC. It was found that in 10 of 14 runs studied, the cycle with the maximum peak pressure did a small percentage more work than the minimum peak pressure cycle with the average trace falling between the two extremes. This led to the thought that peak cycle pressure and imep were related. Thus the hybrid computer was used to calculate imep based on 720 crankangles for each individual cycle for 350 cycles. The results of these calculations showed that the standard deviation of the imep was approximately 1% of the average imep. As a representative example, for data run no. 3 at 2000 rpm, wide open throttle, 23 BTDC ignition timing, and 1.1 equivalence ratio the average imep for 350 cycles was 119 psi with a standard deviation of 1.05 psi. The maximum and minimum imep's were 121.7 psi and 114.0 psi. An attempt to correlate imep's and the peak cycle pressure was made, but the imep data were randomly distributed in relation to the peak cycle pressure. Consequently, it was concluded that the imep and peak pressure are not simply related.

One other point is that although large cyclic variations occurred in the cylinder pressure the imep's for the various cycle were nearly the same. For example, for data run no. 3, the spread in peak cycle pressures was from 351 to 583 psia while the imep ranged from 114.0 to 121.7 psi.

EFFECT OF CYCLIC VARIATIONS ON BURNING

Since the combustion representation employed for this project used experimental pressure-time data directly, it was necessary to investigate the effect on the mass burning rate caused by cyclic cylinder pressure variations. Figure 6 shows the difference in shape of the mass burned fraction versus crankangle curve for calculations made using the average cycle, cycle with maximum peak pressure, and the cycle with the minimum peak pressure for a representative data run (no. 7), made at 2000 rpm, 20 BTDC ignition timing, 1.18 equivalence ratio and a manifold pressure of 11.4 psia. The mass burning rate is closely related to the pressure derivative; thus one has reasonable assurance that the burning curves for the maximum and minimum peak pressure cycles on Fig. 6 form an envelope for the burning curves for all the cycles at

that engine condition. One can see from Fig. 6 that the low peak pressure cycle had a much smaller burning rate initially after the spark than did the maximum peak pressure cycle. This effect was probably caused by differences in mixture motion near the spark plug at ignition (4). One can also see that the burning rate of the low peak pressure cycle continued to be lower than the high peak pressure cycle even after combustion was well under way. It is not known whether this later burning rate reduction was caused by a factor such as reduced bulk mixture motion in the cylinder or if it was caused in some way by the relatively late start in burning as compared to the high peak pressure cycle. Because of this cyclic variation in burning rates it is necessary to either choose a particular rate of burning curve for use in the combustion model or to combine several curves in some statistical manner.

For engine simulation the average pressure trace should be used because it yields the average power output. This procedure has the advantage that by taking an average of many cycles, random noise introduced into the data by instrumentation is nearly eliminated. However, if small, nonrepeatable fluctuations in the pressure data were caused by actual combustion phenomena they would be lost in the averaging process.

In addition, the cylinder pressure enters the Eichelburg heat transfer coefficient in a nonlinear manner. An investigation of this problem based on the fluctuation of the pressure at a given crankangle showed that the average heat transfer and the heat transfer calculated using the average pressure were different by only a small percentage. This difference was believed to be less than the accuracy of the Eichelburg correlation itself. As a result of the investigation on cyclic combustion rates it was decided to use average cylinder pressure traces to calculate the heat release curves for this study.

EFFECT OF ENGINE VARIABLES ON BURNING

The effect of fuel-air ratio, engine speed, spark timing, and engine load on mass burning rates was studied.

Over the range of fuel-air ratios studied, changes in the fuel-air ratio appeared to have a rather small effect on the mass burning rates. Figure 7 shows how the mass burned fraction versus crankangle plots changed with fuel-air ratio. It can be seen that the burning rates of the runs near stoichiometric were slightly higher than the rich and lean runs. One additional run at 1000 rpm and F = 0.84 was made which showed an even slower mass burning rate. Millar, Uyehara and Myers (13) show a plot similar to Fig. 7 in which isooctane was used as a fuel. They also show the trend that data runs near stoichiometric burn faster than rich and lean runs. However, they show a larger influence of fuel-air ratio on mass burning rates than shown here. Consequently, the possibility exists that fuel choice or other experimental variables affect the way the mass burning rate changes with fuel-air ratio.

The effect of engine speed on the mass burned fraction versus crankangle can be seen in Fig. 8. Before any comparisons are made it should be noted that the spark timing for the 2000 rpm run was 3 deg earlier than the other two runs. It can be seen that the 1000 rpm and 2000 rpm runs both burned at about the same rate while the 3000 rpm run burned slightly slower on a crankangle basis. The fact that the mass burning rate essentially keeps up with increased engine speed is generally credited to increased mixture turbulence. Also, Trumpy (2) states that changes in end gas temperatures also serve to increase the flame speed at the high speed operating conditions. The differences in the final mass burned fraction is within the range of experimental accuracy.

Four data runs were made to test the effect of spark timing. The results of these computations are shown in Fig. 9. The shape of the mass burned fraction versus crankangle curve changed with spark timing. As the timing was retarded, the burning rate slowed down. This trend was evident in all four data runs. Also, the rate of burning changed rapidly near the end of the combustion period. This change occurred at lower mass burned fractions for the early timings. In addition, a slightly greater percentage of mass was calculated to have been consumed during the retarded timing runs. However, this small difference in mass burned fraction is within the range of experimental error and one can not be certain if it is real or not.

Engine load was the fourth engine variable that was altered to test its effect on the mass burning rate. The results of the calculations for these runs are shown on Fig. 10. Note that the spark timing of the full load cycle was 3 deg earlier than the other runs. The low load cycles had burning rates that were slower than the full load cycles. This was true to a great extent initially after the spark occurred. One possible reason for this might be a reduced flame velocity at low load due to a larger residual fraction left from the previous cycle. A second reason could be reduced mixture motion in the combustion chamber because of the small flow rates at low load.

CONCLUSIONS

The results of this project show that the shape of the mass burned fraction versus crankangle curve does change as engine operating conditions are altered. Consequently, one should not use one curve to represent the combustion for all conditions. Although large cyclic cylinder pressure variations exist in actual engine data the differences in work output between the various cycles is quite small. Thus, in the present study significant power gains could not be expected by eliminating cyclic combustion rate variations.

With respect to the procedure used here to calculate mass burning curves it was found that the technique is very sensitive to the initial amount of fuel-air mixture in the combustion chamber and to the accuracy of the cylinder pressure measurements while it was less sensitive to the heat transfer rate. The authors suspect, but are not certain, that either the pressure or mixture flow rates or both of these variables may have been consistently in error, consequently causing the final calculated mass burned fractions to be about 0.9 in general. Since the heat transfer rate would have to be increased by roughly 50% or more to account for the unburned fuel, it was thought that this was probably not the source of the large unburned fraction. A small percentage error in the pressure and flow rate values would not significantly alter the shape of the mass burned fraction versus crankangle curve, but it would change the final mass burned fraction. Thus, although roughly 10% of the system's combustible mass was in general calculated to be unburned, it is believed that the general shape of the computed curves is correct although the magnitudes of the mass burned fractions may be low.

ACKNOWLEDGMENTS

This activity was conducted under contract to, and with the technical assistance of, the Systems Propulsion Lab. of the U.S. Army Tank and Automotive Command. Gratitude is also expressed to our colleagues at the University of Wisconsin particularly P.S. Myers and O.A. Uyehara who aided with advice and criticism.

REFERENCES

1. G.M. Rassweiler and L. Withrow, "Motion Pictures of Engine Flames Correlated with Pressure Cards." SAE Transactions, Vol. 33 (1938).
2. D.K. Trumpy, "The Preknock Kinetics of Ethane in a Spark-Ignition Engine." PhD Dissertation, University of Wisconsin, 1969.
3. G. Walker, "Heat Transfer in a Gasoline Engine." The Engineer, Nov. 24, 1967, pp. 690-695.
4. D.J. Patterson, "Cylinder Pressure Variations, a Fundamental Combustion Problem." Paper 660129, presented at SAE Automotive Engineering Congress, Detroit, January 1966.
5. D.E. Cole and W. Mirsky, "Mixture Motion-Its Effect on Pressure Rise in a Combustion Bomb: A New Look at Cyclic Variation," Paper 680766, presented at SAE Fuels and Lubricants Meeting, Tulsa, October 1968.
6. B.D. Peters, "The Determination of Spark-Ignition Engine Apparent Heat Release Using Experimentally Obtained Pressure-Time Data." M.S. Dissertation, University of Wisconsin, 1969.
7. E.F. Obert, "Internal Combustion Engines." Scranton, Pa.: International Textbook Co., 1968, 3rd Edition.
8. S.E. Bonamy, "A Modified Constant-Volume Fuel-Air Cycle." Automobile Engineer, January, 1966, pp. 5-9.

9. J.K. Goodwine and H.E. Pickett, "Computer Modeling the Ideal Otto Cycle." Paper 633B, presented at SAE Automotive and Engineering Congress, Detroit, January 1963.

10. R.G. Krieger and G.L. Borman, "The Computation of Apparent Heat Release for Internal Combustion Engines." ASME Diesel and Gas Power Div., 39th Conference Proceedings, 1967.

11. P.H. Schweitzer, "Discussion of the Paper, The Computation of Apparent Heat Release for Internal Combustion Engines." ASME Diesel and Gas Power Div., 39th Conference Proceedings, 1967.

12. J.L. Bascunana, "Burning Rate Development in a Closed Vessel of Arbitrary Shape and Variable Volume for Variable but Uniform Pressure." ASME Paper 68-WA/DGP-1, 1968.

13. G.H. Millar, O.A. Uyehara, and P.S. Myers, "Practical Application of Engine Flame Temperature Measurements." SAE Transactions, Vol. 62 (1954).

14. G. Walker, "Effect of the Rate of Combustion on Gasoline Engine Performance." Journal of the Institute of Fuel, June, 1964.

15. M.H. Edson, "The Otto Cycle Engine...A Mathematical Model of Combustion." Industrial and Engineering Chemistry, December, 1960, pp. 1007-1010.

16. P. Huber and J.R. Brown, "Computation of Instantaneous Air Flow and Volumetric Efficiency." Paper 812B, presented at SAE Automotive and Engineering Congress, Detroit, January 1964.

17. F.M. Strange, "An Analysis of Ideal Otto Cycle, Including the Effects of Heat Transfer, Finite Combustion Rates, Chemical Dissociation, and Mechanical Losses." Paper 633D, presented at SAE Automotive and Engineering Congress, Detroit, January 1963.

18. D.J. Patterson, "A Comprehensive Cycle Analysis and Digital Computer Simulation for Spark-Ignited Engines." PhD Dissertation, University of Michigan, 1962.

19. T. LeFeuvre, P.S. Myers, O.A. Uyehara, and J.H. Shipinski, "A Tape Recording and Computer Processing System for Instantaneous Engine Data." Paper 680133, presented at SAE Automotive and Engineering Congress, Detroit, January 1968.

20. J.W. Alyea, "The Development and Evaluation of an Electronic Indicated Horsepower Meter." PhD Dissertation, University of Wisconsin, 1968.

APPENDIX A

Table A-1 Engine Data Conditions

Run No.	Speed, rpm	Equivalence Ratio	Spark Timing, BTDC	bhp	Residual Fraction, %
1	2000	0.958	23	8.3	7
2	2000	1.05	23	8.5	7
3	2000	1.12	23	8.5	7
4	2000	1.22	23	8.4	7
5	2000	1.31	23	8.25	7
6	2000	1.16	20	2.6	12
7	2000	1.18	20	5.25	9
8	2000	1.16	20	0.5	14
9	1000	1.25	20	4.0	5
10	2000	1.14	5	5.3	7
11	2000	1.16	5 ATDC	4.6	6
12	2000	1.13	40	5.5	8
13	3000	1.08	20	8.8	8

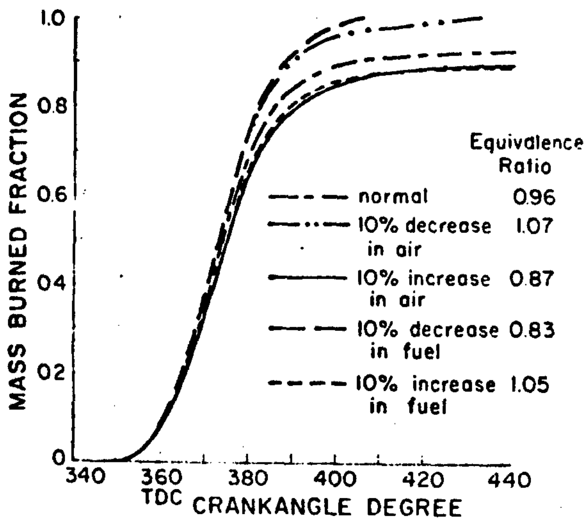

Fig. 1 Mass burned fraction versus crankangle-effect of changing amounts of fuel and air using the average pressure-time diagram of data run No. 1 (See Appendix A for engine operating conditions).

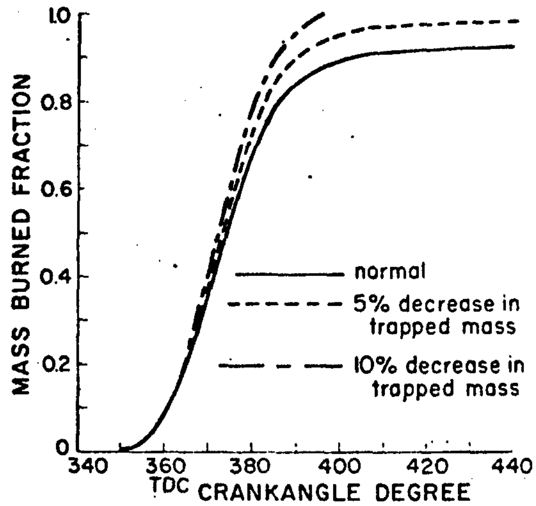

Fig. 2 Mass burned fraction versus crankangle-effect of changing amount of trapped mass using average pressure-time diagram of data run No. 1 with constant residual mass.

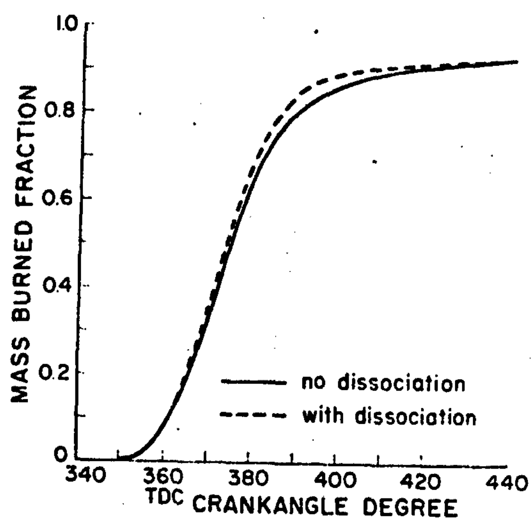

Fig. 3 Mass burned fraction versus crankangle-effect of dissociation using average pressure-time diagram of data run No. 1.

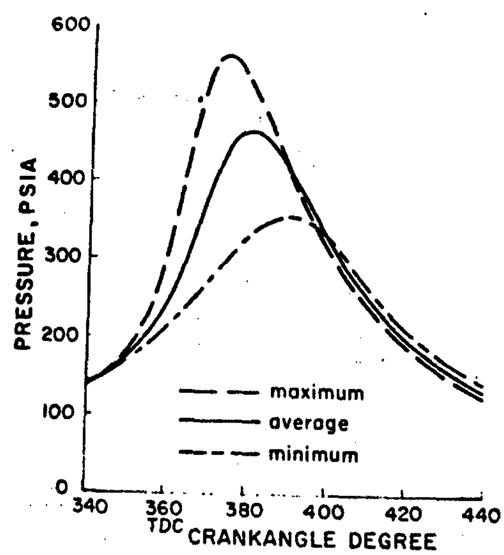

Fig. 4 Pressure-time curves for data run No. 1.

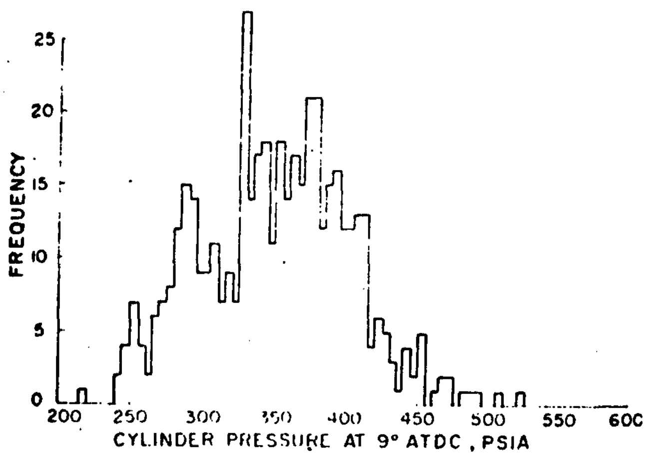

Fig. 5 Frequency plot of cylinder pressure for data run No. 1.

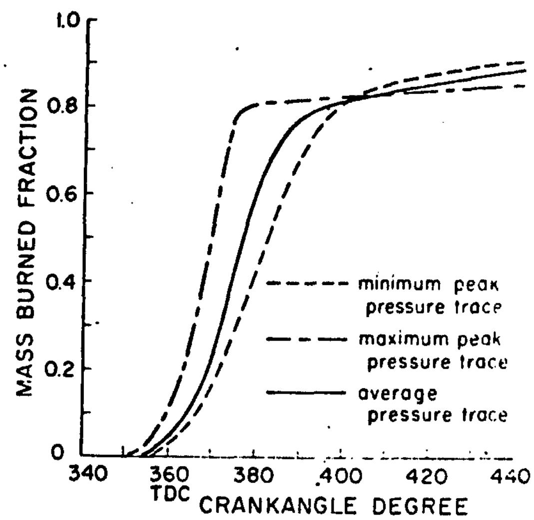

Fig. 6 Mass burned fraction versus crankangle for three cycles of data run No. 7.

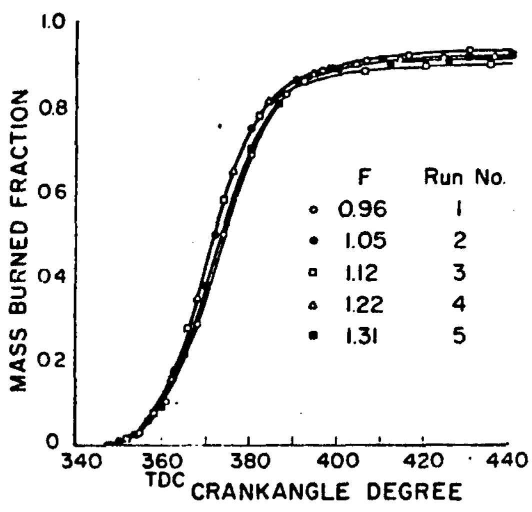

Fig. 7 Mass burned fraction versus crankangle for different fuel-air ratios using average pressure-time diagrams.

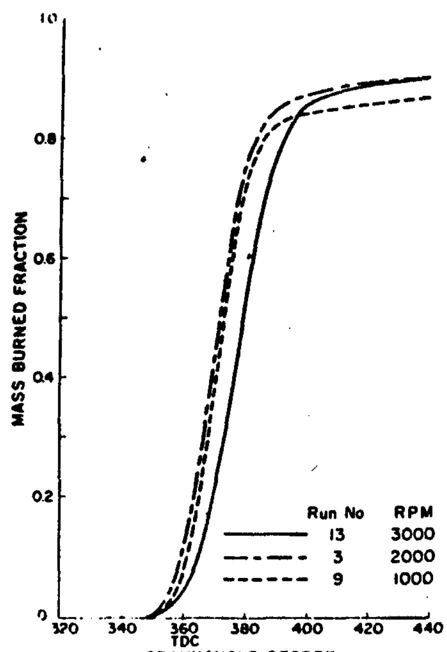

Fig, 8 Mass burned fraction versus crankangle for different engine speeds using average pressure-time diagrams.

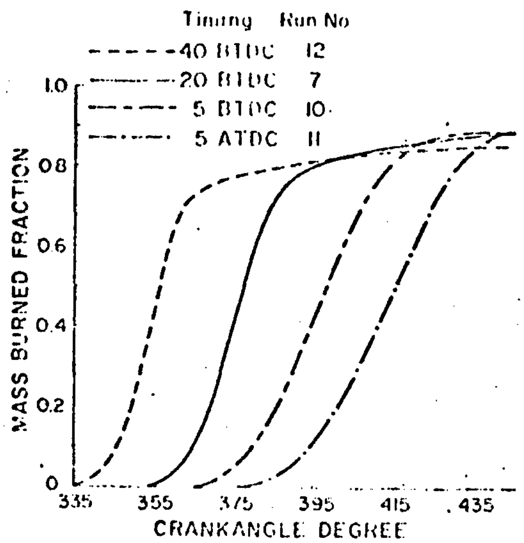

Fig. 9 Mass burned fraction versus crankangle for different spark timings using average pressure-time diagrams.

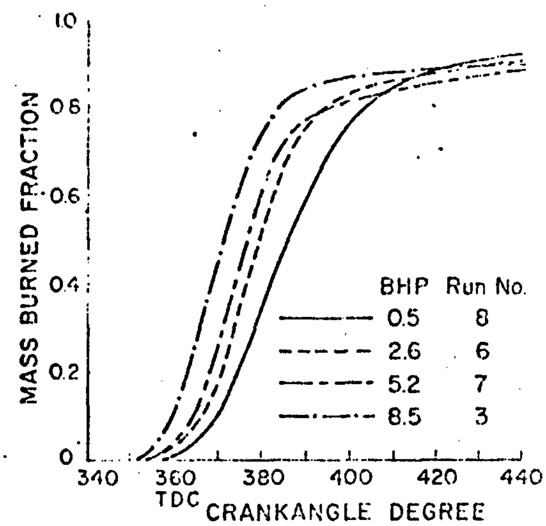

Fig. 10 Mass burned fraction versus crankangle for different engine loads using average pressure-time diagrams.

APPENDIX VI

C

Experimental Correlation Between Rate-of-Injection and Rate-of-Heat-Release in a Diesel Engine

J.H. Shipinski, P.S. Myers and O.A. Uyehara
Mechanical Engineering Dept.
University of Wisconsin

ABSTRACT

The recent development of very large, high-speed computers has encouraged attempts to simulate, in detail, internal combustion engines. In the simulation of the diesel engine, the preferred procedure would be to start with the injection system geometry, compute a rate-of-injection and, from this, compute a rate-of-heat-release and a cylinder pressure-time diagram. The primary objective of the work presented in this paper was to obtain a relationship between the rate-of-injection and the rate-of-heat-release. Rates-of-heat-release and rates-of-injection computed from experimentally obtained engine data are presented. These data have been correlated and expressions for these correlations are given. The single-cylinder open-chamber diesel engine used to obtain data for the correlation was run at speeds of from 1000 to 2500 rpm, with loads of from 60 to 330 psi motored indicated mean effective pressure. Indicated specific outputs of up to 1 hp/cu in. were observed. Injection rates and heat-release rates obtained while varying speed, inlet manifold pressure, fuel-air ratio, injection advance, and the injection system components are illustrated and compared graphically. A mathematical representation of the smoothed heat-release rate curve is developed. Mathematical expressions relating the heat-release rate to the engine operating conditions, injection system, and fuel are presented.

INTRODUCTION

The simulation of a fired compression-ignition engine (CIE) on a digital computer requires knowledge of the rate-of-heat-release (ROHR) during combustion. In the past, when simulations were used for prediction purposes (1)*, ROHR was estimated from prior experience and included as an input to the simulation. A preferred procedure would be to start with the injection-system geometry and a simulation of the injection system plus a relationship between rate-of-injection (ROI) and ROHR and predict ROHR as the simulation progresses through the cycle. Information on the simulation of injection systems is available (2,3,4). Thus, the primary objective of this investigation was to obtain a relationship between ROI and ROHR in a diesel engine. Use of the term "heat release" or "rate-of-conversion of chemical energy" are more precise.

Although the need for a correlation between the cycle-simulation program's ROI and ROHR provided the direct impetus for the present work, there are other uses for the relationship. Control of combustion has been a goal of diesel-engine builders since the time of Rudolph Diesel himself. The tailoring of injection systems to engines is a time-consuming and expensive process. Currently, the development engineer must rely upon intuition, experience, and the results of tests which are expensive to perform. Indeed, much of the design and development of engines is done in this manner: a minimum of theory, as much empirical knowledge as is available and, finally, cut-and-try on the test stand and on the endurance bed. Hopefully, a knowledge of the relationship between ROI and test stand and on the endurance bed. Hopefully, a knowledge of the relationship between ROI add ROHR would decrease development time and costs.

*Underlined numbers in parentheses designate References at the end of the paper.

A detailed theoretical relationship between ROI and ROHR is extremely complicated since combustion in a diesel engine is heterogeneous, and there are different rate-controlling mechanisms for different parts of the combustion period. Determination of the spatial and temporal variation of the composition, temperature, and motion of the cylinder contents has not been, so far, amenable either to analytic or experimental techniques.

The computation of an apparent rate-of-heat-release (AROHR) from a given pressure-time (p-t) diagram is a simple thermodynamic problem (5,6). The computed AROHR may include (7) both combustion and heat transfer (AROHRHT) although the computational technique may compute and separate out heat transfer and thus approximate the actual ROHR. However, as pointed out by Schweitzer (5) and Krieger and Borman (6), extremely accurate p-t histories are required. It is well known that accurate p-t histories are difficult to obtain (8,9 10). In addition, accurate values of mass-flow rates and other engine-performance data are required.

PREVIOUS STUDIES

Experimental AROHR Measurements

One of the earliest computations of AROHRHT is that of Schweitzer (5) in 1926. In his technique, an energy balance yields the algebraic sum of heat release (HR) from combustion and heat losses from heat transfer (HT) to the cylinder walls. The computation of AROHRHT was not the primary objective of Schweitzer's work' thus, he did not emphasize the results arising from this techique.

Zinner (11) presented HR rates obtained from experimental p-t diagrams from a prechamber engine of nearly 100-cu in. displacement at speeds up to 2000 rpm and loads up to 120 mep. The computations for the prechamber engine are complicated by the mass flow (MF) between the pre- and main chambers. Unfortunately, Zinner did not present his computation technique, so it is not known how this MF was included, and also whether his data are AROHRHT or AROHR. Zinner also reported ROI for a few runs.

Uyehara and Myers (7) computed AROHRHT from experimental pressure histories using a technique similar to Schweitzer's. Uyehara and co-workers used a small precombustion chamber engine and measured p-t histories in the prechamber. HR rates were presented for speeds of around 1200 rpm and loads up to 100 mep.

The Pischingers (12) collected graphs of experimental HR rates obtained by various German investigators during the late 1930's. It is not clear whether these data show AROHRHT or AROHR. The reported results were obtained on diesel engines which ranged in size from 60 to nearly 8000 cu in. and included both open and precombustion chambers. Speeds of from 200 to 2000 rpm and various loads were investigated. Most tests were run under naturally aspirated conditions. Some ROI are included in these data. The Pischingers comment on the wide range and different shapes of curves reported.

The only known attempt to relate AROHR to ROI was part of an extensive study by Austen and Lyn (13,14,15). A balanced-pressure indicator was used to obtain a smoothed and averaged p-t history. The difference between the computed AROHRHT obtained from these data and the energy added as fuel for an average cycle was assumed to be the HT during the burning period. This HT then was added to the computed AROHRHT at a uniform rate during the combustion period to obtain an AROHR. Pioneering in nature, this technique can be criticized for at least two reasons:

1. There is no independent energy balance made so that errors in the cumulative HR and absorbed into the HT term.
2. The actual heat flux varies markedly during the HR period. LeFeuvre (16) presents experimental data showing a variation of as high as seven-to-one in the heat flux during the combustion period. It is possible, however, that the effect of flux and area may combine to yield a nearly constant total HT.

Lyn's and Austen's experiments were done at relatively low speeds (700-1500 rpm) and low loads (40-90 bmep). These values are of minimum interest for modern automotive-engine development work where 3000 rpm and 300 bmep are reasonable intermediate term goals and where 600 bmep is possible by the use of the VCR piston (17).

Whitehouse et al. (18), while presenting very little experimental data, indicate that an irregular AROHR is obtained from the pressure diagram. They smooth the curve and then further simplify the resulting "reasonable" HR for use in the simulation program. These investigators reported:

> Frequently diagrams are obtained which are not sufficiently accurate for such analysis. Impossible results are obtained such as heat release during the compression stroke before fuel is available, too much or too little total heat release and imep. If the inaccuracies are simply in the position of tdc and of the zero pressure line, corrections may be made to adjust these positions.

Detailed descriptions of the assumptions, equations, and computer programs needed to calculate an apparent combustion HR have been presented by Borman, Woschni, Lange, and Krieger (19,20,21,6). Different HT correlations were used to estimate the HT rate during the cycle. These workers presented only a few examples of AROHR to illustrate their method. They did not consider ROI.

Goudie (22) obtained AROHR in an M-combustion chamber engine at 1100 and 1700 rpm and with loads ranging from 11 to 135 bmep. Goudie used a piezoelectric pressure transducer and apparently computed HR from a unsmoothed p-t trace. He smoothed the resulting AROHR. Goudie did not present ROI data. A few HR rates (presumably AROHRHT) have been presented by Toda et al. and Broeze (23,24) for large marine two-stroke cycle engines.

Attempted Predictions of ROHR from ROI

Lyn (25) divided the ROI diagram into a plurality of elements. Various burning rate laws for these elements were tried in an attempt to find a burning-rate law that would match the AROHR. Lyn assumed that the same preparation-to-burn and rate-of-burning laws applied to all of the fuel increments in a given injection. Thus, from a droplet-burning standpoint, Lyn assumed the same Sauter Mean Diameter (SMD) and droplet-burning coefficient for each increment of fuel.

Cook (26) presented a paper on diesel-engine cycle analysis and the relationships of fuel injection and combustion efficiency. He defined a "digitalized" fuel which is characterized by the physical properties influencing evaporation and some of the combustion characteristics, in particular, ignition delay (ID). Cook summarized his method as follows:

> Automatic digital combustion is accomplished by three steps; first, the conversion of the fuel injection schedule to a schedule of fuel distribution in compressed air reaching boiling points for the various fractions of fuel; second, a calculation of the percent ignition delay accumulated for each fraction of fuel; third, a conversion of the second schedule of summation of pounds of fuel fractions reaching 100% accrued ignition delay.

Held (27) applied Lyn's method to other combustion chambers without any consideration of droplet sizes. Nagao et al. (28) considered in detail the ID of each increment of fuel injected. His method of dividing the ROI curve into increments according to the crank angle (CA) of injection was similar to that proposed and used by Lyn (15) and followed by Cook and Held. Nagao assumed complete combustion of each fuel increment during the 1 CA following the end of the ID period for that increment. Thus, he gave no explicit consideration to droplet-size distribution, droplet mean diameter, or finite droplet-evaporation and droplet-burning rates.

The following conclusions can be drawn on the basis of the foregoing brief summary of the literature:

1. With the exception of Lyn, (a) very little actual HR data have been presented and (b) almost no effort has been made to relate AROHR to ROI
2. There are no experimental or predicted HR rates at high specific outputs (i.e., around 1 hp/ cu in.).

The two conclusions are rather surprising in view of the otherwise well-developed cycle simulations and in view of the current interest in very high specific output diesel engines. This is because the required experimental data are difficult, time consuming, and expensive to obtain; and the HR process is extremely complex, and, thus, not readily amenable to analysis and modeling.

TABLE 1

Engine Geometry and Standard Operating Conditions

Engine	
Displacement	71.57 cu in.
Bore	4.5 in.
Stroke	4.5 in.
Compression Ratio	16:1 (nominal)
Operating Conditions	
Speed	2000 ± 10 rpm
Start of Injection (dynamic)	20 ± 0.5 deg btc
Intake Temperature	100 ± 3 deg F
Intake Pressure	60 ± 1 in. Hg abs
Exhaust Pressure	60 ± 2 in. Hg abs
Fuel	
Cetane Number	47.1
Specific Gravity at 60 F	0.787

EXPERIMENTAL PROCEDURE

Experimental Setup

A fixed engine configuration, secondary reference fuel (SRF), and standard engine operating conditions (EOC) were selected as described in detail in Tables 2, 3, and 4 in the Appendix. Thus, only the deviations from these are mentioned in presenting the data. All other variables for a particular run are held to the limits listed in Tables 2, 3, and 4.

For convenience, a brief listing of the more important standard operating conditions (SOC) and engine and fuel specifications abstracted from Tables 2, 3, and 4 is given in Table 1. With the SOC listed in Table 1, the cylinder gases follow a p-t and temperature-time (t-t) history which approximates that in an eight compression-ratio engine with 150 in. Hg abs manifold pressure and 240 F manifold temperature. Detailed cycle simulation (29) shows nearly 600 bmep obtainable under these latter conditions. Table 6 in the Appendix gives a complete listing of observed engine operating conditions and combustion performance.

A complete description of the data-processing system is presented by LeFeuvre (16). Briefly, the pressures and wall temperatures which vary during the cycle were recorded on a high-speed, 14-channel tape recorder. These data were digitized with the analog-to-digital converter interface of an SDS 930 hybrid computer. The digitized data were processed with a CDC 1604 computer.

AROHR

Borman's (19) concept of an AROHR was accepted; thus, a one-to-one compatibility was maintained with the previous cycle-simulation work at the University of Wisconsin. In this concept, energy absorbed from the cylinder gases by vaporizing and heating fuel reduces the AROHR because of the "homogeneous combustion" or "distributed heat source" assumption. The model for computation considers three energy terms: (a) work crossing the boundary of the system as p dv work on the piston, (b) HT across the boundary of the system, (c) internal energy of a homogeneous mixture of products of combustion and air. The equations used to compute the AROHR from the experimental data were presented by Krieger (6).

There are cycle-to-cycle variations in the p-t diagram from the engine as well as random noise from the data-recording process. Since the brake horsepower is an average value for many cycles, it was judged desirable to obtain an average of the AROHR for many cycles. This average can be obtained in two ways:

1. Compute the AROHR for individual p-t diagrams and average these results to obtain an average AROHR.
2. Average p-t diagrams for several cycles and compute an averaged AROHR from this averaged p-t diagram.

Each computation of AROHR from a p-t diagram takes about one minute of computer time on a CDC 1604. In the second method in the preceding paragraph, only one computation of AROHR from an average pressure trace is required, whereas in the first method as many computations are required as there are number of cycles to be averaged. As explained by LeFeuvre (16), a single p-t diagram representing the average of as many as 50 cycles of the data recorded on the magnetic tape can be obtained in a few seconds from the SDS 930. An average AROHR is then computed from this average p-t diagram. This procedure is much faster and more economical of computer time than averaging AROHR computed from individual p-t diagrams.

It is necessary to take the derivative of the p-t diagram in order to compute AROHR. This derivative can be obtained from the discrete, experimentally obtained, averaged points. If a curve-fitting routine is used, the derivative can also be obtained from the resulting smoothed p-t diagram. Figure 1 shows AROHR computed using the discrete, experimentally obtained, averaged points.

It can be seen in Fig. 1 that the AROHR (discrete p-t) curve is very irregular and contains many spikes and dips. The curve labeled AROHR (smooth p-t) was obtained from a smoothed p-t diagram. It is not clear whether the spikes and dips in the AROHR (discrete p-t) curve are real or are caused by the data-processing technique. In order not to lose detail at this point, the AROHR (discrete p-t) was used; however, as explained in the next paragraph, a smooth curve was fitted to these AROHR data.

There was loss in detail (the value of the detail is unknown); but, in order to characterize and compare the AROHR curves, an equation based on Wiebe's (30) semi-empirical dimensionless "Brenngesetz" was used. The equation is

$$x = 1 - \exp\left[-C2(y)^{(C1+1)}\right] \tag{1}$$

where

x = ratio of fuel burned at any instant to total fuel present

$C2$ = efficiency of-combustion coefficient

y = dimensionless time function

$C1$ = coefficient for shape of the rate-of-burning (ROB) curve

The derivative of this equation is a smooth curve for the ROHR and was used to put a smooth curve through the experimental AROHR. The form of the derivative of Wiebe's function which was used is:

$$\mathrm{HRR}(Y) = (C)\,(C2)\,(C1+1)\left(Y^{C1}\right)\exp\left[-C2\left(Y^{C1+1}\right)\right] \tag{2}$$

where

$HRR(Y)$ = smoothed heat-release rate (milli-Btu CA deg at normalized CA)

Y = normalized CA which equals $\frac{(CA-C3)}{(310-C3)}$

$C = \frac{(WFCY)(HV)1000}{(310-C3)}$

WFCY = experimentally obtained, time averaged weight of fuel per cycle (lb_m)

HV = higher heating value (Btu lb_m)

$C3$ = Wiebe parameter corresponding to CA at which ignition occurs

It should be noted that when using the Wiebe function, the abrupt initial rise observed in the AROHR (discrete p-t) curve is retained. Use of the AROHR (smoothed p-t) procedures gives a much more gradual rise in the curve. Both the AROHR (smoothed p-t) and Wiebe functions fail to show the high initial peak or spike. The spike is believed to be real, especially when operating naturally aspirated, but is believed to decrease in magnitude with increasing supercharge.

Figure 2 shows the AROHR (discrete p-t) as well as the curve computed from Equation (2) with the best values of the coefficients $C1$, $C2$, and $C3$ as determined by a least-sum-of-squares fit. It was judged that this procedure yielded the most consistent, impartial, simple, smooth representation of the AROHR. An additional significant advantage of the technique is that an AROHR may be characterized completely by the three coefficients, $C1$, $C2$, and $C3$.

Although Wiebe indicates that there is some theoretical basis for his equation, the authors are unable to ascribe any theoretical significance to the coefficients. Nevertheless, as well be shown later, correlation between the coefficients and certain overall combustion parameters is possible. In addition, as also will be explained later, a combustion model based on spray-droplet size distribution and single-droplet burning rates was developed.

EXPERIEMNTAL DATA

Effect of Speed

The effect of speed on the smoothed AROHR is illustrated by Fig. 3.

Within the accuracy of the data, Fig. 3 indicates that combustion is speeded up nearly in proportion to the increase in engine speed and that the point of ignition (IP) clearly advances with increasing engine speed; but this is at least partially a result of variations in injection (INJ) timing. An attempt was made to set INJ timing at 160 CA deg for these runs; however, a variation in this value occurred due to play in the pump drive and other factors. Because of a lack of sufficient channels on the tape recorder, the start of INJ was recorded photographically from an oscilloscope screen. The IP and the ignition delay (ID) in CA deg are:

Speed (rpm)	INJ (CA deg)	IP (CA deg)	ID (CA deg)	(millisec)
1002	162	165	3	0.500
1508	160	166	6	0.664
1991	161	167	6	0.504
2545	162	168	6	0.393

Thus, no clear trend of ID with speed can be deduced.

The shape of the ROI diagram varies with engine speed. This is a result of the compressibility of the fuel and the elasticity of the INJ system.

Inspection of the ROI plots in Fig. 3 shows that the initial ROI, in terms of engine CA, is higher at low engine speeds and that the duration of INJ is longer at high engine speeds due to compressibility and elastic effects. The HR rates show the same trend; the rate is higher early in the cycle at low speeds, and higher late in the cycle for high speeds. Thus, qualitatively, the ROI and the AROHR appear to be related. Note in Fig. 3 that there is a scale factor of 0.5 on the ROI; thus, the peak ROI is more than twice the peak AROHR.

The most important conclusion to be drawn from Fig. 3 is that the ROHR in terms of CA deg stays nearly constant with different engine speeds. At least two factors can be proposed which tend to increase the mass ROB (in terms of real time) with an increase of speed. The first is the belief that the speed of the air motion inside the cylinder is directly proportional to piston speed or engine rpm. Thus, an increased rate of mixing (ROM) should occur at higher engine speeds. This is in accord with the belief that the ROM of fuel and air is one of the major rate-limiting processes during diesel combustion.

The second factor which may contribute to the increased ROB with increased engine speed is the INJ spray-droplet size distribution. The INJ pressure is theoretically quadrupled for a doubling of the engine speed and a constant delivery per CA deg. (In practice, a constant delivery per CA deg is not maintained.) According to the dependence of SMD on INJ pressure as reported by Knight (31), the SMD of the droplets at 2000 rpm is about two-thirds of the value at 1000 rpm if the pressure is quadrupled. Tanasawa (32) has developed a relationship showing the distribution about the SMD. The combination of these two expressions shows that the entire droplet-size distribution changes toward smaller droplets at higher speeds. If the spray ROB concept proposed by Probert (33) and Tanasawa (32) is accepted, the ROB is nearly proportional to the reciprocal of the square of the SMD of the spray in accord with experimentally observed single-droplet burning rates (34,35,36).

Effect of Density Ratio

The effect of inlet manifold density ratios of 1.0, 1.6, 2.0, and 2.5 with a nearly constant equivalence ratio are shown in Fig. 4.

The variation in the shape and position of the AROHR curves with density ratio (DR) in Fig. 4 is not straightforward or regular. Several factors which might explain this lack of a trend are: techniques of data processing; changes in the INJ process and liquid spray development; and complex and interacting changes in the combustion process with increasing DR.

If the curve at 1.6 DR is disregarded, a more orderly variation of the HR shape with increased DR can be observed. During Run 82, the INJ advance adjustment broke, and the lever was held manually for the rest of the run. A great deal of cycle-to-cycle variation in the point of INJ was observed. Despite this, the data were processed and the AROHR computed from an average of 50 pressure traces. The cumulative apparent HR for the average of 50 pressure cycles is only 0.8 percent less than the heat added in the form of fuel for the average cycle.

In addition, Fig. 4 shows that the IP for Run 82 falls in order with the other three DRs plotted. Thus, there are arguments both for ignoring and for using the data from Run 82, the 1.6 DR run.

Effect of Equivalence Ratio

The trend in the shape of the smoothed AROHR with equivalence ratio (ER)—or fuel-air ratio—is quite apparent in Fig. 5 although the experimental ROI does vary regularly. The lack of regular variation in the ROI is believed to be a result of the elasticity of the INJ system and illustrates again the difficulty in controlling the variables in an experiment of this complexity. The results presented in Fig. 5 indicate that the relationship between AROHR and ROI is quite complex since irregular appearing variation in the ROI results in a more ordered variation in the smoothed HR.

In comparing the ROI and the AROHR curves, two factors may be noted. The first of these is the dependence of the later part of the AROHR curve on the end of the ROI. The second factor which can be proposed for the greater afterburning in the case of the higher ERs is: It is possible that the fuel spray cone has nearly the same shape and extent for a certain range of ERs. Wakuri et al. (37) report that the spray cone angle has been found to be only a function of the nozzle-tip geometry and the DRs of the liquid fuel and cylinder gases. In addition, his momentum analysis of the spray shows that the spray penetration is proportional to the one-quarter power of the differential pressure across the nozzle. Thus, it is possible that a locally rich region exists in or near the fuel spray cones especially at higher ERs (38). As the overall fuel-air ratio (F/A) is increased, the fuel in this rich region undoubtedly has more and more difficulty finding oxygen.

The effect of varying the ER using CIE fuel is shown in Fig. 6.

In Fig. 6, the gross relationships late in the HR period are nearly the same as with the SRF. There is a significant difference, as compared to the SRF, in the height and width of the peak HR. The maximum AROHR does not vary nearly as much with ER when using CIE fuel as it did when using SRF. In addition, the curves are significantly narrower, particularly at lower ERs.

There appear to be two separate causes for this result; i.e., the CIE fuel had a longer ID and a higher ROI. In the case of the 0.257 ER with CIE fuel, the somewhat longer ID allows a significant portion of the fuel to become premixed with air. The wide distillation range of the CIE fuel and the relatively low cetane number (CN) probably contribute to this effect.

In the case of the 0.480 ER using CIE fuel, the ROI is nearly 25 percent higher than for the corresponding SRF run. For equal ID periods, 25 percent more fuel is accumulated in the cylinder. The longer ID and greater volatility of the CIE fuel can cause the fraction of the fuel which becomes premixed to be even greater than the expected fraction due to the 25 percent greater fuel accumulation. This is assuming that adiabatic saturation does not occur.

A comparison of Figs. 5 and 6 shows that burning ends significantly earlier with the CIE fuel than with the SRF at 0.257 ER, ends somewhat earlier at 0.5 ER, and ends nearly the same at 0.75 ER. This substantiates the thought that at the highest F/A, locally rich regions exist and the fuel is having such difficulty finding air that differences in fuel properties are not as significant as at lower ERs.

One other characteristic of both of the variable F/A comparisons is the nearly constant or decreasing initial slope of the ROHR curve with increasing F/A. This occurs in spite of the overall trend toward higher initial ROI with increasing F/A. This result is contrary to the more or less direct relationship between ROI and AROHR which might be expected. The lack of increased initial slope of the AROHR curve with increased ROI can be ascribed to:

1. Shorter ID and higher ERs tending to reduce the amount of premixed fuel and air.
2. The possibility of adiabatic saturation occurring for a greater portion of the fuel to higher ROI (38).
3. The possibility that some portion of the HR by early combustion is absorbed in heating and vaporizing the larger amount of liquid fuel present with high ROI.

Effect of Swirl

The effect of swirl on smoothed HR with CIE fuel at an ER of 0.49 is shown in Fig. 7.

The values of swirl ratio in Fig. 7 were obtained on a steady-flow tests stand (29). The HR rate is higher and the duration of burning slightly shorter with the higher swirl rate. The observed fuel consumption is 0.276 and 0.280 lb/mihphr for the high and low swirl runs, respectively. Both the fuel consumption and HR rates are in accord with the theory that an ordered air motion strips vapor from around the spray, thus aiding the mixing of fuel vapor and air. The initially higher HR rate with higher swirl results from the larger amount of fuel which is vaporized, mixed and thus prepared to burn by the end of the ID period. The shorter period of HR is a result of faster and improved mixing of the last portions of the fuel to evaporate.

A greater variation in swirl might show different effects; unfortunately, at the time Runs 57 and 58 were made, only these two values of swirl rate could be obtained due to an inadequate lock on the swirl vane.

Figure 8 shows the (unsmoothed) apparent HR at 0.73 ER with three swirl ratios when using SRF.

The unsmoothed HR is plotted in Fig. 8 since, for SRF, the difference in the AROHR curves is extremely small and the deviation of the experimental data from the least-squares fitted curve could be larger than the differences between the curves. It is realized that the possible sum of the experimental errors and the assumptions made in the computation of apparent HR are also much greater than the differences between the three curves. However, the runs were made and completely processed back-to-back; therefore, the data are consistent. The presence of nearly the same wiggles in each of these curves is quite surprising, particularly when it is recalled that each of these curves is computed from a pressure-CA history which is the average of 50 cycles.

There are several possible explanations for these wiggles. If the CA-deg markers were not uniformly spaced or if there was a repeatable deviation of the command to sample, the observed results would be obtained. Also, repeatable combustion variations or oscillations due to the passage between the combustion chamber and the pressure pickup could be the cause. Since the data were reduced to smoothed HR curves, the exact cause for the wiggles was not determined.

Injection Advance

The effect of INJ advance with a low ROI pump and the standard 0.0138 nozzle tip is illustrated in Fig. 9. The ROI for Run 83 is presented in Figs. 12 and 14.

It can be seen that this Fig. 9 combination of pump and nozzle yields an ROI which is essentially equivalent to a "pilot" INJ, followed by a "main" INJ nearly 15 CA deg later. This pilot INJ effect was maintained over the range of INJ advances reported in Fig. 9. The curves for Runs 83 and 86 are for the same operating conditions and, thus, are one measure of the repeatability of the engine and the data-processing technique. The observed (on the oscilloscope screen) start of needle lift is at 160 ± 2 CA deg for both of these runs. The start of INJ computed from the recorded data is 162 CA deg for both runs. Despite this, the IP is nearly 2 CA deg later for Run 83 than for 86.

The engine had been shut down for installation of a new fuel INJ pump just before the series of runs shown in Fig. 9 were made. The oil, water and inlet-air temperatures were brought up to standard values, were held there for about 20 min, and appeared to be at steady-state conditions during Run 83. Run 86 was made after the engine had been operating about 1 to 2 hr. The shift in the HR curve of Run 83 to CAs nearly 2 CA deg later is a consequence of either not reaching equilibrium after the shutdown of the engine for installation of the new INJ pump or of rapid initial changes in the new pump.

The trends of the curves in Fig. 9 are quite consistent, however, and certain conclusions may be drawn. The shift in the peak of the HR rate curve is nearly 1.5 times the change in INJ advance. The same relationship is seen also in Fig. 10 for the CIE fuel with the high ROI system, and it holds in spite of the longer IDs with increasing INJ advance.

Thus, the increase in the ROB during the early part of the HR period more than offsets the increased ID due to large INJ advances. Then the peak ROHR advances more rapidly than the INJ curve as the INJ curve is advanced. This relationship is significant for purposes of cycle simulation. For example, it might be supposed that the effects of longer delay and faster initial burning with increased INJ advance nearly cancel one another. Then the whole HR curve might simply be shifted to earlier CAs in order to "simulate" a given greater INJ advance. The data just presented show that a misleading result could be obtained from the simulation due simply to shifting the AROHR along the CA axis.

The effect of INJ advance on AROHR with CIE fuel can be seen in Fig. 10. Here the ROI is nearly constant, and the INJ advance, IP, and ID are:

Run	INJ Advance	IP	ID
64	172	176	4
65	162	168	6
66	151	163	12

The AROHR has the highest value for the longest ID and the HR continues later in the cycle with later INJ. The "tail" of the AROHR curve for later INJ lags a similar curve at earlier INJ by about 1.25 times the difference in INJ cutoff CAs. These data indicate that for a fixed shape of the ROI curve, there is a dependence of the later part of the AROHR curve on the CA position (timing) of the fuel INJ curve.

The dependence of the shape of the early part of the AROHR on the ROI is expressed most explicitly by the use of the Wiebe parameter, $C1$. The values of $C1$ obtained by a least-squares fit to the experimental AROHR are:

Run	INJ Advance	$C1$
64	10-deg btc	0.78098
65	20-deg btc	0.47825
66	30-deg btc	0.15361

It is seen that there is a monotonic variation of $C1$ with INJ advance in this range.

Figure 10 illustrates that with very long IDs the very approximate rule that the peak AROHR is nearly one-half the peak ROI for the SOC selected for this investigation does not hold. For the early INJ advance run with relatively low CN but high volatility CIE fuel, the amount of fuel participating in the premixed combustion is apparently quite large; 67.8 percent of the total fuel added is injected before ignition occurs (percent of fuel injected before ignition = $Fuel_{pibi}$).

Another interesting conclusion that can be drawn from an examination of Figs. 9 and 10 concerns the trends of the slopes of the curves. Turning first to Fig. 9 with the very low ROI, a distinct trend with later INJ timing toward lower slopes for the initial rise of the AROHR curves is observed. A much less distinct trend is observed in the slopes of the AROHR at the end of combustion. If a mean slope for the later part of the AROHR curves (say between about 45-60 and 5-10 milli-Btu) is estimated, this slope becomes increasingly more negative with later INJ timing.

The effect of variation of INJ timing with a low ROI pump and a small nozzle tip (0.0118) is shown in Fig. 11.

A somewhat wider range of INJ timings than those shown in Figs. 9 and 10 is covered in Fig. 11, in which the experimentally obtained ROI varies somewhat through Runs 89, 90, and 91. This is due to the larger difference in cylinder pressure resulting from the larger range of INJ timing.

The trends which have been observed with different INJ advances in the previous two figures are followed. An exception to the general rule relating the peak HR rate and the peak ROI is seen again in Fig. 11; i.e., with large values of ID, the early portion of the HR curve is determined by the amount of fuel accumulated rather than by the ROI. This dependence is enhanced by the smaller droplets produced by the INJ system with 0.0118 in. nozzle tip as used in Fig. 11.

Injection System Changes

While the effect of INJ advance in the previous section was under study, incidental changes in the INJ system were made. This section presents the previous tests plus those where the INJ system was changed. The effect of the INJ system changes on the experimentally obtained ROI and on the resulting HR rates is shown in Figs. 12, 13, 14, and 15. It should be emphasized that the EOC were held at the

SOC listed in Table 2; thus, the observed effects result solely from the specified changes in the INJ system.

The INJ pumps which have been used for this work are described in Table 5. One of the pumps has a nominal delivery rate of 10 cu mm/CA deg and the other a rate of 5 cu mm/CA deg. This two-to-one ratio in the nominal delivery rates led to the use of the high ROI and low ROI designations although it is recognized that the pump, the system volume, and the nozzle together determine the ROI. This nomenclature is somewhat misleading as can be seen in Fig. 12. The maximum actual ROI obtained only differs by about 15 percent due to elasticity and compressibility effects.

The shape of the ROI curve in Fig. 12 is quite different although all other variables have been held nearly constant. Thus the average ROI is significantly lower for the low rate system. Again, for the operating conditions, where the amount of premixed combustion is small enough so that the AROHR is controlled by the ROI, the approximate relationship—that the peak AROHR is nearly one-half the peak ROI —is observed. Therefore, the peak ROI and the peak AROHR are nearly the same for the two curves in Fig. 12 despite a two-to-one ratio in the nominal delivery rate of the INJ pumps and a nearly two-to-one ratio in the mean delivery rate.

The main effect of the difference in INJ pumps is the significantly different shape of the AROHR. Again, this is an extremely strong indication that the AROHR is controlled to some degree by the ROI. For example, the peak AROHR lags the peak ROI by nearly the same amount in the two cases shown in Fig. 12 despite large differences in the shape of the respective ROI diagrams.

Another interesting result in the independent confirmation of the findings of Lyn and Valdmanis (39) concerning the weak dependence of ID upon spray characteristics. This weak dependence is observed in Figs. 12, 13, 14, and 15. Some of the computed liquid spray characteristics for the curves of Fig. 12 are:

Run	ROI	SMD (μ)	Spray Penetration (in.)	$Fuel_{Pibi}$	ID
76	high	22	1.7	31	6
83	low	36	1.6	12	6

With the exception of the spray penetration, the above numbers span a wide range of the liquid spray variables. Nevertheless, the ID is the same for these very different spray conditions. This is in accord with Lyn's conclusions on the weak effect of physical factors on ID.

Figure 13 shows the effect the size of the nozzle-tip hole has on the ROI and the resulting AROHR.

The initial separation of the AROHR curves in Fig. 13 is almost certainly a result of the corresponding difference in the start of INJ. If, for comparison purposes, the curves for the 0.0148-in. nozzle tip are shifted 2 CA deg to the left, certain conclusions can be drawn. First, the one-to-two ratio between the peak AROHR and the peak ROI is observed again. Secondly, the ending of INJ is nearly 6 deg earlier with the larger nozzle tip. However, on the shifted scale, the ending of HR is only 2 CA deg earlier with the larger nozzle tip. The larger SMD resulting from the larger nozzle orifices may account for this result.

The effect of nozzle-tip size on the ROI and the resulting AROHR with the low ROI pump is illustrated in Fig. 14.

In Fig. 14, the nozzle-tip size has a significant effect on the ROI obtained. In addition to the effect of nozzle size on ROI, the effect of nozzle size on the droplet sizes is reflected in the shape of the AROHR curve. By comparing the areas under the ROI curves before ignition, it is seen that more fuel has been injected before ignition in the case of the larger nozzle tip. Despite this, the slope of the AROHR curve after ignition is lower. An approximate average of the computed droplet sizes of the fuel injected before ignition is:

Run	Nozzle Size	SMD
83	0.0138	40μ
90	0.0118	30μ

Thus, although slightly more fuel has been injected before ignition in the case of the 0.0138 nozzle, the surface area of the spray is only about three-quarters as great. This indicates that the influence of surface area on the preparation-to-burn rate of fuel droplets may be significant.

Two of the extremes in ROI which have been obtained in this work are compared in Fig. 15.

The two extremes are obtained with the high ROI pump and large nozzle tip and with the low ROI pump and standard tip. The latter combination gives the pilot INJ effect previously mentioned. A quite different ROI and AROHR have been obtained for the two different INJ systems. Despite these large differences, certain relationships between the ROI and the AROHR are maintained. For example, in Fig. 15 the rule relating the amplitude of the peak AROHR to the amplitude of the ROI is followed.

General Observations

The experimental results presented in this section can provide some insight into the question of which mechanisms or processes are controlling during various stages of HR. Considerable caution must be used in generalizing since these results were obtained on a given engine with fixed combustion-chamber geometry and air motion.

The initial slope and height of the AROHR curve is determined by the amount of fuel injected and vaporized during the ID period. The shape and height of the later part of the AROHR curve also are highly dependent on the amount of fuel participating in this "premixed" combustion phase. Possible reasons for this include:

1. The obvious fact that if the fuel is burned during the early part of the HR period, it is unavailable for burning during the later part.
2. A temperature or pressure dependence of the droplet-evaporation rate, or of the chemical-reaction rate.
3. A combustion-induced turbulence promoting mixing.

Results from a spray-droplet model, which are presented later, indicate that an increase of the droplet-evaporation rate with instantaneous, mass averaged gas temperature will produce the above trends.

It is possible that some liquid droplets which are subjected to high temperatures may become heated to the thermodynamic critical point. This may, in effect, give a very rapid "evaporation" rate and may result in the rapid HRs which are observed to occur after the premixed combustion period for long IDs. If the liquid temperature is not above the critical temperature, adiabatic equilibrium (38) may occur in the spray core. The longer HR period with higher F/A is another indication that a fuel-rich spray core exists under certain conditions.

The observation that the peak AROHR is nearly one-half the peak ROI has been mentioned previously. Figures 14 and 15 indicate that this is correct if all other factors are held constant at the standard engine conditions of this investigation. If the ID becomes long, then the amount of fuel injected and evaporated before ignition determines the height of the peak of the AROHR. If the F/A is changed, the changed rate-of-evaporation (ROE)—again possibly due to the adiabatic equilibrium—can have significant influence.

MATHEMATICAL EXPRESSIONS FOR AROHR

The twofold objectives of this study were:

1. To obtain experimental data and to understand the relationship between ROI and AROHR.
2. To obtain theoretical and mathematical relationships for the AROHR given the ROI.

Although the details of the theoretical development of the single-droplet model are given in (29), it was judged desirable for the sake of completeness to repeat here the expressions developed. The correlation developed for the constants of Wiebe's expression also is presented.

Correlation of Wiebe Parameters

The values of the numbers obtained for the parameters in Wiebe's (30) semi-empirical "burning law" are presented in this section. These numbers, obtained by a a least-squares fit of Wiebe's function to the experimentally obtained AROHR are listed in Table 6 and again under the designation *Experimental* in Table 7.

As mentioned previously, a correlation between the $C1$, $C2$, and $C3$ coefficients and certain overall combustion parameters was developed. The correlations are:

$$C1 = 0.1496 - 0.2715 \text{ Pibi} \tag{3}$$

$$C2 = 0.5 \, A/F \tag{4}$$

$$C3 = \mathrm{CA_{INJ}} + \left(\frac{40}{\mathrm{CN}}\right)^{0.69}\left(\frac{6\mathrm{RPM}}{1000}\right)\left(\frac{0.0271}{P^{0.586}}\right)\exp\left(\frac{8360}{T}\right) \tag{5}$$

Niel Watson

where

Pibi = percent of total fuel injected before ignition

A/F = overall, experimentally obtained, air-fuel ratio

$\mathrm{CA_{INJ}}$ = experimentally observed CA at which INJ starts

CN = cetane number of fuel

RPM = experimentally observed engine speed

P = arithmetic average of instantaneous, experimentally measured, cylinder gas pressure at the $\mathrm{CA_{INJ}}$ and at the ignition CA

T = arithmetic average of instantaneous, computed mass averaged, cylinder gas temperature at the $\mathrm{CA_{INJ}}$ and at the ignition CA

The values computed with Eqs. (3), (4) and (5) are listed in Table 7 under *Predicted*. It should be noted that the factor $(40/\mathrm{CN})^{0.69}$ in Eq. (5) was not developed from the data obtained during this investigation but from a replot of data from Tsao et al. (40).

It is probable that the "predictor equations" for the Wiebe parameters can be improved by the addition of some (yet unknown) terms. However, the correlation of the Wiebe parameters (as well as the Wiebe representation itself) is quite empirical. Thus, there is no consideration of many of the intermediate steps in the HR process. The method may be useful for interpolation between certain operating conditions and for limited extrapolation, given a fixed INJ system.

Spray-Droplet Burning Model

There are considerable experimental data which indicate that ROB of a liquid fuel droplet is controlled by ROE from the droplet. The Wiebe relationships contain no explicit consideration of droplet size.

It is believed that an approach to a correlation which includes a consideration of droplet sizes is much more fundamental and, thus, eventually will be used for the simulation of the HR in a diesel engine. The procedures and expressions developed in (29) are given in the following section.

Prediction of ROHR Curve from ROI Curve

Following the authors' approach, the simulation of the combustion rate in an open-chamber direct INJ engine consists of:

1. The division of the injected fuel (ROI) into discrete packets or increments, based on the time interval of INJ. The amount of fuel in an increment was that amount injected during 1 CA deg.
2. The computation of an SMD for each increment of fuel using the following form of Knight's (1955) equation:

$$SMD = 220(\Delta P)^{-0.458}(\dot{Q})^{0.209}(\nu)^{0.215}\left(\frac{A_{orf}}{A(t)_{eff}}\right)^{0.916} \tag{6}$$

where

SMD = Sauter Mean Diameter, microns

ΔP = difference between instantaneous INJ pressure and instantaneous cylinder gas pressure, psi

$\dot{Q}$ = mass-flow rate through the nozzle, lb_m/hr

ν = kinematic viscosity of fuel, centistokes

A_{orf} = exit orifice area, sq in.

$A(t)_{eff}$ = effective orifice area across which ΔP is measured, sq in.

3. The computation of a droplet-size distribution, for each increment of fuel injected, using Tanasawa's distribution which is combined into the spray-burning expression, see Step 5.

4. The computation of an ID for each increment of fuel injected using Wolfer's (1938) formula, modified to fit experimental data, and modified to account for changes in cylinder gas pressure and temperature during the ID period of the fuel increment:

$$ID = \left(\frac{6\ RPM}{1000}\right)\left(\frac{0.0271}{P^{0.386}}\right)\left(\frac{40}{CN}\right)^{0.69} \exp\left(\frac{8360}{T}\right) \tag{7}$$

where

ID = ignition delay, CA

RPM = engine speed

P = linear average of cylinder gas pressure at time of INJ and at time of ignition, psi

CN = cetane number of fuel

T = linear average of cylinder gas temperature at time of INJ and at time of ignition, deg R

5. The computation of the ROHR of each increment of fuel injected using a droplet-size distribution. The following equation includes Godsave's value of 790 for the single-droplet burning coefficient, and the experimentally observed effect of cylinder gas temperature on the spray-burning rate:

$$HR = -DWF(K)(DTDT)(DFDT) \cdot \exp\left[-3(TANA^{0.75})(1-TANA)^{-0.25}\right] \tag{8}$$

where

HR = fuel ROB, lb_m/CA

$DWF(K)$ = mass of fuel in K'th increment injected, lb_m

$$DTDT = \frac{\{DT1 + [CA1 - CA(K)]DT2\}}{[SMD(K)]^2}$$

$$DT1 = \frac{4(790)(T^{0.33})}{6\ RPM}$$

T = instantaneous cylinder gas temperature, deg R

RPM = engine speed

CA1 = engine CA corresponding to current position of piston

CA(K) = engine CA when K'th increment of fuel injected

$$DT2 = \frac{4(790)(0.33)\left(\frac{T}{T}\right)(T^{0.33})}{6\ RPM}$$

ΔT = change in cylinder gas temperature between previous CA and current CA, deg R

SMD(K) = Sauter Mean Diameter of K'th increment of fuel injected

$$DFDT = 2.25(TANA)(1-TANA)^{0.25} + 0.75\ TANA^{0.75}(1-TANA)^{-1.25}$$

$$TANA = \frac{4(790)[CA1 - CA(K)]T^{0.33}}{6\ RPM[SMD(K)]^2}$$

6. Sum the HRs at each CA and multiply by fuel heating value to get the total HR rate at each CA.

CONCLUSIONS

1. Despite the extreme practical difficulties, experimental data which are suitable for the computation of HR rates can be obtained from a CIE high in speed and in specific output.

2. The use of a high-speed multichannel data-acquisition system to record engine data which vary during the cycle not only is practical but also is almost a necessity in a study of this kind.

3. The initial slope and height of the AROHR curve is determined by the amount of fuel injected and vaporized during the ID period.

4. For moderate IDs, the peak AROHR is approximately one-half the peak ROI.

5. The relationships which are observed between the ROI and the ROHR are explainable in terms of the many physical processes occurring in the engine during the HR period.

6. For a fixed combustion chamber and EOC, the HR rate is determined by (a) ROI, (b) ID, (c) spray characteristics of the INJ system, (d) inlet manifold DR and temperature, (e) F/A for the cycle, and (f) a large number of other secondary factors.

7. A correlation for the three parameters of the Wiebe equation was developed.

8. An expression for the AROHR derived from expression for the ROB of single-fuel droplets and modified by a spray-burning coefficient is presented.

9. The concept of a spray burning at a rate corresponding to single-droplet burning coefficients, which has been proposed by Probert and Tanasaw, is physically more descriptive of the events occurring in the engine than the Wiebe-type correlation.

ACKNOWLEDGMENTS

This work was done under technical direction of the Propulsion System Laboratory at the Army Tank—Automotive Command (ATAC). The work was done as part of the ATAC research program in support of the development of high-output military engines. Scholarship support from Cummins Engine, Caterpillar Tractor, and General Motors is deeply appreciated.

REFERENCES

1. K.J. McAulay et al., "Development and Evaluation of the Simulation of the Compression-Ignition Engine," Society of Automotive Engineers, Paper 650451 presented at Chicago, Ill., May 18, 1965.

2. E. Giffen and A. Muraszew, "The Atomization of Liquid Fuels," TP343 65, Chapman & Hall, London, 1953.

3. B.E. Knight, "Fuel Injection System Calculations," Institution of Mechanical Engineers, Automotive Division Proceedings, No. 1, 1960-61, pp. 25-33.

4. P.I.G. Becchi, "The Analytical Investigation of Phenomena Concerning the Fuel Injection in the Fast Diesel Engines, Carried out at the Design Stage by Means of the Electronic Computer," FIAT, Technical Bulletin, Vol. XV, No. 2, April-June 1962.

5. P.H. Schweitzer, "The Tangent Method of Analysis for Indicator Cards of Internal Combustion Engines," Pennsylvania State University Engineering Experiment Station, Bulletin 35, September 1926.

6. R.B. Krieger and G.L. Borman, "The Computation of Apparent Heat Release for Internal Combustion Engines," ASME paper 66-WA/DGP-4 presented at New York City, November 28, 1966.

7. O.A. Uyehara and P.S. Myers, "Diesel Combustion Temperatures—Influence of Fuels of Selected Composition," SAE Transactions, Vol. 57, 1949.

8. J.D. McCullough, "Engine Cylinder Pressure Measurements," SAE Transactions, Vol. 61, 1953, pp. 557-573.

9. W.T. Lyn, A.J. Stockwell, and C. Wang, "Accuracy in Cylinder Pressure Measurement," Institution of Mechanical Engineers, Vol. 180, Part 3G, 1965-66, pp. 8-16.

10. W.L. Brown, "Methods for Evaluating Requirements and Errors in Cylinder Pressure Measurement," SAE Paper 670008 presented at Detroit, Mich., January 9, 1967.

11. K. Zinner, "Gemischbildung, Verbrennungsablauf und Wirkungsgrad beim Schnellaufenden Dieselmotor," VDI—Sonderheft Dieselmaschinen, VII, 1938, pp. 58-63.

12. A. Pischinger and F. Pischinger, "Gemischbildung und Verbrenning im Dieselmotor," (Die Verbrennungskraftmaschine Band 7) Springer-Verlag, Vienna, 1957.

13. A.E.W. Austen and W.T. Lyn, "Relation Between Fuel Injection and Heat Release in a Direct-Injection Engine," Proceedings, Institution of Mechanical Engineers, 1960-61, pp. 47-62.

14. W.T. Lyn, "Calculations of the Effect of Rate of Heat Release on the Shape of Cylinder-Pressure Diagrams and Cycle Efficiency," Institution of Mechanical Engineers, Automotive Division Proceedings, No. 1, 1960-61, pp. 34-36.

15. W.T. Lyn, "Study of Burning Rate and Nature of Combustion in a Diesel Engine," Ninth Symposium (International) on Combustion, 1962.

16. T. LeFeuvre, "Instantaneous Metal Temperatures and Heat Fluxes in a Diesel Engine," PhD Thesis, Department of Mechanical Engineering, University of Wisconsin, 1968.

17. W.P. Mansfield and W.S. May, "Diesel Combustion at High MEP with Low Compression Ratio," SAE, SP280, May 1966.

18. N.E. Whitehouse, et al., "Method of Predicting Some Aspects of Performance of a Diesel Engine Using a Digital Computer," Institution of Mechanical Engineers, Vol. 176, 1962, pp. 195-217.

19. G.L. Borman, "Mathematical Simulation of Internal Combustion Engine Processes and Performance Including Comparisons with Experiment," PhD Thesis, Department of Mechanical Engineering, University of Wisconsin, 1964 (reprinted as CAE Report 954 submitted to Detroit Arsenal, August 1964).

20. G. Woschni, "Computer Programs to Determine the Relationship Between Pressure Flow, Heat Release and Thermal Load in Diesel Engines," SAE Paper 650450 presented at Chicago, Ill., May 1965.

21. W. Lange and G. Woschni, "Thermodynamische Auswertung von Indikator-Diagrammen, elektronisch gerechnet," Motor Technisch Zeitschrift, 25/7, 1965.

22. G.C. Goudie, "A Preliminary Study of Heat Release in the M-Engine Combustion System," Eleventh Symposium (International) on Combustion, August 1966.

23. N. Toda and T.O. Kushiyama, "On a Method of Calculating Characteristics of Exhaust Gas Turbocharged Two-Stroke Diesel Engine," Bulletin, Japan Society of Mechanical Engineers, Vol. 9, 1966, pp. 7-580.

24. J.J. Broeze, "Combustion in C.I. Engines," Engineering, Vol. 169, 1965, p. 618.

25. W.T. Lyn, "Study of Burning Rate and Nature of Combustion in a Diesel Engine," Ninth Symposium (International) on Combustion, 1962.

26. H.A. Cook, "Diesel Engine Cycle Analysis of Relationships of Fuel Injection to Fuel Compression Ignition Characteristics and Best Fuel Compression Ignition Characteristics and Best Fuel Utilization," SAE Paper 650449 presented at Chicago, Ill., May 18, 1965.

27. G. Held, "Welchen Aufschluss geben Einspritz-und Brenngesetz Uber die wirkliche motorische Verbrennung?" Motor Technisch Zeitschrift, 27/12, 1966, pp. 480-484.

28. F. Nagao, M. Ikegami, and K. Oshima, "An Analysis of Combustion Knock in a Diesel Engine," Bulletin, JSME, Vol. 10, No. 39, 1967, pp. 532-542.

29. J.H. Shipinski, "Relationships Between Rates-of-Injection and Rates-of-Heat Release in Diesel Engines," PhD Thesis, Department of Mechanical Engineering, University of Wisconsin, June 1967.

30. I. Wiebe, "Halbempirische Formel für die Verbrennungs-geschwindigkeit," Verlag der Akademie der Wissenschaften der VdSSR, Moscow, 1956.

31. B.E. Knight, "Communication on the Performance of a Type of Swirl Atomizer," Proceedings, Institution of Mechanical Engineers, 1955, pp. 104-105.

32. Y. Tanasawa, "On the Combustion Rate of a Group of Fuel Particles," Technology Reports of Tohoku University, Vol. 18, No. 1, 1953, pp. 61-74.

33. R.P. Probert, "The Influence of Spray Particle Size and Distribution in the Combustion of Oil Droplets," Philosophical Magazine, Series 7, Vol. 37, No. 265, February 1946, pp. 94-105.

34. G.A.E. Godsave, "Studies of the Combustion of Drops in a Fuel Spray," Fourth Symposium (International) on Combustion, 1953.

35. A.R. Hall and J. Diederichsen, "An Experimental Study of the Burning of Single Drops of Fuel in Air at Pressures up to Twenty Atmospheres," Fourth Symposium (International) on Combustion, Williams and Wilkins, Baltimore, 1953, pp. 837-846.

36. H.L. Hottel, G.C. Williams, and H.C. Simpson, "Combustion of Droplets of Heavy Liquid Fuels," Fifth Symposium (International) on Combustion, 1954.

37. Y. Wakuri et al., "Studies on the Penetration of Fuel Spray in a Diesel Engine," Bulletin, JSME, Vol. 3, No. 9, 1960, p. 123.

38. M.M. El-Wakil, P.S. Myers, and O.A. Uyehara, "Fuel Vaporization and Ignition Lag in Diesel Combustion," SAE Transactions, Vol. 64, 1956, p. 712.

39. W.T. Lyn and E. Valdmanis, "The Effects of Physical Factors on Ignition Delay," Institution of Mechanical Engineers, Automotive Division, presented at London, November 1966; see also: SAE Paper 680102 presented at Detroit, Mich., January 8-12, 1968.

40. K.C. Tsao, P.S. Myers, and O.A. Uyehara, "Gas Temperatures During Compression in Motored and Fired Diesel Engines," SAE Transactions, Vol. 70, 1962, pp. 136-145.

APPENDIX

The SOC for the engine are listed in Table 2. Any departure from these conditions is indicated in the text.

TABLE 2

Standard Engine Operating Conditions

Compression Ratio	15.4:1 (measured)
Speed	200 ± 10 rpm
Dynamic Injection Timing	20 ± 0.5 deg btc
Intake Temperature	100 ± 3 deg F
Intake Pressure	60 ± 1 in. Hg abs
Exhaust Pressure	60 ± 2 in. Hg abs
Jacket Coolant Temperature	
In	180 ± 10 deg F
Out	190 ± 10 deg F
Rise	3.5 - 12 deg F
Lubricating Oil	SAE 30 Series III
Temperature	
In	180 ± 10 deg F
Out	200 ± 10 deg F
Rise	6 - 17 deg F
Valve Timing	
Intake Valve Opens	20 deg btc
Intake Valve Closes	50 deg abc
Exhaust Valve Opens	50 deg bbc
Exhaust Valve Closes	20 deg atc
Valve Overlap	40 deg
Injection System	
Plunger Diameter	9 mm
Cam Profile	26/2X tangential
Nozzle Holder	AB AKF 100S X5059A
Nozzle Tip	4-0.0138 in. holes
Nozzle Opening Pressure	3000 psi

TABLE 3

Engine Specifications*

Displacement	71.57 cu in.
Bore	4.5 in.
Stroke	4.5 in.
Compression Ratio	16:1 (nominal)
Connecting Rod Length	9.0 in.
Crankcase	LABECO C. L.R. S/N DI-7
Combustion Chamber	Open bowl in piston
Inlet System Length	19 in. (port + pipe)
Pipe Length	13 in.
Inside Diameter	2.5 in.
Tank Volume	7600 cu in.
Exhaust System Length	19½ in. (port + pipe)
Pipe Length	13 in.
Inside Diameter	2 in.
Tank Volume	7600 cu in.
Injection System	
Pump	AB APE 1B-90P-4843A
Line	(24½ L)(0.062 id)
Nozzle Holder	AB AKF 100S X5059A
Nozzle Tip	AB ADB-145S-131-7

TABLE 4

Fuel Specifications

	CIE Fuel	47.1 CN SRF
API Gravity at 60 F	47.3	48.7
Specific Gravity at 60 F	0.791	0.787
Distillation, F		
IBP	160	371
10%	231	404
50%	372	433
90%	456	481
	501	565
Composition and Volume		
Saturates	78.6	89.5
Olefins	7.3	4.5
Aromatics	14.1	6
Cetane Number	37.5	47.1

TABLE 5

High Rate and Low Rate Injection Pumps

Pump	Plunger	Camshaft	Maximum Ideal Rate
High Rate	PPK 1/3 Z (9 mm)	PAC 26/2X (tangential 6/4)	10 mm^3/CA
Low Rate	PPK 1/1 Z (7 mm)	PAC 26/1X (basic metric 6/1)	5 mm^3/CA

*Cylinder head (including ports, valves, and springs), sleeve, piston, pin, rod, and valve train from International Harvester DT 429 six-cylinder engine.

TABLE 7

Experimental and Predicted Wiebe Parameters

	Experimental			Predicted		
Run	C1	C2	C3	C1	C2	C3
64	0.781	16.2	176	0.667	15	175
65	0.478	14.8	168	0.445	15	166
66	0.154	13.3	163	0.305	15	158
67	0.485	9.20	167	0.599	10	166
68	0.393	29.4	169	0.311	29	167
73	0.519	13.1	167	0.473	17	164
74	0.389	9.80	166	0.453	16	164
75	0.509	14.6	165	0.588	16	166
76	0.416	10.6	167	0.441	17	167
77	0.531	42.5	167	0.317	35	167
79	0.468	8.08	168	0.537	11	166
82	0.706	18.7	170	0.326	16	167
83	1.17	14.1	168	0.714	14	166
85	0.987	17	161	0.675	14	160
86	1.09	13.3	166	0.844	14	167
87	1.30	12	170	1.16	14	172
88	0.657	12.7	158	0.665	14	156
89	0.349	8.38	160	0.488	15	153
90	0.618	7.20	168	0.816	15	165
91	0.066	5.66	159	0.377	15	160
99	0.452	14.3	167	0.416	10	168
100	0.436	13.6	167	0.367	10	168
102	0.372	6.56	166	0.508	15	167
103	0.531	11.7	167	0.508	15	165
109	0.438	10.4	166	0.548	15	165
115	0.451	17	167	0.393	29	169
116	0.677	11	165	0.708	10	165
117	0.702	11.5	165	0.743	10	165
118	0.682	11.4	165	0.660	10	165
120	0.737	8.64	164	0.779	12	167

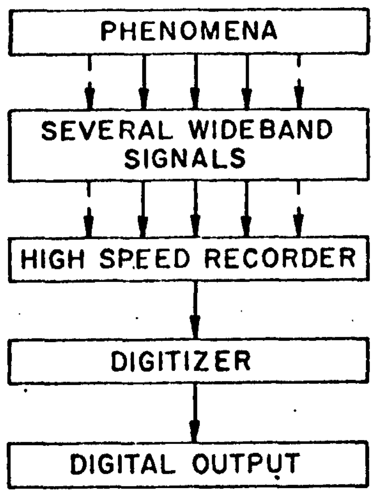

Fig. 1 Conceptual view of overall system.

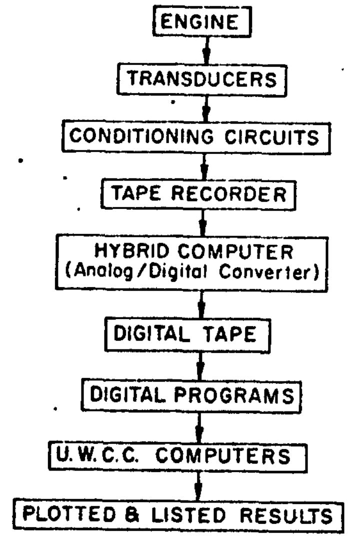

Fig. 2 Overall system used.

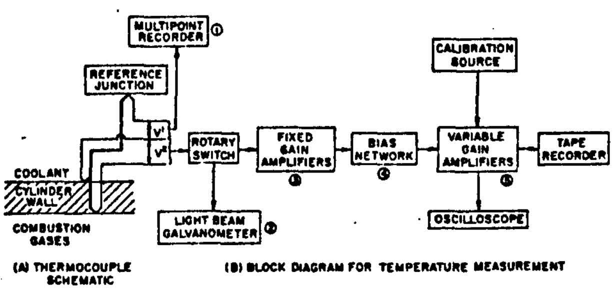

Fig. 3 Thermocouple schematic and instrumentation for surface temperature measurement.

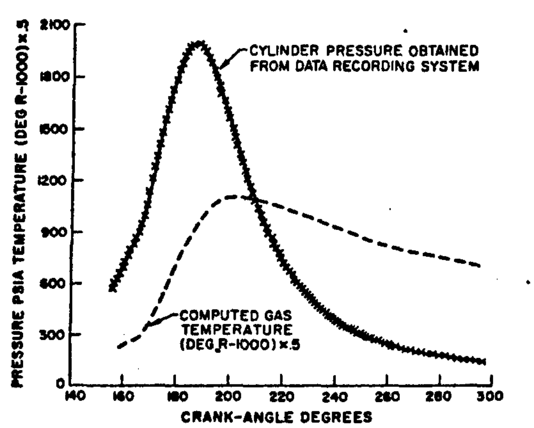

Fig. 4 Cylinder pressure plot obtained from data recording and processing system.

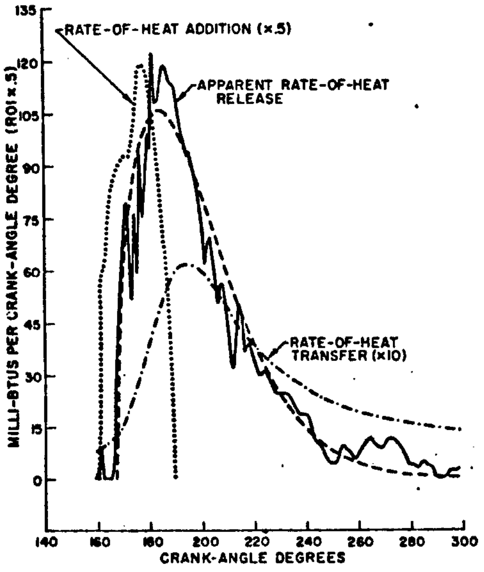

Fig. 5 Computed results from CDC 1604 computer and Calcomp plotter.

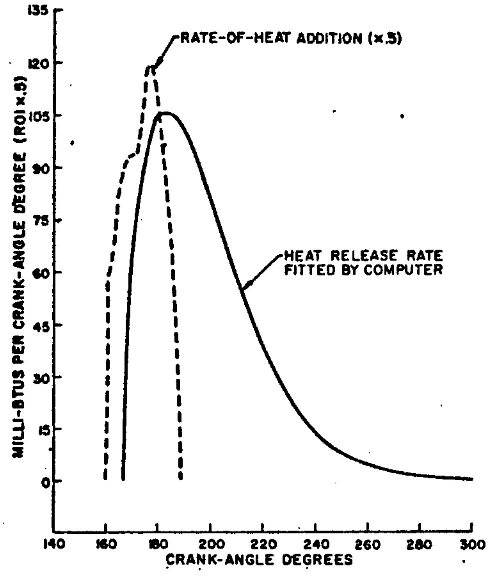

Fig. 6 Wiebe's function as fitted to apparent heat release rate by Program GAUSHAUS.

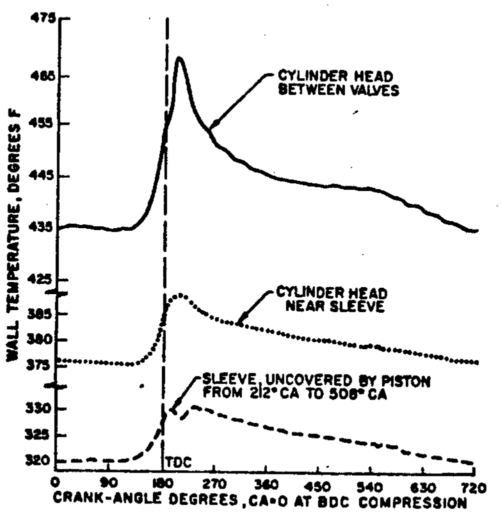

Fig. 7 Surface temperature cyclic variation for three positions in cylinder.

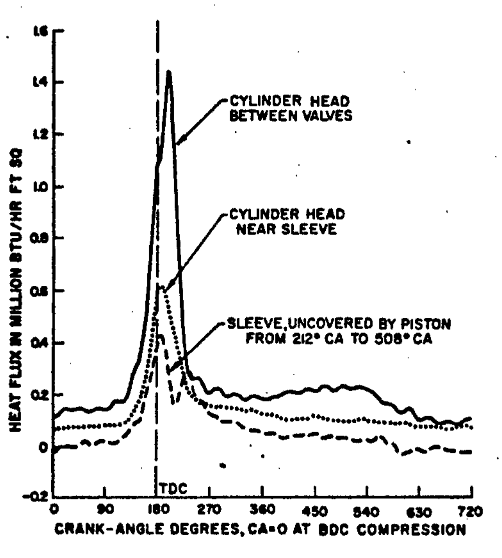

Fig. 8 Surface heat flux for three positions in cylinder.

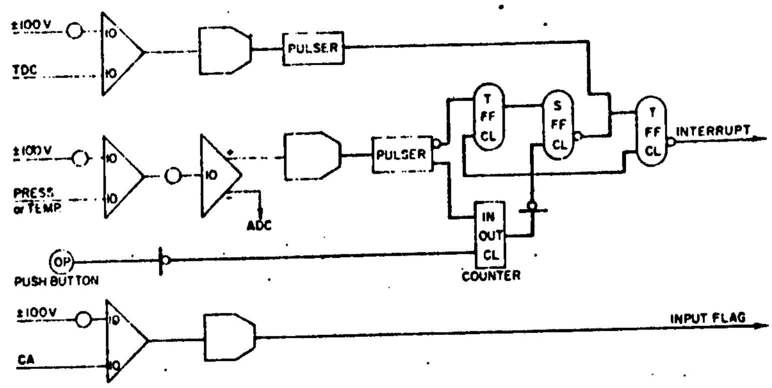

Fig. C-1 Analog and logic schematic, hybrid computer.

APPENDIX VI

D

A Spray-Droplet Model for Diesel Combustion

J. Shipinski, P.S. Myers and O.A. Uyehara
Mechanical Engineering Dept.
University of Wisconsin

ABSTRACT

A spray-burning model (based on single-droplet theory) for heat release in a diesel engine is presented. Comparison of computations using this model and experimental data from an operating diesel engine indicate that heat release rates are not adequately represented by single-droplet burning rates. A new concept is proposed, i.e. a burning coefficient for a fuel spray. Comparisons between computations and experimental data indicate that the numerical value of this coefficient is nearly independent of engine speed and combustion-chamber pressure. However, the instantaneous value of the spray burning coefficient is approximately proportional to the instantaneous mass-averaged cylinder gas temperature to the one-third power.

INTRODUCTION

The availability of very large, high-speed digital computers has encouraged efforts to simulate in detail both spark-ignition (s.i.) and compression-ignition (c.i.) engines (1)-(7)*. In the case of the s.i. engine, attempts have been made to simulate the combustion or heat release process (8)(9). In the case of the c.i. engine the rate of heat release (ROHR) was usually estimated from past experience and included as an input to the simulation. However, Lyn (4) attempted to use Spaulding's (10) single-droplet results to predict burning rates in an engine. Lyn did not explicitly consider droplet sizes in his work. However, implicit in his work is the assumption of the same drop size distribution and mean droplet diameter for every increment of fuel in the injection process. Cook (11)(12) postulated a model for combustion in a diesel engine, based on a partial distillation of each fuel increment and an infinite burning rate after an ignition delay (i.e.) computed for each distilled fraction. Held (13) extended Lyn's method without any consideration of droplet sizes and without presenting any well-defined correlation. Nagao (14) considered in detail the i.d. of each increment of fuel injected. His method of dividing the rate of injection (ROI) into increments according to the crank angle (CA) of injection was similar to that proposed and used by Lyn (4) and followed by Cook (12) and Held (13). Nagao assumed combustion of each fuel increment during the 1 crank angle following the end of the i.d. period for that increment. Thus, he gave no explicit consideration to droplet size distribution, droplet mean diameter, or finite droplet evaporation and burning rates.

The occurrence of finite evaporation rates during the i.d. period (15), in addition to finite burning rates (16)-(19) for single droplets, has been well established by experiment. Burning rates can also be predicted from heat and mass transfer theory (15)(16). The concept of a finite-spray burning rate based on single-droplet theory and experiment was proposed by Probert (20) and extended by Tanasawa (21). Probert combined the Rosin-Rammler particle distribution function and single-droplet burning rates to obtain a spray burning rate. He also assumed that single-droplet evaporation and burning coefficients were valid in the spray; that is, either there was no interaction between droplets or the interaction did not significantly affect the result.

Tanasawa replaced the Rosin-Rammler distribution with a drop size distribution experimentally obtained from a gas turbine nozzle spray. He combined this distribution with the single-droplet burning coefficient C_b and obtained an empirical formula by fitting a curve to the results of these computations. Tanasawa also assumed

*Numbers in parentheses designate References at end of paper.

no interaction between droplets burning in a spray. Neither Probert nor Tanasawa proposed their model for use in dense sprays, such as those present during diesel combustion.

OBSERVED ENGINE BURNING RATES

The phenomena which a burning rate model must describe in detail are usually observed only indirectly. The overall performance of the engine is highly dependent on the burning rate, but the relationship between rate of burning and rate of injection is not well established. Because of this lack of established relationships, engine combustion chamber development is accomplished by observing engine performance data and, in some cases, pressure-time (p-t) diagrams.

An apparent ROHR can be computed from a p-v diagram (22) or a p-t diagram (23). The work from which this paper is drawn (24) is based upon the p-t approach. The use of the term 'heat release' is only a convenient notation, and the terms 'energy release' or 'rate of conversion of chemical energy to sensible energy' are more precise.

The experimental ROHR which were used for comparisons with the model were obtained on a 4.5 in. × 4.5 in. open-chamber diesel engine. Experimental p-t diagrams were recorded for loads of from 60 to 330 lb/in.^{2} motored indicated mean effective pressure (m.i.m.e.p.), and speeds from 1000 to 2500 rev/min. The maximum output was over 1 indicated hp/in.^{3}.

The p-t diagrams were recorded on a high-speed magnetic tape recorder (25). These records were digitized at every crank angle by the analog-to-digital (A/D) interface of a hybrid computer. A p-t diagram which was the average of from 20 to 50 cycles was obtained as output. A typical average p-t diagram is illustrated in the upper part of Fig. 2.1. The ROHR computed from this p-t diagram is shown in the lower portion of Fig. 2.1. It is seen that a very irregular ROHR curve results from a relatively smooth p-t curve. It is possible that these irregularities actually occur in the engine. However, it is also possible that they were unintentionally introduced in the ROHR curve. This introduction could occur either because discrete points rather than a continuous curve were used or because a finite number of p-t curves were averaged.

In addition to the random irregularities there is a fairly consistent sharp peak or initial spike in the ROHR curve. This has been observed by Lyn (26). This spike appears to be the result of a very rapid pre-mixed combustion of fuel vaporized during the i.d. period. This spike is dependent on engine operation conditions and may disappear with high supercharge.

As an aid to understanding and describing the phenomena, it is convenient to divide the ROHR curve into four stages, as illustrated in Fig. 2.2: (1) an i.d. stage, (2) premixed combustion stage, (3) vaporization-limited combustion stage, and (4) mixing-reaction-rate-limited combustion stage.

The titles of these four stages roughly indicate the rate-limiting phenomena believed to be occurring during this portion of the ROHR curve. The boundaries between these stages are not well delineated, either for the ROHR curve as a whole or for an individual increment of fuel.

In the combustion model finally developed, the i.d. stage is described by an i.d. correlation: the pre-mixed combustion stage was described by an arbitrarily selected burning rate; the vaporization-limited combustion stage was described by the drop size distribution model necessarily developed for use during the previous two stages and modified by a spray burning coefficient (C_E); the mixing-reaction-rate-limited combustion stage was described by C_E. In arriving at this final model, models previously described in the literature were evaluated to determine if they adequately described the phenomena. Shipinski (24) presents the details of this evaluation, but the models that are helpful to an understanding of the final model are presented here.

WIEBE MODEL

The first model was simply an empirical curve fit of the experimentally obtained ROHR curves (27). In order to do this Wiebe's (28) semi-empirical dimensionless 'Brenngesetz' was used. The equation used for the ROHR is

$$HRR(Y) = (C)(C2)(C1+1)(Y^{C1})\exp[-C2(Y^{C1+1})] \tag{2.1}$$

where HRR(Y) is the smoothed heat release rate (milli-Btu crank angle degree at normalized crank angle); Y the normalized crank angle, i.e. (CA-C3)/(310-C3); C equals [(WFCY)(HV)1000]/(310-C3); WFCY the experimentally obtained, time-averaged weight of fuel per cycle, lbm; HV the higher heating value (Btu/lbm); C1 the Wiebe shape coefficient; C2 the Wiebe efficiency-of-combustion coefficient; and C3 the Wiebe parameter corresponding to crank angle at which ignition occurs.

As discussed by Shipinski (27), an approximate, but unsatisfactory, correlation with operating variables was obtained for the constants in equation (2.1). As an approach which included consideration of droplet sizes and the processes occurring was considered more fundamental, no more work was done on correlation of Wiebe parameters. Instead, various different single-droplet models as described below were investigated.

MODELS TANASAWA AND TANAS I

As Probert (20) and Tanasawa (21) had shown the importance of drop sizes on the rate of burning of a spray, a model which included a variable Sauter mean diameter (SMD) but a constant drop size distribution was constructed and evaluated. This model is designated as model Tanasawa.

The expression which Tanasawa obtained by fitting empirical curves to the results of graphical calculations is:

$$\frac{w_b}{w_o} = 1 - \exp\left[\left(-3\,\frac{C_b t}{4\bar{x}^2}\right)^{0.75}\left(1 - \frac{C_b t}{4\bar{x}^2}\right)^{-0.25}\right] \tag{2.2}$$

where w_b/w_o is the mass fraction burned at time t; t the time, ms; C_b the burning coefficient, μ^2/ms; μ is microns; and $\bar{x}$ is the Sauter mean diameter, microns.

This equation was the basis for model Tanasawa. The experimentally obtained ROI was divided into 1 crank angle degree increments. The fuel for each of these increments was treated as an individual packet and its atomization, spray penetration, ignition delay, vaporization, and burning history computed. For each fuel increment a SMD was computed from Knight's (29) equation, and its vaporization rate was then computed from the differentiated form of equation (2.2). Note that equation (2.2) includes a drop size distribution and the realistic assumption that the largest drop in the spray is twice the SMD. Although an ignition delay was computed for each increment using Wolfer's (30) equation, it was assumed that vaporization did not start until the end of the delay period, and that once vaporization started, the vaporization and burning rates were equal, i.e. there was no fuel accumulation during the i.d. period. The burning rate for each fuel increment was then determined by the spray size distribution and the single-droplet burning law. The sum of the burning rates for all of the increments forms an envelope which is the predicted ROHR.

Two parameters which were adjusted by the computer for best correlation with experimental results were introduced. The first parameter corresponds to C_b in Tanasawa' equation. The second parameter corresponds to the coefficient in Wolfer's delay equation. (Wolfer's recommended value of 16,600 Btu/lb-mole was used for the apparent activation energy in the i.d. equation.)

The 'predicted' ROHR from model Tanasawa, using the least-squares-fitted parameters, decreases more rapidly than the experimental values during the mixing-reaction-rate-limited stage, as shown in Fig. 2.3. The similarity to and the difference from similar plots by Lyn may be seen in Fig. 2.3. Each line in the heat release rate envelope delineates the rate of heat release of the fuel injected during a single crank angle increment. The 'predicted' heat release curve is not wide enough

during the second stage of heat release and has a too high rate during the after-burning stage. It was thought that this might be caused by the assumption of no vaporization during the delay period. Accordingly, Model Tanas I was constructed and evaluated.

In Model Tanas I, fuel began to evaporate and prepare to burn during the i.d. period at a rate predicted by equation (2.2). This evaporated fuel was accumulated ready-to-burn until the i.d. for that particular increment had elapsed. During the next crank angle after the ignition of an increment, the accumulated ready-to-burn fuel for that particular increment was burned. From this point on, the fuel increment burned according to the spray burning rate formula.

Model Tanas I, however, gave results similar to those shown in Fig. 2.3. It was ultimately judged that this occurred because neither model had mixing or reaction rate relations built into it and, as a result, the least-squares fit could not fit both the vaporization-limited and the mixing-reaction-rate-limited stages.

Experience with Models Tanasawa and Tanas I indicates that:

1. Neither of these models, as described above, will predict a reasonably correct ROHR. The vaporization-limited stage of the predicted curve is always too narrow and the mixing-reaction-rate-limited stage is too drawn out.
2. Tanas I does predict an initial sharp peak or spike as a result of the pre-mixed combustion.
3. The capability of Tanas I to predict the initial peak or spike in the ROHR curve does not decrease its ability to be adjusted to the subsequent portions of the ROHR curve.
4. The single-droplet model must be modified to include more than single-droplet vaporization phenomena in order to predict the observed ROHR.

MODEL TANAS II

The approach was then modified in the following way:

1. Efforts were concentrated on Model Tanas I, the model which accumulates prepared-to-burn fuel during the i.d. period of each increment of fuel.
2. A new combustion or burning coefficient was defined: C_E is a combustion or burning coefficient for the fuel spray in Model Tanas II (the model for combustion of a fuel spray in a diesel engine)--the effects of droplet interaction in the spray, mixing, and chemical reaction rates as well as all other variables, with the exception of those explicitly included, were included implicitly in C_E. The product of $C_b C_E$ is used for C_b in equation (2.2). Shipinski (24) includes C_b of equation (2.2) in his C_E. Thus his coefficient C_E has different numerical values (by the factor C_b), although the concept is the same. The C_E used here is dimensionless. Thus, if the above effects are negligible, C_E is unity.

The possibility of the variation of C_E during the cycle, due to factors not included in the model but which affect the spray, is recognized.

From a practical standpoint, as C_E includes the effects of so many phenomena it is of limited utility if it is a function of many variables. This is especially true, as one can talk about either instantaneous or time-averaged values of the variables.

CORRELATION FOR C_E

Inasmuch as changes in the spray factors not included in the model were observed only indirectly by their effect on cylinder pressure, temperature, and equivalence ratio, an attempt was made to correlate C_E with these variables.

PRESSURE DEPENDENCE ... In order to obtain a burning rate dependent on instantaneous gas pressure, the value of C_b observed by Spaulding (10) was used and the relationship C_E = constant × $P^{0.25}$ was used. The pressure dependence of 0.25 was reported by Hall (17) for single-droplet experiments. The value of the constant was

then computed by the computer as the value which gave the best least-squares fit to the experimental data. The heat release rate computed by the model and the experimentally obtained ROI and ROHR are given in Fig. 2.4. It is seen that the 'predicted' heat release rate curve is too 'narrow' and has a too long 'tail'.

As this discrepancy could be caused by an incorrect pressure dependence, the model was slightly changed, allowing C_E to be dependent on cylinder gas pressure raised to a power determined by a least-squares fit. The computer-determined power was -0.12. A comparison of 'predicted' ROHR using the exponent of -0.12 with the experimental curve is shown in Fig. 2.5. It is seen that a different 'predicted' curve is obtained. Although the correlation between the 'predicted' and 'experimental' curve is improved in some areas, it is worse in other areas.

To make an additional check for pressure dependence, additional comparison runs were made at 1.0, 1.6, 2.0, and 2.5 inlet manifold pressure ratios at a constant inlet-air temperature. Again, the experimental data and a least-squares program were used to 'predict' a dependence of burning rate on instantaneous cylinder pressure. The results showed a scattered, but very weak, dependence on pressure. In addition, the correlation between the 'predicted' and experimental rates for these additional runs was no better than than shown in Fig. 2.5. As these data cover a wide range of cylinder pressures, it appears that the dependence of the coefficient C_E on pressure is very small.

DEPENDENCE ON OXYGEN ... As C_b is a vaporization and not a burning coefficient, C_E must go to zero at the time when all the available oxygen is consumed (i.e. in Borman's (6) terminology, at a burned mixture having an equivalence ratio, F, of one). Accordingly, the dependence of C_E on available oxygen as presented in the literature and also as derived from simple kinetic theory was substituted into the model. Deletion of the pressure dependence and inclusion of the dependence upon the equivalence ratio did not significantly change the shape of the predicted curve or improve the agreement with the experimental curve.

As a matter of interest, even though no improvement in correlation was found by including the instantaneous variation in equivalence ratio during the cycle, an improved correlation was found when the variation in average equivalence ratio (i.e. variation in equivalence ratio with load) was included. The dependence found for the mean coefficient for the entire heat release period was

$$C_E = 0.0166 \times A/F \tag{2.3}$$

where A/F is the overall air/fuel ratio. The range of air/fuel ratios over which this relationship was observed is from 20:1 to 60:1. At high air/fuel ratios the numerical value of C_E obtained from equation (2.3) is nearly unity. The numerical value of C_E at the lowest air/fuel ratio observed is only about 0.333. A possible reason for this is droplet interaction in the fuel-rich spray at low air/fuel ratios.

On the basis of this result, the instantaneous value of C_E was assumed to be a function of the instantaneous ratio of the oxygen present to that present during compression. Several functional relationships were tried in the model in an attempt to predict a more nearly correct heat release rate. None of these produced any improvement in the 'predicted' shape. Next, the computer program was allowed to pick its own dependence on instantaneous oxygen ratio, subject only to the restriction that the instantaneous burning coefficient C_E must decrease with decreasing oxygen content. The result indicated that there is no dependence on oxygen ratio. This result is puzzling in view of the very strong dependence of the overall burning coefficient for the cycle on the air/fuel ratio for the cycle.

Because of this seeming inconsistency as to the effect of oxygen ratio on C_E, and because, as will be described later, a temperature effect on C_E was found, no effect of oxygen on C_E was included. Limited part-load runs indicate that this procedure is satisfactory.

SPEED DEPENDENCE ... The technique of allowing the computer program to 'pick' the best time-average value of C_E was employed over the range of speeds encountered. The results indicate a very weak dependence of C_E on engine speed. The result indicates single-droplet relationships must explain any speed effects and that the well-accepted fact that the combustion period is nearly constant in terms of crank angle

degrees is explained by the change in mean drop size with a change in speed. The change in mean drop size is a result of increased injection pressures with increased speed.

TEMPERATURE DEPENDENCE ... The evaporation rate of a liquid droplet in high temperature surroundings is related to the rate of heat transfer. Thus C_E may vary with gas temperature during the cycle. The technique of allowing the dependence of C_E to selected by the program was again used to determine the dependence of C_E on temperature. That is, C_E was set equal to mT^n, where m and n were adjusted by the computer program to give the best least-squares fit. The results are given in Table 2.1. The data indicate that the instantaneous spray burning rate is nearly proportional to the one-third power of T and that m may vary with engine configuration. It should be remembered, however, that the ROHR curve is a function of

$$\frac{C_E}{(\text{Sauter mean diameter})^2}$$

The best correspondence between experimental and computed heat release rates is illustrated in Fig. 2.6.

NUMERICAL VALUE OF C_E

For the engine used, the equation for C_E is:

$$C_E = \frac{mT^n}{250} \tag{2.4}$$

where m is the constant for given engine configuration--for the engine used, m falls from from 4 to 8; T the instantaneous mass averaged cylinder gas temperature, [°R]; n the exponent of T obtained from this experiment--for the engine used, n falls from 0.30 to 0.35.

Table 2.1 Dependence of C_E on temperature

Run	n	m	Equiv. ratio	Fuel	Swirl
1	0.32	7.42	0.75	CIE	Normal
2	0.32	6.97	0.49	SRF	Normal
3	0.35	6.11	0.26	SRF	Normal
4	0.33	3.91	0.719	SRF	Low

PREDICTION OF ROHR CURVE FROM ROI CURVE

Following the authors' approach, the simulation of the combustion rate in an open-chamber, direct-injection engine consists of the following steps. The values for the constants used by the authors are shown for illustrative purposes.

(a) The division of the injected fuel (ROI) into discrete packets or increments, based on the time interval of injection. The amount of fuel in an increment is that amount injected during 1 crank angle degree.

(b) The computation of a Sauter mean diameter (SMD, microns) for each increment of fuel using the following form of Knight's (29) equation:

$$\text{SMD} = 220(\Delta P)^{-0.458}(Q)^{0.209}(\nu)^{0.215}\left(\frac{A_{orf}}{A(t)_{eff}}\right)^{0.916} \tag{2.5}$$

where ΔP is the difference between instantaneous injection pressure and instantaneous cylinder gas pressure, lb/in.^{2}; Q the mass flow rate through the nozzle, lb/h; v the kinematic viscosity of fuel, cS; A_{orf} the exit orifice area, in.^{2}; $A(t)_{eff}$ the effective orifice area across which ΔP is measured, in.^{2}.

(c) The computation of an i.d. for each increment of fuel injected using Wolfer's (30) formula, modified to fit experimental data, and modified to account for changes in cylinder gas pressure and temperature during the ignition delay (i.d., crank angle) period of the fuel increment:

$$\text{i.d.} = \left(\frac{6\text{RPM}}{1000}\right)\left(\frac{0.0271}{P^{0.386}}\right)\left(\frac{40}{\text{CN}}\right)^{0.69}\exp\left(\frac{8360}{T}\right) \tag{2.6}$$

where RPM is the engine speed, rev/min; P the linear average of cylinder gas pressure at time of injection and at time of ignition, lb/in^2; T the linear average of cylinder gas temperature at time of injection and at time of ignition, °R; CN the cetane number of fuel.

(d) The computation of the rate of heat release of each increment of fuel injected, using Godsave's value of .790 for C_b, a value of 4 for m and a value of 0.33 for n:

$$\text{HR} = -\text{DWF(K)} \times \text{DTDT} \times \text{DFDT} \times \exp(-3.\times\text{TANA}^{0.75}\times(1.-\text{TANA})^{-0.25}) \tag{2.7}$$

where
HR = rate of burning of fuel, lb/crank angle
DWF(K) = mass of fuel in Kth increment injected, lb
DTDT = $\{\text{DT1}+[\text{CA1}-\text{CA(K)}]\times\text{DT2}\}/(\text{SMD(K)})^2$
DT1 = $4 \times 790 \times T^{0.33}/6 \times \text{RPM}$
T = instantaneous cylinder gas temperature, °R
RPM = engine speed, rev/min
CA1 = engine crank angle corresponding to current position of piston
CA(K) = engine crank angle when Kth increment of fuel injected
DT2 = $4. \times 790. \times 0.33 \times \frac{\Delta T}{T} \times T^{0.33}/(6.\ \text{RPM})$
ΔT = change in cylinder gas temperature between previous crank angle and current crank angle, °R
SMD(K) = Sauter mean diameter of Kth increment of fuel injected
DFDT = $-2.25 \times (\text{TANA})^{-0.25} \times (1.-\text{TANA})^{-0.25} + 0.75\ \text{TANA}^{0.75} \times (1-\text{TANA})^{-1.25}$
TANA = $4. \times 790. \times [\text{CA1}-\text{CA(K)}] \times T^{0.33}/[6.\times\text{RPM}\times(\text{SMD(K)})^2]$

(e) Sum the heat rates at each crank angle and multiply by fuel heating value to get the total heat release rate at each crank angle.

CONCLUSIONS

1. The concept of Probert and Tanasawa of a spray burning at a rate corresponding to single-droplet burning coefficients cannot be used without modification to predict the heat release rate in a c.i. engine.
2. Modification of single-droplet burning rate by a coefficient C_E for a spray burning in an engine is proposed. The value of this coefficient is determined by the conditions within the engine.
3. If C_E is considered to be constant during combustion, it is dependent on the overall fuel/air ratio for the cycle.
4. If C_E is considered to be variable during combustion, the instantaneous value for the spray is proportional to the one-third power of the instantaneous mass-averaged gas temperature and has no dependence on pressure and fuel/air ratio.
5. Using the above concepts ROHR curves in an open-chamber diesel engine can be predicted from ROI curves and injector pressures.

REFERENCES

1. Olson, D.R., "Simulation of a Free-piston Engine," S.A.E. Trans., 1958, 66, presented at S.A.E. Annual Meeting, Detroit, 14th January 1958.
2. Brown, D.H., "Criteria for Diesel Cylinder Design Based on Cylinder Heat Transfer," Int. Congress of Combustion Engines, 1959.

3. Cook, H.A., "Digital Computer Analysis and Interpretation of Turbocharged Diesel Engine Performance," S.A.E. Trans., 1959, 67.
4. Lyn, W.T., "Calculations of the Effect of Rate of Heat Release on the Shape of Cylinder-pressure Diagrams and Cycle Efficiency," Proc. Auto. Div. Instn. Mech. Engrs. 1960-61, (No. 1), 34.
5. Huber, P. and Brown, J.R., "Computation of Instantaneous Air Flow and Volumetric Efficiency," S.A.E. Paper No. 812B, presented at Detroit, 1964 (17th January).
6. Borman, G.L., "Mathematical Simulation of Internal Combustion Engine Processes and Performance including Comparisons with Experiment," PhD thesis, Mech. Eng. Dept., University of Wisconsin, 1964; reprinted as C.A.E., Rept. No. 954, submitted to Detroit Arsenal, 1964 (August).
7. McAulay, K.J., Wu, T., Chen, S., Borman, G.L., Myers, P.S. and Uyehara, O. O.A., "Development and Evaluation of The Simulation of the Compression-ignition Engine," S.A.E. Paper No. 650451, presented at Chicago, 1965 (18th May).
8. Edson, M.H., "A Mathematical Model for Combustion," Ind. Eng. Chem., 1960, 52 (No. 12), 1007.
9. Phillipps, R.A. and Orman, P.L., "Simulation of Combustion in A Gasoline Engine Using a Digital Computer," Cranfield Int. Symp. Series, 1966, 8.
10. Spaulding, D.B., *Some Fundamental of Combustion*, 1955, (Academic Press, New York).
11. Cook, H.A., "Appraisal of Effects of Operating Conditions and Engine Design on Combustion in Reciprocating Engines by Engine Cycle Calculations," S.A.E. Paper No. 633C, 1963.
12. Cook, H.A., "Diesel Engine Cycle Analysis of Relationships of Fuel Injection to Fuel Compression-ignition Characteristics and Best Fuel Utilization," S.A.E. Paper No. 650449, presented at Chicago, 1965 (18th May).
13. Held, G., "Welchen Aufschluss Geben Einspritz- und Brenngesetz uber die wirkliche Motorische Verbrennung?" Motor Technisch Zeitschrift 1966, 27/12, 480.
14. Nagao, F., Ikegami, M. and Oshima, K., "An Analysis of Combustion Knock in A Diesel Engine," Bulletin J. Soc. Mech. Engrs 1967, 10, (No. 39), 532.
15. El-Wakil, M.M., Myers, P.S. and Uyehara, O.A., "Fuel Vaporization and Ignition Lag in Diesel Combustion," S.A.E. Trans. 1956, 64, 712.
16. Godsave, G.A.E., "Studies of the Combustion of Drops in A Fuel Spray," Fourth Symp. (Int.) on Combustion 1953.
17. Hall, A.R. and Diederichsen, J., "An Experimental Study of the Burning of Single Drops of Fuel in Air at Pressures up to Twenty Atmospheres," Fourth Symp. (Int.) on Combustion, 1953, 837 (Williams and Wilkins, Baltimore).
18. Hottel, H.L., Williams, G.C. and Simpson, H.C.,""Combustion of Droplets of Heavy Liquid Fuels," Fifth Symp. (Int.) On Combustion, 1954.
19. Wood, B.J. et al. "Heterogeneous Combustion of Multi-component Fuels," Combust. Flame, 1960, 4, 235.
20. Probert, R.P., "The Influence of Spray Particle Size and Distribution in The Combustion of Oil Droplets," Phil. Mag. Ser. 7, 1946, 37, (No. 265), 94.
21. Tanasawa, Y., "On the Combustion Rate of A Group of Fuel Particles," Tech. Rept Tohoku Univ., 1953, 18, (No. 1), 61.
22. Schweitzer, P.H., "The Tangent Method of Analysis for Indicator Cards of Internal Combustion Engines," Bull. No. 35, 1926, (September) (Penn. State Eng. Exp. Sta.).
23. Krieger, R.B. and Borman, G. "The Computation of Apparent Heat Release for Internal Combustion Engines," A.S.M.E. Paper 66-WA/DGP4, presented at Winter Annual Meeting, 1966 (28th November).
24. Shipinski, J.H., "Relationships between Rates-of-injection and Rates-of-heat-release in Diesel Engines," Ph.D. Thesis, Dept. Mech. Eng., University of Wisconsin, 1967 (June).
25. LeFeuvre, T., Myers, P.S., Uyehara, O.A. and Shipinski, J., "A Tape Recording and Computer Processing System for Instantaneous Engine Data," S.A.E. Paper 680133, presented at Detroit, 1968 (12th January).
26. Lyn, W.T., "Study of Burning Rate and Nature of Combustion in a Diesel Engine," Ninth Symp. (Int.) on Combustion, 1962.
27. Shipinski, J.H., Uyehara, O.A. and Myers, P.S., "Experimental Correlation Between Rate-of-injection and Rate-of-heat-release in A Diesel Engine," A.S.M.E. Publ. 68-DGP-11, presented at Diesel and Gas Power Conf. and Exhibit, Houston, Tex. 1968 (12th-16th May).
28. Wiebe, I., Halbempirische Formel fur die Verbrennungsgeschwindigkeit, 1956 (Moscow, Verlag der Akademie der Wissenschaften der VdSSR).
29. Knight, B.E., "Communication on The Performance of A Type of Swirl Atomizer," Proc. Instn mech. Engrs, 1955, 104.
30. Wolfer, H.H., "Ignition Lag in The Diesel Engine," (Der Zundverzug im Dieselmotor), VDI ForschHft. No. 392 1938, 15.

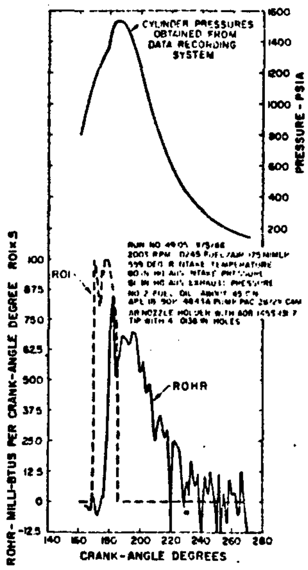

Fig. 2.1 (a) Typical p-t diagram.
(b) ROI and ROHR.

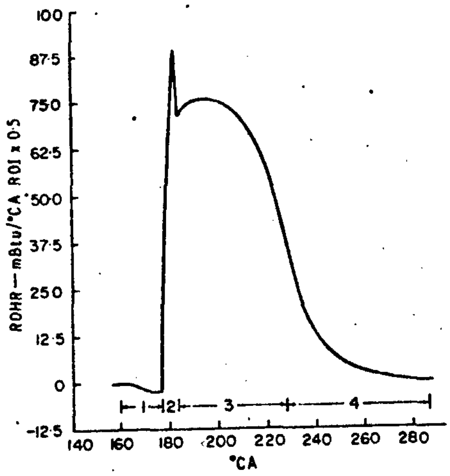

Fig. 2.2 Division of ROHR curve into four stages according to rate-limiting processes.

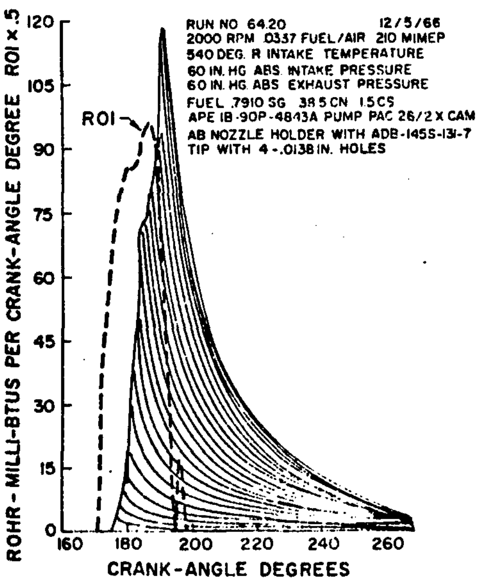

Fig. 2.3 ROHR for fuel injected during each degree crankangle and total heat release curve.

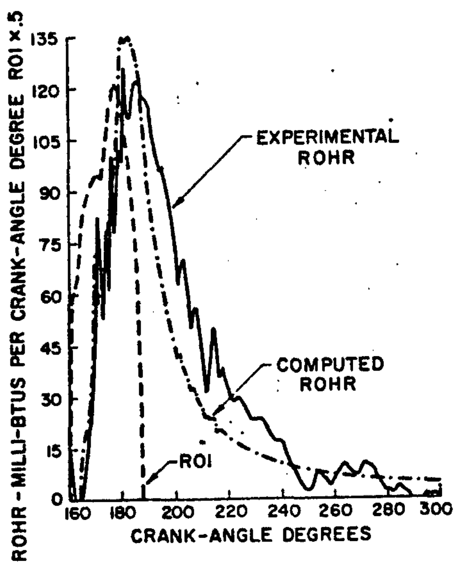

Fig. 2.4 Comparison of ROHR predicted by Model Tanas II with $C_E \propto P^{0.25}$ and experimental ROHR.

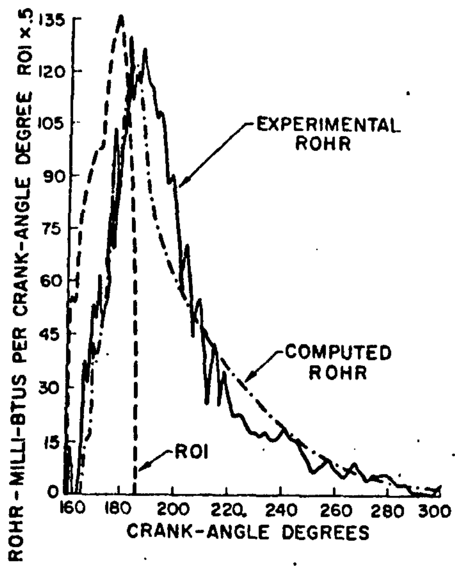

Fig. 2.5 Comparison of ROHR predicted by Model Tanas II with $C_E \propto P^{-0.12}$ and experimental ROHR.

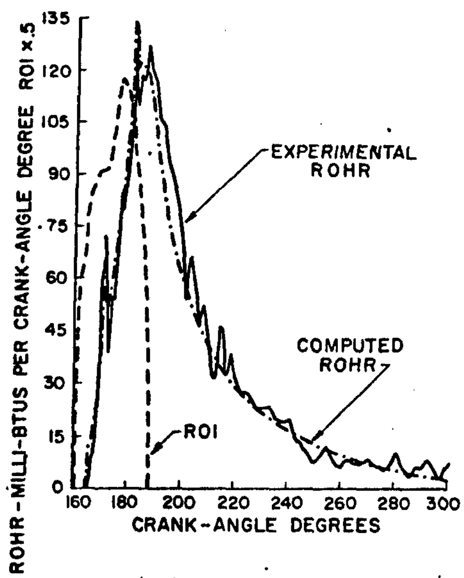

Fig. 2.6 Comparison of ROHR predicted with Model Tanas II with $C_E \propto T^{0.33}$ and experimental ROHR.

APPENDIX VII

The Simulation of Single Cylinder Intake and Exhaust Systems

M. Goyal, G. Scharpf and G. Borman
Mechanical Engineering Dept.
University of Wisconsin

ABSTRACT

A detailed description of a numerical method for computing unsteady flows in engine intake and exhaust systems is given. The calculations include the effects of heat transfer and friction. The inclusion of such calculations in a mathematically simulated engine cycle is discussed and results shown for several systems. In particular, the effects of bellmouth versus plain pipe terminations and the effects of a finite surge tank are calculated. Experimental data on the effect of heat transfer from the back of the intake valve on wave damping are given and show the effect to be negligible. Experimental data on wave damping during the valve closed period and on the temperature rise of the air near the valve are also given.

INTRODUCTION

One of the basic parts of the detailed mathematical simulation of a single cylinder engine is the simulation of the unsteady flow processes which occur in the intake and exhaust systems (1)*. For single cylinder work, each of these systems usually consists of a valve and port plus a section of straight pipe. The open end of the pipe often terminates in a large volume surge tank. The problem of computing the effects of the pressure pulsations is thus one of applying the basic equations of mass, momentum, and energy to the gas system. The equations are considerably simplified if one assumes one-dimensional flow so that the only independent variables are time and distance along the pipe. Such unsteady one-dimensional flow calculations have been the subject of numerous investigations and a list of references may be found in Ref. 2.

Although the one-dimensional flow assumption precludes a detailed description of the flow in the bend in the port, the effect of this bend may be at least partially accounted for by the appropriate addition of frictional effects. In addition to the port bend effect, friction between the gas and pipe may be important in some cases. Heat transfer between the gas and the various metal surfaces can also play a role in complicating the flow problem. Proper inclusion of the effects of friction and heat transfer is made difficult by the fact that good correlations for unsteady flows are not generally available and one must depend primarily on correlations obtained from steady flow experiments. Fortunately in the intake system the fluid velocities and temperatures are often so low that the effects of friction and heat transfer on the pressure waves are small. Nevertheless, the influence of heat transfer on the volumetric efficiency is quite important because the volumetric efficiency is approximately proportional to the gas density.

The higher velocities and temperatures encountered in the exhaust system cause both the heat transfer and friction to be more important. In particular, it is known that frictional effects can play an important role in the exhaust systems of two-cycle engines.

Because of these differences between the intake and exhaust systems, two types of analysis will be presented here. For the intake system the direct effects of friction and heat transfer will be neglected in calculating the unsteady flow. The exhaust system analysis, on the other hand, includes both frictional and heat transfer effects.

*Numbers in parentheses designate References at end of paper.

The intake and exhaust system equations are coupled to the rest of the cycle by the boundary conditions at the valve ends of the systems. The valve lift, which determines the valve flow area at any instant, is a known function of crank-angle. The instantaneous cylinder pressure is calculated from equations of energy and mass continuity for the cylinder (1).

As explained in Ref. 1, the heat transfer in the intake port is accounted for by treating the port as a thermodynamic system. This thermodynamic analysis assumes that the gas in the port is at a pressure and temperature uniform with distance but varying with time. The port pressure is computed as a space average pressure obtained from the unsteady flow analysis. The gas temperature is then calculated using an energy equation which includes terms of instantaneous heat transfer from the back of the valve and the port surface.

In performing cycle computations which included unsteady flow effects in the intake manifold as discussed above, a number of difficulties were encountered when comparisons were made with experimental data. Most obvious among these difficulties was the failure of the theory to predict the correct damping rates for the intake pressure waves during the time when the intake valve was closed. The second discrepancy was that calculated volumetric efficiencies were always higher by a few per cent than the experimental values although the correct trends of volumetric efficiency variation with engine speed and load were predicted. One suggested cause of these discrepancies was the effect of heat transfer from the back of the valve on the damping and flow rates. An experimental program was thus conducted (3) to determine the effect of heat transfer from the valve on the unsteady flow and to measure the rise in port gas temperature during the valve-closed period.

This paper first describes in some detail the method used for calculating the unsteady flow. Then, some results and comparisons are given based on these calculations. Lastly, the results of the heat transfer experiments are given and their relationship to the calculation results discussed.

BASIC EQUATIONS

The well-known differential equations for one-dimensional unsteady flow through a straight pipe of constant area with friction and heat transfer are:

Continuity Equation -

$$\frac{\partial \rho}{\partial t} + \rho \frac{\partial u}{\partial x} + u \frac{\partial \rho}{\partial x} = 0 \tag{1}$$

Momentum Equation -

$$\frac{\partial u}{\partial t} + u \frac{\partial u}{\partial x} + \frac{1}{\rho} \frac{\partial p}{\partial x} + F = 0 \tag{2}$$

where

$$F = \frac{4f}{D} \frac{u^2}{2} \frac{u}{|u|}$$

represents the frictional force per unit mass. The frictional force changes its direction when the velocity u changes sign.

Energy Equation -

$$(\gamma-1)\rho(q+uF) = \frac{\partial p}{\partial t} + u \frac{\partial p}{\partial x} - a^2\left(\frac{\partial \rho}{\partial t} + u \frac{\partial \rho}{\partial x}\right) \tag{3}$$

where q is the rate of heat added per unit time and per unit mass of gas.

The entropy of a gas particle changes because of the energy q added and the work of friction uF. Thus one can show that along a path line

$$\frac{dp}{dt} = \frac{2}{\gamma - 1} \frac{p}{a} \frac{da}{dt} - \rho(uF+q) \tag{4}$$

BOUNDARY CONDITIONS, ENGINE VALVE END

Figure 1 shows a schematic diagram of the system analyzed. When the valve is closed, the boundary condition is given by

$$u_n = 0. \tag{5}$$

During the valve open period, the exhaust process has two phases of flow. Initial blowdown is choked at the valve, hence the flow is sonic at the minimum section and the boundary condition is

$$u_n = a_c\left[-G + \sqrt{G^2 + \frac{2}{\gamma - 1}}\right] \tag{6}$$

where

$$G = \frac{1}{\gamma - 1}\left(\frac{\gamma+1}{2}\right)^{\frac{\gamma + 1}{2(\gamma-1)}} \frac{1}{\phi}\left(\frac{P_n}{P_c}\right)$$

For the subsonic flow in the minimum section

$$u_n = a_c\left[-F + \sqrt{F^2 + \frac{2}{\gamma - 1}}\right] \tag{7}$$

where

$$F = \frac{1}{\gamma - 1}\,\frac{1}{\phi}\left(\frac{P_n}{P_c}\right)^{\frac{\gamma - 1}{2\gamma}}\left[\left(\frac{2}{\gamma-1}\right)\left(\frac{P_c}{P_n}\right)^{\frac{\gamma - 1}{\gamma}} - 1\right]^{-1/2}$$

The boundary condition for flow from the pipe to the cylinder is

$$u_n = -a_n\sqrt{\frac{2}{\gamma - 1}\left[1 - \left(\frac{P_c}{P_n}\right)^{\frac{\gamma - 1}{\gamma}}\right]\Bigg/\left[\left(\frac{P_c}{P_n}\right)^{-2/\gamma}\phi^{-2} - 1\right]} \tag{8}$$

At the open end of the pipe the flow is considered to be either directly to the atmosphere or to the atmosphere through a finite tank. In the case of no tank or a very large tank,

$$p_t = p_{ambient} = p_0.$$

For the flow from the pipe to the tank

$$p_n(x=L) = p_t. \tag{9}$$

Two shapes of the open end are analyzed (Fig. 2). The plain open end gives the boundary condition as

$$u_n(x=L) = a_t\sqrt{\frac{2}{\gamma - 1}\left[\frac{1 - (p_n/p_t)}{1 + \frac{\gamma+1}{\gamma-1}(p_n/p_t)}\right]} \tag{10}$$

and the flared end (bellmouthed end) gives

$$u_n(x=L) = a_t\sqrt{\frac{2}{\gamma - 1}\left[1 - (p_n/p_t)^{\frac{\gamma - 1}{\gamma}}\right]}$$

where in Eqs. 10 and 11, $p_n = p_n(x=L)$.

The flow from the atmosphere to the tank is assumed to be restricted by an orifice of known area. Thus for flow from the tank to the atmosphere

$$u_{or} = a_t\sqrt{\frac{2}{\gamma - 1}\left[1 - (p_0/p_t)^{\frac{\gamma - 1}{\gamma}}\right]} \tag{12}$$

and for flow from the atmosphere to the tank

$$u_{or} = a_0\sqrt{\frac{2}{\gamma - 1}\left[1 - (p_t/p_0)^{\frac{\gamma - 1}{\gamma}}\right]} \tag{13}$$

CHARACTERISTIC EQUATIONS

Solution of the first order quasi-linear partial differential equations by the method of characteristics has been presented in various publications (4-6) giving

$$\left.\frac{dx}{dt}\right]_{1,2} = u \pm a \qquad \text{(Mach line)} \tag{14}$$

$$\frac{dx}{dt} = u \qquad \text{(Path line)} \tag{15}$$

Equations 1-3 can thus be reduced to

$$dp + \rho\ a\ du - (\gamma-1)\rho(q+uF)dt + \rho\ aF\ dt = 0 \tag{16}$$

along the $u + a$ line, and

$$dp - \rho\ a\ du - (\gamma-1)\rho(q+uF)dt - \rho\ aF\ dt = 0 \tag{17}$$

along the $u - a$ line.

In dimensionless form, the Mach line Eqs. 16 and 17 and path line Eq. 4 read:

$$\frac{1}{\gamma}\ dP + \rho^*\ AdU - (\gamma-1)\rho^*\left(\frac{qL}{a_0^3} + \frac{4fL}{2D}\ U^3\ \frac{U}{|U|}\right)dz + \rho^*\ A\ \frac{4fL}{2D}\ U^2\ \frac{U}{|U|}\ dz = 0. \tag{18}$$

along $u + a$ line.

$$\frac{1}{\gamma}\ dP + \rho^*\ AdU - (\gamma-1)\rho^*\left(\frac{qL}{a_0^3} + \frac{4fL}{2D}\ U^3\ \frac{U}{|U|}\right)dz - \rho^*\ A\ \frac{4fL}{2D}\ U^2\ \frac{U}{|U|}\ dz = 0, \tag{19}$$

along $u - a$ line.

$$\frac{1}{\gamma}\ dP - A^2 d\rho^* - \rho^*(\gamma-1)\left(\frac{qL}{a_0^3} + \frac{4fL}{2D}\ U^3\ \frac{U}{|U|}\right)dz = 0, \tag{20}$$

along u line.

For gas flow in a straight pipe of uniform cross-section without friction and heat transfer (for example intake system), the friction and heat transfer terms in Eqs. 18-20 can be dropped. Equations 18-20 then reduce to

$$\frac{1}{\gamma}\,dP + \rho^*\,A dU = 0 \qquad \text{along } u + a \text{ line} \qquad (21)$$

$$\frac{1}{\gamma}\,dP - \rho^*\,A dU = 0 \qquad \text{along } u - a \text{ line} \qquad (22)$$

$$\left.\frac{dP}{d\rho^*}\right]_s = A^2 \qquad \text{in isentropic flow, that is, the sonic velocity equation.}$$

METHOD OF SOLUTION

Very little data are available as to how the coefficient of friction (f) and the heat transfer coefficient (h) vary for pulsating flow. As the velocity, pressure, and temperature in the pipe vary not only with time but also with distance, any values for f and h based on steady flow conditions may be different from the true values under pulsating flow. In a four-stroke engine, the valve is closed for approximately 3/4 of the cycle and during this period the gas continues to flow back and forth. These continual and rapid reversals of flow prevent the development of any significant boundary layer probably resulting in an increase in the heat transfer coefficient far beyond that obtained under steady flow conditions and based on local instantaneous velocity.

Jackson, et al (7), working with small amplitude pressure waves (of the order of 162.5 db) at frequencies in the range 150-300 cps, found that the heat transfer coefficient varied periodically between the nodes and antinodes of the resonant sound waves. The maximum overall increase in the heat transfer coefficient was only 20%, but the local variations were considerably larger. Marec and Harrje (8), working with large pressure oscillations (of the order of 50% peak to peak of the steady state pressure), found an increase in heat transfer coefficient up to 200%. The increase in the heat transfer coefficient was found to be a function of the amplitude of the local velocity oscillations, the frequency of the oscillations, the steady state pressure, and the Mach number. No general engineering type correlations are known to the authors. The correlations reported by various investigators are more or less correlations for their own apparatus, thus having a limited usefulness.

Jenny (6) used the steady state friction coefficient value of $f = 0.0045$ in his calculations of exhaust flows and found reasonable agreement with experimental data. In the absence of more accurate data for friction coefficient based on tests under unsteady flow, $f = 0.0045$ was assumed.

Heat transfer coefficients were used as reported in Refs. 1 and 2. When the valve is open, the flow of gas is essentially uni-directional and the steady pipe flow formula was applied.

$$h = \frac{0.023}{D}(\text{Re})^{0.8}(\text{Pr})^{0.4}$$

where k is the thermal conductivity of the gas and the Reynolds number is based on the port hydraulic diameter D.

When the valve is closed, the Eichelberg coefficient (9) was applied

$$h = 0.0001(V_p)^{1/3}(pT)^{1/2}\text{Btu/hr-in}^2\text{-F}$$

where:

V_p = Mean piston speed, fpm

p = Pressure, psia

T = Temperature, R

The pressure and temperature were taken to be the port values. The Eichelberg coefficient was found to be very nearly equal to the coefficient given by the steady pipe flow formula based on average flow velocity. In an attempt to make the heat transfer coefficient more realistic during the valve closed period during which flow reversals take place, the Eichelberg coefficient was arbitrarily increased by a factor of three. During the valve open period, the larger of the two values was used, that is, coefficient given by the steady flow pipe formula was used until the "modified" Eichelberg coefficient was larger than the former.

The method of computation used was based on the finite difference scheme of Courant, Isaacson, and Rees (10,11) Fig. 3 shows a portion of the time-distance plane. The time increment Δz corresponds directly to the compression-ignition engine cycle simulation program of Ref. 1, as the exhaust and intake process programs were coupled to it. The cycle used a one crank angle degree increment. Pipe length L was divided into an integer number of equal lengths Δx, where Δx was obtained from the stability criterion for the method of solution used. Finite difference methods, when applied to hyperbolic systems, are conditionally stable. The Courant-Friedrichs-Lewy (12) stability criterion was applied in the form

$$\frac{\Delta x}{\Delta z} > (|U|+A).$$

At an engine speed of 2000 rpm, Δx was taken as 3 in.

Consider all points along a line of constant time, say the line $t = t_0$ in Fig. 3. Assume that all properties such as pressure, temperature, density, velocity, and speed of sound at each of the points $X(1), X(2), \ldots, X(N)$ along $t = t_0$ are known. It is desired to obtain the properties of the gas at time $t = t_1$. Let the properties of the gas at $t = t_1$ and $X(G)$ be $P2(G)$, $\rho^*2(G)$, $U2(G)$, $A2(G)$, and $T2(G)$, and at $t = t_0$ and $X(G)$ be $P1(G)$, $\rho^*1(G)$, $U1(G)$, $A1(G)$, and $T1(G)$. It is assumed, as a first approximation, that the slope of the characteristics $U + a$, $U - a$ at point $(t_1, X(G))$ is the same as at point $(t_0, X(G))$ and that the characteristic curves passing through each point along $t = t_1$ are straight lines, that is, by Euler type difference method (for first approximation)

$$X(G) - XJ(G) = (U1(G) + A1(G))\Delta z$$
$$X(G) - XK(G) = (U1(G) - A1(G))\Delta z \tag{23}$$

Equations 23 can be solved at each point to obtain $XJ(G)$ and $XK(G)$. The values of P and U at $XJ(G)$ and $XK(G)$ can be obtained by linear interpolations. The heat transfer term is now computed for a given pipe wall temperature and the mean gas temperature $T(G)$, where

$$T(G) = (T1(G) + T1(G))/2,$$

but for the first approximation

$$T(G) = T1(G).$$

For the friction term, the velocities U at points $XJ(G)$ and $XK(G)$ are used. Let the terms

$$(\gamma-1)\rho^*\left(qL/a_0^3 + \frac{4fL}{2D}U^3\frac{U}{|U|}\right)dz = Q^*\Big]_{J,K}$$

and

$$\rho^* A\frac{4fL}{D}U^2\frac{U}{|U|}\,dz = F^*\Big]_{J,K},$$

then the finite difference approximations for Eqs. 18 and 19 become

$$\frac{1}{\gamma}(P2(G) - PJ(G)) + \rho^* A(U2(G) - UJ(G)) - Q_J^* + F_J^* = 0 \tag{24a}$$

$$\frac{1}{\gamma}(P2(G) - PK(G)) - \rho^* A(U2(G) - UK(G)) - Q_K^* - F_K^* = 0 \tag{24b}$$

where ρ^* and A are arithmetic means of $\rho^*1(G)$ and $\rho^*2(G)$, and $A1(G)$ and $A2(G)$, respectively.

For the first approximation, however, $\rho^* = \rho^*1(G)$ and $A = A1(G)$. The unknown $P2(G)$ and $U2(G)$ can be obtained from the solution of Eqs. 24.

Now from the path line characteristic and using an Euler type difference formula, we have

$$X(G) - XM(G) = U2(G)\Delta z \tag{25}$$

From Eq. 25, $XM(G)$ can be obtained and the properties P and ρ^* at $XM(G)$ can be computed by linear interpolation. Here it must be noted that the point $XM(G)$ on the path line characteristic may lie on the left or right of point $X(G)$ depending on the sign of $U1(G)$. So for $XM(G)$ on the left of $X(G)$, the linear interpolation is between $X(G)$ and $X(G-1)$; however, for $XM(G)$ on the right of $X(G)$, the linear interpolation will be between $X(G)$ and $X(G+1)$. The finite difference approximation for Eq. 20 gives

$$\frac{1}{\gamma}(P2(G) - PM(G)) - A^2(\rho^*2(G) - \rho^*M(G)) - Q^*_M = 0 \tag{26}$$

Equation 26 can be solved for the only unknown $\rho^*2(G)$. Now knowing $P2(G)$, $U2(G)$, $\rho^*2(G)$, at point $(t_1, X(G))$, $A2(G)$ and $T2(G)$ can be obtained using the perfect gas law.

The slope of characteristics $u + a$ and $u - a$ at point $(t_1, X(G))$ is now computed from the computed properties $U2(G)$ and $A2(G)$ thus giving

$$X(G) - XJ(G) = (U2(G) + A2(G))\Delta z$$

$$X(G) - XK(G) = (U2(G) - A2(G))\Delta z \tag{27}$$

Equations 24, 25, and 26 are solved again. The solution at point $(t_1, X(G))$ is iterated until the difference between the computed properties at $(t_1, X(G))$ during two consecutive solutions is within preset limits. Similarly properties of the gas can be obtained at all the interior points along $t = t_1$.

The boundary points require separate treatment. For the valve end boundary only the $u - a$ characteristic can be drawn. The $u + a$ characteristic lies outside the solution domain. Four boundary conditions, flow from engine cylinder to pipe, sonic flow at minimum section and subsonic flow at minimum section, flow from pipe to engine cylinder, and closed valve (flow velocity = 0) are considered. The values of $XK(1)$ and $U2(1)$ are obtained by simultaneous solution of Eq. 24b and the appropriate boundary condition. $\rho^*2(1)$ and $T2(1)$ depend on the boundary conditions. For flow from the engine cylinder to the pipe, these are based on the properties of the gas in the cylinder. Point $XM(1)$ coincides with point $X(1)$ when the valve is closed for $U2(1) = 0$. During flow from the pipe to the cylinder, the point $XM(1)$ lies on the right of point $X(1)$ and the solution is obtained from Eq. 26.

Only the $u + a$ characteristic can be drawn at the point $X(N)$, the open end. Boundary conditions considered here are flow from pipe to the atmosphere and flow from atmosphere to the pipe. The values of $XJ(N)$, $PJ(N)$, and $UJ(N)$ can be obtained as before, $P2(N)$ and $U2(N)$ are computed by simultaneous solutions of Eq. 24a and the appropriate boundary conditions. For flow from the pipe, the path line characteristic falls within the solution domain and $\rho^*2(N)$ and $T2(1)$ can be obtained from the solution of Eq. 26. $\rho^*2(N)$ and $T2(N)$ are based on the ambient properties for the gas flow into the pipe. This gives all the properties of the gas at time $t = t_1$. The solution is quite general and can be followed for computation of properties at $t = t_2$, the starting point being the properties of the gas at $t = t_1$.

When a tank is attached to the open end of the pipe, the open end boundary requires further simultaneous solution and iteration to include the tank and the boundary conditions for the orifice between the tank and the ambient air. The pressure in the tank is assumed uniform throughout, only varying with time, and the temperature and the volume of the tank are constant.

$$\frac{p_2(t)}{p_1} = \frac{m_2(t)}{m_1} = 1 + \frac{1}{m_1} \int_{t_0}^{t} (\dot{m}_p + \dot{m}_{or})\,dt \tag{28}$$

where:

$p_2(t), m_2(t)$ = Pressure and mass in the tank at time t

p_1, m_1 = Pressure and mass in the tank at time t_0

$\dot{m}_p$ = Mass flow from pipe into tank (>0 for flow into tank)

$\dot{m}_{or}$ = Mass flow through orifice (>0 for flow into tank)

CALCULATION RESULTS

Computed crankangle pressure diagrams for the pressure outside the exhaust valve for the entire cycle and cylinder pressure during the exhaust process are presented in Figs. 4-6 for the International Harvester ER-1 engine as reported in Ref. 1 running at an engine speed of 2000 rpm. Figure 4 shows pressure data for the engine running at full load with the exhaust pipe, including the port, 15 in. long, while Fig. 5 shows data with the exhaust system 30 in. long. Data for the motored engine with a 15 in. long exhaust system are shown in Fig. 6.

Comparing Figs. 4 and 5, the maximum pressure outside the exhaust valve during blowdown was 19.8 psia for the short system and 24.1 psia for the longer exhaust system. The pressure wave from the start of blowdown is transmitted and reflected back to the exhaust valve earlier for the shorter exhaust system; the reflected wave (an expansion wave) reduces the pressure at the valve. The effect of the reflected wave can be observed at a later crankangle, when the reflection of the high amplitude compression wave creates a large depression at the valve. The depression for the longer exhaust system is larger because the amplitude of the compression wave was larger compared to the amplitude in the case of shorter exhaust system. Pressure waves for the shorter exhaust are damped down to zero amplitude because the amplitude was not large at the start and because these waves had twice as reflections as for the longer exhaust system. In Fig. 5 however, the pressure waves can be seen even at the time of next E.V.O.

Figure 6 for motoring has a different shape altogether because the pressure and temperature in the cylinder at the time of exhaust valve opening are not high. This gives waves of very small amplitude and the damping very soon brings the pressure in the exhaust system down to the ambient conditions.

Some further studies were made with the computer programs simulating the exhaust and intake systems. For these studies the programs were run independent of the diesel engine cycle simulation program. These studies were prompted by the fact that some experimental data on the intake system of the International Harvester ER-1 engine showed a rate of wave amplitude damping during the valve closed period which was much less than that predicted by the calculations (1).

The first nonengine system considered was a pipe filled with air to a known pressure and with both ends initially closed. When one end is suddenly opened to the atmosphere or to a tank at essentially atmospheric pressure, the air flows from the pipe with subsequent flow reversals. Two situations were investigated. In situation (a) the end is opened to the atmosphere. The effects caused by a bellmouth end as compared to a plain end were computed. In situation (b) a plain open end is connected to a tank of finite size. The tank is also connected to the atmosphere through an orifice of known size.

Turning to situation (a), the pipe was 24.5 in. long with a cross-sectional area of 2.54 in.^{2}. The initial pressure was 4 psig. Figure 7 shows the gage pressure at the valve end plotted against time after the opening of the other end. It is evident from this that a plain open end results in more loss than a bellmouthed end and hence, a higher rate of damping. The reason for this can be seen by examining Fig. 2; inflow from the atmosphere to the pipe in the case of a plain end forms a Venturi at the entrance, restricting the flow, while a bellmouthed end has no restrictions.

Now considering situation (b), Fig. 8 shows the effect of connecting a tank of 2200 cu in. volume, with an orifice of 0.7 in.^{2} area between the tank and the atmosphere, to the open end of a pipe 18.92 in. long and having an area of 2.54 in.^{2}. The initial pressure in the pipe was 4 psig and the initial tank pressure was 0 psig. The computed gage pressure at the valve end for the cases with and without tank is shown in an expanded scale. Even when the maximum rise in tank pressure is only 0.085 psi, the amplitude of the pressure waves is affected detectably.

The effect of a simplified engine intake stroke, running at 2000 rpm, using the same pipe and tank system as given for Fig. 8 is shown in Fig. 9. The continued suction stroke of a long duration (from 540 to 720 crankdegrees) brings down the tank pressure by about 0.4 psi. The large effect of adding the tank volume on the shape of the pressure trace and the amplitude of the pressure waves can be seen.

Calculations of the complete engine cycle with both intake and exhaust dynamics showed that for the ER-1 engine, the effect of exhaust dynamics was to increase the volumetric efficiency by several per cent over the case of computations with an assumed constant exhaust port pressure. No conclusions could be drawn by comparison with the experimental values, however, since the experimental exhaust pipe was not a simple configuration.

Calculations of exhaust dynamics with various levels of friction and heat transfer were also made. The calculations showed only very slight differences, leading to the conclusion that for the cases studied, heat transfer and friction were not very important. Further studies and comparisons will be necessary however, before any conclusive statements can be made.

COMPARISONS WITH EXPERIMENTAL DATA

Comparisons of calculated and experimental intake port pressures showed that the predicted damping of the pressure waves during valve closed period was larger than found experimentally. Figure 10 shows some typical comparisons for the ER-1 engine. Several reasons for the discrepancy were postulated.

1. The losses at the open end of the tube might be smaller than expected. This has already been illustrated in the calculations comparing straight and bellmouthed end configurations.
2. A finite tank volume can interact with the unsteady pipe flow.
3. It is known that acoustic vibrations in pipes can be reinforced by heating one end of the pipe. Such heating occurs in the intake port because of the presence of the hot valve surface and might reinforce the pressure waves.

Of these three effects, the third was least well understood. Thus an experimental investigation of the effects of valve heating was initiated.

EXPERIMENTAL APPARATUS

The experimental apparatus consisted of a valve, port and intake pipe attached to a duct system which was pumped by a single stage steam ejector. A schematic of diagram of the apparatus is shown in Fig. 11. The bottom face of the 2 in. diameter valve was heated electrically and the temperature of the valve was measured by means of a thermocouple located in the center of the face. Figure 12 shows the construction. Heat transfer up the valve stem was reduced by a transite spacer located 1/2 in. up the stem from the head. The port consisted of a 90 deg copper elbow having a 1-5/8 in. inside diameter, a 2-5/16 in. centerline radius bend, and an overall

length of 6 in. The port and valve seat were thermally insulated from the valve by mounting the seat in a transite plate. Various lengths of 1-1/2 in. inside diameter copper tubes with straight or flared ends were attached to the port. This pipe was open to the atmosphere at its upstream end.

Figure 13 is a photograph of the valve actuating mechanism and port with a pipe attached. Threaded onto the top of the valve stem, the roll follower (B) rode on a hardened steel cam (C) having a 1 in. base circle and a total lift of 0.47 in. The cam was designed such that the motion during closing was the same as that used in the I.H. test engine. The closing period of 60 deg cam rotation was preceded by 70 deg of rotation during which the valve was held wide open and was followed by 60 deg of rotation during which the valve was fully closed. The valve was opened again using a smooth connecting ramp. The cam, which was keyed to the camshaft and held in place by spacers, could be easily replaced with ones having different profiles. The camshaft was driven via a belt drive by a 1/2 hp a-c electric motor (D) with the speed controlled by a mechanical speed control (E) using spring loaded and manually controlled sheaves. The speed range extended 700 to 2000 rpm and was measured with a hand tachometer.

Geared to the camshaft was a second shaft on which was keyed a timing cam (F) running at 1/100 the camshaft speed through use of a speed reducer (G). When in operation, the valve was held open by a pivoting arm (H) while the motor was brought up to speed. A pin on the spring-loaded arm followed the timing cam allowing the arm to swing away and release the valve at the proper moment for the follower to contact the cam. The valve then closed following the cam profile and continued to cycle open and shut until the motor was turned off.

The pressure waves caused by the valve closing were measured by pickups mounted in adaptors at either end of the port at distances of 1-1/2 and 6-1/4 in. respectively from the bottom of the valve seat. The temperature rise of the port air was measured by a probe also located 1-1/2 in. from the seat bottom.

The pressure pickups used for measuring the waves were Kistle 601L transducers. Before being displayed on the scope, the pressure signals were amplified using Kistler 566 Multi-Range Charge amplifiers. The temperature rise was measured using a DISA 55A35 hot-wire resistance probe as one leg of a Wheatstone bridge circuit. The characteristics of the probe as given by the manufacturer were as follows:

Wire and mounting	-	Platinum plated tungsten welded to gold-plated nickel supports.
Wire diameter	-	0.005 mm.
Wire length	-	1 mm.

This resistance wire probe was identical to those used in hot-wire anemometers for measuring the velocities of fluids. However, instead of maintaining a constant wire temperature, the current passing through the wire remained approximately constant. Then as the fluid temperature changed, the wire temperature also changed. Since the wire resistance was proportional to its temperature and the current was constant, the voltage drop across the probe changed with temperature. The change in the bridge circuit output voltage could then be measured. In order to measure the air temperature accurately, the current passing through the probe had to be extremely low, approximately 0.5 m-amps or less.

Since the output was a function of the probe temperature, the probe had to be nearly at the same temperature as the air, within about 0.5F to record a 10-20 F change. Therefore, in order to keep the wire self-heating as low as possible, a very small current was used in the circuit. Furthermore, any change in the air velocity had little effect on the wire temperature since the rate of heat transfer between the wire and air was small due to the small temperature difference. With this in mind, a bridge circuit was designed to operate with a current of 0.28 m-amps in each leg using 1.5 v dry cell as power source. The bridge output for a 20F temperature rise was approximately 20 μ v. This output signal was then amplified before being displayed by using an Astrodata Model 885 differential d-c amplifier.

In addition to the experimental apparatus described above, a small bench test apparatus was used for some pressurized pipe experiments. As seen in Fig. 14 it consisted of a 1 in. diameter copper tube 24.5 in. in length attached to a solid copper bar approximately 2 in. in diameter and 6 in. long. The copper bar was

heatel by means of a Bunsen burner to temperatures of 600 F or above, the temperature being measured with a Conax copper-constantan thermocouple. Nine inches from the closed end and mounted on an adaptor was a Kistler 601L pressure pickup for measuring the pressure waves.

WAVE DAMPING RESULTS

Three basic types of experiments were conducted using the apparatus described above. The first type of experiment used the cam mechanism to close the valve. In the second type, the valve was allowed to snap closed with no cam control. Such closing insured that the valve would stay closed and was devised to allow a longer time for observing the pressure oscillations. The third type of experiment utilized the pipe system of Fig. 14. In this experiment, the copper bar was heated and after the heated air was blown out of the pipe, the open end was sealed with a rubber stopper through which a tube from a compressed air tank passed. The pipe was then pressurized to a few psig and the rubber stopper pulled out quickly.

Damping rates were observed for all three experiments with and without heating. In all cases the damping rates were essentially unchanged by the heat transfer. In order to study the damping rates, an average logarithmic decrement was used. The decrement for successive peaks is defined as

$$\delta = \ell n(y_n/y_{n+1}) \tag{31}$$

where y_n is the amplitude of the n-th peak.

The decrement varied somewhat with the wave number, n, so an average value was used. The amplitude ratios were averaged over six cycles and the decrements for the upper and lower peaks were then averaged. Figure 15 shows this average decrement as obtained by snap closing of the valve. The differences, if any, caused by heat transfer lie within the experimental scatter. The lines shown are averages of the points at any one initial mass flow value.

Since the valve temperature had no effect on the rate of damping, the average logarithmic decrement for each pipe length as a function of mass flow rate is shown replotted in Fig. 16. On the same graph for comparison purposes is a plot of the decrement as computed from I.H., ER-1 engine data. Two points obtained on a similar U.W. test engine are also shown. Two reasons can be given for the lower damping values of the engine test data.

1. The engine data had lower initial peak pressures.
2. The engine overall intake system length was 18 in.

Extrapolation of the snap closing data to zero mass flow and a 12 in. pipe still, however, gives a decrement value of about 0.14 which is considerably higher than the engine values. The higher values of damping encountered in both the calculated and experimental snap closing data are thus still unexplained.

TEMPERATURE RISE IN INTAKE PORT

The data used in the study of the temperature rise in the port were obtained from the experiments run with the snap closing of the intake valve. This method allowed a sufficient interval for observation of the air temperature without the valve opening again. Upon closing of the valve, the temperature fluctuated initially with the pressure in the port, lagging by 1 or 2 ms since the hot-wire probe was longer time constant than the pressure transducer. These fluctuations decreased in magnitude quite rapidly after five or six wave cycles while the mean temperature rose during this interval. The temperature in the port stabilized about 30-40 ms after valve closing and all measurements were made at a time of 40 ms. As more time elapsed, convection currents were generated by the hot valve and the motion of the heated gas particles around the probe created large fluctuations in the temperature as observed on the oscilloscope. Figure 17 shows a sample of the pressure and temperature data obtained.

The results of the tests are shown in Fig. 18 where the temperature rise is plotted as a function of mass flow rate and valve temperature. This mass flow rate would correspond in the actual engine to that occurring just at the start of valve closing. This is slightly below the maximum but quite a bit above the mean flow rate for the engine. Test runs were made for a given flow and valve temperature for each of the three intake pipe lengths. No effect was observed due to the different pipes. As expected, the average temperature rise increased as the valve temperature increased. However, this rise decreased for a given valve temperature as the flow increased. This occurred because the valve was heated under no-flow conditions. A few seconds elapsed between the time the flow was established and the moment when the valve was closed and the run conducted. During this interval, the surface of the valve cooled down somewhat from the measured interior temperature, more so at the higher flow rates. Because of this cooling, the actual temperature difference between the valve surface and the port air was lower at the higher flows and the temperature rise was correspondingly lower.

A study of the temperature traces indicated that a significant temperature rise did occur due to the heat transferred from the back surface of the valve. This rise was approximately 13-23 F at the lower flow rates and 10-20 F at the higher rates. It can therefore be concluded that the air entering an engine cylinder upon valve opening has been warmed considerably above the ambient temperature, about 15-20 F. Though not studied, heat port walls at a temperature of about 170 F could also be expected to contribute to a temperature increase, but to a lesser degree than the valve.

This investigation showed that using a hot-wire resistance thermometer is a good method for measuring the air temperature in the simulated port and intake system of an engine. It has a very fast response, with a time constant on the order of 1 ms, several times faster than the best thermocouple. However, the small bridge circuit output required a high amplifier gain of 1000, causing a large noise-to-signal ratio and making it difficult to get accurate measurements from the enlarged temperature traces. This was a result of the small current required in the circuit to keep the hot-wire self-heating at a minimum. This explains the scatter that appears in Fig. 18. With further work, though, the bridge circuit could be modified to have a larger output without increasing the current through the probe. It should then be possible to get good transient temperature measurements of the port air.

CONCLUSIONS AND FUTURE WORK

We have seen that the intake and exhaust dynamics for a single cylinder engine can be joined with a detailed mathematical cycle simulation program. The computations can include heat transfer and friction effects as well as the effects of various pipe terminations. More comparisons are necessary, however, between experimental and simulated exhaust systems before a good evaluation of the exhaust dynamics program can be given. In addition, more basic work on heat transfer and friction coefficients for unsteady flow is needed.

Calculations of the intake dynamics do not perfectly match engine data. Experiments with valve heating have shown that the valve heat transfer does not cause this discrepancy even though the temperature rise in the port during the valve closed portion of the cycle is significant.

The experimental temperature measuring technique used could be tried on an actual engine to determine the temperature rise in the intake system. Such measurements would be particularly useful in helping to determine heat transfer rates and the effects of port heating on volumetric efficiency.

ACKNOWLEDGMENTS

This activity was conducted under contract to and with the technical assistance of the Systems Propulsion Laboratory of the U.S. Army Tank and Automotive Command. Acknowledgment is given to the International Harvester Co. for the experimental data supplied. The authors also wish to thank Profs. P.S. Myers and O.A. Uyehara for their many helpful suggestions.

NOMENCLATURE

a = Sonic speed, in./sec
A = a/a_0
D = Inside diameter of pipe, in.
f = Coefficient of friction
L = Length of pipe, in.
p = Pressure, psi
P = p/p_0
q = Transfer of heat per unit of mass and time, $in.^2/sec^2$
t = Time, sec
T = Temperature, R
u = Particle velocity in direction of x, in./sec
U = u/a_0
x = Distance along pipe, in.
X = x/L
y_n = Amplitude of nth pressure peak, psi
Z = a_0t/L
ρ = Density, $lb_m/in.^3$
ρ^* = ρ/ρ_0
ϕ_v = Effective area of valve, $in.^2$
ϕ_n = Cross-sectional flow area of pipe, $in.^2$
ϕ_{or} = Effective area of orifice, $in.^2$
ϕ = ϕ_v/ϕ_n
γ = Ratio of specific heats

Subscripts
0 = Reference state
c = Cylinder
n = Pipe
t = Tank
or = Orifice

REFERENCES

1. K.J. McAulay, G.L. Borman and T. Wu, "Development and Evaluation of the Simulation of the Compression Ignition Engine." Part 1; Part 2, by S.K. Chen, P.S. Myers, and O.A. Uyehara, SAE Paper 650451, May 1965, SAE Transactions, 1966.
2. G.L. Borman, "Mathematical Simulation of Internal Combustion Engine Processes and Performance Including Comparisons with Experiment," PhD Thesis, M.E. Dept. University of Wisconsin, Madison, Wis., 1964.
3. G. Scharpf, "Experimental Study of Heat Transfer from the Valve and Unsteady Flow in a Simulated Engine Intake System," MS Thesis, M.E. Dept., University of Wisconsin, Madison, Wis., 1966.
4. R.S. Benson, "Some Recent Research on Non-Steady Flows in Engine Exhaust Systems with Particular Reference to Numerical Solution Using Digital Computers." Lecture given at Eidg. Technische Hochschule, Zurich, February 1963.
5. A.H. Shapiro, "The Dynamics and Thermodynamics of Compressible Fluid Flow," Vol. II, New York: Ronald Press, 1954.
6. E.Jenny, "Unidimensional Transient Flow with Consideration of Friction, Heat Transfer, and Change of Section," The Brown Boveri Review, November 1950, pp. 447.
7. T.W. Jackson, K.R. Purdy, C.C. Oliver, "The Effects of Resonant Acoustic Vibrations on the Nusselt Number for a Constant Temperature Horizontal Tube." Second International Heat Transfer Conference, August 1961.
8. J.P. Marec and D.T. Harrje, "Heat Transfer is Oscillating Flow." Progress Report for the Period to June 30, 1963, Princeton University Aeronautical Engineering Report No. 483-e.
9. G. Eichelberg, "Some New Investigations on Old Combustion Engine Problems," Engineering, London, Vol. 148, 1939, p. 603.
10. R. Courant, E. Isaacson and M. Rees, "On the Solution of Non-Linear Hyperbolic Differential Equations by Finite Differences," Commun. Pure Appl. Math 5, 1952, pp. 225-243.
11. L. Fox, "Numerical Solutions of Ordinary and Partial Differential Equations," ADlWES International Series in Engineering Sciences, Pergamon, Addison-Wesley, London.
12. Courant, Friedrichs, Lewy, "Uber die Partiellen Differenzen Gleichungen der Mathematischen Physic." Math Ann. Vol. 100, 1928, pp. 32-74 (484).

DISCUSSION

FRANK J PEKAR
Mack Trucks, Inc.

The basis of my comments on a previous paper by Prof. Borman* and the ones being presented now is a computer simulation incorporating the same mathematical methods used by the authors. The objective of this digital analysis was to simulate actual engine performance close enough to reduce the number of experimental tests in normal engine development. To check the simulation accuracy, a number of controlled engine tests were made, and the results of both compared. Based on this comparison, my conclusions paralleled the authors'. The computer results can accurately predict relative differences, such as volumetric efficiency changes as a function of engine speed, inlet pipe length, effective valve flow area, and cam timing. It cannot predict absolute volumetric efficiency close enough to the experimental results at a given condition to be of any value. These absolute differences that occurred between the experimental and calculated results were attributed to neglecting friction and heat transfer. Heat transfer effects appear to be most influential at the lower engine speeds and friction effects at the higher engine speeds. While it was realized that heat transfer was a factor, there was no way of knowing whether or not the predominant heat addition to the incoming air took place in the inlet manifold and port or in the cylinder. The authors' paper seems to have conclusively proved that heat transfer in the port and from the inlet valve is of little consequence since the pressure-time history remained practically unchanged with the omission or addition of port and inlet valve heat transfer effects.

In light of these findings, I reviewed my previous calculated and experimental data and believe the same conclusions can be drawn. A brief outline of my test program is as follows:

Both motoring and full load volumetric efficiencies were measured at a series of test engine speeds that corresponded to calculated engine speeds. At each speed the engine was first motored cold, that is, after setting for an entire night, to guaranteeing that all parts attained room temperature. Then the engine was quickly motored to the particular test rpm, and the volumetric efficiency was observed as a funciton of time. At the lower piston speeds very little change occurred in the volumetric efficiency until the engine was switched from motoring to full load operation. At this point the volumetric efficiency dropped appreciably after a few seconds. Because cold water was still circulating through the engine, it can be concluded that inlet manifold port and probably inlet valve temperatures did not appreciably change in this few seconds, but that the combustion chamber surface temperatures of both the exhaust valve and piston did. This rapid rise in exhaust valve and piston surface temperature is, in my opinion, responsible for the decrease in volumetric efficiency due to heat transfer during the inlet cycle. At first it was believed that possibly the increase in cylinder pressure at the start of the inlet cycle accompanying the switch from motoring to full load conditions was responsible for at least some of the decreased volumetric efficiency. Additional computer runs were made that included increased pressure and temperature at the start of the inlet cycle to simulate the change to full load with very little effect on the calculated volumetric efficiency. Based on this fact and the authors' findings, the discrepancy seems to lie in the heat transfer that takes place in the cylinder during the inlet cycle.

T. WU AND K.J. McAULAY
International Harvester Co.

Clarity and simplicity in the presentation of numerical solutions of the problem by the authors is indeed a contribution to the engine simulation literature. Our comments are as follows:

1. Intake Port Pressure - First we want to discuss the intake port pressure traces in Fig. 10 of the paper. The general shape of the pressure trace over a cycle depends on the initial pulse duration, i.e., the effective

---

*G.L. Borman, K.J. McAulay, and T. Wu, "Development and Evaluation of the Simulation of the Compression-Ignition Engine." Presented at SAE Mid-Year Meeting, Chicago, May 1965, paper 650451.

valve open period and the time required for the pulse to travel to the end of pipe and back. The number of waves during the valve closed period, therefore, approximately coincides with the natural frequency of the intake pipe with one end closed and one end open. This checks well the results shown in Fig. 10 of the paper. According to the results of the present paper, the large decay of the wave amplitude is largely due to wave interaction of finite tank volume and an excessive energy loss at the tank end of the pipe. Since the solution of the wave equations depend on boundary and initial conditions, we would like to ask the following questions:

a. What loss considerations have been used in the derivation of the tank end pipe condition (Eq. 10 of the paper)?

b. Due to the inertia effect of gas at the pipe open end, some authors have used an end correction equal to $\pi D/8$ which was added to the pipe length. Have the authors made such a modification?

2. Effect of Exhaust Flow - Figure A is a set of intake pressure traces taken from a single cylinder engine at full load and three different engine speeds. The engine variables are controlled so that only the effect of exhaust valve timing on intake port pressure is to be examined. It is seen that there are considerable differences in the intake port pressure traces as the exhaust valve timing is changed from 10 deg CA advance to 10 deg CA retard from the normal setting. It should be pointed out at this time that the exhaust timing was changed by means of an offset key on the exhaust cam. The tdc and bdc marks, shown in Fig. A, represent the induction stroke of the cycle. The vertical grid length corresponds to 2 psi pressure. As the exhaust valve timing is retarded 10 deg CA from nominal exhaust timing, the magnitude of the intake pressure during the intake valve opening is decreased, and the engine volumetric efficiency is increased (about 2%). This result can be explained by the change in combined flow area of both exhaust and intake valves during overlap period. This test data also shows that both intake and exhaust gas dynamics are interrelated. Therefore, considering intake dynamics along does not in general give a complete simulation of the engine. This fact may explain some of the discrepancies between experimental and computed data reported in the authors' Ref. 1 and also in Fig. 10 of their paper. In Ref. 1 the intake port pressure was computed assuming a constant exhaust port pressure without considering unsteady flow gas dynamics.

3. Exhaust Port Pressure - We do not have the corresponding experimental data to make an exact comparison with the authors' computed data as shown in Fig. 4 of the paper. However, the computed data matched the experimental data in general shape, except that test data indicated a first peak during blow down which was slightly later than that shown in Fig. 4 of the paper.

4. Intake System Design Parameters - One shortcoming of the numerical solution is that a generalized correlation cannot be readily obtained. On the other hand, by using dimensional analysis it is possible to obtain the following parameters for the correlation of engine breathing:

$$(Z_{iv}) = \text{Intake gulp factor} \equiv \left(\frac{1}{C_i}\right)\left(\frac{B}{d_{iv}}\right)^2\left(\frac{C_m}{C_o}\right)$$

C_i = Intake valve average flow coefficient $\approx 1.2\left[\frac{h_{max}}{d_{iv}}\right]$

h_{max} = Maximum intake valve lift

d_{iv} = Intake valve OD

(L/S) = Dimensionless pipe length = Pipe Length from valve/stroke

(D/B) = Dimensionless pipe ID = Pipe ID/bore

$\left(\frac{C_m}{C_o}\right)$ = Dimensionless mean piston speed = $\frac{\text{Mean piston speed}}{\text{Engine inlet sonic speed}}$

$\frac{\theta_{ivc}}{180}$ = Dimensionless intake valve closing

θ_{ivc} = Intake valve closing in °CA after tdc

A set of optimum criteria of pipe length and pipe ID equations can then be derived from past experimental data. This method gives a quick and rationalized guidance for initial engine design.

Although we have raised questions about several details of the paper, in general we agree with the approach taken to the exhaust and intake dynamics. There are still many problem areas which complicate diesel engine computer simulation, namely, the multi cylinder engine application, variable area piping, and possible shock wave interaction. We would like to encourage the authors to carry out further experimental and analytical work on the gas dynamics of reciprocating engines so as to improve our understanding of the processes taking place in the engine.

AUTHORS' CLOSURE TO DISCUSSION

The authors would first like to thank the discussors for their careful review of the paper and their encouraging remarks. In particular, the authors would like to acknowledge the rigorous review of the theoretical equations by Dr. Wu and Mr. McAulay.

Turning to Mr. Pekar's remarks, we are in general agreement that the heat transfer from the cylinder surfaces during intake is an important factor in determining volumetric efficiency. However, the authors do not agree that heat transfer from the valve and port can be neglected. It is true that such heat transfer does not seem to affect the pressure waves, but it nevertheless can have an important effect by simply heating the air and thus reducing the mass intake.

Next, taking up the questions of Wu and McAulay, we agree that many other engine factors, such as the exhaust dynamics, influence the volumetric calculations. We still feel, however, that the intake calculations are a major cause of the discrepancies noted in the paper. The equations for the open pipe end are based on steady-flow theory and were not corrected by the addition of the $\pi D/8$ length which is obtained from acoustic theory. The plain end is treated essentially as an orifice, but other corrections for, say, frictional losses or unsteady effects are not included. Since the loss terms were too high, one might conclude that the bellmouth equations should be used. More recent engine tests with a clearly plain end pipe show the same difficulties, however. Further studies of open end unsteady flows thus needed to establish the correct equations.

Lastly, we agree with the discussors that the "gulp factor" equations can be quite useful and compliment the computer studies when extensive experimental data are available to the designer.

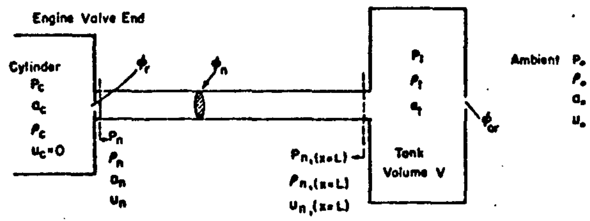

Fig. 1 Schematic diagram of simplified intake or exhaust system of single cylinder engine.

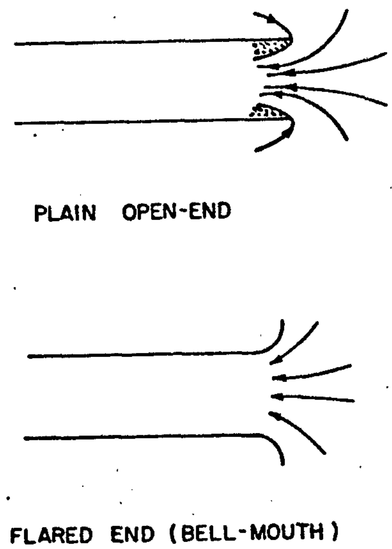

Fig. 2 Diagram showing inflow at plain and flared end of a pipe.

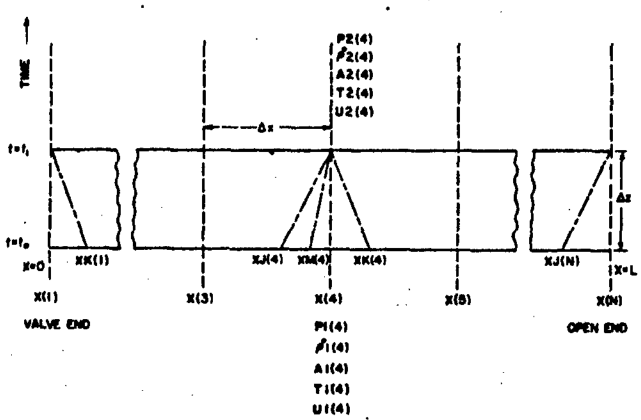

Fig. 3 Diagram showing finite difference notation in time-distance plane.

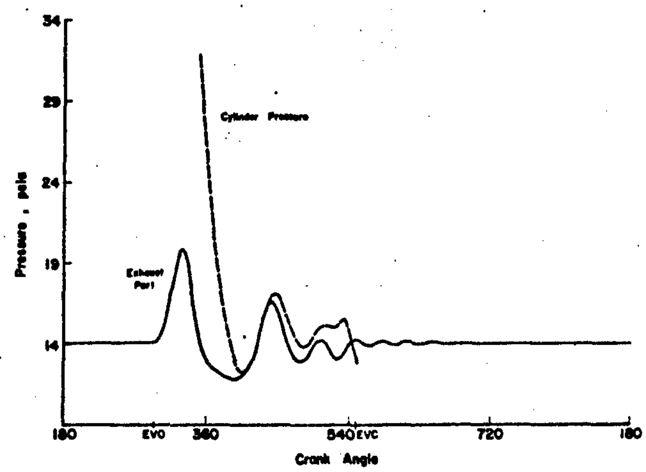

Fig. 4 Cylinder and exhaust port pressures for full load, 2000 rpm, exhaust system 15 in. long.

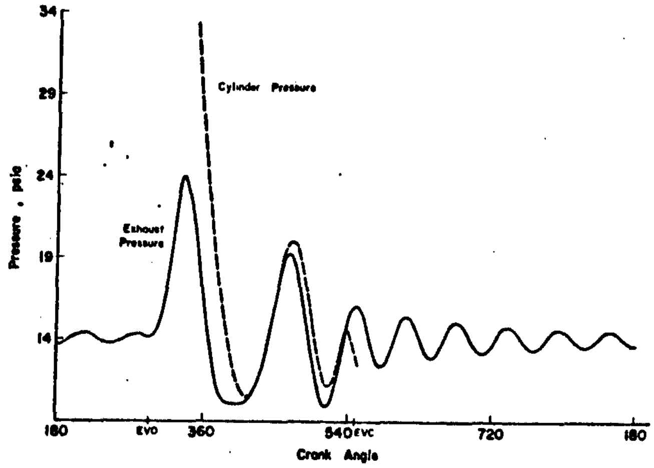

Fig. 5 Cylinder and exhaust port pressures for full load, 2000 rpm, exhaust system 30 in. long.

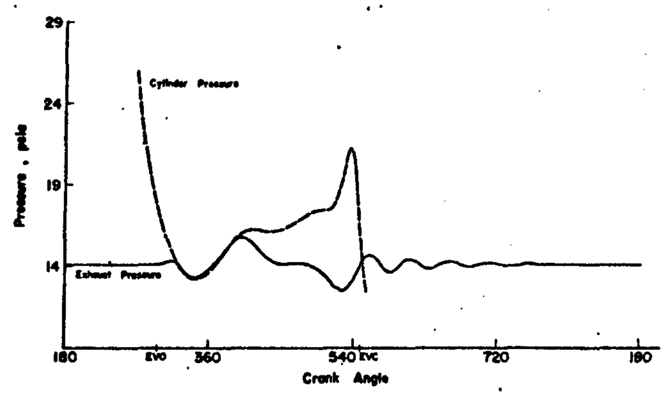

Fig. 6 Cylinder and exhaust port pressures for motored engine, 2000 rpm, exhaust system 15 in., long.

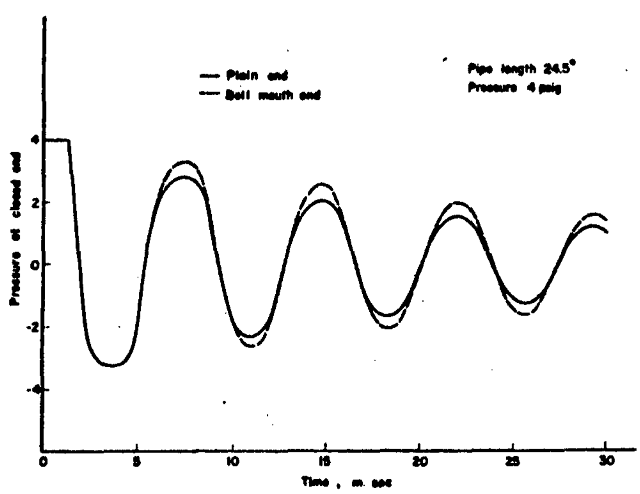

Fig. 7 Effect of plain open end and bell mouth open end on emptying of a straight pipe closed at one end.

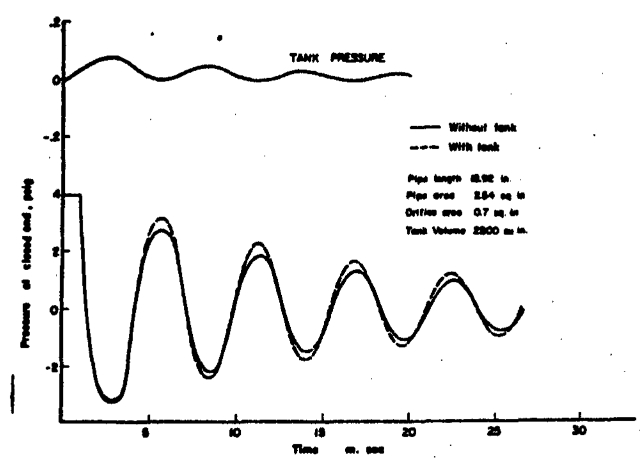

Fig. 8 Effect of finite tank on emptying of straight pipe.

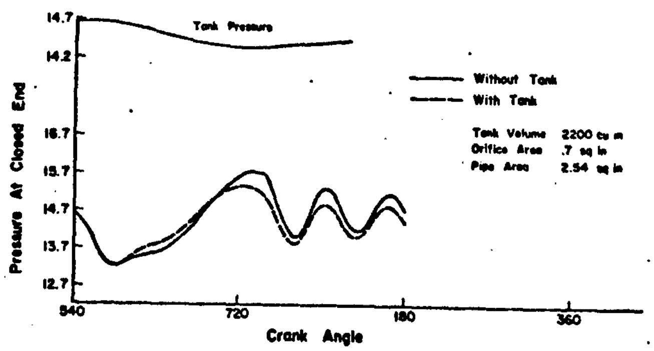

Fig. 9 Effect of finite tank on simplified engine intake.

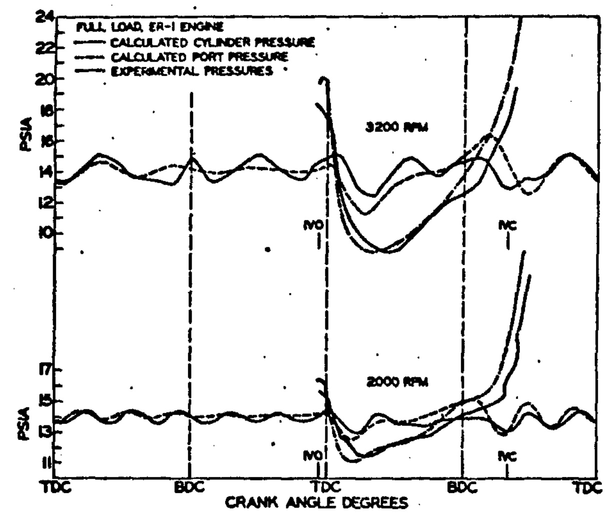

Fig. 10 Some comparisons of experimental and calculated intake port pressures. (International Harvestor Co. Data, Ref. 1).

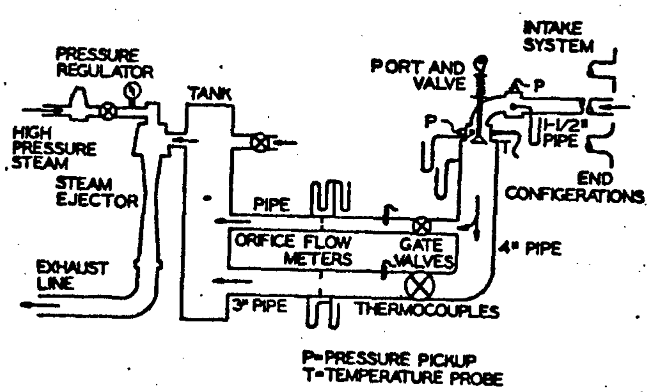

Fig. 11 Schematic diagram of flow system apparatus.

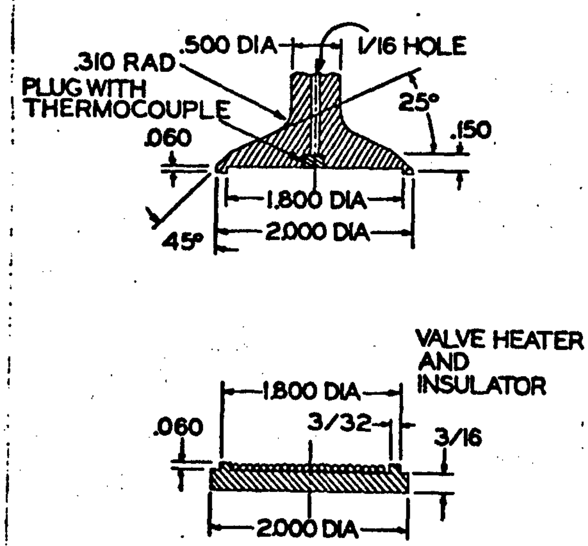

Fig. 12 Diagram of valve and valve heater.

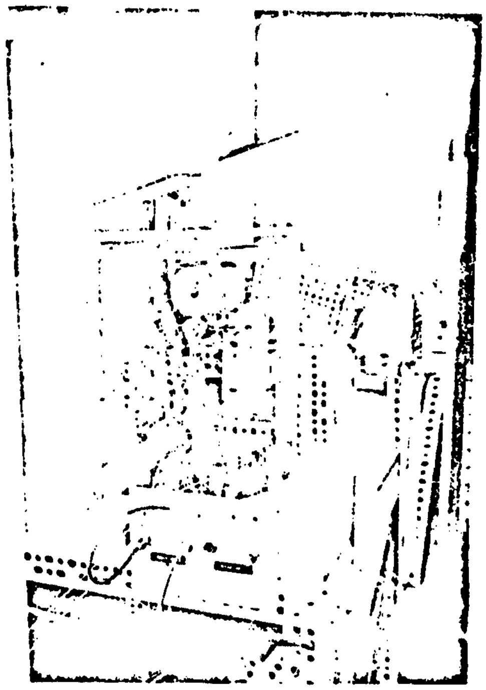

Fig. 13 Photograph of valve actuating mechanism and port with pipe attached.

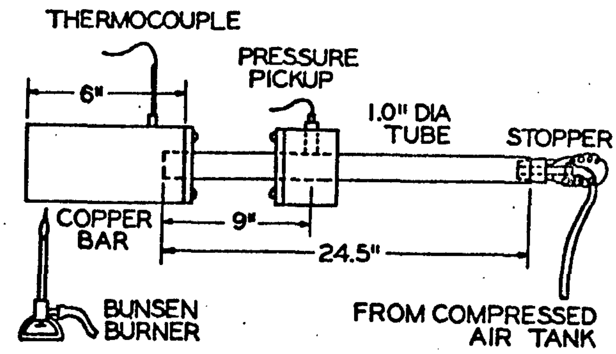

Fig. 14 Schematic of pressurized pipe bench test apparatus.

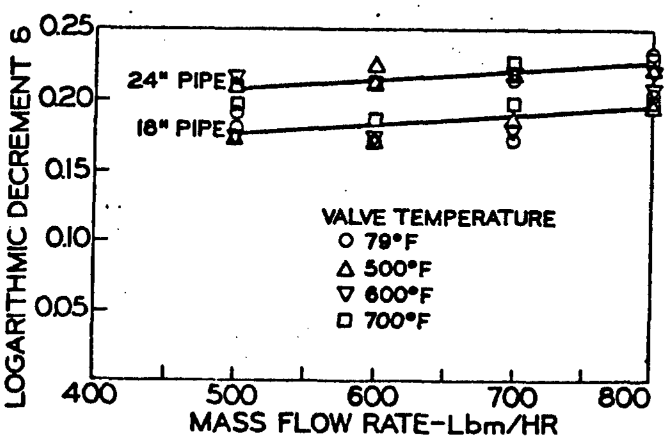

Fig. 15 Effect of valve temperature on wave damping.

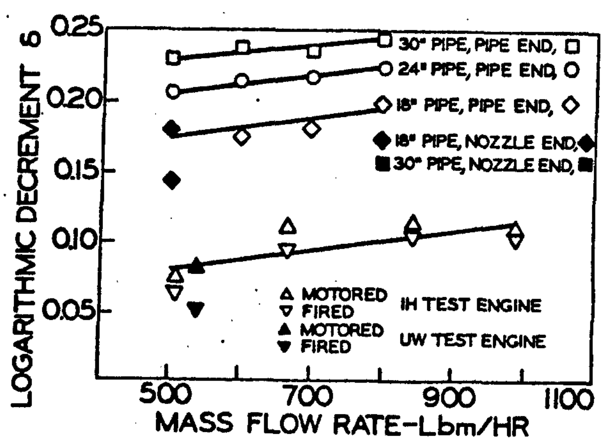

Fig. 16 Wave damping as function of mass flow rate.

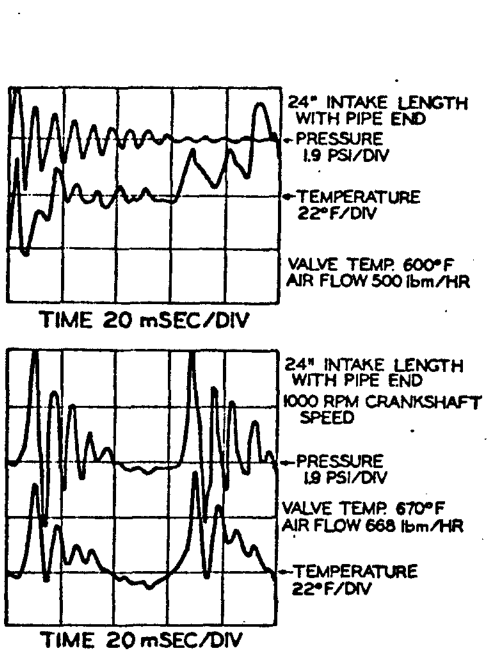

Fig. 17 Examples of pressure and temperature signals viewed on oscilloscope,

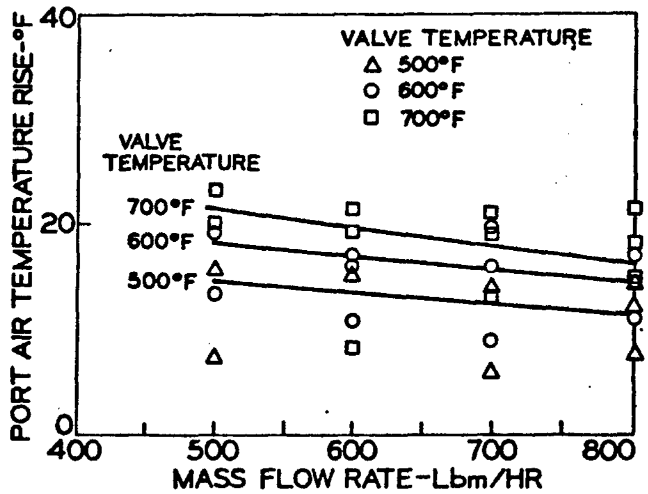

Fig. 18 Air temperature rise in port as function of valve temperature and mass flow rate.

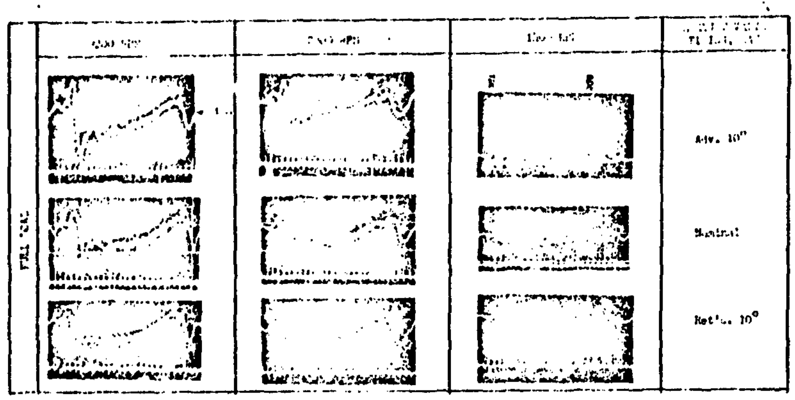

Fig. A Intake port dynamic pressure as influenced by exhaust valve timing (constant intake valve timing).

APPENDIX VIII

Some Problem Areas in Engine Simulation

G.L. Borman, P.S. Myers and O.A. Uyehara
Mechanical Engineering Dept.
University of Wisconsin

ABSTRACT

Problem areas in engine simulation where the required information is lacking are discussed. The need for improved heat transfer, combustion, friction, and turbocharger models is discussed as are instrumentation needs for measurements of accurate pressure, radiant heat transfer, time-varying cylinder velocities, and instantaneous mass flow rates.

INTRODUCTION

Ideally, an engine design should be optimized for each application. However, building and testing the many combinations required for this optimization is prohibitively expensive--both in time and money. Consequently, from the first conception of the internal combustion engine, a mathematical model of the fluid flow, heat transfer, and thermodynamic behavior of the engine (variously called cycle analysis, engine simulation, etc.) has been used to minimize optimization costs.

The usefulness of an engine simulation varies directly with its detail and complexity. For example, air-standard cycle analysis is mathematically simple but predicted details (such as the pressure-time diagram) are in poor agreement with observed values. Thus the analysis has limited utility. On the other hand, computation costs of engine simulation as well as the cost of obtaining necessary relationships increase rapidly with the detail and complexity included. Thus for a given stage of engine development there is a corresponding optimum engine simulation program from a cost-benefit standpoint.

Because of the complexity of the time-varying rate phenomena such as heat transfer, chemical kinetics, and gas dynamics occuring in the engine, the relatively sophisticated engine simulation programs in use today are still inadequate in many areas because systemized information is simply not available. This paper is an attempt to point out these problem areas, to summarize the information available, and to point out needed additional information. Space limitations dictate that the paper concentrate primarily on instrumentation, heat transfer, and combustion where the authors have specific knowledge and expertise, although brief commentaries are included on friction and turbochargers because they are important problem areas.

If information concerning the basic concepts of engine simulation is desired, see Refs. 1-3.

INSTRUMENTATION

Evaluation of the engine simulation programs and of new models for these programs requires accurate performance data plus instantaneous values of pressure, mass flow, heat transfer, etc. In the following section shortcomings of some of the instruments used and the need for new instruments to obtain experimental data are presented.

PRESSURE MEASUREMENTS ... Accurate measurement of indicated work depends primarily upon the accuracy of the pressure transducer (4)*. The pressure in the combustion chamber varies from approximately 1 to 200 atmospheres and the temperature

*Numbers in parentheses refer to References at end of paper.

from atmospheric to 4500 F. Rates of change of both temperature and pressure are large and highly variable.

In the construction of pressure transducers the diaphragm serves to keep the combustion gases from coming in contact with the sensing device and to keep a preload on the sensing element that is at least equal to atmospheric pressure, since without preload the transducer is unable to measure a vacuum. Brown (5) and Alyea (4) have shown the effect of transient heat transfer on this diaphragm. Their apparatus alternately subjected the diaphragm to the intense heat of flame and to the room atmosphere. This alternate heating and cooling caused temperature gradients and, even though the diaphragm was thin, relieved some of the preload on the sensing device. False signal outputs as high as 10 psi were measured.

Figure 1 was obtained by mounting two pressure transducers in the same fired engine cylinder. One diaphragm was coated with a silicone rubber compound while the other was uncoated. The trace labelled ΔP is the difference between the two outputs, while the trace labelled P is the output of the coated transducer. Alyea (4) fed the output signal from the pressure transducer to an IMEP meter. With the coated transducer the IMEP meter read 108 psi, whereas with the uncoated transducer the meter read 91.6 psi.

Instead of preload a mechanical connection can be made between the diaphragm and the sensing element. This is difficult to do with a transducer of the piezoelectric type, but in a strain tube type pressure pick-up the diaphragm can be easily connected to the strain tube. Pressures greater than atmospheric cause the diaphragm to push on the sensing element; pressures less than atmospheric pull on the sensing element. A design of this type has been made by Matsuoka (6).

HEAT TRANSFER MEASUREMENTS ... A heat transfer sensor should generate a signal that can be manipulated to give instantaneous heat flux data preferably without changing the normal heat transfer paths in an engine. Overbye (7) and LeFeuvre (8) employed an evaporated film thermocouple approximately 1.6 mm in diameter and threaded through the combustion chamber wall so that the thermocouple surface was flush. The body of the thermocouple was made of low carbon steel having approximately the same thermal characteristics as the combustion chamber wall and thus did not disturb normal heat transport. The evaporated film, approximately 1 micron thick, followed the surface temperature of the combustion chamber. From the generated voltage instantaneous values of heat flux could be computed.

Some of the problem areas are the effect of deposits from the combustion process as well as oil film coating that may alter the signal output. Overbye (7) showed that deposits can significantly affect heat transfer.

As will be pointed out later, radiation from carbon particles may contribute significantly to total heat flux. Ebersole (9) measured time-averaged values, but instantaneous values are needed.

Flynn (10) is developing a radiation spectrometer using an infrared solid-state radiation detector at liquid nitrogen temperature in an attempt to obtain instantaneous radiation intensities. Engine radiation is compared with radiation from broad ribbon tungsten lamp although the "radiation spectrometer" has been calibrated with a black body source.

VELOCITY MEASUREMENTS ... Instrumentation (sensors) to measure instantaneous velocities is sorely needed. Ohigashi (11) used a spark discharge to produce a 500-3000 μ sec. duration arc which travels with the air motion to a probe located a known distance down-stream. Since the distance from the gap to the probe is known, the velocity can be computed. The method is applicable to one-dimensional velocities, but obtaining velocities in three dimensions would be difficult. Instead of a continuous arc, Nakajima (12) used high-frequency, high-voltage electric pulses with each succeeding discharge essentially following along the moving path of the first discharge. With many pulses separated by known time intervals, the air motion can be followed photographically. This method requires a transparent window in the combustion chamber and presents measurement problems when three-dimensional motion is present.

Haffaker (13) continued the development of a system that uses the Doppler effect and light from a laser. The laser light is scattered from small particles in the air stream. Because of the Doppler effect, the frequency of the scatter light is slightly different than the frequency of the incident light. The two frequencies are hetrodyned to give a lower frequency which is proportional to velocity. The problem of equipping a diesel engine with a quartz cylinder head, which will allow transmission of the laser beams without optical distortion, could be difficult.

MASS FLOW RATE MEASUREMENTS ... Mass fuel flow rates are needed for prediction of heat release rates. Shipinski (14) mounted a small strain-gage-type pressure transducer near the tip of the injection nozzle to obtain the fuel injection pressure. He obtained the needle lift motion by having the needle vary the carrier frequency of the frequency modulated oscillator. This procedure, however, does not directly give mass fuel flow rates.

There is no satisfactory way to measure instantaneous mass flow rates in manifolds. Some of the techniques discussed under velocity measurements could be used for manifold velocity measurements, but some technique for measuring or calculating density would then be needed. Our capabilities of measuring instantaneous enthalpies are in an equally unsatisfactory condition.

HEAT TRANSFER

The high temperatures used in internal combustion engines to reduce irreversibilities, as well as the sequence of events, requires cyclic operation with consequent heat transfer to and from the walls. The desirability and importance of this heat transfer is highly variable both during the cycle for a particular engine and between different types and applications of engines.

While there are heat transfer problems on the water side and in calculating conduction in complicated engine shapes where heat fluxes are a function of space as as well as time, space limitations confine us to convective and radiant heat transfer on the gas side of the cylinder.

Figure 2 was prepared from engine simulation calculations (runs A and J of Ref. 1). Run A is for a naturally aspirated engine using a heat transfer correlation of the type suggested by Annand (15); in run J the heat transfer coefficient was arbitrarily increased by 30%. The first number is the percentage of the fuel input energy; the number in parentheses is the part temperature in F. Table 1 presents additional heat transfer data as well as approximate values for events affected by heat transfer.

Figure 2 and Table 1 show that: The largest single heat rejection item is to the piston; the heat rejection to the exhaust port is equal to or larger than the heat rejection to the head and valves; heat transfer significantly changes the gas temperatures involved; and factors other than heat transfer have a singificant fect on the gas temperature at the time the intake valve closes.

It can also be shown from the calculations that decreasing the heat transfer by one Btu per ihp-min (keeping all else constant) results in a 1.3 IMEP increase in IMEP, while decreasing the piston temperature 21 F, the head 18 F and the intake valve 29 F. While an increase of 1.3 IMEP may be desirable, a decrease of some 15-30 F for parts that are highly loaded from a thermal standpoint may be crucial to engine life.

Engine heat transfer is further complicated because heat fluxes measured simultaneously in the head of an open-chamber diesel engine vary considerably with position as illustrated in Fig. 3(8). Note the reversal of heat transfer at the two thermocouple locations between fired and motored conditions.

Figure 3 raises many questions. Is the large variation of heat flux with position caused by convective or radiant heat transfer? How does one model convective and radiant heat transfer to predict instantaneous heat fluxes that vary with position while still retaining reasonable computational simplicity? Is the best procedure to speak of an instantaneous space-averaged heat transfer coefficient and, if so, how is it evaluated and correlated?

RADIANT HEAT TRANSFER ... Radiant heat transfer is a function of the radiating and absorbing temperatures, the emissivity of the flame, and the absorptivity and configuration of the absorbing surfaces. It can be shown from Fig. 2 that, with the possible exception of the exhaust valve, the fourth power of the part temperatures is relatively small in comparison with combustion temperatures. Also, with the exception of the sleeve, part absorptivities are relatively constant. Thus we will concentrate on the temperature and emissivity of the radiating material.

Radiation may contribute significantly to heat transfer. Ebersole (9), in the only radiant heat transfer measurements known to the authors, obtained the time-averaged values of radiant heat transfer shown in Fig. 4. A study by Flynn (10) is currently underway at Wisconsin to measure instantaneous radiant heat transfer. Preliminary and unconfirmed results suggest that as much as 70% of the heat transfer during combustion is due to radiation. Clearly, further experimental data are necessary.

Radiation may come from either the gas itself or soot particles in the gas. Although more experimental data are needed, the authors believe gas radiation to be comparatively small. Overbye (7) shows data (Fig. 13) for an SI engine and states, "Thermocouple 3 does not respond until late in the cycle even though it is 'looking' at the flame front travelling across the combustion chamber; this suggests that radiant heat transfer* is not significant during combustion."

If gas radiation is small and Ebersole"s data are correct, particle radiation must be significant. The only particle emissivity measurements in engines known to the authors are those reported by Myers (16), who found emissivities up to 0.3-0.5 in a prechamber engine using a relatively short path length of about 1.5 in. An emissivity of 0.5 and a temperature of 5000 R gives radiant heat transfer rates of about 0.5×10^6 Btu per hr-ft^2 (compare with Fig. 3). Note that assuming the total number of particles is fixed, the sleeve sees a variable number of particles during expansion; the head and piston see a constant number.

Radiant heat transfer is extremely sensitive to source temperature. Most engine simulations have assumed homogeneous combustion; in practice the heterogeneous combustion exists. The homogeneous assumption will inevitably markedly underestimate radiant heat transfer for heterogeneous combustion. Is a more detailed combustion model necessary if reasonably accurate radiant heat transfer predictions are to be made?

The possibility that during heterogeneous combustion soot particles are formed at a relatively constant temperature must be recognized. This would occur if soot particles were formed at essentially a constant air-fuel ratio independent of wide variations in the overall fuel-air ratio. Evidence for this relatively constant and higher radiation temperature as compared to a space-averaged temperature is in the discussion of Uyehara (17).

CONVECTIVE HEAT TRANSFER ... The unusual convective heat transfer problems found in reciprocating engines are primarily a result of compression and expansion of the boundary layer and time-varying velocities which are induced by the piston motion, by the intake process, by the compression as a result of chamber configuration, and by combustion.

Pfriem (18), Elser (19), Overbye (7), and Oguri (20) recognized that compression and expansion of the boundary layer affects the profile of gas temperature versus distance.

To illustrate this effect, picture the temperature profile in the boundary layer of a motored engine at top center. As expansion takes place, the gas temperature everywhere will be reduced, except right at the wall where it will remain essentially constant. Expansion cooling may reduce the temperature of the gas close to the wall below the wall temperature, even though the bulk gas is considerably hotter than the wall. This distortion of the boundary layer temperature profile due to compression and expansion inevitably affects heat transfer rates.

---

*His work and comments are clearly limited to nonluminous flames.

Three experiments and corresponding calculations have been conducted at Wisconsin in an attempt to clarify the existence and magnitude of this effect. Goluba (21) measured the instantaneous heat flux at the stagnation point of a flow experiencing high-amplitude, steep-fronted pressure oscillations in air. Wendland (22) used an essentially closed cylinder to compress and expand the same air over and over. LeFeuvre (8) motored an open chamber diesel engine. As a part of their work all three made a one-dimensional conduction-compression model for flow and conduction in the gas. Excellent agreement between theory and experiment was found by Goluba; Wendland predicted theoretically about 50% of the experimentally measured heat transfer; LeFeuvre predicted theoretically only about 20% of the experimentally measured values. In spite of these experiments, the relative importance of compression and expansion in determining temperature profiles in practical situations is not clearly established.

Since most forced convection heat transfer correlations involve the Reynolds number as a measure of boundary layer thickness, the use of Reynolds number in engine heat transfer correlations is not surprising. However, the fluid velocity and characteristic dimension to be used is neither obvious nor probably constant during one cycle. LeFeuvre (8) estimated that establishment of a new boundary layer thickness when the gas velocity is changed occurs in times ranging 0.5-2.5 crank angle deg. Thus the assumption of quasi-steady conditions and the use of fluid velocities variable during the cycle seem appropriate.

Unfortunately, measurements of fluid velocities in an engine are rare. Semenov (23) measured turbulence intensity in an engine having a cylindrical combustion chamber and found that during compression turbulence intensity varied approximately linearly with engine speed. Other evidence for a linear relation between turbulence and speed comes from the known fact that flame speeds in SI engines vary approximately linearly with engine rpm. Also, if volumetric efficiency is constant with rpm inlet velocities must vary directly with rpm. Thus most heat transfer correlations have used mean piston speed as the appropriate velocity in the Reynolds number.

However, piston motion generates several velocities. The velocities perpendicular to the head and piston face are those used in the one-dimensional conduction-compression model (22). During intake the port and valve are often designed to produce a swirling gas motion about the axis of the cylinder bore. On compression near top center, piston and head cavities for combustion or valve purposes produce additional velocities. During blowdown gas velocities are not related to mean piston velocities.

Combustion can also produce gas motion. Woschni (24) recognized this possibility and included a combustion velocity term in his heat transfer expression. Even in flat cylindrical chambers, expansion of the hot burned gases with consequent compression and motion of the relatively cold unburned gases occurs. In divided chamber engines gross gas velocities are caused by combustion.

As our need for more sophisticated simulations increases, more detailed analyses and heat transfer correlations will be necessary.

COMBUSTION

The design and development of combustion systems is done experimentally with maximum dependence on past experience and minimal use of theory. Even the criteria for optimum design is a matter of judgment because of the many factors of performance such as fuel consumption, smoke level, thermal loading, peak pressure, rate-of-pressure rise, and exhaust emissions which must be balanced among themselves as well as over a range of speed, load, boost pressure, and applications. The simulation of combustion is probably the weakest link in cycle simulation.

APPARENT HEAT RELEASE RATES ... The approach used in most simulations has been an analysis of combustion based on experimentally obtained pressure-time histories. A true synthesis of the combustion process would require only those inputs which are available prior to actual construction and testing, but it is highly unlikely that a satisfactory universal combustion model of such a basic nature will ever be achieved. It may be expected, however, that progress will be made to the point where a combination of experimental analysis and combustion simulation will reduce

the cost and time needed to develop a specific engine. We will present a review of the current status of combustion simulation and point out the problems which must be overcome in moving toward a more complete synthesis.

Various approaches have been used to obtain the rate of heat release from an analysis of pressure-time diagrams. Schweitzer (25), Pischinger (26), Whitehouse (27), Krieger (28), and Goudie (29), among others, have applied a first law energy balance to the cylinder gas assuming a homogeneous system. Basically, all of these analyses use an equation of the form:

$$\frac{dU}{dt} + p\,\frac{dV}{dt} + \frac{dQ}{dt} = \frac{dQc}{dt}\ ;$$

where the terms on the left represent the time rate of change of internal energy, work, and heat transfer, respectively, and the term on the right represents the rate of energy generation caused by combustion. If the pressure is experimentally measured, the work term can be easily evaluated. By using a mass-average temperature obtained from the ideal gas law and an empirical heat transfer relationship, the heat transfer term can be estimated. Fortunately, the left hand side of the equation is not very sensitive to the heat transfer so that an error of even 50% in heat transfer will cause only a 5% change in the predicted total energy released by combustion. To evaluate the internal energy accurately, we must know the local composition and temperature throughout the combustion chamber. To illustrate this fact, imagine the chamber to be divided into a number of small volumes each of equal mass. If we could calculate the internal energy of each volume and then add up the energies, we would obtain the internal energy of the system. If, however, we assume a homogeneous composition and uniform temperature throughout the chamber and then calculate the internal energy, we shall be in error because we have used the mass average temperature. The error arises from the nonlinearity of the internal energy and equilibrium composition with temperature. This difficulty in correctly modeling the internal energy is further compounded by the difficulty in experimentally obtaining local values of either composition or temperature. One concludes, therefore, that the shape of the heat release curve predicted by the homogeneous model assumption is only an apparent shape.

If the experimental and calculated amounts of fuel burned do not agree, some adjustment must be made prior to using the heat release schedule in the simulation program. If one simply scales the entire heat release curve, considerable error may result in the subsequent calculation of the cylinder pressure. If the disagreement is caused by errors in only the last half of the pressure record, but the entire heat release is scaled up (or down), the resulting calculated pressure may be grossly in error and the predicted peak pressure and maximum rate-of-pressure-rise will be incorrect. The solution to this problem lies in improving the accuracy of the data or in theoretically correcting the data for transducer error.

Fortunately, the shape of the heat release curve has only a small influence on the IMEP, heat transfer per cycle, etc., (1,30). The cycle analysis can thus be used with fairly inaccurate heat release curves and still have utility in predicting the effects of changing valve size, manifold geometry, etc. The heat release curves in themselves also have utility in helping to understand the effects of experimental changes in the design of the combustion system. Such analysis may be aided by the use of the semi-empirical curve fitting procedure formulated by Wiebe (31) and further studied by Lange (32). Shipinski (33) was only moderately successful in correlating the coefficients used in the Wiebe equation and the extent to which his correlation can be accurately applied to other engines is currently unknown.

FUNDAMENTAL APPROACHES ... To obtain a true synthesis of the combustion process one should start with injection rate and predict the temperature, composition, and pressure as a function of time. In their pioneering work on diesel combustion Austen and Lyn (34) tried to connect the injection rate to the heat release rate by a simple empirical burning law. Held (35), Nagao (36), and Cook (37) further elaborated on the work of Lyn. In these models, as an increment of fuel is injected it is first assumed to undergo an ignition delay and then assumed to burn following some prescribed burning rate. The models do not explicitly account for such factors as droplet size distribution, spray penetration, air motion, etc.

Shipinski (14) has attempted to include more factors in a semi-empirical burning rate model by the application of droplet vaporization and burning theory. Starting from the injection pressure, a mean droplet diameter is calculated. The droplets

are assumed to vaporize according to a simple steady-state formula for single droplets in the air. Ignition delay is calculated by an empirical ignition delay formula. At the end of the delay period the vaporized fuel is arbitrarily assumed to burn in one crank angle deg. The unvaporized fuel is assumed to burn according to a spray burning law developed by Tanasawa for gas turbine spray. The mass burning rate so obtained is used in a homogeneous combustion model, such as that proposed by Borman (38), and can thus be compared directly to the burning rate curves obtained by use of experimental pressure-time data and a homogeneous first law combustion model. Such comparisons showed rather unsatisfactory agreement and led Shipinski to propose various empirical modifications to the spray burning law. While the proposed modification improve the Shipinski model, they are neither of a universal nature nor are they able to bring about completely satisfactory results. This is not unexpected since the Shipinski model does not explicitly account for the mixing process caused by air motion and spray penetration or for the fact that a diesel spray is both unsteady and dense. Furthermore, the model for the premixed burning does not bring in the reaction rate and other factors which determine flame propagation. Lastly, the model predicts a burning rate to be used with the assumption of homogeneous energy release and thus can be criticized on this basis. Despite these critical remarks, it is encouraging that a relatively simple phenomenological model showed some success in predicting diesel combustion over a fairly wide range of engine conditions. In particular, it appears that further work is justified especially to include modeling of these phenomena for which Shipinski found a group empirical correction necessary. In addition, it seems desirable to remove the homogeneous restriction from the combustion model. For example, one might divide the chamber into two reaction zones (rich diffusion burning and premixed burning), a mixing zone and an unmixed air zone. Application of first law energy balances to such a model might provide further insight into the nature of the combustion as well as to predict such factors as radiation heat transfer, smoke, and NO formation.

It should be pointed out that the above discussion concentrates on modeling of the diesel combustion based on various thermodynamic and fundamental phenomenological approaches. One could attack the problem from a completely experimental view point by conducting an extensive set of statistically designed experiments and then empirically correlating the results using curve-fitting procedures. Such an approach could be used directly during the design process and would replace the mathematical simulation approach in so far as the combustion part of the cycle is concerned.

In conclusion, the modeling of the combustion process needs work on all fronts. Better instrumentation is needed to both provide data for modeling and to provide a method of evaluating the models. Basic information is needed on diesel sprays, engine air motion, and droplet burning under diesel conditions. Models which remove the assumption of homogeneous heat release as well as models which try to incorporate basic theory into a phenomenological synthesis are needed. Lastly, better data obtained from statistically designed experiments are needed in order to provide a sound basis for evaluation of the theoretical efforts.

FRICTION

Before engine output (brake hp) can be computed from piston work (indicated hp), information on engine friction is required. Some writers include cylinder and crankcase pumping losses with friction. However, since these losses are predicted by the simulation program we shall consider only rubbing between surfaces as engine friction. Although power requirements for accessories must also be subtracted from the indicated work, we shall not discuss these losses because of space limitations.

Rubbing friction depends on many factors: surface roughness, oil film thickness, surface loading (inertia and gas), etc. Many of these are highly variable during the cycle as well as with engine conditions. In general, instantaneous values of friction do not seem to be necessary for simulation purposes.

Gish (39), using statistically averaged pressures obtained with a balanced diaphragm pressure pick-up, computed IMEP values. Using these and measured BMEP values he obtained FMEP values. He found that FMEP varied with peak pressure and that motored FMEP trends and values differed from fired FMEP trends and values. The data did not permit correlation of FMEP trends with engine design.

Bishop (40) attempted to analyze the friction of different engine components such as bearings, rings, pistons, etc. as a function of engine rpm and cylinder pressures using data from four spark-ignition engines. The general applicability of the relationship he found has not been established. Blair (41) attempted a similar procedure for a compression-ignition engine. He gives a mathematical formula for friction horsepower. Alyea (4) using his IMEP meter, studied FMEP for a single cylinder engine as a function of warm-up time maintaining a constant crankcase oil temperature. He found that FMEP decreased by 50% over the period of 1 hr after the engine was started.

Again, one must conclude that adequate data do not exist. FMEP is an important factor in engine performance and simulation, and is a fruitful area for imaginative research.

TURBOCHARGERS

The analysis of a multicylinder turbocharged engine depends on the simulation of the incylinder events, on the simulation of the gas dynamics of the manifold and on calculations of the turbocharger performance. We have already indicated some of the major problems in simulating the incylinder events. The problem of simulating the gas dynamics in the manifolds has been treated by many authors including papers by Benson (3). Manifold simulations use a one-dimensional analysis and only approximate multidimensional effects which can occur at junctions and in curved sections. Friction is also included only in an approximate form by use of steady flow formulas. As was pointed out in the previous discussion of heat transfer, the heat transfer in the exhaust port can be very important in determining the energy available to the turbine. The expressions which are used for heat transfer in the exhaust system are very approximate and thus also limit the accuracy of the gas dynamic analysis. Despite these approximations the one-dimensional analysis gives reasonably a accurate results. The complexity of the analysis, however, causes large increases in the computation time and presents a cost-effectiveness problem.

From the simplest point of view, the turbine can be represented as an orifice at the end of the manifold with appropriate coefficients obtained from experimental analysis of the turbine. If, in fact, the engine produced a steady flow of constant pressure gas to the turbine, the accuracy of the analysis would be limited only by the accuracy of the steady-flow turbine map. Unfortunately, the engine in most cases produces a pulsating flow. Thus numerous unanswered questions arise. Because of inertia the turbine operates at a constant speed during steady-state running of the engine. The pressure ratio across the turbine at any instant may thus not correspond to any steady-state point on the turbine map. Under extreme cases the pressure ratio may even be momentarily reversed. The instantaneous mass flow and efficiency are unknown under conditions of pulsating flow. A quasi-steady flow analysis can be used which will partially correct for the pulsations, but complete data for such analysis is also unavailable. For example, one could drive the turbine at a steady speed (by supplying power to the shaft if necessary) while maintaining an arbitrarily constant pressure ratio. While the authors are not aware of any extensive analysis of this type, there have been experiments performed with unsteady flows produced by cold gas pulsation generators (42,43). Quasi-steady flow analysis (QSF) based on experimental data was used by both authors and compared with measured performance. Several of the conclusions of the two papers are in disagreement. Wallace found the swallowing capacity reduced and Benson found it increased under nonsteady flow conditions. Benson explains this difference on the basis of the pressure fluctuations downstream of the turbine which were neglected by Wallace. A second discrepancy which seems unresolved arose in the effect on measured power. Wallace found the measured power to be less than indicated by QSF analysis, while Benson found the opposite to be true. In addition to these full admission results, Benson found that "the quasi-steady flow analysis using partial admission test data would grossly underestimate the mass flow rate and power output of the turbine." The magnitude of the unsteady flow effects was found to be dependent on the pulse frequency and turbine speed. The effect of wave shape is not so clear. For example, some manifolds are short enough to be treated by a filling and emptying analysis rather than a wave analysis. One would expect that systems produce less steep pressure changes and thus may be more accurately approximated by a QSF analysis of the turbine. It should also be pointed out that the effects of unbalanced pressure and flows in the two scrolls of the divided housing in radial flow turbines is a further cause of complexity in the analysis. In this regard, axial flow turbines may

present a simpler problem and indeed some evidence exists (44) that QSF analysis can be successfully applied to axial flow turbines.

The problems in predicting nonsteady flow effects in turbines can be equally applied to compressors (45). Both the surge point and efficiency are influenced by nonsteady conditions. From these effects, it is clear that steady flow data for matching conditions will lead to inaccuracies in the match point.

In conclusion, it is clear that much additional work is required before the accurate simulation of turbochargers can be carried out. The solution to these problems is made difficult by the lack of experimental methods for measuring instantaneous mass flows and efficiencies.

REFERENCES

1. K.J. McAulay, Tang Wu, Simon K. Chen, G.L. Borman, P.S. Myers, and O.A. Uyehara, "Development and Evaluation of the Simulation of Compression Ignition Engines." SAE Transactions, Vol. 74 (1965), paper 650451.
2. R.B. Krieger, R.R. Booy, P.S. Myers, and O.A. Uyehara, "Simulation of Crankcase Scavenged, Two Stroke, SI Engine and Comparisons with Experimental Data, Paper 690135 presented at SAE International Automotive Engineering Congress, Detroit, January 1969.
3. R.S. Benson, ASME paper 69-WA/DGP-9, 1969.
4. J.W. Alyea, P.S. Myers, and O.A. Uyehara, "The Development and Evaluation of an Electronic Indicated Horsepower Motor." Paper 690181 presented at SAE International Automotive Engineering Congress, Detroit, January 1969.
5. W.L. Brown, "Methods for Evaluating Requirements and Errors in Cylinder Pressure Measurement." SAE Transactions, Vol. 76, paper 670008.
6. S. Matsuoka, Private Communication, 1967.
7. V.D. Overbye, J.E. Bennethum, O.A. Uyehara, and P.S. Myers, "Unsteady Heat Transfer in Engines. SAE Transactions, Vol. 69 (1961), paper 201-C.
8. T.L. LeFeuvre, P.S. Myers, and O.A. Uyehara, "Experimental Instantaneous Heat Fluxes in a Diesel Engine and Their Correlation." Paper 690464 presented at SAE Mid-Year Meeting, Chicago, May 1969.
9. George D. Ebersole, P.S. Myers, and O.A. Uyehara, "The Radiant and Convective Components of Diesel Engine Heat Transfer." Paper 701-C presented at SAE International Summer Meeting, Montreal, June 1963.
10. Patrick F. Flynn, PhD Thesis, Mech. Engr. Dept., Univ. of Wisc., To be completed in 1970.
11. S. Ohigashi, Y. Hamamoto, and S. Tanabe, "A New Digital Method for Measuring Gas Flow Velocity by Electric Discharge." Paper 690180 presented at SAE International Automotive Engineering Congress, Detroit, January 1969.
12. K. Nakajima, et al, Bul. JSAE, 1969.
13. R.M. Huffaker, "Application of Laser Doppler Velocity Instrumentation to the Measurement of Jet Turbulence." Paper 690266 presented at SAE International Automotive Engineering Congress, Detroit, January 1969.
14. J.H. Shipinski, PhD Thesis, Mech. Engr. Dept., Univ. of Wisc., 1967.
15. W.J.D. Annand, Proc. Inst. of Mech. Eng., Vol. 177, No. 36, 1963.
16. P.S. Myers and O.A. Uyehara, "Flame Temperature Measurements--Electronic Solution of the Temperature Equations." SAE Quarterly Transactions, 1947.
17. O.A. Uyehara and P.S. Myers, "Diesel Combustion Temperatures--Influence of Fuels of Selected Composition." SAE Quarterly Transactions, 1949.
18. H. Pfriem, Forschung, Geb. Eng., Vol. 13, pp. 150-164, 1942.
19. K. Elser, Mitt 15, Inst. Thermodyn., Verbrennungsmotorenbrau, ETH, Zurich, 1954.
20. T. Oguir, B-1. Jap. Soc. Mech. Engrs., Vol. 3, pp. 363 & 370, 1960.
21. R.W. Goluba and G.L. Borman, Int. J. Heat Mass Transfer, Vol. 12, pp. 1281-1293, September 1969.
22. D.W. Wendland, PhD Thesis, Mech. Engr. Dept., Univ. of Wisc., 1968.
23. E.S. Semenov and A.S. Sokolik, IZV. An SSR Otd. Tehn. n. No. 8, p. 130, 1958.
24. G. Woschni, "A University Applicable Equation for the Instantaneous Heat Transfer Coefficient in the Internal Combustion Engine." SAE Transactions, Vol. 76 paper 670931.
25. P.H. Schweitzer, Penn. State Univ. Engr. Expt. Station, Bul. 35, September 1926.

26. A. Pischinger and F. Pischinger, Die Verbrennungskraft maschine Band 7, Springer-Verlag, Vienna, 1957.
27. N.E. Whitehouse, et al., I.M.E., Vol. 176, pp. 195-217, 1962.
28. R.B. Krieger and G.L. Borman, ASME paper 66-WA/DGP-4, November 1966.
29. G.D. Goudie, Eleventh Int. Sym. on Comb., 1966.
30. H. Weber and G.L. Borman, "Parametric Studies Using a Mathematically Simulated Diesel Engine Cycle." SAE Transactions, Vol. 76, paper 670480.
31. I. Wiebe, Verlag der Akademie der Wissenchaften der VdSSR, Moscow, 1956.
32. W. Lange and G. Woschni, MTZ 25/7, 1965.
33. J.H. Shipinski, O.A. Uyehara, and P.S. Myers, ASME paper 68-DGP-11,1968.
34. A.E.W. Austen and W.T. Lyn, Proc. I.M.E., 1960-61, pp. 47-62.
35. G. Held, MTZ 27/12, 1966, pp. 480-484.
36. F. Nagao, M. Ikegami, and K. Oshima, Bul. JSME, Vol. 10, No. 39, (1967), pp. 532-542.
37. H.A. Cook, "Diesel Engine Cycle Analysis of Relationships of Fuel Injection to Fuel Compression Ignition Characteristics and Best Fuel Utilization." Paper 650449 presented at SAE Mid-Year Meeting, Chicago, May 1965.
38. G.L. Borman, PhD Thesis, Mech. Engr. Dept., Univ. of Wisc., 1964.
39. R.E. Gish, J.D. McCullough, J.B. Retzloff, and H.T. Mueller, "Determination of True Engine Friction." SAE Transactions, Vol. 66 (1958)
40. I. Bishop, "Effect of Design Variables on Friction and Economy." SAE Transactions, Vol. 73 (1965), paper 812-A.
41. L.W. Blair, Midwestern Simulation Council Meeting--NASA, Cleveland, 1965.
42. R.S. Benson and K.H. Scrimshaw, Proc. I.M.E., 1965-66, Vol. 180, Part 3J, paper 23/66.
43. F.J. Wallace and G.P. Blair, ASME paper 65-GTP-21, 1965.
44. J.H. Horlock and R.S. Benson, Proc. Sixth Int. Cong. Combustion Engines, Copenhagen, 1962.
45. R.S. Benson and A. Whitfield, Proc. I.M.E., 1965-66, Vol. 180, Part 1, paper P27/66.

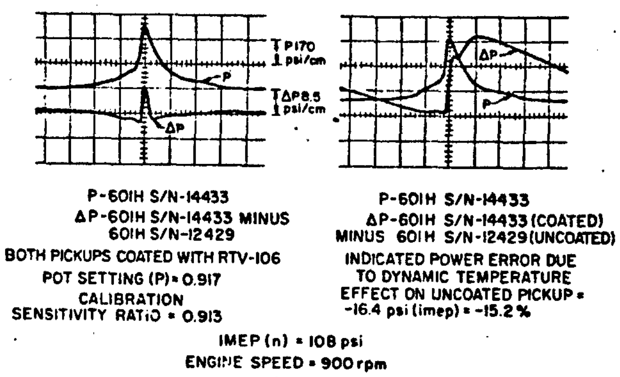

Fig. 1 Transient heat transfer effect on measured pressure.

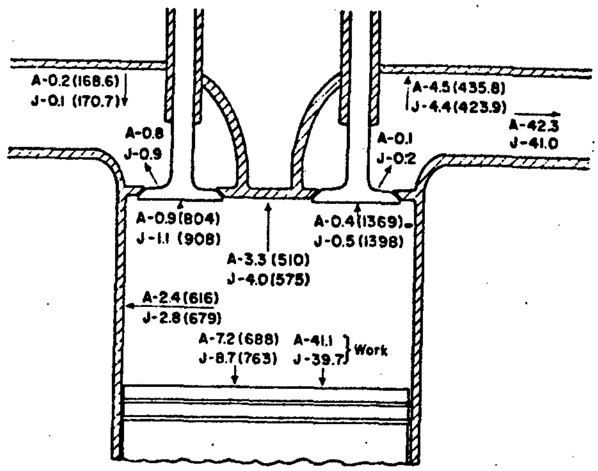

Fig. 2 Comparison heat transfer data for cylinder head.

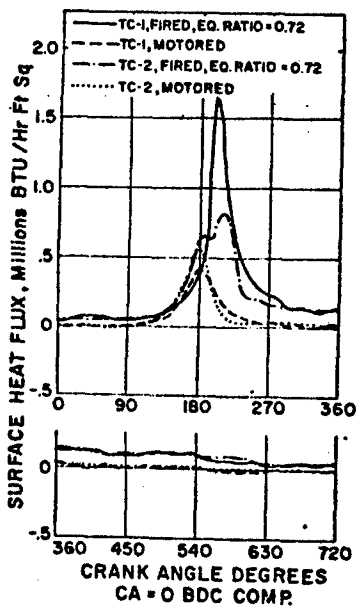

Fig. 3 Effect of thermocouple location on surface heat flux.

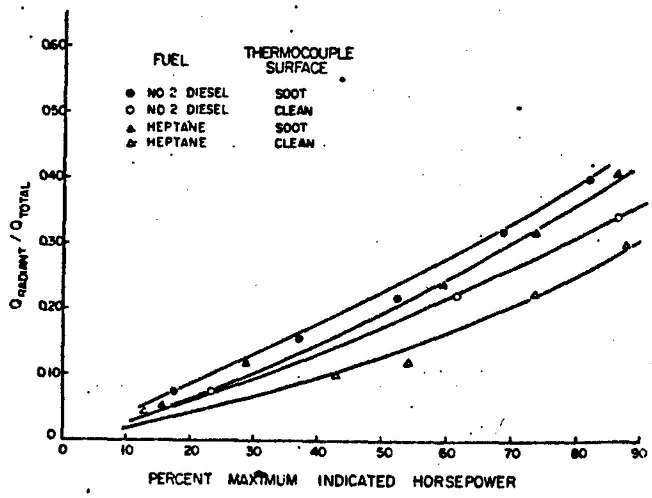

Fig. 4 Time-averaged radiant heat transfer in a diesel engine.